

**Faculty of Science and Engineering**

**Department of Civil Engineering**

**Characterisation of Static Liquefaction of Sand with  
Different Mixtures of Fines**

**Ayad Salih Sabbar**

**This thesis is presented for the degree of**

**Doctor of philosophy**

**of**

**Curtin University**

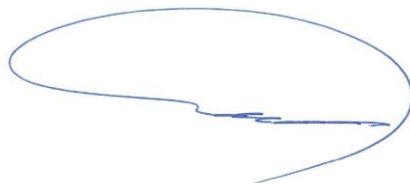
**April 2018**

# Declaration

To the best of my knowledge and belief, this thesis contains no materials previously published by any other person except where due acknowledgement has been made.

This thesis contains no material which has been accepted for the award of any other degree or diploma in any university.

**Signature:**

A handwritten signature in blue ink, consisting of a large, sweeping oval shape followed by a horizontal line and a small flourish.

**Date: 4/4/2018**

# Abstract

This research provides a comprehensive study of the static liquefaction behaviour of sand with various amounts of fines (slag, clay and a combination of slag and clay). The work was performed in two stages. In the first stage, the experiments were conducted under conditions of undrained static triaxial compression. Then, the results of the experimental work were used to develop artificial neural network (ANN) and genetic programming (GP) models for predicting the liquefaction susceptibility of clean sandy soils and sand–fines mixtures.

Conventional undrained triaxial compression tests were conducted using isotropically consolidated specimens under different testing conditions. The samples were prepared by the dry mixing of clean Perth sand with three amounts of slag (2%, 4% and 6%), two amounts of bentonite (3% and 5%), two amounts of kaolinite (3% and 5%), and sand containing combinations of slag and clay. Samples were prepared at three relative densities (10%, 50% and 90%) and sheared under three initial confining pressures (100, 150 and 200 kPa). Some of the clean sand tests were performed on partially saturated samples to investigate the effect of the degree of saturation on the liquefaction behaviour of sandy soils. The experimental results showed that the complete static liquefaction with zero effective stress occurred in clean sandy soils at a very low relative density and the lowest confining pressure. The deviatoric stresses of clean sandy soil were increased, and the pore water pressure ratios decreased with an increase in the initial confining pressure indicating ‘reverse behaviour’. An increase in the relative density significantly improved the shear strength of clean sandy soils, and its behaviour shifted from reverse to normal when the relative density increased. The undrained behaviour of sandy soil significantly improved with a decrease in the degree of saturation, and the samples with the lowest degree of saturation exhibited the highest deviatoric stress and the lowest pore water pressure ratio. The experimental results also showed that the liquefaction behaviour of sand–fines mixtures were profoundly dependent upon the type (i.e. plastic or non-plastic) and the amounts of fines. The liquefaction susceptibility of clean sandy soils decreased significantly when sand was mixed with slag, and the mixture of sand–4% slag showed the lowest value. The effect of the slag content on the liquefaction behaviour of sandy soils was hindered by an increase in the relative density. Furthermore, the presence of slag in sandy soils

enhanced the ability of the soil to generate the reverse behaviour. The positive effect of slag on the liquefaction susceptibility of sandy soils could be related to the role of slag particles in enhancing the soil fabric, which reduced the ability of the soil to generate pore water pressure. The results of the undrained triaxial tests conducted on the sand–clay mixtures demonstrated that the clay mineralogy might play a substantial role in the liquefaction behaviour of sandy soils. The presence of the fines content increased the ability of sandy soils to liquefy. The liquefaction susceptibility of the sand–3% bentonite mixture was lower than that of sand–5% bentonite. The presence of bentonite also increased the ability of sandy soil to generate the reverse behaviour. The role of the low bentonite content in producing unstable soil fabric may be responsible for increasing the liquefaction susceptibility of the sand–bentonite mixtures. The liquefaction susceptibility of sandy soils reduced when they were mixed with kaolinite clay, and the mixture of sand–3% kaolinite exhibited lower liquefaction susceptibility than sand–5% kaolinite. In both of these sand–clay mixtures, the liquefaction susceptibility decreased when the clay content was 3%; then, it increased with an increase in the clay content to 5%. Furthermore, the mixtures of sand–kaolinite exhibited lower liquefaction susceptibility than the sand–bentonite mixtures. The liquefaction susceptibility of sandy soil decreased considerably when the sandy soil was mixed with a combination of slag and clay, and the mixtures of sand–4% slag–3% kaolinite had the lowest values of the undrained brittleness index and the pore water pressure. The results of this study indicated that the undrained brittleness index, state parameter at the start of the test and stress ratio at the instability line could be efficiently used to evaluate the liquefaction susceptibility of sandy soil. The ANN and GP results revealed that both of these approaches could well predict the liquefaction susceptibility of clean sandy soils and sand–fines mixtures with the lowest values of the coefficient of determination and the root mean square error.

# Publications

The following publications have resulted from this research.

## Refereed published journal papers:

- 1- Sabbar, A., Chegenizadeh, A., & Nikraz, H. (2016). A review of the experimental studies of the cyclic behaviour of granular materials: Geotechnical and pavement engineering. *Australian Geomechanics Journal*, 51(2), 89-103.
- 2- Sabbar, A. S., Chegenizadeh, A., & Nikraz, H. (2017d). Static liquefaction of very loose sand–slag–bentonite mixtures. *Soils and Foundations*, 57, 341-356. Doi: <https://doi.org/10.1016/j.sandf.2017.05.003>.
- 3- Sabbar, A. S., Chegenizadeh, A., & Nikraz, H. (2017c). Prediction of liquefaction susceptibility of clean sandy soils using artificial intelligence techniques. *Indian Geotechnical Journal*. Doi: 10.1007/s40098-017-0288-9.
- 4- Sabbar, A. S., Chegenizadeh, A., & Nikraz, H. (2017a). Effect of fines content on static liquefaction susceptibility of sandy soil. *World Academy of Science, Engineering and Technology, International Journal of Geotechnical and Geological Engineering*, 4(11).
- 5- Sabbar, A. S., Chegenizadeh, A., & Nikraz, H. (2017b). Experimental investigation on the shear strength parameters of sand-slag mixtures. *World Academy of Science, Engineering and Technology, International Journal of Geotechnical and Geological Engineering*, 11(3), 198-203.
- 6- Sabbar, A. S., Chegenizadeh, A., & Nikraz, H. (2018). Effect of slag and bentonite on shear strength parameters of sandy soil. *Geomechanics and Engineering*, 15(1), 659-668.

## **Refereed published conference papers:**

- 1- Sabbar, A. S., Chegenizadeh, A., & Nikraz, H. (2017, November 28-29). *Effect of fines content on static liquefaction susceptibility of sandy soil*. Paper presented at the 19<sup>th</sup> International Conference on Geotechnical Planning, Design, Analysis and Research. Melbourne, Australia.
- 2- Sabbar, A. S., Chegenizadeh, A., & Nikraz, H. (2017d, 10-12 December). *Influence of slag content on liquefaction susceptibility of sandy soils*. Paper presented at the One Curtin International Postgraduate Conference, Miri, Sarawak, Malaysia.
- 3- Sabbar, A. S., Chegenizadeh, A., & Nikraz, H. (2017, March 05-06). *Experimental investigation on the shear strength parameters of sand-slag mixtures*. Paper presented at the 19th International Conference on Ground Improvement Methods for Stabilization of Different Soils. Rome, Italy.

## **Awards**

- 1- Best paper award at the 19<sup>th</sup> International Conference on Geotechnical Planning, Design, Analysis and Research. Melbourne, Australia, November 28-29, 2018.
- 2- Best paper award at the 19<sup>th</sup> International Conference on Ground Improvement Methods for Stabilization of Different Soils. Rome, Italy, March 05-06, 2017.

# ACKNOWLEDGEMENTS

I would like to extend my sincere gratitude and profound respect to my supervisor, Professor Hamid Nikraz, for his patience, advice, support and encouragement during my study. I am greatly indebted to him for his timely advice, hearty concern for my research and the intensive, regular meetings to guide me throughout my time as his student.

I would also like to express my gratitude to Dr Amin Chegenizadeh, my co-supervisor, for his invaluable suggestions, motivation, stimulating discussions and perpetual direction throughout my study time in our regular meetings. His guidance and support have been invaluable on both personal and academic levels.

I would like to extend my appreciation to the Higher Committee for Education Development in the Republic of Iraq for sponsoring me and giving me this great opportunity to study for my PhD degree at such a well-known university the Curtin University.

I would like to convey my gratitude to Dr Ranjan Sarukalige for being the chairperson of my thesis committee. I sincerely thank the Department of Civil Engineering at Curtin University for providing a pleasant research environment, with specific thanks to Dr Megan Walske for her assistance. I would also like to extend my gratitude to the technicians of Geomechanics lab for their helping me in doing my experiments. Also, I would like to thank the staff of Microscopy and Microanalysis Facility for their help in doing SEM and EDS tests.

Finally, I would like to express my deepest love to my family in Iraq for their sincere prayers which have kept me on the path to success. Sincere thanks and great appreciation to my beloved wife for her support and love in good and bad times.

# Table of Contents

Declaration	i
Abstract	ii
Publications	iv
ACKNOWLEDGEMENTS.....	vi
Table of Contents.....	vii
List of Figures.....	x
List of Tables	xvii
List of Acronyms, Abbreviations, and Notations .....	xvii
Chapter 1: Introduction .....	1
1.1 Background of the Study.....	1
1.2 Research Objectives.....	7
1.3 Significance.....	8
1.4 Thesis Organisation .....	9
Chapter 2: Literature review .....	11
2.1 Introduction .....	11
2.2 Undrained behaviour of sandy soil .....	11
2.2.1 Types of undrained behaviour.....	12
2.2.2 Critical and steady-state conditions .....	17
2.3 Liquefaction and instability of sandy soils.....	24
2.4 Static liquefaction of clean sandy soils .....	33
2.4.1 Effect of initial state .....	33
2.4.2 Effect of stress mode .....	38
2.4.3 Effect of sample preparation method.....	39
2.4.4 Effect of degree of saturation.....	41
2.4.5 Effect of compositional characteristics .....	44
2.5 Static liquefaction of sandy soils with fines .....	46
2.6 Liquefaction susceptibility .....	57
2.7 Evaluation of liquefaction of sand using Artificial Intelligence approaches.....	65
2.8 Link between static and cyclic liquefaction .....	73
2.9 Summary .....	74
Chapter 3: Materials and Methods .....	76
3.1 Introduction .....	76
3.2 Materials.....	77



3.2.1 Sand .....	77
3.2.2 Slag .....	79
3.2.3 Bentonite.....	81
3.2.4 Kaolinite .....	84
3.3 Triaxial testing system .....	86
3.3.1 General description.....	86
3.3.2 Specimen preparation .....	91
3.3.3 Saturation .....	95
3.3.4 Consolidation .....	96
3.3.5 Shearing .....	97
3.3.6 Corrections to triaxial test data .....	98
3.3.6.1 Membrane corrections .....	98
3.3.6.2 Sample detail corrections .....	100
3.4 Artificial intelligence analysis .....	101
3.4.1 Artificial neural network (ANN) models .....	101
3.4.2 Genetic programming (GP) models.....	104
3.5 Testing program.....	107
Chapter 4: Static Liquefaction Behaviour of Sand–Fines Mixtures.....	110
4.1 Introduction .....	110
4.2 Static liquefaction behaviour of clean sand.....	111
4.2.1 Effect of confining pressure .....	111
4.2.2 Effect of relative density .....	120
4.2.3 Static liquefaction behaviour of partially saturated sandy soils .....	128
4.2.4 Liquefaction susceptibility of fully saturated sandy soil .....	132
4.3 Effect of slag on liquefaction behaviour of sandy soil.....	144
4.4. Effect of bentonite on liquefaction susceptibility of sandy soils .....	166
4.5. Effect of kaolinite on liquefaction susceptibility of sandy soils .....	185
4.6. Influence of clay mineralogy on liquefaction susceptibility of sandy soils.....	206
4.7 Summary .....	210
Chapter 5: Static Liquefaction Behaviour of Sand–Slag–Clay Mixtures.....	211
5.1 Introduction .....	211
5.2 Liquefaction behaviour of sand–slag–bentonite mixtures.....	212
5.3 Liquefaction behaviour of sand–slag–kaolinite mixtures.....	225
5.4 Summary .....	243
Chapter 6: Modelling of Liquefaction Susceptibility Using Artificial Intelligence Approaches.....	244
6.1 Introduction .....	244

6.2 Modelling of liquefaction susceptibility of clean sand soils .....	245
6.2.1 Artificial neural network (ANN) models .....	245
6.2.2 Genetic programming model.....	253
6.2.3 Parametric study .....	257
6.3 Modelling of liquefaction susceptibility of sand–fines mixtures.....	258
6.3.1 Artificial neural network (ANN) models .....	258
6.3.2 Genetic programming model of sand–fine mixtures .....	269
6.4 Summary .....	272
Chapter 7: Conclusions and recommendations .....	274
7.1 General .....	274
7.2 Conclusions .....	274
7.3 Recommendations.....	280
References	282
Appendix	294

# List of Figures

Figure 1.1 Soil liquefaction (Rapti, 2016).....	2
Figure 1.2 Proposed flow chart for the assessment of soil liquefaction (Robertson & Fear, 1995) .....	3
Figure 1.3 Aerial photograph of the Merriespruit tailings dam failure (Fourie, Blight, & Papageorgiou, 2001) .....	5
Figure 1.4 Aerial photograph of the Aberfan disaster (Hutchinson, 1986) .....	5
Figure 2.1 Types of undrained behaviour of saturated sandy soil under static loading: (a) stress–strain relationships, (b) stress paths, and (c) excess pore pressure–strain relationships (adapted and modified from (Chern, 1985) and (Bobei, 2004)) .....	14
Figure 2.2 Behaviour of dense sands under undrained static loading after large strains (adopted and modified from (Chern, 1985)) .....	17
Figure 2.3 Typical states of the undrained loading behaviour of saturated sandy soil: (a) stress–strain relationships and (b) stress paths (adapted and modified from (Murthy et al., 2007)) .....	18
Figure 2.4 Steady state and isotropic consolidation lines of sandy soil (Thevanayagam & Mohan, 2000) .....	21
Figure 2.5 Effect of non-plastic silt content on the position of CSL of Ottawa sand in the $e - \log p'$ space (Murthy et al., 2007) .....	22
Figure 2.6 Undrained behaviour of sandy soils (Yamamuro & Lade, 1998).....	26
Figure 2.7 Difference between collapse surface and flow liquefaction line (Yang, 2002) .....	29
Figure 2.8 Instability line and zone of potential instability defined by undrained and drained tests for loose sandy soil (Chu & Leong, 2002).....	32
Figure 2.9 Effect of relative density on undrained behaviour of sandy soil (Poulos et al., 1985).....	35
Figure 2.10 Undrained static behaviour of isotropically consolidated sample (Alarcon-Guzman et al., 1988).....	36
Figure 2.11 Critical state line for triaxial tests and plane–strain tests (Wanatowski & Chu, 2007).....	39
Figure 2.12 Effect of sample preparation method on the monotonic undrained behaviour of sandy soil (Vaid & Sivathayalan, 2000) .....	41
Figure 2.13 Relationships between the peak deviator stress and the B value for Toyoura sand (Ishihara et al., 2004) .....	43
Figure 2.14 Ranges of liquefaction-susceptible soils (Ishihara, Troncoso, Kawase, & Takahashi, 1980).....	45
Figure 2.15 Schematic representation of loose silty sand showing the particle structure hypothesis (Yamamuro & Lade, 1997b) .....	51
Figure 2.16 Effect of fine content on the particle structure of binary mixtures (Yamamuro & Covert, 2001) .....	52
Figure 2.17 Classification of granular sand (Thevanayagam & Martin, 2002) .....	52

Figure 2.18 Factors affecting liquefaction susceptibility of soil .....	58
Figure 2.19 Schematic representation of liquefaction susceptibility of soils: a) small susceptibility to liquefaction and b) high susceptibility to liquefaction (Verdugo & Ishihara, 1996) .....	59
Figure 2.20 Description of the modified state parameter (Bobei et al., 2009).....	62
Figure 2.21 Typical structure of ANN (Das, 2013) .....	67
Figure 2.22 Flowchart for major stages in the development of ANN models (Maier & Dandy, 2000) .....	68
Figure 2.23 Example of GP tree illustrating $(2/x_1 + x_2)^2$ (Javadi, Rezania, & Nezhad, 2006) .....	71
Figure 3.1 Structure of materials and experimental and analytical work .....	76
Figure 3.2 Sand used in this study: (a) normal image, (b) SEM image, and (c) EDS image.....	78
Figure 3.3 Particle size distribution curve of sand.....	79
Figure 3.4 Particle size distribution curve of slag.....	80
Figure 3.5 Slag used in this study: (a) normal image, (b) SEM image, and (c) EDS image.....	81
Figure 3.6 Bentonite used in this study: (a) normal image, (b) SEM image, and (c) EDS image.....	83
Figure 3.7 Kaolinite used in this study: (a) normal image, (b) SEM image, and (c) EDS image.....	85
Figure 3.8 Illustrative arrangement of the triaxial testing system .....	86
Figure 3.9 LCD and keypad of TRAIX 100. ....	88
Figure 3.10 Typical arrangement of triaxial cell (ELE, 2004).....	89
Figure 3.11 Schematic representation of DPVC (GDS, 2017) .....	90
Figure 3.12 General view of triaxial testing system.....	91
Figure 3.13 Moist tamping procedure .....	94
Figure 3.14 Sample preparation steps .....	94
Figure 3.15 Membrane penetration correction procedure .....	99
Figure 3.16 View of created network.....	102
Figure 3.17 Mean squared error during training stage .....	103
Figure 3.18 Linear regression of ANN.....	104
Figure 3.19 HeuristicLab interface .....	105
Figure 3. 20 Visualisation of HeuristicLab model .....	106
Figure 4.1 Undrained behaviour of very loose clean sand samples: (a) stress–strain relationships and (b) effective stress paths.....	112
Figure 4.2 Undrained behaviour of very loose clean sand samples: (a) effective stress ratio vs. axial strain and (b) pore water pressure ratios vs. axial strain	114
Figure 4.3 Wrinkles in the membrane surrounding the sample during static liquefaction.....	116

Figure 4.4 Excess pore water pressures of very loose clean sand samples tested at different initial confining pressures .....	117
Figure 4.5 Stress ratio ( $q_{min}/q_{peak}$ ) vs. initial confining pressure of very loose clean sand .....	118
Figure 4.6 Post-consolidation void ratio of very loose clean sandy soil sheared at three initial confining pressures. ....	119
Figure 4.7 Undrained behaviour of medium ( $D_{ri}$ 50%) clean sand at three confining pressures: (a) stress–strain relationships, (b) effective stress paths, and (c) pore water pressure ratios vs. axial strain.....	122
Figure 4.8 Undrained behaviour of dense ( $D_{ri}$ 90%) clean sand at three confining pressures: (a) stress–strain relationships, (b) effective stress paths, and (c) pore water pressure ratios vs. axial strain.....	125
Figure 4.9 Effect of relative density on the undrained behaviour of sandy soil tested at initial confining pressure of 100 kPa: (a) stress–strain relationships, (b) effective stress paths, and (c) slope of effective stress paths.....	127
Figure 4.10 Effect of relative density on undrained behaviour of sandy soil tested at initial confining pressure of 100 kPa: (a) effective stress ratio vs. axial strain, and (b) pore water pressure ratio vs. axial strain .....	128
Figure 4.11 Undrained behaviour of partially saturated very loose sandy soil sheared at initial confining pressure of 100 kPa: (a) stress–strain relationships, (b) effective stress paths, (c) pore water pressure ratio vs. axial strain, and (d) effective stress ratio vs. axial strain.....	130
Figure 4.12 Types of liquefaction behaviours of soils .....	133
Figure 4.13 Liquefaction susceptibility of clean sandy soil prepared at different relative densities and tested at three initial confining pressures: (a) brittleness index vs. initial confining pressure, (b) brittleness index vs. relative density, and (c) brittleness index vs. pore water pressure ratio .....	137
Figure 4.14 Brittleness index against the stress ratio at the instability line of clean sandy soil prepared at different relative densities and tested at different initial confining pressures .....	139
Figure 4.15 Pore water pressure ratio against stress ratio at the instability line of clean sandy soil prepared at different relative densities and tested at different initial confining pressures .....	140
Figure 4.16 Pore water pressure ratio against state parameter at the start of the test of clean sandy soil.....	142
Figure 4.17 Brittleness index against state parameter at the start of the test of clean sandy soil.....	142
Figure 4.18 Stress ratio at the instability line against the state parameter at the start of the test of clean sandy soil.....	143
Figure 4.19 Undrained behaviour of very loose sand–slag samples: (a) stress–strain curves with $p_0 = 100$ kPa, (b) strain curves with $p_0 = 150$ kPa, and (c) strain curves with $p_0 = 200$ kPa .....	147
Figure 4.20 Undrained behaviour of very loose sand–slag samples: (a) effective stress path with $p_0 = 100$ kPa, (b) effective stress path with $p_0 = 150$ kPa, and (c) effective stress path with $p_0 = 200$ kPa.....	150

Figure 4.21 Undrained behaviour of very loose sand–slag samples: (a) pore water pressure ratio–strain with $p_0 = 100$ kPa, (b) pore water pressure ratio–strain with $p_0 = 150$ kPa, and (c) pore water pressure ratio–strain with $p_0 = 200$ kPa .....	152
Figure 4.22 Undrained behaviour of sand–slag samples prepared at the relative density of 50%: (a) stress–strain relationships, (b) effective stress paths, and (c) pore water pressure ratio–strain.....	155
Figure 4.23 Undrained behaviour of sand–slag samples prepared at the relative density of 90%: (a) stress–strain relationships, (b) effective stress paths, and (c) pore water pressure ratio–strain.....	157
Figure 4.24 Effect of slag content on undrained behaviour of sand–slag mixtures: (a) stress ratio vs. slag content (effect of initial confining pressure), (b) stress ratio vs. slag content (effect of relative density), and (c) pore water pressure ratios vs. slag content .....	159
Figure 4.25 Effect of slag content on the brittleness index of sand–slag mixtures: (a) brittleness index vs. initial confining pressure, (b) brittleness index vs. slag content, and (c) brittleness index vs. relative density.....	162
Figure 4.26 Effect of slag content on state parameter at start of the test of sand–slag mixtures: (a) brittleness index vs. state parameter at start of the test and (b) state parameter at start of the test vs. relative density.....	164
Figure 4.27 Effect of slag content on stress ratio at instability line of sand–slag mixtures.....	165
Figure 4.28 Undrained behaviour of very loose sand–bentonite samples: (a) stress–strain curves with $p_0 = 100$ kPa, (b) strain curves with $p_0 = 150$ kPa, and (c) strain curves with $p_0 = 200$ kPa.....	169
Figure 4.29 Undrained behaviour of very loose sand–bentonite samples: (a) effective stress path with $p_0 = 100$ kPa, (b) effective stress path with $p_0 = 150$ kPa, and (c) effective stress path with $p_0 = 200$ kPa.....	171
Figure 4.30 Undrained behaviour of very loose sand–bentonite samples: (a) pore water pressure ratio–strain with $p_0 = 100$ kPa, (b) pore water pressure ratio–strain with $p_0 = 150$ kPa, and (c) pore water pressure ratio–strain with $p_0 = 200$ kPa .....	173
Figure 4.31 Undrained behaviour of sand–bentonite samples prepared at relative density of 50%: (a) stress–strain relationships, (b) effective stress paths, and (c) pore water pressure ratio–strain .....	175
Figure 4.32 Undrained behaviour of sand–bentonite samples prepared at relative density of 90%: (a) stress–strain relationships, (b) effective stress paths, and (c) pore water pressure ratio–strain .....	177
Figure 4.33 Effect of bentonite content on state parameter at start of the test of sand–bentonite mixtures: (a) state parameter at start of the test vs. initial confining pressure and (b) brittleness index vs. state parameter at start of the test .....	179
Figure 4.34 Effect of bentonite content on brittleness index of sand–bentonite mixtures: (a) brittleness index vs. initial confining pressure and (b) brittleness index vs. bentonite content .....	181

Figure 4.35 Effect of bentonite content on state parameter at start of the test of sand–bentonite mixtures: (a) state parameter at start of the test <i>vs.</i> initial confining pressure and (b) brittleness index <i>vs.</i> state parameter at start of the test .....	182
Figure 4.36 Effect of bentonite content on stress ratio at instability line of sand–bentonite mixtures: (a) stress ratio at instability line <i>vs.</i> bentonite content and (b) stress ratio at instability line <i>vs.</i> state parameter at start of the test .....	184
Figure 4.37 Undrained behaviour of very loose sand–kaolinite samples: (a) stress–strain curves with $p_0 = 100$ kPa, (b) strain curves with $p_0 = 150$ kPa, and (c) strain curves with $p_0 = 200$ kPa.....	188
Figure 4.38 Undrained behaviour of very loose sand–kaolinite samples: (a) effective stress path with $p_0 = 100$ kPa, (b) effective stress path with $p_0 = 150$ kPa, and (c) effective stress path with $p_0 = 200$ kPa.....	190
Figure 4.39 Undrained behaviour of very loose sand–kaolinite samples: (a) pore water pressure ratio–strain with $p_0 = 100$ kPa, (b) pore water pressure ratio–strain with $p_0 = 150$ kPa, and (c) pore water pressure ratio–strain with $p_0 = 200$ kPa.....	192
Figure 4.40 Undrained behaviour of sand–kaolinite samples prepared at the relative density of 50%: (a) stress–strain relationships, (b) effective stress paths, and (c) pore water pressure ratio–strain .....	195
Figure 4.41 Undrained behaviour of sand–kaolinite samples prepared at the relative density of 90%: (a) stress–strain relationships, (b) effective stress paths, and (c) pore water pressure ratio–strain .....	198
Figure 4.42 Effect of kaolinite content on undrained behaviour of sand–kaolinite mixtures: (a) stress ratio <i>vs.</i> kaolinite content and (b) pore water pressure ratios <i>vs.</i> kaolinite content .....	199
Figure 4.43 Effect of kaolinite content on brittleness index of sand–kaolinite mixtures: (a) brittleness index <i>vs.</i> initial confining pressure and (b) brittleness index <i>vs.</i> kaolinite content .....	201
Figure 4.44 Effect of kaolinite content on state parameter at start of the test of sand–kaolinite mixtures: (a) state parameter at start of the test <i>vs.</i> confining pressure and (b) brittleness index <i>vs.</i> state parameter at start of the test.....	203
Figure 4.45 Effect of kaolinite content on stress ratio at instability line of sand–kaolinite mixtures: (a) stress ratio at instability line <i>vs.</i> kaolinite content and (b) stress ratio at instability line <i>vs.</i> state parameter at start of the test.....	205
Figure 4.46 Effect of clay type on liquefaction behaviour of sandy soil: (a) brittleness index <i>vs.</i> clay content and (b) pore water pressure ratio <i>vs.</i> clay content.....	207
Figure 4.47 Effect of clay content on liquefaction behaviour of sandy soil: (a) stress ratio at instability line <i>vs.</i> clay content; (b) state parameter at start of the test <i>vs.</i> clay content.....	209
Figure 5.1 Undrained behaviour of very loose sand–3% bentonite–slag samples: (a) stress <i>vs.</i> strain curves with $p_0 = 100$ kPa, and (b) effective stress path with $p_0 = 100$ kPa.....	214

Figure 5.2 Undrained behaviour of very loose sand–slag–3% bentonite mixtures: (a) effective stress ratios vs. strain with $p_o = 100$ kPa and (b) pore water pressure ratio vs. strain with $p_o = 100$ kPa.....	216
Figure 5.3 Undrained behaviour of very loose sand–5% bentonite–slag samples: (a) stress vs. strain curves with $p_o = 100$ kPa and (b) effective stress path with $p_o = 100$ kPa.....	218
Figure 5.4 Undrained behaviour of very loose sand–slag–5% bentonite mixtures: (a) effective stress ratios vs. strain with $p_o = 100$ kPa and (b) pore water pressure ratio vs. strain with $p_o = 100$ kPa.....	220
Figure 5.5 Stress ratios of sand–slag–bentonite mixtures .....	222
Figure 5.6 Undrained brittleness index of sand–slag–bentonite mixtures .....	223
Figure 5.7 Pore water pressure ratios of sand–slag–bentonite mixtures .....	224
Figure 5.8 Undrained behaviour of very loose sand–slag–kaolinite samples: (a) stress vs. strain with $p_o = 100$ kPa and (b) effective stress path with $p_o = 100$ kPa .....	227
Figure 5.9 Undrained behaviour of very loose sand–slag–3% kaolinite mixtures: (a) effective stress ratios vs. strain with $p_o = 100$ kPa and (b) pore water pressure ratio vs. strain with $p_o = 100$ kPa.....	229
Figure 5.10 Undrained behaviour of very loose sand–5% kaolinite–slag samples: (a) stress vs. strain curves with $p_o = 100$ kPa and (b) effective stress path with $p_o = 100$ kPa.....	231
Figure 5.11 Undrained behaviour of very loose sand–slag–5% kaolinite mixtures: (a) effective stress ratios vs. strain with $p_o = 100$ kPa and (b) pore water pressure ratio vs. strain with $p_o = 100$ kPa.....	233
Figure 5.12 Stress ratios of sand-slag-kaolinite mixtures .....	237
Figure 5.13 Undrained brittleness index of sand-slag-kaolinite mixtures .....	238
Figure 5.14 Pore water pressure ratio of sand–slag–bentonite mixtures .....	239
Figure 5.15 Undrained brittleness index of all the mixtures.....	240
Figure 5.16 Pore water pressure ratio of all the mixtures.....	241
Figure 6.1 Schematic representation of an artificial neural network.....	246
Figure 6.2 Measured vs. predicated stress ratio for ANN model 1 .....	250
Figure 6.3 Measured vs. predicated stress ratio for ANN model 2 .....	250
Figure 6.4 Measured vs. predicated stress ratio for ANN model 3 .....	251
Figure 6.5 Measured vs. predicated stress ratio for ANN model 4 .....	251
Figure 6.6 Measured vs. predicated stress ratio for ANN model 5 .....	252
Figure 6.7 Measured vs. predicated stress ratio for all the ANN models .....	252
Figure 6.8 Measured values of the stress ratio vs. those predicted by the developed GP model .....	255
Figure 6.9 Normalised stress ratio vs. that predicted by the developed GP model for all the datasets .....	256
Figure 6.10 Tree of the developed GP model .....	256
Figure 6.11 Stress ratio measured by experimental tests vs. that predicted by the developed GP model .....	258



Figure 6.12 Schematic representation of the structure of ANN .....	263
Figure 6.13 Measured vs. predicated stress ratio for ANN model 1 of sand–fines mixtures.....	266
Figure 6.14 Measured vs. predicated stress ratio for ANN model 2 of sand–fines mixtures.....	266
Figure 6.15 Measured vs. predicated stress ratio for ANN model 3 of sand–fines mixtures.....	267
Figure 6.16 Measured vs. predicated stress ratio for ANN model 4 of sand–fines mixtures.....	267
Figure 6.17 Measured vs. predicated stress ratio for ANN model 5 of sand–fines mixtures.....	268
Figure 6.18 Measured vs. predicated stress ratio for all the ANN models of sand–fines mixtures.....	268
Figure 6.19 Measured values of the stress ratio vs. those predicted by the developed GP model of sand–fines mixtures.....	271
Figure 6.20 Normalised stress ratio vs. that predicted by the developed GP model for all the datasets of sand–fines mixtures.....	271
Figure 6.21 Tree of the developed GP model of sand–fines mixtures	272

# List of Tables

Table 2.1 Types of undrained behaviour of saturated sandy soil under static loading .	15
Table 2.2 Silt content thresholds of some studies reported in the literature .....	53
Table 2.3 Comparison between the main chemical components of Portland cement and slag (Ika Putra, 2014).....	56
Table 3.1 Physical properties of sand.....	78
Table 3.2 Chemical components of GBFS .....	80
Table 3.3 Chemical components of bentonite.....	82
Table 3.4 Chemical components of kaolinite .....	84
Table 3.5 Technical specifications of TRIAX 100 (Controls, 2005) .....	87
Table 3.6 Technical specifications of DPVC (GDS, 2017).....	90
Table 3.7 Summary of static triaxial tests performed during the present study .....	107
Table 4.1 Results of undrained tests conducted on clean sand samples .....	111
Table 4.2 Physical properties of sand–slag mixtures .....	144
Table 4.3 Results of undrained tests conducted using sand–slag samples .....	145
Table 4.4 Physical properties of sand–bentonite mixtures .....	166
Table 4.5 Results of undrained tests conducted on sand–bentonite samples.....	167
Table 4.6 Physical properties of sand–kaolinite mixtures .....	185
Table 4.7 Results of undrained tests conducted on sand–kaolinite mixtures.....	186
Table 5.1 Physical properties of sand–slag–bentonite mixtures .....	212
Table 5.2 List of undrained tests conducted on sand–slag–bentonite mixtures .....	213
Table 5.3 Physical properties of sand–slag–kaolinite mixtures .....	225
Table 5.4 List of undrained tests conducted on sand –slag-kaolinite mixtures ....	226
Table 6.1 Properties of the sands used .....	247
Table 6.2 Statistical distribution of each parameter in the database .....	247
Table 6.3 Performance and details of the ANN models .....	249
Table 6.4 Symbolic regression parameters .....	253
Table 6.5 Coefficients of Equation (6-1).....	254
Table 6.6 Performance of the $q_{min}/q_{peak}$ model for the training and testing datasets...	255
Table 6.7 Details of tests included in the database for modelling the liquefaction susceptibility of sand–fines mixtures .....	259
Table 6.8 Statistical analysis of input dataset .....	262
Table 6.9 Performance of ANN models of sand–fines mixtures .....	265
Table 6.10 Symbolic regression parameters .....	269
Table 6.11 Coefficients of Equation (6-2).....	270
Table 6.12 Performance of the $q_{min}/q_{peak}$ model for the training and testing datasets	270

# List of Acronyms, Abbreviations, and Notations

The following is a list of acronyms, abbreviations and notations used in this thesis.

$(S_r)_{crit}$	Corresponding degree of saturation
$(V_a)_{crit}$	Critical limit of the volume of the air
$\Delta \sigma_3$	Change in cell pressure
$\Delta u$	Change in pore water pressure
$\Delta v_s$	Actual volume change of specimen
$\Delta v_m$	Unit membrane penetration
Ac	Area of contraction behaviour
$A_c$	Consolidated cross-sectional area of specimen
Ad	Area of dilation behaviour
AI	Artificial Intelligence
ANN	Artificial neural network
$A_o$	initial cross-sectional area of specimen
B	Skempton's coefficient
BPNN	Back-propagation neural networks
CPT	Cone penetration test
CRR	Cyclic resistance ratio
CS	Critical state
CSL	Critical state line
CSR	Critical state ratio
CT	Characterization threshold
$C_u$	Coefficient of uniformity
$D_{ri}$	Initial relative density
e	Void ratio
EA	Evolutionary algorithm
$e_{cs}$	Post-consolidation void ratio
EDS	Energy dispersive X-ray spectrometer
$e_g$	Granular void ratio

$e_{ge}$	Equivalent granular void ratio
$e_{max}$	Maximum void ratio
$e_{min}$	Minimum void ratio
$e_o$	Initial void ratio
$e_{skeleton}$	Sand skeleton void ratio
$e_{ss}$	Void ratio at steady state
$e_{thre}$	Threshold void ratio
$e_{uf}$	Void ratio of upper limit
$f_c$	Fine content
$F_{cthr}$	Threshold fines content
FL	Factor of safety against liquefaction
FLL	Flow liquefaction line
GA	Genetic algorithm
GEP	Gene expression programming
GP	Genetic programming
$G_s$	Specific gravity of soil
$I_B$	Undrained brittleness index
ICL	Isotropic consolidation line
IL	Instability line
$I_p$	State pressure index
$k_s$	Bulk modulus of soil
$k_w$	Bulk modulus of water
$L_c$	Consolidated length of sample
LGP	Linear genetic programming
$L_o$	Initial length of sample
$L_p$	Liquefaction potential
M	Slope of critical / steady state line
m	Mass of soil
MEP	Multi expression programming
$m_f$	Mass of fines
MGGP	Multi gene genetic programming
MLP	Multi-layer perceptron

MSGP	Multi-stages genetic programming
$n$	The soil porosity
$P_{cs}^{\prime}$	Mean effective stress at critical state
$p_{CSL}^{\prime}$	Mean effective stress at critical state
$P_o^{\prime}$	Initial confining pressure
$P_{pt}^{\prime}$	Effective stress at phase transformation
$P_a$	Atmosphere pressure
PI	Plasticity index
PNN	Probabilistic neural networks
PT	Phase transformation state
$q_{CSL}$	Deviatoric stress at critical state
$q_{min}$	Minimum deviatoric stress
$q_{min}/q_{peak}$	Stress ratio
$q_o$	Deviatoric stress at $B=0$
$q_{peak}$	Peak deviatoric stress
QSS	Quasi steady state
$R^2$	Coefficient of determination
$R_c$	Relative of contractiveness
RMSE	Root mean square error
$R_u$	Pore water pressure ratio
SEM	Scanning electronic microscopy
SOM	Self-organizing map
SPT	Standard penetration test
$S_r$	Degree of saturation
SS	Steady state
SSL	Steady state line
$S_u$	Undrained steady state shear strength
$S_{u(LIQ)}$	Shear strength of liquified soil
$S_{u(yield)}$	Yield strength of soil
SVM	Support vector machine
$U_{excess}$	Excess pore water pressure
$U_f$	Maximum pore water pressure ratio

UIS	Undrained instability state
USC	Unconfined compression strength
$v_c$	Consolidated volume of sample
$v_o$	Initial volume of sample
$v_s$	Corrected volume change of specimen
$V_T$	Total volume of sample
$\epsilon v_c$	Volumetric strain after consolidation
$\eta$	Stress ratio at instability line
$\xi_R$	Relative state parameter index
$\rho_d$	Desired dry density
$\rho_{dmax}$	Maximum dry density
$\rho_{dmin}$	Minimum dry density
$\rho_w$	Density of water
$\sigma'_1 / \sigma'_3$	Maximum effective principle stress ratio
$\sigma'_3$	Effective stress
$\sigma'_{liq}$	Effective stress at liquefaction
$\sigma_1 - \sigma_3$	Stress difference / deviatoric stress
$\sigma_{1s}$	Major principal stress at steady state
$\sigma_{3s}$	Minor principal stress at steady state
$\tau_d$	Applied shear stress
$\phi_{CS}$	Critical state friction angle
$\phi_{FLL}$	Flow liquefaction angle
$\phi_s$	Mobilised internal friction angle
$\Psi$	State parameter
$\Psi_m$	Modified state parameter
$\Psi_{m(o)}$	Modified state parameter at start of the test
$\Psi_o$	State parameter at start of the test

# Chapter 1: Introduction

## 1.1 Background of the Study

Liquefaction is one of the most complicated and debated topics in geotechnical engineering because it is used to define various contrasting but related phenomena (Kramer, 1996). The term liquefaction, was initially used by (Hazen, 1918, 1920) to explain the behaviour of granular soils responsible for the failure of the Calaveras Dam. Thereafter, (Terzaghi & Peck, 1948) used the term 'spontaneous liquefaction' to explain the contractive behaviour of very loose saturated granular soils under undrained monotonic loading. Bjerrum, Kringstad, and Kummeneje (1961) stated that in 1950s, the researchers at U.S. Waterways Experiment Station were the first to achieve static liquefaction via laboratory tests. Then, Bjerrum et al. (1961) conducted stress-controlled triaxial compression tests on anisotropically consolidated specimens of soil involved in the flow slides in the Norwegian fjords; they reported that 'it was surprising to see, however, the small increase in deviator stress required to cause failure in the undrained tests'. While, Seed and Lee (1966) were the first researchers who investigated the pore pressure development in sandy samples under cyclic loading.

Liquefaction is a phenomenon of a sudden reduction in shear strength due to an abrupt increase in the pore water pressure in saturated cohesion-less soils when subjected to undrained monotonic or cyclic loading such that the soils move as a viscous liquid (Castro, 1969; Castro & Poulos, 1980; El Mohtar, Bobet, Drnevich, Johnston, & Santagata, 2013; Jafarian, Ghorbani, Salamatpoor, & Salamatpoor, 2013; Kramer, 1996; NRC, 1985; Olson & Stark, 2002; Srbulov, 2008; Vaid & Sivathayalan, 2000; Verdugo & Ishihara, 1996; Yamamuro & Lade, 1997b).

The reduction in shear strength is associated with the rearrangement of sand particles under the action of shear stresses generated by external loading, which is prevented by the existence of water under the condition of no drainage, i.e. the 'undrained condition'. The state of no drainage occurs when the permeability of the material is low and the rate of loading is faster than the time required for the pore water pressure to dissipate; for example, construction on the clayey soil, in this case, the induced pore

pressure may affect the stability of the buildings. Another situation related to the no drainage case with quick action is an instance in which earthquake loading may damage buildings constructed on a sandy soil. Under the undrained condition, the pore pressure may increase because of the transmission part of the load to water, causing a reduction in the effective stress. Consequently, the shear strength decreases. The undrained condition was simulated in laboratory tests carried out on soil specimens by preventing the drainage out of the sample by closing the drainage valve. Figure 1.1 shows a simple illustration of soil liquefaction (Rapti, 2016).

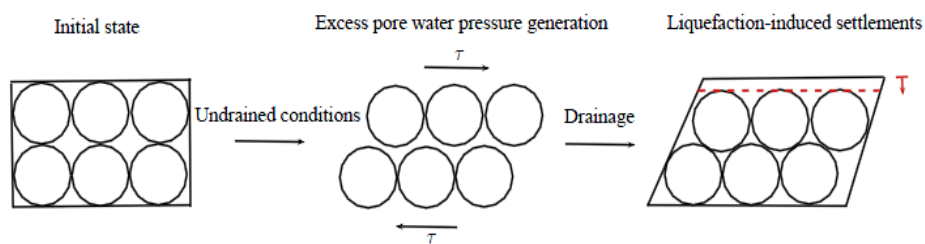


Figure 1.1 Soil liquefaction (Rapti, 2016)

Liquefaction has received considerable attention from researchers because of its engineering importance and destructive nature of failures, and a vast amount of work has been performed to analyse its basic mechanism and identify the factors affecting it. There are two leading causes of liquefaction: the first is earthquakes, and the second is a rapidly applied surcharge (dead weight). The liquefaction generated by an earthquake is called cyclic liquefaction, and the criteria of liquefaction failure are referred to as cyclic mobility. However, surcharge-triggered liquefaction is called static liquefaction, and the criteria of liquefaction failure are called flow liquefaction. Both cyclic and static liquefaction are crucial in any assessment of liquefaction hazard. In the field, cyclic liquefaction occurs more often than static liquefaction, but the consequences of static liquefaction are usually far more drastic (Kramer, 1996). The existing studies linking static and cyclic liquefaction showed that static and cyclic liquefaction are firmly connected (Mohamad & Dobry, 1986). Vaid and Sivathayalan (2000) argued that cyclic liquefaction occurred when the mobilised friction angle reached a value that triggered static liquefaction. Yang, Sze, and Heung (2009) stated that large deformations occurred under cyclic loading when the effective stress path achieved the instability line under monotonic loading. Moreover, previous studies



have shown that sample preparation methods do not significantly affect the connection between static and cyclic liquefaction. Robertson and Fear (1995) proposed a flow chart for the assessment of static and cyclic liquefaction, as shown in Figure 1.2. This thesis is committed to static liquefaction only.

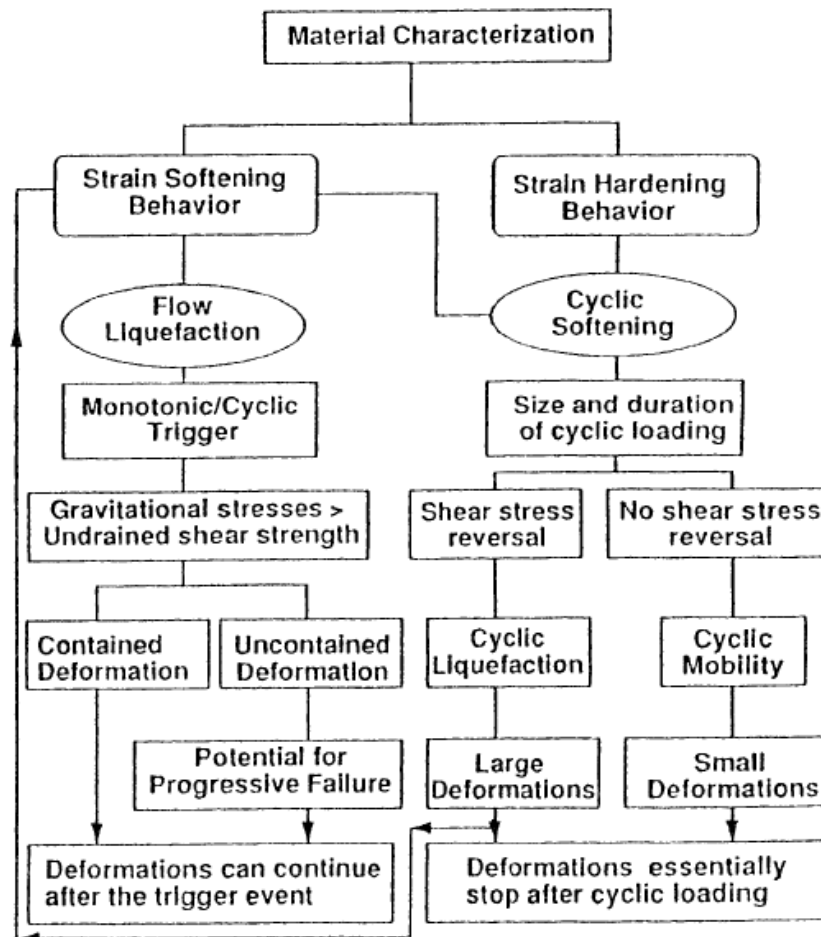


Figure 1.2 Proposed flow chart for the assessment of soil liquefaction (Robertson & Fear, 1995)

Static liquefaction is considered an essential design point for large geotechnical applications, such as earth dams and main tailing impoundments (Robertson, 2009). Flow liquefaction may occur when the static shear stresses applied to soil are greater than the shear strength in the liquefied state (Kramer, 1996; NRC, 1985). Static liquefaction produces the most devastating effects of all the liquefaction types, and massive instabilities are termed ‘flow failure’ (Kramer, 1996; NRC, 1985). The static liquefaction is distinguished by its unexpected origin, quick development of pore

pressure and deformations, and the long length up which the liquefied soil usually flows (Kramer, 1996). Static liquefaction can occur in saturated, loose, sandy soil deposits because of human causes such as a statically increased shear load (e.g., construction loading, rapid sediment accumulation, raising of embankment heights, and over stepping slopes), or it can occur naturally in coastal and offshore soil deposits (Sadrekarimi, 2014c). The induced pore water pressure may reduce the bearing capacity of the sandy soil, thereby jeopardising the stability of geotechnical applications. The damages in geotechnical applications due to static liquefaction vary according to the nature of the applications. Under level grounds, the damage caused includes cracking, inclining or breakdown of the buildings, and lateral extension of the overlying embankments. However, under slopes, the damages caused include flow slides. In the past few decades, there have been many dramatic examples of catastrophic effects associated with liquefaction instabilities, such as the 1994 flow slide failure of the Merriespruit gold mine tailing dam in Virginia, South Africa. This calamity killed 17 people and destroyed 280 houses as a result of the release of 600,000 m<sup>3</sup> of waste tailing over more than 2 km. Further, the 1966 collapse of the Colliery spoil tip in the welsh village of Aberfan, South Wales, killed 116 children under the age of 10 years and 28 adults as 40000 m<sup>3</sup> of soil travelled to the village within minutes. In the case of the failures in Calaveras Dam in California in 1918, the soil travelled for 200 m. Further, failures in soil layers which supported the off-shore oil platforms in the Canadian Beaufort Sea, the failures of Coal tailing dumps in British Columbia, and the failures of the North Dyke of the Wachusett Dam in Massachusetts in April 1907, where the soil travelled approximately 100 m without any disaster, are some of the examples which have raised some concerns about static liquefaction (Andrade, 2009; Dawson, Morgenstern, & Stokes, 1998; Jeyapalan, Duncan, & Seed, 1983; Olson, 2001; Sladen, D'Hollander, Krahn, & Mitchell, 1985). Muhammad (2012); Olson (2001) reported many other examples of flow failures. Figures 1.3 and 1.4 show some of the catastrophic effects of flow liquefaction.



Figure 1.3 Aerial photograph of the Merriespruit tailings dam failure (Fourie, Blight, & Papageorgiou, 2001)



Figure 1.4 Aerial photograph of the Aberfan disaster (Hutchinson, 1986)

Numerous techniques are now available to evaluate the liquefaction susceptibility of sandy soils; some of these techniques are as follows: (1) experimental work (Ishihara, 1993; Mulilis, Townsend, & Horz, 1978; Sivathayalan & Vaid, 2004); (2) numerical simulation of soil constitutive models (Robertson, 2009; Seed, 1987); (3) empirical correlations with field tests (Byrne, 1991; Byrne, Jitno, & Salgado, 2004); and (4) a

combination of experimental work with empirical correlations or of experimental work with numerical simulations (Beatty & Byrne, 2008; Robertson, 2004). Our basic understanding of static liquefaction is based on the undrained triaxial compression tests. Nevertheless, the behaviour of soil is very complex because it is inelastic and nonlinear; further, soil behaviour depends on certain factors such as the initial state, the magnitude and direction of the effective principal stresses, stress/strain history, and stress path during undrained shearing. Moreover, the presence of fines in sandy soil deposits adds some complexity to the mechanical response of sandy soils under monotonic and dynamic loadings. The effect of fines on the liquefaction susceptibility of sandy soils was not considered in the earlier studies because the first thought was that the pore pressure, which relates to soil liquefaction, could not be generated in fine soils. Nevertheless, recent research has shown that many of the types of sandy soils have a significant size of fines (materials passing sieve no. 200). Therefore, the role of the fines content in determining the liquefaction susceptibility of sandy soil has been included in the current liquefaction susceptibility measurements. Studies on static liquefaction using other testing instruments such as triaxial extension tests (Hyodo, Tanimizu, Yasufuku, & Murata, 1994; Vaid, Chung, & Kuerbis, 1990; Vaid & Thomas, 1995) and plane-strain tests (also referred to as “biaxial tests” in the literature) (Han & Vardoulakis, 1991; Wanatowski & Chu, 2007) are limited. The results of triaxial compression and extension tests showed that the shear strength in triaxial compression is higher than in triaxial extension and that a high density is required to prevent the reduction in shear strength during undrained loading. Numerous studies (Alarcon-Guzman, Leonards, & Chameau, 1988; Andrade, 2009; Delia, 2010; El Mohtar et al., 2013; Fourie et al., 2001; Hird & Hassona, 1990; Lade & Yamamuro, 2011; Rahman & Lo, 2014; Sadrekarimi, 2014c; Salamatpoor & Salamatpoor, 2014; Wei & Yang, 2014; Yamamuro & Lade, 1997b) have reported that the static liquefaction of sandy soils depends on a large number of factors such as relative density, particle size distribution, sample preparation method, stress history, confining pressure, degree of saturation, magnitude and type of loads (isotropic or anisotropic), and fines content. The previous studies on the effects of fines content on the undrained static behaviour of sandy soils revealed some discrepancies; some of them showed positive effects, and the others reported negative effects.

Most previous studies have focused mainly on clean sand (sand with no fines content). However, few studies are available on the effect of fines on the liquefaction behaviour of sandy soils, and the findings of these studies have been inconsistent and contradictory. Some of these studies have reported that the presence of fines can have a positive effect on the liquefaction behaviour of sandy soils (Pitman, Robertson, & Sego, 1994; Seed, Idriss, & Arango, 1983). In contrast, Yamamuro and Lade (1998) and Zlatovic and Ishihara (1997) stated that clean sand might be less liquefiable than sand with fines. Moreover, most previous studies have focused on using one type of fines, either plastic (clay) or non-plastic (silt) fines. However, very little attention has been paid to the effects of mixing of two types of fines on the static behaviour of sandy soils under undrained conditions. An increasing amount of waste materials has encouraged researchers to find alternative ways to use them in different applications. Reusing these materials has substantial, positive environmental effects involving resource conservation and reductions in greenhouse emissions. The research on the effect of waste materials on the static liquefaction of sandy soils is limited. Moreover, the use of artificial intelligence (AI) techniques for predicting the static liquefaction of sandy soils has been less extensive. To address these gaps, this research will extend the experimental and theoretical work on the static liquefaction of clean sandy soils and sand–fines mixtures. The behaviour of clean sand, sand–slag mixtures, and clayey sand–slag mixtures under isotropic undrained static loadings are considered. This research will also investigate the effect of relative density, confining pressure, and degree of saturation on the behaviour of materials under undrained static shear. The experimental results will be used to predict the static liquefaction of materials by using artificial neural network (ANN) and genetic programming (GP) techniques.

## **1.2 Research Objectives**

Based on the background mentioned previously, the primary aims of this research are to do the following:

- 1- Characterise the static liquefaction behaviour of clean sandy soils in an isotropic undrained compression triaxial test under various conditions such as three confining pressures, three relative densities, and various degrees of saturation.

- 2- Investigate the effect of different fines contents such as three percentages of slag content, two percentages of kaolinite, and two percentages of bentonite on the static liquefaction susceptibility of sandy soils under different test conditions such as confining pressure and relative density.
- 3- Investigate the effect of clay mineralogy on the behaviour of sandy soil and sand–slag mixtures in isotropic undrained compression triaxial tests.
- 4- Investigate the effect of combination of two types of fines on liquefaction susceptibility of sandy soils.
- 5- Integrate the practical results obtained from the experimental work of the present study with the results of theories often discussed in geotechnical engineering.
- 6- Predict the static liquefaction susceptibility of materials by using ANN and GP, including the use of data obtained from the experimental part to develop liquefaction susceptibility models.

### **1.3 Significance**

The findings of this research will help to develop our understanding on the static liquefaction of sandy soils by addressing some important points:

- 1- The current study contributes to the extant literature by providing more detailed investigations regarding the effect of the fines content on the static liquefaction behaviour of sandy soils; in particular, previous studies have reported contradictory results.
- 2- The results of this research will help to investigate the effect of mixing sandy soil with two different types of fines on the behaviour of sandy soil in a undrained compression triaxial test under various test conditions.
- 3- This research will provide an alternative method to use waste materials such as slag in geotechnical applications which could bring economic and environmental benefits.
- 4- This research will also provide a model for predicting the static liquefaction susceptibility of sand–fines mixtures.
- 5- The results of this research will provide relevant data on the static liquefaction behaviour of sandy soils with fines to help develop the current databases for future studies when dealing with the same soils.

- 6- The experimental results of this research will provide an initial indicant on the effect of slag and mixtures of slag and clay on the cyclic liquefaction of sandy soils.

## **1.4 Thesis Organisation**

To establish the research objectives, this thesis is divided into seven chapters, and the content of Chapters 2 to 7 are briefly outlined as follows.

Chapter 2 of this thesis presents a review of previous studies that reported on the static liquefaction of clean sandy soils and sand with fines. A critical review of the results of earlier work is presented to explain the analyses conducted in this research. It also presents the types of behaviour exhibited under undrained static loading and the mechanisms triggering static liquefaction. The factors affecting the static liquefaction behaviour of sandy soils are discussed. Moreover, the methods used to identify the static liquefaction susceptibility of sandy soils are addressed. The numerical and theoretical studies used to predict the static liquefaction of sand soils are presented as well.

Chapter 3 presents the types of materials and equipment utilised in this study, sample preparation method, testing program, and description of the ANN and GP analysis. The properties of sand, slag, kaolinite, and bentonite are presented, as well as the description of the triaxial apparatus and the testing procedure adopted in the current research are also discussed.

Chapter 4 presents the results of the strain-controlled undrained compression triaxial tests done on clean sand specimens. The effects of different factors such as confining pressure, relative density, and degree of saturation, which is simulated by using Skempton's pore pressure coefficient ( $B$ ), on the static liquefaction behaviour are discussed. Moreover, the liquefaction susceptibility of clean sand is presented. This chapter includes a discussion on the experimental results for the effect of the fines content on the static liquefaction behaviour of sandy soil. The effects of three percentages of slag, two percentages of kaolinite,

and two percentages of bentonite were investigated. The effects of the fines content, confining pressure, and relative density were studied. Moreover, the effects of the kaolinite content and the bentonite content on the behaviour of sandy soils in undrained static triaxial compression tests are compared. The liquefaction susceptibility of the sand–slag, sand–kaolinite, and sand–bentonite mixtures is discussed.

Chapter 5 presents the experimental results of the effect of mixing two different types of fines on the static liquefaction behaviour of sandy soils. Chapter 4 considered the effect of the slag content on the liquefaction behaviour of clean sandy soils (zero fines content). Therefore, the purpose of this chapter is to simulate the effect of the slag content on the unclean sandy soils (sand with different types and contents of fines). The experimental results for the sand–slag–kaolinite mixtures and the sand–slag–bentonite mixtures were discussed. The liquefaction susceptibility of the sand–slag–clay mixtures was investigated.

Chapter 6 presents the prediction of the static liquefaction susceptibility of the sand–slag–clay mixtures by using AI approaches. Therefore, two AI approaches were used. ANN was used to build models by using the experimental results presented in Chapters 4 and 5 for predicting the stress ratio, which was adopted in many of the previous studies to distinguish between liquefiable and non-liquefiable soils. Then, GP was used to build other prediction models by using the ANN results.

Finally, conclusions drawn on the basis of the experimental and empirical results and recommendations for future studies are presented in Chapter 7.



# Chapter 2: Literature review

## 2.1 Introduction

In the recent decades, liquefaction has attracted considerable research attention in the area of soil mechanics because of its catastrophic effects on geotechnical applications. Extensive experimental, numerical, and post-liquefaction field tests have been conducted to gain a better understanding of this phenomenon and to identify the main factors affecting it. This chapter reviews the existing studies related to the static liquefaction of sandy soils. It draws attention on the possible types of undrained static behaviour of sandy soil, and the corresponding terms are reviewed. Moreover, concepts such as quasi-steady state (QSS) Alarcon-Guzman et al. (1988), steady state (SS) Poulos (1981), collapse surface Sladen, D'hollander, and Krahn (1985), flow liquefaction line (Kramer and Seed 1988), and instability line (Lade and Pradel 1990) are comprehensively reviewed as they will be mentioned in the later chapters. Furthermore, the significant effects of several parameters such as the initial state (i.e. relative density and confining pressure), fines content, fines types (i.e. plastic or non-plastic), degree of saturation, drainage conditions, and type of consolidation (i.e. isotropic or anisotropic) on the static liquefaction behaviour of cohesionless soils are reviewed. The methods which have been adopted in the literature to investigate the liquefaction susceptibility of sandy soils such as the ratio of the minimum deviator stress to the initial peak deviator stress (Yamamuro and Lade 1997b), relative contrastiveness (Verdugo and Ishihara 1996), and brittleness index (Bishop 1971) are reviewed. Attention is then drawn to the numerical and empirical studies which have been used to evaluate the static liquefaction potential on the basis of field or laboratory tests.

## 2.2 Undrained behaviour of sandy soil

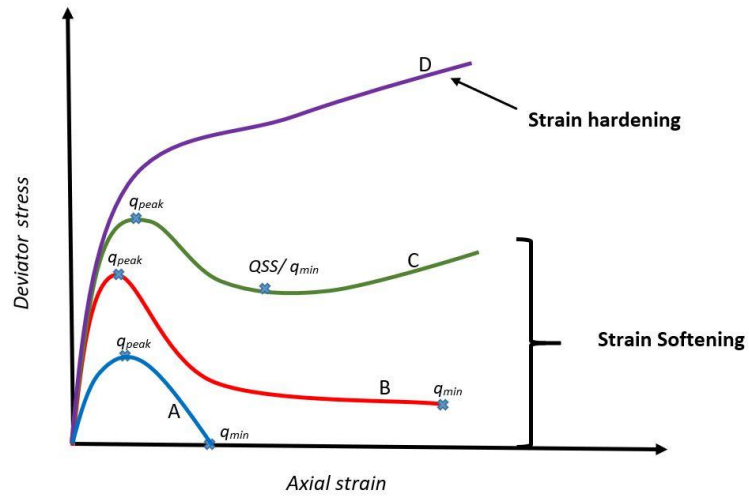
A good understanding of the undrained behaviour of sandy soils under static or cyclic loading is a key factor in the evaluation of liquefaction susceptibility and the estimation of the deformations during and after liquefaction. As mentioned in Chapter

1, the laboratory tests represent the major base of our knowledge of the behaviour of sandy soils under undrained conditions. The undrained behaviour of sandy soils has been previously investigated by using different techniques such as conventional triaxial compression tests, extension triaxial tests, and plane strain tests. The outcomes of conventional triaxial compression tests are a pillar of our knowledge of the liquefaction phenomena. The behaviour of saturated soils is only concerned with the evaluation of undrained behaviour because the development of pore pressure that is accompanied with a significant reduction in shear strength and large deformations occurred only in fully saturated samples under both static and cyclic loadings. Kramer (1996) reported that liquefaction is most frequently observed close to rivers, bays, and other water bodies because it only exists in saturated soils. Srbulov (2008) listed the major factors that affect the undrained shear strength of soil under a static condition; of these factors, the most important are density, degree of overconsolidation, consistency, and plasticity. The term ‘spontaneous liquefaction’ has been used by Terzaghi and Peck (1948) to explain the rapid deformation in loose cohesionless soils under undrained conditions.

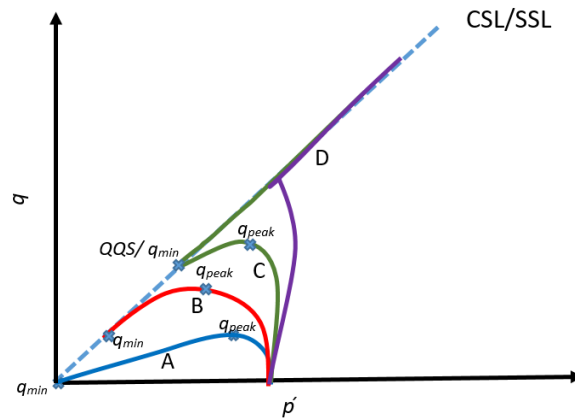
### **2.2.1 Types of undrained behaviour**

The behaviour of saturated sandy soils under undrained monotonic loadings has been widely investigated in triaxial compression tests (Alarcon-Guzman et al., 1988; Castro, 1969; Della, Arab, & Belkhatir, 2011; Ishihara, 1993; Mohamad & Dobry, 1986; Park & Jeong, 2015; Rahman & Lo, 2014; Riemer & Seed, 1997; Verdugo & Ishihara, 1996; Yoshimine, Robertson, & Wride, 1999), using remoulded samples that were prepared using different sample preparation methods. Alarcon-Guzman et al. (1988) stated that the state diagram of the undrained behaviour of sandy soil could be divided into three regions. The first one is the strain softening characterised by the decrease in the stress–strain curve under low strain conditions and the increase in the pore water pressure. The second one is the strain hardening in the region where the sand exhibits an increase in the shear strength and a decrease in the pore water pressure. The final region is the transition region between the two abovementioned regions. Ibsen (1998) noted that the volume change plays a significant role in the behaviour of sandy soil under both undrained and drained conditions. The volume changes could be dilative or contractive depending upon the stress magnitude and density. The dilative behaviour appeared in

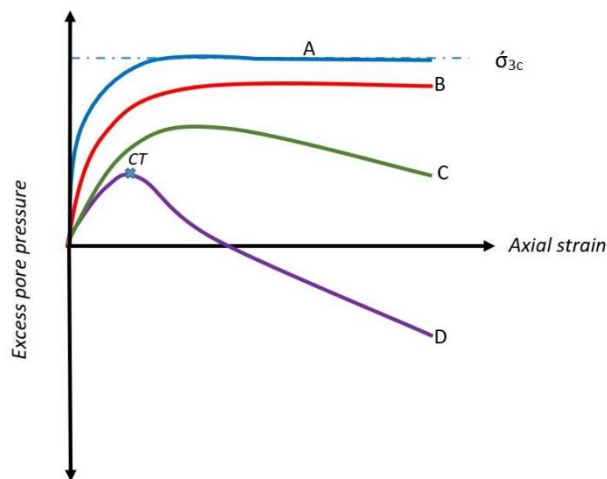
dense samples at a low confining pressure and a high stress level, and a transformation from the contractive behaviour to the dilative behaviour occurred through the straight line; this line is called the characteristic line under the drained condition. The typical behaviours of isotropically consolidated saturated sand in undrained triaxial compression tests are shown in Figure 2.1 and listed in Table 2.1. Figures 2.1(a), (b), and (c) show the stress–strain relationship, stress path, and excess pore water pressure–strain relationship, respectively. The variation in behaviour from type A to type D depends on the changes in the initial state (i.e. relative density and confining pressure) as listed in Table 2.1. Additionally, these types of behaviours are observed in anisotropically consolidated samples. Types A, B, and C are strain softening behaviour associated with a reduction in the shear strength after attaining the peak value. The decrease in the shear strength continues until the minimum value is reached at the state of continuous deformation at constant volume and shear and effective stresses. This state has been defined as the steady state (SS), residual state, or critical state (CS), and the shear strength at this state is called the undrained steady state strength or residual strength (Castro, 1975; Vaid & Chern, 1983b). Jefferies and Been (2015) and Verdugo and Ishihara (1996) argued that these three states represent the same phenomenon. The reduction in the shear strength after attaining the initial peak depends on the initial relative density and confining pressure. Types (A) and (B) are a strain-softening response with extensive and unidirectional deformations. These behaviours are associated with very loose and loose sandy soils and exhibit the peak deviatoric stress ( $q_{peak}$ ) at a small shear strain followed by a rapid reduction in the shear strength until the minimum deviator stress ( $q_{min}$ ) is reached. Both types (A) and (B) are recognised as flow liquefaction or flow failure (Alarcon-Guzman et al., 1988; Vaid & Chern, 1983a). Flow liquefaction is characterised by a quick reduction of the shear strength accompanied with the rapid development of positive pore water pressure and large shear strains, as shown in Figures 2.1(a), (b), and (c). Casagrande (1975); Poulos, Castro, and France (1985); Vaid et al. (1990); Sladen, D'hollander, and Krahn (1985); and Yamamuro and Lade (1997a) labelled the type B response with the following different names: actual liquefaction, static liquefaction, collapse behaviour, and undrained instability, respectively.



(a)



(b)



(c)

Figure 2.1 Types of undrained behaviour of saturated sandy soil under static loading: (a) stress–strain relationships, (b) stress paths, and (c) excess pore pressure–strain relationships (adapted and modified from (Chern, 1985) and (Bobei, 2004))

Table 2.1 Types of undrained behaviour of saturated sandy soil under static loading

Behaviour type	Initial state		Undrained behaviour	Liquefaction classification
	Relative density	Initial confining pressure level		
A	Very loose	Low	Strain softening	Complete liquefaction
B	Loose	Low/very high	Strain softening	liquefaction
C	Medium	Medium	Strain softening	Limited liquefaction
D	Dense	Low/high	Strain hardening	No flow

Type A represents a particular type of flow failure called complete static liquefaction (Yamamuro & Lade, 1997b). This type of response is associated with the very loose state and characterised by abrupt increases in the positive pore water pressure until a value equal to the initial effective confining pressure at this point is reached; then, the soil loses its shear strength completely because the effective stress is equal to zero ( $\sigma'_3 = 0$  or  $\sigma_1 - \sigma_3 = 0$ ) as shown in Figures 2.1(a), (b), and (c). Type B is associated with the loose state and represents the flow failure as well, but the differences between this type and type A are attributed to the fact that the minimum shear strength did not reach zero with a slight difference between the generated excess pore water pressure and the initial confining pressure. The flow failure behaviours, types A and B, have been consistently reported in many previous studies (Castro, 1969; Ishihara, 1993; Murthy, Loukidis, Carraro, Prezzi, & Salgado, 2007; Seed, Lee, Idriss, & Makdisi, 1975; Vaid & Chern, 1985; Yang, 2002). These studies pointed out that the dramatic effects of the flow failure type of behaviour make it one of the most dangerous types of liquefaction-related phenomena in geotechnical applications. Strain-softening behaviour types A and B are called contractive behaviours. The type C response is a strain softening with limited unidirectional strain. This type of response is associated with medium to loose sands and is characterised by the initial peak shear strength attained at a small strain. Then, the shear strength decreases to the minimum value at moderate strain. After minimum shear strength is attained, the shear strength increases to its maximum value and the pore water pressure drops to its minimum value in the case of a large strain. It is important to mention that the behaviour of soil at the minimum shear strength could

be linked to the steady state of deformation because it showed continuous deformations under constant normal and shear stresses. The constant volume is satisfied by the undrained condition and the strain-controlled triaxial system meets the condition of constant velocity. The minimum shear strength is called the quasi-steady state point (QSS) and is defined as the point when the undrained behaviour changes from contractive to dilative (Alarcon-Guzman et al., 1988; Ishihara, 1993; Yamamuro & Lade, 1998), while the state achieved at a large strain is linked with the SS condition. The shear stress mobilised at SS is larger than the stress mobilised at QSS. In contrast, the strain level required for the QSS is considerably lower than the strain associated with SS. In the case of behaviour type C, the shear strength at QSS is less than the shear strength at the ultimate state with considerably larger deformations. Therefore, a serious question is raised here about which of the two strengths should be adopted as SS or the residual shear strength. Ishihara (1993) argued that the answer to this question depends on the conditions experienced in the field; further, the shear strength at QSS can be used to define the SS conditions as reported in many of the previous works. Type C behaviour was defined as limited liquefaction by (Castro, 1969). Type D behaviour represents the strain-hardening response. This type of behaviour is associated with a dense state and characterised by a continuous increase in the shear strength without the appearance of the initial peak. This increase in the shear strength is accompanied with a reduction in the pore water pressure after reaching the maximum value, as shown in Figure 2.1(C). Sand exhibiting such a response is called dilative. This type of behaviour does not reach SS at the end of a test. Luong (1980) defined the start point of the reduction in the pore water pressure as the characterisation threshold (CT), which was similar to QSS explained earlier. Luong (1980) stated that CT can be used as a boundary condition between contractive and dilative behaviours, and is independent of the relative density but occurs at the same effective stress ratio. The type D response is called the non-flow behaviour. A strain-hardening response may change into a strain-softening response, as shown in Figure 2.2, but the shear strength and strains required to generate this behaviour are very large and are not of practical interest (Chern, 1985).

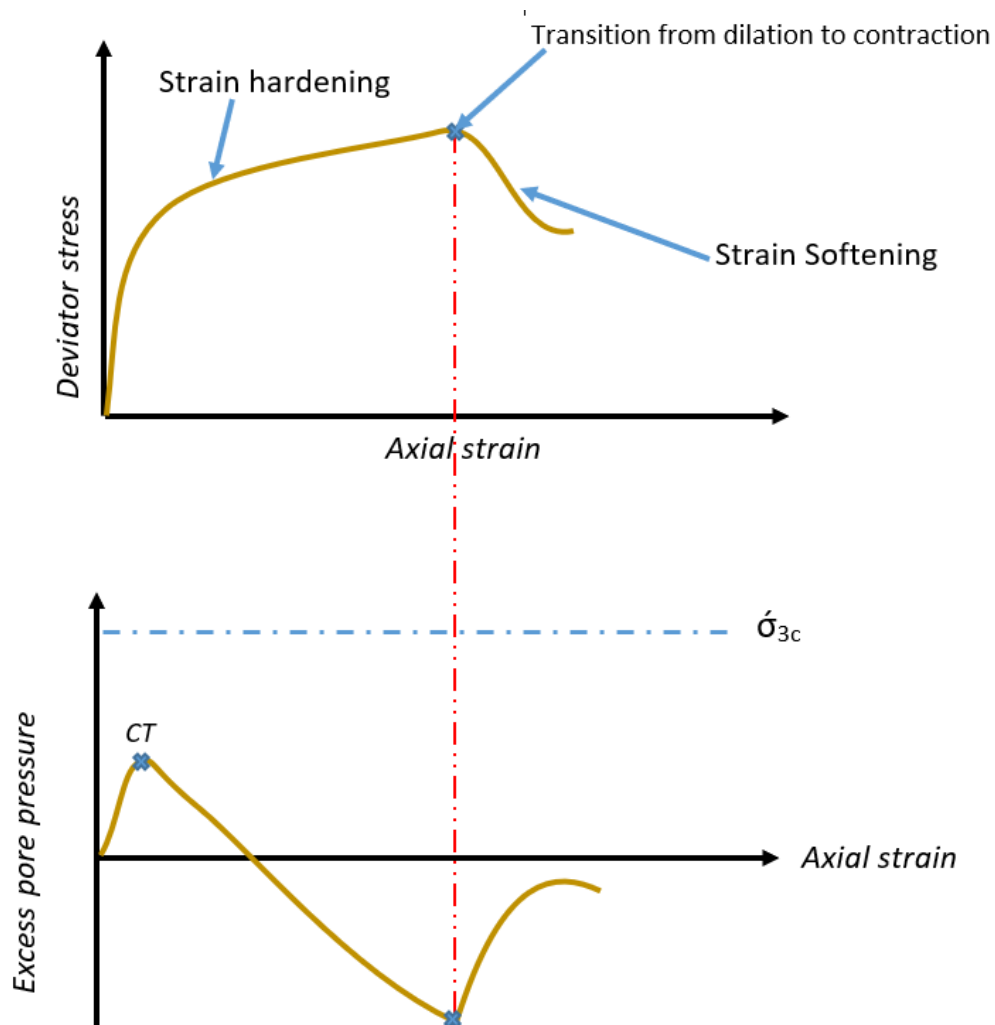


Figure 2.2 Behaviour of dense sands under undrained static loading after large strains (adopted and modified from (Chern, 1985))

### 2.2.2 Critical and steady-state conditions

CS soil mechanics is one of the most important frameworks used previously to model the soil response. This framework builds on the central idea that the soil reaches an ultimate state under a particular combination of void ratios and effective stress, irrespective of the shearing history or the stress path (Murthy et al., 2007). The ultimate state is called the critical state (CS) and is defined as the state when the soil shows continuous deformations under a constant void ratio and constant stress (Castro, 1975; Roscoe, Schofield, & Wroth, 1958; Vaid & Chern, 1983b). The conditions that explain the critical state of soils have been presented in many of the previous studies. Casagrande (1940) reported that reaching the critical state under drained conditions

could require the void ratio and the normal stresses to stay constant under continued loading. However, the critical state is attained under undrained conditions when the effective stress and pore pressure remain constant at a high strain. Seed and Lee (1967) reported another definition of the critical state condition as a combination of the void ratio after consolidation and the confining pressure that generated zero volumetric strain at the maximum deviator stress under drained conditions. Under undrained conditions, the critical state can be defined as a combination of the void ratio after consolidation and the effective confining pressure at the peak failure. These two critical state concepts presented by Seed and Lee (1967) produce two different critical state lines. Failure of the effective stress at a large strain indicates the critical state conditions in sandy soils (Casagrande, 1940). According to the critical state concept, the sands with a low relative density exhibit contractive behaviour, while those with a high relative density shows dilative behaviour, and at an appropriate confining pressure, the void ratio is changed from the initial value to the critical void ratio. Murthy et al. (2007) reported that depending on the initial relative density and the initial confining pressure, the states of the undrained behaviour of sandy soils in monotonic triaxial tests can be classified into four different types: critical state (CS), phase transformation state (PT), quasi-steady state (QSS), and undrained instability state (UIS), as shown in Figure 2.3.

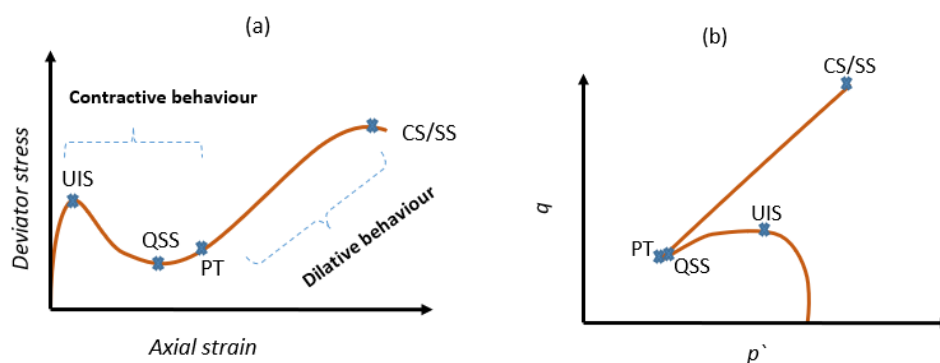


Figure 2.3 Typical states of the undrained loading behaviour of saturated sandy soil: (a) stress–strain relationships and (b) stress paths (adapted and modified from (Murthy et al., 2007))



As can be seen from Figure 2.3, CS is the state at which the sample deforms at zero change in the deviator stress, mean effective stress, and void ratio. PT represents the state when the behaviour of the soil changes from contractive to dilative, and in undrained tests, it is associated with the minimum mean effective stress. QSS is defined as the state when the deviatoric stress reaches the minimum value at undrained shearing. Experimental studies showed that QSS is not identical to PT but the two are very close in terms of the stress path. The phase transformation state occurs at an axial strain higher than that required for the quasi-steady state (Murthy et al., 2007). However, the deviator stresses at PT and QSS are almost identical. UIS is defined as the state at which the deviator stress reaches the initial peak before dropping to the minimum value; UIS is associated with the onset of static liquefaction. There is a connection between UIS and QSS because the sample that shows QSS also exhibits UIS. Therefore, UIS and QSS have received considerable attention from researchers because they exhibit the initial peak and the minimum undrained shear strength of granular soils at small deformation levels. The critical state of sandy soils is used widely in the liquefaction analysis method, mentioned as the steady state (SS) method (Castro, 1969; Castro & Poulos, 1977; Poulos et al., 1985). Poulos (1981) and Yamamuro and Lade (1998) defined the steady state as the state in which the soil mass is constantly deforming under undrained constant shear stress, constant volume, and constant excess pore water pressure. Moreover, the steady-state condition is observed when the deviator stress becomes constant at a large strain in the stress–strain response. The critical state is determined using the drained tests; however, the steady state is determined using undrained tests. CS and SS approaches provide a valuable framework for studying the monotonic strength of fine and coarse soils, respectively (Srbulov, 2008). Poulos et al. (1985) indicated that the soil reaches the steady-state condition after a complete change of its own fabric, which is a result of the orientation change of all the particles generated by the particle breakage. The soil fabric can be defined as the normal orientation distribution of sand particles (Dafalias & Manzari, 2004). Laboratory investigations of the undrained behaviour of sand showed that both the steady state and the critical state are almost the same, and the concept of critical state can be used to model them (Been, Jefferies, & Hachey, 1991; Jefferies & Been, 2015; Li & Wang, 1998; Poorooshasb, 1989; Verdugo & Ishihara, 1996). The results of undrained monotonic triaxial compression tests indicated that the points when the soil samples reach the critical state (CS) or the steady state (SS) are located on a

straight line passing through the origin of the stress path and called the critical state line (CSL) or steady state line (SSL), as shown in Figure 2.1(b). CSL or SSL in the stress path ( $q - p'$  space) can be represented as follows:

$$q_{CSL} = M \times p'_{CSL} \quad (2-1)$$

in which  $q_{CSL}$  and  $p'_{CSL}$  are the deviatoric stress and the mean effective stress at the critical state, respectively;  $M$  is the slope of CSL/SSL. Equation (1) can be written for the triaxial tests as proposed by Schofield and Wroth (1968) as follows:

$$\sin \phi_s = \frac{3 \times M}{6 + M} \quad (2-2a)$$

Alternatively, Equation (2a) can be written as proposed by Ishihara (1993) as follows:

$$\left(\frac{q}{p'}\right)_{CSL} = \frac{6 \times \sin \phi_s}{3 - \sin \phi_s} \quad (2-2b)$$

where  $\phi_s$  is the mobilised internal friction angle.

For a given sand sample, we can use the critical or steady state concept to differentiate between contractive and dilative behaviours by drawing the CSL or SSL from a plot of the void ratio after consolidation versus the log of the confining pressure, as shown in Figure 2.4 (Jafarian, Ghorbani, et al., 2013). Castro (1969) stated that the steady-state strength was only a function of the relative density of sand. The position of steady-state strength in a state diagram is represented by a unique line called the steady-state line. According to the relation of  $e - \log p'$  proposed by Terzaghi, the void ratio ( $e$ ) is considered the most relevant state variable to characterise the behaviour of soils. The undrained behaviour of soils depends on the position of the initial state of the soils on the steady state line in the  $e - \log p'$  curve (Bobei, Lo, Wanatowski, Gnanendran, & Rahman, 2009; Thevanayagam & Mohan, 2000). The undrained behaviour was contractive (C in Figure 2.4) when the initial state was located above the steady-state line. However, when the location of the initial state was below the steady-state line, the behaviour was dilative (D in Figure 2.4). If the initial state was close to the steady-state line, the behaviour was initially contractive, followed by dilation (C–D in Figure 2.4).

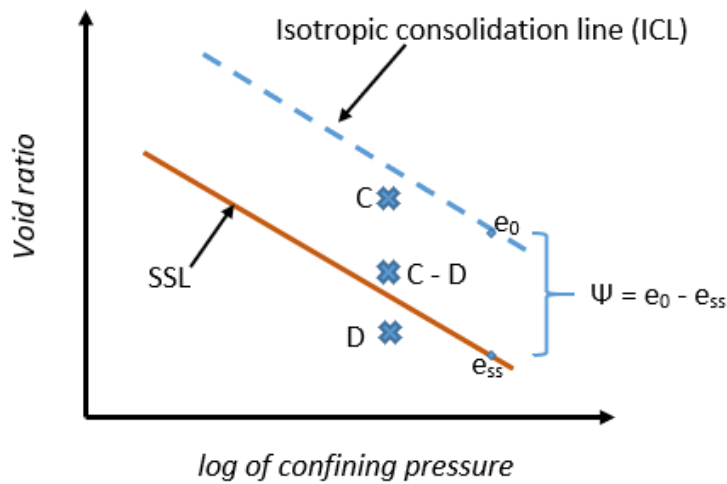


Figure 2.4 Steady state and isotropic consolidation lines of sandy soil (Thevanayagam & Mohan, 2000)

Despite the lack of a theoretical difference between CS and SS, the uniqueness of CSL and SSL in the  $e - \log p'$  space needs to be studied. The discussion about the uniqueness of CSL and SSL arises because of the fact that different results have been reported in many of the experimental studies. Been et al. (1991); Chu (1995); Ishihara (1993); Leong, Chu, and Teh (2000); Poulos, Castro, and France (1988); Verdugo and Ishihara (1996); and Yoshimine and Ishihara (1998) argued that the CSL and SSL of clean sand are identical in the  $e - \log p'$  space. However, Alarcon-Guzman et al. (1988); Konrad (1990), and Vaid et al. (1990) stated that the CSL and SSL are different. The difference between CSL and SSL could be related to the different test conditions adopted to measure them. The shapes of CSL and SSL also represent another aspect that needs to be considered while evaluating the uniqueness of the two lines. Been and Jefferies (1985) and Konrad (1990) reported that the shape of both CSL and SSL is straight. However, Verdugo and Ishihara (1996) and Thevanayagam and Mohan (2000) stated that the shapes of the two lines bent at a low confining pressure. Note that the presence of fines in sandy soils has a significant effect on the position of CSL and SSL in the  $e - \log p'$  space. Non-plastic fines content and the isotropic consolidation line (ICL) had a considerable effect on the position of SSL (Thevanayagam & Mohan, 2000; Yamamuro & Lade, 1998). Murthy et al. (2007) pointed out that the location of the

critical state in the  $e - \log p'$  space shifted downward, and the scatter in the data increased with an increase in the fines content. This could be associated with a decrease in the uniformity of the samples with an increase in the silt content, as shown in Figure 2.5. Moreover, Murthy et al. (2007) argued that the critical states in the undrained and drained tests were identical. Notwithstanding, Yamamuro and Lade (1998) stated that the initial confining pressure had a strong effect on the drained and undrained steady-state lines. The two steady-state lines diverged at a low confining pressure, while both of them synchronised at medium-to-high confining pressures. A possible explanation of this difference is related to the fact that the samples in the drained tests are loaded at a high strain, where the soil dilates considerably to reach the steady state (Yamamuro & Lade, 1998).

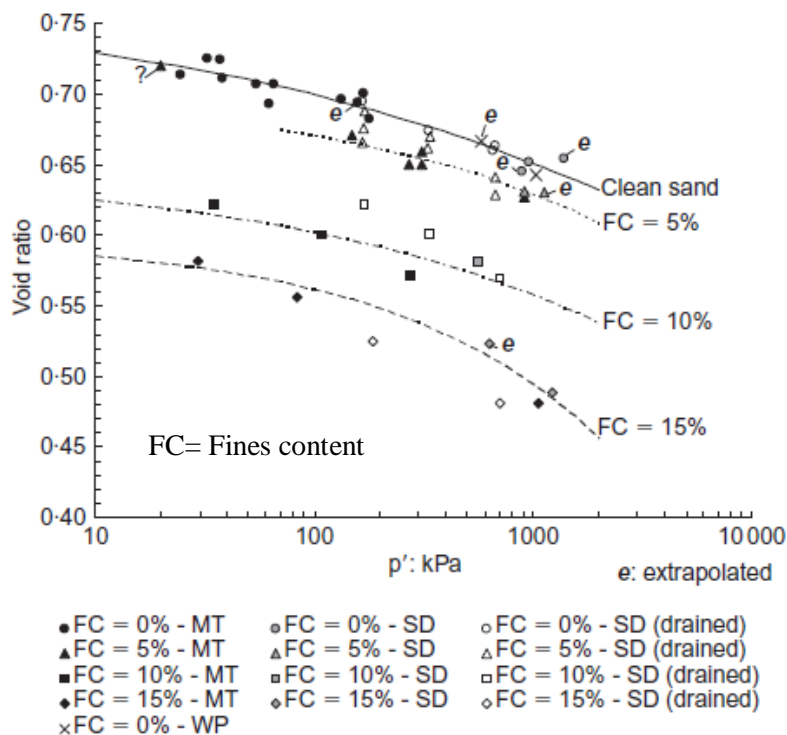


Figure 2.5 Effect of non-plastic silt content on the position of CSL of Ottawa sand in the  $e - \log p'$  space (Murthy et al., 2007)

Many previous studies have reported that the position of the critical state in the  $e - \log p'$  space is influenced by certain factors. These factors include the drainage state, the initial state (initial relative density and initial confining pressure), the type of consolidation (isotropic or anisotropic), the magnitude of the principal effective

stresses, and the sample deposition techniques used (Murthy et al., 2007). However, Been et al. (1991); Ishihara (1993); Verdugo and Ishihara (1996) stated that the initial state (initial void ratio and initial confining pressure) does not affect the critical state of specimens. The critical state concept has been effectively adopted in the literature to formulate the constitutive models and calculate the mechanical response of cohesionless soils. Therefore, various parameters have been suggested to describe the differences between the normal state and the critical state. Murthy et al. (2007) argued that among the many critical state parameters, the most popular one is the state parameter ( $\Psi$ ). (Been & Jefferies, 1985) defined the state parameter as the difference between the initial void ratio ( $e_0$ ) and the critical state void ratio ( $e_{ss}$ ) corresponding to the mean effective stress at the critical state  $p'$ , as shown in Figure 2.4. Negative values of ( $\Psi$ ) indicate dilative behaviour. However, positive values indicate contractive behaviour. Murthy et al. (2007) stated that irrespective of the materials and the sample preparation method used, the effect of the initial fabric can be considered just at the early stages of loading, with the consequences omitted at a large shear strain. This conclusion is based on their experimental results which showed that there was no difference in the strength of the samples prepared using slurry deposition methods and the moist tamping method, at the critical state, phase transformation state, and quasi-steady state. However, the difference exists at the undrained instability state. The same conclusion was reported by Ishihara (1993); Poulos et al. (1985); Verdugo and Ishihara (1996); they stated that the fabric of a sample is completely remoulded when it reaches the steady state. Therefore, the sample preparation method which controls the original fabric has no effect on the slope or the position of the steady-state line. Verdugo and Ishihara (1996) reported that the quasi-steady-state line can be used to distinguish between contractive and dilative behaviours. All of the points located above the quasi-steady state line represent a contractive response, while the points under the quasi-steady-state line showed dilative behaviour; the initial confining pressure caused a slight difference in the positions of the points. They also stated that the quasi-steady state could be a particular case of phase transformation where a temporary reduction in the deviator stress occurs at limited levels of shear strains. They argued that the development of the shear strength during a quasi-steady state is associated with the frictional resistance between the grains of the soil. The steady-state line is uninfluenced by the initial state as long as the soil mass is uniform.

## 2.3 Liquefaction and instability of sandy soils

The liquefaction phenomenon has been recognised in the early stage of soil mechanics development. Terzaghi and Peck (1948) proposed the term ‘Spontaneous liquefaction’ to describe the sudden changes in the properties of sandy soils that flowed as a liquid, triggered by a slight disturbance. This phenomenon was adopted in analysing slope failures likely to happen in saturated deposits of silty sands. In 1953, (Mogami & Kubu) reported a similar phenomenon called ‘liquefaction’ and used it to describe the failure conditions of the deposits of sandy soils during earthquakes; this phenomenon has since been treated as an issue of engineering significance. The quantity of excess pore pressure, the amount of generated deformation, or the mechanism that leads to a significant strain are the three different criteria previously adopted to define the liquefaction of soils on the basis of the loading types. As the present work focuses only on static liquefaction, only the criteria of the amount of excess pore water pressure and the mechanism responsible for the large deformations are discussed in this thesis.

Two major points should be well addressed when dealing with liquefaction. The first is the stress conditions required to trigger liquefaction, and the second is the consequences of liquefaction regarding possible deformations and possible slidings (Seed, 1987). Many previous studies, such as Alarcon-Guzman et al. (1988); Ishihara (1993); Vaid and Sivathayalan (2000); Wanatowski and Chu (2007); Yamamuro and Lade (1997b), have reported that the behaviour of sandy soils under undrained static loadings is considerably dependent on the initial void ratio and the initial confining pressure. On the basis of the initial state of a sandy soil, Yamamuro and Lade (1998) classified the undrained behaviour of sandy soils into the following five different regions, as shown in Figure 2.6:

- 1- Liquefaction region: This region occurs at low confining pressure with high contraction tendency that causes complete liquefaction (zero effective stress) (Bobei et al., 2009; Poulos et al., 1985). This aspect is confirmed by the static and earthquake-produced liquefaction investigations which revealed that the occurrence of liquefaction in very deep soil layers is rare.
- 2- Temporary or limited liquefaction region: This region is characterised by an increase in the stability of soils with an increase in the initial confining pressure. Further, this area includes a broad range of confining pressure. The

mechanism of contractions in this region is related to the particle rearrangements during consolidations.

- 3- Stable or non-flow region: This region represents the case when there is no reduction in the deviator stress in the undrained effective stress path (no quasi-steady-state point). This region could occur at a very narrow range of confining pressure and depends on the type of sand and density.
- 4- Temporary instability region: This area occurs at a high confining pressure and represents the case when the stability of the soil reduces with an increase in the confining pressure. The difference between temporary liquefaction and temporary instability is that in the case of temporary liquefaction, the soil strength increases with an increase in the confining pressure. In contrast, the soil strength decreases with an increase in the confining pressure during temporary instability (Yamamuro & Lade, 1997b).
- 5- Instability region: This region represents the case when the initial peak deviator stress is higher than the deviator stress under steady-state conditions. Further, it represents the liquefaction area, but the stresses is too high to simulate. Thus, the liquefaction should be studied at a small confining pressure in soils with a low relative density.

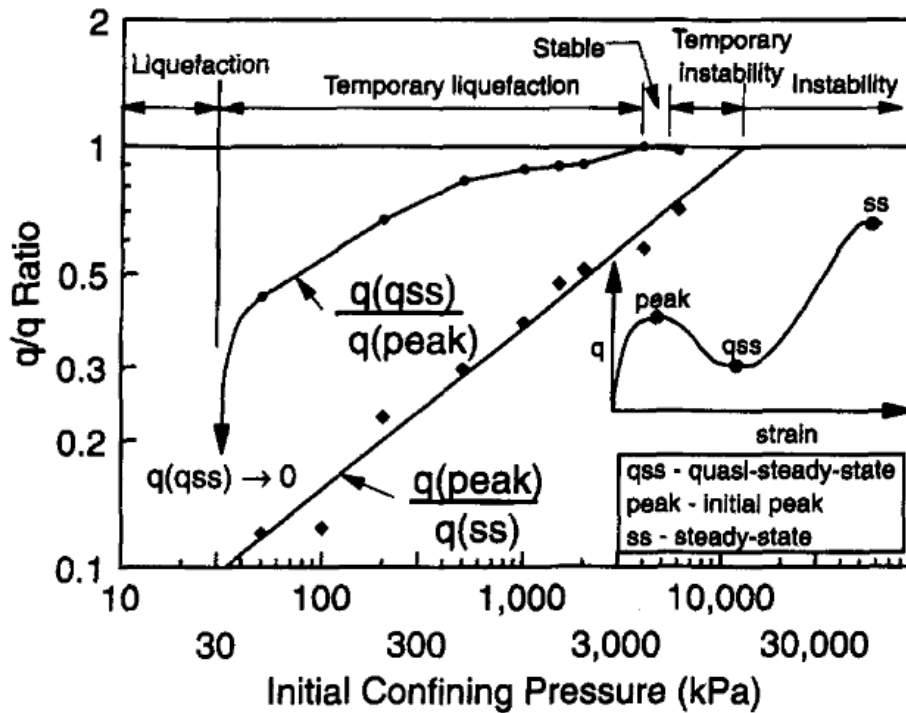


Figure 2.6 Undrained behaviour of sandy soils (Yamamuro & Lade, 1998)

Yamamuro and Lade (1997b) argued that the stress magnitude and the characteristics of the stress paths play a major role in the variation between the patterns. Both the liquefaction behaviour and the temporary liquefaction behaviour are referred to as static liquefaction. The source of volumetric contraction in cases of liquefaction and temporary liquefaction is particle rearrangement, whereas particle crushing is the source of volumetric contraction in cases of temporary instability and instability. The steady-state line shown in Figure 2.4 can be used to distinguish between the first three types of undrained behaviour of sandy soils. The initial state which is located well above the steady-state line is classified as the liquefaction behaviour. However, the non-flow response is associated with initial state located well below the steady-state line. Limited liquefaction is related to the initial state slightly above or below the steady-state line. The decrease in the shear strength during shearing is associated with the volumetric change tendency and the drainage condition (Poulos et al., 1985). Liquefaction occurs only in contractive soils (i.e. soils that show a decrease in volume during loading) when the applied shear stresses in the field are adequate to trigger liquefaction in the undrained state. However, dilative soils (i.e. soils that tend to



increase in volume during shearing) are not susceptible to liquefaction even under undrained shearing because their shear strength in the undrained state is greater than that in the drained state (Poulos et al., 1985). Static liquefaction is triggered in saturated loose sandy soils when the static driving shear stress exceeds the undrained peak shear strength of the soils (Sadrekarimi, 2014a). Various cases (such as overstepping of the slope, increasing embankment height, and weight of the construction/repair equipment) show some of the monotonically increasing shear load conditions that lead to static liquefaction on a sloping ground or beneath an embankment. In addition, static liquefaction has been observed in naturally deposited soils (Bjerrum 1971), man-made fills (Cornforth, Worth, and Wright 1974), and mine tailing piles (Eckersley 1985). Casagrande (1975) stated that the considerable contractive behaviour during liquefaction could be attributed to the flow structure which consists of 'soil grains rolling over each other with minimum resistance'. Liquefied soils undergo significant unidirectional shear strain and behave as a liquid until the applied shear stress is lower than the shear strength (Poulos et al., 1985). During the reduction of the effective stress path, the undrained behaviour of sandy soil is considered unstable and the sand is unable to sustain a constant deviator stress. The shear strength at the steady state plays a fundamental role in the determination of whether liquefaction will occur. If the shear strength at the steady state is lower than the applied shear stress, the susceptibility to liquefaction will increase with an increase in the possibility of the occurrence of large deformations (Sadrekarimi, 2014c). In contrast, if the applied shear stress is less than the shear strength at the steady state, then the liquefaction cannot occur because the associated large unidirectional deformations are not possible. Seed (1987) presented another condition for liquefaction triggering; he stated that the liquefaction in soil could be triggered when the pore pressure builds up to a high value (e.g. the value of the pore pressure ratio  $r_u > 60\%$ , where  $r_u = U_{excess}/\text{initial confining pressure}$ ). In case there is no high pore pressure build-up, the liquefaction will not be triggered in the soil and no problems of sliding and deformation will arise. Thus, the disastrous consequences of liquefaction can be avoided by designing geotechnical applications such that the generated pore pressure is small ( $r_u < 100\%$ ). To understand and describe the flow liquefaction behaviour, (Sladen, D'hollander, & Krahn, 1985) proposed the concept of a collapse surface. This concept is based on the peak points of the effective stress path of samples which are consolidated at the same void ratios but different confining pressures located

on a straight line passing through the steady-state points on the stress path, as shown in Figure 2.7(a). Liquefaction occurred when the soil state reached the collapse surface under undrained conditions, and the shear strength exceeded the steady-state shear strength (Sladen, D'hollander, & Krahn, 1985). Moreover, Sladen, D'hollander, and Krahn (1985) reported that the slope of the collapse surface does not change with a change in the initial void ratio, but it is offset according to its steady-state intercept. Yang (2002) stated that the collapse surface or line is a continuation of the steady-state concept and is unique for loose soil. Ishihara (1993) arrived at the same conclusion in that loose Toyoura sand had a unique collapse line in the stress path space. However, other studies by Vaid and Chern (1985); Vaid and Chern (1983b), and Lade (1993) revealed that the onset of flow liquefaction under static or cyclic loadings is controlled by the effective stress ratio  $\eta_L(q/p')$  and that the peak points in the effective stress path are located on the straight line passing through the origin instead of through the steady-state points, as shown in Figure 2.7(b). This line was defined as the flow liquefaction surface or line (FLL) by Yang (2002), critical state ratio (CSR) by Vaid and Chern (1985), peak envelope by Konrad (1993), and instability line by Lade (1992). Vaid and Chern (1985); Vaid and Chern (1983b), and Lade (1993) also proposed that the FLL is unique for loose soils. This differs from the conclusion of Vaid and Chern (1985) and Lade (1993) derived from Yang (2002), that the FLL depends on the initial state of the sand (initial void ratio and initial confining pressure) and is not unique for loose sand, but changes with the stress level. The slope of instability line decreases with an increase in the confining pressure. This line could be used to characterise the onset of flow liquefaction or instability by separating the liquefaction behaviour into an unstable and stable response in the  $p' - q$  space. The flow liquefaction behaviour is a trigger, and the shear strength will decrease rapidly to the steady state when the stress conditions reach this line (Yang & Wei, 2012). The flow liquefaction line is dependent on the state parameter ( $\Psi$ ) which defined as the difference between initial void ratio and void ratio at the steady state, and the flow liquefaction angle can be computed using the state parameter as suggested by (Yang, 2002) as follows:

$$\left(\frac{q}{p'}\right)_{peak} = \frac{M}{B} \exp(A\Psi) \quad (2-3)$$

where  $M$  is the stress ratio at the steady state,  $A$  is less than zero, and  $B$  is an additional parameter that is anticipated to change within a limited range. On the basis of Equation (3), the flow liquefaction angle can be defined as follows:

$$\sin\phi_{FLL} = \frac{3 \times \left[ \frac{M}{B} \exp(A\Psi) \right]}{6 + \left[ \frac{M}{B} \exp(A\Psi) \right]} \quad (2-4)$$

According to Equation (3), Equation (4) can be rewritten as follows:

$$\sin\phi_{FLL} = \frac{3 \times \left( \frac{q}{p} \right)_{peak}}{6 + \left( \frac{q}{p} \right)_{peak}} \quad (2-5)$$

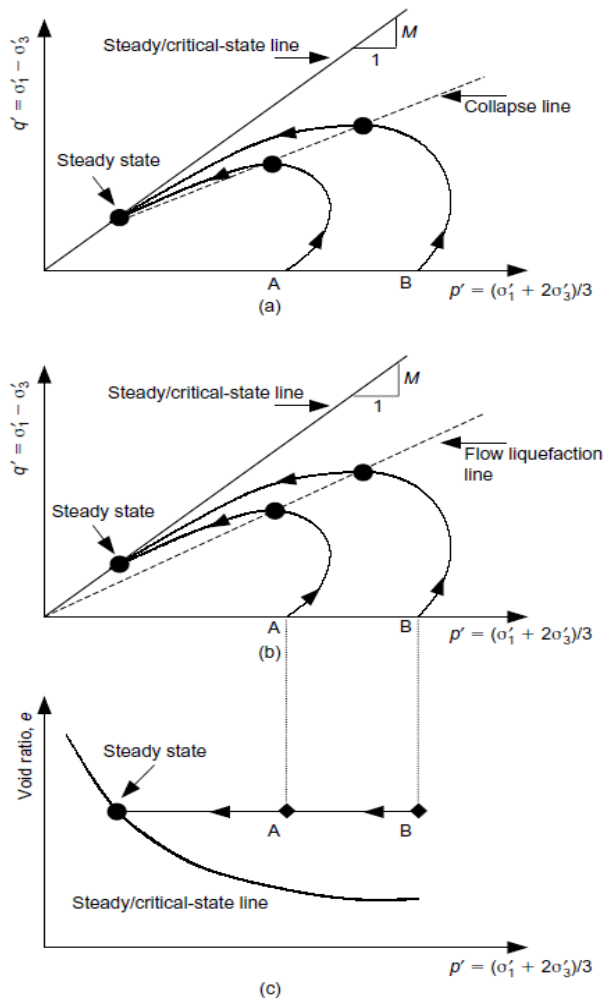


Figure 2.7 Difference between collapse surface and flow liquefaction line (Yang, 2002)

The FLL concept can be used to explain the trigger conditions of flow failure under both cyclic and static loading. Lade (1992); Vaid and Chern (1985), and Konrad (1993) reported that the flow failure behaviour could be initiated when the cyclic stress path reached FLL or when the cyclic stress state reached the collapse surface. Hyodo et al. (1994) stated that the strain softening behaviour under cyclic loading conditions was

observed when the deviatoric stress in cyclic loading was larger than the deviatoric stress in static loading at the phase transformation. Another condition for the initiation of strain softening was presented by Ishihara, Verdugo, and Acacio (1991); they stated that the flow failure under cyclic loading starts when the cyclic stress path crosses the monotonic undrained stress path. The experimental results showed that the flow liquefaction angle increased with a decrease in the state parameter; the denser the sand was, the higher was the flow liquefaction angle. The slope of the collapse line and the flow liquefaction line is a constant irrespective of the state of the soil. Lade, Nelson, and Ito (1988) stated that under undrained conditions, the decrease in shear stresses which are accompanied by large plastic strains could lead to unstable behaviour. In this case, two criteria control the instability response. The first is that the failure occurs when the maximum effective principal stress ratio ( $\sigma'_1/\sigma'_3$ ) is reached, and the second is that the instability line passes through the maximum deviatoric stress. In drained tests, both of these criteria are met simultaneously. However, in undrained tests, the maximum deviatoric stress could occur before the maximum effective principal stress ratio. In this case, the instability could be generated before the stress state reached the failure surfaces; as a result, the geometry of a failure surface helps to produce plastic deformations under diminishing stresses. Contrary to the conventional stability concept which assumes that the soil mass remains stable unless the failure strength is achieved, some experimental studies have reported that sandy soils exhibited unstable behaviour before reaching the failure state (Chu, Lo, & Lee, 1993; Lade, 1992; Pradel & Lade, 1990; Sasitharan, Robertson, Segoo, & Morgenstern, 1994). Lade and Pradel (1990); Pradel and Lade (1990) conducted undrained triaxial tests to investigate the probability of instabilities in loose sandy soils. The results showed that the instability occurs below the failure line under certain kinematic circumstances. Moreover, Pradel and Lade (1990) pointed out that the instability associated with liquefaction occurs at the maximum point of the stress path, which leads to the collapse of the sample. Lade (1992) argued that the existence of the instability line indicates the onset of possibly unstable stress conditions. Leong et al. (2000) stated that the instability behaviour of soil is characterised by the abrupt development of pore water pressure and axial strain in the load-controlled shearing state. Further, Leong et al. (2000) argued that despite the fact that instability and liquefaction occur in very loose granular fills under undrained conditions, the conditions for the occurrence of both of them are different. Liquefaction is mainly controlled by the relative density and the effective confining

pressure. However, instability occurs when the stress level falls within the instability zone. Lade (1993) and Olson, Stark, Walton, and Castro (2000) reported that many failures in geotechnical applications such as flow slides or the collapse of sandy soil slopes are related to instability. The term instability can be used to point out the behaviour of soil when there is a sudden development in the deformations as a result of the inability of the soil element to sustain an external load or stress (Chu & Leong, 2002). It was found that the instability did not occur under drained conditions irrespective of the stress state if it was above or below the peak stress ratio at the onset of the instability. However, the instability was observed in the loose sand under undrained conditions, and the occurrence of instability was considerably affected by the stress level (Leong et al., 2000). Lade and Pradel (1990) argued that instability occurs when the stress states are in the stress path space above the instability line (IL). Lade (1993) defined the instability line (IL) as a straight line which connects the peak deviatoric stress points on the effective stress path and passes through the origin, as shown in Figure 2.8. They stated that the slope of IL increases with a decrease in the void ratio. Yamamuro and Lade (1998) reported that the stress ratio, i.e. the deviator stress at the initial peak divided by the deviator stress at the steady state point, is used to evaluate the instability of samples. Small values of this ratio with stable behaviour are observed at low confining pressures, while the unity value of this ratio with unstable behaviour is observed at a high confining pressure. Further, the confining pressure at the unity value represents the lower values required for a stable response; a confining pressure beyond this value will cause complete instability. Sadrekarimi (2014a) argued that the onset of static liquefaction followed by the strain-softening behaviour is triggered when the undrained stress path crosses the IL. The reduction in the shear strength continues until a steady state is reached at  $q_{min}$ . The IL is used to differentiate between the stable and the unstable behaviours of sandy soils under undrained conditions. Figure 2.8 shows that the area between IL and CSL is called the zone of potential instability (Lade, 1993) or the zone of instability (Leong et al., 2000). Leong et al. (2000) argued that the location of the stress state of the soil element within the zone of instability is a necessary but not a sufficient condition because instability might not occur if the stress state is located within this zone and the other conditions are not met. Despite the fact that both static liquefaction and instability occur in loose granular materials under undrained conditions, the results showed that the conditions for the development of instability were different from those for static liquefaction.

Lade (1992) stated that instability is essential for liquefaction; however, they are not the same thing, even though both cause disastrous events. Static liquefaction is dominated more by the void ratio than the stress level, but note that the instability behaviour is affected by the void ratio as well. The instability line is not unique and depends on the initial state of the soil, and the relationship between the instability line and the void ratio after consolidation is a reverse relationship; the lowest void ratio produced the highest instability line (Chu & Leong, 2002). The unstable behaviour of granular materials is associated with the degree of saturation and the drainage conditions (Andrade, 2009; Lade & Pradel, 1990; Pradel & Lade, 1990). Moreover, the onset of liquefaction instability is a function of the sand state, not of material properties (Andrade, 2009). Further, stable behaviour is always obtained under drained conditions irrespective of the stress path direction and the sign of the second increment of work (Andrade, 2009; Pradel & Lade, 1990). Lade and Pradel (1990) pointed out that the following three conditions trigger the unstable behaviour of granular materials: (1) the negative value of the second work increment, (2) fully or nearly fully saturated samples that compress, and (3) undrained conditions. Under these circumstances, the pore pressure can build up openly, which produces the unstable behaviour. In contrast, a stable response is presented under all of the other conditions of the second work increment, drainage conditions, and degree of saturation.

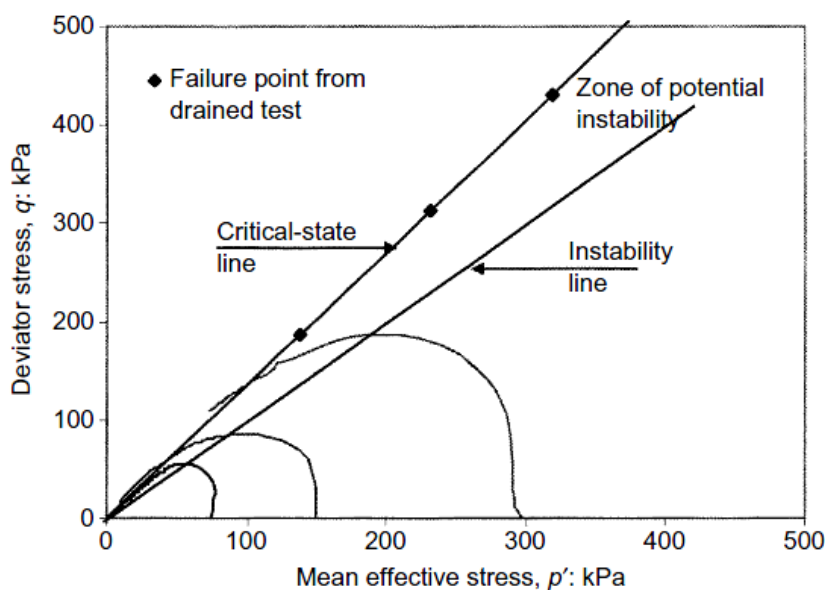


Figure 2.8 Instability line and zone of potential instability defined by undrained and drained tests for loose sandy soil (Chu & Leong, 2002).

## **2.4 Static liquefaction of clean sandy soils**

Because of the disastrous effect of the liquefaction phenomenon on the infrastructure, this phenomenon has received considerable attention among geotechnical researchers, and many studies have been conducted to clarify its basic mechanism and the factors affecting it. Previously, researchers have reported that various factors affect the liquefaction behaviour of soils. Evaluation of these factors may provide sound knowledge of the causes and effects of liquefaction. Moreover, precise understanding of the influence of some factors is required because of contradictory conclusions and inconsistent results reported in some of the past studies. A considerable amount of previous research on soil liquefaction has focused on relatively clean sand because the pore pressure can quickly build up in sandy soils, while the cohesive soils are considered non-liquefiable soils. However, more recent studies have reported that liquefaction failures can exist in sandy soils containing fines (materials passing sieve no. 200) (Miura, Yagi, & Kawamura, 1995; Perlea, Koester, & Prakash, 1999; Perlea, 2000). A large volume of published studies exists on the analysis of the static liquefaction in sandy soil and the factors affecting it, carried out using different apparatus and methodologies. These studies have reported that the liquefaction behaviour of clean sandy soils is considerably affected by many factors such as initial state (i.e., relative density and initial confining pressure), stress mode, sample preparation method, degree of saturation, compositional characteristics, and fines content. Some studies have expressed relative density in terms of the void ratio. The initial state is one of the most significant factors dominating the liquefaction behaviour of soils (Della et al., 2011; Ishihara, 1993; Konrad, 1990; Kramer & Seed, 1988; Leong et al., 2000; Miura & Toki, 1982; Mohamad & Dobry, 1986; Poulos et al., 1985; Riemer & Seed, 1997; Saikia & Chetia, 2014; Vaid & Thomas, 1995; Verdugo & Ishihara, 1996; Yamamuro & Lade, 1997b, 1998; Yoshimine & Ishihara, 1998).

### **2.4.1 Effect of initial state**

The behaviour of saturated sandy soils under undrained monotonic stress is profoundly dominated by the initial state (i.e. relative density and initial confining pressure) (Salamatpoor & Salamatpoor, 2014; Salem, Elmamlouk, & Agaiby, 2013). However,

it was dominated more by the void ratio than the stress level, but note that the instability behaviour is affected by the void ratio as well (Leong et al., 2000). Garga and Zhang (1997) stated that the volumetric changes during the saturation of the sample in the triaxial test increased as the relative density decreased and the confining pressure increased. The effect of the relative density is not separate from the applied stress level. This is evident when the high-relative-density samples showed strain-softening behaviour at the high confining pressure (Vaid & Sivathayalan, 2000). In addition, the effect of relative density may dominate the undrained behaviour of sandy soil more than the other factors. Complete static liquefaction (zero effective stress) behaviour can occur at a very low relative density and confining pressure (Yamamuro & Covert, 2001; Yamamuro & Lade, 1997a). Saikia and Chetia (2014) stated that liquefaction could exist in the saturated clean sand or silty sands have relative density up to 50%. However, non-flow behaviour can occur beyond 75% relative density. The occurrence of static liquefaction at low values of the initial states is associated with the field observations that recorded the liquefaction usually exist within the depth less than 20 m, which coincides with the vertical effective overburden pressure of 200 kPa in the completely saturated and level ground (Jafarian, Ghorbani, et al., 2013). Similarly, Krim, el Abidine Zitouni, Arab, and Mostéfa (2013) found that at a low confining pressure, the loose sample exhibited a reduction in the liquefaction potential when the confining pressure increased up to 200 kPa. Moreover, they added that the behaviour of sandy soil changed from flow behaviour to limited liquefaction when the relative density increased. The peak deviator stress required to trigger the strain softening decreased with the increasing void ratio (Konrad, 1990). Verdugo and Ishihara (1996) and Sivathayalan and Vaid (2004) argued that the different relative densities led to different behaviours. A high relative density resulted in dilative behaviour, while low relative densities led to contractive behaviour, and the effect of the initial confining pressure decreased with increasing relative density. Loose sandy soil samples are quite sensitive to changes in the relative density; even a small increase in the relative density can lead to a rather large variation in the behaviour of the samples from contractive to dilative behaviour, as shown in Figure 2.9 (Poulos et al., 1985). Figure 2.9 shows that small increases such as an increase of 3% in the relative density are sufficient to modify the behaviour of the samples. Similarly, the shear strength at the steady state increased with increasing relative density. This sensitivity



to changes in the relative density could be linked to the effect of the variation in the relative density on the soil fabric (Polito & Martin, 2003).

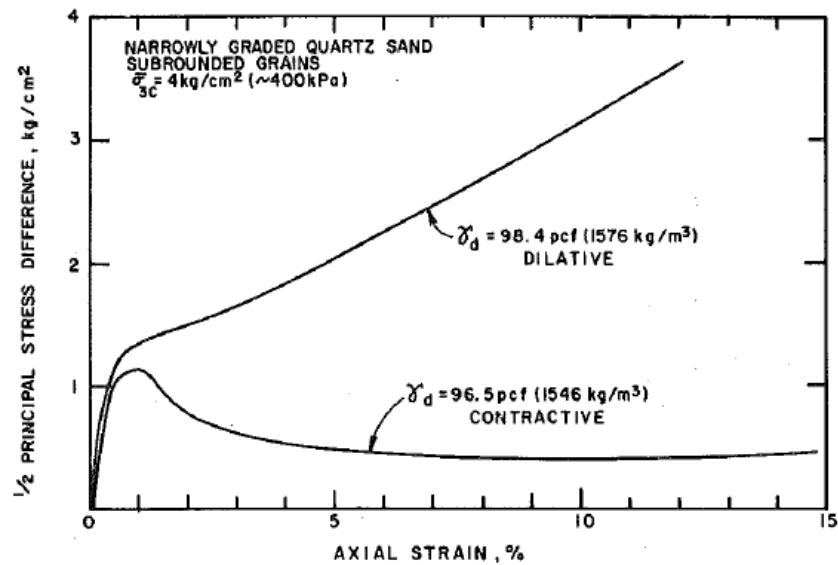


Figure 2.9 Effect of relative density on undrained behaviour of sandy soil (Poulos et al., 1985)

The effect of the initial confining pressure on the static liquefaction behaviour of clean sandy soil is associated with the relative density. At a given confining pressure, the behaviour of sandy soils under undrained static shearing could be changed from the flow response to the non-flow behaviour with increasing relative density. However, the sample tested at a high confining pressure showed a sharper reduction in the deviator stress than the sample tested at a low confining pressure (Sladen, D'hollander, & Krahn, 1985). In addition, at a high confining pressure, the liquefaction potential decreased for both loose and dense sands (Krim et al., 2013). The stress level at which the samples are consolidated in both triaxial compression and extension has a strong influence on the measured QSS strength; the higher the stress is, the higher is the QSS strength, and in triaxial compression, the drainage conditions during shearing do not affect the steady state (Riemer & Seed, 1997). Based on initial state, different frameworks have been used to explain the behaviour of sandy soil under undrained static loading. Alarcon-Guzman et al. (1988) proposed the 'structural collapse' concept to explain the undrained behaviour of sands. According to this concept, cohesionless materials have unstable fabric in a loose state, and the contacts between the sand particles can be lost during undrained loading because of the abrupt particle rearrangements. However, the short time of applying the load prevents the water from

flowing out of the soil. Therefore, the water is trapped and prevents the sand particles from moving closer together. Consequently, the pore water pressure increases, which in turn decreases the contact between the soil particles leading to a loss of strength, which causes the flow liquefaction behaviour. The generation of excess pore water pressure depends on the changes in the potential volume and the tendency to collapse. The sudden change in compressibility concerning a small shear strain is considered the key factor in the collapse concept. The occurrence of a ‘kink’ in the pore water pressure curve as shown by point (c) in Figure 2.10 refers to the collapsed structure of loose sandy soil during shearing (Alarcon-Guzman et al., 1988). This is supported by Konrad (1990), who reported that the change in the curvature of the excess pore pressure curve could be used to identify the onset of the structural collapse in the sand samples. In contrast, Been and Jefferies (2004) argued that the hypothesis for structural collapse could not explain the static liquefaction of sandy soil, as the flow failure response could be related to the changes in the plastic strain rates than to sudden particle rearrangements. They built their conclusion on the basis of the assumption of the effective stress instability criterion (e.g. stress ratio at collapse  $\eta_L$  or the ratio of  $q/p'$ ) cannot be used as a soil property because these ratios are less than the ratio of  $q/p'$  at the critical state despite the lack of densification of the specimen. Andrade (2009) also observed that liquefaction phenomena are a function of the state of the sand rather than the characteristics of the sand.

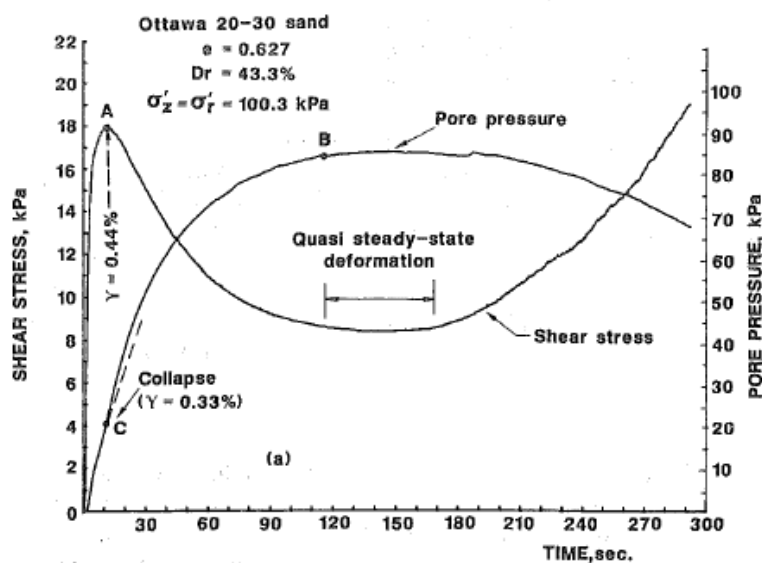


Figure 2.10 Undrained static behaviour of isotropically consolidated sample (Alarcon-Guzman et al., 1988)

The literature on the undrained behaviour of sandy soil has highlighted two different types of behaviour. The first one is called the normal behaviour of clean sand which is characterised by more strength at a low confining pressure and no increase in the positive pore pressure (Yamamuro & Lade, 1997b). However, at a high confining pressure, more contractive behaviour is observed with positive pore water pressure, thereby reducing the soil strength. While the second is the response of very loose sand, which was entirely different from the first type of behaviour on many sides as the soil strength increased with increasing confining pressure. This behaviour has been defined as 'reverse soil behaviour' by (Yamamuro & Lade, 1997b). There are two main reasons to explain the reverse soil behaviour of loose sandy soil; the first is that the compressibility of soil decreased with increasing confining pressure, which produce strong soil fabric and dilatant behaviour; in other words, the soil densified under a high confining pressure. The second reason is that under a high confining pressure, there is a chance to absorb the generated pore water pressure. Kramer and Seed (1988) defined the static liquefaction resistance as the undrained shear stress required the initiation of static liquefaction; they also reported that this resistance increased with increasing relative density and initial confining pressure. Additionally, Kramer and Seed (1988) stated that at any given relative density, the liquefaction behaviour of sandy soil is a function of the relationships between the initial and the steady-state confining pressure and that the liquefaction resistance decreases with increasing confining pressure. Sladen, D'hollander, and Krahn (1985) stated that the behaviour of soil in the triaxial compression test is affected by its initial state in relation to the steady state. The effective stress states at the steady state considerably depend on the void ratio. For the samples that had a different void ratio, the shape of the stress path will be similar, but the steady-state end point will differ. In contrast, Sivathayalan and Vaid (2002) argued that the steady-state strength is not associated with the void ratio alone. Some previous studies showed that the mode of stress might reduce the effect of the initial state on the liquefaction behaviour of sandy soils (Vaid & Thomas, 1995). At any given relative density, the effect of increasing the initial confining pressure in the triaxial compression test offsets the effect of the increasing relative density, while the opposite is true during extension loading. Vaid and Thomas (1995) also added that even loose sandy samples showed dilative behaviour under a confining pressure of up to 1000 kPa in the static compression triaxial tests. However, different densities of up to 60% resulted in contractive behaviour in the static extension triaxial tests. Yoshimine et al.

(1999) observed that the ratio of the shear strength to the initial effective stress was strongly related to the relative density and the shear mode. The effect of the initial state may dominate the behaviour of sandy soils more than the other factors. Igwe, Sassa, and Fukuoka (2004) observed that the liquefaction susceptibility depends on the relative density rather than on the gradation of sand. At low relative densities, sands with different gradation showed very close values of the peak and the residual strength. However, the values of the peak and the residual shear strength differed significantly when the relative density increased.

### **2.4.2 Effect of stress mode**

The effect of the stress mode or the type of loading (e.g. triaxial extension, triaxial compression, or simple shear) on the undrained behaviour of saturated sandy soil under monotonic loading has been reported in many studies. Sadrekarimi (2014b) and Yoshimine et al. (1999) reported that the undrained monotonic behaviour of loose saturated cohesionless soil is considerably dependent on the mode of shear stress irrespective of the sample preparation method and the fines content. The highest, intermediate, and lowest undrained shear strength mobilised in the triaxial compression tests, simple shear tests, and triaxial extension tests, respectively. Robertson and Fear (1995) observed that the QSS strength of triaxial extension is lower than the QSS of a triaxial compression test, and the response in compression is more brittle than in extension. Yoshimine and Ishihara (1998) stated that the maximum excess pore water pressure is significantly affected by the stress condition during deformation such as the direction of the principal stress and the magnitude of the intermediate principal stress. Sadrekarimi (2014b) also found that increasing the anisotropic consolidation stresses and increasing the intermediate principal stress parameter may trigger the static liquefaction and strain softening of sandy soil. The difference in the undrained behaviour between triaxial extension and triaxial compression is attributed to the effect of anisotropy on the behaviour of sandy soils (Arthur & Menzies, 1972). Anisotropy plays a significant role in the behaviour of loose sandy soil under static undrained shearing (Uthayakumar & Vaid, 1998). There are two types of anisotropy: the first one is attributed to the particle sedimentations and the second is stress-persuaded anisotropy. The behaviour of loose sand was dilative when the direction of load was the same as the sedimentation direction. In contrast,

the behaviour was contractive when the loading direction was perpendicular to the sedimentation direction. The strain softening appeared in anisotropically consolidated samples when the initial confining pressure increased at constant  $\sigma'_1/\sigma'_3$  or  $\sigma'_1/\sigma'_3$  increased at constant confining pressure, irrespective of the significant increases in relative density. Vaid and Thomas (1995) and Bishop (1966) also reached the same conclusion. The undrained behaviour of sand in the triaxial test is similar to that under plane strain. However, the critical state line (CSL) in both the  $e - \log p'$  and  $q - p'$  spaces is different, as shown in Figure 2.11, which could be related to the effect of the intermediate principal stress (Wanatowski & Chu, 2007). Konrad (1990) stated that there was an insignificant effect of the loading mode on the steady state strength, while the samples tested under step loading showed a slightly higher deviator stress than the constant rate.

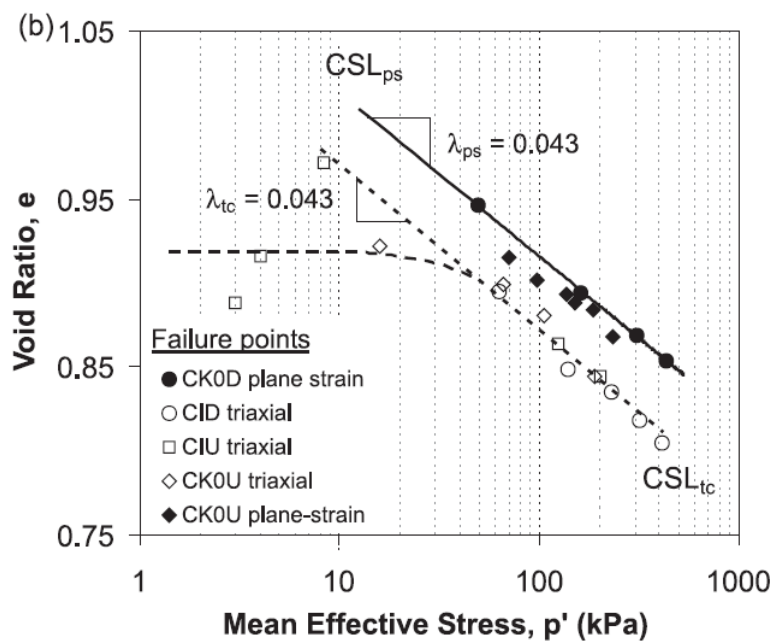


Figure 2.11 Critical state line for triaxial tests and plane-strain tests (Wanatowski & Chu, 2007)

### 2.4.3 Effect of sample preparation method

Various specimen preparation methods have been used in the previous studies to simulate the sand mass in the field by replication of a uniform sand sample at the specific relative density and the effective stress. Vaid and Sivathayalan (2000) stated that the sample preparation method might dominate the ensuing fabric of sandy soil.

The soil fabric has a significant influence on the undrained response at the intermediate level of strain (e.g. 1%–15%). However, this effect significantly decreases at large strains (Been et al., 1991; Ishihara, 1993). Miura and Toki (1982) added that the sample preparation methods could be considered a type of strain or stress history. The friction angles mobilised at the steady state or the phase transformation strength are invariant with respect of the specimen preparation method (Vaid, Sivathayalan, & Stedman, 1999). Stark and Mesri (1992) reported that the sample preparation method does not affect the slope of the critical strength line and the slope is the same for the disturbed and undisturbed samples. Tamping and pluviation are the most common techniques utilised in previous studies.

The different results that have been reached by researchers have made the effect of the sample preparation method on the undrained static behaviour of sandy soils a controversial topic. Zlatovic and Ishihara (1997) reported that the sedimentation method produced fewer liquefied samples than dry funnel pluviation and wet deposition as all the sample preparation methods produced different fabric characteristics. Konrad (1990) stated that the moist tamping method could be the best method to obtain the loose state in a laboratory. In contrast, the dry funnel method used to produce high-relative-density samples (Yamamuro & Wood, 2004; Yamamuro, Wood, & Lade, 2008). Many studies have indicated that the samples prepared using the wet deposition method showed more liquefaction resistance than those prepared using the dry funnel pluviation method (Mulilis, Arulanandan, Mitchell, Chan, & Seed, 1977; Yamamuro & Wood, 2004). In contrast, a different conclusion has been reached by other researchers: the dry funnel pluviation method produced more stable and dilatant behaviour than wet deposition (Benahmed, Canou, & Dupla, 2004; Della et al., 2011; Ishihara, 1993; Krim et al., 2013; Vaid et al., 1999). In addition, according to Vaid and Sivathayalan (2000), the samples prepared using the moist tamping method appeared to be potentially collapsible and more liquefiable than those prepared using other sample preparation methods as shown in Figure 2.12. The moist tamping method produced a weak fabric as a honeycomb which generated a substantial reduction in the void ratio during saturation. Moreover, the residual shear strength was very sensitive to the sample preparation method. Samples prepared using the dry funnel deposition method showed higher residual strength than the wet deposition samples (Della et al., 2011). However, Konrad (1993) stated that the peak shear strength was independent of the sand fabric in the moist tamping method and that the

steady-state strength depended on the stress state at the start of the flow failure. The effect of the sample preparation method on the static undrained behaviour of sandy soils decreased with increasing relative density and fines content (Wood, Yamamuro, & Lade, 2008).

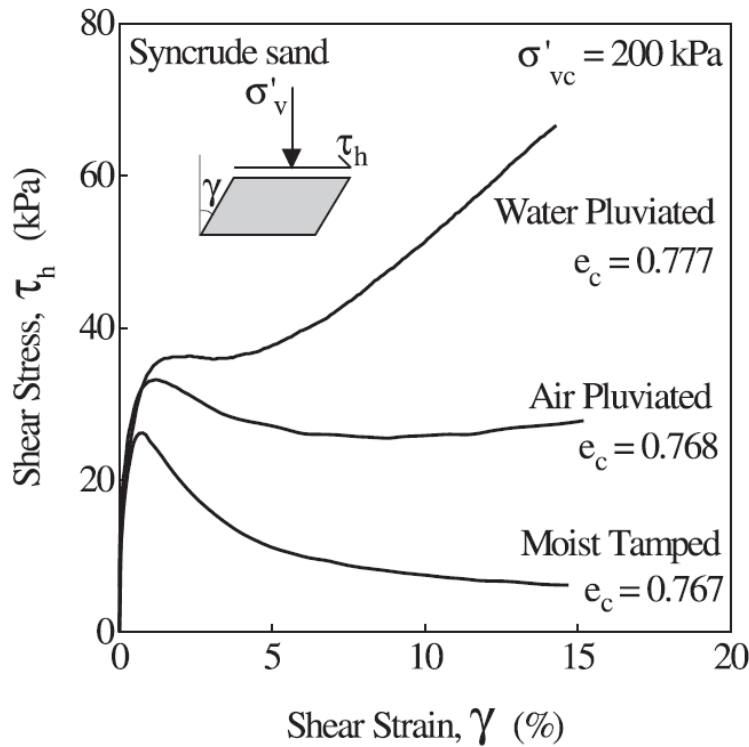


Figure 2.12 Effect of sample preparation method on the monotonic undrained behaviour of sandy soil (Vaid & Sivathayalan, 2000)

#### 2.4.4 Effect of degree of saturation

The degree of saturation ( $S_r$ ) plays a significant role in the stability of granular materials under undrained conditions. It is well-known that soil is composed of three phases, i.e., solid soil particles, water, and air. The degree of saturation refers to the relative amount of water included in the voids. In the increasing number of studies on the liquefaction of sand under different loading conditions, the influence of the degree of saturation on the liquefaction behaviour of sandy soils has already been reported. Some investigators have reported that a slight shift in the degree of saturation is sufficient to bring about a significant change in the liquefaction behaviour of sand. It is difficult to precisely measure  $S_r$ , particularly if the soil is partially saturated and

close to being fully saturated. In this case, Skempton's coefficient ( $B$ ), which is defined as the ratio between the generated pore water pressure to the applied cell pressure, can be adopted to identify the degree of saturation (Ishihara, Tsukamoto, & Kamada, 2004). The level of saturation can be easily simulated in the laboratory by using Skempton's coefficient ( $B$ ), and it is adequately precise to determine the condition of partial saturation. However, Ishihara et al. (2004) argued that one of the disadvantages of using the  $B$  value to identify the degree of saturation was that this parameter cannot be measured in the field. Samples are considered saturated when the  $B$  value is  $\geq 0.95$ , whereas they are considered partially saturated when the  $B$  values are less than 0.95. The instability of soils decreased with a decreasing degree of saturation because the development of the pore pressure is prevented by the presence of the compressible gas to hinder an unstable, runaway condition, as shown in Figure 2.13 (Delia, 2010; Ishihara, Tsuchiya, Huang, & Kamada, 2001; Pradel & Lade, 1990; Yang, Savidis, & Roemer, 2004). Figure 2.13 shows the relationship between the peak deviator stress at an axial strain of 10% and the  $B$ -value for Toyoura sand samples prepared at different relative densities and using different sample preparation methods. Figure 2.13 shows that the peak deviator stress decreased with an increase in the  $B$  value for the loose samples. However, the peak deviator stresses increased with increasing relative densities irrespective of the  $B$  value of the dense samples (Ishihara et al., 2004). Furthermore, Ishihara et al. (2004) argued that the relationship between the peak deviator stress and the  $B$  value can be represented by a straight line for each relative density. The straight line can be defined as follows:

$$q = q_0 e^{\alpha B} \quad (2-6)$$

where  $q_0$  is the value of the deviatoric stress at the point of  $B = 0$ ,  $e$  is the mathematical constant and  $\alpha$  is the slope of the straight line. Xia and Hu (1991) also added that the decrease in the level of saturation did not significantly affect the liquefaction resistance when the degree of saturation was less than 99%. Furthermore, the increasing back pressure considerably increased the liquefaction resistance. Eseller-Bayat, Yegian, Alshawabkeh, and Gokyer (2013) reported that samples with a degree of saturation of less than 90% did not achieve initial liquefaction. Mulilis et al. (1978) argued that the liquefaction potential was not significantly affected by a variation of the  $B$  values



between 0.91 and 0.97. Lade and Pradel (1990) indicated that the undrained behaviour of the partially saturated sand depended on the volume of the air bubbles inside the sample. The critical limit of the volume of the air  $(V_a)_{crit}$  and the corresponding degree of saturation  $(S_r)_{crit}$  can be used to distinguish between the stable and the unstable behaviour of the partially saturated samples. Furthermore, Lade and Pradel (1990) added that any change in the relative density and in the level of shear could significantly affect  $(S_r)_{crit}$ . The samples exhibited an unstable behaviour when the degree of saturation was more than or equal to the critical degree of saturation  $(S_r)_{crit}$ . This result indicates that full saturation increases the instability of the soil element. Consequently, this double jeopardy of the soil structure has been investigated.

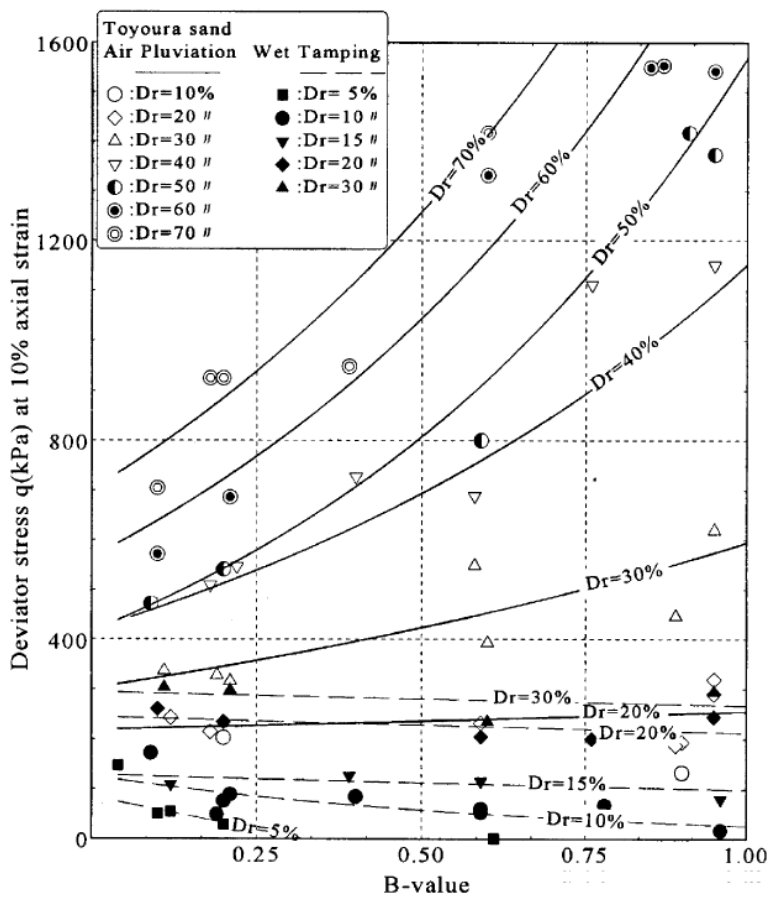


Figure 2.13 Relationships between the peak deviator stress and the B value for Toyoura sand (Ishihara et al., 2004)

## 2.4.5 Effect of compositional characteristics

Compositional features such as particle size, shape, and gradation have a significant effect on the liquefaction susceptibility of soil (Kramer, 1996). All the geological environments that produce a uniform grain size distribution and a loose state increase the susceptibility to liquefaction of these deposits. Kuerbis, Negussey, and Vaid (1988); Monkul, Etminan, and Şenol (2016); and (Pitman et al., 1994) argued that the variation of sand gradation had a negligible effect on the drained and undrained behaviour of sandy soils. Some scholars, however, have reported that sand gradation could affect the undrained behaviour of sandy soils (Igwe et al., 2004; Kokusho, Hara, & Hiraoka, 2004). Igwe et al. (2004) reported that at a given relative density, the static liquefaction resistance increased when the coefficient of uniformity  $C_u$  increased. Kokusho et al. (2004) also found that the cyclic liquefaction resistance was independent of the soil gradation, while the static liquefaction resistance increased with increasing  $C_u$ . On the basis of the grain size distribution curve, Tsuchida (1970) proposed a range of the most liquefiable soils and potentially liquefiable soils, as shown in Figure 2.14. A well-graded soil is less susceptible to liquefaction than poorly graded soils because smaller particles fill the space between the larger particles, which reduces the pore pressure under the undrained condition and reduces the volumetric changes under the drained conditions (Kramer, 1996). Soil with rounded particles is more susceptible to liquefaction than soil with angular particles. Rounded particles can densify and produce more considerable volumetric changes than angular particles (Alarcon-Guzman et al., 1988; Hird & Hassona, 1990; Kramer, 1996). Furthermore, Hird and Hassona (1990) added that the slope of the collapse surface in the  $q-p'$  space strongly depends on the grain shape and decreases with increasing sphericity. Flaky particles can enhance the compressibility of sand mixtures, which makes the sand less susceptible to liquefaction. Rounded particles can exist in fluvial and alluvial environments. Kramer (1996) also reported that the age of the soil deposits could affect the soil behaviour; older soil deposits exhibit more liquefaction than newer soil deposits. Previous research has established that the liquefaction behaviour of soil is affected by the size of the soil particles. Soil with a high percentage of gravel exhibited high shear strength during shearing because the dissipation of the pore water pressure is more rapid than in sand. However, Chang (1978); Evans and Seed (1987); Youd, Harp, Keefer, and Wilson (1985) reported that liquefaction could exist in gravel soils

and membrane penetration could be responsible for the high liquefaction resistance of gravelly soils. Seed (1968) also added that liquefaction could occur in loose gravelly soils when the gravel layer is enclosed by an impenetrable layer. Ishihara (1985) stated that the liquefaction behaviour of fine-grained soil is associated with plasticity characteristics rather than size. Wang (1979) argued that the fine-grained soils can be classified as susceptible to liquefaction if they satisfy each of the following four Chinese criteria:

Fraction finer than 0.005  $\leq$  15%

Liquid limit, LL  $\leq$  35%

Natural water content  $\geq$  0.9 LL

Liquidity index  $\leq$  0.75

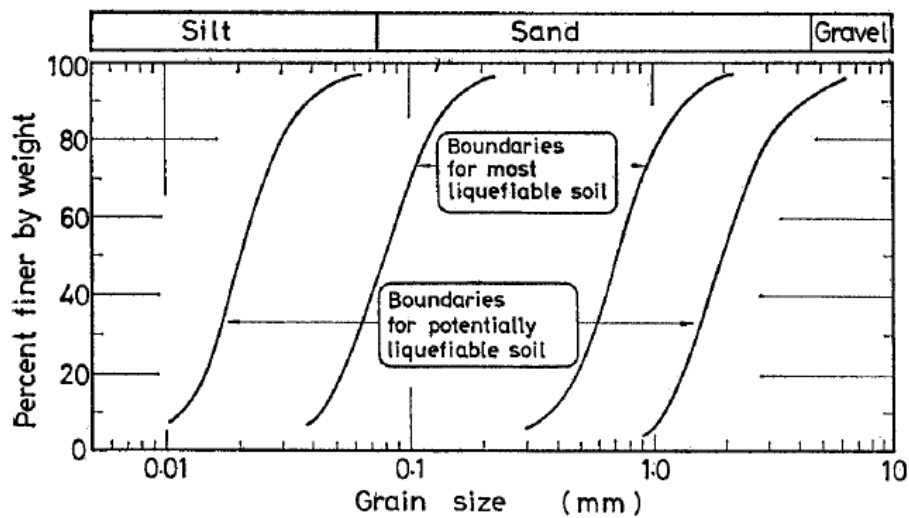


Figure 2.14 Ranges of liquefaction-susceptible soils (Ishihara, Troncoso, Kawase, & Takahashi, 1980).

A survey of the experimental studies which have been conducted on different types of sand showed that the liquefaction behaviour could be affected by other factors. Park and Jeong (2015) and Goto and Tatsuoka (1988) reported that the shear strength of dense sand increased and the strength of loose sand decreased with increasing sample size. Park and Jeong (2015) also reported that at constant relative density, the friction

angle of the sample was influenced by the sample size. For evaluating the friction angle of sand under the undrained condition, it is better to use a large specimen to the greatest extent possible. Yamamuro, Abrantes, and Lade (2011); Yamamuro and Lade (1998) pointed out the effect of the strain rate on the liquefaction behaviour of sandy soil. They found that the axial strain at the peak deviator stress decreased, while the dilation and the secant modulus increased with an increase in the strain rate.

## **2.5 Static liquefaction of sandy soils with fines**

Early studies on the liquefaction behaviour of soils primarily concentrated on clean sandy soils because the researchers at that time believed that liquefaction occurs only in clean sandy soils. Later, laboratory and field observations revealed that liquefaction can also occur in natural granular materials that have a considerable amount of fines (passing sieve no. 200). Even a small fines content is sufficient to significantly affect the behaviour of sandy soils as is shown in numerous studies (Georgiannou, Burland, & Hight, 1990; Thevanayagam, 1998). Thus, a substantial amount of research has been conducted on the effect of the fines content on the static stress–strain behaviour, cyclic response, collapse potential, and steady-state strength of mixtures of sand with fines (Chang, 1990; Chu & Leong, 2002; Georgiannou, 2006; Georgiannou et al., 1990; Thevanayagam, 1998; Yoshimine et al.; Zlatović & Ishihara, 1995). The influence of the fines content on the response of sandy soil under monotonic and cyclic loadings is an area of uncertainty because of the differing results obtained in previous studies. Some studies reported that the presence of the fines reduced the ability of the sandy soil to liquefy. In contrast, other studies concluded that the strength of sandy soil decreases with increasing fines content, as the presence of fines increases the soil compressibility by reducing the contact between coarse particles. Other studies have proposed a threshold around which the proportion of the fines content has a positive or adverse effect. Moreover, some field studies evaluated the effect of fines on the liquefaction resistance and the post-liquefaction strength of the sand–fines mixtures (Seed et al., 1983; Stark & Olson, 1995). The existence of fines notably influence the engineering characteristics and the liquefaction behaviour of sandy soils. The reason for this strong effect can be related to the relative density, plasticity index of fines, the fabric of the sand–fines mixtures, grain size distribution, and stress conditions. Bobei et al. (2009) stated that the sand with fines was more compressible than clean sand

because the fines shifted the position of the isotropic consolidation line (ICL) and the critical state line (CSL) downwards, while the CSL showed a higher downward shift. Moreover, the presence of fines effects the shape of ICL. However, the form of CSL was similar to that in the cases of clean sand and sand with fines. Rahman and Lo (2014) also reported that adding fines shifted the ICL and SSL downwards. However, the shift of SSL was greater than that of ICL. The effect of various types of fines such as plastic and non-plastic fines on the undrained static behaviour of sandy soils has been investigated in the last few decades. Silt is one of the non-plastic fines commonly used in these studies. However, the results showed some variation regarding the influence of silt on the mechanical behaviour of sandy soils. The earlier studies on the phenomenon of liquefaction assumed that the behaviour of clean sand is the same as that of silty sand. Some of these studies reported that the presence of fines in sandy soils leads to increase in undrained shear strength (Ishihara & Koseki, 1989; Yasuda, Wakamatsu, & Nagase, 1994). Moreover, the silt content did not affect the residual shear strength of sandy soil because the particles of fines and sand grains were the same and there was no magnetic force acting on their surfaces (Ishihara, 1993). Furthermore, a number of studies on the effect of silt on the mechanical behaviour of sandy soils indicated that silt does not contribute to the undrained shear strength of mixed soils because of their properties (e.g. size, nature, and position), and fines should be treated as voids. This led to the definition of the concept of the intergranular void ratio. On the basis of this concept, the fines which occupied the spaces between the large sand grains were considered nonactive. Kuerbis et al. (1988) stated that the effect of fines could be neglected and the behaviour of the sand fines–mixtures was controlled by the sand skeleton only. The sand skeleton’s void ratio can be calculated by using the following equation (Kuerbis et al., 1988):

$$e_{skeleton} = \frac{V_T G_s \rho_w - (M - M_f)}{(M - M_f)} \quad (2-7)$$

where  $V_T$ ,  $G_s$ ,  $\rho_w$ ,  $M$ , and  $M_f$  are the total volume of the sample, specific gravity of the soil, density of water, mass of soil, and mass of fines, respectively. Mitchell (1976) and Kenney (1977) proposed a new index known as the granular void ratio ( $e_g$ ), which can be computed as follows:

$$e_g = \frac{\text{volume of actual voids} + \text{volume of fines}}{\text{volume of coarse material}} \quad (2-8)$$

$$e_g = \frac{e + f_c}{1 - f_c} \quad (2-9)$$

where

$$f_c = \frac{\text{volume of fines}}{\text{total volume of solids}}$$

Furthermore,  $e$  is the void ratio.

Ni, Tan, Dasari, and Hight (2004) argued that the relationship between the granular void ratio and the undrained shear strength of mixed soils was not the same as that of the host sand. Their results showed that the presence of plastic fines increased the contraction tendency of the sand–fines mixtures, whereas the presence of non-plastic fines had a positive contribution to the undrained shear strength of mixed soils. Thevanayagam, Shenthan, Mohan, and Liang (2002) introduced new parameter called the equivalent granular void ratio ( $e_{ge}$ ) to evaluate the different contributions of fines and can be computed as follows:

$$e_{ge} = \frac{e + (1-b)f_c}{1 - (1-b)f_c} \quad (2-10)$$

where  $b$  is defined as ‘the portion of fines that contributes to the active intergrain contact’ (Thevanayagam et al., 2002). The value of  $b$  can be calculated by using the semi-empirical equation proposed by (Rahman, Lo, & Gnanendran, 2008):

$$b = \left(1 - e^{-2.5(f_c)^2/k}\right) \cdot \left(\frac{rf_c}{f_{cth}}\right) \quad (2-11)$$

where  $k = 1 - r^{0.25}$ ,  $r = X^{-1}$ ,  $X = D_{10}/d_{50}$ , and  $f_{cth}$  = threshold fines content. The values of  $b$  ranged between 0 and 1. Fines completely act as voids when the  $b$  value = 0. However, fines behave like the host sand when  $b = 1$ . Chu and Leong (2002) observed that when the fines content exceeds a certain percentage (20%–30%), the concept of the granular or intergranular void ratio is not applicable to the silty sand because the fine grains completely occupied the voids between the sand particles and efficiently

contributed to the mechanical behaviour. Moreover, when the fines content was less than a certain percentage (20%–30%), the instability curve which represents the relationship between the stress ratio at the onset instability and the global or intergranular void ratio was identical for clean sand and silty sand if the intergranular void ratio was used. However, some experimental work shows that important differences do exist; albeit, these findings are somewhat contradictory. Yamamuro and Lade (1997b) stated that the presence of a small percentage of silt (6%) enhanced the static liquefaction and ‘reverse behaviour’ of loose Nevada sand. They argued that the major reason for this behaviour was that the particle structure of silty sand was completely different from that of clean sand. A particle structure hypothesis was postulated on the basis of the interaction between the sand grains and the fines particles. According to this hypothesis, the presence of fines increases the compressibility of the sand–fine mixture more than that of the clean sand; even the relative density of the mixture was higher. Then, the liquefaction potential and the reverse behaviour improved as a result of the increased compressibility. Figure 2.15 shows an illustration of the particle structure hypothesis. As shown in Figure 2.15(a), the voids between the sand grains in the loose state are occupied by the fine particles; the fine particles could increase the relative density, but they have an insignificant effect on sand behaviour because they just occupy the voids. Moreover, the fine particles may locate in the contact points between the sand particles. During isotropic compression and shearing, as shown in Figure 2.15(b), the fine particles located near the sand grains contact sliding into the void space, which increases the volumetric strain and consequently, the liquefaction potential under the undrained condition (Yamamuro & Lade, 1997b, 1998). Regarding the reverse behaviour, the sliding of the small particles into the void space between the sand grains enhanced the contact between the large grains, which reduces the compressibility and increases skeleton stiffness when the confining pressure increases. The nature of deposition of clean sand makes a strong contact between the sand grains even in the loose state and hinders the development of the particle structure. Therefore, the clean sand is less compressible than the sand with fines (Yamamuro & Lade, 1997b). Rahman, Lo, and Dafalias (2014) observed that the location of the isotropic consolidation line (ICL) relative to the location of the steady-state line (SSL) plays a major role in whether the reverse behaviour will occur. The occurrence of the reverse behaviour is associated with ICL located above SSL. However, the normal behaviour is associated with the ICL located

below the SSL but finally, crosses the SSL at a high effective confining pressure. Further, Kuerbis et al. (1988); Pitman et al. (1994), and Thevanayagam (1998) reported that the quantity of fines affected the particle structure of the sand–fines mixture. The particle structure of a large amount of fines is different from that of a small amount of fines. Figure 2.16 shows the various types of particle structures at different silt contents. The relative density increased with an increase in the fines content from point A to point B as a result of the voids between the large sand grains fully occupied by the fines particles. A significant amount of fines completely separated the larger grains of soil until the small particles were present at point C, as shown in Figure 2.17. Thevanayagam and Martin (2002) proposed a classification system for the sand–fine mixtures based on the fines content, as shown in Figure 2.17. Numerous studies have reported that the liquefaction susceptibility of the sand–silt mixtures increased with increasing silt content. However, beyond a particular fine content called the threshold fines content  $F_{C_{thr}}$ , the behaviour transmitted from contraction to dilation with an increase in the silt content (Bayat & Bayat, 2013; Belhouari, Bendani, Missoum, & Derkaoui, 2015; Hsiao & Phan, 2016; Kuerbis et al., 1988; Pitman et al., 1994; Thevanayagam, Ravishankar, & Mohan, 1996; Xenaki & Athanasopoulos, 2003; Yang, Sandven, & Grande, 2006; Zlatović & Ishihara, 1995). However, there is some variation in these studies regarding the values of the fines content threshold  $F_{C_{thr}}$ . The reported values of  $F_{C_{thr}}$  in the literature ranged between 20% and 50%, as shown in Table 2.2. The threshold value is not unique, but it could depend on the properties of the coarse and the fine grains (Xenaki & Athanasopoulos, 2003). Thevanayagam and Mohan (2000) stated that when the fines content is equal to the threshold fines content, the matrix of the soil changes from a fine in the sand to sand in the fines soil matrix. The variation in the values of  $F_{C_{thr}}$  reported in the previous work could be attributed to two reasons. The first is that the nature of sand and silt may add some complexity of the value of  $F_{C_{thr}}$  because both of them are granular materials and they individually interact with each other during loading. The second is the shape and size of the host sand grains and silt particles. Yang and Wei (2015) investigated the effects of the particle shape and size on the static liquefaction behaviour of cohesionless soil. The results showed that a large difference between the sand particles and the fines leads to a large strength reduction as the fine grains may roll into the voids between the sand particles and make no contribution to resisting the external stresses. In addition, the shape of the sand particles and the fine grains plays a significant role in determining



the static liquefaction behaviour. Further, the fabric of the rounded sand particles is less stable than that of the angular sand particles. Moreover, the angular fine grains increased the stability of the sand fabric even when mixed with the rounded sand particles. In addition, Yang and Wei (2015), Wei and Yang (2014) reported that crushed glass beads showed higher strength than rounded glass beads. They added that the critical state friction angle  $\phi_{CS}$  for the sand–granular bead mixtures was more than the  $\phi_{CS}$  of the mixtures of sand–rounded glass beads and the shape of the fines was more influential on the behaviour of the mixtures than the hardness of the fines. Yang and Wei (2012) also added that in addition to the effect of the fines shape, the shape of the host sand particles plays a significant role in determining the overall behaviour of the sand–fines mixtures because the interparticle contact depends on the shape of both the sand and the fine particles. Monkul et al. (2016) observed that silty sand showed the lowest static liquefaction resistance when the host sand became coarser. They defined the static liquefaction resistance as ‘positive excess pore pressure generation capacity of the specimen, where greater liquefaction resistance implies smaller positive excess pore pressure generation capacity’. They added that the effect of the base sand gradation reduced with an increase in the fines content. When  $C_u \leq 2.5$ , the reduction in the undrained shear strength of sandy soil with a small amount of silt was very sharp with minor increases of the  $C_u$  samples showing stable and temporary liquefaction. However, when  $C_u$  was increased from 2.5 to 5, the shear strength decreased gradually, and all the samples showed complete static liquefaction when  $C_u \geq 5$  for the sand mixed with different percentages of silt.

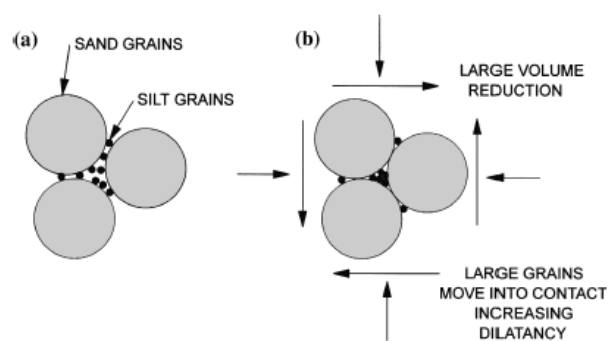


Figure 2.15 Schematic representation of loose silty sand showing the particle structure hypothesis (Yamamuro & Lade, 1997b)

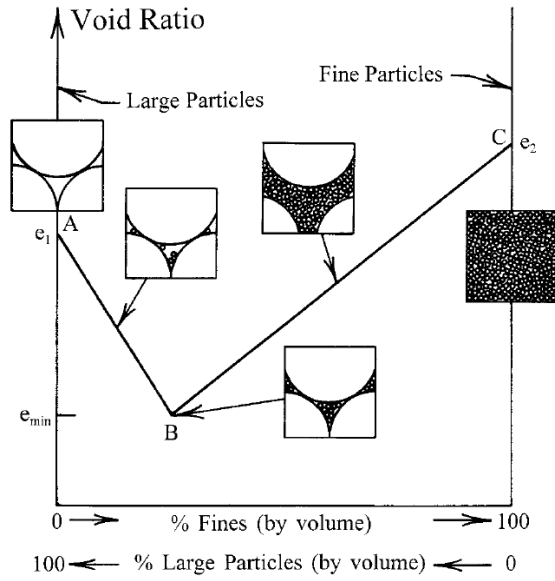


Figure 2.16 Effect of fine content on the particle structure of binary mixtures (Yamamuro & Covert, 2001)

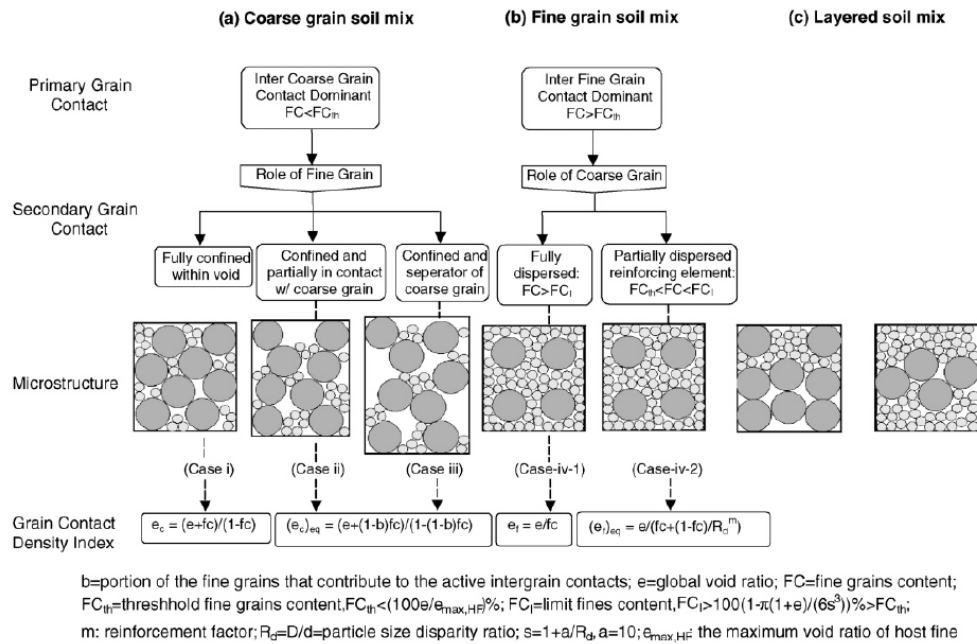


Figure 2.17 Classification of granular sand (Thevanayagam & Martin, 2002)

Table 2.2 Silt content thresholds of some studies reported in the literature

<i>No.</i>	<i>F<sub>c</sub><sup>thr</sup> value (%)</i>	<i>References</i>
1	20	(Kuerbis et al., 1988)
2	20–30	(Pitman et al., 1994; Thevanayagam et al., 1996; Zlatović & Ishihara, 1995)
3	30	(Belhouari et al., 2015; Yang, Sandven, et al., 2006)
4	35	(Bayat & Bayat, 2013)
5	44	(Xenaki & Athanasopoulos, 2003)
6	50	(Hsiao & Phan, 2016)

Murthy et al. (2007) reported that the presence of a small amount of silt in the clean sand might increase the contractions of the sample. Further, they added that the critical state friction angle  $\phi_{CS}$  increased with increasing silt content as a result of the angular shape of silt and that the rounded shape of the sand particles produced a good fabric and thus increased  $\phi_{CS}$ . However, some studies found differences for the effect of fines on  $\phi_{CS}$ . They indicated that the  $\phi_{CS}$  was insensitive to the fines content. Monkul et al. (2016) observed that adding silt to sandy soil made it more liquefiable than clean sand because silt made the gradation of the sand more gap graded. The non-plastic fines content and the size of the fine particles are the major factors considered during the investigation of the effect of non-plastic fines on the liquefaction behaviour of sandy soil. However, many factors such as the plasticity of fines, clay mineralogy, and pore water chemistry have to be studied well in the case of plastic fines (Abedi & Yasrobi, 2010). A vast amount of experimental work has been conducted on the liquefaction of clayey soil over the past few decades, and a number of different outcomes have been obtained (Tang, Ma, & Shao, 2013). Bray et al. (2004) and Boulanger, Meyers, Mejia, and Idriss (1998) reported that the clayey soils showed high susceptibility to liquefaction when the plasticity index (PI) was close to 12 and 17, respectively. One of the most significant findings of such research is that the effect of the clay content on the liquefaction behaviour of sandy soils is associated with a particular content called the critical value of the clay content; above the critical content, the liquefaction potential increased, and below it, the liquefaction susceptibility trend was reversed

(Tang, Ma, & Shao, 2013). Abedi and Yasrobi (2010) stated that the instability of the sand–plastic fines mixtures decreased with an increase in the plastic fines content to more than 10%–15%. The peak shear strength decreased with increasing fines content, but the reduction rate of the shear strength decreased with increasing fines content and the shear strength became stable at a relatively high fines content. Furthermore, Abedi and Yasrobi (2010) added that the instability zone became larger when the fines content increased up to 10%, and after 20%, it decreased. Many studies have reported that the presence of kaolinite in sandy soils reduced the stability of the fabric of sand and consequently, reduced the undrained shear strength at the quasi-steady state. In this case, the fines did not act as voids but were worse than voids (Georgiannou, 2006; Georgiannou et al., 1990; Pitman et al., 1994; Thevanayagam & Mohan, 2000). Ni et al. (2004) reported that the contribution of plastic fines in the undrained shear strength of mixed soil is a function of the stress history. For instance, the plastic fines acted worse than voids in normally consolidated samples. However, the contribution of plastic fines changed to a positive effect in the overconsolidated specimens. Moreover, they stated that most of the clay minerals are in the form of platy particles, which make them adjust their position and get out of the force-carrying skeleton in the clayey sand. Tang, Ma, and Shao (2013) and Tang, Ma, and Dieudonné (2013) reported that samples with a bentonite content of 5% showed higher liquefaction tendency than clean sand, while the liquefaction susceptibility decreased when the bentonite content was increased to 10% and 15%. They added that when the clay content was between 5% and 10%, the samples were the most vulnerable to liquefaction. The possible reason for the negative effect of the clay content was the unstable fabric produced by mixing the clean sand with a low clay content because the clay particles accumulated at the sand particles' contact points, which caused connectors with a low strength that quickly broke during shearing. However, with an increase in the clay content, the clay particles spread around the sand grains, filling the voids between the particles, and contributed along with the sand particles to the bearing loading. Consequently, the clay particles helped to stabilise the sample fabric. The above findings are consistent with the findings of (Gratchev, Sassa, Osipov, Fukuoka, & Wang, 2007). Gratchev et al. (2007) examined the effect of the bentonite content on the cyclic liquefaction resistance of sandy soil. A small amount of bentonite negatively affected the soil structure and resulted in unstable fabric, causing rapid cyclic liquefaction. However, at a high bentonite content, the liquefaction resistance increased as a result of the clay

matrix produced with a high bentonite content. Research findings by Bayat, Bayat, Aminpour, and Salarpour (2014) also pointed toward both bentonite and kaolinite having an adverse effect on the shear strength at a low fines content. However, increasing the kaolinite content to more than 20% leads to an increase in the peak shear strength of the mixtures. Bentonite has a more considerable effect on the behaviour of sandy soils than on the behaviour of the sand–kaolinite mixtures, and the samples of the sand–bentonite mixtures showed a slightly dilatant behaviour when the bentonite content increased to more than 5%. El Mohtar et al. (2013) investigated the effect of the presence of a small amount of bentonite on the pore pressure generation in loose sand in three different tests. The resonant column, cyclic, and static triaxial tests were conducted. The overall results indicated that the presence of a small amount of bentonite had a considerable effect on the behaviour of sand at all the strain levels. The results of the static triaxial tests showed that the contractive tendency of the sand–bentonite samples was more than that of the clean sand samples before the change in behaviour and the start of dilation. Moreover, the 5% bentonite sample showed lower excess pore pressure than the 3% bentonite sample at any strain level. The negative effect of the presence of bentonite on the behaviour of sand could be related to the bentonite grains being trapped between the sand particles during sample preparation and the formation of unstable fabric, but with continued shear, the contact between the sand particles developed, eventually changing the behaviour from contraction to dilation.

Nowadays, there is a global interest in utilising waste materials for different engineering applications because of the huge amount of these materials produced and their problematic disposal. An increasing amount of waste materials has encouraged researchers to find alternative ways to use them in different applications. Reusing these materials has substantial, positive environmental effects involving resource conservation and reductions in greenhouse emissions. Slag is one of the waste materials that have been utilised in different civil engineering applications in the last few decades. The main reasons for using slag are environmental and economic considerations because it is cheaper than another cementing agent as it is a by-product material. Moreover, the level of energy consumption and the amount of carbon dioxide generated from producing slag are very low compared to those while producing cement or lime (Veith, 2000). The production of one ton of Portland cement consumes 5000 MJ/ton of energy and 1.5-ton limestone and clay as well as generates 0.95 tons of CO<sub>2</sub>;

however, the production of the same amount of slag needs 1300 MJ/ton of energy and produces 0.07 tons of CO<sub>2</sub> (Yi, Liska, & Al-Tabbaa, 2014). Slag is a by-product of the iron and steel industry, with millions of tonnes of slag being produced annually worldwide. According to the Australian Slag Association (2011), 3.4 million tonnes of iron and steel slag products were manufactured in Australia in 2009, with 80% of them utilised in the construction of buildings and roads. The main chemical components of Portland cement and slag are almost the same as those listed in Table 2.3 (Ika Putra, 2014).

Table 2.3 Comparison between the main chemical components of Portland cement and slag (Ika Putra, 2014)

Chemical components	Portland cement	Granulated slag
Calcium oxide ( <i>CaO</i> )	65%	40%
Silica, amorphous ( <i>SiO<sub>2</sub></i> )	20%	35%
Aluminium oxide ( <i>Al<sub>2</sub>O<sub>3</sub></i> )	5%	10%
Magnesium oxide ( <i>MgO</i> )	2%	8%

When slag makes contact with water, it reacts like Portland cement; however, it needs more time to achieve a full reaction, which is why it is sometimes mixed with a chemical activator. Ouf (2001) stated that the long reaction time of slag provides additional time to finalise the stabilisation work in the field. Matsuda, Shinozaki, Ishikura, and Kitayama (2008) argued that granulated blast furnace slag could be used in geotechnical applications for liquefaction resistance because its shear strength increases with time. They added that its geotechnical characteristics (high internal friction angle, light weight, and high permeability) make it useful for the backfilling of quay wells, sand mats, and lightweight embankments. Slag has been used extensively in the stabilisation of clayey soils. However, published research on the use of slag on its own for stabilising sandy soils is difficult to find. Ouf (2001) observed that the unconfined compressive strength (UCS) of expansive soil with a curing time of 7 and 28 days increased with the addition 6% of slag. Cokca, Yazici, and Ozaydin (2009) reported that the swelling potential of expansive soil decreased upon the addition of slag and cement. Lu, Modmoltin, and Onitsuka (2004) also reported that the UCS of cement-stabilised clayey soil increased upon the addition of slag. Yadu

and Tripathi (2013) stated that the plasticity index (PI) of soft clayey soil decreased from 17% to 13% upon the addition of 9% of slag. Budihardjo, Chegenizadeh, and Nikraz (2015) performed small direct shear tests on the sand–slag mixtures. They found that the internal friction angle of sandy soil increased upon the addition of 1%, 2%, and 3% of slag. Several studies have reported that the shear strength of slag-stabilised sandy soils can be increased by using chemicals to activate the slag (Park, Choi, & Nam, 2014; Rabbani, Daghigh, Atrechian, Karimi, & Tolooiyan, 2012) (Yi et al., 2014). It appears from the aforementioned investigations that numerous investigations of the effects of fines on the static liquefaction behaviour of sandy soils have been conducted. Most of the open literature on the static liquefaction behaviour of sand–fines mixtures is focused mainly on the silt, whereas few studies have investigated the effect of plastic fines. These experimental data showed controversial results, and there was no agreement on the effect of fines on the static liquefaction behaviour of sandy soils. In addition to these primary data, systematic studies on the liquefaction behaviour of sandy soils are required for a better understanding of the influence of the other fines types such as waste materials. Examining the effect of waste materials such as slag on the liquefaction behaviour of sandy soils, which may extend the work on the effect of fine materials on the static liquefaction of sandy soils and provide an alternative way to use waste materials in geotechnical applications, was the motivation behind the present study. Moreover, another motivation for this study was to investigate the effect of mixing two different types of fines on the liquefaction behaviour of sandy soils because in most of the cases, the tests were performed on mixtures of sand with one type of fines.

## **2.6 Liquefaction susceptibility**

Although the liquefaction susceptibility of granular materials has been extensively investigated by using experimental, theoretical, and empirical methods, few geological studies and field observations have been reported in the literature. These studies have listed many factors affecting the liquefaction susceptibility of sandy soils. Figure 2.18 shows a flowchart of the factors that influence liquefaction susceptibility (Chheda et al., 2014). The determination of liquefaction susceptibility is one of the soil stability analysis techniques. However, different determination methods were adopted in the literature. Some of the determination methods used the grain size distribution curves

to determine whether the sandy soil was susceptible to liquefaction (Ishihara et al., 1980; Tsuchida, 1970). Figure 2.14 shows the boundaries between liquefiable and non-liquefiable sand. In contrast, Verdugo and Ishihara (1996) reported that the liquefaction susceptibility of sandy soils does not depend only on the shape of the particle size distribution curve; there are other factors that affect it, such as particle shape, particle hardness, fines content, and plasticity of fines.

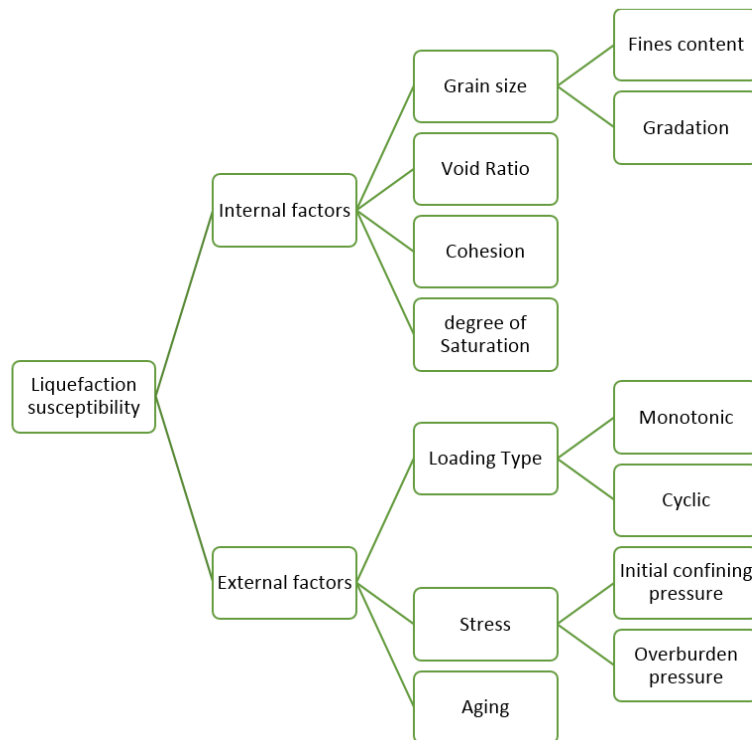


Figure 2.18 Factors affecting liquefaction susceptibility of soil

Verdugo and Ishihara (1996) argued that the isotropic consolidation lines (ICLs) for the loosest and the densest states provide boundaries for any possible soil behaviour and the position of the steady-state line (SSL) with respect to these limits could be used to distinguish between the states of contractive and dilative behaviours, as shown in Figure 2.19. As illustrated in Figure 2.19(a), if the position of the SSL is close to the ICL of the loosest states, the area of states associated with contractive behaviour denoted by  $A_c$  is small. However, Figure 2.19(b) shows that in soils with SSL close to ICL of the densest state, the area of dilative behaviour denoted by  $A_d$  is small. In this case, the liquefaction susceptibility of the soil deposit is high. Consequently, we can evaluate the liquefaction susceptibility of a soil deposit depending on the position of the steady-state line with respect to the positions of the isotropic consolidation lines of



the loosest and the densest states. The ICL for the loosest and the densest states merge with each other at high pressures. Therefore, the behaviour is fully contractive. While at a low pressure and in the dense state, the behaviour is dilative. To evaluate the liquefaction susceptibility of soils, Verdugo and Ishihara (1996) proposed an index property called relative contrastiveness,  $R_c$ , which can be expressed as follows:

$$R_c = \frac{e_{max} - e_{ss}}{e_{max} - e_{min}} \quad (2-12)$$

where  $e_{max}$ ,  $e_{min}$ , and  $e_{ss}$  represent the maximum, minimum, and steady-state void ratios at the steady-state mean effective stress. The relative contrastiveness  $R_c$  is considerably dependent on the particle composition and not used to specify the state of the soil. Note that the state of soils significantly affects the actual liquefaction resistance.  $R_c$  may have values between 0 and 1. The initial state associated with contractive behaviour has  $R_c = 1$ ; however,  $R_c = 0$  represents all the initial states that will always have a dilative behaviour. Verdugo and Ishihara (1996) reported that the presence of fines might increase the contractive tendency of cohesionless soils because the value of relative contrastiveness increased with an increase in the fines content.

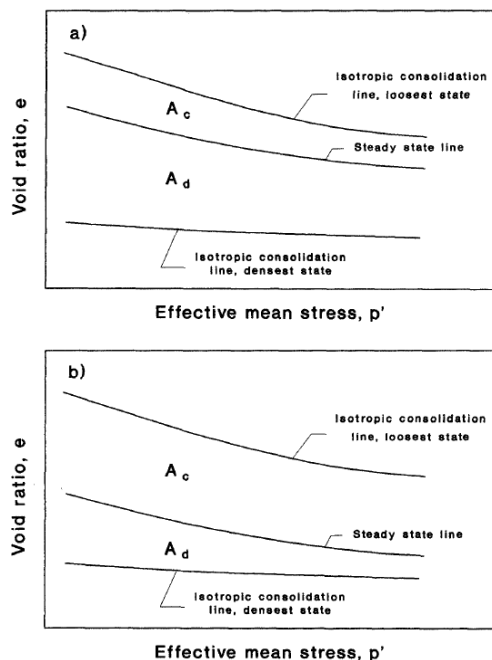


Figure 2.19 Schematic representation of liquefaction susceptibility of soils: a) small susceptibility to liquefaction and b) high susceptibility to liquefaction (Verdugo & Ishihara, 1996)

Poulos et al. (1985) stated that the determination of the liquefaction susceptibility of soils requires that the shear stress in situ and the shear strength be determined. For the liquefaction analysis, the undrained steady-state shear strength is required. The shear strength is difficult to determine precisely because it is considerably dependent on the void ratio. Poulos et al. (1985) added that the liquefaction susceptibility could be evaluated by using the factor of safety against liquefaction (FL). The factor of safety against liquefaction is the ratio of the undrained steady-state shear strength to the shear stress required to maintain static liquefaction.

$$FL = \frac{S_u}{\tau_d} \quad (2-13)$$

$$S_u = q_s \cos \phi_s \quad (2-14)$$

$$q_s = \frac{\sigma_{1s} - \sigma_{3s}}{2} \quad (2-15)$$

where  $S_u$  is the undrained steady-state shear strength,  $\tau_d$  is the applied shear stress,  $\sigma_{1s}$  is the major principal stress at steady state, and  $\sigma_{3s}$  is the minor principal stress at steady state. The factor of safety should be greater than 1 to be considered safe for sand and silt. If the FL is less than 1 and  $S_u < \tau_d$ , most of the soil will be in an unstable equilibrium and any disturbance such as the toe of the slope, foundation settlement, or earthquake may trigger liquefaction. The susceptibility to liquefaction is not dependent on the type of driving shear stress, and the liquefaction may occur because of static loads and not any temporary loads such as an earthquake or a blasting load. The undrained steady-state strength is a function only of soil and its in-situ relative density. It does not depend on the magnitude or nature of temporary loading that may cause liquefaction. Thus, cyclic tests are not required to evaluate the susceptibility to liquefaction. Moreover, the undrained steady-state strength is not related to the soil structure and the effective in-situ stress (Poulos et al., 1985).

Other studies used the state parameter  $\Psi$  to evaluate the susceptibility to liquefaction of soils. Been and Jefferies (1985) have defined the state parameters as the difference between the initial void ratio  $e_o$  and the void ratio at the steady state  $e_{ss}$ .

$$\Psi = e_o - e_{ss} \quad (2-16)$$

The state parameters at the start of shearing are denoted by  $\Psi(0)$ , which can be used to predict the response trend during undrained loading qualitatively (Bobei et al., 2009). The positive values of  $\Psi(0)$  are associated with the static liquefaction behaviour, while the negative values are related to the non-flow response (Bobei et al., 2009). The framework of the state parameters shows the normal behaviour of clean sandy soils when its values changed from negative to positive with an increase in the confining pressure. However, the behaviour of sandy soils with fines does not imply the same framework (Bobei et al., 2009). Wang, Dafalias, Li, and Makdisi (2002) proposed an alternative framework to predict the liquefaction behaviour of sandy soils, called the state pressure index  $I_p$  and defined as  $(p'/p'_{CS})$ , where  $p'_{CS}$  is the effective mean stress at the critical-state line at the same void ratio. Been et al. (1991) argued that the use of the state parameter and the state pressure index for explaining the behaviour of sandy soils requires an equivalence between the critical-state and the steady-state lines. Many experimental studies support the assumption of the equality and uniqueness of the CS and SS lines of sandy soils. However, the uniqueness and equality of sand with the fines are still questioned, which is impeding the use of state parameters for describing the soil response. The results showed that the undrained behaviour of samples changed from flow failure to limited flow when the confining pressure increased. The pore pressure remained constant after reaching the minimum deviator stress. Moreover, Bobei et al. (2009) reported that the samples tested under medium initial confining pressure reached the SS at strains (3%); however, samples tested under high confining pressure reached the SS at strains (13%), which indicated that the liquefaction susceptibility reduced with an increase in the confining pressure; the same results were reported by (Yamamuro & Lade, 1997b, 1998). Bobei et al. (2009) reported that the CSL and SSL for sand with fines are equivalent and unique because the CSL and SSL points are located on the single curve irrespective of the test type and the stress history. They also stated that the state parameter did not provide an adequate explanation of the change in behaviour from flow to limited flow. Thus, they proposed the modified state parameter  $\Psi_m$  for any stress state as defined by Figure 2.20 and the equations below:

$$\Psi_m = \Psi \left| \frac{\Delta p'}{p'} \right| e \quad (2-17)$$

The factor  $\Delta p/p'$  can be replaced by the state pressure index  $I_p = p/p'_{cr}$

$$\frac{\Delta p}{p} = \frac{p - p'_{cr}}{p} = 1 - \frac{1}{I_p} \quad (2-18)$$

when  $e > e_{thre}$  where  $e_{thre}$  is threshold void ratio, the modified state parameter can be modified as follows:

$$\Psi_m = \Psi e \quad (2-19)$$

Bobei et al. (2009) also observed that the modified state parameter at the start of loading  $\Psi_m(0)$  could be a good predictor of the liquefaction behaviour of sand with fines irrespective of the initial state.  $\Psi_m(0)$  can be calculated by using the initial void ratio  $e_o$  and the initial effective stress  $p'_o$  from Equations (17)–(19).

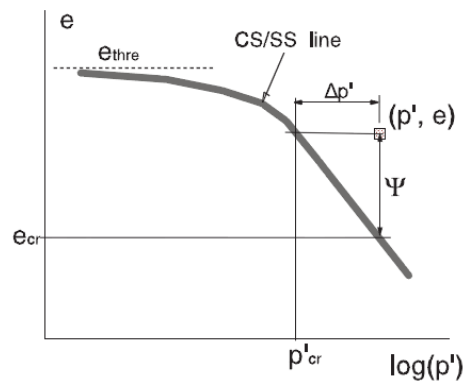


Figure 2.20 Description of the modified state parameter (Bobei et al., 2009)

Konrad (1990) presented another modification of the state parameter. He argued that there should be an upper limit of the steady-state strength and a lower limit of steady-state strength. The modified state parameters  $\Psi_i$  can be defined as the difference between the void ratio after consolidation  $e_c$  and the void ratio of the upper limit  $e_{UF}$  of the steady-state strength line for the same stress condition.

$$\Psi_i = e_c - e_{UF} \quad (2-20)$$

Konrad (1990) reported that the modified state parameter played a significant role in the evaluation of the liquefaction susceptibility of saturated sandy soils under monotonic loading in the field state.

(Yamamuro & Lade, 1997b) Yamamuro and Lade (1998) argued that the stress ratio ( $q_{min}/q_{peak}$ ) which includes the deviator stress at the quasi-steady state point divided by the deviator stress at initial peak could be used to distinguish between liquefiable and non-liquefiable soils. A stress ratio value of zero represents the case of complete liquefaction (deviator stress at steady-state condition = zero), and the non-liquefaction or stable behaviour is indicated by the unity value of the stress ratio. However, the stress ratio which includes the deviator stress at the initial peak divided by the deviator stress at the steady-state point is used to evaluate the instability of the samples (Yamamuro & Lade, 1998). Small values of this ratio with stable behaviour are observed at a low confining pressure, while the unity value of this ratio with unstable behaviour is observed at a high confining pressure; the confining pressure at the unity values represents the lower values required for a stable response, and a confining pressure beyond this value will cause complete instability (Yamamuro & Lade, 1998). Ishihara (1993) and (Lade & Yamamuro, 2011) reported that the  $q_{min}/q_{peak}$  ratio could be used to compute the liquefaction potential defined as follows:

$$\frac{q_{peak} - q_{min}}{q_{peak}} = 1 - \frac{q_{min}}{q_{peak}} \quad (2-21)$$

Rahman and Lo (2014) pointed out that the ratio of  $q_{min}/q_{peak}$  can be correlated to the state parameter to normalise the amount of strain softening in the samples. Casagrande (1976) proposed the liquefaction potential  $L_p$  as a measure of the contractions of sand. The liquefaction potential of soil can be expressed as follows:

$$L_p = \frac{\sigma'_{3c} - \sigma'_{3us}}{\sigma'_{3us}} \quad (2-22)$$

where  $\sigma'_{3c}$  and  $\sigma'_{3us}$  are the initial effective stress and the effective stress at the steady state. The complete liquefaction is associated with  $L_p > 5-7$ . However, limited liquefaction and non-liquefaction behaviours are associated with a positive value of  $L_p$

< 3 and negative values, respectively. Based on the Mohr–Coulomb strength criterion, Castro and Poulos (1977) rewrote the  $L_p$  equation, which was proposed by Casagrande (1976), in terms of the angle of friction of the sand and the pore pressure parameter  $A$  during the steady-state flow as follows:

$$L_p = A \frac{2 \sin \phi}{1 - \sin \phi} \quad (2-23)$$

Kramer and Seed (1988) stated that the above equation indicates that at a given relative density, the liquefaction behaviour is a function of the relationship between the initial and the steady- state confining pressure and that the liquefaction potential increases with an increase in the confining pressure. Consequently, other factors such as the initial shear stress level do not influence the liquefaction potential. Some scholars used the brittleness index,  $I_B$ , which was proposed by Bishop (1971), to characterise the amount of reduction in the undrained shear strength during liquefaction.

The undrained brittleness index,  $I_B$ , can be expressed as follows:

$$I_B = \frac{q_{peak} - q_{min}}{q_{min}} \quad (2-24)$$

The values of  $I_B$  are in the range of 0–1, and non-flow or non-brittle behaviour (where a non-strength decline occurs during undrained static shear) is observed when  $I_B = 0$ . However, brittle soil behaviour or complete static liquefaction is associated with  $I_B = 1$ . Sadrekarimi (2014a) proposed an empirical approach to estimate liquefaction-triggering strength of the strain-softening, saturated sand soils exhibit to statistically increasing shear load and take into account effect of the soil-contraction tendency as follows:

$$I_B = \exp \left( \frac{2.1 \mp 0.9}{1.72 \mp 1.00 - \sigma_c / \sigma'_{liq}} \right) - 0.03 \quad (2-25)$$

where  $\sigma'_c$  and  $\sigma'_{liq}$  are the initial effective stress and the effective stress at the liquefaction state, respectively.

Yoshimine and Ishihara (1998) argued that the maximum excess pore water pressure ratio  $U_f$  achieved in the undrained static shearing test can be used as an index to

evaluate the flow potential of soils. The maximum excess pore water pressure ratio  $U_f$  is defined as follows:

$$U_f = \left(1 - \frac{p'_{PT}}{p'_c}\right) \times 100 (\%) \quad (2-26)$$

where  $p'_{PT}$  and  $p'_c$  are the mean effective principal stress at phase transformation state and mean isotropic effective confining stress respectively. Also, they added that in addition to the initial state the maximum excess pore water pressure ratio  $U_f$  is strongly influenced by the stress state through deformation, for example, the direction of principal stresses and level of intermediate principal stress. Konrad (1988) proposed the relative state parameter index  $\xi_R$  which can be used to recognise the liquefaction susceptibility of granular soils and it is more appropriate than state parameter in the in situ state:

$$\xi_R = \frac{1}{Q - \ln(\dot{p}/p_a)} - D_r \quad (2-27)$$

where  $\dot{p}$  is the initial mean effective confining pressure,  $p_a$  is the atmospheric pressure, and  $Q$  is the empirical constant. The contractive behaviour is associated with the positive values of  $\xi_R$ , while the negative values are associated with dilative behaviour.

## 2.7 Evaluation of liquefaction of sand using Artificial Intelligence approaches

There are many limitations for using the results of experimental tests on disturbed specimens directly in field situations. One of these constraints is that these tests do not take into account all the actual properties of natural soils, such as fabric, cementation, strain history, and overconsolidation (Jafarian, Vakili, & Abdollahi, 2013). Next, the experimental tests are often costly and time consuming. Similarly, analytical methods such as the finite element method which is utilised to analyse many geotechnical engineering problems are constrained as these techniques need a large number of parameters to obtain an accurate constitutive model for complex problems such as liquefaction (Das, 2013). Therefore, artificial intelligence AI approaches have been used to reduce these difficulties and provide an easy technique for evaluating complex issues in different applications (Hanna, Ural, & Saygili, 2007; Kim & Kim, 2008).

Over the past few decades, there has been an increasing amount of literature on the use of AI in many civil engineering applications because of its heuristic problem-solving capacity (Hanna et al., 2007). Artificial Neural Network ANN belongs to the class of AI techniques and can be categorised as ‘machine learning’. ANNs consist of interconnected computational elements called neurons that have unique features similar to those of biological neurons. These neurons enable ANN to simulate the learning capacities of the human brain by automating the methods of data gathering and mining (Hanna et al., 2007). This similarity between the ANN structure and the brain structure increases the ability of ANN to analyse many parameters that include intuitive judgement and have a high degree of complexity. Note that the number of neurons in the human nervous system is around  $3 \times 10^{10}$ , while ANNs have a few hundreds of neurons and the number of neurons required in geotechnical engineering is less than 100 (Das, 2013). Based on the architectural differences, ANNs can be categorised into back-propagation neural networks (BPNNs), categorical learning (unsupervised) networks (self-organising maps (SOMs), and probabilistic neural networks (PNNs) (Hagan, Demuth, & Beale, 2002). Das (2013) argued that BPNNs are the best architecture for geotechnical engineering. ANNs consist of a group of nodes that are set out in layers: an input layer, an output layer, and one or more hidden layer, as shown in Figure 2.21, which shows the typical structure of ANNs. This structure was called 4-3-2 with four input-layer neurons, three hidden-layer neurons, and two output-layer neurons. The input layer did not implement any calculations on the input data received from an external environment (Farrokhzad, JanAliZadeh, & Barari, 2008). The hidden layers processing the data received from the input layer by using weights, biases, and transfer functions, and the results are sent to the output layer. The output layer connects the output of the ANN model to the user data using neurons. This ANN structure is generally mentioned as a fully interconnected feed-forward multi-layer perceptron (MLP).



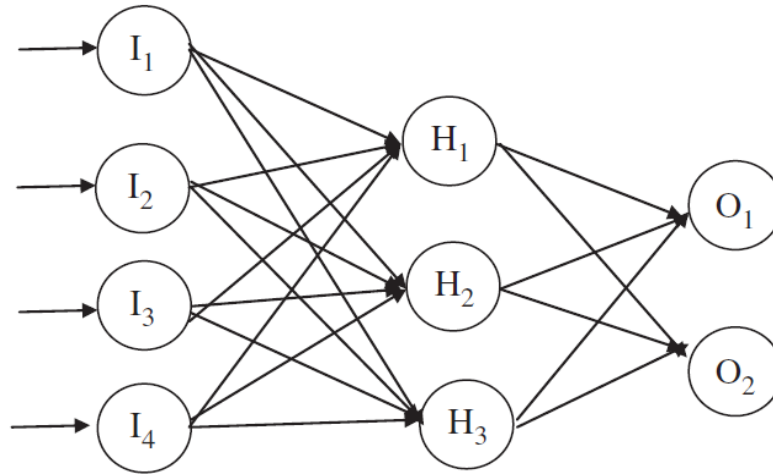


Figure 2.21 Typical structure of ANN (Das, 2013)

Goh (1994) pointed out that one or two hidden layers were found to be highly effective for many problems, and the number of hidden layers and the number of neurons in the hidden layers depend on the nature of the problem. The maximum number of hidden neurons should not exceed  $(2I + 1)$ , where  $I$  is the number of input variables. The number of nodes in the hidden layer can be set to be equal to the total number of output nodes and input nodes divided by two. Furthermore, the degree of complexity in the connection among the operation parameters and the quality responses influences the number of hidden layers; if the connection is difficult to determine, the two hidden layer can be utilised. Choobbasti, Farrokhzad, and Barari (2009) stated that the ability of ANN model to make an accurate prediction reduced when the number of hidden layers was very high because of the overfitting which affected the generalisation. Further, they added that the back-propagation algorithm is the best training algorithm for ANNs and is still one of the most useful. ANNs have the ability to learn from data given to them, generalising the predicted interrelationships for a future solution, and self-updating (Elhag & Wang, 2007; Farrokhzad et al., 2008). Detailed information on ANNs is provided in (Das, 2013; Hagan et al., 2002). The main steps of the development of the ANN model are shown in Figure 2.22. The process of training a neural network includes adjusting the weights of the parameters inside the hidden layers until the lowest difference is reached between the predicted output and the actual output. The dataset was split into three groups, namely training, testing, and validation.

The percentage of each group can be identified on the basis of some factors such as the number of input and output points and the nature of the problem. However, the percentages of 70%, 15%, and 15% for training, testing, and validation, respectively, were used in many previous studies. The training data are used to modify the connection weights. The testing dataset is adopted to avoid the overfitting, and the validation set is used to investigate the estimation ability of the model. The model can be considered an optimal model if it combines three conditions: (i) perfect performance in the testing set, (ii) a minimum number of hidden neurons, and (iii) good performance in the training, testing, and validation sets.

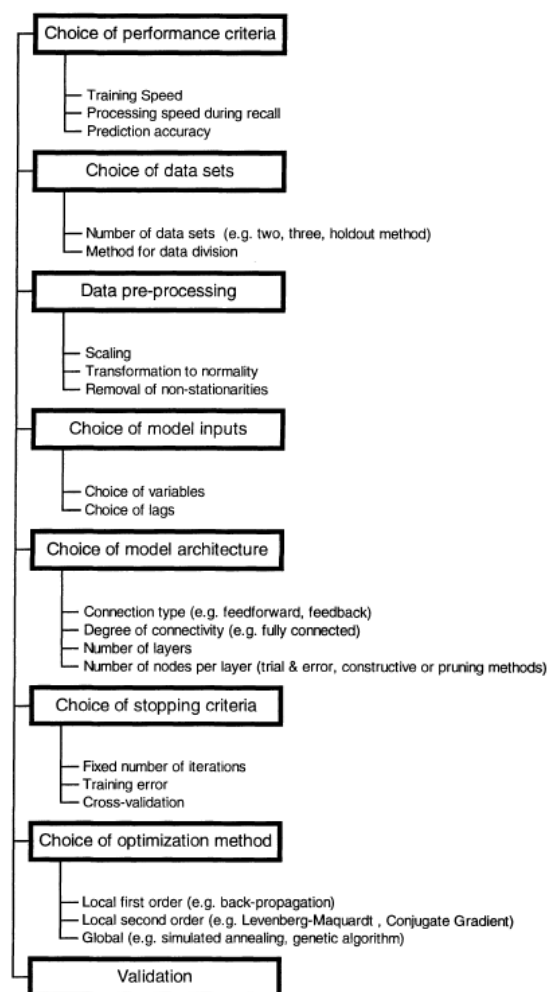


Figure 2.22 Flowchart for major stages in the development of ANN models (Maier & Dandy, 2000)

The performance of the ANN model was investigated by Root Mean Square Error (RMSE), and coefficient of determination ( $R^2$ ), as follows:

$$RMSE = \sqrt{\frac{1}{n} \sum_{i=1}^n (y_i - x_i)^2} \quad (2-28)$$

$$R^2 = \left[ \frac{\sum_{i=1}^n (x_i - \bar{x})(y_i - \bar{y})}{\sqrt{\sum_{i=1}^n (x_i - \bar{x})^2 \sum_{i=1}^n (y_i - \bar{y})^2}} \right]^2 \quad (2-29)$$

where  $x_i$  are the input data,  $y_i$  is the model estimation,  $n$  is the number of data points, and  $\bar{x}$  and  $\bar{y}$  are the mean values of the observed data model estimation. The best performance of the ANN models is achieved through trial and error until an  $R^2$  value of around 90% is obtained. After completing training and testing the model, a sample dataset is used to test the accuracy of the model. ANN has been found to be more dependable than analytical techniques such as traditional empirical and statistical methods because of two reasons. The first one is that ANNs can learn from the input data examples given to them. The second reason is the ability of the ANNs to recognise the precise practical relationships between the input data even though the fundamental relationships are unrecognised. However, this technique is called the black-box system because it cannot produce the complete model equation (Goh, Kulhawy, & Chua, 2005). Tung, Wang, and Wong (1993) stated that the simplicity, lowest prior analysis of data collection, accumulative learning and flexible abilities, and the automatic combination of the hidden data structure are the most important properties of ANNs. In recent years, there has been an increasing amount of literature on the use of ANNs in the evaluation of the liquefaction potential of soils. Goh (1994) developed a BPNN model to evaluate seismic soil liquefaction by using actual field data. He stated that neural networks could be considered feasible tools for the soil liquefaction evaluation and that they are simpler to apply than the other methods and the standard penetration test SPT and fine content the major input parameters in potential liquefaction assessment. Ural and Saka (1998) used the BPNN model to assess seismic liquefaction on the basis of a database of earthquakes from North and South America, Japan, and China. Hanna et al. (2007) developed general regression neural network models to predict the liquefaction conditions of soils on the basis of in situ datasets from two major earthquakes that occurred in Turkey and Taiwan in 1999. In all, 620 sets of data involving 12 soil and seismic variables were used in the model. Hanna et al. (2007) showed that the GRNN model could be effectively used to predict the occurrence/non-occurrence of soil liquefaction at these sites. The results also indicated that the GRNN model could be used to explore the complex relationship between the liquefaction

conditions and the main contributing parameters. Goh (1996) adopted the BPNN method to predict the seismic liquefaction potential of soils by using the cone penetration test and seismic data were collected from five earthquakes that took place in Japan, United States, China, and Romania between 1964 and 1983. He stated that one of the most significant benefits of the neural network technique is the ability to improve the performance of the ANN model by adding new data. Tung et al. (1993) developed an ANN model for the prediction of the soil liquefaction potential on the basis of the data collected from the 1976 Tangshan Earthquake. Omar (2013) adopted the ANN to predict the liquefaction potential of soils using a database of cone penetration tests (CPT). Further, he argued that the pre-processing, normalising, or calibration of the data before evaluating the liquefaction potential was not necessary. Farrokhzad, Choobbasti, and Barari (2010) developed ANN models to predict the seismic liquefaction potential of soils using data gathered from field tests (30 boreholes). Baziar and Nilipour (2003) used multi-layer perceptrons associated with the back-propagation algorithm to develop an ANN model for the prediction of the liquefaction potential on the basis of the CPT data and the seismic records. Young-Su and Byung-Tak (2006) developed a back-propagation ANN model to predict the liquefaction cyclic resistance ratio (CRR) using data obtained from undrained cyclic triaxial and cyclic simple shear tests. The results showed good agreement between the predicted and the measured CRR, which indicated the strong ability of the ANNs to capture the liquefaction resistance under different test conditions. Additionally, ANN has been adopted to assess many problems in the area of geotechnical engineering, such as prediction of scours at bridge piers, unsaturated shear strength of soil, safety of a typical artificial slope subjected to earthquake forces, horizontal ground displacement generated by earthquakes, maximum dry density and permeability of various types of soils, and residual friction angle of clayey soils (Das & Basudhar, 2008; Erzin & Cetin, 2012; Kaya, 2010; Lee, Lee, & Kim, 2003; Sinha & Wang, 2008; Wang & Rahman, 1999). Recently, genetic programming GP, which is defined as the next generation of AI techniques, has been used as an alternative AI method. GP is the second version of the genetic algorithm (GA), which is considered to be an evolutionary algorithm (EA). An EA uses the principle of genetic and natural selection in computing search techniques. In these methods, the computer performed a number of the natural evolutionary mechanisms (such as mutation, crossover, and selection). GP was first used by Cramer (1985) and then developed by (Koza, 1992). GP is a

process of developing computer programs called individuals or chromosomes to solve a particular problem. It depends on the evolutionary algorithms to provide a good approximate solution to problems by unexpectedly creating populations of computer applications presented by a tree structure, as shown in Figure 2.23. There are different types of GP, such as linear genetic programming (LGP), multi-stage genetic programming (MSGP), multi-expression programming (MEP), gene expression programming (GEP), and multi-gene genetic programming (MGGP) (Gandomi & Alavi, 2011, 2012; Hossein Alavi & Hossein Gandomi, 2011).

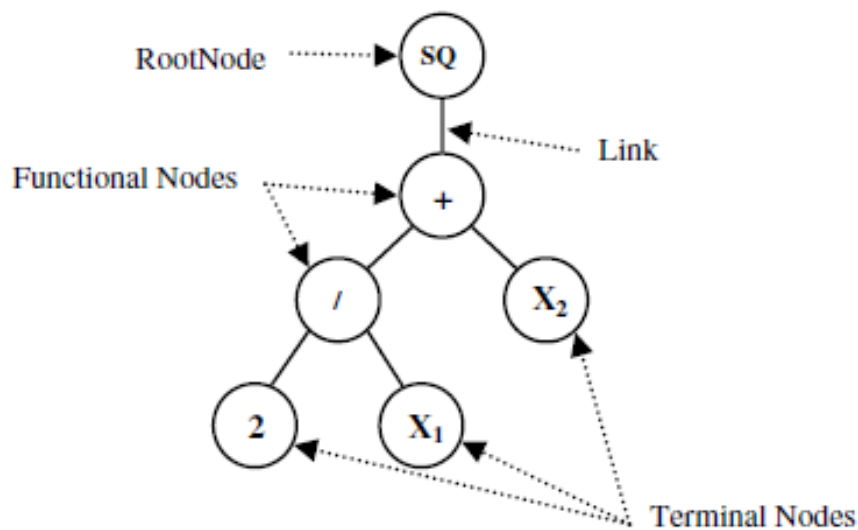


Figure 2.23 Example of GP tree illustrating  $(2/x_1 + x_2)^2$  (Javadi, Rezanian, & Nezhad, 2006)

The first stage of the solution by GP uses random sets of terminals and functions to create an initial population of computer programs. The terminals may include variables, numerical constants, and/or logical constants, while functions may include basic mathematical factors (e.g. /, x, -, and +), Boolean logic functions (e.g. AND, OR, and NOT), trigonometric functions (e.g. sin and cos, etc.) and/or any other user-known functions. Each program is executed, and its fitness is assessed with respect to the real solution. Then, new groups of computer programs are generated by reproduction, mutation, and crossover; the result of the GP is the best computer program that appears in any of the generations. Reproduction is the replication of the computer program from the current population to the new population unaccompanied by changes. Crossover is genetically reconnecting random parts of a two-computer

program. Mutation is a process of changing an arbitrarily chosen terminal or functional node with another from the same terminal or function set. The process of evaluating the fitness of the current population and producing a new population continues until the termination criteria are met. The termination criteria may include an acceptable error or a maximum number of generations. The performance of the GP model can be examined by using statistical precision parameters such as RMSE and  $R^2$  (equations (28) and (29)). The structure and the operation of GP have been described in detail by numerous authors such as (Koza, 1990) (Johari, Habibagahi, & Ghahramani, 2006) (Muduli & Das, 2014a) (Rezania & Javadi, 2007). The GP technique is distinguished from the other AI techniques and statistical methods by the possibility of predicting compact and explicit prediction model equations in terms of various model parameters (Muduli & Das, 2014a). Although the GP technique has been successfully used to predict some of the complex parameters of soil mechanics, the application of this technique to the evaluation of the liquefaction potential has been very limited (Das & Muduli, 2011; Gandomi & Alavi, 2012; Muduli & Das, 2014a; Muduli & Das, 2014b). Das and Muduli (2011) investigated the liquefaction potential of soil by using GP based on the cone penetration test data collected after the Chi-Chi earthquake that occurred in Taiwan in 1999. They reported that the results of the GP model and the statistical method including the liquefaction index showed that the developed GP model performed better than the statistical procedure in differentiating between liquefaction and non-liquefaction cases. Muduli and Das (2014a) used MGGP to predict the liquefaction potential of soils by using the standard penetration test (SPT) dataset. The results showed that the liquefaction potential model, which was developed using MGGP, was more accurate than the models developed using ANN and Support Vector Machine (SVM) when the same database was used. They also argued that the model of CRR which was developed by MGGP on the basis of the SPT data in association with the cyclic stress ratio  $CSR_{7.5}$  could be adopted to estimate the factor of safety versus liquefaction development. Muduli and Das (2014b) developed two different MGGP models to predict the liquefaction potential of soils on the basis of the liquefaction index based on the CPT database. Although the SPT is widely used, the consistency, repeatability, and ability to recognise a constant soil profile have made the CPT more acceptable than the SPT. The results showed that the performance of both the models was better than that of the ANN and SVE with a high accuracy of learning the complex relationship between the liquefaction index and the major

contributing variables. The results also indicated that the cone tip resistance was the most important parameter in the prediction of the liquefaction index in both the models. Javadi et al. (2006) developed a new approach to evaluate the liquefaction-induced lateral displacement of soil by using GP and the data from SPTs. Johari et al. (2006) developed a GP model to predict the soil–water characteristics curve based on the plate tests conducted on different types of soils. However, note that all of the previous studies on AI have been included in the open literature on the liquefaction behaviour of sandy soils. To the best of my knowledge, the case of using ANN and GP in the prediction of the static liquefaction behaviour of sandy soils on the basis of experimental data has not been given considerable attention by the researchers in the past, and this motivated the present study.

## **2.8 Link between static and cyclic liquefaction**

Several studies have revealed that static behaviour should be considered while analysing the undrained cyclic behaviour of saturated sands (Ibsen, 1998). A sound knowledge of the effective stress conditions at which static liquefaction is triggered will provide a good understanding of the cyclic liquefaction behaviour of soils (Kramer, 1996). Both static and cyclic liquefaction are closely related, and the effect of the initial shear stress on the cyclic liquefaction resistance is dominated by the static stress–strain response (Mohamad & Dobry, 1986). Konrad (1993) stated that the contractive flow deformation under static and cyclic loadings is initiated under the same effective stress condition. Moreover, the peak shear strength line which passes through the origin of the  $p'$ - $q$  space is unique for isotropically static and anisotropically cyclic undrained loadings. Alarcon-Guzman et al. (1988) and Zlatovic and Ishihara (1997) argued that the state boundary that controls the start of the flow failure under undrained cyclic loading can be constituted by using the static stress path in the static undrained shear. Yoshimine and Ishihara (1998) stated that the static undrained shear test utilised for the assessment of the flow failure of sandy soil as a result of the flow failure of the slightly to the moderately sloped ground is controlled more by the static gravitational force than by the cyclic deformation generated by shaking. In general, as observed from prior studies, the cyclic behaviour of sandy soil is strongly dependent on the static liquefaction behaviour, and a good understanding of the cyclic

liquefaction of the sand–fines mixtures requires further study of the static liquefaction of the sand–fines mixtures. These were the other motivations behind the present study.

## **2.9 Summary**

A detailed review of the experimental and analytical published work was performed with respect to the liquefaction behaviour of clean sandy soil and the mixtures of sand with different types and contents of fines. A general review of the undrained behaviour of clean sand and sand with fines categorised the undrained behaviour into four categories, namely complete liquefaction, flow failure, limited liquefaction, and non-flow categories of liquefaction. It was pointed out that the initial state (i.e. initial void ratio and confining pressure) determined the undrained behaviour of sandy soils. Furthermore, the undrained behaviour of sandy soils was dependent on other factors such as stress mode, sample preparation method, degree of saturation, compositional characteristics, and fines content. It was also indicated that the critical state concept had been effectively used to evaluate the liquefaction behaviour of sandy soil and of sand with fines. In the existing literature on the liquefaction behaviour of sandy soils, the relative importance of fines has been subjected to considerable discussion. Many studies have reported that the effect of fines on the static liquefaction behaviour of sandy soils is considerably controversial and uncertain. Although a significant number of previous studies have investigated the effect of fines such as silt on the static liquefaction behaviour of sandy soil, there is little research on sand with waste materials. In general, it appears that factors such as fines content, confining pressure, relative density, and degree of saturation have to be considered and additional laboratory work is required to further assess the effect of waste materials on the liquefaction behaviour of sandy soil. Several parameters have been used in the literature to examine the liquefaction susceptibility of sandy soils such as the state parameter, stress ratio, brittleness index, maximum excess pore water pressure ratio, state parameter index, and relative contrastiveness. Moreover, several studies have reported that the triggering mechanism of static liquefaction is an effective tool to evaluate the liquefaction during cyclic loading. This motivated me to thoroughly examine the static undrained behaviour of clean sandy soils and sand with fines. AI approaches such as ANN and GP have been widely used to evaluate many complex problems in geotechnical engineering, such as cyclic liquefaction. However, developing models for static liquefaction on the basis of experimental results still



needs more attention. This justified the aim of this thesis to develop ANN and GP models for the static liquefaction behaviour of clean sandy soils and sand–fines mixtures.

# Chapter 3: Materials and Methods

## 3.1 Introduction

This chapter introduces the details of the materials along with the experimental, ANN, and GP procedures used in the current work. The physical and chemical properties of materials, sample preparation method, undrained static triaxial compression test procedure, ANN procedure, and GP procedure are described. The details of some of the standard tests such as particle size distribution, standard compaction, minimum dry density, and specific gravity are not presented here. The ANN and GP software programs utilised to model the static liquefaction behaviour of materials are also discussed in this chapter. The organisation of this section is depicted in Figure 3.1.

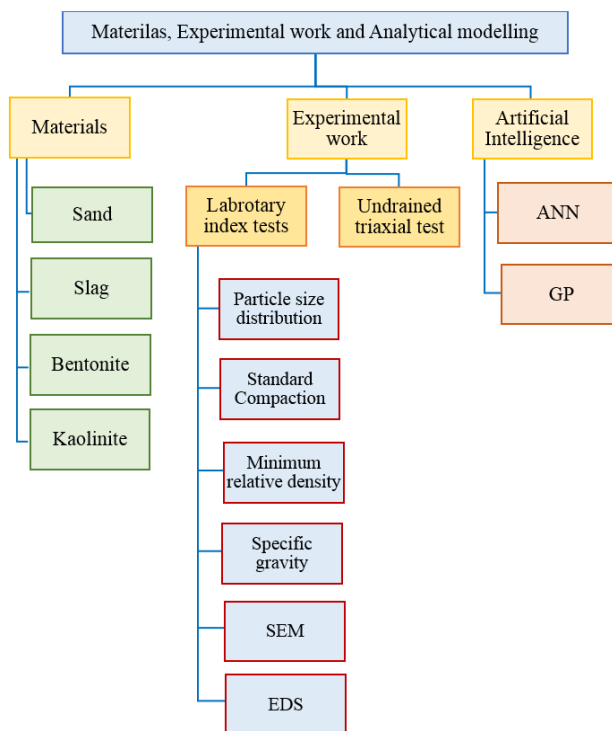


Figure 3.1 Structure of materials and experimental and analytical work

## 3.2 Materials

The previous chapter showed that the influence of fines on the liquefaction behaviour of sandy soils has mostly been investigated using sand with non-plastic fines. However, other fines types such as plastic fines and waste materials need to be investigated further. Therefore, this study was designed to examine the static liquefaction behaviour of clean sandy soils and mixtures of sand with different contents of slag, bentonite, and kaolinite under different test conditions by conducting experimental and analytical work. Materials were chosen from local sources because of their extensive availability and use in various applications in Perth, Western Australia.

### 3.2.1 Sand

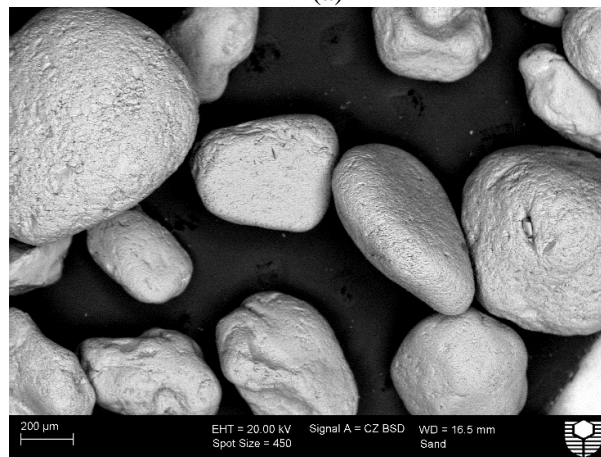
Sand used in the present work was collected from the Baldivis area, approximately 50 km south of Perth, Western Australia. This sand has been widely utilised in geotechnical applications for making concrete and mortar and footing in Western Australia. This sand is also called yellow sand because of its colour, as shown in Figure 3.2(a). Figures 3.2(b) and (c) show the images of scanning electronic microscopy (SEM) and energy dispersive X-ray spectrometry (EDS) images of the sand. As can be seen from Figure 3.2(b), the sand particles had almost the same size with a round and subrounded shape. Figure 3.2(c) shows that silicon was a significant component of the sand. The particle size distribution curve of the sand used in the experiments was estimated using a sieve analysis according to AS 1289.3.6.1–2009, as shown in Figure 3.3. The Baldivis sand was clean sand (i.e. 99.80% sand and 0.2% silt) and was classified as poorly graded sand according to the unified soil classification system (USCS). Tsuchida (1970) proposed the boundaries for potentially liquefiable soils and the most liquefiable soil. Figure 3.3 shows that the particle size distribution curve of the used sand is located inside the limits for the most liquefiable soil which indicates the high liquefaction susceptibility of the used sand. A small percentage of carbon (C) appeared in the EDS image; this was not a component of the sand but might be related to the coating of the samples before the SEM and EDS tests. The properties of the used sand are listed in Table 3.1.

Table 3.1 Physical properties of sand

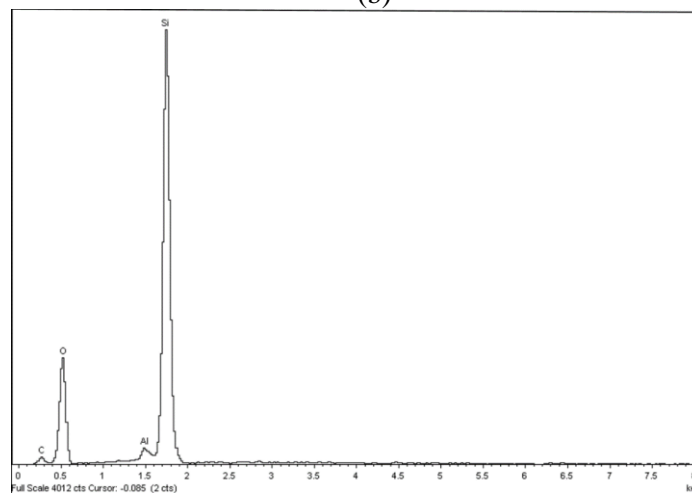
$D_{50}$	$C_u$	$G_s$	$\rho_{dmax}$	$\rho_{dmin}$	$e_{max}$	$e_{min}$
0.35 mm	2.235	2.58	1.67 g/cm <sup>3</sup>	1.56 g/cm <sup>3</sup>	0.675	0.544



(a)



(b)



(c)

Figure 3.2 Sand used in this study: (a) normal image, (b) SEM image, and (c) EDS image

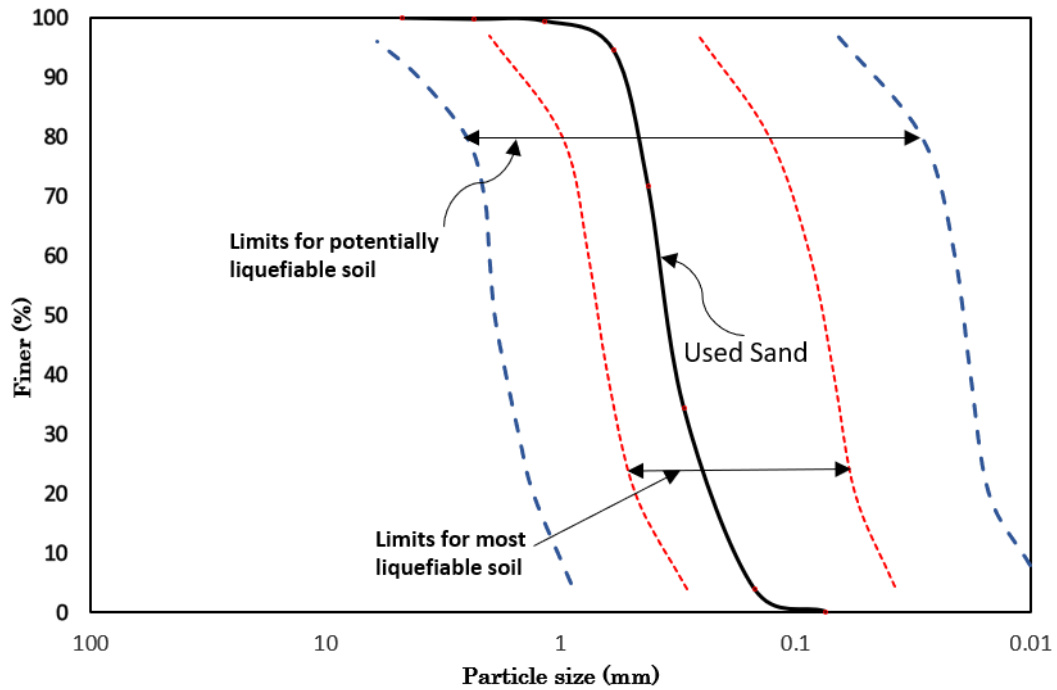


Figure 3.3 Particle size distribution curve of sand

### 3.2.2 Slag

Slag can be defined as a by-product of the iron- and steel-making operations. Based on the techniques used to produce iron, slag can be classified as blast furnace slag, steel furnace slag, or electric arc furnace slag. Blast furnace slag is a by-product of iron made in a blast furnace; it comes in three forms, namely, air-cooled, granulated, and expanded. The slag used in this study was granulated blast furnace slag (GBFS), manufactured by BGC Cement in Western Australia. It was a coarse off-white granular solid, odourless, alkaline, and insoluble in water, with a specific gravity of 2.8–3.1, a bulk density of loose state of 1–1.1 tonne/m<sup>3</sup>, a relative density of 2.85–2.95, and a surface area of 400–600 m<sup>2</sup>/kg. The chemical composition of the slag was similar to that of Portland cement; it contained aluminium oxide (Al<sub>2</sub>O<sub>3</sub>), calcium oxide (CaO), silica amorphous, and sulphur, as shown in Table 3.2. The particle size distribution curve of the slag is illustrated in Figure 3.4.

Table 3.2 Chemical components of GBFS

Ingredient	Calcium oxide (CaO)	Sulphur	Silica, amorphous	Aluminium oxide (Al <sub>2</sub> O <sub>3</sub> )
Content (%)	30–50	<5	35–40	5–15

SEM and EDS images of the slag are presented in Figures 3.5(b) and (c). As can be seen, the slag had angular particles of different sizes, and silicon (Si), calcium (Ca), aluminium (Al), magnesium (Mg), titanium (Ti), and oxygen (O) were its main components.

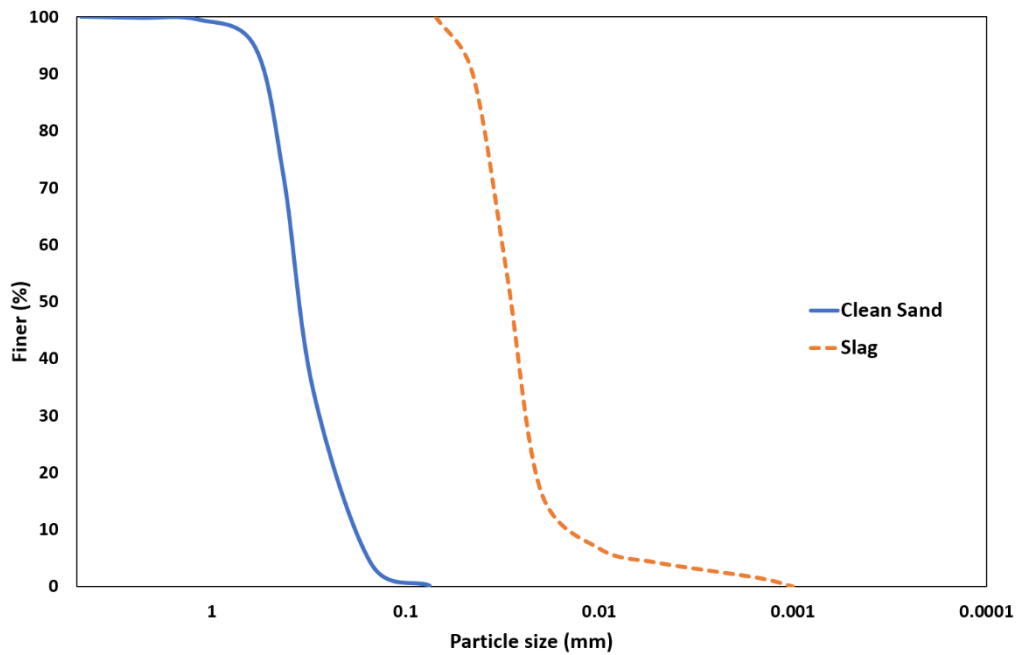
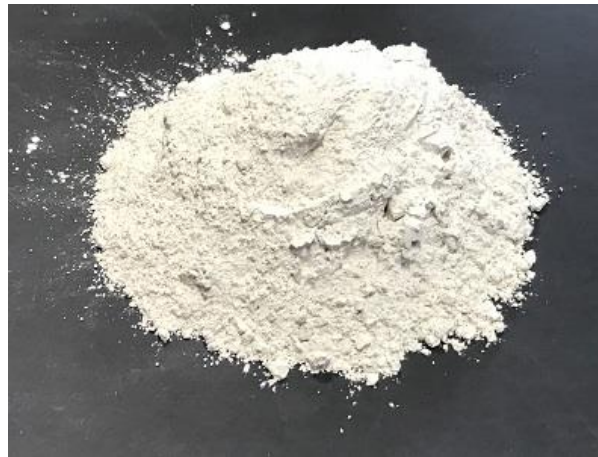
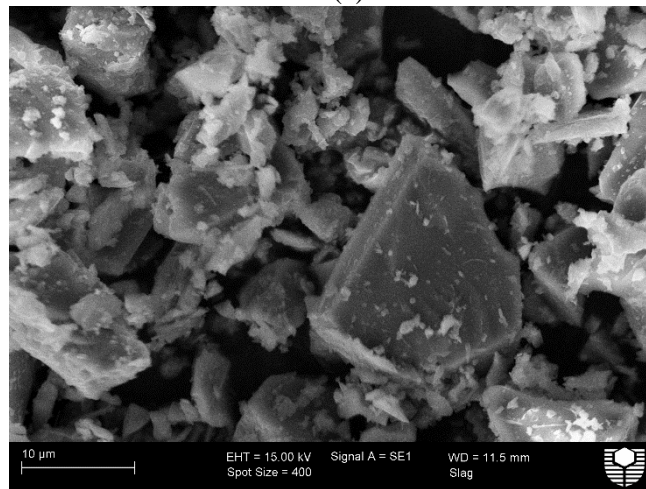


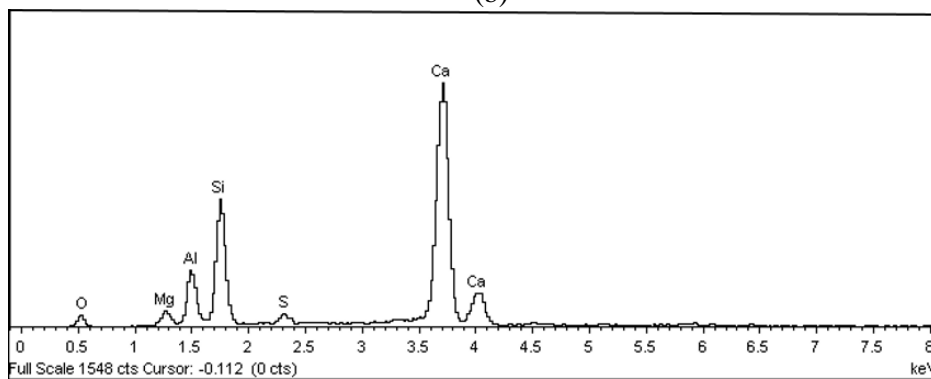
Figure 3.4 Particle size distribution curve of slag



(a)



(b)



(c)

Figure 3.5 Slag used in this study: (a) normal image, (b) SEM image, and (c) EDS image

### 3.2.3 Bentonite

Bentonite is an absorptive aluminium phyllosilicate clay consisting mainly of montmorillonite. Bentonite is a product of the weathering of volcanic ash in the presence of water. On the basis of the dominant component, bentonite can be classified

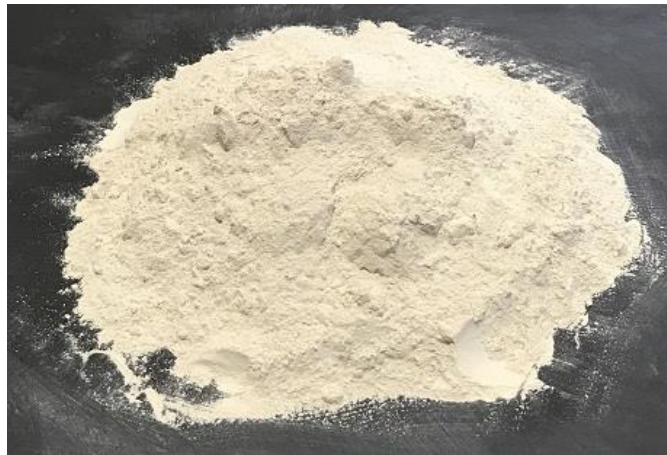
into potassium-, sodium-, calcium-, or aluminium-based bentonite. For industrial purposes, just two types of bentonite exist, namely calcium and sodium bentonite. Sodium bentonite swells when it touches water, absorbing moisture many times more than in its dry condition. The colloidal property makes sodium bentonite a suitable drilling mud for boreholes in geotechnical investigations, gas wells, and oil wells (Odom, 1984). Moreover, the swelling property of sodium bentonite provides a low permeability and self-sealing barrier which makes it useful as a sealant. The bentonite used in the present work was a powdered sodium-based bentonite containing a high proportion of the active mineral species montmorillonite; it was manufactured by Unimin Australia Limited, Queensland. It was an off-white impalpable powder with no distinct odour, formed colloidal suspensions in water, and had high thixotropic properties; its pH was 7–9 (20% aqueous slurry); at least 78% of the sample passed a 75-micron sieve. The sample had bulk density of loose 1.0 t/m<sup>3</sup> and a specific gravity of 3.3. The chemical composition of bentonite is presented in Table 3.3.

Table 3. 3 Chemical components of bentonite

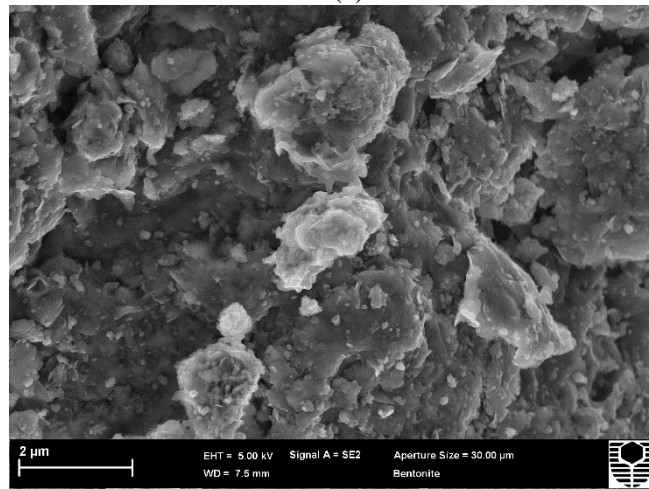
Chemical component	Content %
Silicon dioxide (SiO <sub>2</sub> )	63.6
Aluminium oxide (Al <sub>2</sub> O <sub>3</sub> )	14.6
Titanium dioxide (TiO <sub>2</sub> )	0.4
Iron oxide (Fe <sub>2</sub> O <sub>3</sub> )	2.8
Calcium oxide (CaO)	0.3
Sodium oxide (Na <sub>2</sub> O)	1.3
Magnesium oxide (MgO)	2
Potassium oxide (K <sub>2</sub> O)	0.5
Loss on ignition	14.5

The SEM and EDS images of bentonite are presented in Figures 3.6(b) and (c). As shown in Figure 3.6(c), the main elements of bentonite are silicon (Si), oxygen (O), aluminium (Al), magnesium (Mg), sodium (Na), iron (Fe), calcium (Ca), and potassium (K).

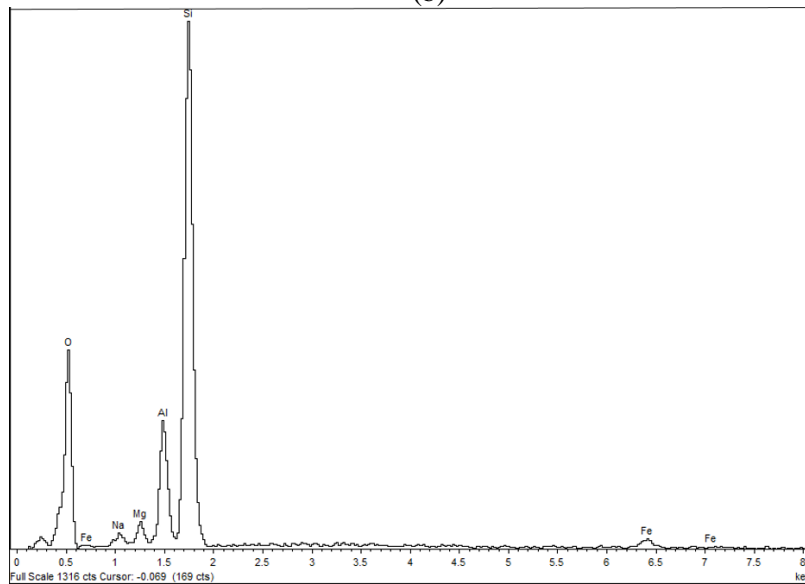




(a)



(b)



(c)

Figure 3.6 Bentonite used in this study: (a) normal image, (b) SEM image, and (c) EDS image.

### 3.2.4 Kaolinite

Kaolinite is a clay mineral, an element of the set of industrial minerals. Clay minerals are complex aluminium silicates consisting of two fundamental components: (1) alumina octahedron and (2) silica tetrahedron (Das & Sobhan, 2014). Kaolinite is composed of repeating layers of basic silica–gibbsite sheets in a 1:1 lattice. Kaolinite is produced by the chemical weathering of aluminium silicate minerals such as feldspar. Kaolinite has a low shrink–swell capacity at different water contents and does not exchange the iron or magnesium cations. Kaolinite is quite effective for making relatively high-quality clay products. Kaolinite used in the present study is called Prestige NY and was collected from Sibelco Australian Limited Factory in Western Australia. It was white to cream powder with the following properties: earthy odour, insoluble, specific gravity of 2.58, pH of 9.2 (20% aqueous slurry), and surface area of 16 m<sup>2</sup>/g. The grain size analysis showed that 99.4% of the sample passed a 0.053-mm sieve, 97.8% passed a 0.02-mm sieve, 95.9% passed a 0.01-mm sieve, 90.3% passed a 0.005-mm sieve, 75.7% passed a 0.002-mm sieve, and 63.6% passed a 0.001-mm sieve. The chemical composition of kaolinite is presented in Table 3.4.

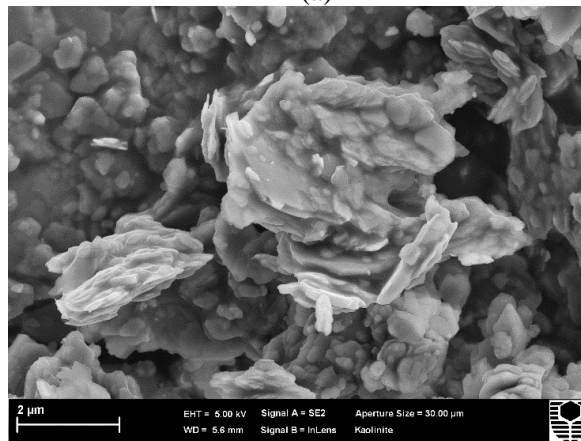
Table 3.4 Chemical components of kaolinite

Chemical component	Content %
Silicon dioxide (SiO <sub>2</sub> )	46.6
Aluminium oxide (Al <sub>2</sub> O <sub>3</sub> )	36.1
Titanium dioxide (TiO <sub>2</sub> )	0.8
Iron oxide (Fe <sub>2</sub> O <sub>3</sub> )	0.9
Calcium oxide (CaO)	0.7
Magnesium oxide (MgO)	0.4
Potassium oxide (K <sub>2</sub> O)	0.4
Sodium oxide (Na <sub>2</sub> O)	0.1
Loss on ignition	14

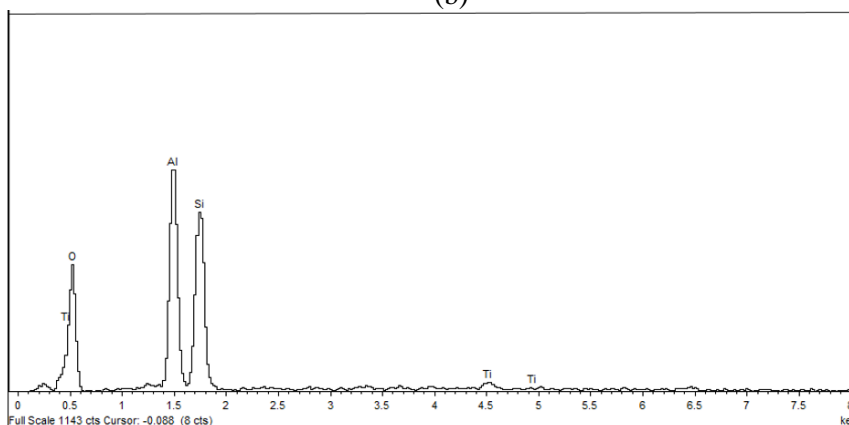
The SEM and EDS images of kaolinite are presented in Figures 3.7(b) and (c). As shown in Figure 3.7(c), the main elements of kaolinite are silicon (Si), oxygen (O), aluminium (Al), and titanium (Ti).



(a)



(b)



(c)

Figure 3.7 Kaolinite used in this study: (a) normal image, (b) SEM image, and (c) EDS image.

## 3.3 Triaxial testing system

### 3.3.1 General description

The conventional triaxial testing system used in the present study consisted of a digital motorised load frame, triaxial cell, load dial gauge, strain dial gauge, and digital pressure/volume controllers, as shown in Figure 3.8. The motorised load frame is a typical device for performing the ‘controlled strain’ triaxial compression test (Head, 2014). Yang and Wei (2015) also stated that the strain-controlled tests provided a dependable set of data for the post-peak response, thereby allowing a clear stress path and stress–strain relationship for a wide range of strains.

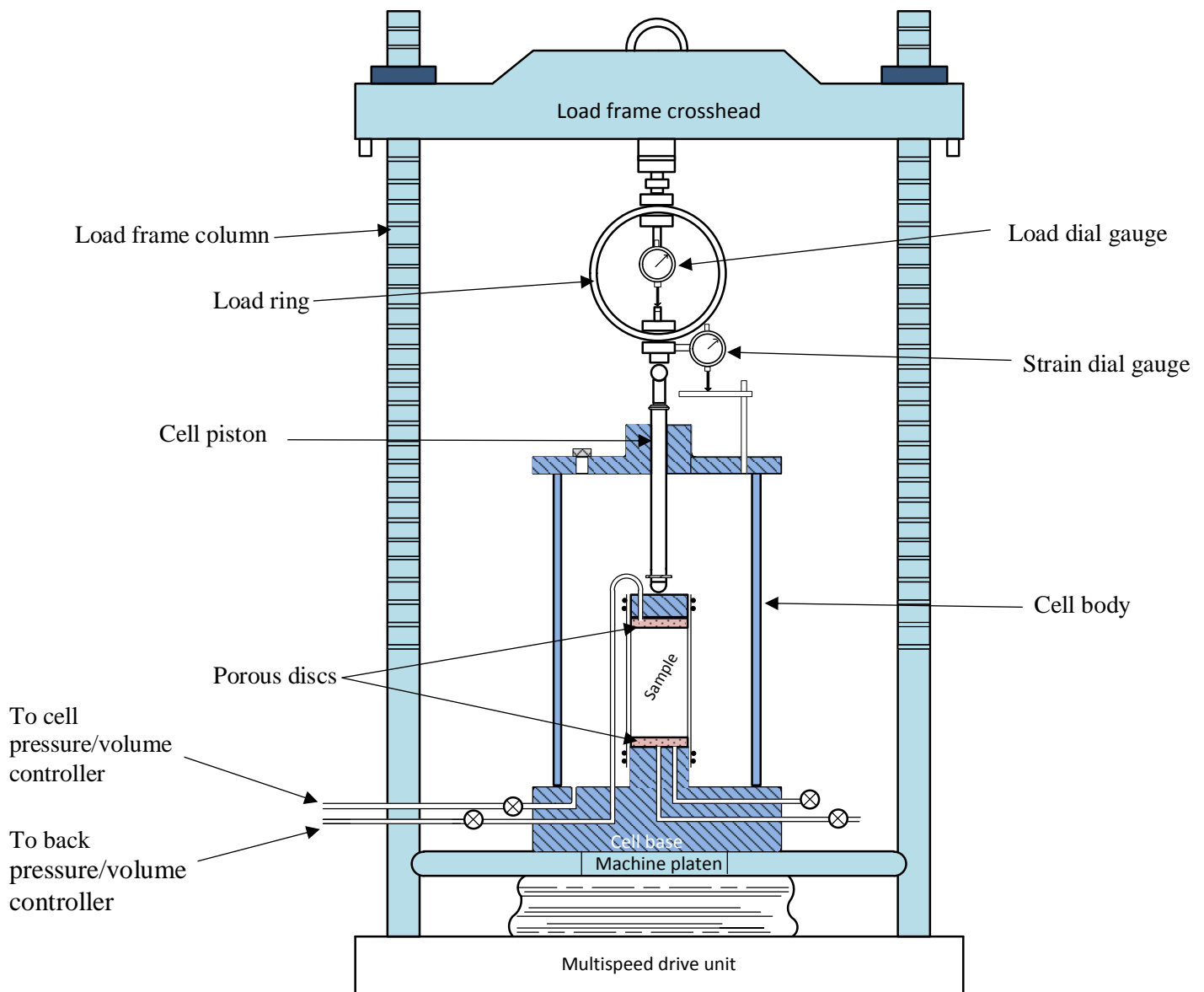


Figure 3.8 Illustrative arrangement of the triaxial testing system

The triaxial testing system contained a cylindrical soil specimen (i.e. 50 mm in diameter and 100 mm in height) inside a cylindrical triaxial cell that was then filled with de-aired water. The bottom of the soil specimen and the triaxial cell were connected to two digital pressure–volume controllers (DPVCs) to control and monitor the water pressure inside the sample and the triaxial cell, respectively. The motor of the load frame moved the base platen at a fixed rate of displacement; thus, the sample was deformed at a constant rate of strain. The axial force resulting from straining the sample and constraining the top of the sample was recorded using a load dial gauge for certain selected periods of time or strain. The digital motorised loading frame was a TRIAX 100 system manufactured by the Controls group (Italy). This loading frame consisted of two columns with a mobile machine platen, load frame crosshead, and a basement which included the mechanical drive system, electric motor, electronic parts, waterproof membrane keyboard, and digital (LCD) display. The drive system was controlled by a microprocessor with a developed stepper motor allowing the user to set any strain rate readily by using the keyboard. The technical specifications of TRIAX 100 are listed in Table 3.5. The LCD of TRIAX 100 is shown in Figure 3.9.

Table 3.5 Technical specifications of TRIAX 100 (Controls, 2005)

<b>Load capacity</b>	<b>100 kN</b>
<b>Max. sample size</b>	150 mm dia
<b>Rate of strain</b>	0.00001–9.99999 mm/min
<b>Rapid approach speed</b>	25 mm/min
<b>Platen diameter</b>	160 mm
<b>Max. platen travel</b>	100 mm
<b>Motor power</b>	250 W
<b>Overall dimensions</b>	1390 mm × 590 mm × 450 mm (height × width × length)
<b>Weight approx.</b>	150 kg
<b>Stroke limiting system</b>	Two electric microswitches plus two digital microswitches
<b>Max. horizontal clearance</b>	458 mm
<b>Max. vertical clearance</b>	1060 mm



Figure 3.9 LCD and keypad of TRAIX 100.

The triaxial cell used in this study was manufactured by ELE international (United Kingdom) and consisted of a transparent Perspex chamber which had a piston collection adapted to the top of the cell. Three assemblies of tie rods and tie rod nuts were used to clamp the upper part of the cell to the base. Moreover, the cell had a base adapter, strain gauge datum, and filler/bleed screw. The base of the cell had five inlet positions for top drainage/back pressure, cell pressure, and pore water pressure and bottom drainage. The cell also had two valves of the no volume change type. The maximum specimen size that could be used in the triaxial cell was 50 mm × 100 mm. The maximum working confining pressure was 1700 kPa, and the maximum piston load was 45 kN. The weight of the triaxial cell was 4 kg, and the required vertical clearance and horizontal clearance was 380 mm and 155 mm, respectively. Figure 3.10 shows a schematic representation of the triaxial cell. The cell pressure and back/pore pressure during the triaxial test were controlled using two digital pressure–volume controllers (DPVCs). The digital controllers used in the present study were manufactured by GDS instruments (United Kingdom). DPVC is a microprocessor regulated screw pump for the accurate control and calculation of the volume change and the pore pressure. The basis of the operation of DPVC is illustrated in Figure 3.11. Pressure was applied to de-aired water by the movement of the piston in the cylinder. The piston was driven by a ball screw turned in a captive ball nut by a stepping motor and a gearbox that shifted straight on the ball slide. The volume change was calculated by counting the steps of the stepping motor. One step of the stepping motor caused a volume displacement of 1mm<sup>3</sup>. The pressure and the volume were presented digitally

on the control panel of the DPVC. The technical specifications of the DPVC are listed in Table 3.6. A general view of the triaxial testing system is shown in Figure 3.12. The axial force and the axial displacement were measured using dial gauges.

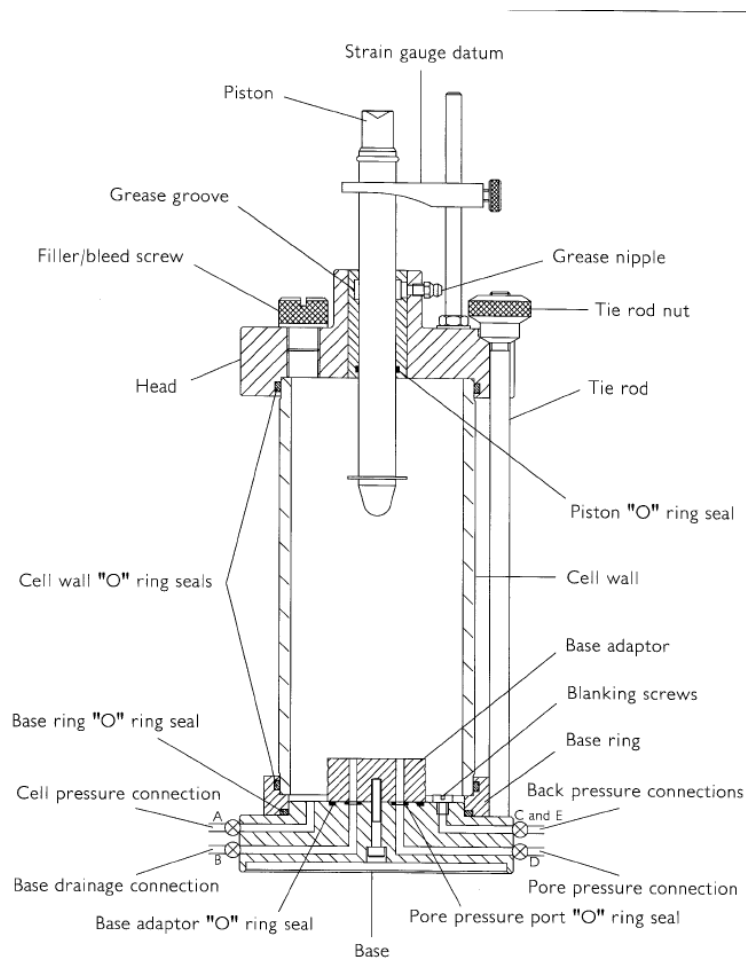


Figure 3.10 Typical arrangement of triaxial cell (ELE, 2004)

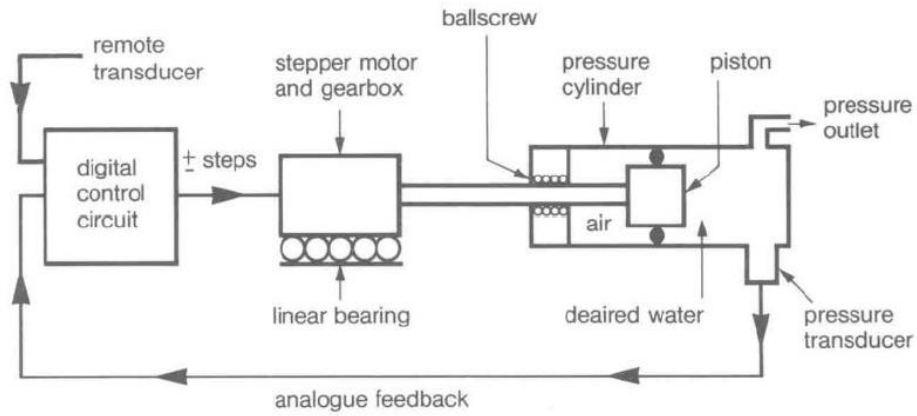


Figure 3.11 Schematic representation of DPVC (GDS, 2017)

Table 3.6 Technical specifications of DPVC (GDS, 2017)

<b>Pressure range</b>	<b>500 kPa–100 MPa</b>
<b>Volumetric capacity</b>	Normal capacity = 200 cc. Optional capacity = 1000 cc for pressures greater than 2 MPa
<b>Weight</b>	20 kg
<b>Size</b>	860 mm × 230 mm × 220 mm
<b>Control panel</b>	16-keypad-membrane touch with audio feedback
<b>Minimum flow rate</b>	0.1 mm <sup>3</sup> /any time
<b>Maximum flow rate</b>	500 mm <sup>3</sup> /s for volume and 250 mm <sup>3</sup> for pressures in the range of 2–32 MPa 100 mm <sup>3</sup> /s for volume and 50 mm <sup>3</sup> for a pressure of 64 MPa



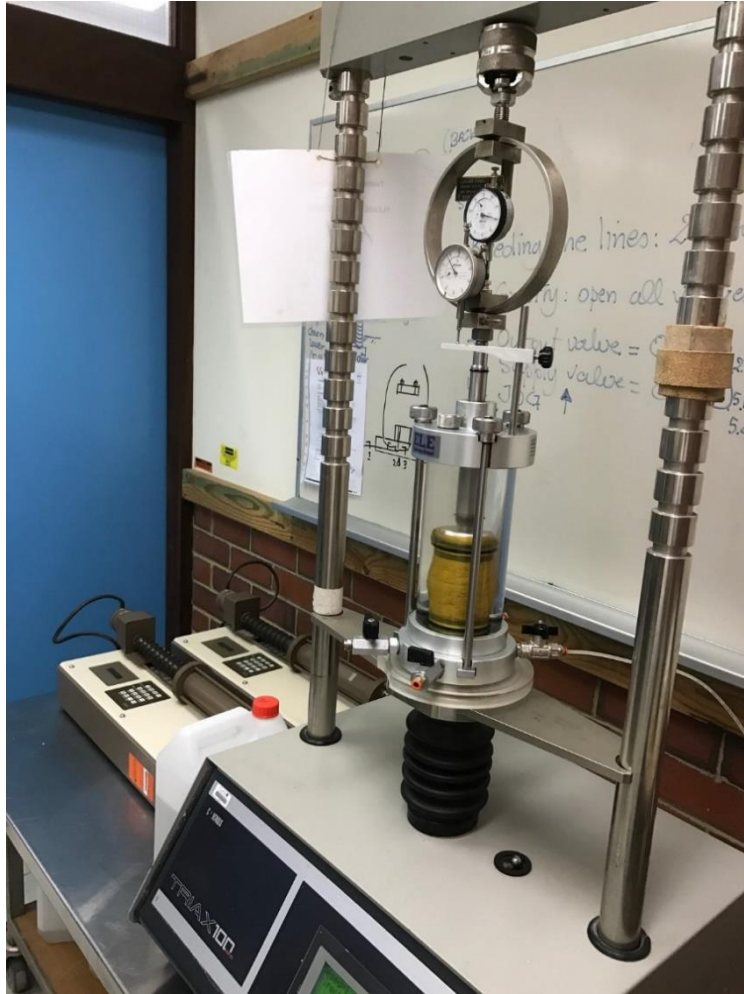


Figure 3.12 General view of triaxial testing system

### 3.3.2 Specimen preparation

Triaxial tests were performed on a cylindrical specimen 50 mm in diameter and 100 mm in height ( $H/D = 2$ ), prepared using a moist tamping technique, which has been utilised in many previous studies (Bobei et al., 2009; Chu & Leong, 2002; Ishihara et al., 2004; Kramer & Seed, 1988; Leong et al., 2000; Liu et al., 2011; Murthy et al., 2007; Ni et al., 2004; Rahman et al., 2014; Riemer & Seed, 1997; Salem et al., 2013; Tang, Ma, & Shao, 2013; Verdugo & Ishihara, 1996; Yamamuro & Lade, 1997b; Yang & Wei, 2012, 2015). This method was chosen firstly to prevent sample segregation and secondly to produce very loose samples. The sample preparation procedure can be described as follows:

- 1- The porous disk and the filter paper were placed on the cell pedestal. The porous disk and the filter paper were thoroughly saturated by immersing them in de-aired water. The diameter of the porous disk was slightly smaller than the diameter of the sample.
- 2- A thin rubber membrane was fixed on the cell pedestal by using two rubber O-rings. For better sealing, the surface of the cell pedestal was rubbed with a small amount of silicon grease. However, the porous disk and the filter paper had to be kept away from possible contamination by the silicon grease.
- 3- The split mould was assembled around the cell pedestal, and before clamping in its position, its matching faces were rubbed with a thin film of grease.
- 4- The membrane was stretched by fitting its top end around the top of the mould; it was secured using two rubber O-rings.
- 5- Approximately  $-15$  kPa of vacuum was applied to ensure that the rubber membrane was completely fitted inside the mould.
- 6- A predetermined amount of oven-dry materials was mixed in a container until a homogenous blend was obtained. Then, 5% of de-aired water was added to the mixture.
- 7- The wet sample was divided into five predetermined equal portions by weight. Next, each part of the wet soil was deposited into the split mould by using a spoon and gently compacted using the small tamper, as shown in Figure 3.13. The diameter of the small tamper was 35% less than that of the specimen. The number of blows during the compaction of each layer was controlled by using a predetermined height to achieve the desired density; each layer was 18 mm in height. The required relative density was computed using the following equation:

$$R_D = \frac{\rho_{dmax} - (\rho_d - \rho_{dmin})}{\rho_d (\rho_{dmax} - \rho_{dmin})} \times 100\% \quad (3-1)$$

where  $R_D$  = relative density,  $\rho_{dmax}$  = maximum dry density,  $\rho_{dmin}$  = minimum dry density, and  $\rho_d$  = desired dry density.

- 8- The top of each compacted layer was scarified to increase the interlocking between the layers. The steps were repeated for all of the five portions.

- 9- The top cap was carefully seated on the upper surface of the sample after placing the filter paper and the porous disk; the membrane was fixed to the top cap and sealed by the two rubber O-rings, as illustrated in Figure. 3.14(a). The split steel tube expander was used to avoid sample damage during the sealing of the rubber membrane onto the top cap. For better sealing, the surface of the top cap was rubbed with a small amount of silicon grease.
- 10- The split mould was carefully disassembled, and the dimensions of the sample (i.e. diameter and height) were measured as shown in Figure. 3.14(b).
- 11- The triaxial chamber was carefully assembled with the cell piston elevated to its highest range to prevent any disturbance caused to the soil sample while clamping the triaxial chamber to the cell base.
- 12- The cell piston was allowed to fall gradually into contact with the top cap, as shown in Figure. 3.14(c).
- 13- The triaxial chamber was filled with de-aired water through a filler/bleed screw from the supply system or the reservoir. Turbulence was not allowed during the filling process.
- 14- The bleed screw was kept open until the application of cell pressure was begun, to keep the cell at atmospheric pressure. Further information about the sample preparation method can be found in (Head, 2014; Head & Epps, 2011). The sample was then ready for running the next stages of the routine tests described in the following sections.

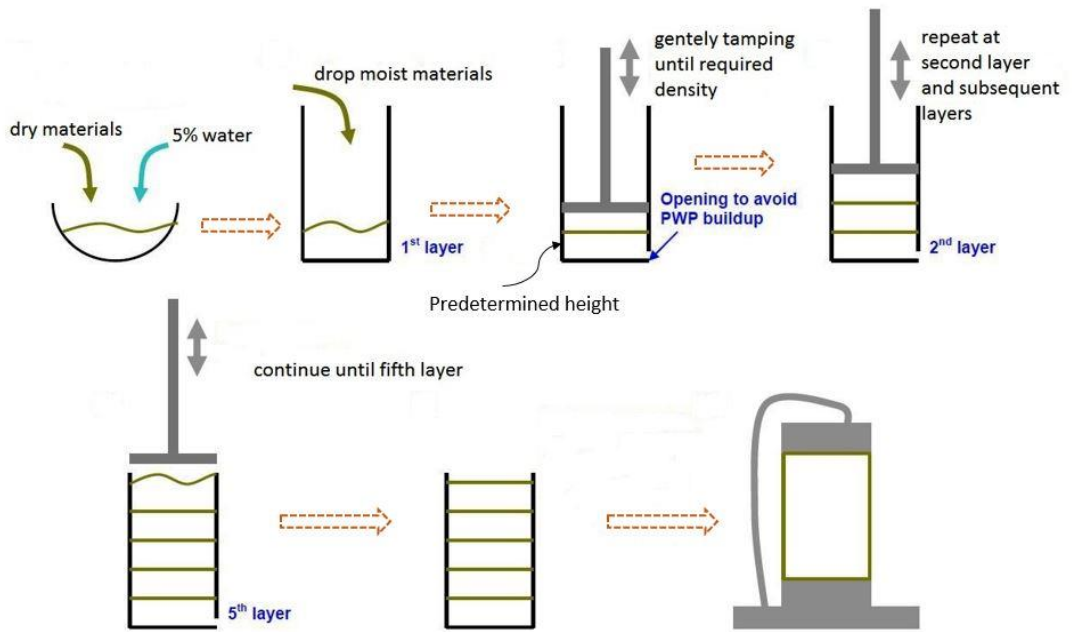


Figure 3.13 Moist tamping procedure



(a)



(b)



(c)

Figure 3.14 Sample preparation steps

### 3.3.3 Saturation

The sample in the triaxial test was saturated by increasing the pore water pressure to an adequate level for all of the air in the void spaces to be dissolved in water. At the same time, the confining pressure was increased to maintain a small effective stress in the sample. Saturation also removed any air bubbles that formed in the pore pressure connections and drainage lines that might not have been flushed out. The cell pressure increments during the saturation stage were less than 50 kPa and did not exceed the effective confining pressure during consolidation. Head (2014) also added that the differential pressure (i.e. the difference between the cell pressure and the back pressure) during saturation should not be higher than 20 kPa and less than 5 kPa. Applying back pressure from the bottom of the sample improved the degree of saturation of the sample by compressing the air bubbles between the sand particles (Delia, 2010). The back pressure saturation procedure described in (Head, 2014) was adopted in the present study. Saturation was implemented by simultaneously increasing the cell pressure and the back pressure while keeping the differential pressure constant at 20 kPa throughout the saturation process. The test was continued by increasing the cell pressure and the back pressure until the sample was fully saturated. The degree of saturation was estimated by computing Skempton's B-coefficient. The B value is the ratio of the pore water pressure generated by increasing the cell pressure to the variation in the cell pressure ( $\Delta u/\Delta\sigma_3$ ). The sample was considered fully saturated when the value of B was  $\geq 0.95$ . The relationship between the degree of saturation and Skempton's coefficient can be represented by the following equation (Lade & Hernandez, 1977):

$$B = \frac{1}{1+nk_s \left( \frac{S_r}{k_w} + \frac{(1-S_r)}{U_a} \right)} \quad (3-2)$$

where  $k_s$  = bulk modulus of soil,  $k_w$  = bulk modulus of water,  $n$  = the soil porosity, and  $U_a$  = pore water pressure. Cell pressure in the present work was applied in three sequences. The first one was applied in 25-kPa increments until the value of B reached 0.5. Then, the increments increased to 50 kPa until the value of B reached 0.8 and 100 kPa thereafter. Some samples of clean sand were tested at B values of 0.25 and 0.5 to investigate the effect of the degree of saturation on the static behaviour of clean Perth

sand. However, a majority of the samples were tested in the fully saturated state with  $B \geq 0.95$ . The back pressure applied to saturate the samples was varied with an increase in the fines content. All the samples were saturated in the range of 800–1000 kPa. The cell volume changes during saturation were recorded in each increment to track the sample volume change during saturation. When a sample achieved a B value of 0.95 or more, the saturation stage was terminated, but before closing the valves, an additional back pressure increment was applied to the sample to allow for any uncertainty; then, all of the valves were closed and the sample was ready for the next stage.

### **3.3.4 Consolidation**

The effective confining pressure at the end of the saturation stage was less than the effective stress required for the compression test. Therefore, the consolidation stage aimed to increase the effective confining pressure up to the required level and then allow the sample to consolidate by the dissipation of the pore water pressure (Head, 2014). Three techniques are used to increase the effective stress: increasing the cell pressure or reducing the back pressure or a mix of both. The increasing cell pressure technique which was used in this study is the most widely used method for consolidating samples because the degree of saturation may reduce when the back pressure is reduced. However, the reducing back pressure technique can be used when the pressure required is larger than the maximum working pressure for the triaxial cell. In the present study, three isotropic consolidation confining pressures were used: 100, 150, and 200 kPa. To begin the consolidation stage, all the valves were closed. Then, the cell pressure was increased to the level at which the differential stress was equal to the required effective confining pressure. The values of the pore water pressure were recorded during the application of the cell pressure. The excess pore water pressure needed for the dissipation was equal to the difference between the final steady pore water pressure and the back pressure at the start of the consolidation stage. The back pressure volume changes were recorded at regular time intervals. The time required for the dissipation of the pore water pressure in the present work varied as different materials were used. The time taken for the consolidation of the clean sand and sand–slag samples was less than the time required for the consolidation of the sand–clay and sand–slag–clay samples. Moreover, the time increased with an increase in the fines

content. The consolidation stage was terminated when the volume changes were constant at least two time intervals. Before the termination of the consolidation stage, the total volume changes were recorded, and the sample was then ready for the shearing stage. Further information on the consolidation stage in the triaxial test is reported in (Head, 2014).

### **3.3.5 Shearing**

The samples were sheared by applying an axial displacement at a constant rate through the upward movement of the load frame platen at a constant cell pressure. The imposed axial load allowed the increase in the pore water pressure; therefore, the change in the effective stress was not equal to the change in the total stress. The rate of the applied axial strain was sufficiently slow to allow the pore water pressure to equalise for the entire sample. All of the undrained compression triaxial tests for the current study were performed under strain-controlled circumstances at a constant strain rate of approximately 1%/min. The first step in this stage was to place the reversing switch of the load frame machine on the upward movement. Before running the motor, the speed controller was set to provide the required strain rate. The motor was stopped when the cell piston was attached to the top cap, and the load dial gauge was adjusted to read zero. The adjustment of the load dial gauge corrected the effect of the cell pressure and the piston friction on the load dial gauge. After checking for appropriate contact between the piston and the top cap, the motor was rerun and the readings of the axial load, axial strain, pore water pressure, and the volume of the cell pressure unit were recorded at regular time intervals. The readings were recorded at 0.2% strain intervals up to 1% strain, and 0.5% strain thereafter. However, the readings were recorded more frequently when they changed rapidly. The tests were allowed to continue until the failure criteria were reached. Two failure criteria were used in the present study. The first one was that the experiments were terminated when the axial strain reached >20% in the case of non-flow behaviour. The second one was that the tests were terminated when the pore water pressure remained constant with increasing strain in the cases of liquefaction and limited liquefaction behaviours. When the sample reached the failure condition, the motor stopped, the back pressure valve closed, and the load frame machine was set on the down movement to unload the sample. The cell pressure was reduced to zero, and the bleeding screw was opened to empty the cell. Finally, the triaxial cell was disassembled, and a small sample was taken from the specimen for

the water content measurement. Further information on the shearing stage in the triaxial test can be found in (Head, 2014).

### 3.3.6 Corrections to triaxial test data

The corrections that were applied to the measured data from the triaxial tests are discussed in this section. Two types of corrections were used in the present study: the first one was the membrane corrections, and the second one was the sample detail corrections after consolidation.

#### 3.3.6.1 Membrane corrections

Membrane corrections were applied to the measured deviator stress and membrane penetration effect on the volume change data through the triaxial test. For the deviator stress, the correction method reported in Head (2014) was used, and the result showed that the correction was apparently small and could be ignored. The effect of the rubber membrane penetration on the volume change data has been studied in many previous studies (Frydman, Zeitlen, & Alpan, 1973; Newland & Allely, 1959; Roscoe, Schofield, & Thurairajah, 1963). Frydman et al. (1973) stated that the main particle size ( $d_{50}$ ) is the primary factor affecting the membrane penetration at any applied confining pressure. However, other factors such as particle size distribution, sample density, and particle shape had a small effect. The experimental procedure proposed by Frydman et al. (1973) was adopted in the present work to minimise the error associated with the rubber membrane penetration. To determine the actual volume change of the sample, the following procedure was used: (a) based on the main diameter of sample  $d_{50}$ , Figure 3.15(a) was used to determine the slope ( $S$ ) of the unit membrane penetration  $\Delta v_m$  line, (b) the straight line of slope  $S$  was drawn from the point of the confining pressure  $\sigma_3$ . The membrane penetration per unit area ( $\Delta v_m$ ) corresponding to a confining pressure was read as shown in Figure 3.15 (b). The volume change ( $\Delta V_m$ ) caused by membrane penetration was calculated as follows:

$$\Delta V_m = \Delta v_m \times A_m \quad (3-3)$$



here  $A_m$  = the area of contact between the specimen and the membrane ( $A_m = \pi \times D \times H$ );  $D$  = diameter of the sample, and  $H$  = height of the sample. The actual volume change of the specimen ( $\Delta V_s$ ) was calculated as follows:

$$\Delta V_s = \Delta V - \Delta v_m \tag{3-4}$$

where  $\Delta V$  = the volume of water drained out of the specimen into the back pressure/volume unit.

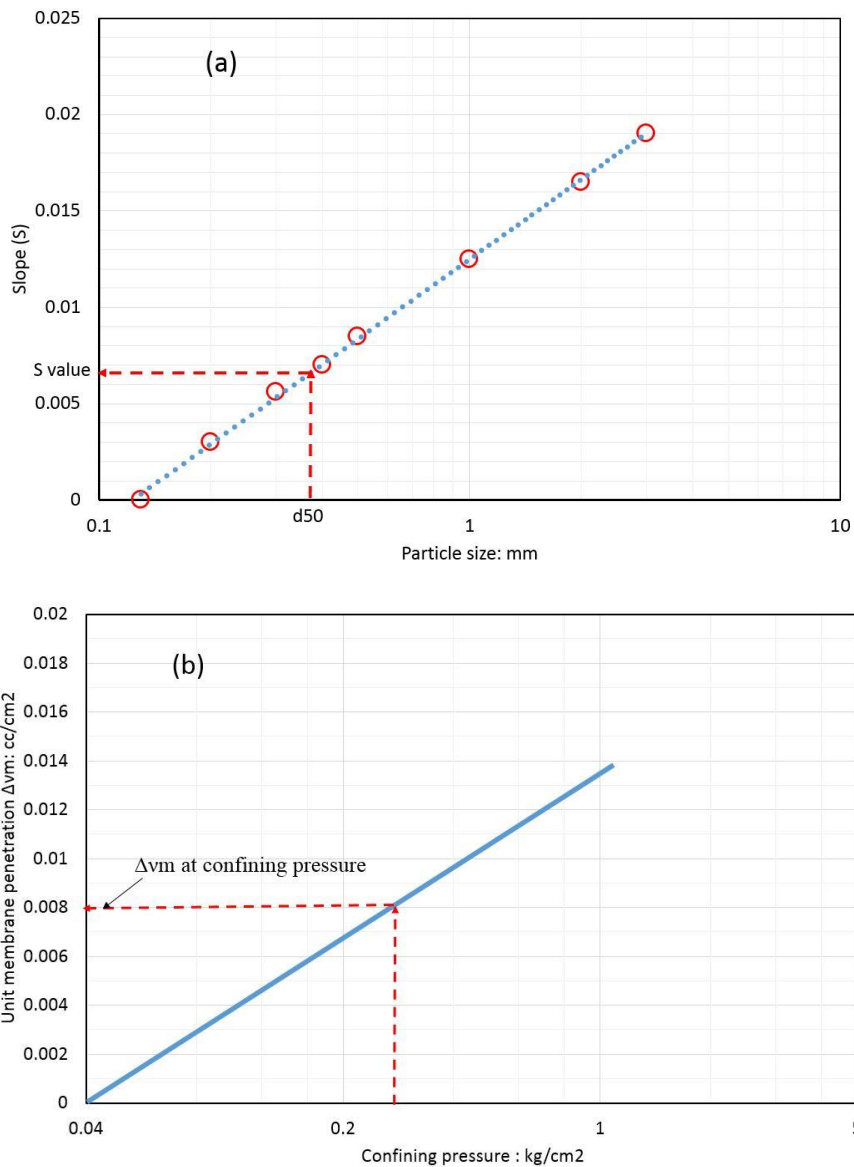


Figure 3.15 Membrane penetration correction procedure

### 3.3.6.2 Sample detail corrections

The volumetric strain after consolidation ( $\varepsilon_{vc}$ ) was calculated as follows:

$$\varepsilon_{vc} = \frac{V_s}{V_o} \times 100\% \quad (3-5)$$

where  $V_s$  = corrected volume change of the specimen and  $V_o$  = initial volume of the sample.

The correction of the sample details (i.e. sample area, length, and volume) at the end of the consolidation stage was calculated as follows. Note that the equations used in this section are dependent upon the elastic theory for a small volume change with Poisson's ratio of 0.5.

$$L_c = L_o \left( 1 - \frac{1}{3} \times \frac{\varepsilon_{vc}}{100} \right) \text{ mm} \quad (3-6)$$

where  $L_c$  = consolidated length used for calculating the axial strain and  $L_o$  = initial length of the sample.

$$A_c = A_o \left( 1 - \frac{2}{3} \times \frac{\varepsilon_{vc}}{100} \right) \text{ mm}^2 \quad (3-7)$$

where  $A_c$  = consolidated cross-sectional area used for calculating the stress in the compression stage and  $A_o$  = initial cross-sectional area of the sample.

$$V_c = \frac{A_c L_c}{1000} = V_o - \Delta V_s \quad (3-8)$$

where  $V_c$  = consolidated volume of the sample ( $\text{mm}^3$ ).

## 3.4 Artificial intelligence analysis

In the present study, an artificial neural network ANN and genetic programming GP were used to predict the liquefaction susceptibility of clean sandy soil and mixtures of sand with fines in terms of the stress ratio  $q_{min}/q_{peak}$ . The datasets for the clean sand models were collected from the literature. However, the liquefaction susceptibility models of the sand–fines mixtures were developed on the basis of the data obtained from the current study. The ANN and GP procedures are described in the following sections.

### 3.4.1 Artificial neural network (ANN) models

In this study, the ANN models were generated using Neural Network Toolbox in MATLAB R2015a provided by Curtin University, Western Australia. The creation of a neural network was based on the determination of the input and output datasets, algorithm type, number of hidden layers, and the number of hidden neurons. Essential factors expected to affect the liquefaction susceptibility of sandy soil were presented to the ANN models as the possible input dataset. These included the coefficient of uniformity  $C_u$ , mean diameter  $D_{50}$ , maximum void ratio  $e_{max}$ , minimum void ratio  $e_{min}$ , initial void ratio  $e_o$ , relative density  $D_r$ , initial effective confining pressure  $p'_o$ , degree of saturation  $B$ , consolidation type  $\alpha$ , and fines content. The stress ratio  $q_{min}/q_{peak}$  was the single model output. In the cases of both clean sand and sand with fines, the number of input variables was varied to examine the efficiency of the ANN models. The architecture of the ANN used in the present work involved a varied number of input parameters and one target parameter; the Levenberg–Marquardt back-propagation algorithm with a varied number of hidden layers and neurons was used. Figure 3.16 shows an example of a neural network. The effect of the sample preparation method was not considered in the input dataset because a majority of the samples used in the present work were deposited by the moist tamping technique.

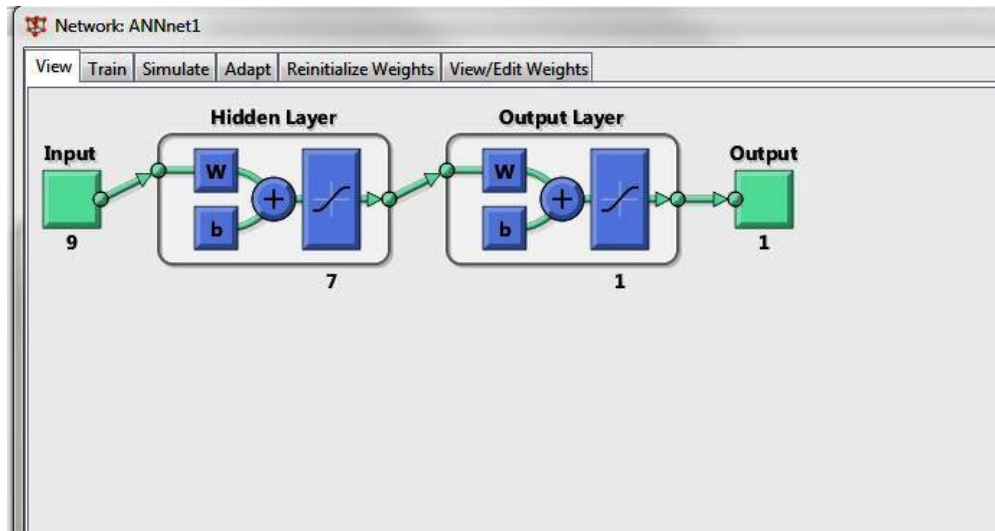


Figure 3.16 View of created network

All the datasets were normalised using MATLAB’s normalisation function, which is a requirement of ANN modelling. Goh (1994) stated that the normalisation of datasets is necessary because the sigmoid transfer function adjusts the output values in the range of 0–1. The dataset in this study was split into three groups, namely training, testing, and validation. The percentage of data in each group was 70%, 15%, and 15% for training, testing, and validation, respectively. After creating a neural network, the training dataset was used until the average sum-squared errors over all of the training sets decreased. The results were considered reasonable when the final mean squared error was small, and the validation set and the test set had the same behaviour, as shown in Figure. 3.17 (Demuth, Beale, & Hagan, 2008).

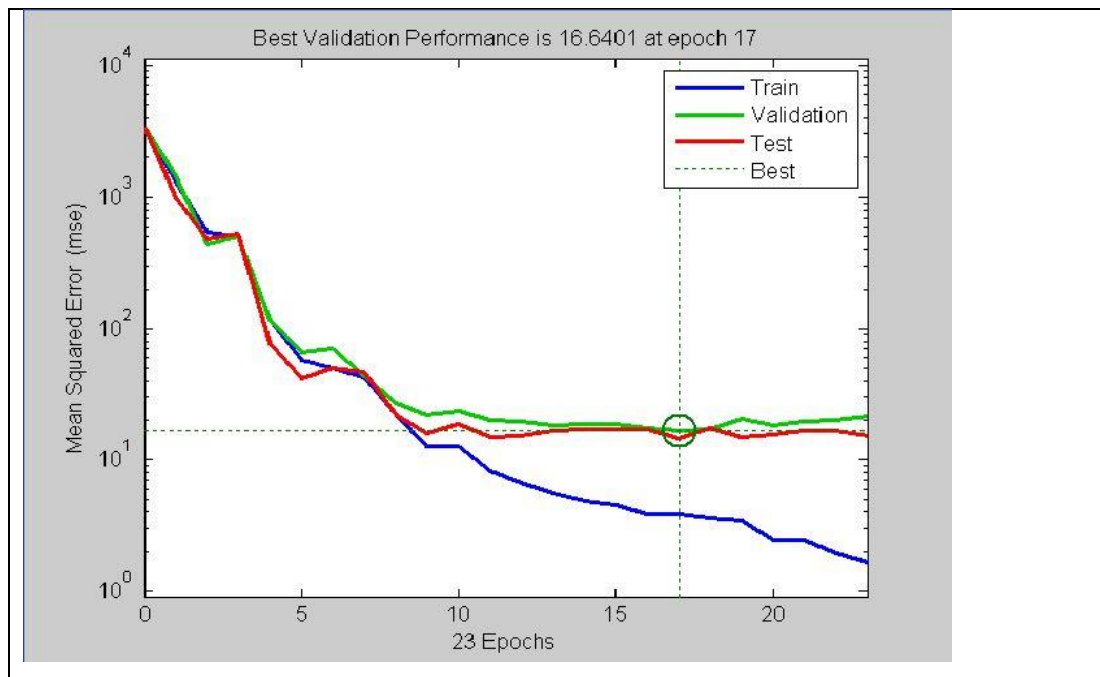


Figure 3.17 Mean squared error during training stage

To obtain better results, the number of layers, number of hidden neurons, number of epochs, and the learning rate were changed during the training stage until the mean squared error achieved the error goal. Moreover, the performance of the ANN models was evaluated by performing a linear regression between the predicted values and the corresponding target for the training, validation, testing, and overall datasets, as shown in Figure 3.18. The outputs were considered reasonably good when the R-values were  $>0.9$  for all the datasets. However, the efficiency of the ANN models was evaluated for the testing datasets as reported in Muduli and Das (2014a) and Das and Basudhar (2008). These scholars stated that the performance of a testing dataset should be used for evaluating the efficiency of the different developed ANN models. After completing the training and testing of the model, a sample dataset was used to test the accuracy of the model.

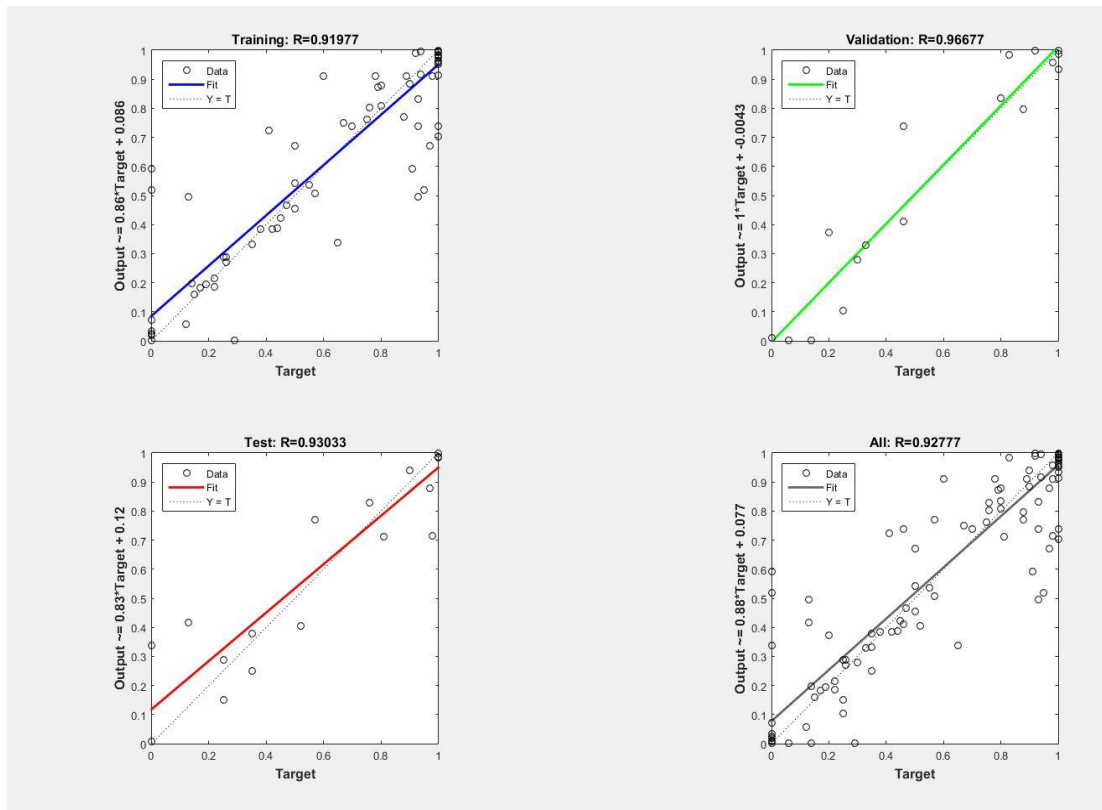


Figure 3.18 Linear regression of ANN

### 3.4.2 Genetic programming (GP) models

In the present work, the HeuristicLab software (Figure 3.19) was used to obtain the predictive equations for the ratio of  $q_{min}/q_{peak}$  of clean sandy soils and sand–fines mixtures based on symbolic regression via genetic programming (GP). Symbolic regression can be defined as a data mining approach used to extract hidden meaningful relationships by using input data and weights. Symbolic regression depends on a tree-based genetic programming (GP) system to develop mathematical equations. HeuristicLab has been used for solving some engineering problems. However, the utilisation of this software in soil mechanics and foundation engineering is still quite rare. HeuristicLab is open-source software based on heuristic and evolutionary algorithms and was created by the Heuristic and Evolutionary Algorithms Laboratory (HEAL) in 2002 at the University of Applied Sciences, Upper Austria. It uses C++ and is based on the Microsoft.Net framework (Wagner et al., 2014). Moreover, it provides a good graphical user interface. HeuristicLab supports a broad range of algorithms such as genetic algorithm, Gaussian process regression and classification, neural

network regression, and classification. Moreover, it helps in solving many types of problems, such as artificial art, classification, clustering, symbolic regression, and symbolic classification. One of the features of HeuristicLab is the ability to simplify a complex model by trimming it to find a good agreement between complexity and accuracy (Wagner et al., 2014). Further details about HeuristicLab are reported in (Wagner et al., 2014).

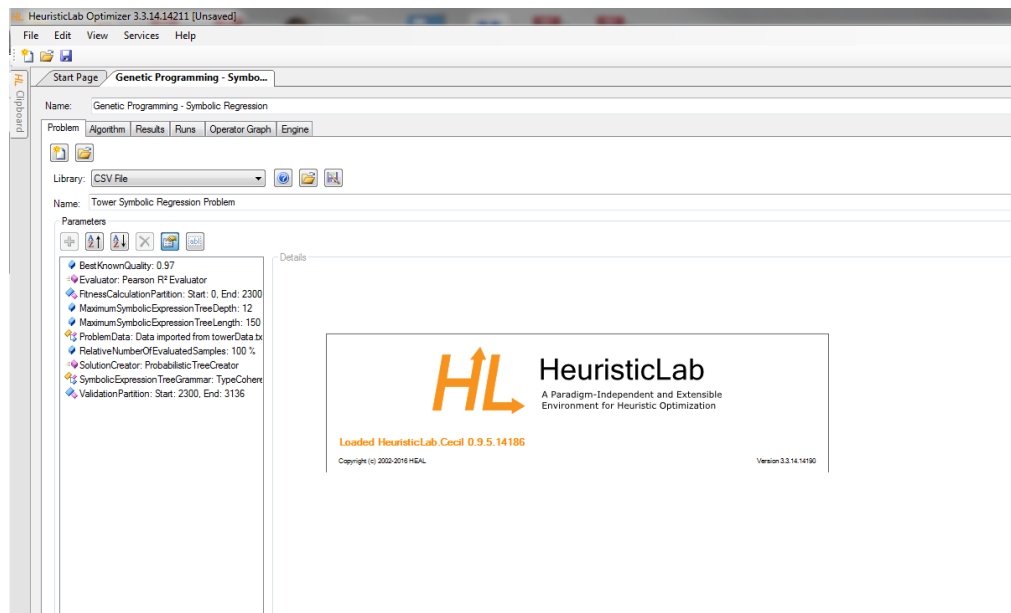


Figure 3.19 HeuristicLab interface

The GP models developed in the current study were based on the results of the best ANN models. The datasets divided into the input dataset included a different number of input variables and one output variable (ratio of  $q_{min}/q_{peak}$ ). The dataset was loaded into the software; then, it was split into training and testing datasets. The data division into subsets (training and testing) prevented over-fitting during the training stage. Typically, over-fitting occurs when data points in the training phase are inadequate (Das, 2013). Ferreira (2006) argued that no specific ratio can be used for each data subset, but in general, 80%–90% of the available data should be utilised as the training set and 10%–20% as the testing set. In this work, datasets were randomly split into 67% for training and 33% for testing. The structure of the GP model included population size, maximum generation, parent selection, crossover, and mutation rate. For a better modelling process, the trial-and-error approach was adopted to identify

appropriate values for the input variables. During each step, runs were performed, and the value of one of the input parameters was varied, while the other parameters were kept constant. At the end of each run, the MSEs for the training and testing sets were checked to determine the smallest MSE. The performance of the GP models was evaluated by minimizing the error (i.e. the difference between the predicted and the measured values). If the error calculated did not satisfy the termination criteria for each model in the population, the evolutionary process continued to create a new generation of models until the minimum error was obtained. The fitness of each model was considered to be reasonably good when the correlation coefficient  $R^2$  values were  $>0.85$  for all the datasets. The procedure was continued until the best model was obtained. After reaching the best performance, the model prediction was visualised as a tree, as shown in Figure 3.20. The colour of the tree indicates the importance of the subtrees with respect to the training quality. A green subtree has a substantial effect on the output, while white subtrees have almost no effect on the output. Finally, the tree was simplified into a mathematical model by replacing the nodes with constants.

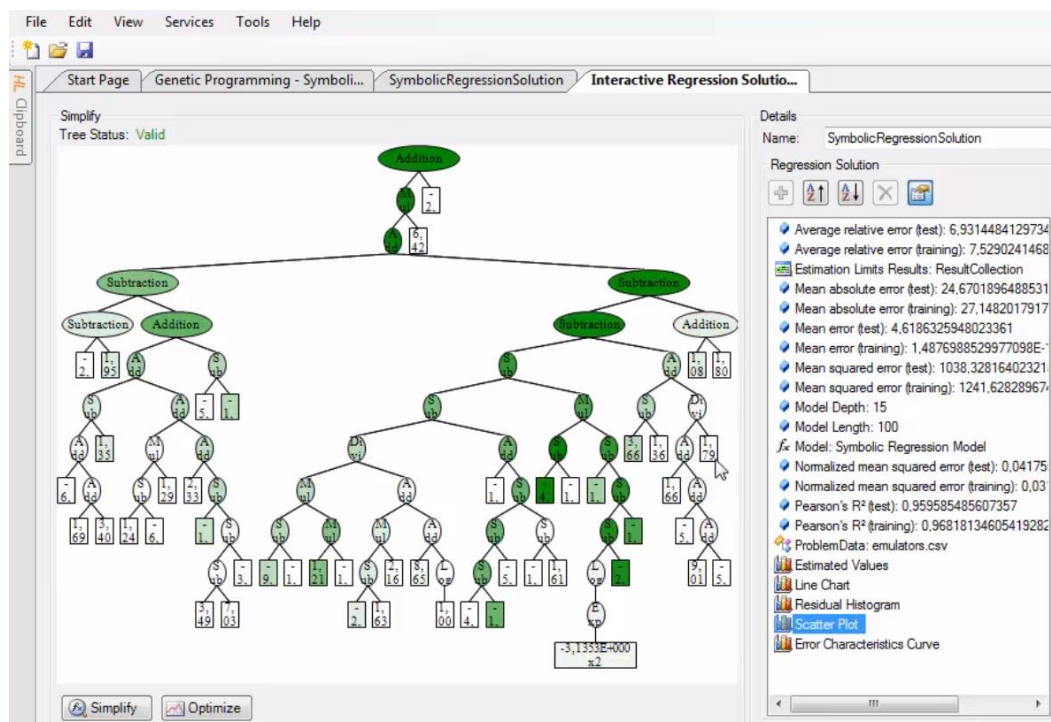


Figure 3. 20 Visualisation of HeuristicLab model



### 3.5 Testing program

In all, 68 undrained static triaxial tests were performed on clean sand and sand with fines under different testing conditions, such as three confining pressures (100, 150, and 200 kPa), three relative densities (10%, 50%, and 90%), three B values (0.95, 0.50, and 0.25) and different fines contents. The testing program included seven binary mixtures and twelve triple mixtures produced by dry mixing clean sand with different contents of slag, bentonite, and kaolinite. The tests are summarised in Table 3.7.

Table 3.7 Summary of static triaxial tests performed during the present study

No.	Materials	Symbol	Relative density (%)	Confining pressure (kPa)	B value
1	100% Sand	CS1	10	100	0.95
2	100% Sand	CS2	10	150	0.95
3	100% Sand	CS3	10	200	0.95
4	100% Sand	CS4	50	100	0.95
5	100% Sand	CS5	50	150	0.95
6	100% Sand	CS6	50	200	0.95
7	100% Sand	CS7	90	100	0.95
8	100% Sand	CS8	90	150	0.95
9	100% Sand	CS9	90	200	0.95
10	100% Sand	CS10	10	100	0.25
11	100% Sand	CS11	10	100	0.5
12	100% Sand	CS12	20	100	0.95
13	100% Sand	CS13	40	100	0.95
14	98% Sand + 2% slag	2%S	10	100	0.95
15	98% Sand + 2% slag	2%S	10	150	0.95
16	98% Sand + 2% slag	2%S	10	200	0.95
17	98% Sand + 2% slag	2%S	50	100	0.95
18	98% Sand + 2% slag	2%S	90	100	0.95
19	96% Sand + 4% slag	4%S	10	100	0.95
20	96% Sand + 4% slag	4%S	10	150	0.95
21	96% Sand + 4% slag	4%S	10	200	0.95
22	96% Sand + 4% slag	4%S	50	100	0.95
23	96% Sand + 4% slag	4%S	90	100	0.95
24	94% Sand + 6% slag	6%S	10	100	0.95
25	94% Sand + 6% slag	6%S	10	150	0.95

No.	Materials	Symbol	Relative density (%)	Confining pressure (kPa)	B value
26	94% Sand + 6% slag	6%S	10	200	0.95
27	94% Sand + 6% slag	6%S	50	100	0.95
28	94% Sand + 6% slag	6%S	90	100	0.95
29	97% Sand + 3% bentonite	3%B	10	100	0.95
30	97% Sand + 3% bentonite	3%B	10	150	0.95
31	97% Sand + 3% bentonite	3%B	10	200	0.95
32	97% Sand + 3% bentonite	3%B	50	100	0.95
33	97% Sand + 3% bentonite	3%B	90	100	0.95
34	95% Sand + 5% bentonite	5%B	10	100	0.95
35	95% Sand + 5% bentonite	5%B	10	150	0.95
36	95% Sand + 5% bentonite	5%B	10	200	0.95
37	95% Sand + 5% bentonite	5%B	50	100	0.95
38	95% Sand + 5% bentonite	5%B	90	100	0.95
39	97% Sand + 3% kaolinite	3%K	10	100	0.95
40	97% Sand + 3% kaolinite	3%K	10	150	0.95
41	97% Sand + 3% kaolinite	3%K	10	200	0.95
42	97% Sand + 3% kaolinite	3%K	50	100	0.95
43	97% Sand + 3% kaolinite	3%K	90	100	0.95
44	95% Sand + 5% kaolinite	5%K	10	100	0.95
45	95% Sand + 5% kaolinite	5%K	10	150	0.95
46	95% Sand + 5% kaolinite	5%K	10	200	0.95
47	95% Sand + 5% kaolinite	5%K	50	100	0.95
48	95% Sand + 5% kaolinite	5%K	90	100	0.95
49	95% Sand + 2% slag + 3% bentonite	2S3B	10	100	0.95
50	95% Sand + 2% slag + 3% bentonite	2S3B	10	150	0.95
51	95% Sand + 2% slag + 3% bentonite	2S3B	10	200	0.95
52	95% Sand + 2% slag + 3% bentonite	2S3B	20	100	0.95
53	95% Sand + 2% slag + 3% bentonite	2S3B	50	100	0.95
54	93% Sand + 4% slag + 3% bentonite	4S3B	10	100	0.95
55	93% Sand + 4% slag + 3% bentonite	4S3B	10	150	0.95
56	93% Sand + 4% slag + 3% bentonite	4S3B	10	200	0.95
57	93% Sand + 4% slag + 3% bentonite	4S3B	20	100	0.95
58	91% Sand + 6% slag + 3% bentonite	6S3B	10	100	0.95
59	91% Sand + 6% slag + 3% bentonite	6S3B	10	150	0.95
60	91% Sand + 6% slag + 3% bentonite	6S3B	10	200	0.95
61	91% Sand + 6% slag + 3% bentonite	6S3B	20	100	0.95
62	91% Sand + 6% slag + 3% bentonite	6S3B	50	100	0.95
63	93% Sand + 2% slag + 5% bentonite	2S5B	10	100	0.95
64	91% Sand + 4% slag + 5% bentonite	4S5B	10	100	0.95
65	89% Sand + 6% slag + 5% bentonite	6S5B	10	100	0.95
66	95% Sand + 2% slag + 3% kaolinite	2S3K	10	100	0.95
67	95% Sand + 2% slag + 3% kaolinite	2S3K	50	100	0.95

No.	Materials	Symbol	Relative density (%)	Confining pressure (kPa)	B value
68	95% Sand + 2% slag + 3% kaolinite	2S3K	90	100	0.95
69	93% Sand + 4% slag + 3% kaolinite	4S3K	10	100	0.95
70	91% Sand + 6% slag + 3% kaolinite	6S3K	10	100	0.95
71	91% Sand + 6% slag + 3% kaolinite	6S3K	50	100	0.95
72	93% Sand + 2% slag + 5% kaolinite	2S5K	10	100	0.95
73	93% Sand + 2% slag + 5% kaolinite	2S5K	50	100	0.95
74	91% Sand + 4% slag + 5% kaolinite	4S5K	10	100	0.95
75	89% Sand + 6% slag + 5% kaolinite	6S5K	10	100	0.95

# Chapter 4: Static Liquefaction Behaviour of Sand–Fines Mixtures

## 4.1 Introduction

The liquefaction behaviour of sandy soil is affected by many factors among which are the relative density, confining pressure, degree of saturation, soil fabric, consolidation stress type, and fines content. The concentration on the effect of the relative density (void ratio) and the mean effective stress has led to the development of some basic concepts such as structural collapse (Alarcon-Guzman et al., 1988) and instability (Lade, 1992). However, as mentioned in the literature review chapter, controversial results have been reported on the effect of fines on the liquefaction behaviour of sandy soil. Therefore, the main objective of this chapter is to discuss the effect of fines on the liquefaction susceptibility of sandy soil by using a logically organised testing program. The investigation emphasised on the effect of the fines type and the fines content on the liquefaction behaviour of sandy soil. In the first stage, the undrained static triaxial tests were conducted on saturated clean sand samples for a range of relative densities and confining pressures to determine the effect of the initial state on the liquefaction behaviour of sandy soils. The influence of the degree of saturation on the liquefaction behaviour of clean sandy soil was also investigated in the first stage by conducting undrained static triaxial tests on partially saturated samples. Moreover, the results of clean sand samples provided adequate details to explain the normal and reverse behaviours of sandy soils. The following investigations were performed to examine the effect of fines on the liquefaction susceptibility of sandy soils. In these experiments, the effect of three slag contents, two bentonite contents, and two kaolinite contents were investigated. The results were also used to investigate the effect of the clay type on the liquefaction susceptibility of sandy soil under static shearing.

## 4.2 Static liquefaction behaviour of clean sand

### 4.2.1 Effect of confining pressure

The undrained test results of very loose clean sand ( $D_{ri}$  10%) are presented in Figures 4.1 and 4.2. They are labelled CS1, CS2 and CS3, and sheared at the initial confining pressure  $\dot{p}_o$  of 100, 150, and 200 kPa. The test results are summarised in Table 4.1.

Table 4.1 Results of undrained tests conducted on clean sand samples

<i>Test name</i>	$\dot{p}_o$	$B$	$D_{ri}$	$e_{cs}$	$q_{peak}$	$R_u$	$q_{min}/q_{peak}$	$I_B$	$\eta$	$\Psi_o$
<i>CS1</i>	100	0.95	10	0.660	6.990	1.000	0.000	1.000	0.129	0.0035
<i>CS2</i>	150	0.95	10	0.656	9.090	0.933	0.346	0.654	0.140	0.0045
<i>CS3</i>	200	0.95	10	0.653	19.000	0.800	0.642	0.358	0.174	0.0055
<i>CS4</i>	100	0.95	50	0.609	40.650	0.630	0.880	0.120	0.751	0.0008
<i>CS5</i>	150	0.95	50	0.608	63.940	0.560	0.852	0.148	0.673	0.0015
<i>CS6</i>	200	0.95	50	0.607	84.590	0.460	0.828	0.172	0.636	0.0022
<i>CS7</i>	100	0.95	90	0.5573	170.000	0.336	0.994	0.006	0.941	-0.0001
<i>CS8</i>	150	0.95	90	0.5575	266.000	0.137	0.992	0.008	0.909	-0.0003
<i>CS9</i>	200	0.95	90	0.5575	358.000	0.059	0.989	0.011	0.875	-0.0004
<i>CS10</i>	100	0.5	10	0.6607	21.200	0.720	0.565	0.435	0.372	0.0008
<i>CS11</i>	100	0.25	10	0.6605	30.000	0.440	0.797	0.203	0.405	0.0010

The stress–strain relationships are illustrated in Figure 4.1(a) as  $q$  versus  $\varepsilon_a$  in which  $q$  is the deviatoric stress =  $\sigma_1 - \sigma_3$  and  $\varepsilon_a$  is axial strain. The effective stress paths (ESPs) for the tests are shown in Figure 4.1(b); they are plotted on the Cambridge  $\dot{p}$ – $q$  space, in which  $\dot{p}$  is the mean effective stress =  $(\sigma'_1 + 2\sigma'_3)/3$ . The stress–strain relationships shown in Figure 4.1(a) indicated that the three samples under the three confining pressures showed flow liquefaction behaviours characterised by a rapid reduction in the deviatoric stress that occurred after reaching the peak deviatoric stress  $q_{peak}$ , obtained in general at small axial strain. The reduction in the deviatoric stress continued until the minimum deviatoric stress  $q_{min}$  was reached under the steady state SS condition. Figure 4.1(a) also demonstrated that the reduction in the deviatoric stress reduced with increasing confining pressure. This was indicated by the increasing values of  $q_{min}$  obtained under SS condition relative to  $q_{peak}$ . The  $q_{min}$  value in the CS1 test increased from zero to 4.97 kPa and to 12.2 kPa in the CS2 and CS3 tests when the initial confining pressure increased to 150 kPa and 200 kPa, respectively. The ESPs

of the CS1 to CS3 tests are shown in Figure 4.1(b). This figure shows that the ESPs for the three tests plummeted toward the origin of the  $q$ - $p'$  space after achieving their particular peak deviatoric stress, which indicated the flow liquefaction behaviour.

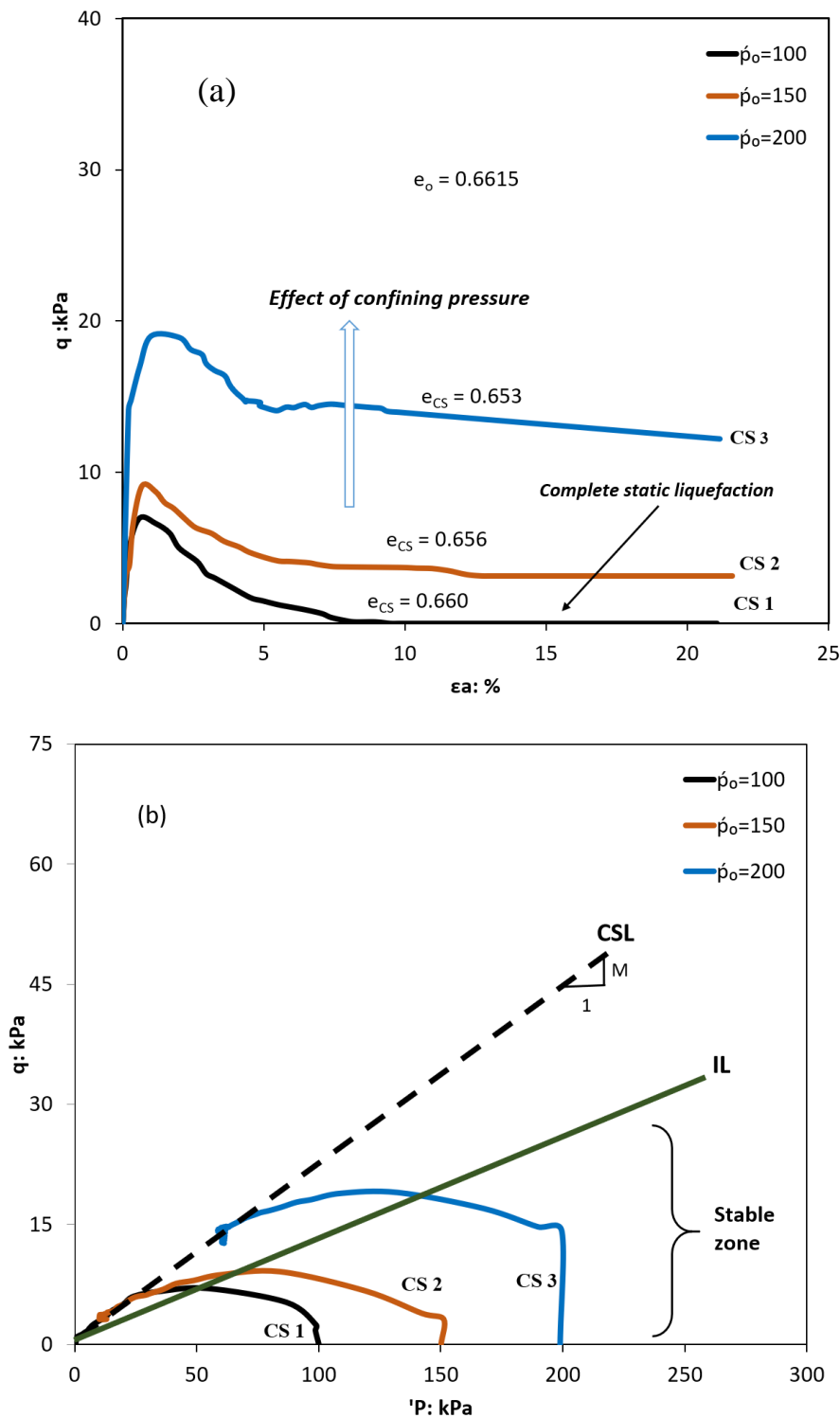


Figure 4.1 Undrained behaviour of very loose clean sand samples: (a) stress–strain relationships and (b) effective stress paths

Previous studies on the undrained monotonic triaxial compression tests showed that the position of the maximum deviator stress of different ESPs at different initial confining pressures with the same initial state fell onto one line called the instability line (IL) or the flow liquefaction line (FLL), which intersected the origin of the  $q$ - $p'$  space as shown in Figure 4.1(b). IL can be used as a state boundary between the stable and the unstable behaviours of soils, in which all the areas under the IL can be considered the stable zone, while the areas above the IL can be considered the unstable zone (Jafarian, Ghorbani, et al., 2013; Leong et al., 2000; Yamamuro & Lade, 1997b). Under undrained conditions, soil instability may occur in the area between the IL and the critical state line (CSL) (Yamamuro & Lade, 1997b). The CSL in the  $p'$ - $q$  stress path can be defined as a straight line which connects the origin and the points when the soil reaches the critical state. In the case of critical-state soils concept, the relationship between the deviatoric stress  $q$  and the effective mean principal pressure  $p'$  can be written as follows:

$$q_{CSL} = M \times p'_{CSL} \quad (4.1)$$

where  $q_{CSL}$  and  $p'_{CSL}$  are the deviatoric stress and the mean effective stress at the critical state, respectively, and  $M$  is the slope of the CSL. According to Schofield and Wroth (1968), Equation (4.1) can be reformulated for the triaxial test cases as follows:

$$\sin \phi_s = \frac{(3 \times M)}{(6 + M)} \quad (4.2)$$

where  $\phi_s$  is the mobilised internal friction angle at the critical state.

The relationships between the axial strain and the normalised effective stress ( $\sigma'_3/p'_0$ ) and the pore water pressure ratio ( $R_u$ ) are shown in Figures 4.2(a) and (b), respectively. The pore water pressure ratio is the ratio of the excess pore water pressure ( $U_{excess}$ ) to the initial confining pressure  $p'_0$ ; the flow behaviour is associated with the positive value of  $R_u$ , and complete static liquefaction is associated with the unity value of  $R_u$ . However, the non-flow behaviour is associated with the negative values of  $R_u$ . The liquefaction behaviour was accompanied by abrupt increases in the pore water pressure ratio  $R_u$  and a sharp reduction in the effective stress  $\sigma'_3$ , as shown in Figures 4.2(a) and (b).

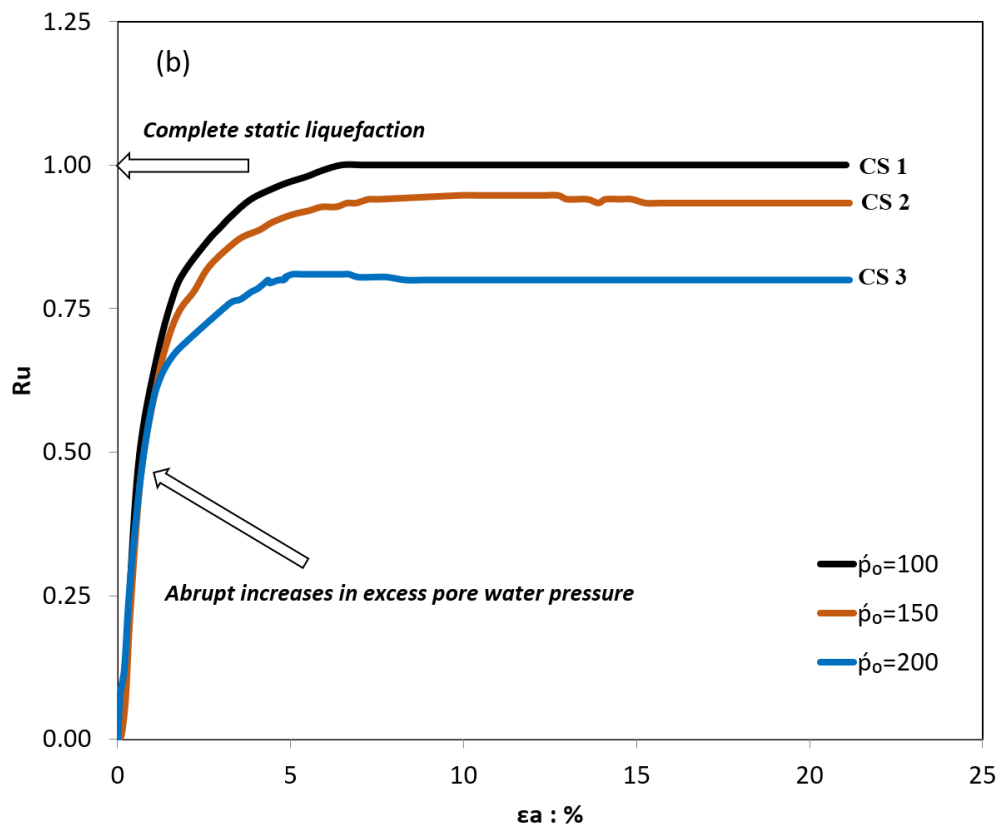
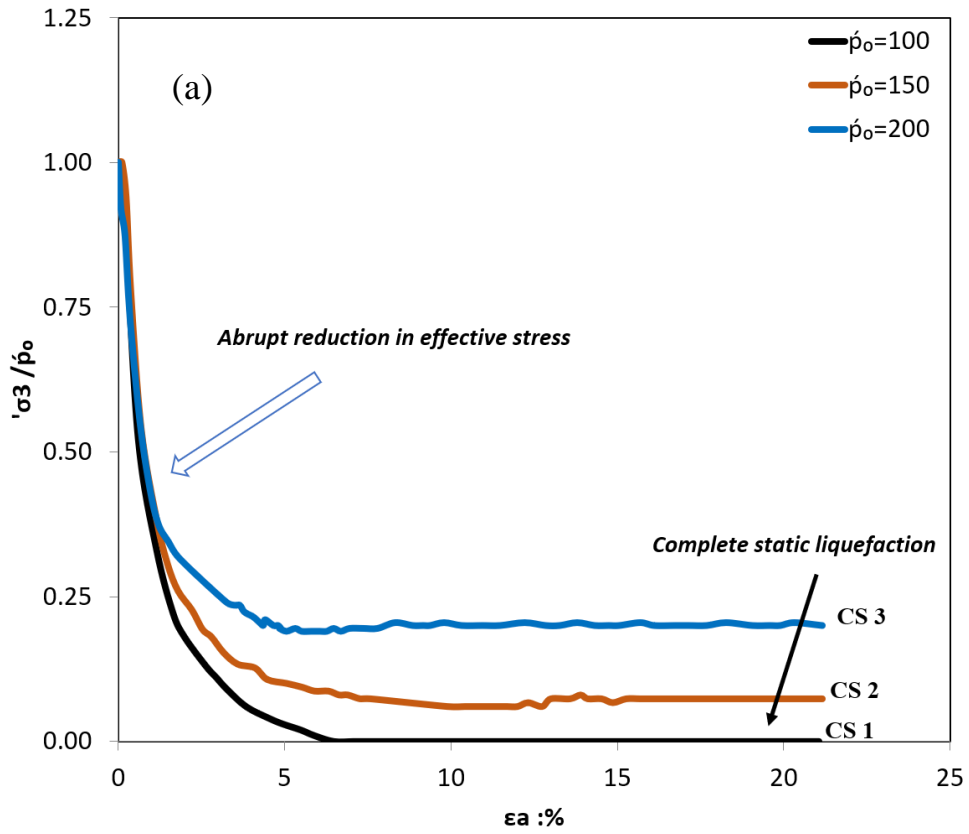


Figure 4.2 Undrained behaviour of very loose clean sand samples: (a) effective stress ratio vs. axial strain and (b) pore water pressure ratios vs. axial strain



From the data shown in Figure 4.2(a), it is apparent that the effective stress of the CS1–CS3 tests rapidly decreased from the initial value at the commencement of the shear to the minimum values obtained at the small axial strain. Figure 4.2(b) shows the pore water pressure variation in the CS1, CS2, and CS3 tests; it is represented as  $R_u - \varepsilon_a$ . Furthermore, Figure 4.2(b) shows that all the samples showed abrupt increases in the pore water pressure at a small axial strain with a positive value of  $R_u$ . Figure 4.2(b) also shows that the  $R_u$  decreased with an increase in the confining pressure.  $R_u$  decreased from 1 at the confining pressure of 100 kPa to 0.93 and 0.8 when the confining pressure increased to 150 and 200 kPa, respectively. The pore water pressure of these three tests remained constant under loading conditions after the samples reached  $q_{min}$ , which satisfied the SS condition. Figures 4.1 and 4.2 show that the CS1 test conducted at the lowest initial confining pressure (100 kPa) exhibited complete static liquefaction behaviour. The term ‘complete static liquefaction’ can be defined as follows:

$$(\sigma_1 - \sigma_3 = 0) \text{ and } (\sigma'_3 = 0) \quad (4-3)$$

The sample exhibited zero effective stress and zero deviatoric stress when the excess pore water pressure was equal to the initial confining pressure  $p'_o$  at this point the soil liquefied as a liquid. Figure 4.1(a) shows that the CS1 test showed a sharp reduction in the deviatoric stress after reaching the peak value at small  $\varepsilon_a < 0.5\%$ . The sharp reduction in  $q$  continued until the zero value was reached at  $\varepsilon_a$  (8.2%). The decreases in  $q$  were accompanied with the rapid development in the pore water pressure ratio  $R_u$ , which reached unity at the same  $\varepsilon_a$  for  $q_{peak}$ , as shown in Figure 4.2(b). This result was consistent with the findings of Ishihara (1993); Riemer, Seed, Nicholson, and Jong (1990); Yamamuro and Lade (1997b), who reported that the very loose sandy soil was liquefied at a low confining pressure of 100 kPa or less. Static liquefaction was accompanied with the generation of large wrinkles in the membrane surrounding the specimens (Figure 4.3); this is indicative of a uniform pattern of internal deformations (Lade, 1992; Yamamuro & Lade, 1997b). A marked feature of the CS1–CS3 tests was that the peak deviatoric stress increased and the excess pore water pressure ( $U_{excess}$ ) decreased with increasing initial confining pressure  $p'_o$ . Figure 4.1(a) shows that the peak deviatoric stress  $q_{peak}$  of the tests at  $p'_o$  of 150 kPa and 200 kPa was greater than

the  $q_{peak}$  at 100 kPa. Furthermore,  $q_{peak}$  increased from 6.99 kPa at  $p'_o$  of 100 kPa to 11.84 and 19 kPa when  $p'_o$  increased to 150 and 200 kPa, respectively.

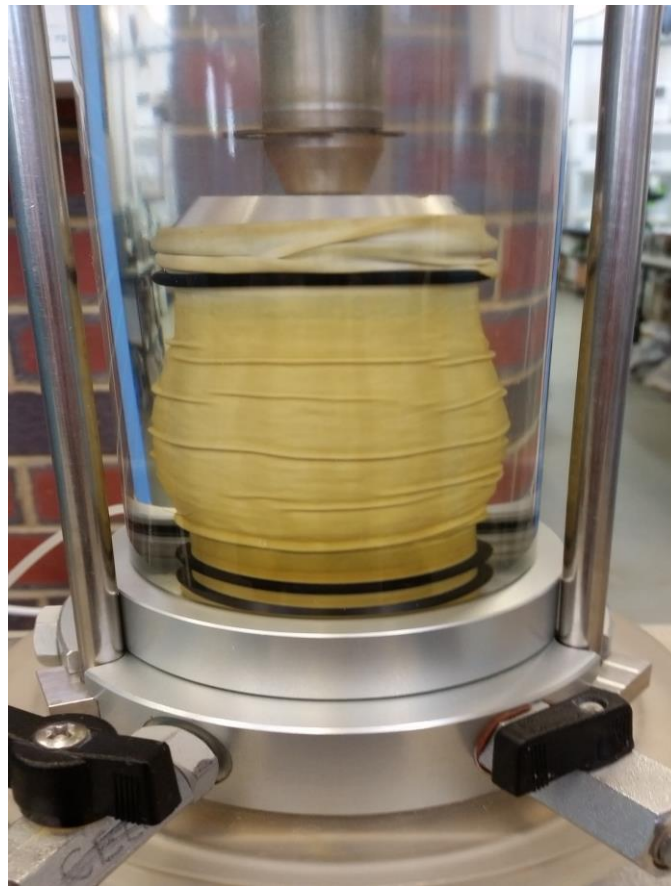


Figure 4.3 Wrinkles in the membrane surrounding the sample during static liquefaction

After the peak value was achieved, the excess pore water pressure of CS2 and CS3 tests reached a value lower than the initial confining pressure and the sample exhibited constant pore water pressure and constant strength as  $q_{min}$  did not reach zero, which satisfied the SS conditions. Moreover, the higher the confining pressure was, the more rapidly was the excess pore water pressure generated (Figure 4.4). Figure 4.2(a) shows that the effective confining pressure rapidly decreased from the initial value at the commencement of shear. Testing at an initial confining pressure of 100 kPa approached the minimum values ( $\sigma'_3 = 0$ ) at 6.5% axial strain because of the tendency of very loose cohesionless materials to compress, which reduced the effective stress and increased the excess pore water pressure. However, samples at confining pressures of 150 and 200 kPa approached the minimum values ( $\sigma'_3 \neq 0$ ) at axial strains of 8%

and 10%, respectively. This was related to the increases in the effective stress and decreases in the excess pore water pressure after increases in the initial confining pressure.

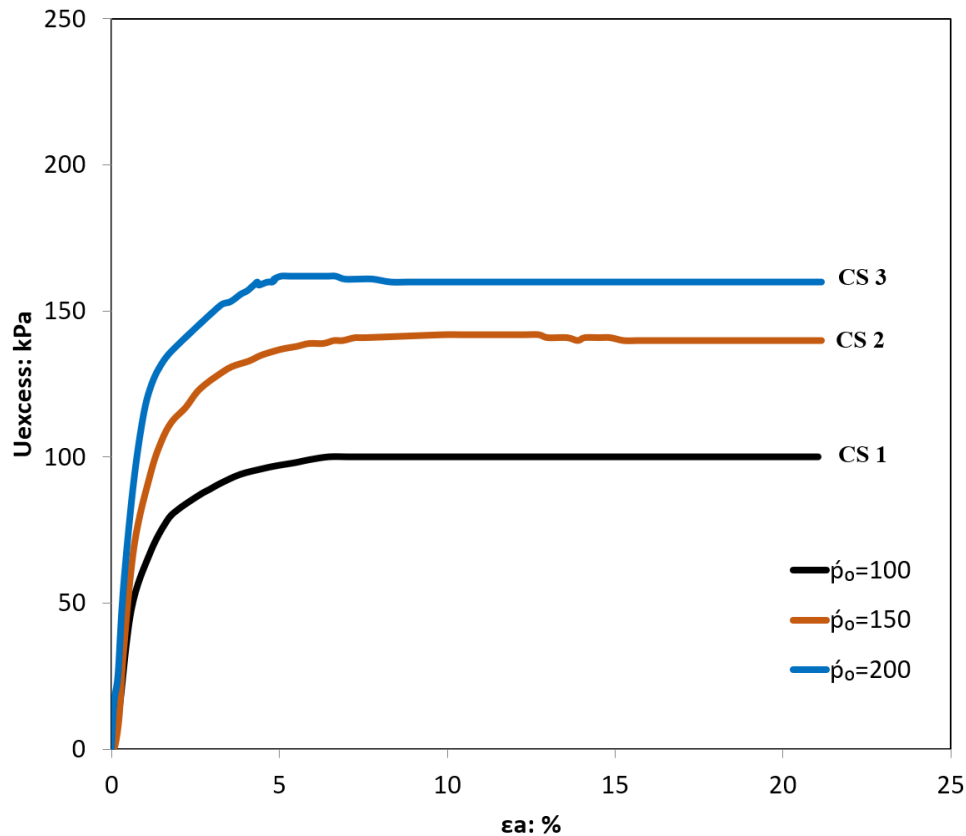


Figure 4.4 Excess pore water pressures of very loose clean sand samples tested at different initial confining pressures

The effect of the confining pressure on the liquefaction behaviour of sandy soils can also be observed by drawing the relationship between the ratio of the minimum deviator stress to the peak deviator stress ( $q_{min}/q_{peak}$ ) and the initial confining pressure. As shown in Figure 4.5, this relationship could be used to show the confining pressure at which liquefaction took place. The  $q_{min}/q_{peak}$  ratio of 0 represented complete static liquefaction, and a ratio of 1 implied a non-flow response. Figure 4.5 shows that the ratio of  $q_{min}/q_{peak}$  was zero at an initial confining pressure of 100 kPa, indicating complete static liquefaction. The ratio then increased at the initial confining pressures of 150 and 200 kPa, indicating that the specimens exhibited flow behaviour with less liquefaction susceptibility. Moreover, Figure 4.5 shows insignificant differences

between the deviator stress ratio and the initial confining pressure in the present study and the previous studies. This was compared with the findings of a previous study conducted on very loose Nevada sand ( $D_r = 12\%$ ) at various initial confining pressures in the range of 25–150 kPa (Yamamuro & Lade, 1997b).

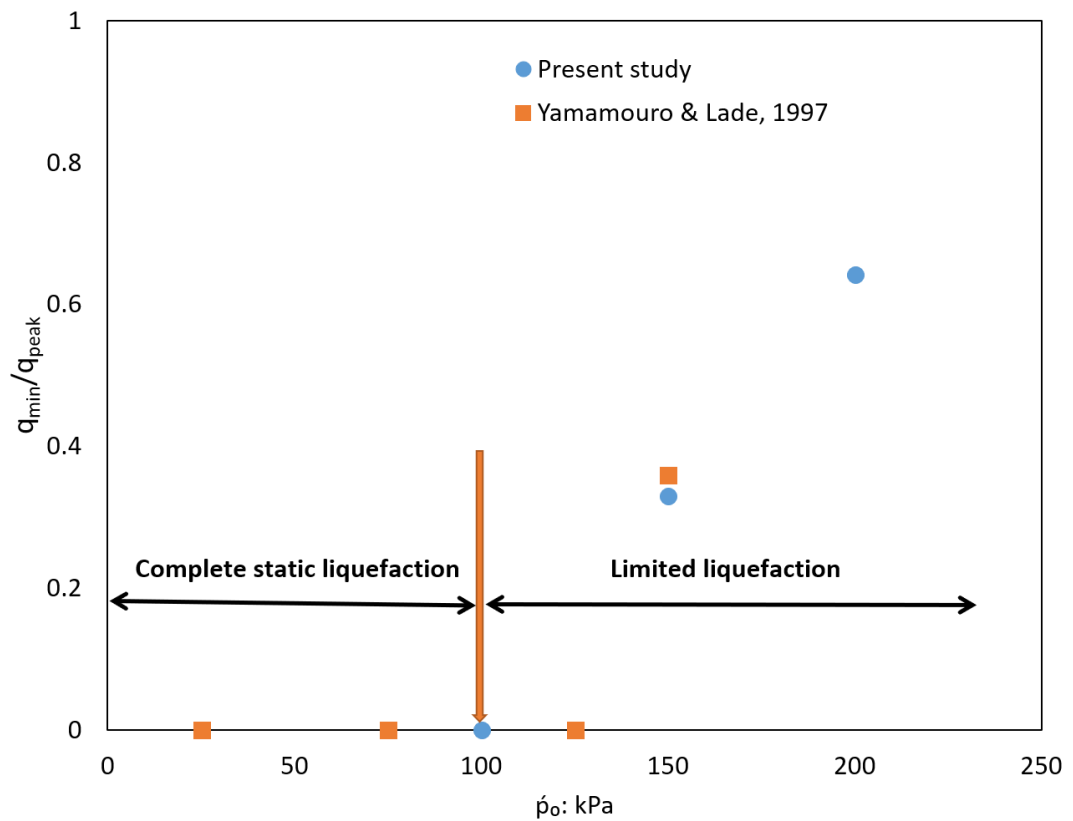


Figure 4.5 Stress ratio ( $q_{min}/q_{peak}$ ) vs. initial confining pressure of very loose clean sand

The effect of the initial confining pressure on the behaviour of very loose C.S samples can be considered anomalous or reverse behaviour. The term ‘*anomalous*’ is used here to describe the behaviour of very loose samples when the shear strength increased with increasing confining pressure. In contrast, normal behaviour is where the strength of the samples decreased with increasing confining pressure, as reported in many previous studies (Alarcon-Guzman et al., 1988; Vaid & Chern, 1985). According to (Yamamuro & Covert, 2001; Yamamuro & Lade, 1997b), the main reasons for the

‘reverse’ behaviour of C.S are related to the densification of samples during their consolidation, because of the rapid decreases in the sample compressibility with increasing initial confining pressure. The reduction in compressibility indicates better contact between the sand particles, which then produces high soil fabric stiffness. Consequently, the excess pore water pressure decreases. The effect of densification during consolidation was observed when the post-consolidation void ratio ( $e_{cs}$ ) decreased with increasing initial confining pressure. The void ratio reduced from the initial value of 0.6615 to 0.660, 0.656, and 0.653 at confining pressures of 100, 150, and 200 kPa, respectively, as shown in Figure 4.6. Kramer and Seed (1988) found that the liquefaction resistance which is defined as the undrained shear strength required to initiate static liquefaction increased with the increasing initial state values (i.e. relative density and initial confining pressure), which agreed well with the results of the present study.

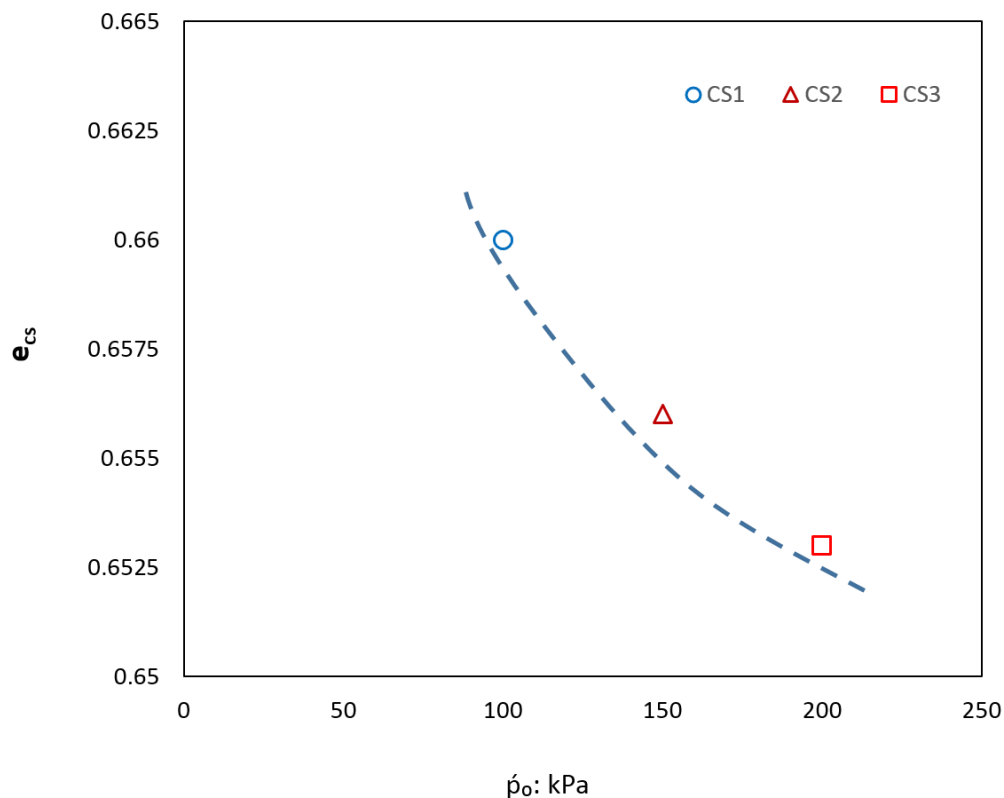
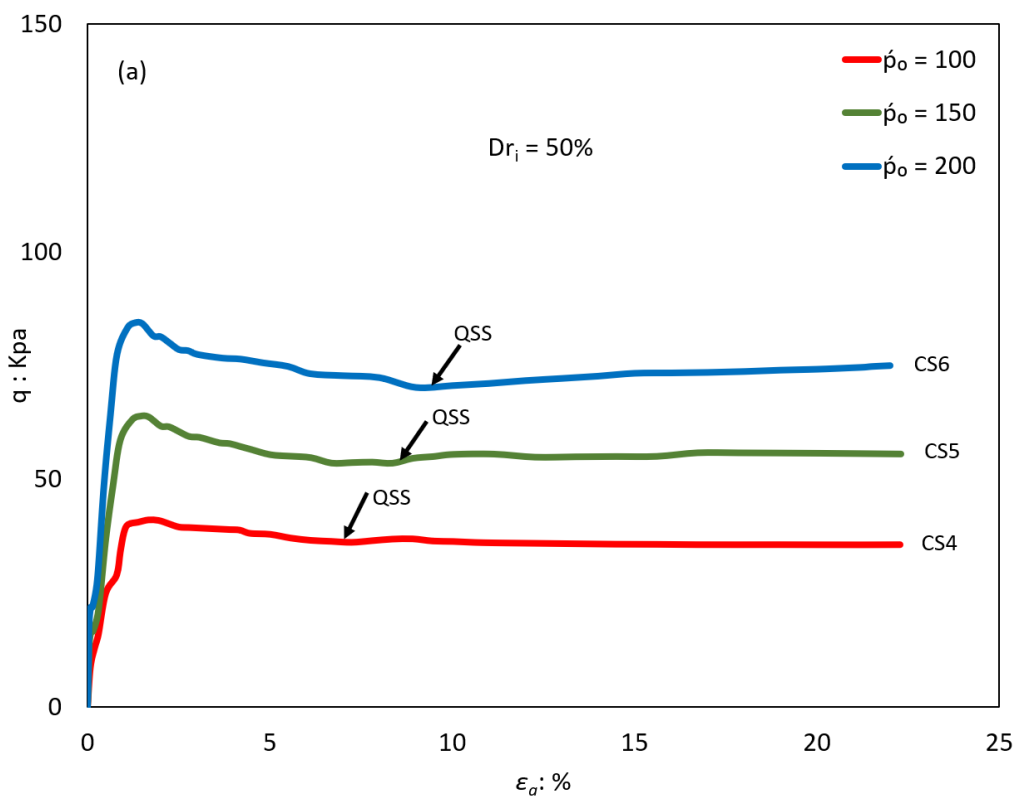


Figure 4.6 Post-consolidation void ratio of very loose clean sandy soil sheared at three initial confining pressures.

## 4.2.2 Effect of relative density

The influence of the increases in the relative density on the liquefaction behaviour of clean sand was examined by conducting undrained static compression triaxial tests on saturated clean Perth sand with initial relative densities of 10%, 50%, and 90%. The results of the three isotropically consolidated undrained triaxial tests CS4, CS5, and CS6 at a relative density of 50% with shearing commencing from the initial confining pressure  $\dot{p}_o$  of 100, 150, and 200 kPa, respectively, are presented in Figures 4.7(a)–(c). Figures 4.7(a) and (b) show that the stress–strain curves and the effective stress paths consisted of three sections, initially tracing toward of the peak deviatoric stress  $q_{peak}$ , then plummeting to the transient minimum value referred to as the quasi-steady state (*QSS*) (Figure 4.7 (a)) after attaining  $q_{peak}$ , and finally bending slightly upwards toward a higher mean stress. This behaviour called limited liquefaction was associated with a reduction in the excess pore water pressure after attaining peak value, as shown in Figure 4.7(c). The  $q_{peak}$  and deviatoric stresses at *QSS* increased with increasing  $\dot{p}_o$ . Furthermore,  $q_{peak}$  increased from 40.65 kPa at  $\dot{p}_o$  of 100 kPa to 63.94 and 84.41 kPa when  $\dot{p}_o$  increased to 150 and 200 kPa, respectively. Figure 4.7(c) also shows that the three tests showed a positive excess pore water pressure ratio  $R_u$  and its value decreased with increasing  $\dot{p}_o$ . Tests for  $D_{ri}$  90% are labelled CS7, CS8, and CS9 and sheared at the initial confining pressure  $\dot{p}_o$  of 100, 150, and 200 kPa, respectively, as shown in Figure 4.8. In Figures 4.8(a) and (b), the three tests exhibited more pronounced non-flow behaviour than the CS1–CS6 tests. This indicated a consistent behavioural trend in that the liquefaction tendency decreased with an increase in the relative density. For the CS7–CS9 tests, the change in the pore water pressure was negative toward the end of the tests. Furthermore, the CS7–CS9 tests exhibited an initial peak in the excess pore water pressure ratio  $R_u$  followed by rapid reduction until the end of the test. Luong (1980) defined the point of start of the reduction in the excess pore water pressure as the characterisation threshold (*CT*), as shown in Figure 4.8(c). The value of *CT* reduced with increasing initial confining pressure, and CS9 exhibited a relatively high negative  $R_u$  value. The abovementioned behavioural trend of  $D_{ri}$  50% and  $D_{ri}$  90% indicated that the deviatoric stresses increased and the pore water pressure ratios decreased with increasing initial confining pressure. The undrained behaviour of 10% relative density was compared with that of 50% and 90% relative density, as shown in Figures 4.9 and 4.10. The undrained shear of all the tests commenced from

the same effective stress state defined by  $p'_o = 100$  kPa. The comparison was made at this initial confining pressure because the samples showed complete static liquefaction at this confining pressure. The relationship of stress versus strain and the stress paths are shown in Figures 4.9 (a)–(c). Figure 4.9(a) shows that the behaviour of the samples transferred from complete static liquefaction to no-flow behaviour when the relative density increased from 10% to 90%. The value of the deviatoric stress at the end of the tests increased from 0 kPa at the relative density of 10% to 35.68 kPa and 170 kPa when the relative density increased to 50% and 90%, respectively.



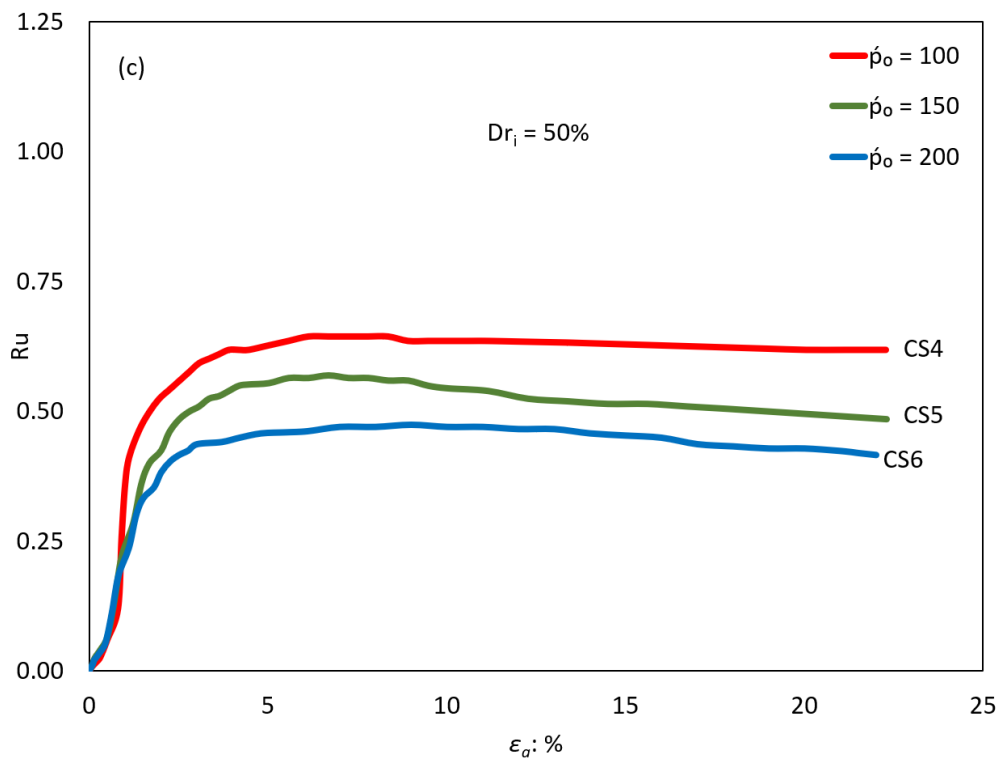
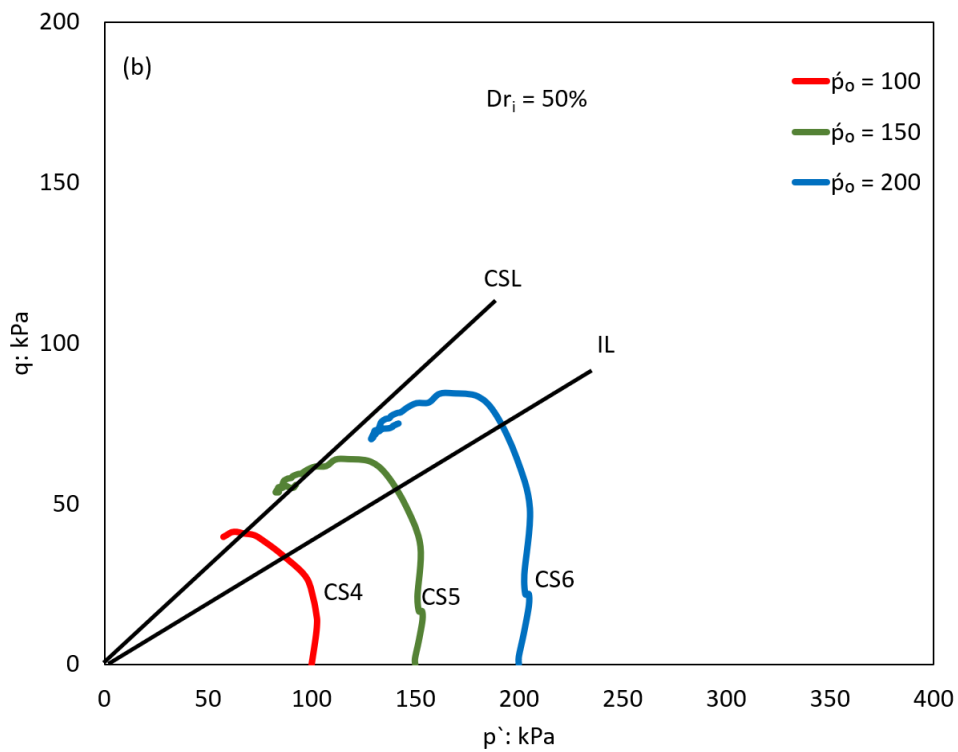
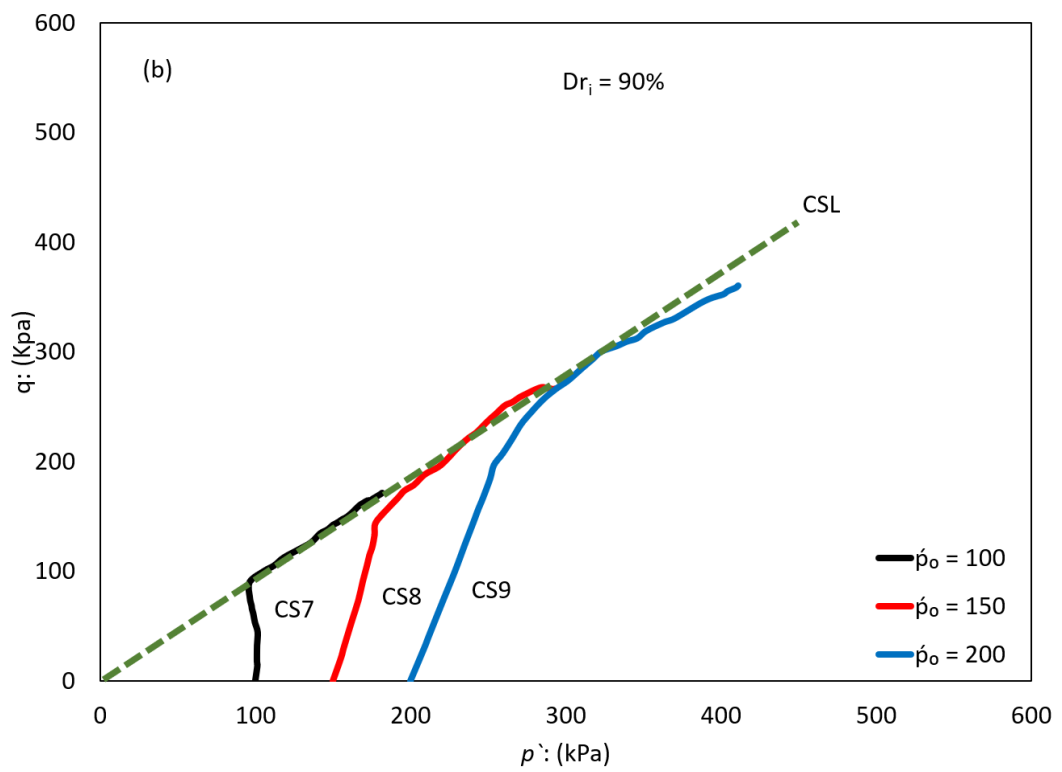
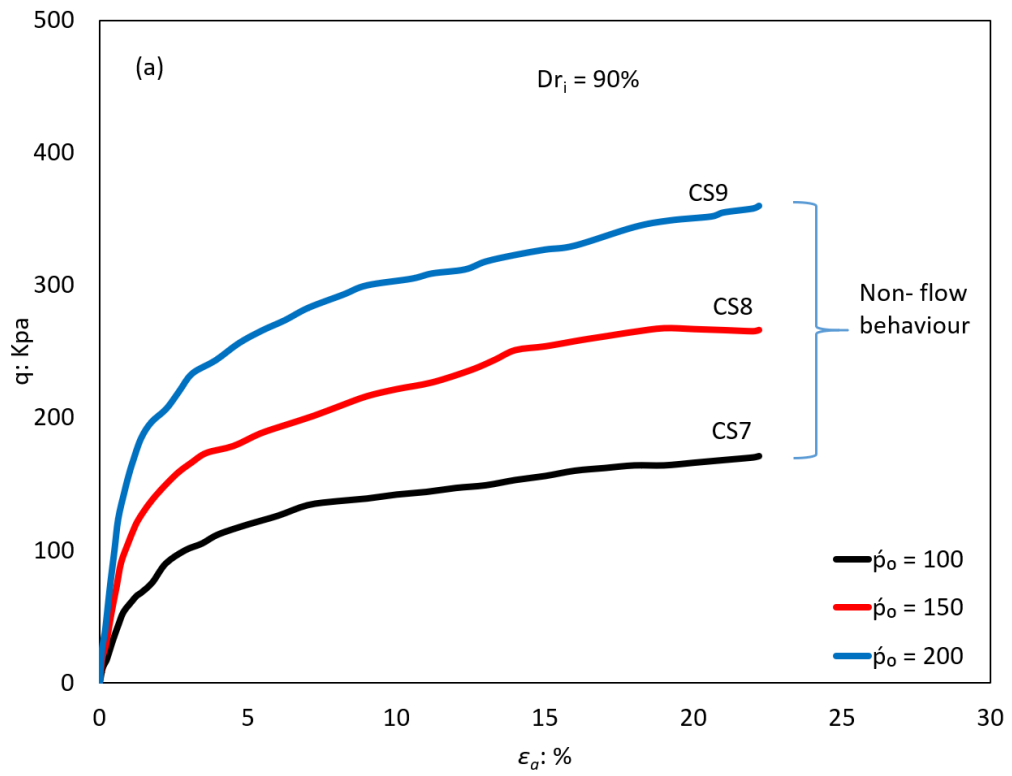


Figure 4.7 Undrained behaviour of medium ( $D_{r_i}$  50%) clean sand at three confining pressures: (a) stress–strain relationships, (b) effective stress paths, and (c) pore water pressure ratios vs. axial strain



Figure 4.9(b) shows that the effective stress path of the samples increased with the increasing relative density of the samples. The effective stress path of the sample at  $D_{ri}$  10% plummeted to the origin after reaching the initial peak deviatoric stress. The sample at  $D_{ri}$  50% showed a reduction in the deviatoric stress after attaining the initial peak value; then, the deviatoric stress increased with further shearing beyond the minimum value to the steady state. However, the dense sample ( $D_{ri}$  90%) showed strain hardening behaviour throughout the loading characterised by the abrupt increases in the deviatoric stress, but the sample did not reach the steady state at the end of the test. The slope of the effective stress paths ( $M$  value) increased with increasing relative density, which indicated that the shear strength of the samples increased with an increase in the relative density. The  $M$  value increased from 0.22 at a relative density of 10% to 0.73 and 0.97 when  $D_{ri}$  increased to 50% and 90%, respectively, as shown in Figure 4.9(c). Figures 4.10 (a) and (b) show a clear trend of increasing effective stress and decreasing excess pore water pressure with increasing relative density. Figures 4.10(a) and (b) show that at the relative density of 10%, the effective stress was dramatically reduced (indicating complete static liquefaction) upon sudden increases in the excess pore water pressure, until it matched the initial confining pressure ( $R_u = 1$ ) at a very low axial stress. However, at a relative density of 50%, the effective stress gradually decreased with slow increases in the excess pore water pressure and then increased as the excess pore water pressure decreased with shearing, indicating limited liquefaction. When the relative density increased to 90%, the sample exhibited abrupt increases in the effective stress with an abrupt reduction in the excess pore water pressure after reaching the initial peak. The reduction in the excess pore water pressure was continued until negative values were reached at the end of the test. The results of the present study were consistent with the findings of Yamamuro and Lade (1997), who reported that the Nevada sand completely liquefied at a very low relative density of 12%, while the samples exhibited limited liquefaction and completely stable behaviour after the relative densities increased. Verdugo and Ishihara (1996) and Sivathayalan and Vaid (2004) also found that the contractive behaviour of sandy soils was associated with low relative densities. However, dilative behaviour was associated with high relative densities, and the effect of confining pressure decreased with increasing relative density.



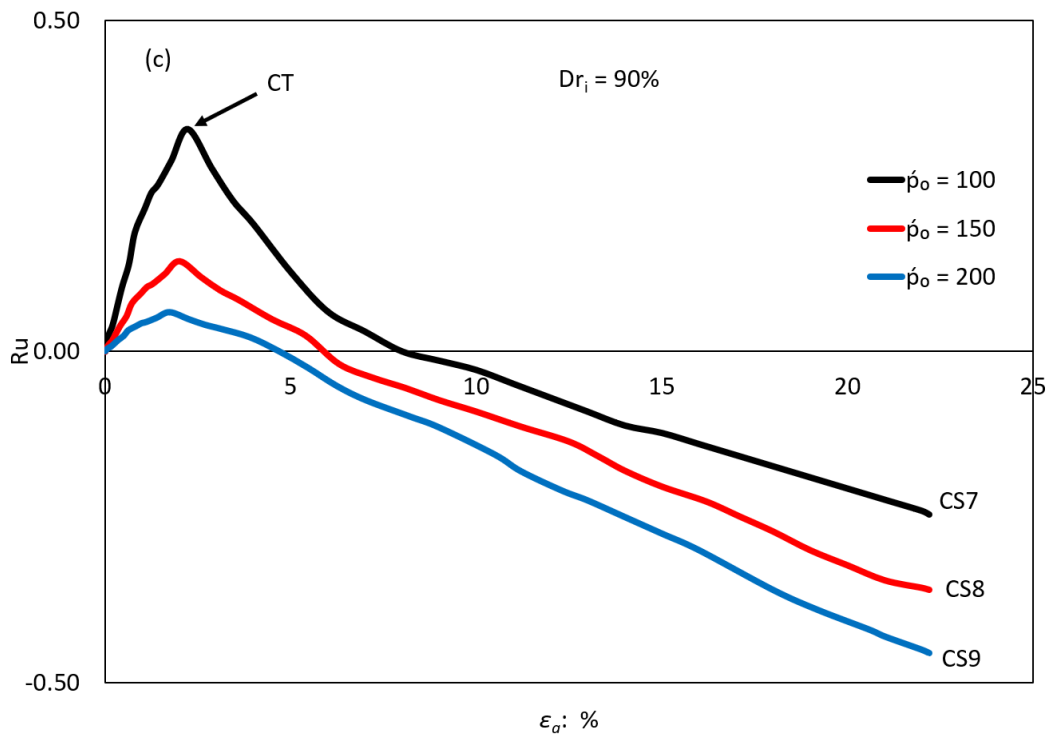
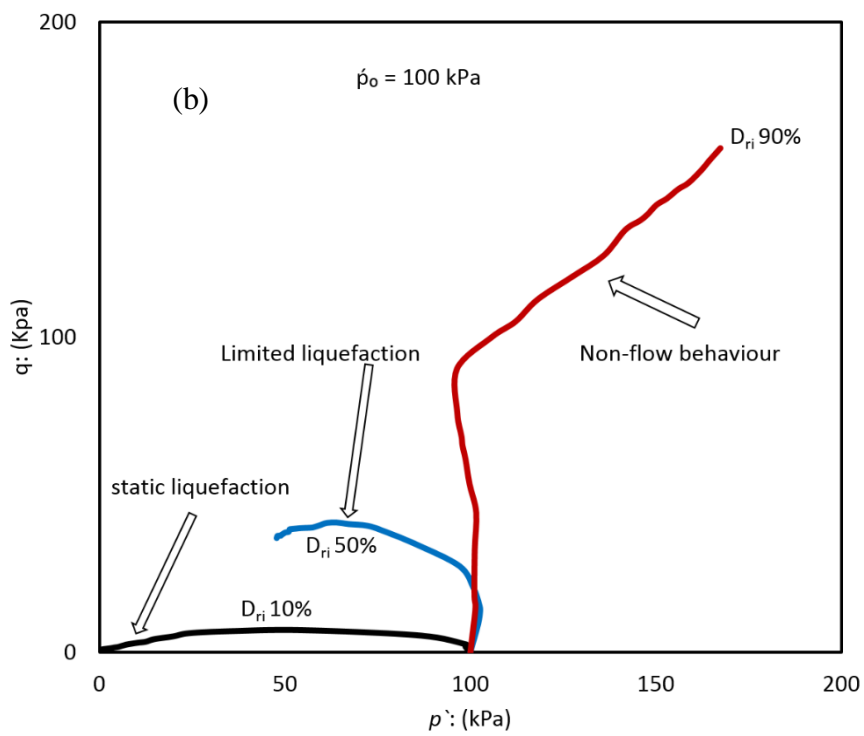
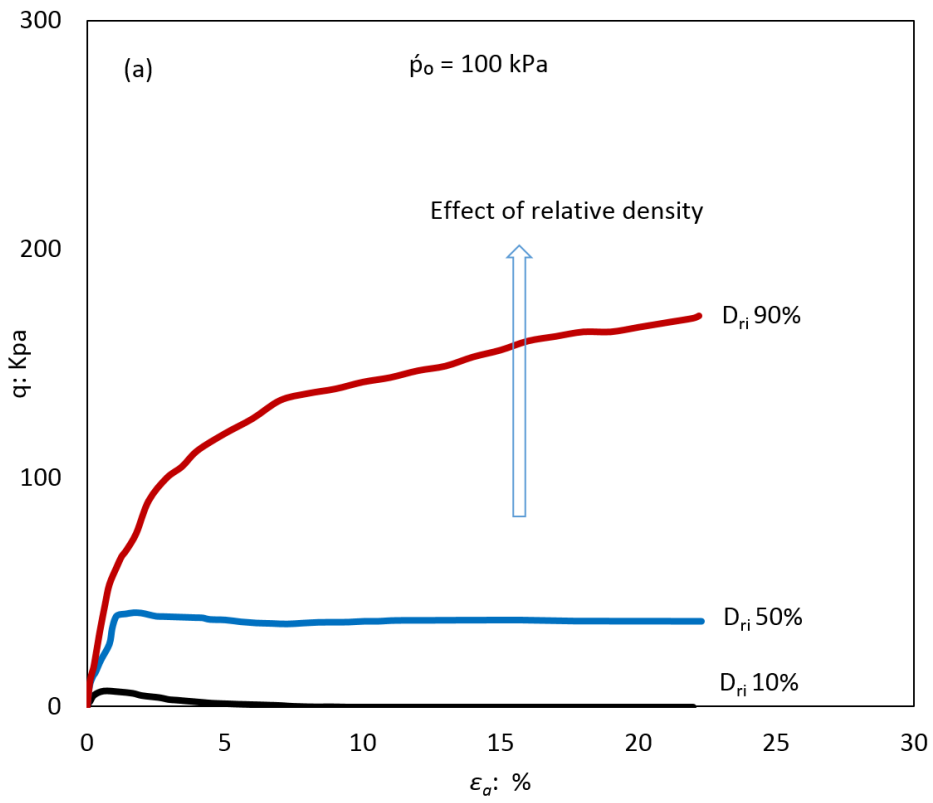


Figure 4.8 Undrained behaviour of dense ( $D_{ri}$  90%) clean sand at three confining pressures: (a) stress–strain relationships, (b) effective stress paths, and (c) pore water pressure ratios vs. axial strain

The improvement of the shear strength of the samples with increasing relative density could be attributed to the stability of the sand fabric, which improved because of the increases in the inter-particle contact and decreases in the sample compressibility. The relationship between the relative density and the compressibility of the samples was observed when the post-consolidation void ratio decreased with increasing relative density. The post-consolidation void ratio reduced from 0.66 at  $D_{ri}$  10% to 0.609 and 0.556 at  $D_{ri}$  50% and 90%, respectively. The stable sand fabric reduced the rate of the pore water pressure and increased the effective stress, finally producing more stable behaviour.



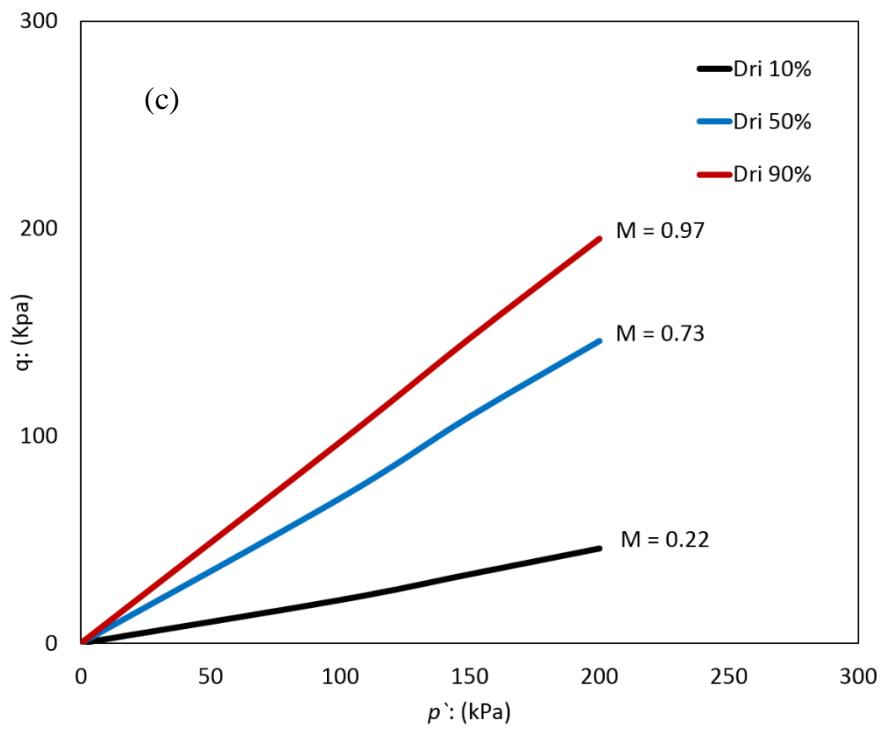
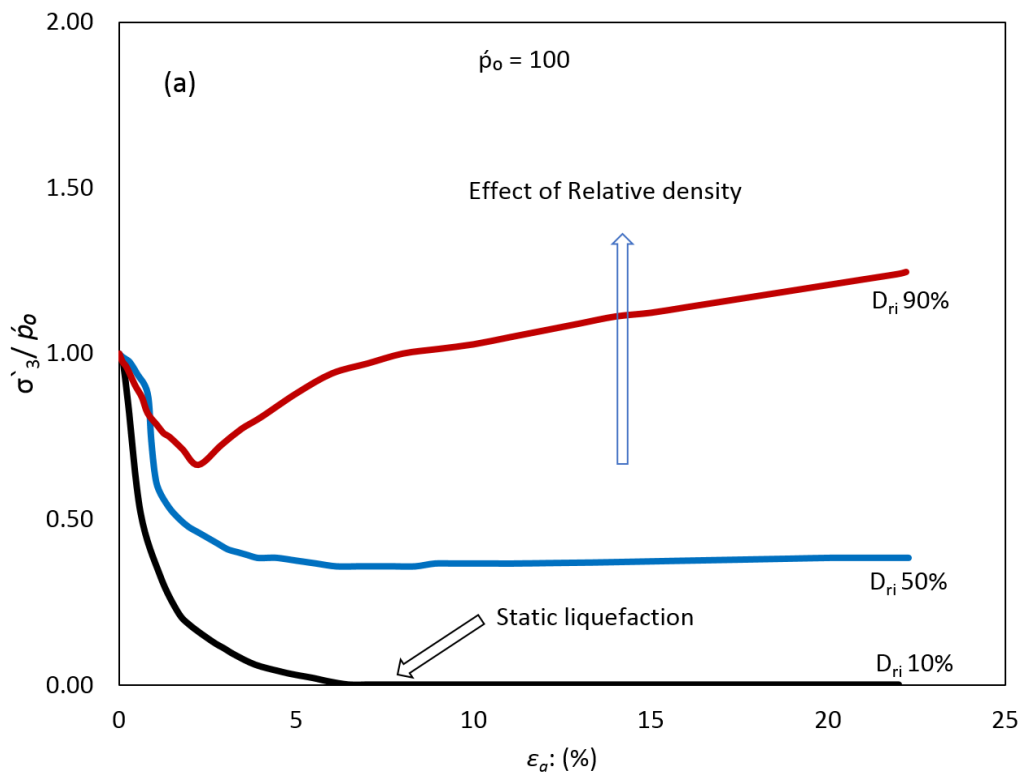


Figure 4.9 Effect of relative density on the undrained behaviour of sandy soil tested at initial confining pressure of 100 kPa: (a) stress–strain relationships, (b) effective stress paths, and (c) slope of effective stress paths.



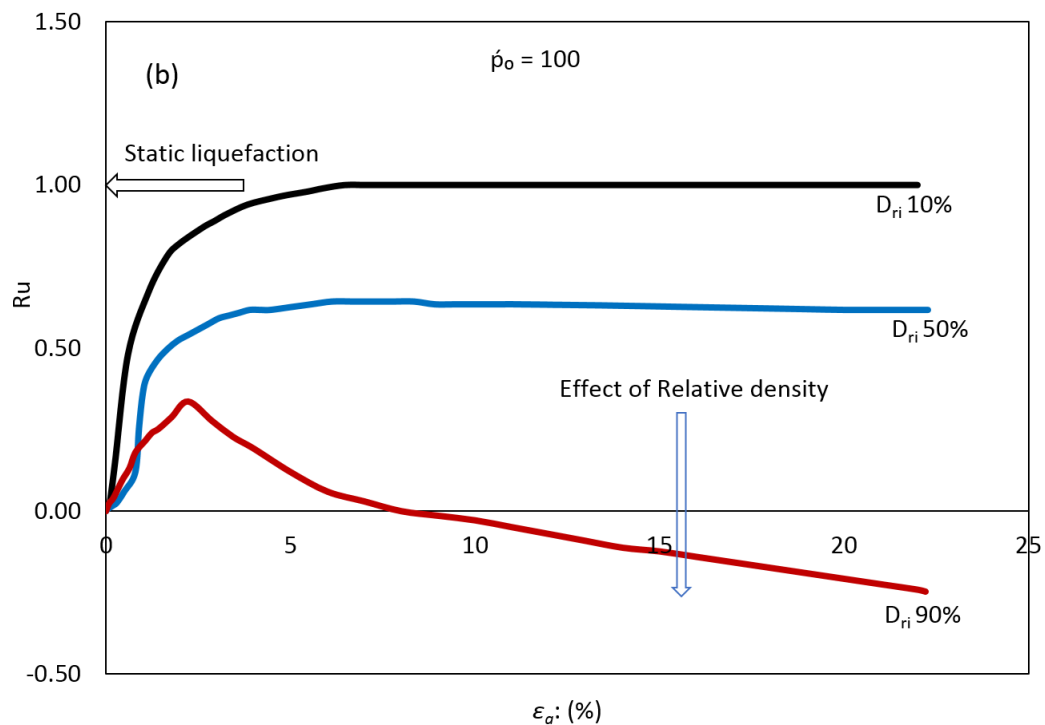
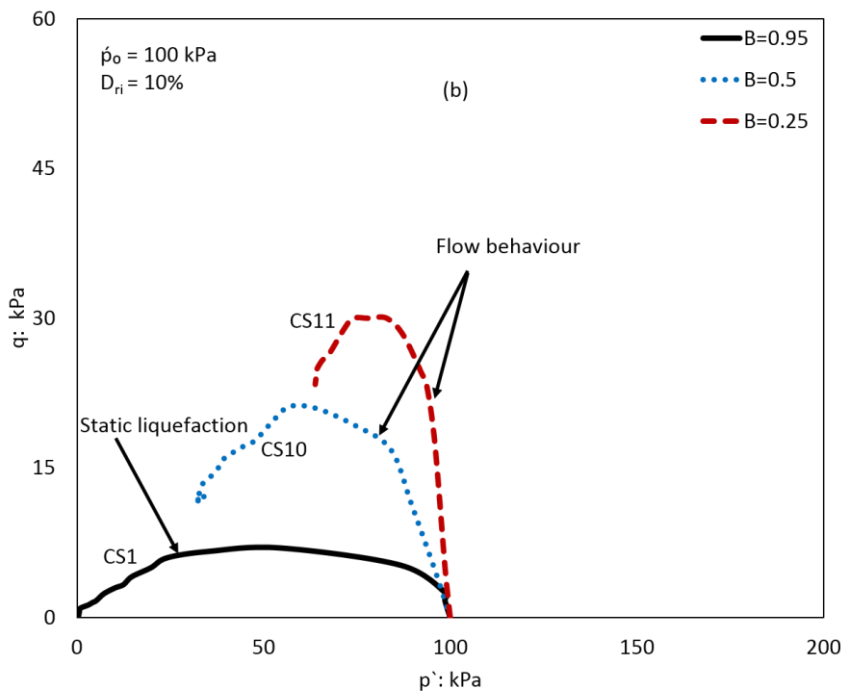
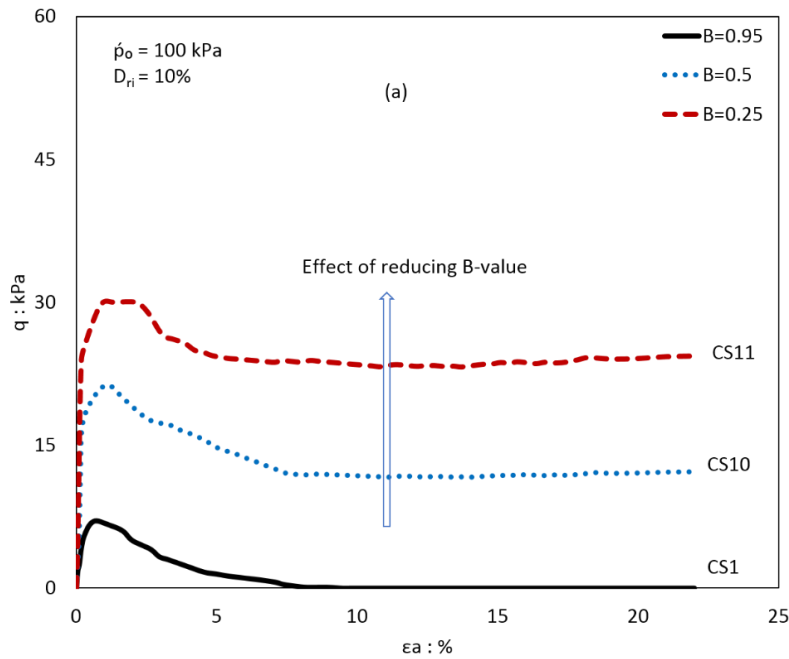


Figure 4.10 Effect of relative density on undrained behaviour of sandy soil tested at initial confining pressure of 100 kPa: (a) effective stress ratio vs. axial strain, and (b) pore water pressure ratio vs. axial strain

### 4.2.3 Static liquefaction behaviour of partially saturated sandy soils

The effect of the degree of saturation on the behaviour of sandy soil was investigated by conducting three monotonic undrained triaxial tests on the loss sand samples ( $D_{ri}$  10%) with shearing commencing at  $p'_o = 100$  kPa. The level of saturation was simulated in these tests by using Skempton's coefficient ( $B$ ). Skempton's coefficient ( $B$ ) can be defined as the ratio between the generated pore water pressures and the applied cell pressure. The samples were considered saturated when the  $B$  value was  $\geq 0.95$ , whereas they were considered partially saturated when the  $B$  values were  $< 0.95$ . Three different Skempton's  $B$  values, namely 0.95, 0.5, and 0.25, were used, and the tests were labelled CS1, CS10, and CS11, respectively. Figure 11(a) shows the stress-strain relationships for the CS1, CS10, and CS11 tests. As can be seen, the three tests showed flow behaviour characterised by a reduction in the deviatoric stress after attaining the initial peak value  $q_{peak}$  and the reduction continued until the minimum

deviatoric  $q_{min}$  stress was reached at the end of the tests. The initial peak value increased with decreasing B values,  $q_{peak}$  increased from 7 kPa at a B value of 0.95 to 21.2 kPa and 30 kPa when the B value decreased to 0.5 and 0.25, respectively. Figure 4.11(a) also shows that the amount of reduction in the deviatoric stress decreased with a decrease in the B value. This was manifested by increasing  $q_{min}$  relative to the peak deviatoric stress.



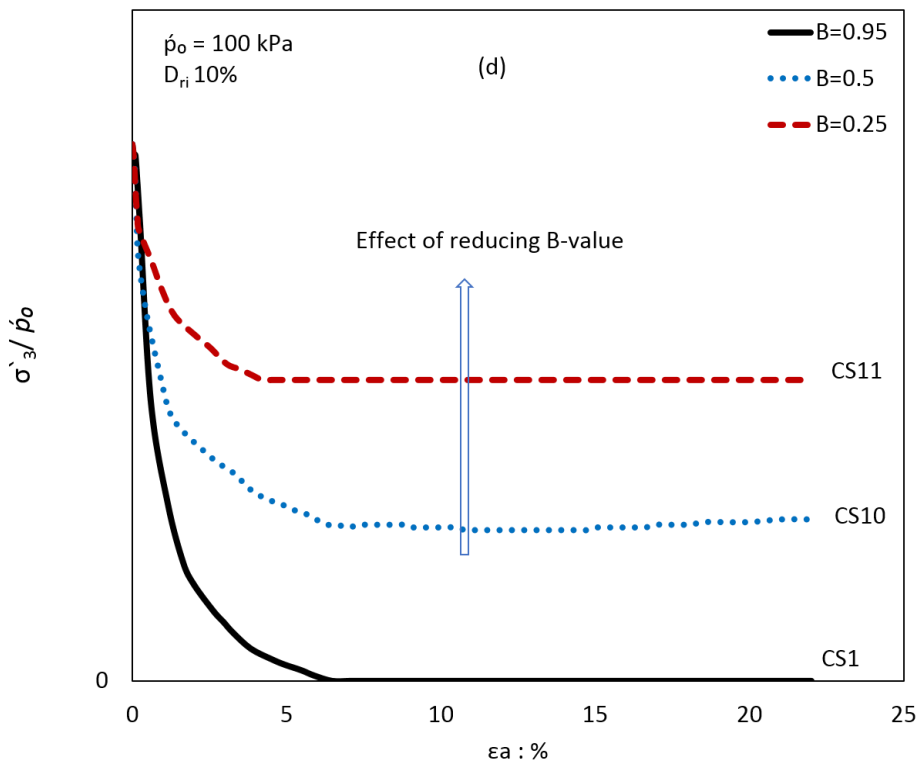
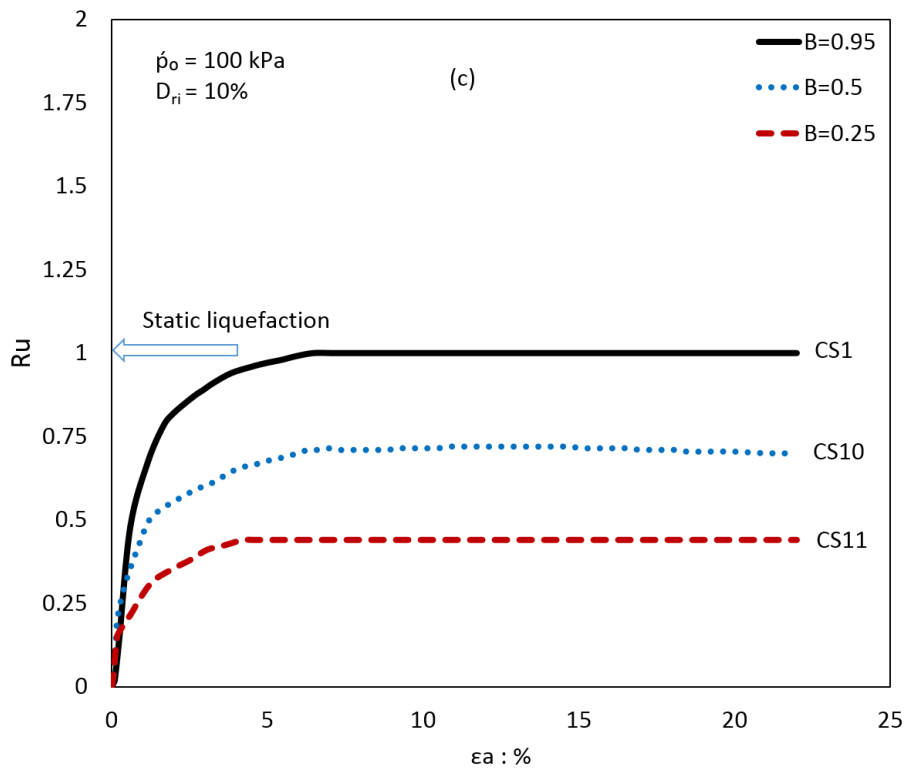


Figure 4.11 Undrained behaviour of partially saturated very loose sandy soil sheared at initial confining pressure of 100 kPa: (a) stress–strain relationships, (b) effective stress paths, (c) pore water pressure ratio vs. axial strain, and (d) effective stress ratio vs. axial strain.



The effective stress paths of the CS1, CS10, and CS11 tests are shown in Figure 4.11(b); here, the three samples showed contractive behaviour when the three effective stress paths plummeted toward the origin of the  $q-p'$  space after reaching their representative  $q_{peak}$  and the slope of effective stress paths increased with a decrease in the  $B$  value, which indicated that the shear strength of soil increased with a decrease in the degree of saturation. This behaviour can also be seen in Figure 4.11(c) wherein all the samples showed a positive excess pore water pressure ratio ( $R_u$ ) and its value increased with an increase in the  $B$  value due to an increase in the pore water pressure.  $R_u$  was 1, 0.7, and 0.4 at the  $B$  values of 0.95, 0.5, and 0.25, respectively. Samples with a  $B$  value of 0.95 showed complete static liquefaction, and their stress difference reached zero. However, samples with  $B$  values of 0.25 and 0.5 exhibited more resistance to liquefaction, as shown in Figures 4.11(a) and (b). Note from Figure 4.11(a) that the undrained tests CS1, CS10 and CS11 reached the steady state SS at a constant excess pore water pressure. However, the value of the axial strain at the steady state decreased with a decrease in the  $B$  value. In Figures 4.11(c) and 5(d), a clear dramatic increase in the generation rate of the pore water pressure and an abrupt decrease in the effective confining pressure at a low strain with  $B = 0.95$  were observed. In contrast, a gradual increase in the rate of the pore water pressure generation and a gradual decrease in the effective confining pressure with a decrease in the  $B$  value were observed. These findings were consistent with those of previous studies in that the liquefaction resistance increased with a decrease in the degree of saturation ( $B$  value), because of the pore water pressure generation in partially saturated samples was lower than that in the fully saturated samples (Delia, 2010; Ishihara et al., 2001; Yang et al., 2004). The generated pore water pressure in the partially saturated samples was lower than that in the fully saturated samples; this could be attributed to the presence of a compressible gas which hindered the development of pore water pressure. Consequently, the instability of the samples reduced with a decrease in the degree of saturation (Pradel & Lade, 1990; Yang et al., 2004).

#### 4.2.4 Liquefaction susceptibility of fully saturated sandy soil

The literature on the liquefaction susceptibility of cohesionless soils has highlighted several techniques, such as experimental, theoretical, and empirical methods, for assessing the ability of a soil to liquefy (Ishihara, 1993; Sadrekarimi, 2014c; Vaid & Sivathayalan, 2000; Yamamuro & Lade, 1997b). Many parameters have been reported in the literature to evaluate the liquefaction susceptibility of soils, such as the brittleness index, liquefaction potential, state parameter, relative contractiveness, and stress ratio (minimum deviator stress  $q_{min}$  to initial peak deviator stress  $q_{peak}$ ). The shear strength of liquefied soil  $Su_{(LIQ)}$  and the yield strength  $Su_{(yield)}$  have been used in several studies to determine the loss in the undrained strength which could occur in sandy soils under undrained conditions. The peak undrained shear strength is represented by  $Su_{(yield)}$ , and  $Su_{(LIQ)}$  represents the residual undrained shear strength. Many techniques, such as laboratory shear tests, numerical analyses including those using constitutive models, and field penetration tests, are available to calculate  $Su_{(yield)}$ , the peak undrained shear strength of sandy soil (Sadrekarimi, 2014c). The  $Su_{(yield)}$  value is considerably dependent on mineralogy, gradation, structure, soil mixing effects, and sample disturbance. Several researchers have developed techniques for estimating the shear strength and the shear strength of liquefied soils (Ishihara, 1993; Olson & Stark, 2003; Poulos et al., 1985). These scholars have defined procedures for calculating the  $Su_{(yield)}$  and  $Su_{(LIQ)}$  values of liquefied soils, as follows:

$$Su_{(yield)} = q_{peak}/2 \quad (4-1)$$

$$Su_{(LIQ)} = q_{min}/2 \times \cos \phi_s \quad (4-2)$$

where  $q_{peak}$  is the initial peak deviatoric stress and  $q_{min}$  is the minimum deviatoric stress, as shown in Figure 4.12.

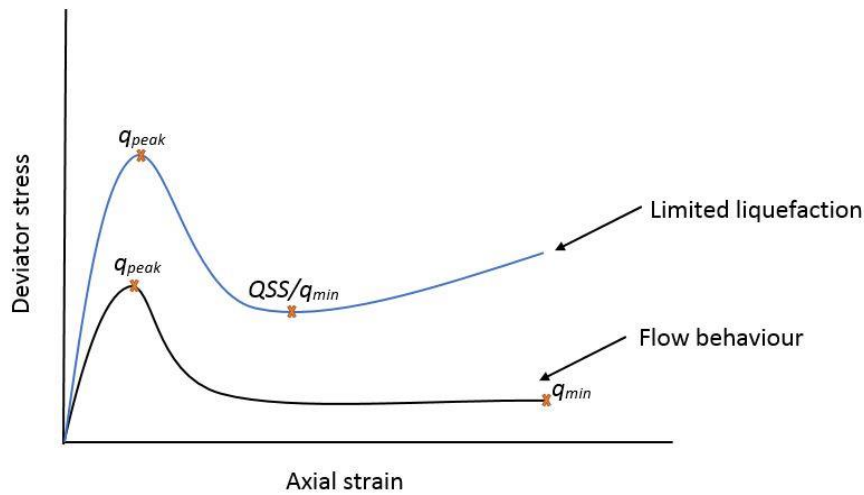


Figure 4.12 Types of liquefaction behaviours of soils

The initial peak deviatoric stress and the minimum deviatoric stress have also been used in the previous studies to measure the magnitude of the decline in the undrained shear strength that occurred following the initiation of static liquefaction. The amount of shear strength lost beyond liquefaction has a significant effect on its consequences (Kramer & Seed, 1988). During liquefaction, the soil element achieved  $q_{peak}$  at a very low strain, and then,  $q_{peak}$  decreased until it reached the minimum deviatoric stress ( $q_{min}$ ). Some of the undrained triaxial static tests showed an increase in the deviatoric stress toward the end of the test after a reduction in the peak deviatoric stress. In this case, the minimum values of the deviatoric stress (occurring after its drop but before its increase) are denoted as QSS (see Figure 4.12) (Ishihara, 1993; Yoshimine et al., 1999). Flow failure may occur when the decline from the peak to the minimum deviatoric stress is considerable. The normalisation between  $q_{peak}$  and  $q_{min}$ , as proposed by Bishop (1971) and used by Sadrekarimi (2014c) and others, was adopted in the present study to analyse the liquefaction susceptibility of clean sandy soils and sand–fines mixtures. The amount of reduction in the undrained shear strength during liquefaction is usually characterised by the undrained brittleness index,  $I_B$ , as shown below (Bishop, 1971):

$$I_B = \frac{q_{peak} - q_{min}}{q_{peak}} \quad (4-3)$$

The values of  $I_B$  are in the range of 0–1, and non-flow or non-brittle behaviour (where a non-strength decline occurs during undrained static shear) is observed when  $I_B = 0$ . However, brittle soil behaviour or complete static liquefaction is associated with  $I_B = 1$ . The brittleness index can also be expressed as follows:

$$\frac{q_{peak} - q_{min}}{q_{min}} = 1 - \frac{q_{min}}{q_{peak}} \quad (4-4)$$

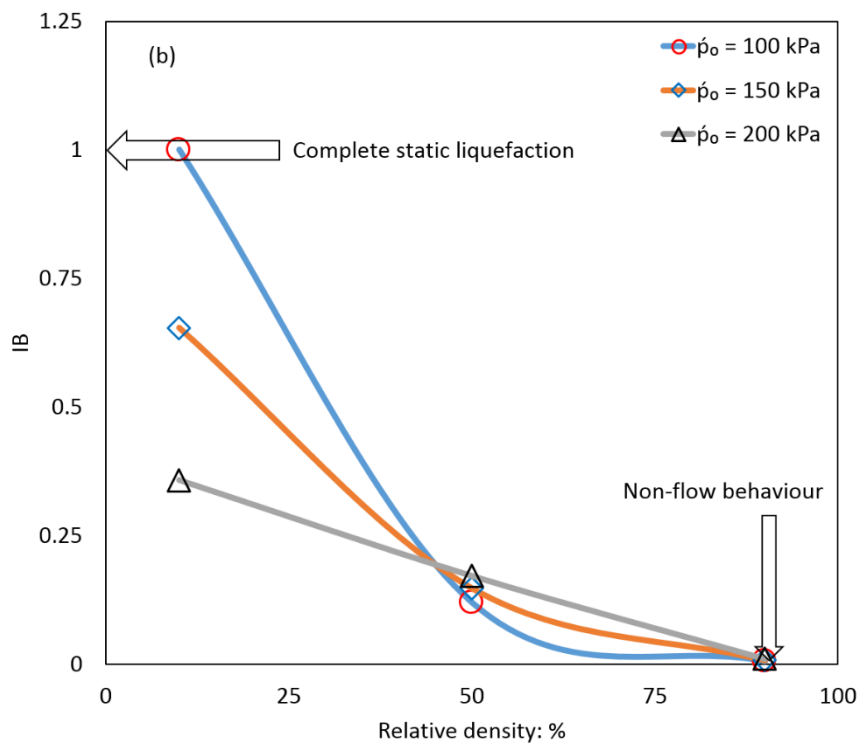
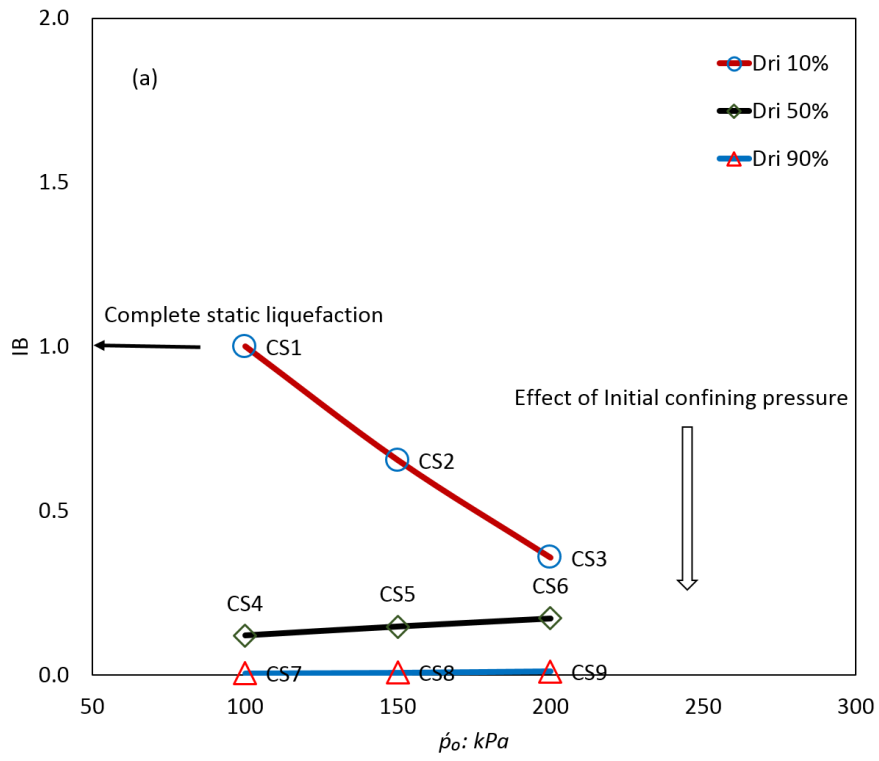
The stress ratio defined as the ratio of the minimum deviatoric stress to the initial peak deviatoric stress ( $q_{min}/q_{peak}$ ) has also been used in the present study to evaluate the liquefaction susceptibility of clean sandy soils and sand–fines mixtures. The stress ratio can also be used to evaluate the liquefaction susceptibility of soils. Complete static liquefaction is associated with a  $q_{min}/q_{peak}$  ratio of zero. Non-flow behaviour is associated with a  $q_{min}/q_{peak}$  ratio of 1 (Ishihara, 1993; Lade & Yamamuro, 2011; Yamamuro & Lade, 1997b). Many previous studies have reported that the instability line (IL) or flow liquefaction line (FLL) can be used to differentiate between the stable and the unstable behaviours of sandy soils. Yang (2002) stated that the flow liquefaction line is dependent on the state parameter. Therefore, this section presents the relationship of liquefaction susceptibility with the instability line and the state parameter. The relationship between liquefaction susceptibility and the instability line was deeply investigated by considering the relationships between  $I_B$  and the stress ratio at the instability line  $\eta$  ( $q_{peak}/p'$ ); here,  $p'$  is the mean effective stress related to the peak deviatoric stress. However, the state parameter at the start of the test ( $\Psi_0$ ) was considered to present the relationship between liquefaction susceptibility and the state parameter. The relationships of the brittleness index  $I_B$  versus the initial confining pressure  $p'_0$  and the brittleness index  $I_B$  versus the relative density  $D_{ri}$  are shown in Figures 4.13(a) and (b), respectively. Figure 4.13(a) shows that the liquefaction susceptibility of very loose samples ( $D_{ri}$  10%) reduced with increasing  $p'_0$ , and  $I_B$  reduced from 1 at  $p'_0 = 100$  kPa to 0.358 when  $p'_0$  increased to 200 kPa. However, the medium-to-dense samples ( $D_{ri}$  50%) and the dense samples ( $D_{ri}$  90%) exhibited a slight increase in  $I_B$  with an increase in  $p'_0$ . The  $I_B$  value of the medium-to-dense samples ( $D_{ri}$  50%) increased from 0.148 at  $p'_0 = 150$  kPa to 0.172 when  $p'_0$  increased to 200 kPa. Figure 4.13(b) shows a clear trend of the significant decrease in  $I_B$  when the relative density increased to 50% and 90%. The behaviour of the sample tested at

$D_{ri}$  10% and  $p'_o = 100$  kPa (CS1 test) changed from complete static liquefaction  $I_B = 1$  to limited liquefaction  $I_B = 0.12$  and non-flow behaviour  $I_B \approx 0$  when the relative density increased to 50% and 90%, respectively, when tested at the same  $p'_o$ . Note that in Figures 4.13(a) and (b), all the tests (CS1–CS9) showed two different behaviours when tested under different relative densities and initial confining pressures. The first one was observed in tests CS1–CS3 conducted at  $D_{ri}$  10%; this behaviour was characterised by the decrease in the liquefaction susceptibility with an increase in the initial confining pressure. This behaviour is called ‘reverse behaviour’ and has been reported in many previous studies (Yamamuro & Lade, 1997b). The second one is called ‘normal behaviour’ and was observed in tests CS4–CS6 conducted at  $D_{ri}$  50% and in tests CS7–CS9 conducted at  $D_{ri}$  90%. The normal behaviour was characterised by a slight increase in the liquefaction susceptibility with an increase in the initial confining pressure. This difference in behaviours with the increasing relative density may prove that the occurrence of reverse behaviour is associated with a low relative density, but an increase in the relative density shifts the behaviour from reverse to normal. Furthermore, the results showed that the undrained behaviour of clean sandy soil was dominated more by the relative density than by the initial confining pressure. Figure 4.13(c) presents the relationship between the brittleness index  $I_B$  and the pore water pressure ratio  $R_u$  ( $R_u = U_{excess}/p'_o$ ). As shown in this figure, the brittleness index  $I_B$  was significantly reduced by the reducing pore water pressure ratio, and the samples prepared at a high relative density ( $D_{ri}$  90%) showed the lowest  $I_B$  and  $R_u$ . Figure 4.13(c) also shows a good correlation between the brittleness index and the pore water pressure ratio; further,  $I_B$  can be computed by using the following equation:

$$I_B = 0.0046 e^{5.42 R_u} \quad (4-5)$$

where  $e$  is the mathematical constant

Although the liquefaction susceptibility of the medium and dense samples increased slightly when the relative density increased; it was still lower than the liquefaction susceptibility of very loose samples.



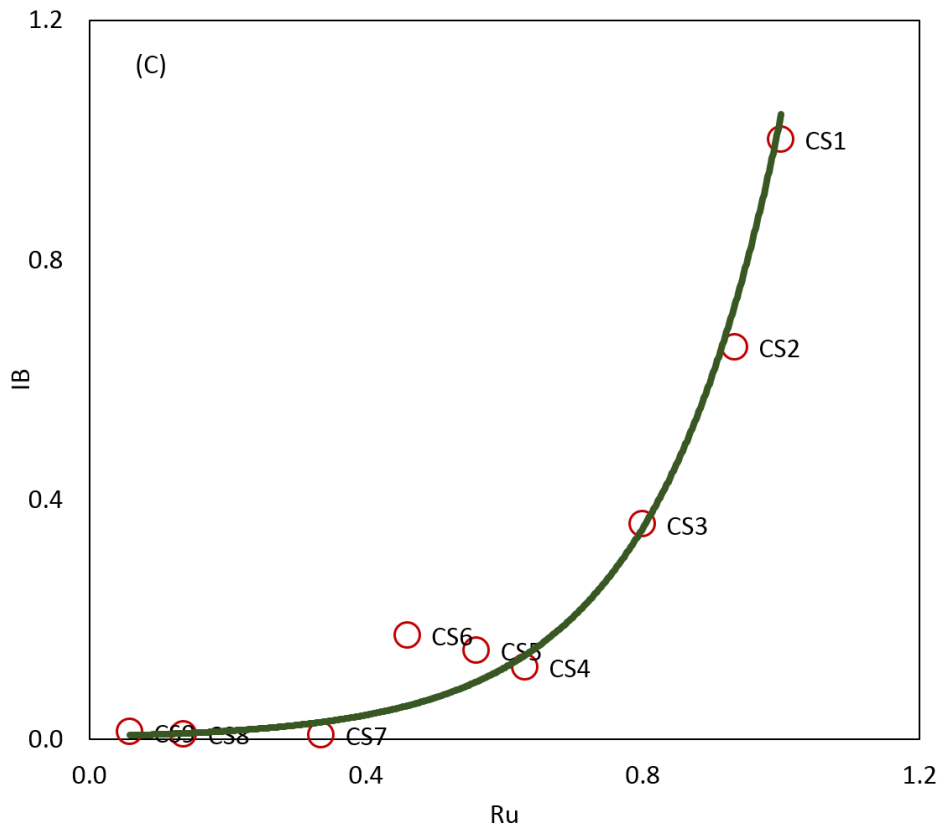


Figure 4.13 Liquefaction susceptibility of clean sandy soil prepared at different relative densities and tested at three initial confining pressures: (a) brittleness index vs. initial confining pressure, (b) brittleness index vs. relative density, and (c) brittleness index vs. pore water pressure ratio

Therefore, the relative density had a positive effect on the behaviour of sandy soils by reducing the liquefaction susceptibility which could reduce the negative consequences of liquefaction on geotechnical applications. A possible explanation for the positive effect of the relative density might be the soil fabric which may change from unstable fabric with a high void ratio at a low relative density to stable fabric with a low void ratio at a high relative density. At a high relative density, the spaces between the sand particles become narrow, which increases the contact between the particles and hinders the generation of the pore water pressure. Consequently, the liquefaction susceptibility is decreased. This view was supported by Vaid and Sivathayalan (2000); Verdugo and Ishihara (1996); Yamamuro and Covert (2001); Yamamuro and Lade (1997b), who reported that different relative densities resulted in different behaviours and that the liquefaction susceptibility of sandy soils decreased with an increase in the relative density. Several researchers have reported that the sand may become unstable even before the stress state achieves the liquefaction state (Chu & Leong, 2002). This type

of instability can be observed in the undrained saturated very loose–loose sand under the undrained condition and in saturated medium-to-dense sand under strain-controlled tests (Lade & Pradel, 1990; Leong et al., 2000). The instability can be represented by the instability line which is defined as a straight line that passes through the origin and connects the peak deviatoric stress in the  $q-p'$  space. To better understand the effectiveness of the instability line on the liquefaction behaviour of clean sandy soils, the stress ratio at the instability line  $\eta$  ( $q_{peak}/p'$ ) was plotted with the brittleness index  $I_B$ . Figure 4.14 shows the results of CS1 to CS9 within the  $I_B$ -  $\eta$  plane; it is apparent that the stress ratio at the instability line  $\eta$  increased with increasing relative density. In the low-relative-density tests CS1–CS3,  $\eta$  increased with an increase in the initial confining pressure. However, the results of the CS4–CS6 tests at  $D_{ri}$  50% and the CS7–CS9 at  $D_{ri}$  90% showed a slight reduction in the values of  $\eta$  with increasing  $p'_o$ . This behaviour implied that the instability of clean sandy soils was dominated more by the relative density than the initial confining pressure because the soil fabric at the high relative density was more stable than that at the low relative density. This was observed when the samples prepared at a high relative density ( $D_r$  90%) exhibited lower values of  $\eta$ . From the data presented in Figure 4.14, we can see that the liquefaction susceptibility ( $I_B$ ) for all the tests (CS1–CS9) reduced with increasing values of  $\eta$  and that  $\eta$  can be used to compute the liquefaction susceptibility by using the following equation:

$$I_B = 1.7972e^{-5.174\eta} \quad (4-6)$$

where  $e$  is the mathematical constant



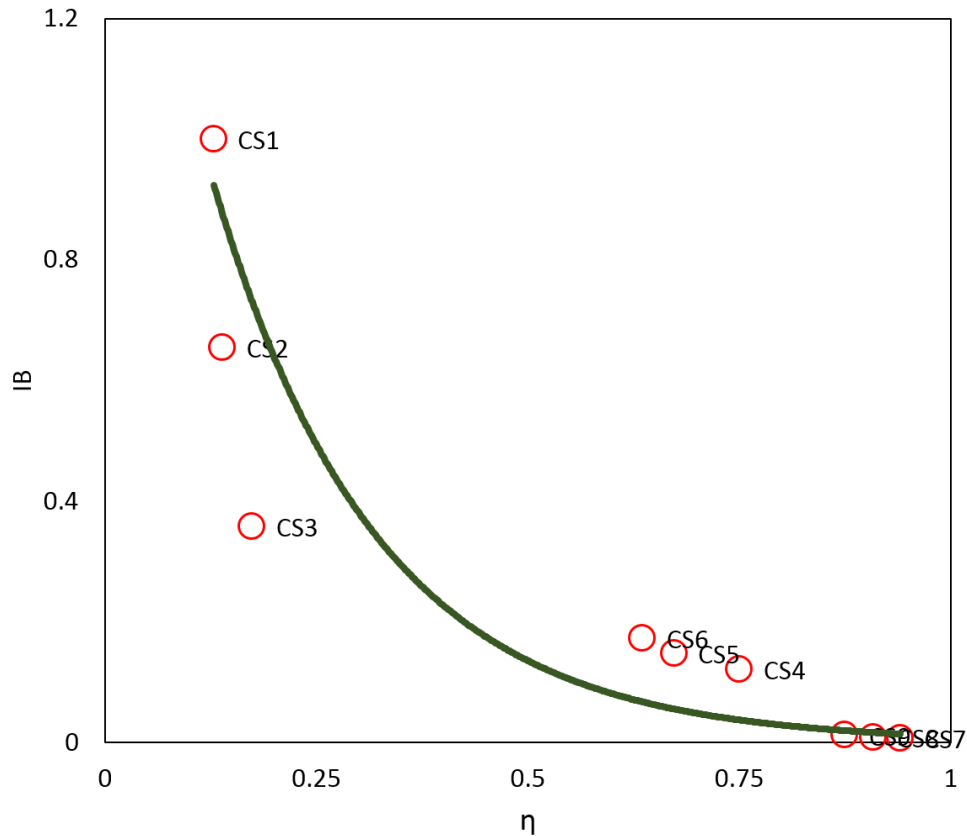


Figure 4.14 Brittleness index against the stress ratio at the instability line of clean sandy soil prepared at different relative densities and tested at different initial confining pressures

The decisive role of the stress ratio at the instability line  $\eta$  in reducing the liquefaction susceptibility was demonstrated when the results of all the tests (CS1–CS9) were plotted in the  $\eta$ – $R_u$  space. In Figure 4.15, a clear decreasing trend of the pore water pressure ratio  $R_u$  is observed with increasing  $\eta$ . The value of  $R_u$  decreased from 1 at  $\eta = 0.129$  to 0.336 when  $\eta$  increased to 0.94. Seed (1987) reported that the liquefaction in soil might be triggered when the value of the pore water pressure ratio  $R_u \geq 60\%$ . From the data presented in Figure 4.15, we can see that the CS1–CS3 tests at  $D_{ri}$  10% and the CS4–CS6 tests at  $D_{ri}$  50% showed  $R_u > 0.6$ . However, the value of  $R_u$  in the CS7–CS9 tests at  $D_{ri}$  90% was lower than 0.6. Therefore, the liquefaction behaviour was triggered in the loose–medium state but not triggered in the dense state. Figure 4.15 shows a clear correlation between  $R_u$  and  $\eta$ ; further,  $\eta$  can be used to compute  $R_u$  by using the following equation:

$$R_u = -0.6221 \eta^2 - 0.2512 \eta + 0.966 \quad (4-7)$$

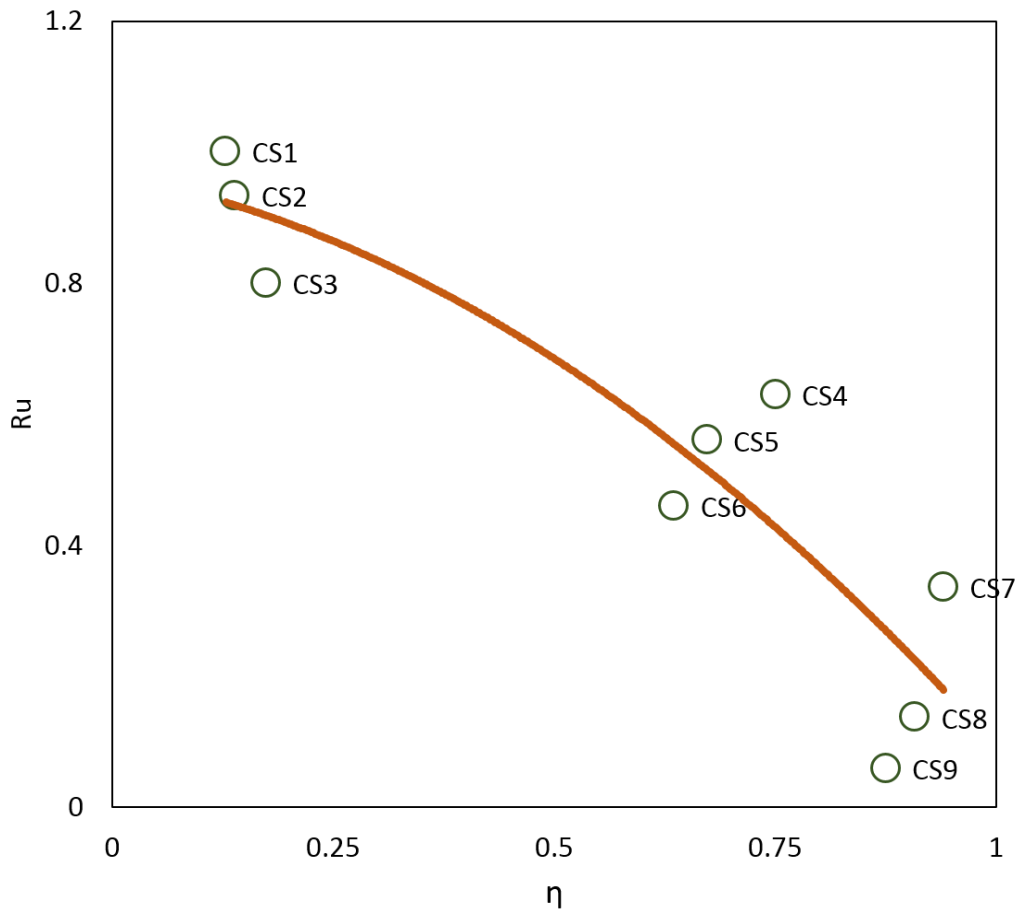


Figure 4.15 Pore water pressure ratio against stress ratio at the instability line of clean sandy soil prepared at different relative densities and tested at different initial confining pressures

The state parameter at the start of the tests, denoted as ( $\Psi_o$ ), was used in the present work to qualitatively estimate the liquefaction behaviour trend in the case of undrained shearing for clean sandy soils under different test conditions. In the case of undrained shearing, the positive  $\Psi_o$  was associated with the flow behaviour; however, the negative values of  $\Psi_o$  were associated with the non-flow behaviour. Figure 4.16 presents the results of the CS1–CS9 tests within the  $\Psi_o$ – $R_u$  plane. On the basis of the values of  $\Psi_o$  and  $R_u$ , Figure 4.16 was divided into three zones. The first zone was the complete static liquefaction zone characterised by the positive values of  $\Psi_o$  and  $R_u \geq 1$ . The second zone was the limited liquefaction zone (lower right quarter) characterised by the positive values of  $\Psi_o$  and  $1 \leq R_u \leq 0.6$ . The final zone was the non-flow zone (lower left quarter) characterised by the negative values of  $\Psi_o$  and  $R_u \leq 0.3$ . Accordingly, one sample (CS1) was located in the complete static liquefaction zone,

and five samples (CS2–CS6) were located in the limited liquefaction zone. The remaining tests (CS7–CS9) were located in the non-flow zone with the negative values of  $\Psi_o$ . Moreover, in all the tests, the values of  $R_u$  decreased with decreasing  $\Psi_o$ , which indicated that the liquefaction susceptibility of clean sandy soil decreased with decreasing  $\Psi_o$ . Figure 4.17 shows a clear decreasing trend of the liquefaction susceptibility  $I_B$  with decreasing  $\Psi_o$ . The value of  $I_B$  decreased from 1 to 0.011 when  $\Psi_o$  reduced from 0.0035 to  $-0.0001$ . Figure 4.16 also shows a good correlation between the  $I_B$  values and  $\Psi_o$  with some scatter in the data of the low-relative-density tests (CS1–CS3). The value of  $\Psi_o$  can be used to compute the liquefaction susceptibility  $I_B$  by using the following equation:

$$I_B = 0.0174 e^{944.09 \Psi_o} \quad (4-8)$$

where  $e$  is the mathematical constant

The effectiveness of using the state parameter at the start of the shearing  $\Psi_o$  for describing the undrained behaviour of clean sandy soils is illustrated by plotting the results of the CS1–CS9 tested in the  $\eta$ – $\Psi_o$  space. The data presented in Figure 4.18 revealed that the stress ratio at the instability line significantly reduced with a decrease in  $\Psi_o$ .

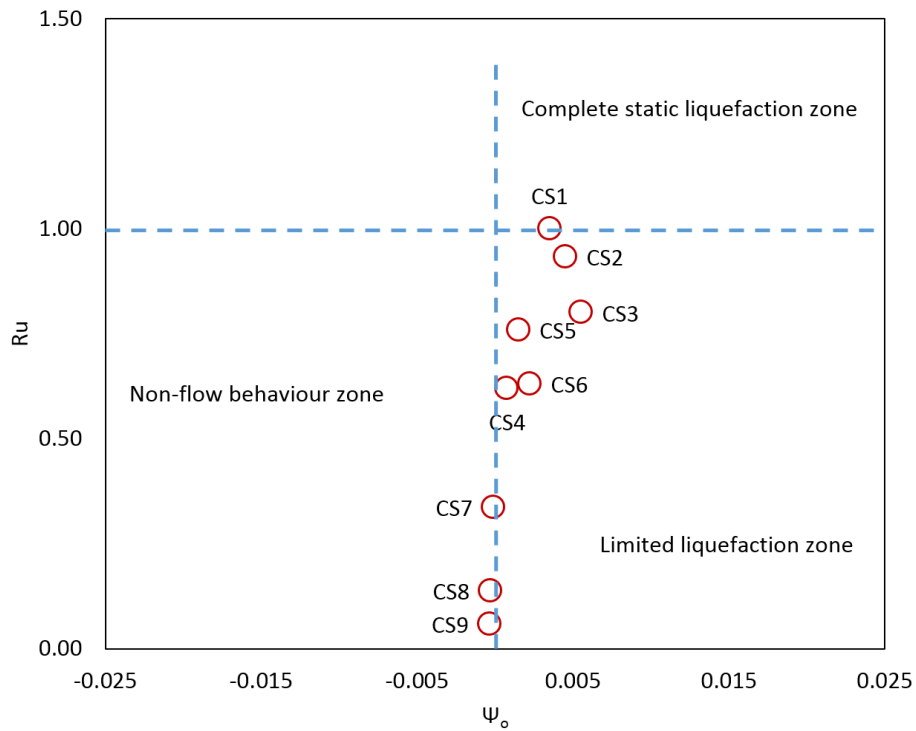


Figure 4.16 Pore water pressure ratio against state parameter at the start of the test of clean sandy soil

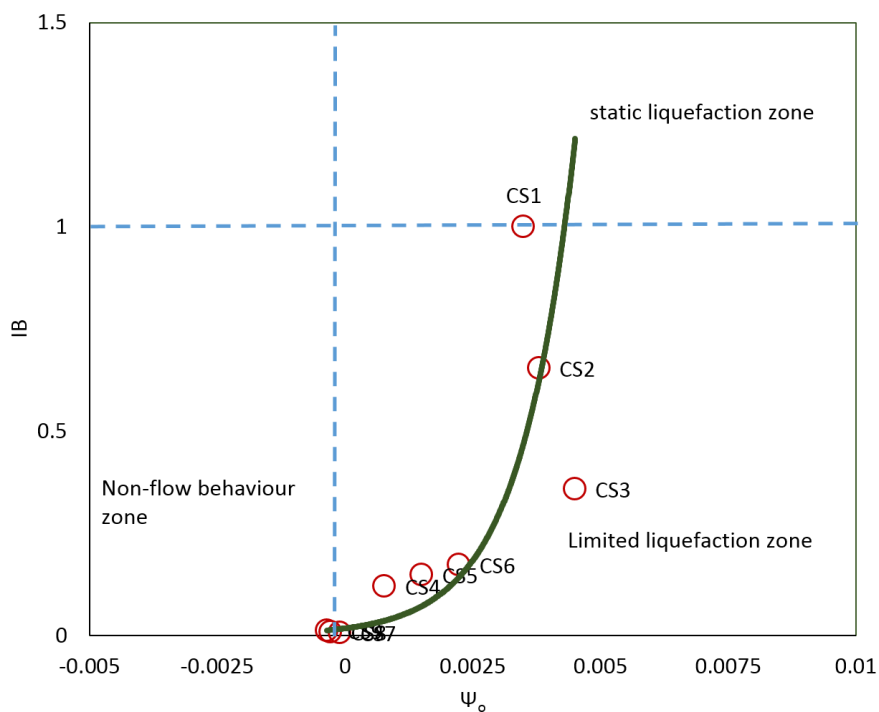


Figure 4.17 Brittleness index against state parameter at the start of the test of clean sandy soil

The values of  $\eta$  increased from 0.129 to 0.941 when  $\Psi_o$  decreased from 0.0035 to  $-0.0001$ . This behaviour indicated that the stability of clean sandy soils increased with a decrease in  $\Psi_o$ . The results of the low-relative-density tests (CS1–CS3) exhibited some scatter data points around the correlation curve, and  $\Psi_o$  was used to compute  $\eta$  by using the following equation:

$$\eta = -9728.1 \Psi_o^2 - 138.05 \Psi_o + 0.8793 \quad (4-9)$$

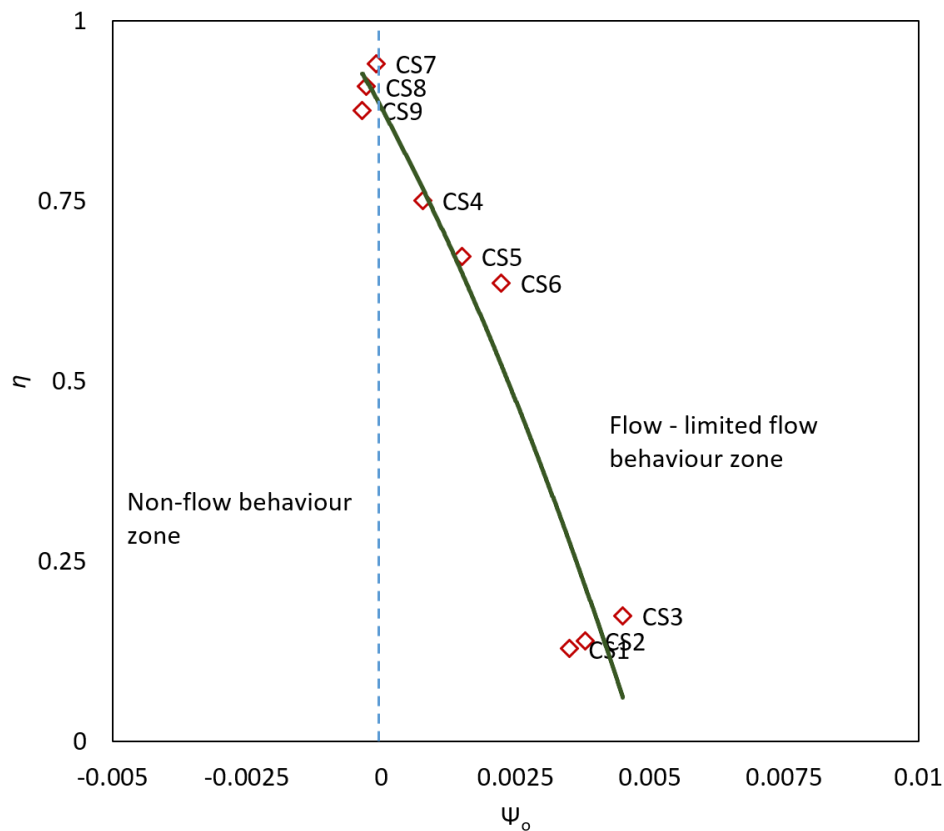


Figure 4.18 Stress ratio at the instability line against the state parameter at the start of the test of clean sandy soil

Although the state parameter has been used in many previous studies to describe the undrained behaviour of sandy soils, Bobei et al. (2009); Jafarian, Ghorbani, et al. (2013), and Ishihara (1993) argued that the use of the state parameter for quantifying the undrained behaviour of sandy soils is more relevant in medium-to-dense sands under a high confining pressure than in loose sands under a low confining pressure. The results of the present study are consistent with the findings of Ishihara (1993) as

the results of the low-relative-density tests (CS1–CS3) showed a scattering trend across the correlation lines, as shown in Figures 4.17 and 4.18.

### 4.3 Effect of slag on liquefaction behaviour of sandy soil

A series of undrained isotropically consolidated monotonic compression triaxial tests were conducted on samples prepared by mixing Perth sand with different slag contents to evaluate the effect of slag on the liquefaction behaviour of sandy soil. The clean Perth sand was mixed with three different slag contents (2%, 4%, and 6%) on the basis of the dry weight of the sand. The physical properties of the sand–slag mixtures used in this study are listed in Table 4.2. Samples were tested under different testing conditions such as three relative densities of 10%, 50%, and 90%; fully saturated with  $B \geq 0.95$ ; 0-day curing time; and three initial confining pressures of 100, 150, and 200 kPa. The tests of samples prepared by mixing sand with 2% slag, 4% slag, and 6% slag were labelled 2%S, 4%S, and 6%S, respectively. The results of these tests are summarised in Table 4.3.

Table 4.2 Physical properties of sand–slag mixtures

Materials	Symbol	$e_{max}$	$e_{min}$	$C_u$	$G_s$
Clean sand	C.S	0.675	0.544	2.235	2.58
Sand + 2% slag	2%S	0.649	0.548	2.209	2.613
Sand + 4% slag	4%S	0.646	0.546	1.902	2.63
Sand + 6% slag	6%S	0.644	0.544	1.93	2.64

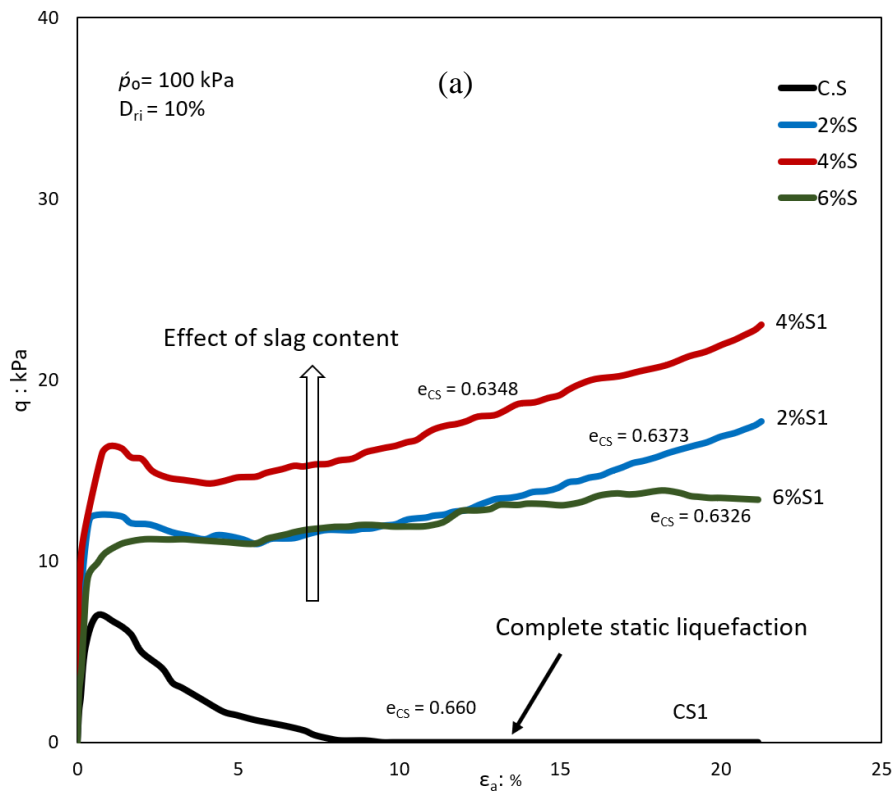
In Table 4.2, there is an evident effect of slag on the physical properties of sand such as the maximum void ratio, minimum void ratio, coefficient of uniformity, and specific gravity, which may affect the mechanical properties as well. It appears from Table 4.2 that the maximum void ratio ( $e_{max}$ ) and the minimum void ratio ( $e_{min}$ ) decreased with an increase in the slag content. In contrast, the specific gravity ( $G_s$ ) of the sand–slag mixtures increased with an increase in the slag content.

Table 4.3 Results of undrained tests conducted using sand–slag samples

Test name	Materials	$\dot{p}_o$	$D_{ri}$ (%)	$e_{cs}$	$R_u$	$I_B$	$q/p'$	$\Psi$
2%S1	Sand + 2% slag	100	10	0.6373	0.6	0.1303	0.2323	0.00156
2%S2	Sand + 2% slag	150	10	0.6338	0.56	0.0465	0.2513	0.00506
2%S3	Sand + 2% slag	200	10	0.6290	0.52	0.0483	0.2646	0.00986
2%S4	Sand + 2% slag	100	50	0.5980	0.44	0.0129	0.8307	0.00077
2%S5	Sand + 2% slag	100	90	0.5583	0.26	0.0012	0.9498	-0.00019
4%S1	Sand + 4% slag	100	10	0.6348	0.44	0.0657	0.2812	0.00109
4%S2	Sand + 4% slag	150	10	0.6324	0.40	0.0030	0.3027	0.00351
4%S3	Sand + 4% slag	200	10	0.6271	0.35	0.0078	0.3364	0.00886
4%S4	Sand + 4% slag	100	50	0.5952	0.19	0.0010	0.6030	0.00058
4%S5	Sand + 4% slag	100	90	0.5563	0.14	0.0015	0.9358	-0.00028
6%S1	Sand + 6% slag	100	10	0.6326	0.74	0.1996	0.2475	0.00128
6%S2	Sand + 6% slag	150	10	0.6293	0.67	0.0204	0.2673	0.00467
6%S3	Sand + 6% slag	200	10	0.6225	0.60	0.0319	0.2702	0.01147
6%S4	Sand + 6% slag	100	50	0.5932	0.33	0.0114	0.5989	0.00074
6%S5	Sand + 6% slag	100	90	0.5542	0.20	0.0053	0.9545	-0.00023

The results of the tests performed on very loose samples ( $D_{ri} = 10\%$ ) and sheared under three initial confining pressures are presented in Figures 4.19–4.21. The stress–strain relationships, effective stress paths, and pore water pressure ratio ( $R_u$ )–strains are shown in Figures 4.19, 4.20, and 4.21, respectively. Figure 4.19(a) compares the stress–strain data of the very loose clean sand (C.S) sample with the very loose sand–slag mixtures tested at  $\dot{p}_o = 100$  kPa. The data presented in Figure 4.19 revealed that complete static liquefaction ( $q = 0$ ) occurred in the C.S samples with the lowest relative density ( $D_{ri} = 10\%$ ) and at the lowest initial confining pressure ( $\dot{p}_o = 100$  kPa), while none of the three mixtures (2%S, 4%S, and 6%S) liquefied at the same confining pressure and relative density. The stress–strain curves of the sand–slag mixtures show that the deviatoric stress did not reach zero as in the test indicating complete static liquefaction, but declined after attaining the peak value and then increased to a level well above the initial peak, indicating the condition of limited liquefaction. Figure 4.19(a) also shows that the initial peak deviatoric stress ( $q_{peak}$ ) increased with an increase in the slag content up to 4%. However, the value of  $q_{peak}$  reduced when the slag content increased to 6% but was still higher than the  $q_{peak}$  value of the C.S samples.

The values of  $q_{peak}$  increased from 7 kPa in the C.S sample to 12.59, 16.59, and 11.31 kPa when the slag content was increased to 2, 4%, and 6%, respectively. The values of the minimum deviatoric stress  $q_{min}$  also increased with increasing slag content;  $q_{min}$  increased from 0 in the C.S sample to 10.95, 15.5, and 9.06 kPa when the slag content increased to 2%, 4%, and 6%, respectively. The initial peak deviatoric stresses  $q_{peak}$  and the minimum deviatoric stresses  $q_{min}$  of all the samples—C.S, 2%S, 4%S, and 6%S increased when the confining pressure increased from 100 kPa to 150 kPa and 200 kPa, and the 4%S mixtures showed the highest initial peak and the minimum deviatoric stress under the three confining pressures, as shown in Figures 4.19(b) and (c).





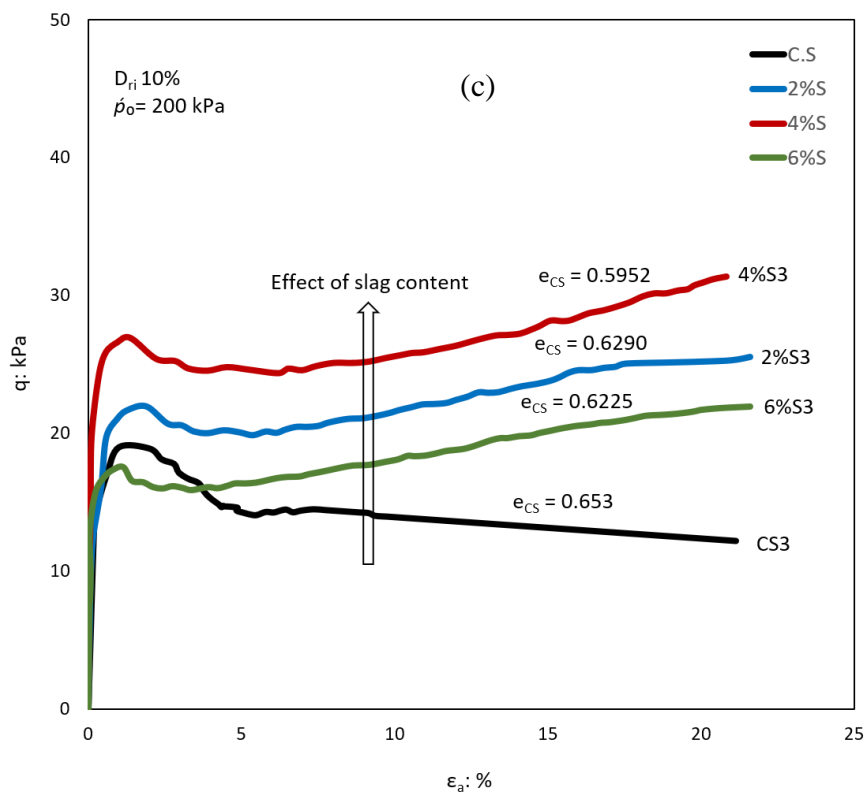
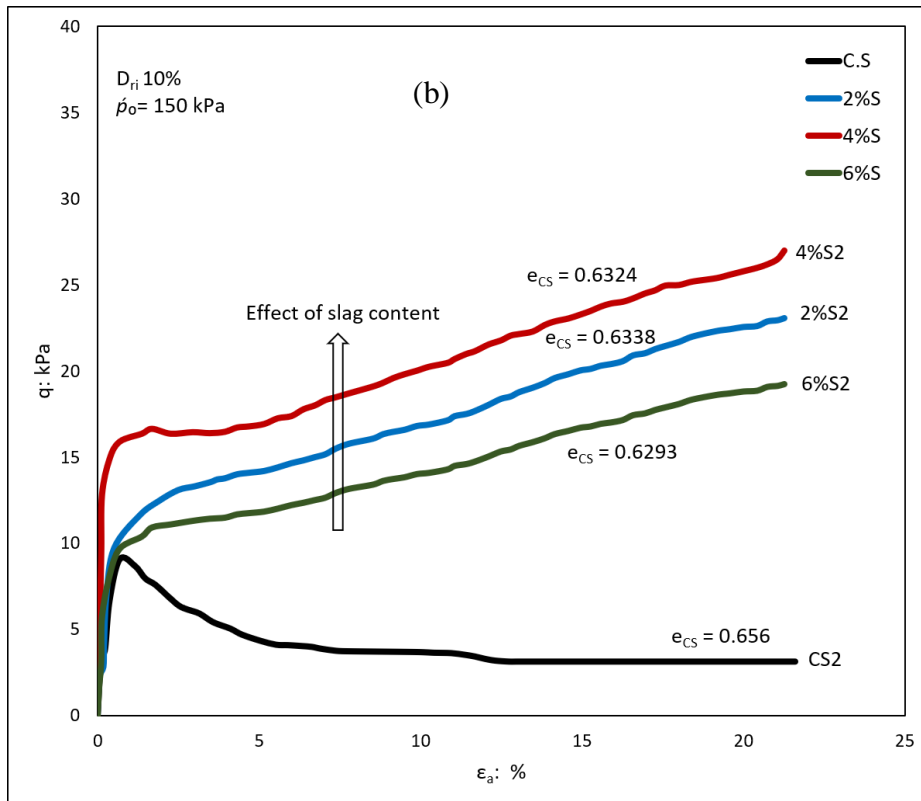
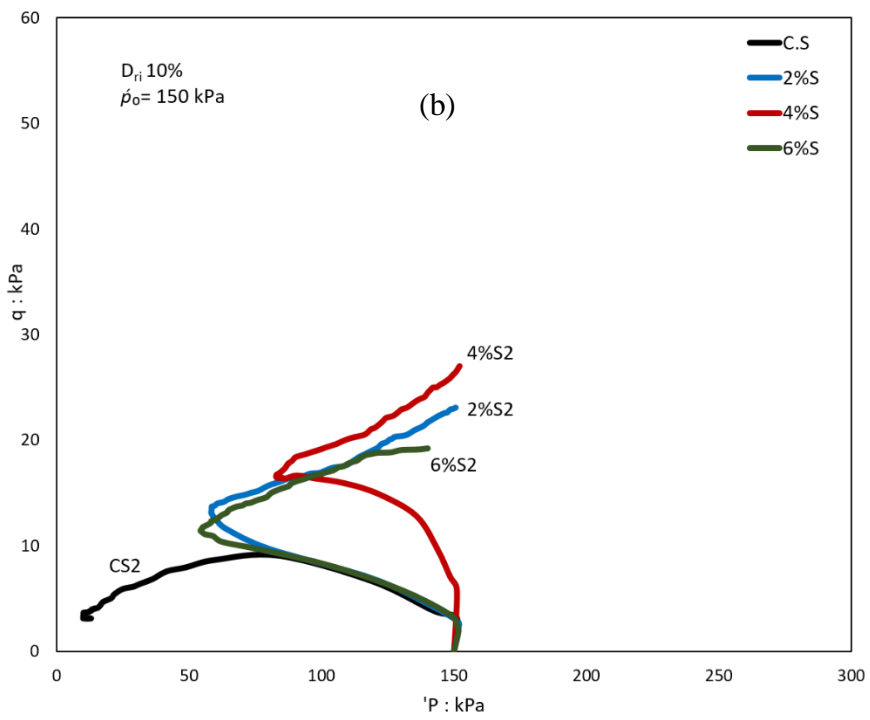
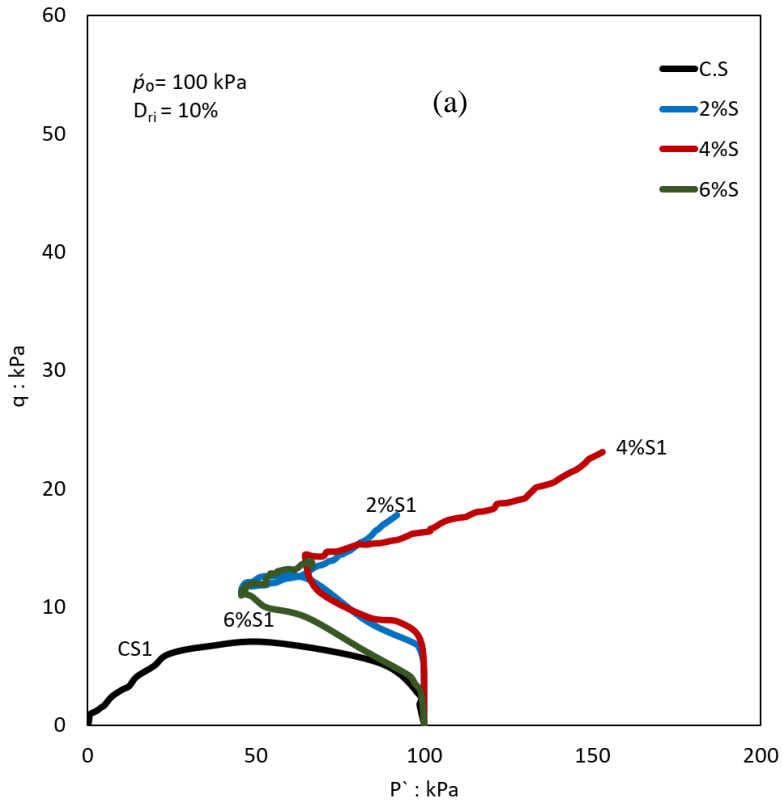


Figure 4.19 Undrained behaviour of very loose sand–slag samples: (a) stress–strain curves with  $p_0 = 100$  kPa, (b) strain curves with  $p_0 = 150$  kPa, and (c) strain curves with  $p_0 = 200$  kPa

The values of  $q_{peak}$  of the 4%S mixture increased from 16.59 kPa at  $p'_o = 100$  kPa to 17 and 27 kPa when  $p'_o$  increased to 150 and 200 kPa, respectively. Figure 4.19(c) shows that at initial confining pressure 200 kPa,  $q_{peak}$  increased with increasing slag content of up to 4%; however, the 6%S sample exhibited  $q_{peak}$  lower than  $q_{peak}$  in the case of the C.S sample, but the behaviour was different. The C.S sample showed a flow behaviour trend, while the 6%S sample showed limited liquefaction behaviour with a significant difference in the deviatoric stresses at the end of the tests. Figures 4.20(a)–(c) present the effective stress paths (ESPs) plotted in the  $p'-q$  spaces of all the mixtures prepared at  $D_{ri}$  10% and sheared under three confining pressures (100, 150, and 200 kPa). As can be seen from Figure 4.20, the slope of ESPs increased when the slag content increased up to 4%. Moreover, the slope of the ESPs of all the mixtures also increased with increasing initial confining pressure. Figure 4.20(a) shows that the ESPs of the C.S sample plummeted toward the origin, which indicated the complete static liquefaction behaviour. However, all sand–slag mixtures showed different behaviours when the ESPs moved to the left and then to the right, indicating a contraction first and then a dilation behaviour. Further, the 4%S mixtures exhibited the highest ESPs slopes at three confining pressures. Figure 4.20(b) indicates that there was a significant difference between the ESPs of 4%S mixture and the ESPs of C.S, 2%S, and 6%S. Figures 4.20(a)–(c) show that the deviatoric stress  $q$  at quasi-steady state point (QSS) increased with increasing slag content up to 4% and initial confining pressure. The samples of the 4%S mixture showed higher values of  $q$  at the QSS point than the other samples. Figures 4.20(a)–(c) also show an insignificant difference between the ESPs of clean sand samples and those of the 6%S samples under three confining pressures, which indicated that increasing the slag content to 6% reduced the shear strength of the sand–slag mixtures.



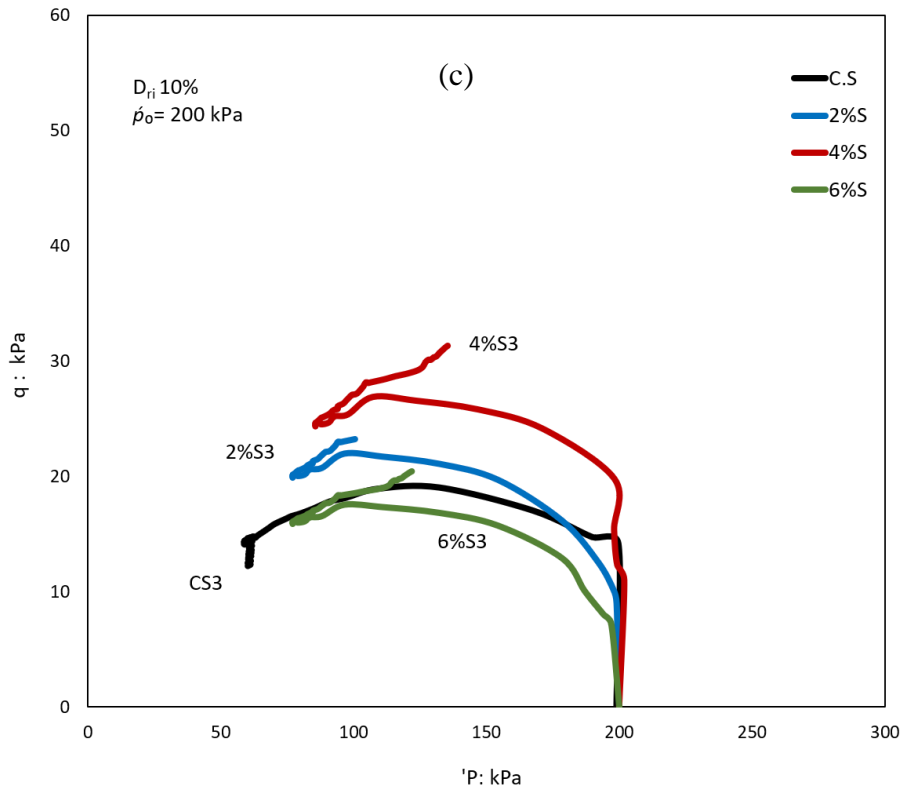
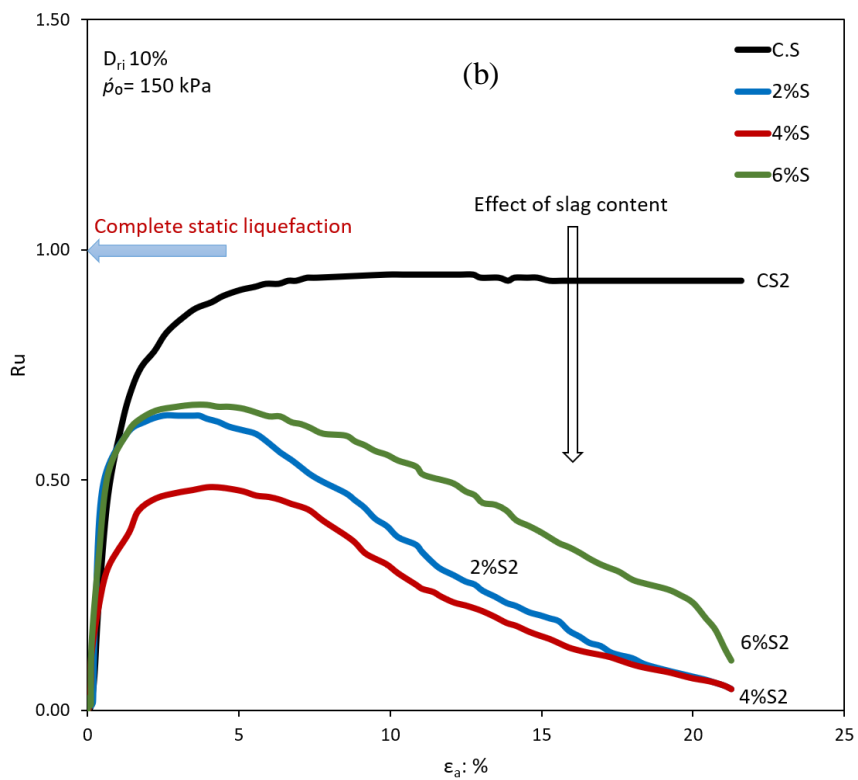
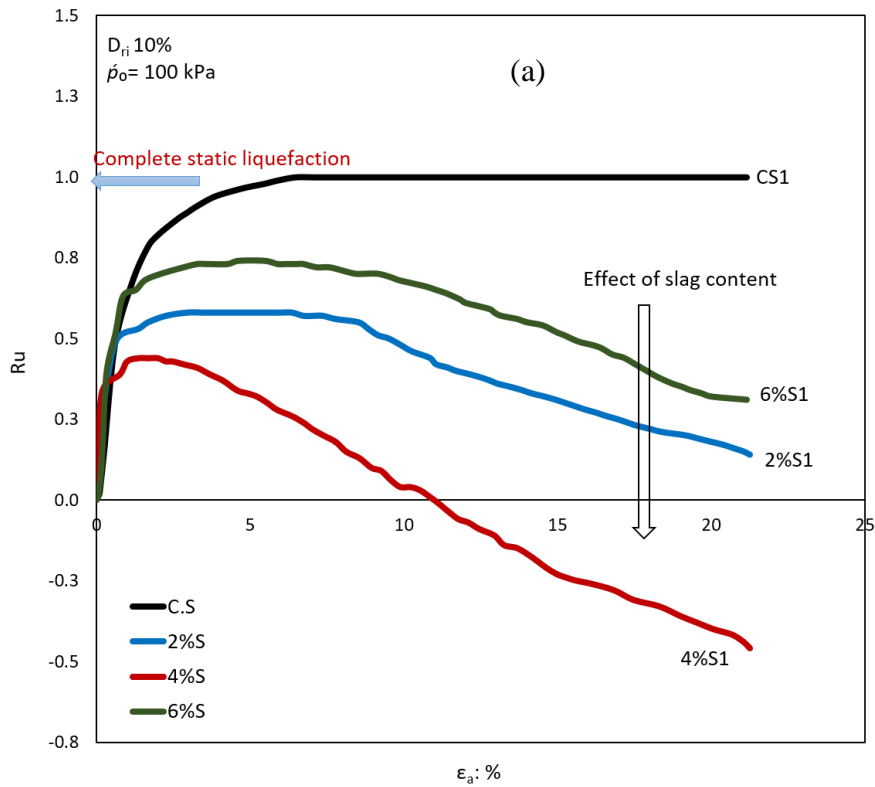


Figure 4.20 Undrained behaviour of very loose sand–slag samples: (a) effective stress path with  $p_0 = 100$  kPa, (b) effective stress path with  $p_0 = 150$  kPa, and (c) effective stress path with  $p_0 = 200$  kPa

The effect of the slag content on the behaviour of sandy soil can be observed in Figures 4.21 (a)–(c), which present the pore water pressure ratio  $R_u$  versus strain relationships of very loose samples under three initial confining pressures. Figures 4.21 (a)–(c) demonstrate that all the mixtures under three confining pressures exhibited a positive pore water pressure ratio  $R_u$  except the 4%S sample tested under  $p_0$  of 100 kPa that showed an initial peak positive  $R_u$  and then reduced to the negative values at the end of the test. From the data shown in Figure 4.21(a), it is apparent that at 100-kPa confining pressure, there was an abrupt increase in the pore water pressure ratio in the C.S sample, whereas the pore water pressure ratio increased gradually in the sand–slag mixtures, and the S.4%S mixture showed the lowest  $R_u$  at the same confining pressure. All the sand–slag mixtures under the three initial confining pressures (100, 150, and 200 kPa) exhibited a reduction in  $R_u$  after attaining the initial peak values. However, the values of  $R_u$  reduced with increasing initial confining pressure. Figure 4.21(a) shows that the  $R_u$  of the sand–slag mixtures at  $p_0 = 100$  kPa reduced when the slag content increased up to 4%. However, the values of  $R_u$  increased when the slag content

increased to 6% but was still lower than  $R_u$  of C.S when tested under the same initial confining pressure of 100 kPa.



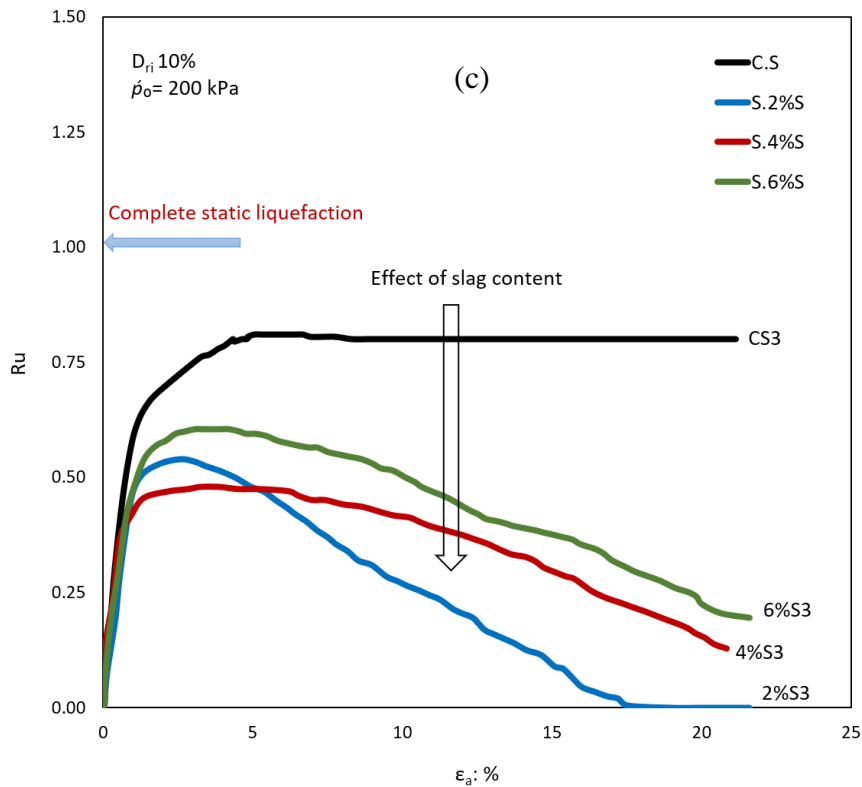
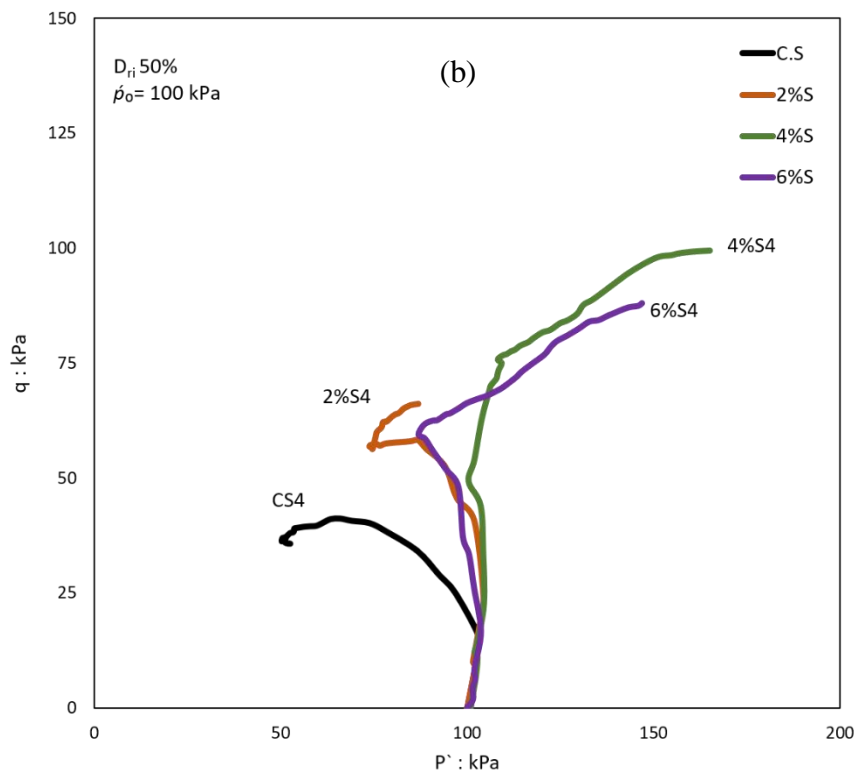
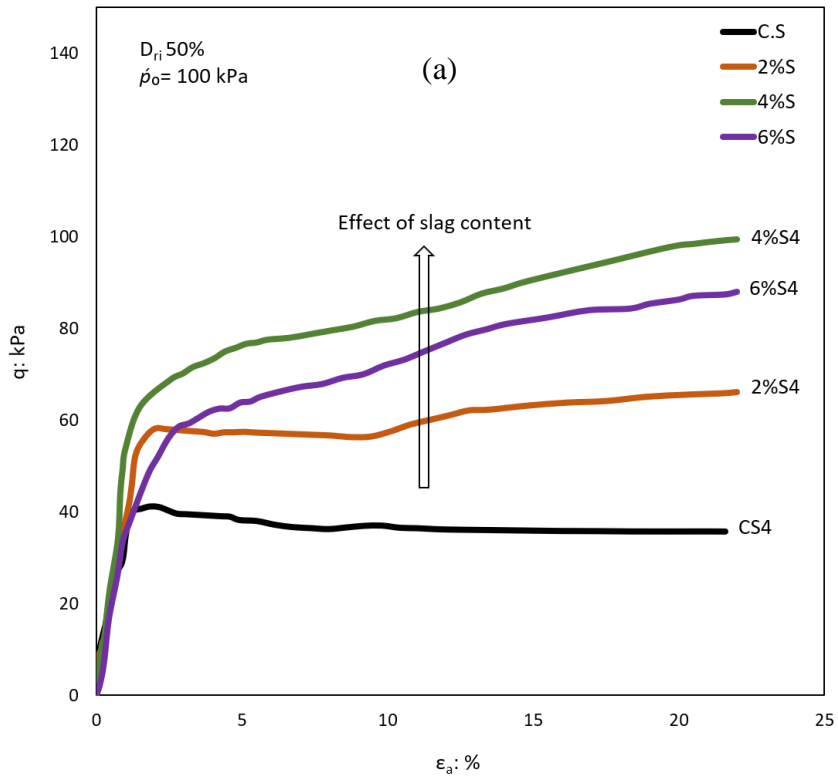


Figure 4.21 Undrained behaviour of very loose sand–slag samples: (a) pore water pressure ratio–strain with  $p_0 = 100$  kPa, (b) pore water pressure ratio–strain with  $p_0 = 150$  kPa, and (c) pore water pressure ratio–strain with  $p_0 = 200$  kPa

The values of  $R_u$  were reduced from 1 in C.S at the 100-kPa confining pressure to 0.6, 0.44, and 0.74 when the slag content increased to 2%, 4%, and 6%, respectively. The values of  $R_u$  were reduced from 0.44 in the 4%S sample at the 100-kPa confining pressure to 0.39 and 0.35 when  $p_0$  increased to 150 kPa and 200 kPa, respectively. The above behaviour trend indicated that the shear strength of the sand–slag mixtures increased with increasing initial confining pressure. This response was in line with the so-called ‘reverse behaviour’ (Yamamuro & Lade, 1997b). To better investigate the effect of the slag content on the liquefaction behaviour of sandy soils, the subsequent experiments were conducted with the same slag content (2%, 4%, and 6%) at two relative densities (50% and 90%) and the confining pressure of 100 kPa. The tests results are shown in Table 4.3. Figures 4.22(a)–(c) provide the stress–strain relationships, effective stress paths, and  $R_u$ –strain relationships of all the mixtures prepared at  $D_{ri}$  50%, respectively. From these figures, we inferred that the behaviour of all the samples was considerably affected by increasing the relative density to 50% and that the 4%S sample showed the highest deviatoric stress and the lowest  $R_u$ . The

behaviour of the C.S sample changed from complete static liquefaction at  $D_{ri}$  10% (Figure 4.19(a)) to limited liquefaction at  $D_{ri}$  50%. However, samples of the sand–slag mixtures exhibited different behaviour trends as compared to the same samples prepared at  $D_{ri}$  10% and tested under the same testing conditions, as shown in Figure 4.19(a). The samples of 2%S and 6%S showed the same behaviour trend (limited liquefaction) in the loose state ( $D_{ri}$  10%) and the medium state ( $D_{ri}$  50%), but the initial peak deviatoric stress  $q_{peak}$  significantly increased with increasing relative density. Moreover, the amount of reduction in the deviatoric stress after attaining  $q_{peak}$  reduced with increasing relative density. The  $q_{peak}$  value of the 2%S and 6%S samples increased from 12.59 kPa and 11.32 kPa at  $D_{ri}$  10% to 57 kPa and 88 kPa when  $D_{ri}$  increased to 50%. However, the behaviour of 4%S was changed entirely from limited liquefaction at  $D_{ri}$  10% to non-flow behaviour at  $D_{ri}$  50%, and the 4%S sample showed a higher  $q_{peak}$  value than the other samples. The  $q_{peak}$  value of the 4%S samples increased from 16.59 kPa at  $D_{ri}$  10% to 99 kPa when  $D_{ri}$  increased to 50%. The effect of the relative density on the liquefaction behaviour of the sand–slag mixtures was also observed in Figures 4.22(b) and (c). Figure 4.22(b) presents the effective stress paths of all the mixtures prepared at  $D_{ri}$  50%. Here, the slope of the effective stress paths increased with increasing relative density and the 4%S sample showed the highest values.





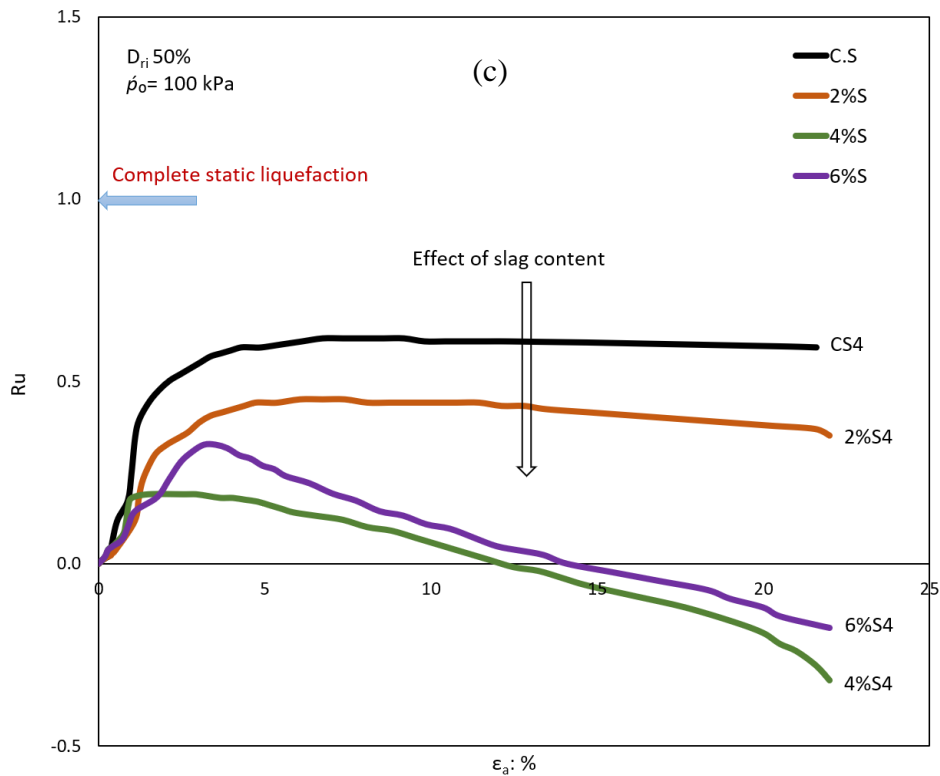
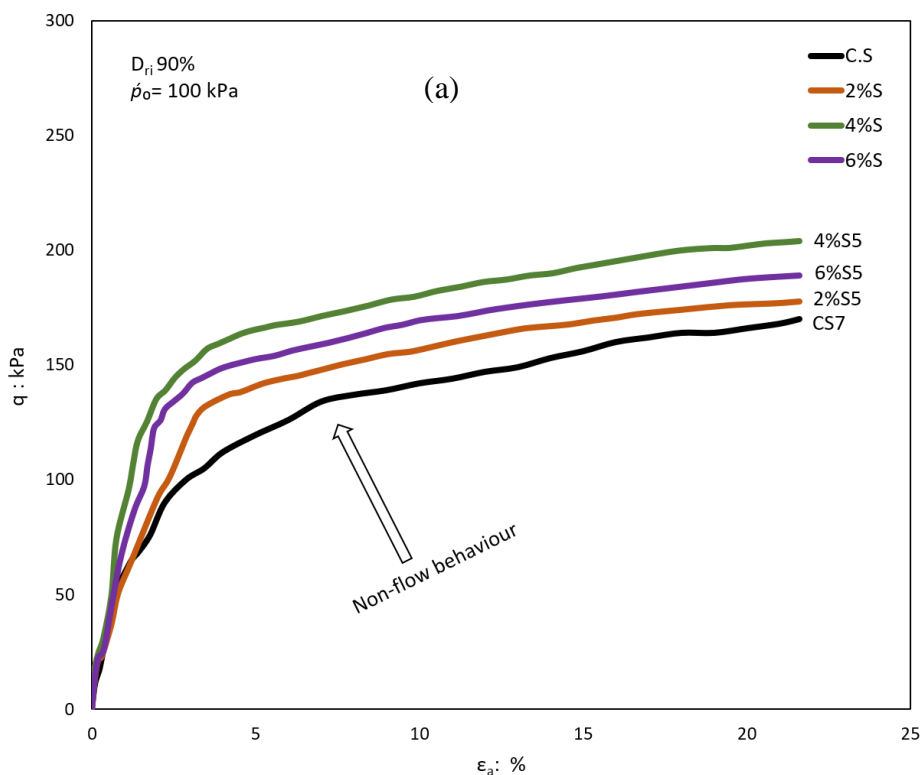


Figure 4.22 Undrained behaviour of sand–slag samples prepared at the relative density of 50%: (a) stress–strain relationships, (b) effective stress paths, and (c) pore water pressure ratio–strain

The effective stress path of the C.S sample moved to the left but did not reach the zero value. The effective stress paths of the 2%S and 6%S samples moved slightly to the left and then to the right, indicating limited liquefaction behaviour. However, the effective stress path of 4%S moved directly to the right with abrupt increases in the deviatoric stresses. Figure 4.22(c) shows that all the mixtures showed a reduction in the pore water pressure ratio after achieving the peak value, but the reduction rate in the C.S and 2%S samples was less than 4%S and 6%S. The values of  $R_u$  reduced from 0.6 in C.S to 0.45, 0.19, and 0.33 when the slag content increased to 2%, 4%, and 6%, respectively. Moreover, both the 4%S and 6%S samples showed negative  $R_u$  at the end of the tests, but the 4%S sample showed the lowest values. Figures 4.23(a)–(c) show the results of the tests performed on dense samples ( $D_{ri}$  90%) and sheared at a single confining pressure of 100 kPa. From the data presented in Figure 4.23(a), it is apparent that all of the samples (C.S, 2%S, 4%S, and 6%S) exhibited non-flow behaviour which was attributed to the gradual increases in the deviatoric stresses until the end of the test. The deviatoric stress increased with increasing slag content, and the 4%S sample showed the highest value. The deviatoric stress increased from 171 kPa in C.S to 177.6

kPa, 204 kPa, and 189 kPa when the slag content increased to 2%, 4%, and 6%, respectively. This behaviour is inferred from Figure 4.23(b), which presents the effective stress paths of all of the mixtures. As seen from this figure, all the mixtures showed the no-flow behaviour when the effective stress paths moved to the right with abrupt increases in the deviatoric stresses. The non-flow behaviour was manifested by sudden decreases in the pore water pressure ratio  $R_u$  after reaching the peak value and the reduction in  $R_u$  continuous until negative values were reached at the end of the test, as shown in Figure 4.23(c). In the data of the tests performed at  $D_{ri}$  50% and 90%, note that the deviatoric stress of 6%S was higher than that of 2%S, and the pore water pressure ratio for 6%S was less than that for 2%S as compared to the data obtained in the case of  $D_{ri}$  10%. This change in behaviour could be attributed to the fact that effect of the fines content on the behaviour of the sandy soil was hindered by the increasing relative density.



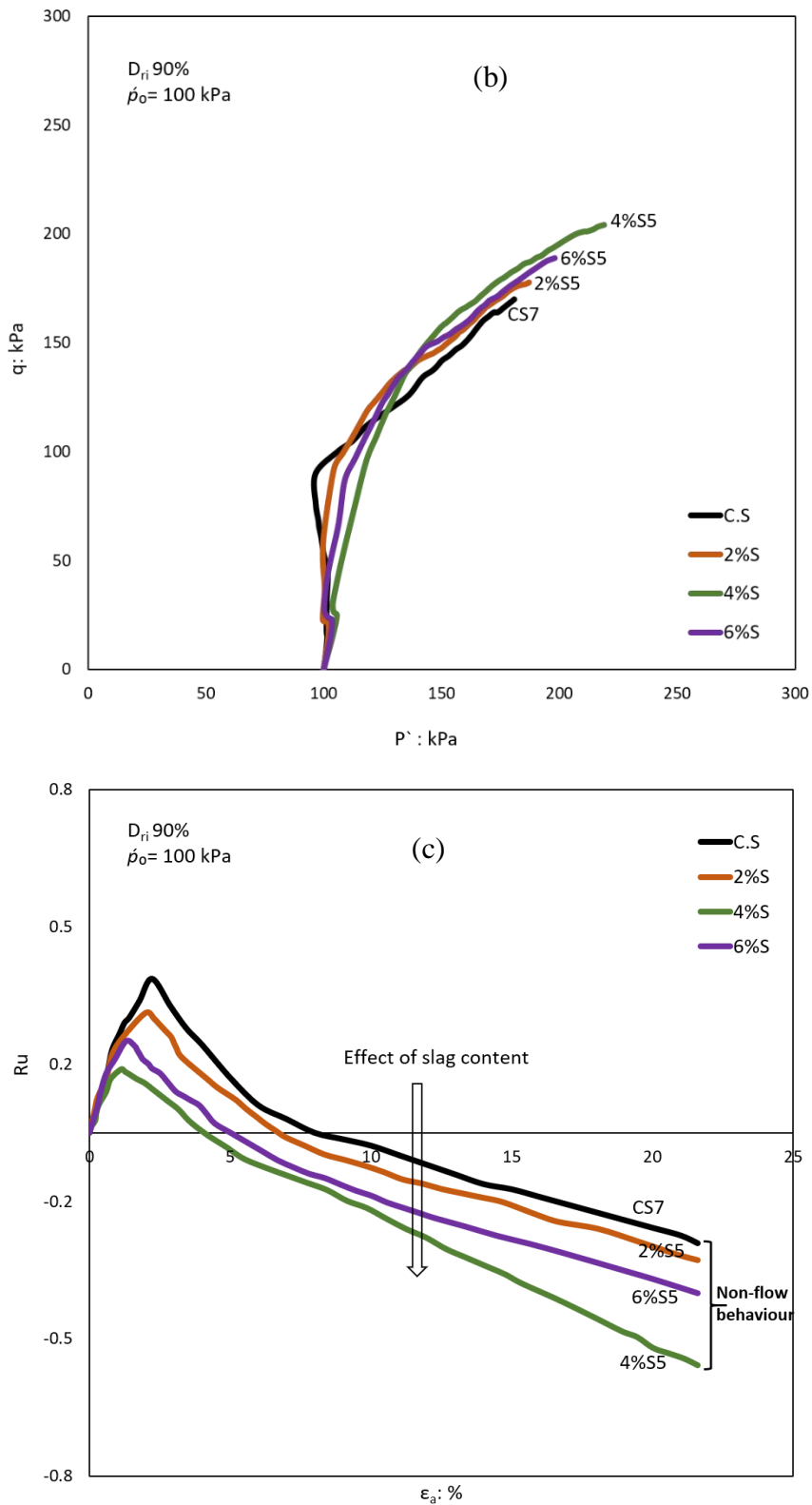
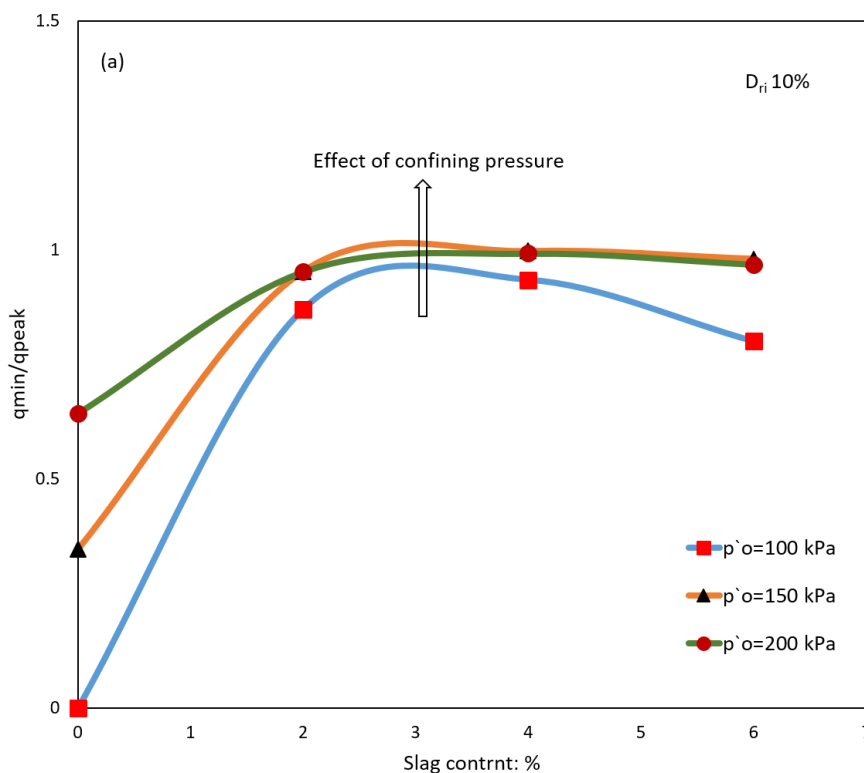


Figure 4.23 Undrained behaviour of sand–slag samples prepared at the relative density of 90%: (a) stress–strain relationships, (b) effective stress paths, and (c) pore water pressure ratio–strain

The influence of the slag content on the liquefaction behaviour of sandy soil can also be shown by examining the relationships between the stress ratio ( $q_{min}/q_{peak}$ ) and the slag content, as shown in Figures 4.24(a)–(c). Figure 4.24(a) presents the relationship between the slag content and the stress ratio  $q_{min}/q_{peak}$  of very loose samples ( $D_{ri}$  10%) tested under three different initial confining pressures (100, 150, and 200 kPa). Figure 4.24(a) shows a clearly increasing trend of the stress ratio  $q_{min}/q_{peak}$  when the slag content increased up to 4%; the ratio decreased when the slag content increased to 6%. The values of the stress ratio  $q_{min}/q_{peak}$  at  $p'_o$  of 100 kPa increased from 0 to 0.87, 0.934, and 0.8 when the slag content increased from 0, 2%, 4%, and 6%, respectively. Moreover, the stress ratio increased with increasing confining pressure and a slight difference in the values of the stress ratio  $q_{min}/q_{peak}$  was observed when the confining pressure increased from 150 kPa to 200 kPa. Moreover, the reduction in the stress ratio  $q_{min}/q_{peak}$  when the slag content increased to 6% slowed down with an increase in the initial confining pressure. Figure 4.24(b) shows the relationships between the stress ratio  $q_{min}/q_{peak}$  and the slag contents for samples tested at three relative densities and sheared at the initial confining pressure  $p'_o$  of 100 kPa.



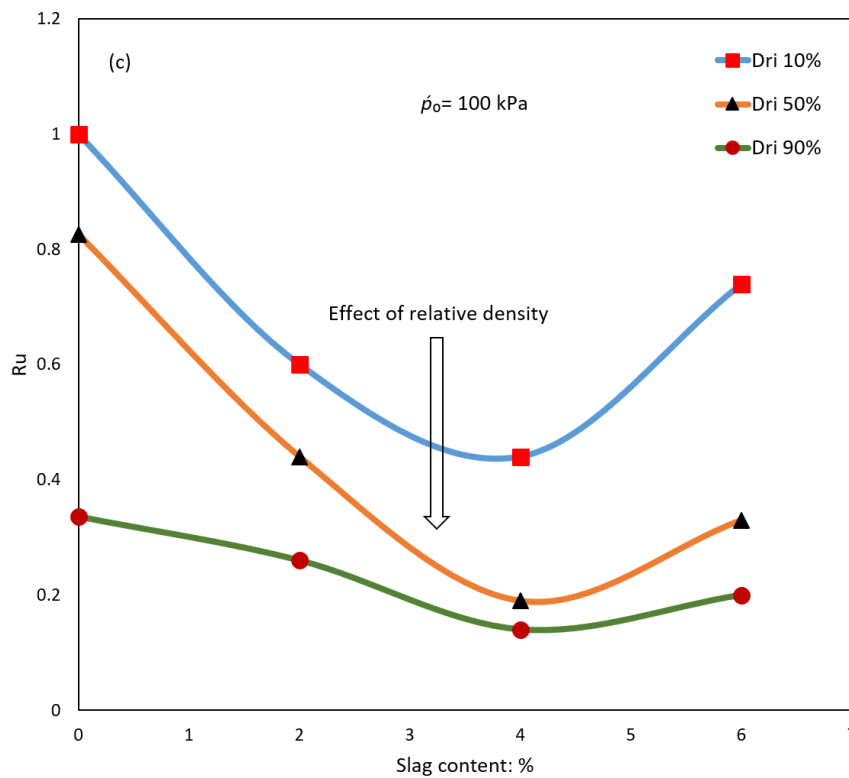
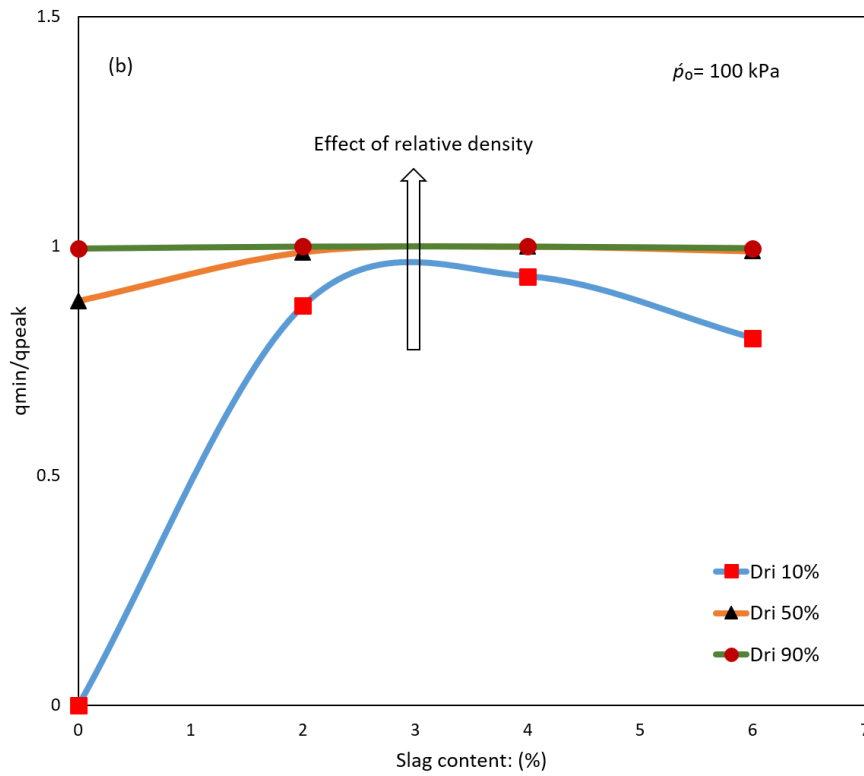
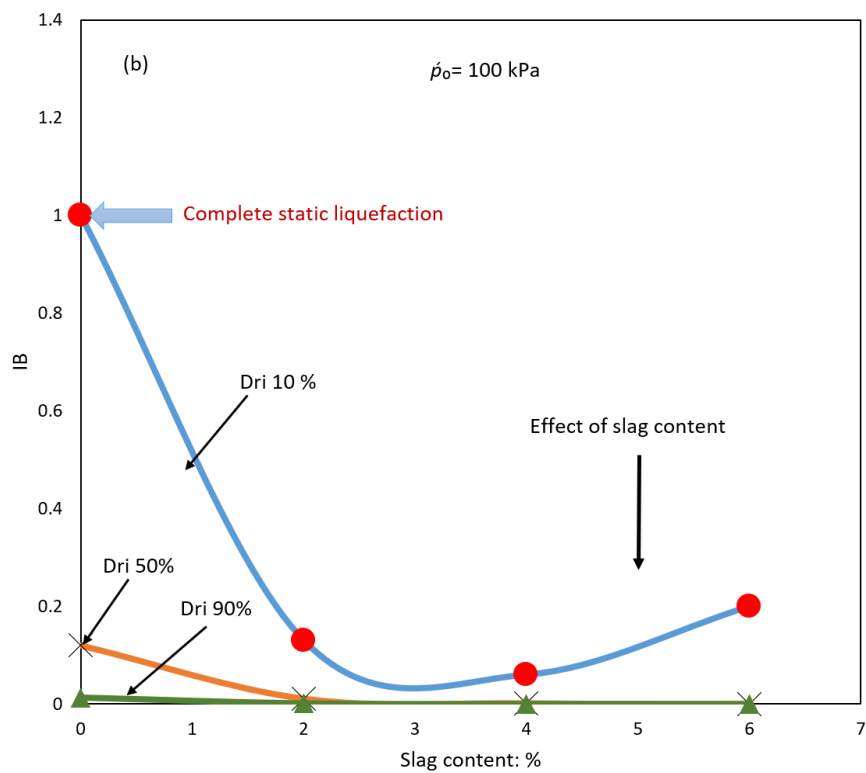
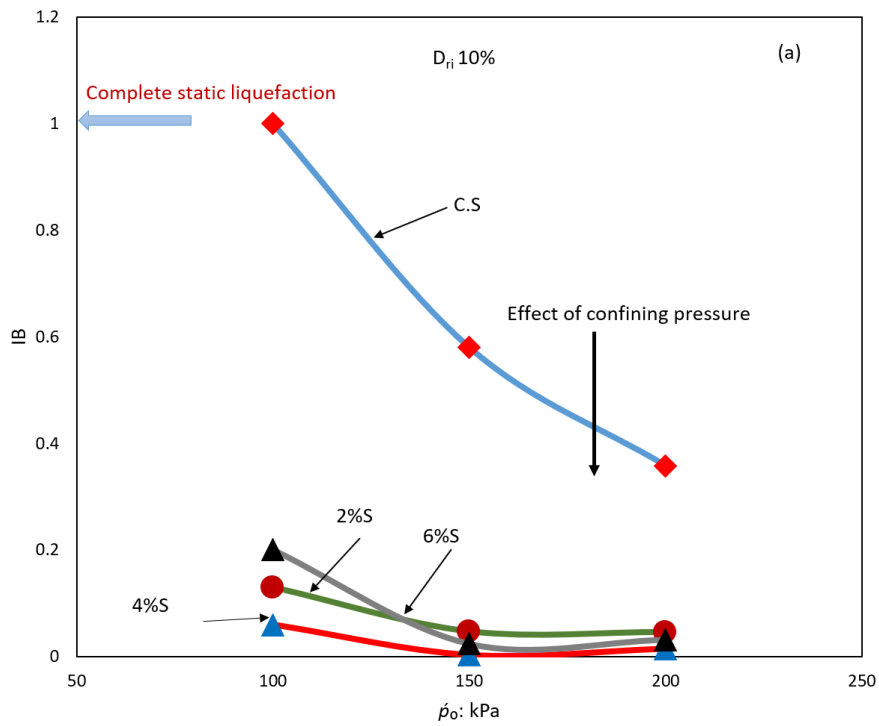


Figure 4.24 Effect of slag content on undrained behaviour of sand–slag mixtures: (a) stress ratio vs. slag content (effect of initial confining pressure), (b) stress ratio vs. slag content (effect of relative density), and (c) pore water pressure ratios vs. slag content

It is apparent from Figure 4.24(b) that the stress ratio  $q_{min}/q_{peak}$  significantly increased when the relative density increased from 10% to 50% and 90%. Figure 4.24(b) also shows that the stress ratio at the relative density of 10% increased when the slag content increased up to 4%. However, at the medium ( $D_{ri}$  50%) and the dense ( $D_{ri}$  90%) states, the increasing rate was lower than that for the very loose samples, which referred to the effect of slag content reduced with an increase in the relative density. This behaviour is shown in Figure 4.24(c) when the pore water pressure ratio reduced with an increase in the slag content up to 4% and then to 6%. The reduction rate of the pore water pressure ratio slowed down with increasing relative density. The effects of the slag content on the liquefaction susceptibility of sandy soils are shown in Figure 4.25–4.27. Figures 4.25(a)–(c) show the relationships between the brittleness index  $I_B$  and the confining pressure, slag content, and relative density. Figure 4.25(a) shows that complete static liquefaction with an  $I_B$  value of 1 occurred in the clean sand sample at the lowest relative density (10%) and the lowest confining pressure (100 kPa). However, none of the three blends (2%S, 4%S, and 6%S) showed complete static liquefaction at the same relative density and confining pressure. Furthermore, there was a significant reduction in the liquefaction susceptibility with increasing slag content, which indicated that adding slag increased the stability of the mixtures and the effect of the slag content reduced with increasing initial confining pressure. The brittleness index  $I_B$  of loose ( $D_{ri} = 10\%$ ) sand–slag mixtures tested at 100-kPa confining pressure reduced from 1 at 0% slag content to 0.13, 0.066, and 0.2 at slag contents of 2%, 4%, and 6%, respectively. Figures 4.25(b) and (c) also show that the liquefaction susceptibility of the sand–slag mixtures reduced with increasing relative density and the increases in the relative density hindered the effect of the slag content on the liquefaction susceptibility. This behaviour was observed in very loose samples when  $I_B$  reduced with increasing slag content up to 4% and then increased when the slag content increased to 6%. However, at a high relative density of 50% and 90%, the  $I_B$  values showed only a slight change with increasing slag content. Figure 4.25(b) shows that the brittleness index  $I_B$  of 4%S reduced from 0.06 at  $D_{ri}$  10% to 0.001 and 0.001 when the relative density increased to 50% and 90%, respectively. These findings were consistent with the findings reported in the previous sections wherein the relative density reduced the effect of the slag content on the stress ratio  $q_{min}/q_{peak}$ . Further, this indicated that the relative density hindered the effect of the fines on the liquefaction susceptibility of sandy soil.



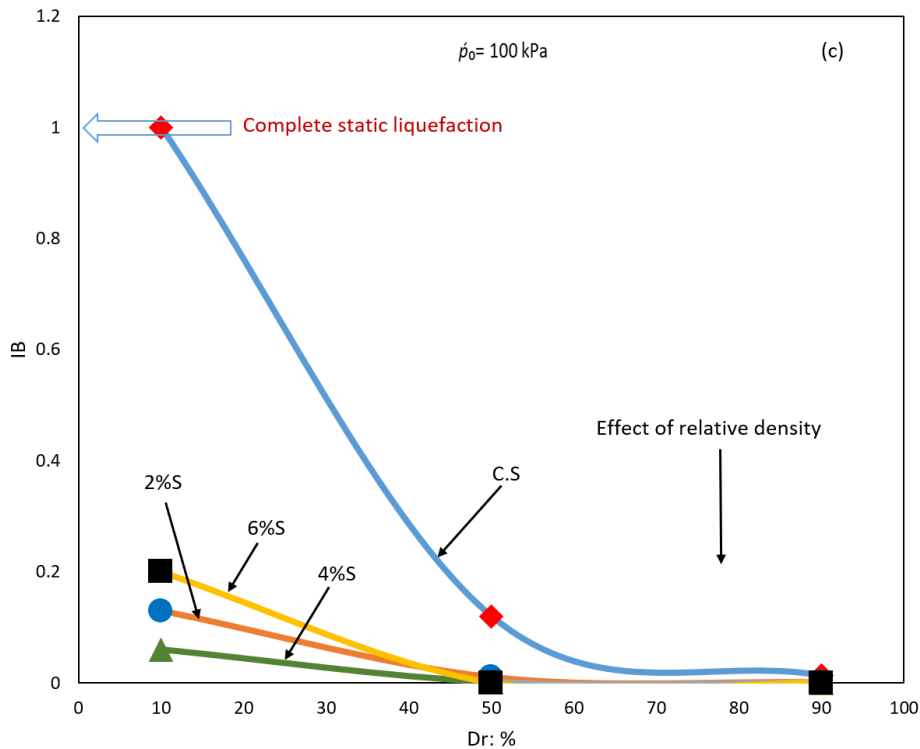
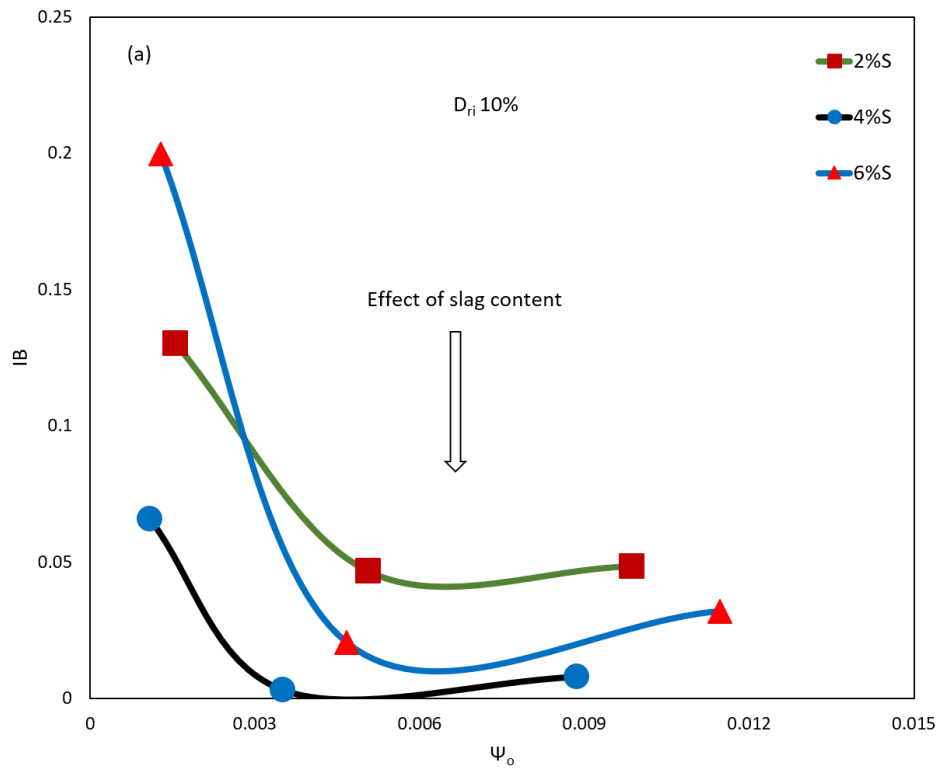


Figure 4.25 Effect of slag content on the brittleness index of sand–slag mixtures: (a) brittleness index vs. initial confining pressure, (b) brittleness index vs. slag content, and (c) brittleness index vs. relative density

The effect of the slag content on the liquefaction susceptibility of clean sandy soils can also be evaluated by examining the relationships between the state parameter at the start of the test  $\Psi_o$  and the other parameters such as brittleness index  $I_B$ , relative density, and slag content, as shown in Figures 4.26(a) and (b). Figure 4.26(a) shows the relationships between the brittleness index  $I_B$  and the state parameter at the start of the test  $\Psi_o$  of very loose samples tested under three initial confining pressures. From this figure, we can see that  $\Psi_o$  decreased with increasing initial confining pressure and the mixture of 4%S showed the lowest values of  $\Psi_o$ . Figure 4.26(a) also shows that 6%S showed the highest  $\Psi_o$  values at  $\dot{p}_o$  of 100 kPa. However, the values of  $\Psi_o$  decreased slightly with increasing initial confining pressure. At the lowest initial confining pressure (100 kPa), the mixture of 6%S exhibited the highest liquefaction susceptibility with the highest  $I_B$  value of 0.2. When the initial confining pressure was increased to 150 kPa and 200 kPa, the mixture of 2%S showed the highest liquefaction susceptibility, but the value of  $\Psi_o$  at  $\dot{p}_o$  of 200 kPa was lower than that for 6%S. The



data presented in Figure 4.26(b) revealed that the values of  $\Psi_o$  significantly reduced from positive values to negative values when the relative density increased from 10% to 90%. Moreover, the major effect of the slag content on  $\Psi_o$  was observed in very loose samples tested at  $p_0$  of 100 kPa.



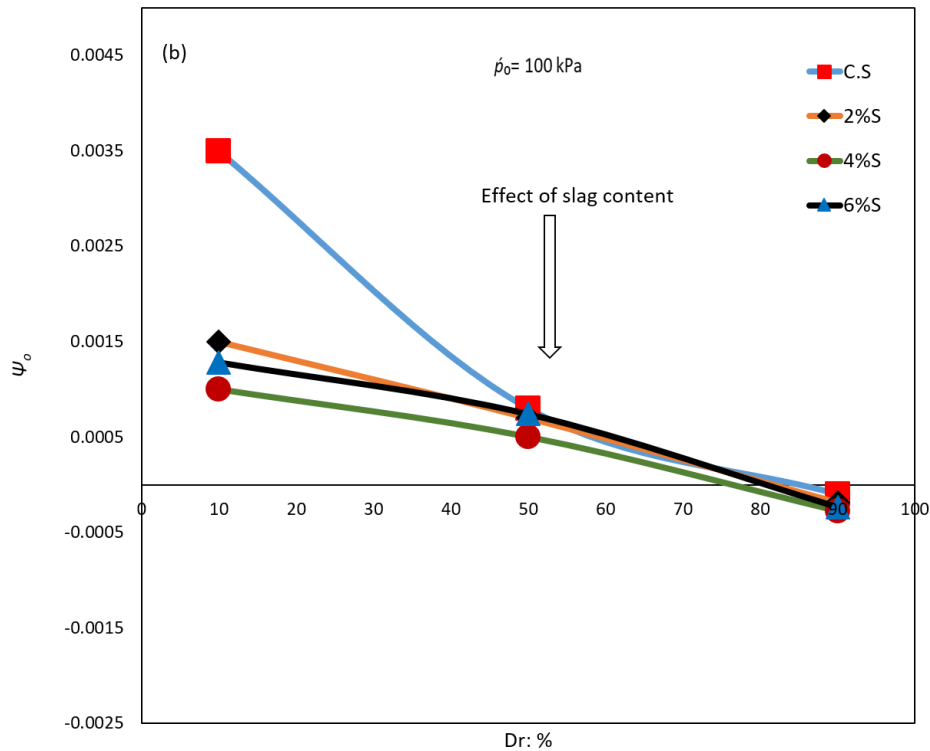


Figure 4.26 Effect of slag content on state parameter at start of the test of sand–slag mixtures: (a) brittleness index vs. state parameter at start of the test and (b) state parameter at start of the test vs. relative density

The values of  $\Psi_o$  reduced from 0.0035 at 0% slag content to 0.0016, 0.0011, and 0.0013 when the slag content increased to 2%, 4%, and 6%, respectively. However, there was a slight difference in  $\Psi_o$  when the relative density increased to the medium state ( $D_{ri}$  50%) and the dense state ( $D_{ri}$  90%). The relationships between the stress ratio at the instability line  $\eta$  and the slag content of very loose samples tested under three confining pressures are illustrated in Figure 4.27. Here,  $\eta$  increased when the slag content increased up to 4% and then decreased when the slag content increased to 6%. This behaviour was attributed to the effect of fines when they comprised more than 4% of the mixture, which was done to increase the compressibility of the samples and, consequently, reduce the liquefaction resistance by increasing the excess pore water pressure and decreasing the effective confining pressure. Figure 4.27 shows that  $\eta$  increased with increasing initial confining pressure and the highest values of  $\eta$  were obtained at 200 kPa. The values of  $\eta$  at  $p'_o$  of 200 kPa increased from 0.174 at 0% slag content to 0.265, 0.336, and 0.27 when the slag content increased to 2%, 4%, and 6%,

respectively. This behaviour was attributed to the role of slag in improving the soil fabric and consequently, reducing the instability of the mixtures.

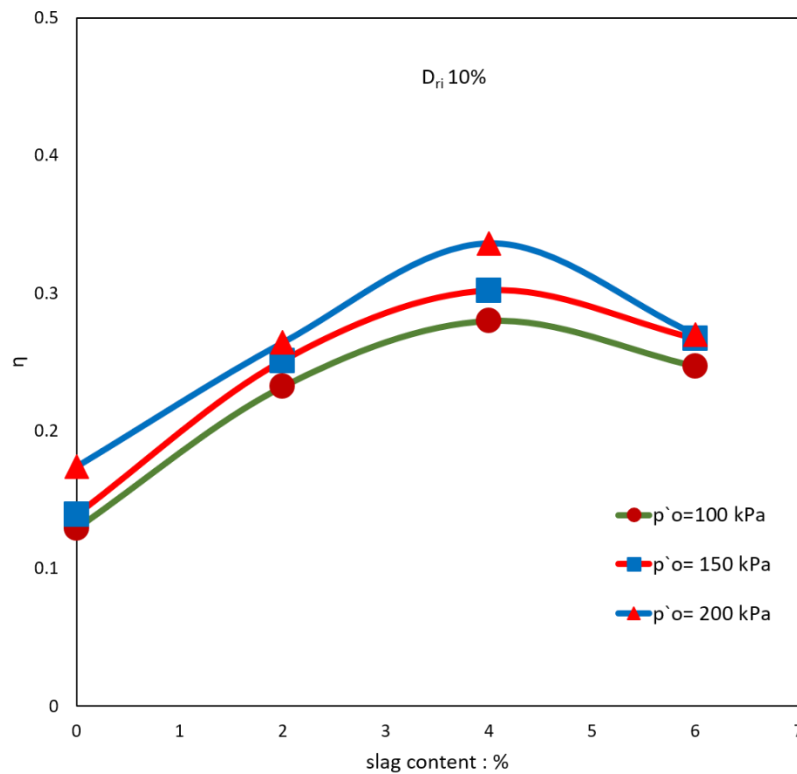


Figure 4.27 Effect of slag content on stress ratio at instability line of sand–slag mixtures

The positive effect of the slag content on the behaviour of sandy soils could be attributed to mechanical, rather than chemical, effects. The slag may react as a chemical additive and increase the soil strength when it is fully hydrated and cured. However, in this study, the tests were conducted without considering the slag curing time because of the complexity of the effect; this can be considered a future work direction. Therefore, the liquefaction susceptibility of sandy soils decreased with a decrease in the fines content because of the role of slag as a fines additive which filled the voids between the sand particles and increased the contact between the sand grains. Hence, slag reduced the pore water pressure and stabilised the sample fabric. Another reason for this positive role of slag is the nature and the shape of the slag particles. Both sand and slag are granular materials, and the angular shape of the slag particles may enhance the contact between the sand particles. Yang and Wei (2015) argued that the angular shape was more stable than the rounded shape and the angular fines with rounded soil particles reduced the liquefaction susceptibility of sandy soils. Ni et al.

(2004) argued that the presence of non-plastic fines contributes positively to the undrained shear strength of mixed soils. However, the negative role of increasing the slag content up to 6% might be related to the compressibility of the samples. Yamamuro and Lade (1997b) stated that the particle structure of the sand–fines mixtures is different from the clean sand structure and that the presence of fines may increase the compressibility of the sand–fines mixtures more than clean sands even when the relative density of the mixtures is higher. The effect of the slag content on the compressibility of the sand–slag mixtures can be noted in Table 4.3, which shows that the post-consolidation void ratio reduced with increasing slag content. Previous studies on the effect of slag on the behaviour of sandy soil are rare, and hence, comparisons cannot be made. Almost all of the previous studies focused on using slag to improve the mechanical properties of soft clays and expansive soils. All of them indicated that slag improved the shear strength of soft clay soils and reduced the expansion of expansive soils.

#### 4.4. Effect of bentonite on liquefaction susceptibility of sandy soils

A series of undrained isotropically consolidated monotonic triaxial tests were conducted to characterise the effect of the bentonite content on the liquefaction behaviour of sandy soils. Samples were prepared by mixing clean Perth sand with two percentages of bentonite (3% and 5%) on the basis of the dry weight of sand. The physical properties of the mixtures used in the present work are presented in Table 4.4.

Table 4.4 Physical properties of sand–bentonite mixtures

Materials	Symbol	$e_{max}$	$e_{min}$	$C_u$	$G_s$
Clean sand	C.S	0.675	0.544	2.235	2.580
Sand + 3% bentonite	3%B	0.657	0.492	2.250	2.614
Sand + 5% bentonite	5%B	0.675	0.502	2.300	2.670

Table 4.4 shows that the maximum ( $e_{max}$ ) and the minimum ( $e_{min}$ ) void ratios decreased when the bentonite content was 3% and then increased when the bentonite content increased to 5%. However, the specific gravity ( $G_s$ ) and the coefficient of uniformity ( $C_u$ ) of all the mixtures increased with increasing bentonite content. The undrained

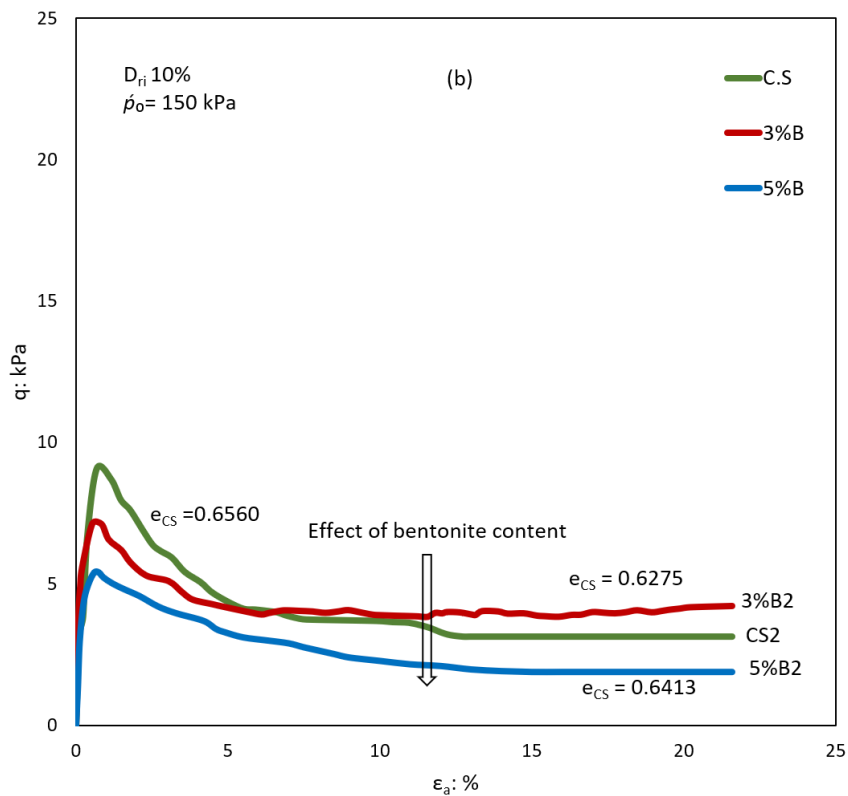
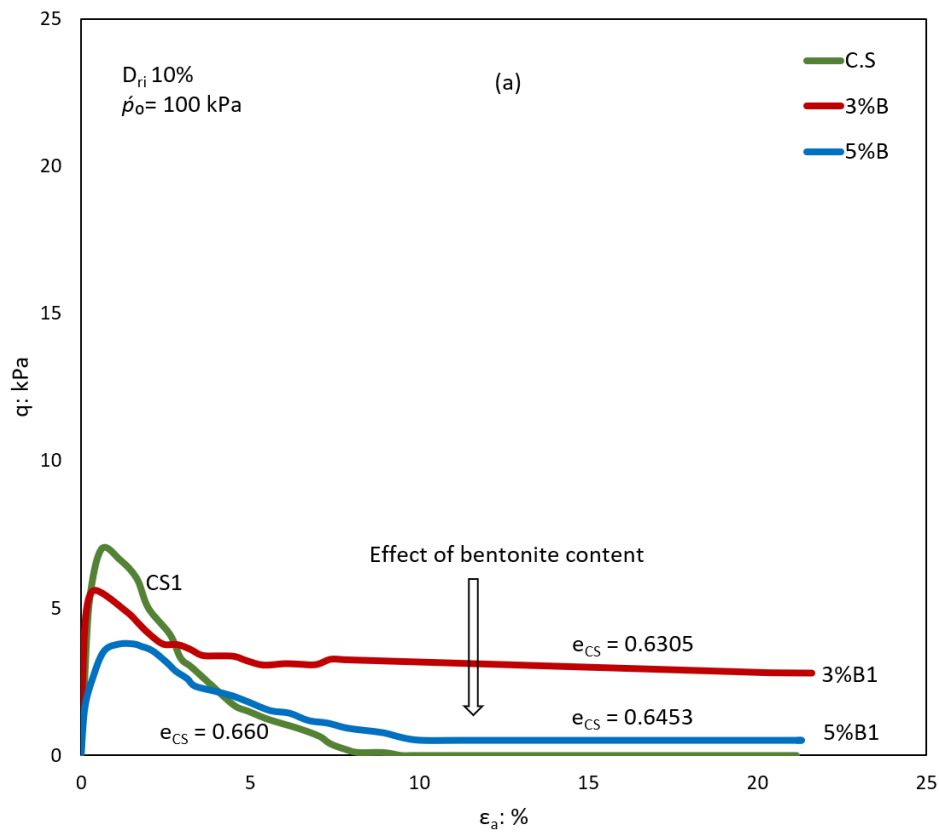
monotonic triaxial tests were run on fully saturated ( $B \geq 0.95$ ) samples with three relative densities ( $D_{ri} = 10\%$ ,  $50\%$ , and  $90\%$ ) and the shearing commencing from the initial confining pressures of 100, 150, and 200 kPa. Tests with samples prepared by mixing the sand with 3% and 5% bentonite were labelled 3%B and 5%B, respectively; the results of these tests are presented in Table 4.5.

Table 4.5 Results of undrained tests conducted on sand–bentonite samples

Test name	$\dot{p}_o$	$D_{ri}$	$e_{cs}$	$q_{peak}$	$R_u$	$q_{min}/q_{peak}$	$I_B$	$\eta$	$\Psi_o$
<b>3%B1</b>	100	10	0.63053	5.61	0.950	0.335	0.665	0.120	0.0099
<b>3%B2</b>	150	10	0.62754	7.12	0.940	0.463	0.537	0.131	0.0129
<b>3%B3</b>	200	10	0.62357	9.77	0.935	0.604	0.396	0.150	0.0168
<b>3%B4</b>	100	50	0.57090	35.91	0.634	0.780	0.220	0.579	0.0029
<b>3%B5</b>	100	90	0.50672	70.00	0.340	0.983	0.017	0.763	0.0018
<b>5%B1</b>	100	10	0.64535	3.78	0.960	0.132	0.868	0.084	0.0120
<b>5%B2</b>	150	10	0.64134	5.40	0.949	0.350	0.650	0.103	0.0160
<b>5%B3</b>	200	10	0.63784	6.40	0.950	0.594	0.406	0.119	0.0195
<b>5%B4</b>	100	50	0.58450	27.60	0.660	0.697	0.303	0.519	0.0038
<b>5%B5</b>	100	90	0.51688	73.00	0.380	0.904	0.096	0.730	0.0028

The results of six isotropically consolidated undrained triaxial tests (3%B1–3%B3 and 5%B1–5%B3) using samples in the very loose state ( $D_{ri} 10\%$ ) with shearing starting from the initial confining pressure  $\dot{p}_o$  of 100, 150, and 200 kPa are presented in Figures 4.28–4.30. Figure 4.28 shows the stress–strain relationships of the sand–bentonite mixtures tested at  $\dot{p}_o$  of 100, 150, and 200 kPa. It is apparent that mixing sandy soil with 3% and 5% bentonite did not improve the shear strength of the sandy soil. This behaviour is shown in Figures 4.28(a)–(c) where the clean sand samples exhibited a higher initial peak deviatoric stress ( $q_{peak}$ ) than the sand–bentonite mixtures at the three confining pressures and the values of  $q_{peak}$  decreased when the bentonite content increased up to 5%. However, the samples of sand–3% bentonite showed the highest minimum deviatoric stress  $q_{min}$ . The values of  $q_{peak}$  decreased from 7 kPa in the clean sand sample to 5.61 kPa and 3.78 kPa when the bentonite content increased to 3% and 5%, respectively. Moreover, the initial peak deviatoric stresses of the sand–bentonite mixtures increased with an increase in the initial confining pressure, while the increase rate of the deviatoric stresses was less than that for the C.S samples. The  $q_{peak}$  value of sand–3% bentonite increased from 5.61 kPa at  $\dot{p}_o = 100$  kPa to 7.12 kPa and 9.77 kPa when the initial confining pressure  $\dot{p}_o$  increased to 150 and 200 kPa, respectively.

Furthermore, note that the minimum deviatoric stress  $q_{min}$  at the end of the tests increased with an increase in the initial confining pressure  $p'_o$ .



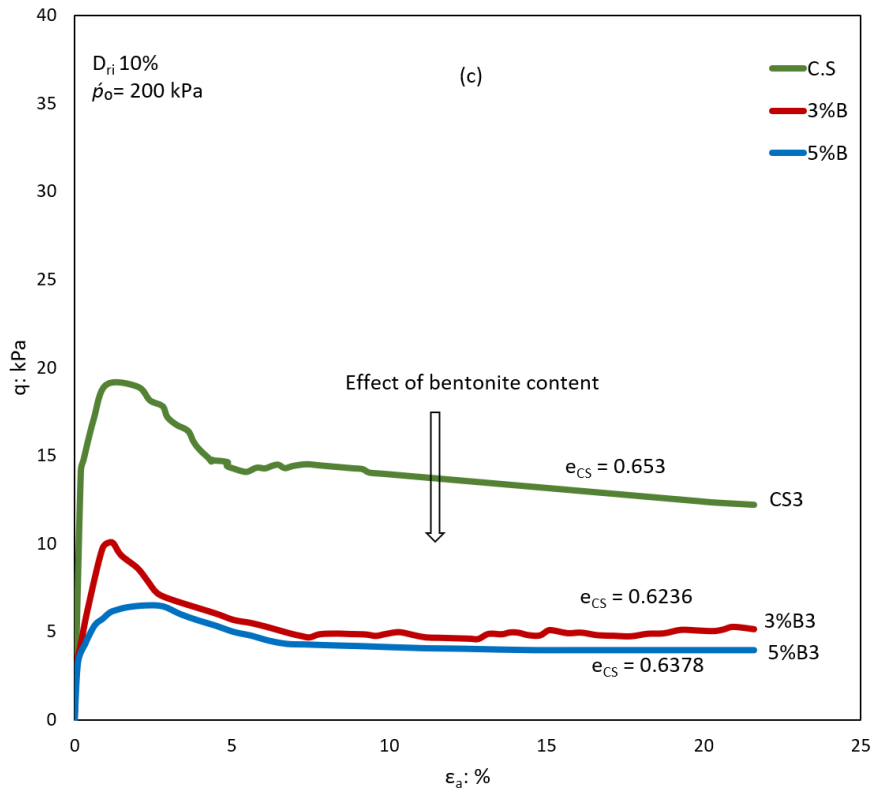
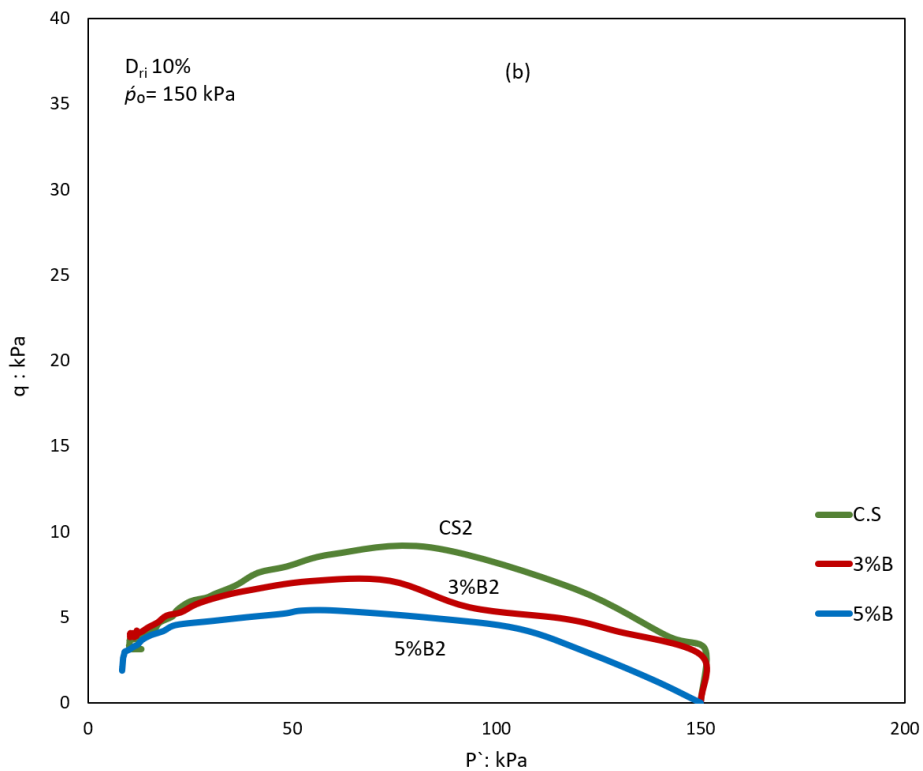
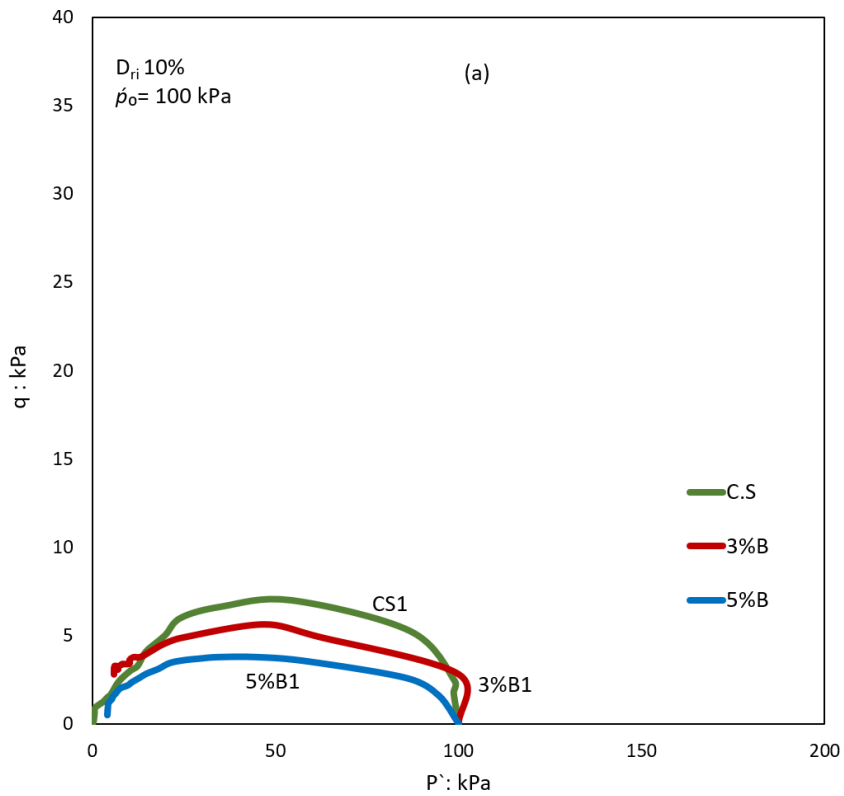


Figure 4.28 Undrained behaviour of very loose sand–bentonite samples: (a) stress–strain curves with  $\dot{p}_0 = 100$  kPa, (b) strain curves with  $\dot{p}_0 = 150$  kPa, and (c) strain curves with  $\dot{p}_0 = 200$  kPa

The effective stress paths of the tests of samples prepared at  $D_{ri}$  10% and sheared under the three initial confining pressures (100, 150 and 200 kPa) are shown in Figures 4.29(a)–(c). For all the tests (clean sand and sand–bentonite mixtures), the effective stress paths plummeted toward the origin of the  $q$ – $p'$  plane after reaching their representative peak deviatoric stress; this indicated the flow behaviour. However, a clean sand sample tested at  $\dot{p}_0 = 100$  kPa showed complete static liquefaction when the deviatoric stress rapidly reduced to zero. The data presented in Figures 4.29(a)–(c) revealed that the slope of the effective stress paths of all the tests increased with increasing initial confining pressure and that the effective stress paths at the initial confining pressure of 200 kPa showed the highest values. At the three initial confining pressures (i.e. 100, 150, and 200 kPa), the slope of the effective stress paths of the C.S samples was higher than that in the case of the sand–bentonite mixtures, and the difference between the slopes of the effective stress paths increased with an increase in the initial confining pressures. Figures 4.29(a)–(c) clearly show the decreasing trend

of the slope of the effective stress paths with an increase in the bentonite content; further, the 5%B samples showed the lowest values.





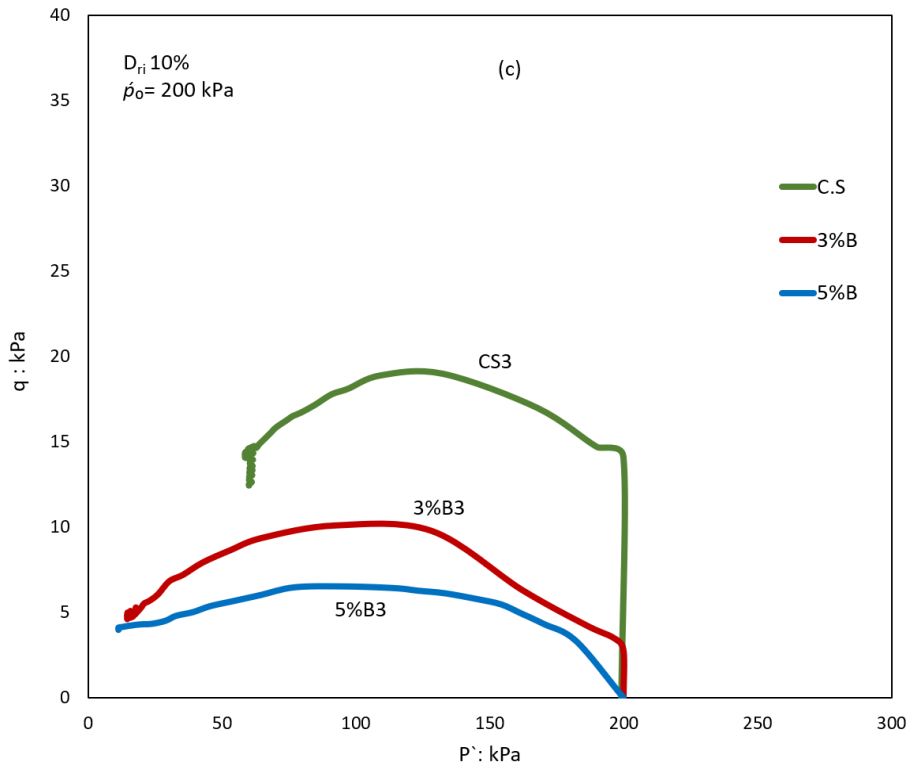
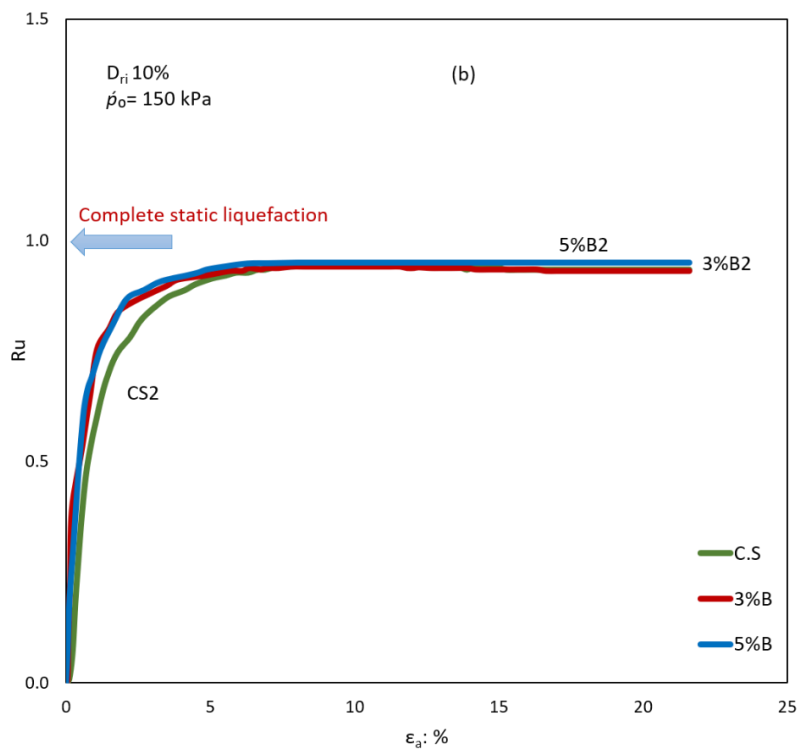
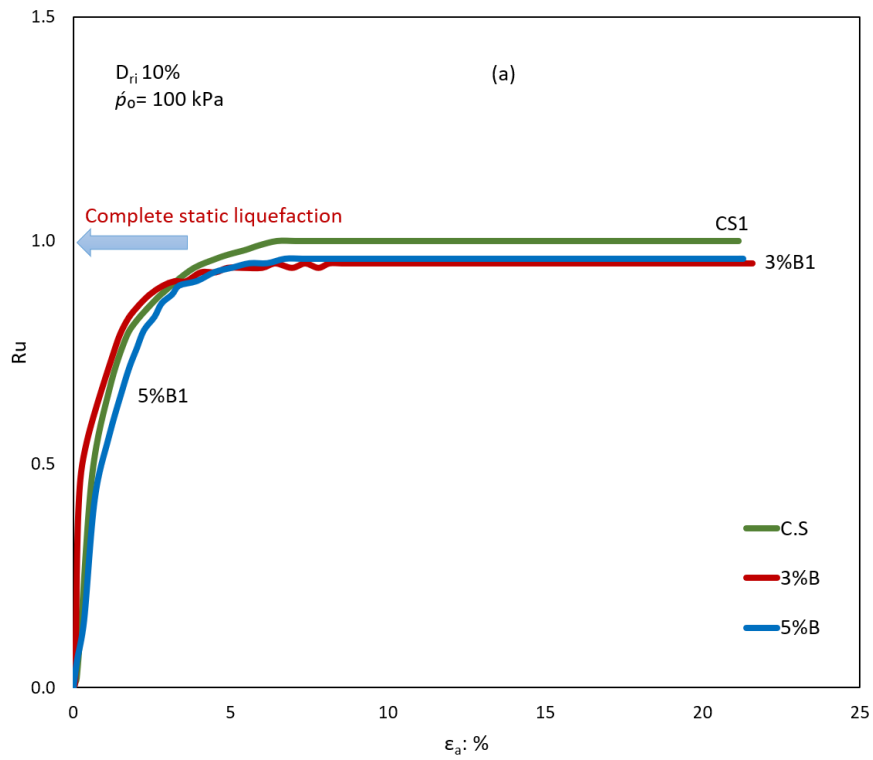


Figure 4.29 Undrained behaviour of very loose sand–bentonite samples: (a) effective stress path with  $p_0 = 100$  kPa, (b) effective stress path with  $p_0 = 150$  kPa, and (c) effective stress path with  $p_0 = 200$  kPa

The negative effect of the bentonite content on the liquefaction behaviour of sandy soil is shown in Figures 4.30(a)–(c). It is apparent from these figures that all of the loose samples (i.e. clean sand and sand–bentonite samples) sheared at the initial confining pressure  $p_0$  of 100, 150, and 200 kPa showed flow behaviour characterised by the positive pore water pressure ratio  $R_u$ . At  $p_0 = 100$  kPa, the  $R_u$  of the clean sand sample slightly reduced with an increase in the bentonite content of up to 3%; then, it slightly increased with an increase in the bentonite content to 5%. The pore water pressure ratio  $R_u$  decreased from 1 in the clean sand sample to 0.95 and 0.96 when the bentonite content increased to 3% and 5%, respectively. The values of the pore water pressure ratios  $R_u$  decreased with an increase in the initial confining pressure  $p_0$  to 150 kPa and 200 kPa, and the 3%B and 5%B samples showed higher  $R_u$  values than the clean sand samples. At  $p_0 = 150$  kPa, the three samples showed almost the same values when  $R_u$  increased from 0.93 in the clean sand sample to 0.94 and 0.95 when bentonite increased to 3% and 5%, respectively. However, the effect of the bentonite content on the generation of the pore water pressure of sandy soils was more pronounced at  $p_0 =$

200 kPa when the clean sand sample exhibited the lowest  $R_u$  values; further,  $R_u$  increased with an increase in the bentonite content. At  $p'_0 = 200$  kPa,  $R_u$  significantly increased from 0.63 for the clean sand to 0.93 and 0.95 when the bentonite content increased to 3% and 5%, respectively.



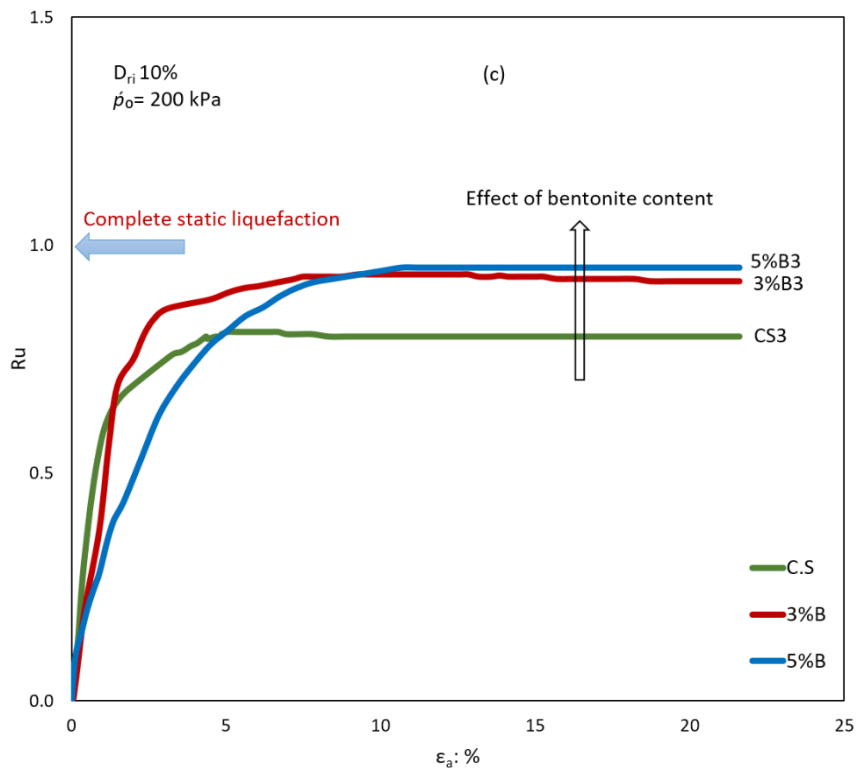
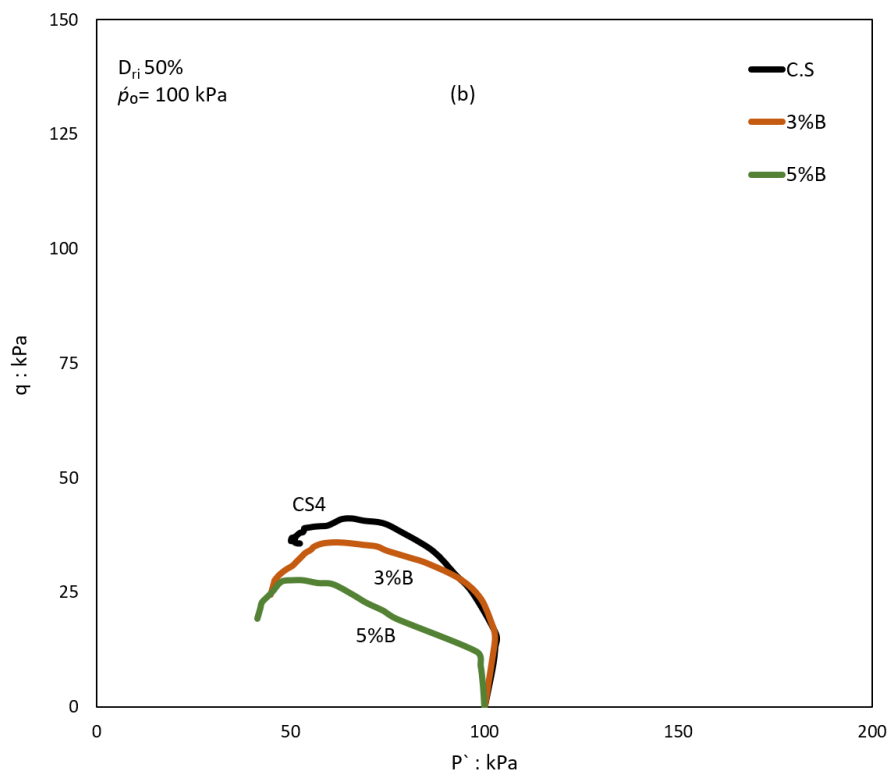
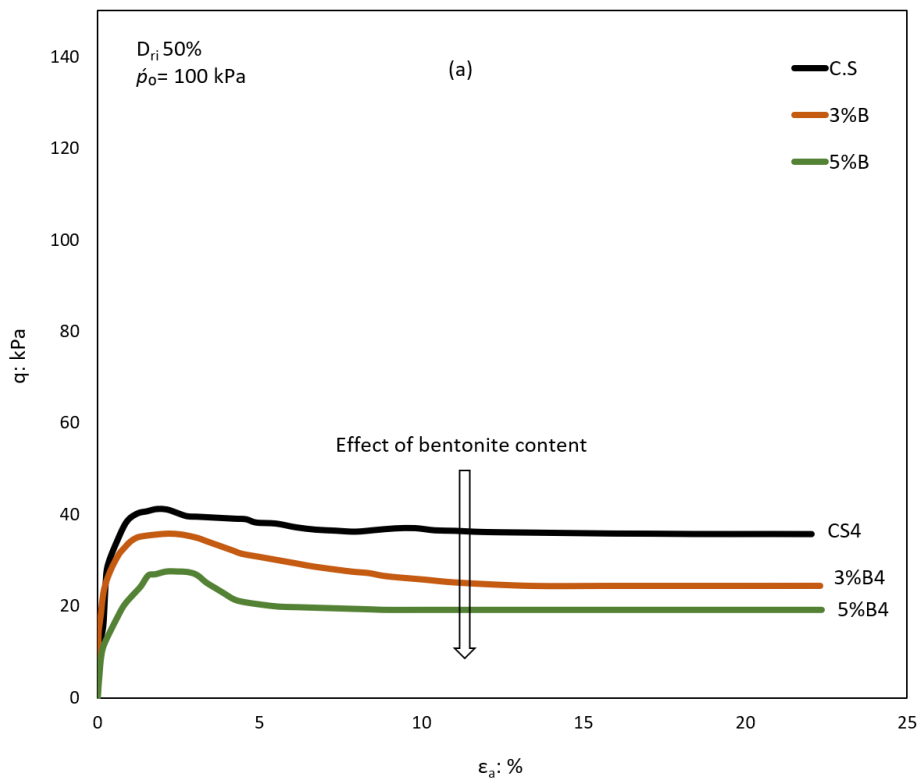


Figure 4.30 Undrained behaviour of very loose sand–bentonite samples: (a) pore water pressure ratio–strain with  $p_0 = 100$  kPa, (b) pore water pressure ratio–strain with  $p_0 = 150$  kPa, and (c) pore water pressure ratio–strain with  $p_0 = 200$  kPa

Note that the  $R_u$  data of the very loose sand–5% bentonite mixtures were obtained because the effect of the increasing initial confining pressure on the generation of the pore water pressure was diminished, which was inferred from the slight reduction in its values with an increase in  $p_0$ , as shown in Table 4.5. The above behaviour trend of the very loose ( $D_{ri}$  10%) clean sand and sand–bentonite mixtures at the three initial confining pressures is in line with the so-called ‘reverse behaviour’ as represented by the increasing initial peak deviatoric stresses, increasing slope of effective stress paths, and reducing pore water pressure ratios with increasing initial confining pressure. Moreover, the presence of bentonite in sandy soil reduces the ability of the soil to induce this type of behaviour. The undrained behaviour of the very loose  $D_{ri}$  10% samples is compared with that of the  $D_{ri}$  50% and 90% samples in Figures 4.31 and 4.32. The undrained shear of all the tests commenced from the same initial confining pressure defined by  $p_0 = 100$  kPa. Figures 4.31(a)–(c) show a comparison of the results of the clean sand sample prepared at  $D_{ri}$  50% with the sand–bentonite mixtures prepared at the same relative density. It was apparent that increasing the relative

density from 10% to 50% enhanced the shear strength of clean sandy soil by changing its behaviour from complete static liquefaction to limited liquefaction.



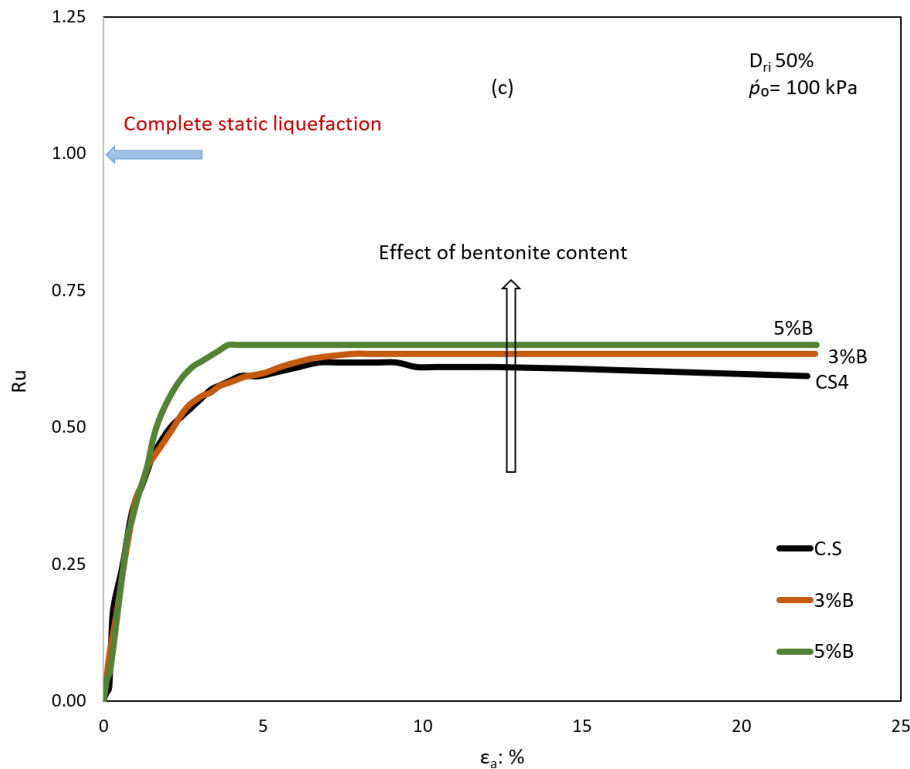
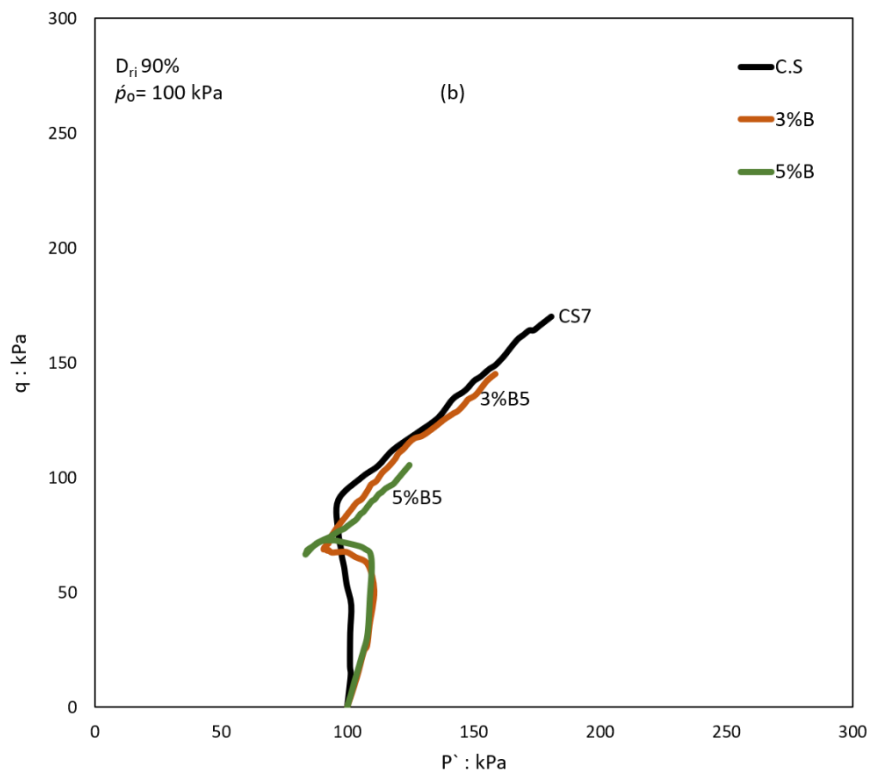
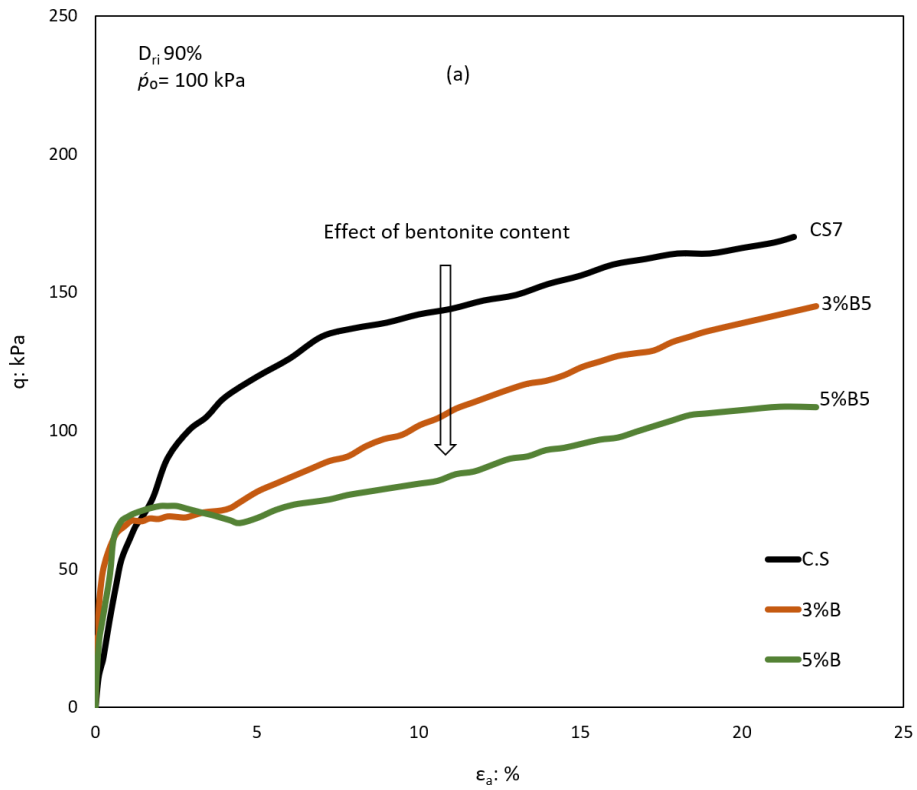


Figure 4.31 Undrained behaviour of sand–bentonite samples prepared at relative density of 50%: (a) stress–strain relationships, (b) effective stress paths, and (c) pore water pressure ratio–strain

Furthermore, increasing the relative density of the sand–bentonite mixtures also enhanced the shear strength of these mixtures, but the behaviour of the very loose mixtures ( $D_{ri}$  10%) and medium mixtures ( $D_{ri}$  50%) exhibited the same trend (flow behaviour). Further, the initial peak deviatoric stresses and the minimum deviatoric stresses increased with an increase in the relative density, as shown in Figure 4.31(a). Moreover, adding the bentonite content to sandy soil enhanced the ability of the constructiveness of sandy soil by reducing the deviatoric stress; the 5%B samples showed the lowest values. The rate of reduction from the initial peak to the minimum deviatoric stresses increased with an increase in the bentonite content. The initial peak deviatoric stresses increased with an increase in the bentonite content. The initial peak deviatoric stress decreased from 40.65 kPa in C.S to 35.9 kPa and 27.6 kPa when the bentonite content increased to 3% and 5%, respectively. Figure 4.31(b) shows that the slope of the effective stress paths of the clean sand and the sand–bentonite mixtures increased with an increase in the relative density; the C.S sample showed the highest slope values. However, adding bentonite to sandy soil reduced the slope of the effective stress path, and sand with 5% bentonite exhibited the lowest values. The effect of increasing the relative density on the pore water pressure of the sand–

bentonite mixtures is shown in Figure 4.31(c). This figure shows that the three samples (i.e. C.S, 3%B, and 5%B) had positive pore water pressure ratios.



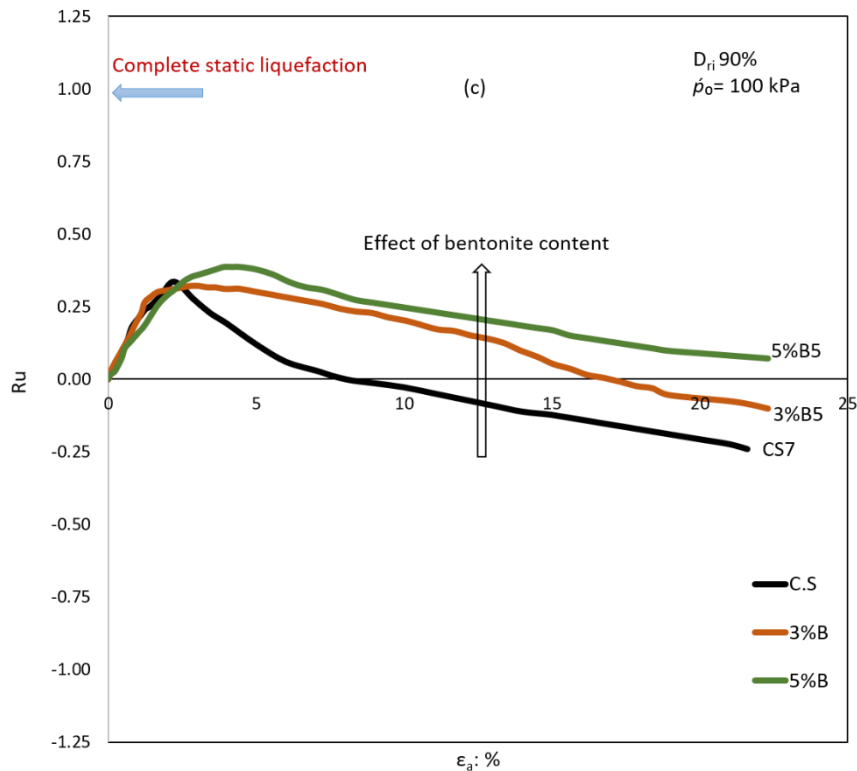


Figure 4.32 Undrained behaviour of sand–bentonite samples prepared at relative density of 90%: (a) stress–strain relationships, (b) effective stress paths, and (c) pore water pressure ratio–strain

The clean sand sample showed a gradual increment in  $R_u$  until the maximum value was obtained; then,  $R_u$  decreased until the end of the test. However, the sand–bentonite mixtures showed a gradual increment in  $R_u$  until the maximum value was reached and then remained constant until the end of the test. The values of  $R_u$  increased from 0.63 in the C.S sample to 0.634 and 0.66 when the bentonite content increased to 3% and 5%, respectively. In addition, the sample of 3%B reached the constant pore water pressure ratio at the axial strain of 6.13%. However, the sample of 5%B reached a constant value at 3.91%. Figures 4.32(a)–(c) show the results of the undrained triaxial tests conducted on the samples of clean sand and sand–bentonite mixtures prepared in the dense ( $D_{ri}$  90%) state. The data presented in Figure 4.32(a) revealed a significant reduction in the deviatoric stress of C.S when mixed with 3% and 5% bentonite. The C.S sample exhibited non-flow behaviour characterised by the gradual increment of the deviatoric stress until the end of the tests. However, both the sand–bentonite mixtures (i.e. 3%B and 5%B) exhibited a reduction in the deviatoric stresses after attaining the initial peak; then, these stresses increased until the end of the tests. Furthermore, a slight difference between the initial peak deviatoric stresses of 3%B

and 5%B was observed, but the deviatoric stress at the end of the test in the 3%B sample was higher than that in the 5%B sample. The initial peak deviatoric stress in 3%B was 70 kPa; it is increased to 73 kPa when the bentonite content increased to 5%. The deviatoric stress at the end of the test reduced from 170 kPa in the C.S sample to 145 kPa and 108.36 kPa when the bentonite content increased to 3% and 5%, respectively. Figure 4.32(b) shows the effective stress paths of the dense clean sand and sand–bentonite mixtures. Further, the effective stress paths of 3%B and 5%B initially showed the flow behaviour, while relatively large strains caused elbowing and the stress path switched to the non-flow behaviour until the end of the tests. However, the C.S samples showed rapid increases in the deviatoric stress, which indicated non-flow behaviour. This behaviour is observed in Figure 4.32(c) when the C.S sample showed an abrupt decrease in the pore water pressure ratio ( $R_u$ ) after achieving an initial peak; the reduction continued until a negative value was obtained at the end of the test. However, both the 3%B and the 5%B samples showed a reduction in the pore water pressure ratio after attaining the peak value, but the reduction rate was less than that of the C.S sample. Moreover, the initial peak of the pore water pressure ratio increased with an increase in the bentonite content, and the 5%B sample exhibited the highest value. A marked feature of the abovementioned Figures 4.28–4.32 is that upon the addition of bentonite to the very loose sandy soil, the sand tended to become softer because of the decreasing deviatoric stresses and the increasing pore water pressure ratios. In contrast, increasing the relative density enhanced the shear strength of the sandy soil and the sand–bentonite mixtures; however, the clean sand samples showed higher strength than the sand–bentonite mixtures, and the increasing relative density hindered the negative effect of bentonite on the liquefaction behaviour of sandy soil, as shown in Figures 4.33(a) and (b). Figure 4.33(a) shows that the stress ratio ( $q_{min}/q_{peak}$ ) of all the mixtures considerably increased with an increase in the relative density from 10% to 50% and 90%. At the relative density of 10%, the stress ratio ( $q_{min}/q_{peak}$ ) increased from zero in the C.S sample to 0.335 and 0.132 when the bentonite content increased to 3% and 5%, respectively. However, at the relative densities of 50% and 90%, a slight difference between the stress ratios of C.S and 3%B was observed, but the stress ratio decreased when the bentonite content increased to 5%. Figure 4.33(b) shows a significant reduction in the pore water pressure ratios when the relative densities increased from 10% to 50% and 90%. Moreover, all the samples



showed insignificant differences in  $R_u$ , and the samples of 5%B exhibited the highest values of  $R_u$  at  $D_{ri}$  50% and 90%.

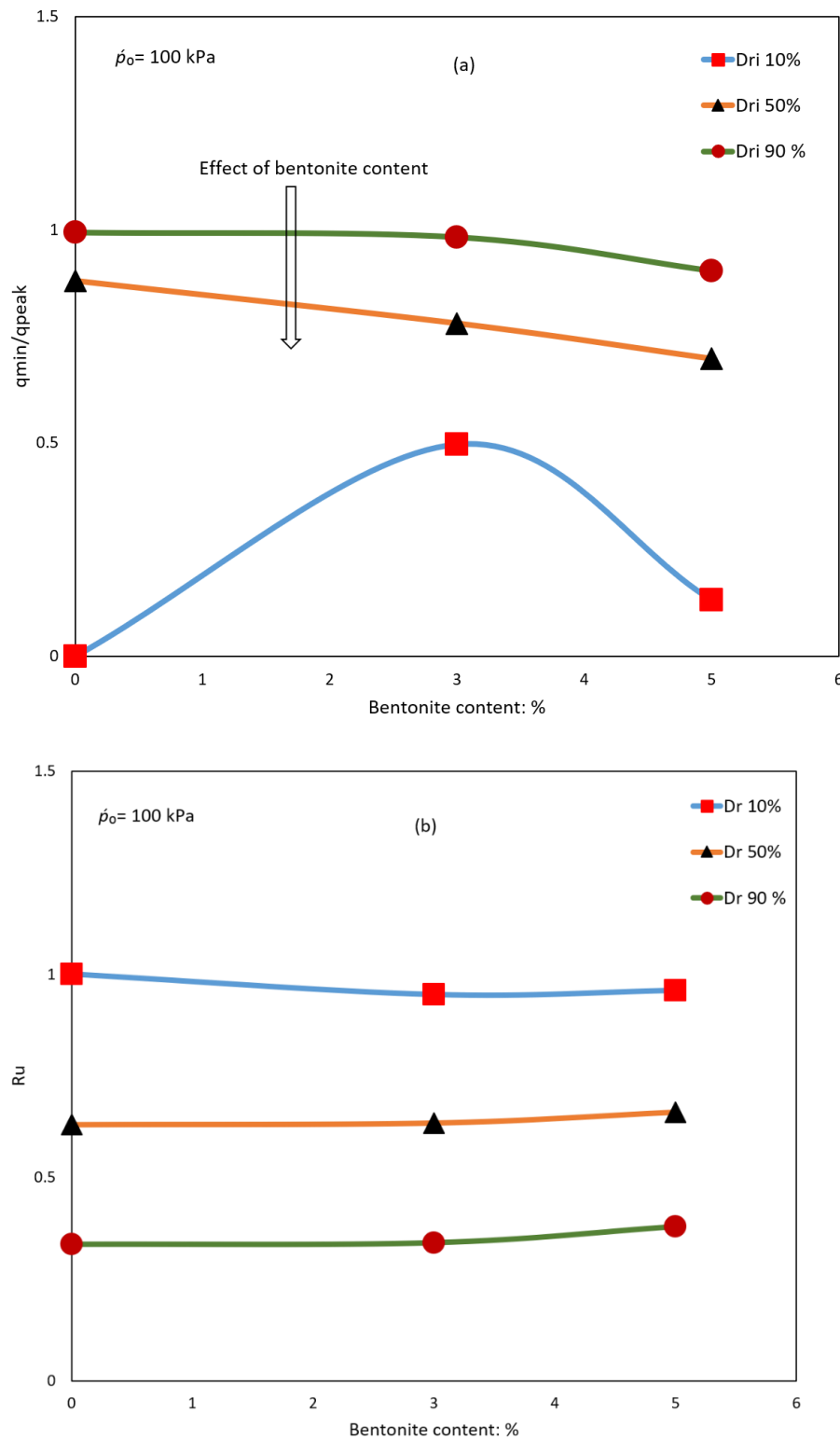
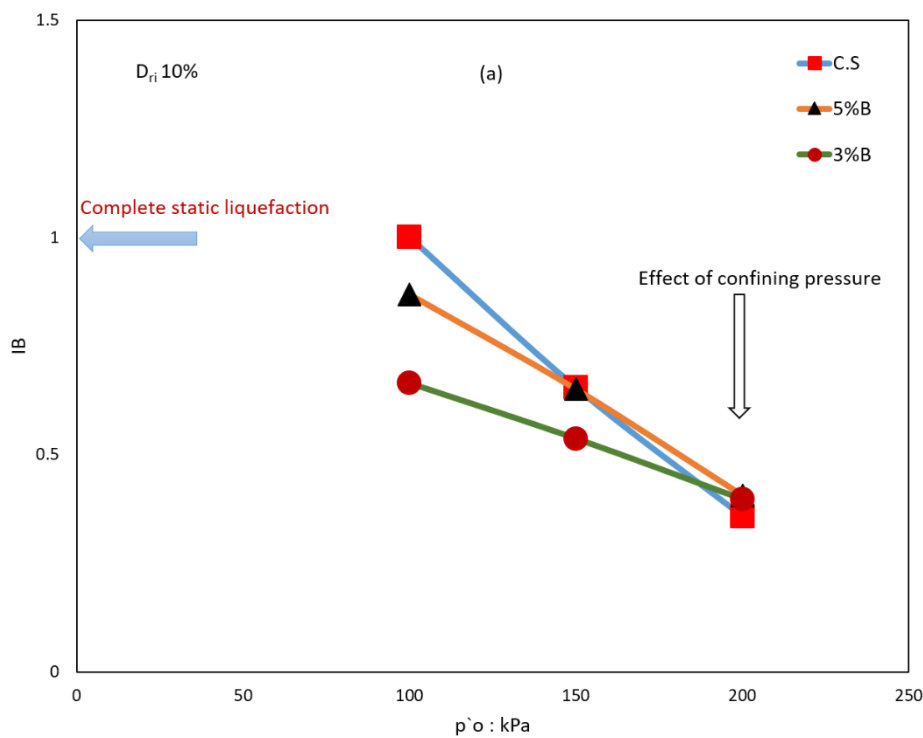


Figure 4.33 Effect of bentonite content on state parameter at start of the test of sand-bentonite mixtures: (a) state parameter at start of the test vs. initial confining pressure and (b) brittleness index vs. state parameter at start of the test

The effect of the bentonite content on the liquefaction susceptibility of sandy soil is shown in Figures 4.34–4.36. Figure 4.34(a) shows the relationships between the brittleness index  $I_B$  and the initial confining pressure  $p'_o$  of the very loose samples. It is apparent from this figure that the liquefaction susceptibility of all the samples decreased with increasing initial confining pressure  $p'_o$  and the sand–bentonite mixtures showed the highest value of  $I_B$  at  $p'_o = 200$  kPa. Moreover, the 3%B samples showed lower liquefaction susceptibility than the 5%B samples. The values of  $I_B$  of the very loose samples at  $p'_o = 200$  kPa increased from 0.358 in the C.S sample to 0.396 and 0.4 when the bentonite content increased to 3% and 5%, respectively. Note that in Figure 4.34(a), the values of  $I_B$  of the very loose sand–bentonite samples exhibited an oscillating trend with an increase in the initial confining pressure. At the lowest confining pressure of 100 kPa, the sand–bentonite mixtures showed a lower  $I_B$  value than the C.S samples. In contrast, with an increase in the initial confining pressure, the  $I_B$  values of the sand–bentonite mixtures increased until they were higher than those of the C.S samples at  $p'_o = 200$  kPa. This discrepancy proved the negative effect of the bentonite content on the sand fabric at a very low relative density.



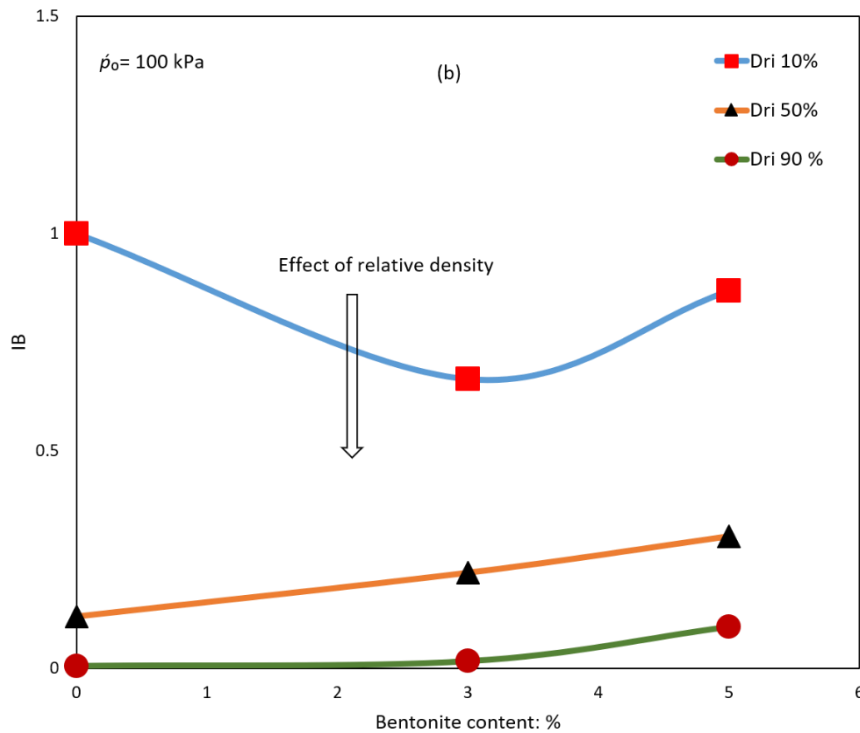


Figure 4.34 Effect of bentonite content on brittleness index of sand–bentonite mixtures: (a) brittleness index vs. initial confining pressure and (b) brittleness index vs. bentonite content

Note that such inconsistency in the relationships between  $I_B$  and the initial confining pressure was not observed when the relative density increased from 10% to 50% and 90%, as shown in Figure. 4.34(b). In this figure, we clearly observed the decreasing trend of  $I_B$  with increasing relative density, and the  $I_B$  values increased with an increase in the bentonite content. Moreover, the samples of 5%B exhibited the highest values of  $I_B$  at the relative density of 50% and 90%. Another investigation of the effect of the bentonite content on the liquefaction susceptibility of sandy soil was carried out by examining the state parameter of all the mixtures at the start of the test ( $\Psi_o$ ). Figure 4.35(a) shows the relationships between  $\Psi_o$  of all the mixtures at  $D_{ri}$  10% and the initial confining pressure. This figure shows that all the mixtures exhibited positive values of  $\Psi_o$ , which indicated the flow behaviour; further, the values of  $\Psi_o$  in all the mixtures increased with an increase in the initial confining pressure. Furthermore,  $\Psi_o$  increased with an increase in the bentonite content, and 5%B showed the highest values. At  $\dot{p}_o = 100$  kPa,  $\Psi_o$  increased from 0.0035 in the C.S sample to 0.0099 and 0.012 when the bentonite content increased to 3% and 5%.

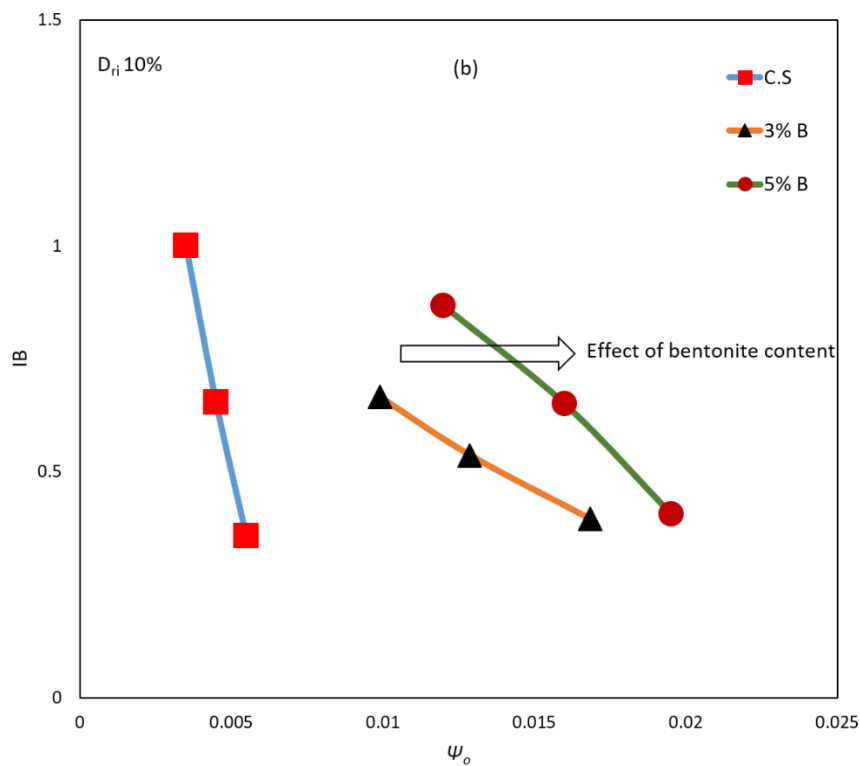
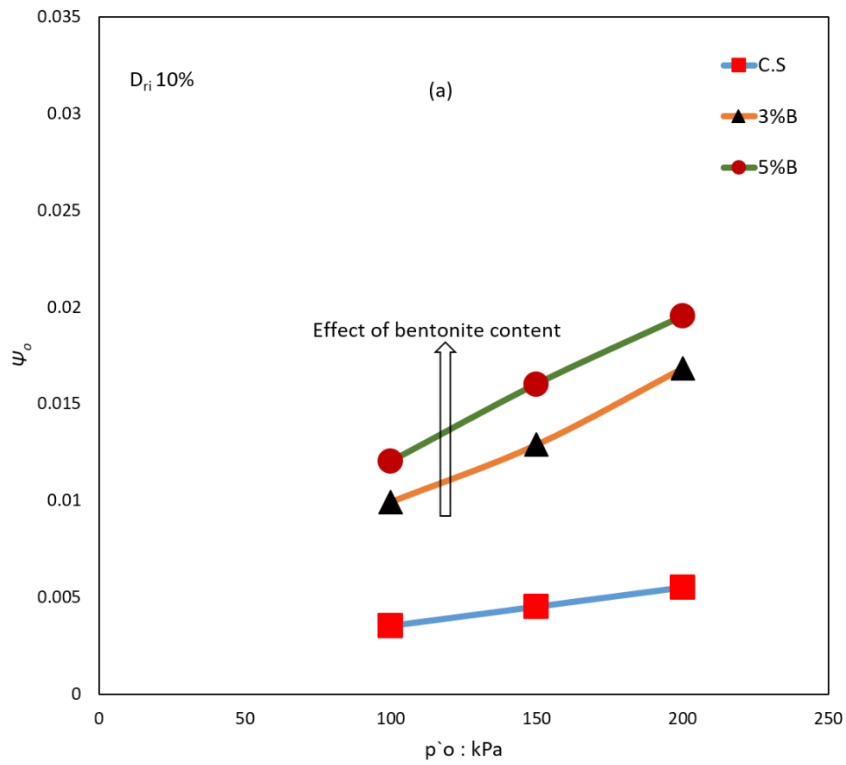
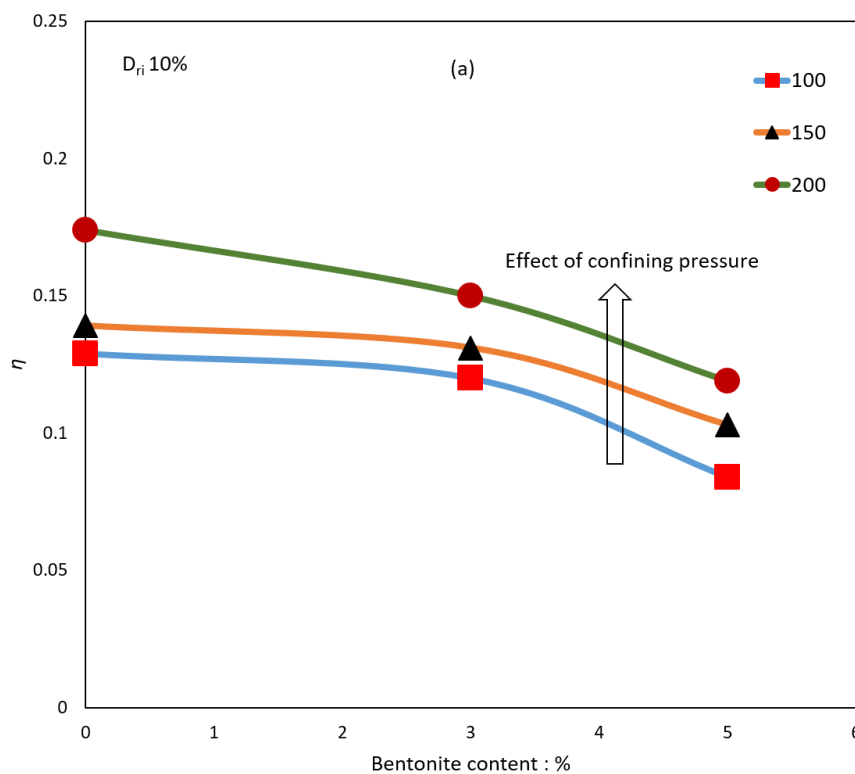


Figure 4.35 Effect of bentonite content on state parameter at start of the test of sand–bentonite mixtures: (a) state parameter at start of the test vs. initial confining pressure and (b) brittleness index vs. state parameter at start of the test

Figure 4.35(b) illustrates the relationship between  $I_B$  and  $\Psi_o$  for all the mixtures. It appears from this figure that the liquefaction susceptibility of the clean sand soil abruptly decreased with a decrease in  $\Psi_o$ ; however, the sand–bentonite mixtures showed a gradual reduction in  $I_B$  with an increase in  $\Psi_o$ . Furthermore, the relationship between  $I_B$  and  $\Psi_o$  shifted to the right, which indicated that the liquefaction susceptibility increased with an increase in the bentonite content and the 5%B samples showed the highest liquefaction susceptibility. Figures 4.36(a) and (b) showed the influence of the bentonite content on the stress ratio at the instability line  $\eta$ . Figure 4.36(a) shows that the  $\eta$  values of all the very loose mixtures increased with an increase in the initial confining pressure. However,  $\eta$  reduced with increasing bentonite content, and the 5%B samples showed the lowest  $\eta$  values at the three initial confining pressures. Moreover,  $\eta$  at  $p_o = 100$  kPa reduced from 0.129 to 0.12 and 0.084 when the bentonite content increased from 3% to 5%.



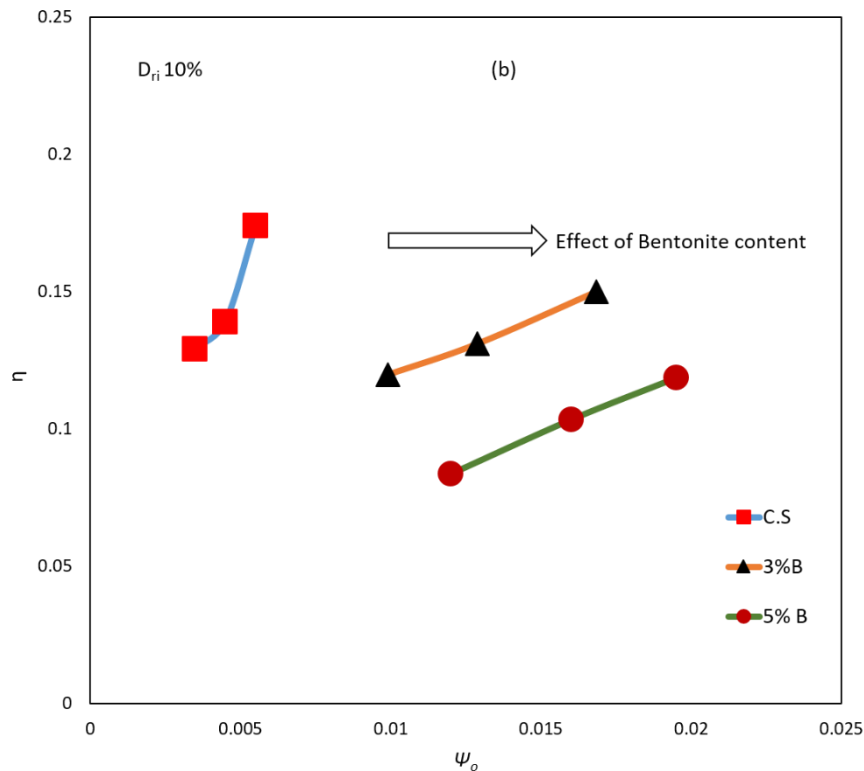


Figure 4.36 Effect of bentonite content on stress ratio at instability line of sand–bentonite mixtures: (a) stress ratio at instability line vs. bentonite content and (b) stress ratio at instability line vs. state parameter at start of the test

This response of  $\eta$  with the increasing bentonite content proved that the addition of bentonite reduced the stability of the sand fabric. This is shown in Figure 4.36(b) when the increasing bentonite content shifted the relationship between  $\eta$  and the state parameter at the start of the test downwards. Further, the shape of the relationship changed from a curve to a straight line with an increase in the bentonite content indicated an increase in the compression tendency for the sand–bentonite specimens, eventually enhancing the potential for static liquefaction. The negative effects of bentonite on the behaviour of sandy soil would be related to its producing an unstable fabric, as a low bentonite content makes the sand grains slippery and increases compressibility. This finding was consistent with those of Tang, Ma, and Shao (2013); Tang, Ma, and Dieudonné (2013), and El Mohtar et al. (2013), who reported that the liquefaction potential increased with the bentonite contents of <5%. However, (Gratchev, Sassa, Osipov, & Sokolov, 2006) reported that artificial clay–sand mixtures exhibited rapid liquefaction when the bentonite content was  $\leq 7\%$ , while the liquefaction susceptibility decreased when the bentonite content was  $\geq 11\%$ . The effect of the curing time on the sand–bentonite mixtures was not explored in this study as it

has already been extensively investigated in the existing literature. These studies reported that the undrained shear strength of the sand–bentonite mixtures increases and the generation of excess pore pressure decreases with an increase in the curing period. El Mohtar et al. (2013) also found that the generation of excess pore pressure in sand mixed with 3% and 5% bentonite decreased with an increase in the curing age.

## 4.5. Effect of kaolinite on liquefaction susceptibility of sandy soils

For the determination of the effect of the clay type on the liquefaction behaviour of sandy soil, a series of undrained triaxial compression tests were performed on sand–kaolinite clay in the present study. All the samples were formed by mixing sandy soil with two proportions (3% and 5%) of kaolinite clay, as shown in Table 4.6. Each sample was monotonically sheared in compression under undrained conditions. The samples were prepared at three relative densities (10%, 50%, and 90%) with the shearing starting from the initial confining pressures  $p'_o$  of 100 kPa, 150 kPa, and 200 kPa. Tests using samples prepared by mixing sand with 3% and 5% kaolinite were labelled 3%K, and 5%K, respectively; the results of these tests are presented in Table 4.7.

Table 4.6 Physical properties of sand–kaolinite mixtures

Materials	Symbol	$e_{max}$	$e_{min}$	$C_u$	$G_s$
Clean sand	C.S	0.675	0.544	2.235	2.580
Sand + 3% kaolinite	3%K	0.739	0.496	1.882	2.640
Sand + 5% kaolinite	5%K	0.767	0.502	1.633	2.670

Table 4.6 shows that the maximum ( $e_{max}$ ) and the minimum ( $e_{min}$ ) void ratios of clean sand decreased when the sand was mixed with 3% kaolinite and then increased when the kaolinite content increased to 5%. The coefficient of uniformity ( $C_u$ ) decreased with increasing kaolinite content. However, the specific gravity ( $G_s$ ) increased when the kaolinite content increased from 3% to 5%.

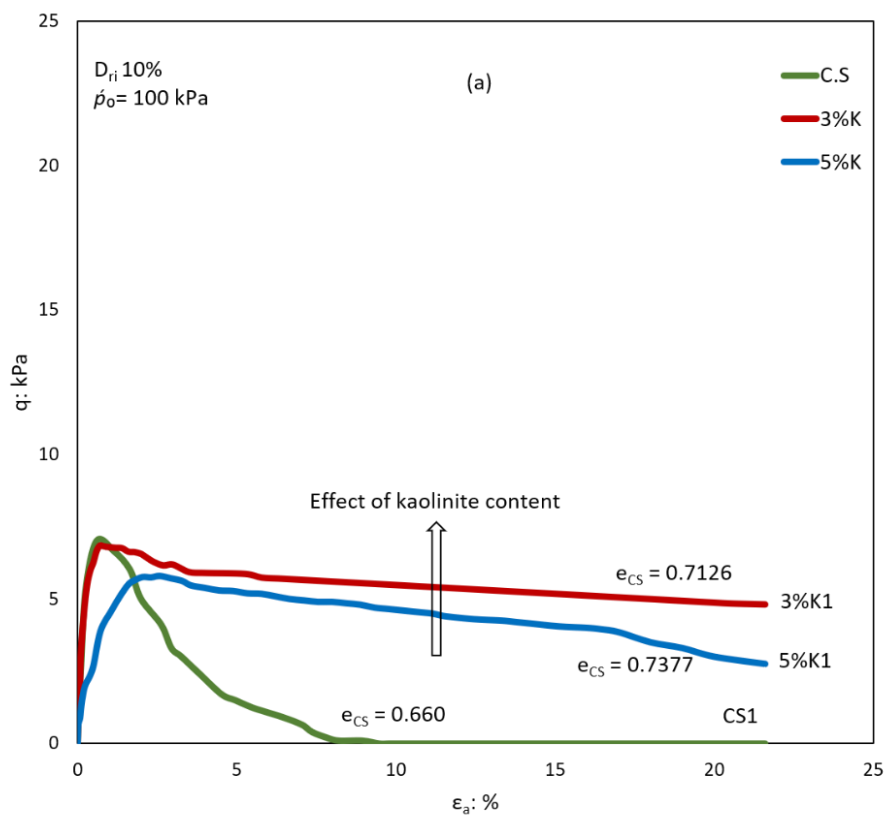
Table 4.7 Results of undrained tests conducted on sand–kaolinite mixtures

Test name	$p'_o$	$D_{ri}$	$e_{cs}$	$q_{peak}$	$R_u$	$q_{min}/q_{peak}$	$I_B$	$\eta$	$\Psi_o$
3%K1	100	10	0.71259	6.84	0.900	0.703	0.297	0.133	0.0021
3%K2	150	10	0.71103	11.78	0.833	0.767	0.233	0.142	0.0036
3%K3	200	10	0.71000	20.9	0.76	0.836	0.164	0.177	0.0047
3%K4	100	50	0.61939	56.00	0.230	0.982	0.018	0.800	-0.0013
3%K5	100	90	0.52106	185.43	0.150	0.998	0.002	0.976	-0.0006
5%K1	100	10	0.73773	5.80	0.940	0.474	0.526	0.126	0.0028
5%K2	150	10	0.73658	8.70	0.887	0.575	0.425	0.138	0.0040
5%K3	200	10	0.73553	17.9	0.83	0.625	0.375	0.175	0.0050
5%K4	100	50	0.63530	53.00	0.340	0.962	0.038	0.768	-0.0010
5%K5	100	90	0.53018	174.90	0.204	0.996	0.004	0.956	-0.0005

Figures 4.37(a)–(c) present the stress–strain relationships of very loose ( $D_{ri}$  10%) sand–kaolinite mixtures sheared under initial confining pressures  $p'_o$  of 100, 150, and 200 kPa. The data presented in Figure 4.37(a) revealed that the three samples (C.S, 3%K, and 5%K) tested at  $p'_o$  100 kPa exhibited a flow behaviour characterised by the reduction in the deviatoric stress after attaining the initial peak  $q_{peak}$  value and the amount of reduction in the deviatoric stress reduced with an increase in the kaolinite content. Furthermore, a slight difference in the initial peak deviatoric stress  $q_{peak}$  was observed for all the samples, and the samples of 5%K showed the lowest values. Moreover,  $q_{peak}$  decreased slightly from 7 kPa in C.S to 6.84 kPa and 5.8 kPa when the kaolinite content increased to 3% and 5%, respectively. However, the minimum deviatoric stresses  $q_{min}$  of the three samples increased when the sand was mixed with 3% kaolinite and then reduced when the kaolinite content increased to 5%. Next,  $q_{min}$  increased from zero in the C.S sample, which indicated complete static liquefaction, to 4.81 kPa in a specimen of 3%K and then reduced to 2.75 kPa in a specimen of 5%K. When the initial confining pressure increased to 150 kPa, all the samples exhibited the same behaviour trend (flow behaviour), but the initial peak deviatoric stress was greater than 100 kPa, as shown in Figure 4.37(b). Furthermore, the reduction rate from the initial peak deviatoric stress to the minimum deviatoric stress decreased with increasing kaolinite content, and the C.S sample showed the lowest value of  $q_{min}$ . A sample of 3%K showed the highest  $q_{peak}$  and  $q_{min}$  stresses. Next,  $q_{peak}$  increased from 9.09 kPa in C.S to 11.78 kPa in a sample of 3%K and then reduced to 8.7 kPa when the kaolinite content increased to 5%. The stress–strain relationships of very loose



sand–kaolinite mixtures sheared at an initial confining pressure  $p'_o$  of 200 kPa are shown in Figure 4.37(c). It is apparent from this figure that all of the samples exhibited the same behaviour trend (flow behaviour), and the initial peak deviatoric stresses increased when the sand was mixed with 3% kaolinite and then reduced when the kaolinite content increased to 5%. However, the C.S sample showed the highest reduction rate of deviatoric stresses. Furthermore, a sample of 3%K showed the highest  $q_{peak}$  and  $q_{min}$ .  $q_{peak}$  in C.S increased from 19 kPa to 20.9 kPa and reduced to 17.9 kPa when the kaolinite content increased to 3% and 5%, respectively.



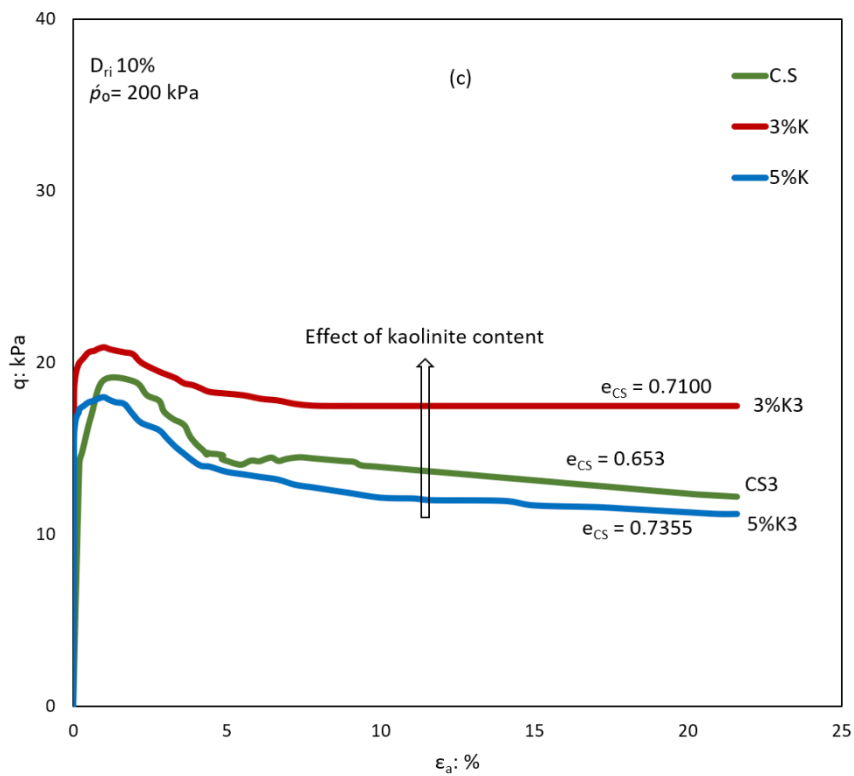
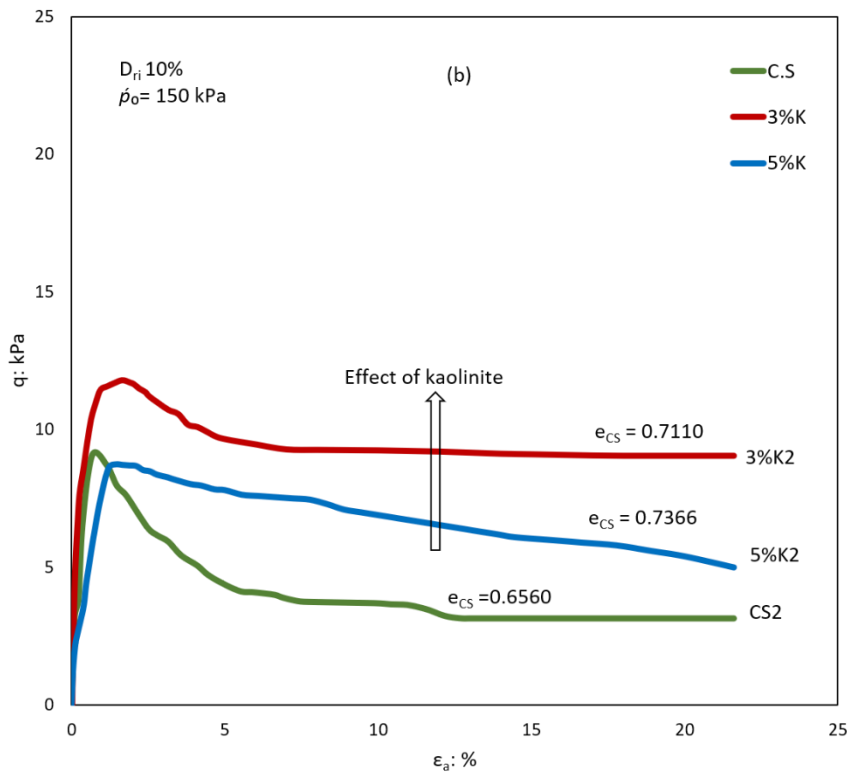
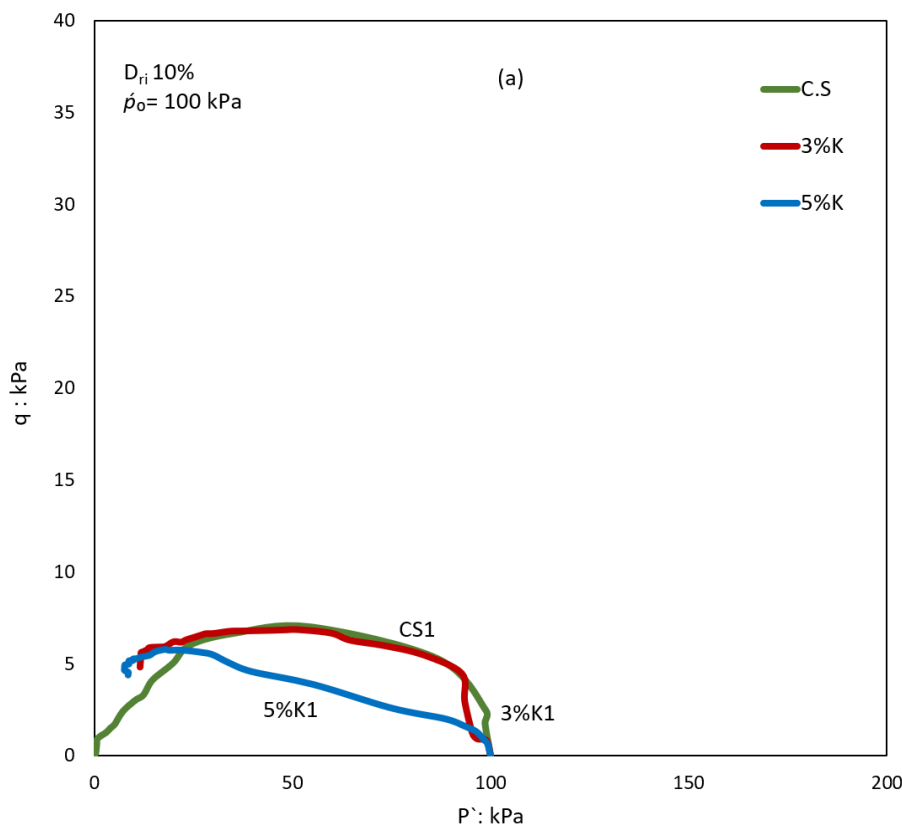


Figure 4.37 Undrained behaviour of very loose sand–kaolinite samples: (a) stress–strain curves with  $p_0 = 100$  kPa, (b) strain curves with  $p_0 = 150$  kPa, and (c) strain curves with  $p_0 = 200$  kPa

The following effective stress paths of the 3%K1–3%K3 tests and the 5%K1–5%K3 tests are shown in Figures 4.38(a)–(c). The effective stress paths of the samples sheared at  $p'_o = 100$  kPa are plotted in Figure 4.38(a); here, the resultant effective stress path plummeted toward the origin of the  $q$ – $p'$  plane after reaching their representative peak deviatoric stress, which indicated flow liquefaction behaviour. The C.S sample sheared at 100 kPa showed complete static liquefaction characterised by the rapid drop of the effective stress path to zero. However, none of the other samples (3%K and 5%K) showed complete static liquefaction at the same initial confining pressure. Figure 4.38(a) also shows a slight difference between the effective stress paths of C.S and the 3%K samples; further, a sample of 5%K showed the lowest values. The flow behaviour was also observed when the initial confining pressure increased to 150 and 200 kPa, but the samples subjected to the highest confining pressure showed the highest deviatoric stresses. The data presented in Figures 4.38(a)–(c) show that the slope of the effective stress paths of the sand–kaolinite mixtures increased with increasing initial confining pressure and that the sample of 3%K showed the highest values at all the three initial confining pressures.



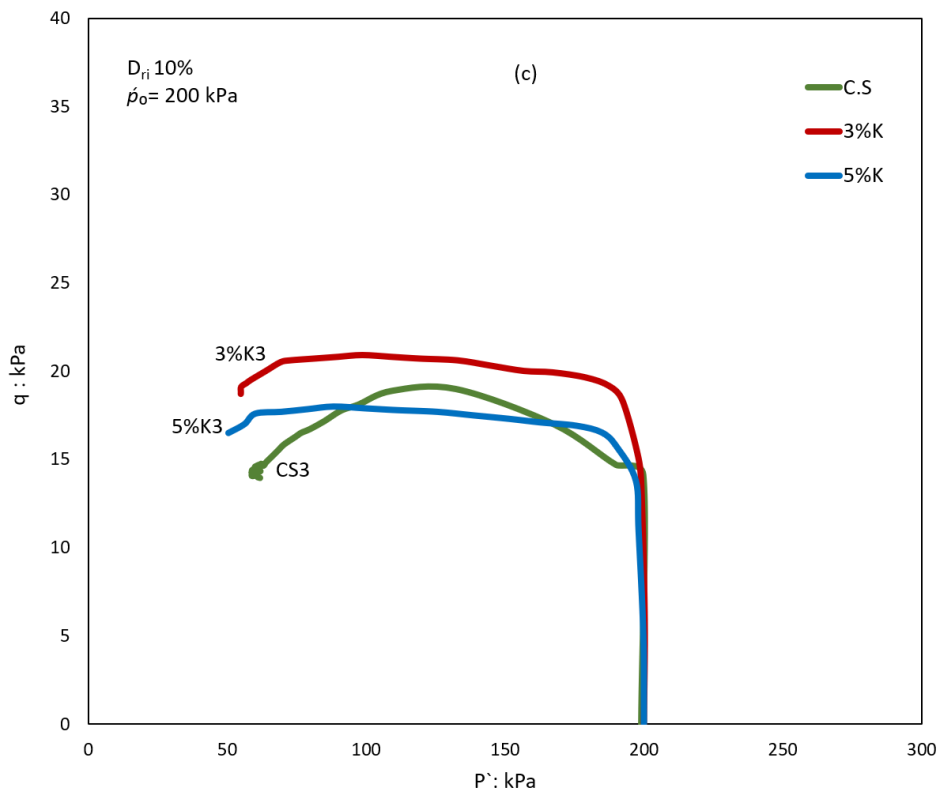
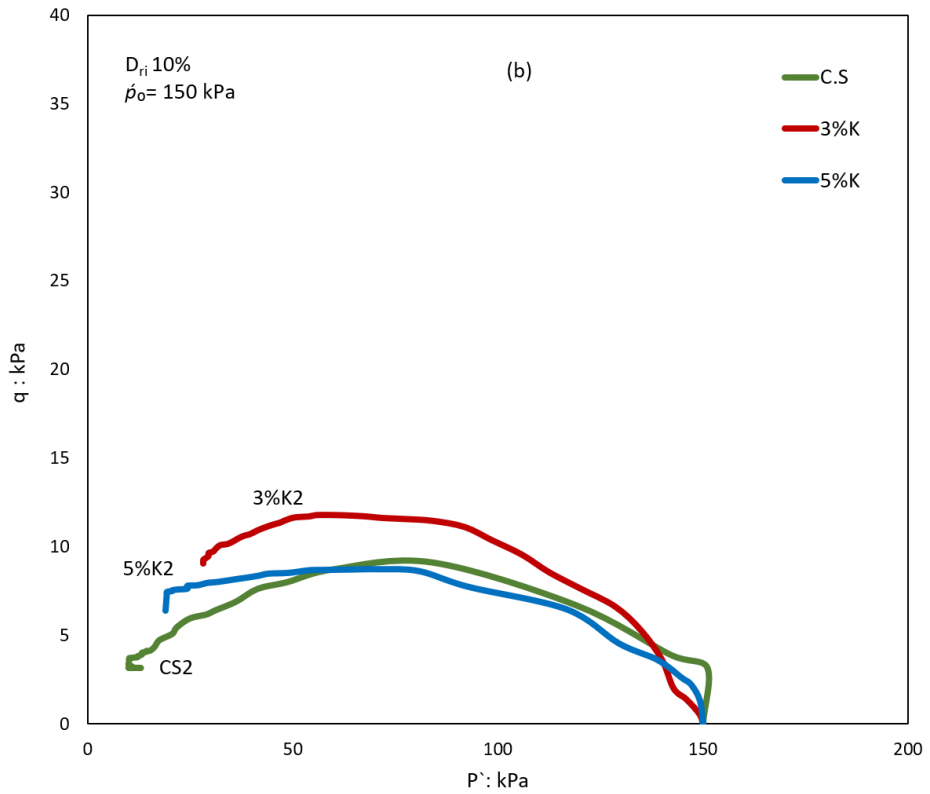
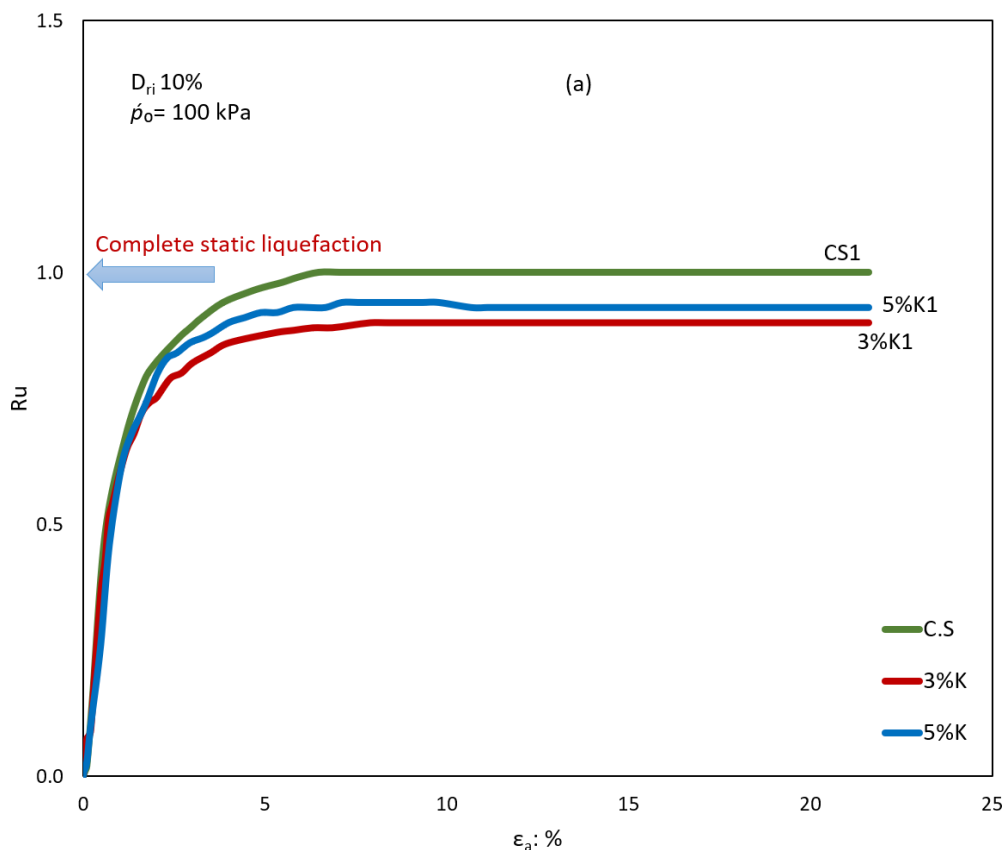


Figure 4.38 Undrained behaviour of very loose sand–kaolinite samples: (a) effective stress path with  $\dot{p}_0 = 100 \text{ kPa}$ , (b) effective stress path with  $\dot{p}_0 = 150 \text{ kPa}$ , and (c) effective stress path with  $\dot{p}_0 = 200 \text{ kPa}$

The effect of the kaolinite content on the liquefaction behaviour of sandy soils can be observed in Figures 4.39(a)–(c), which present the relationships between the pore water pressure ratios  $R_u$  and the axial strain of the very loose samples sheared at the three initial confining pressures. The data presented in Figure 4.39 revealed that all of the samples (C.S, 3% K, and 5% K) sheared at the three initial confining pressures (100, 150, and 200 kPa) exhibited a positive  $R_u$  value, which indicated that the flow behaviour and the pore water pressure ratios in all the tests reduced with increasing initial confining pressure. At the initial confining pressures of 100 kPa and 150 kPa, the C.S samples showed  $R_u$  values higher than those of the sand–kaolinite mixtures. However, when the initial confining pressure increased to 200 kPa, the sample of 5% K showed the highest value of  $R_u$ . At the initial confining pressure  $p'_o$  of 100 kPa,  $R_u$  reduced from 1 in C.S to 0.9 when the sand was mixed with 3% kaolinite; then,  $R_u$  increased to 0.94 when the kaolinite content increased to 5%.



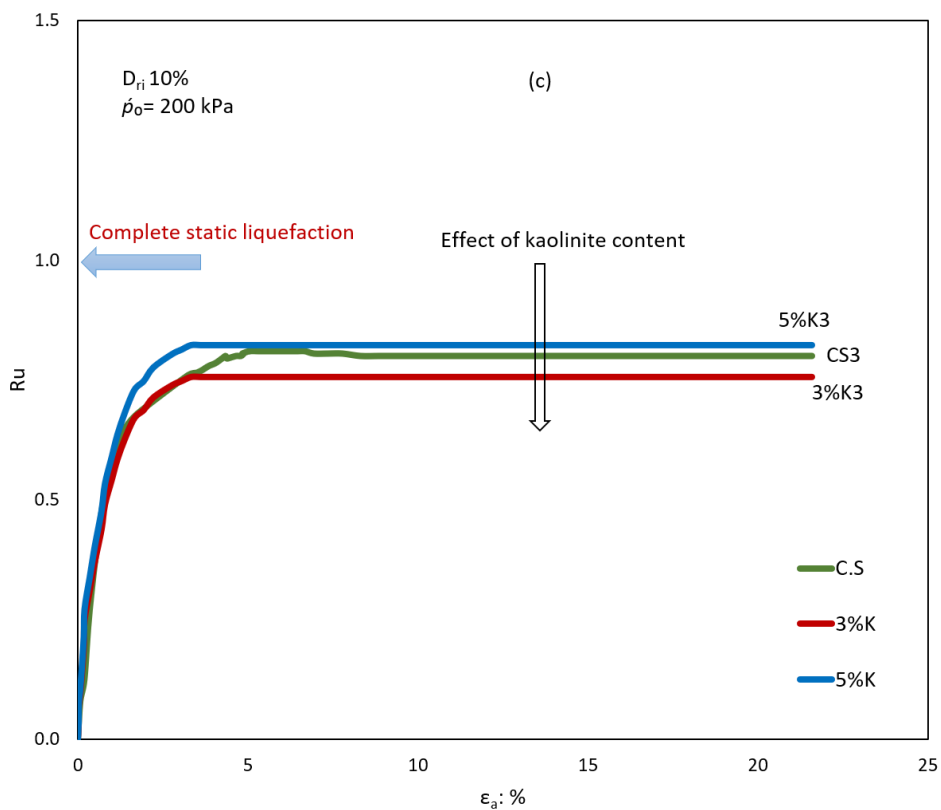
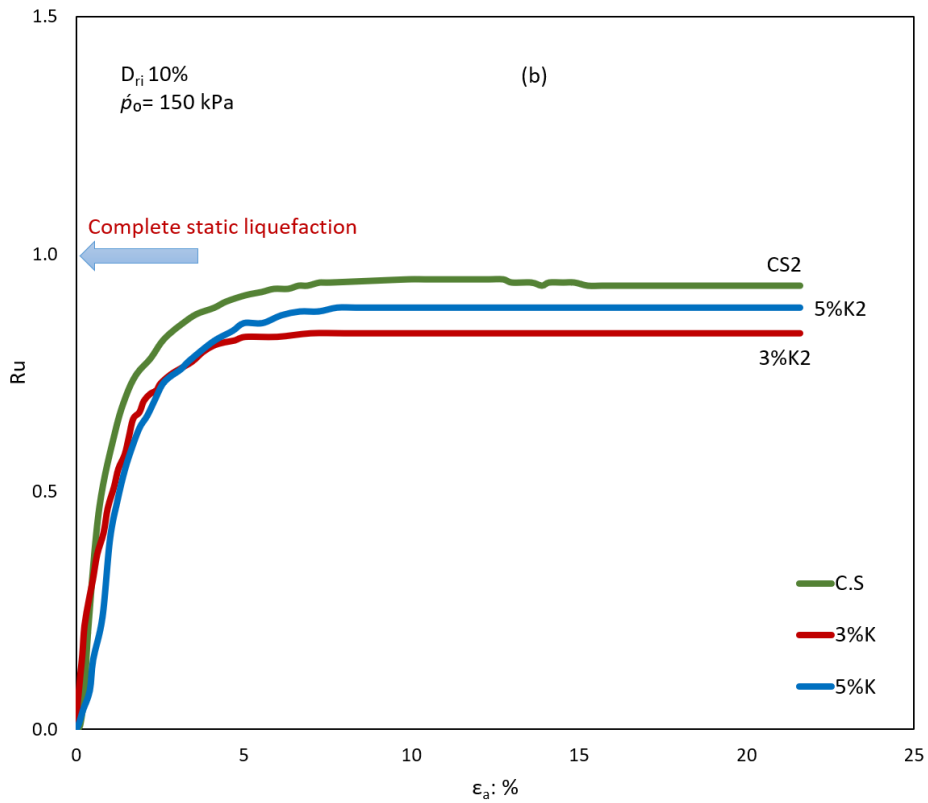
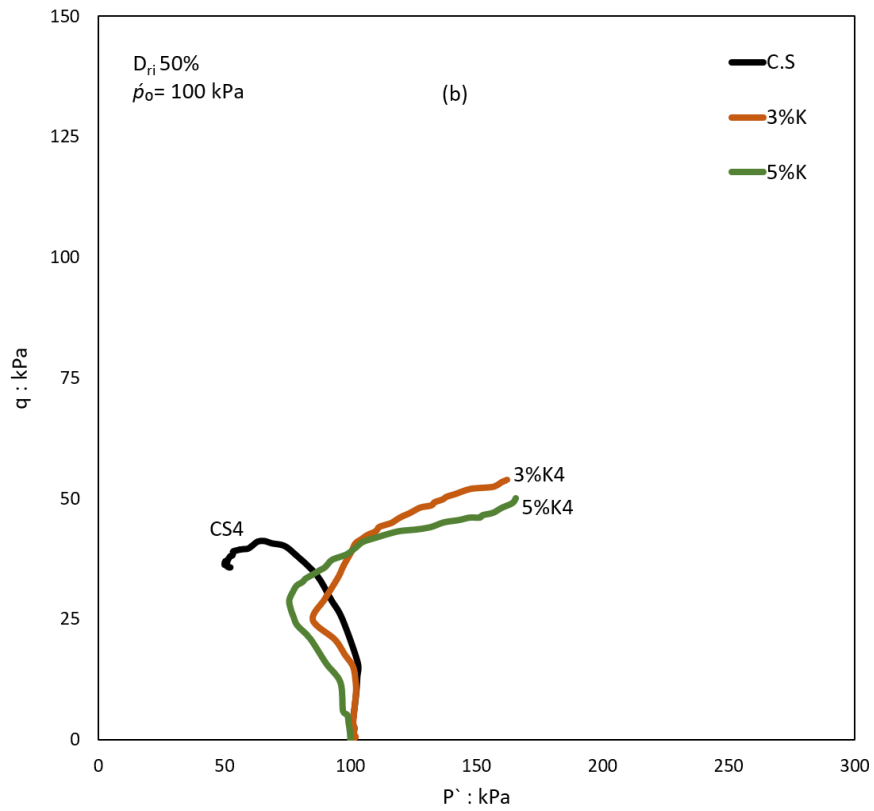
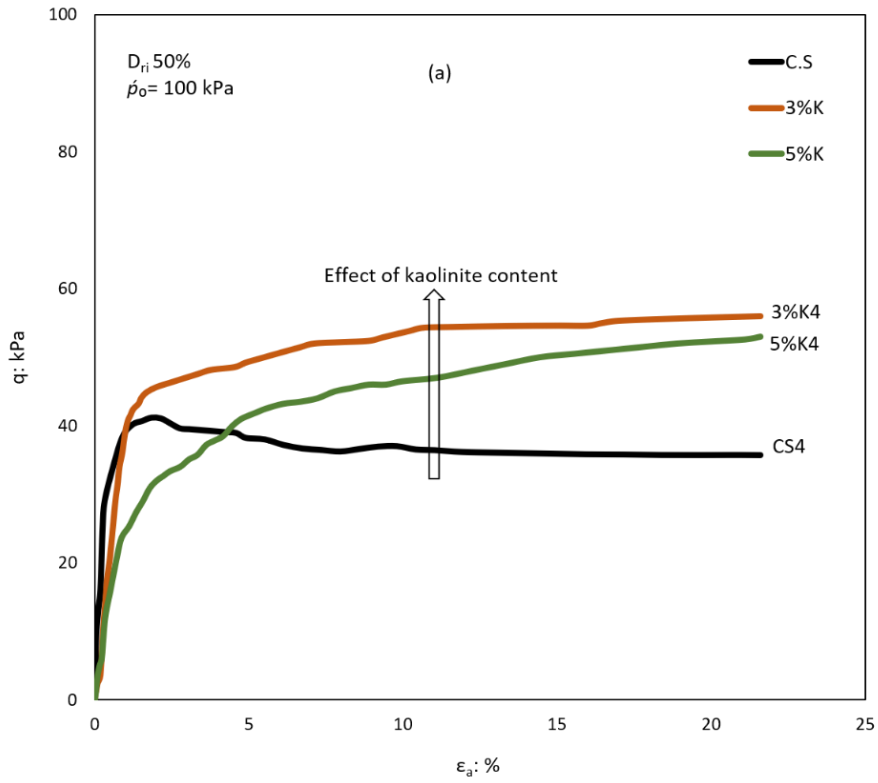


Figure 4.39 Undrained behaviour of very loose sand–kaolinite samples: (a) pore water pressure ratio–strain with  $\dot{p}_o = 100 \text{ kPa}$ , (b) pore water pressure ratio–strain with  $\dot{p}_o = 150 \text{ kPa}$ , and (c) pore water pressure ratio–strain with  $\dot{p}_o = 200 \text{ kPa}$

At the initial confining pressure  $p_o$  of 150 kPa,  $R_u$  reduced from 0.933 in C.S to 0.833 when the sand was mixed with 3% kaolinite; then,  $R_u$  increased to 0.887 when the kaolinite content increased to 5%. However, at the initial confining pressure  $p_o$  of 200 kPa, the behaviour of the pore water pressure ratios was different from that of the other two initial confining pressures when the sample of 5% K showed a higher  $R_u$  value than C.S.  $R_u$  reduced from 0.8 in C.S to 0.76 when the sand was mixed with 3% kaolinite; then,  $R_u$  increased to 0.83 when the kaolinite content increased to 5%. A marked feature of the undrained triaxial compression tests conducted on very loose ( $D_{ri}$  10%) sand–kaolinite mixtures is that the ‘reverse behaviour’ was enhanced by adding kaolinite to sandy soil. This was inferred from the increases in the initial peak deviatoric stresses and the slope of the effective stress paths, and the decrease in the pore water pressure ratio with increasing initial confining pressure for both sand–3% kaolinite and sand–5% kaolinite. These findings proved that kaolinite enhanced the ‘reverse behaviour’ in sandy soil. The influence of the relative density on the liquefaction behaviour of the sand–kaolinite mixtures is shown in Figures 4.40 and 4.41. Figure 4.40(a) shows the stress–strain relationships of the sand–kaolinite mixtures prepared at a relative density of 50% and sheared under a single initial confining pressure of 100 kPa. In Figure 4.40(a), there is an apparent change in the behaviour trends of the samples.





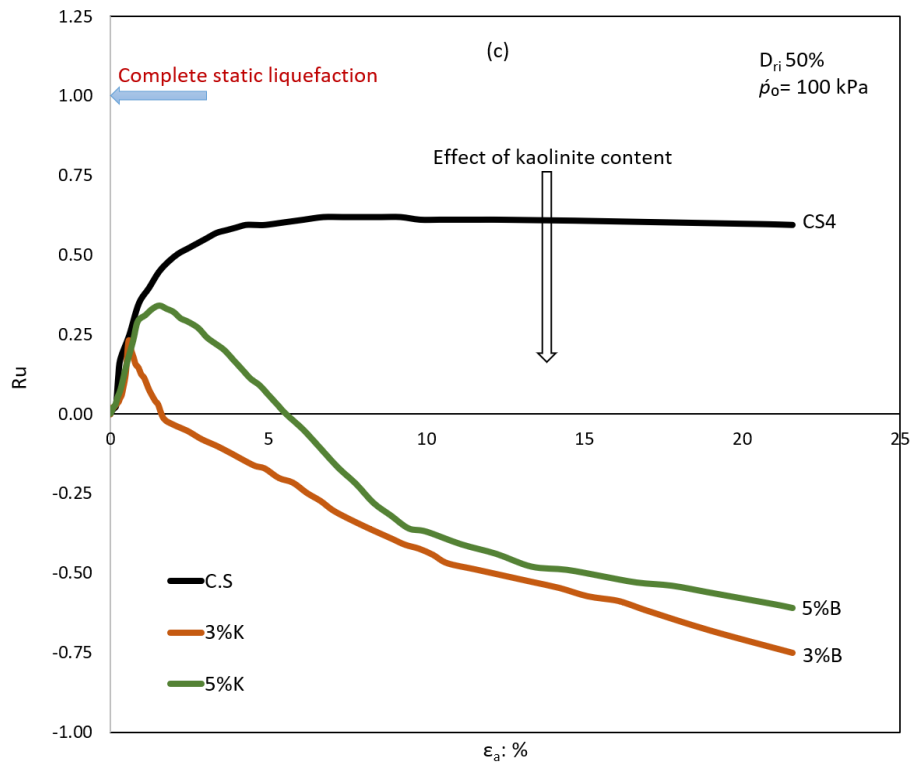
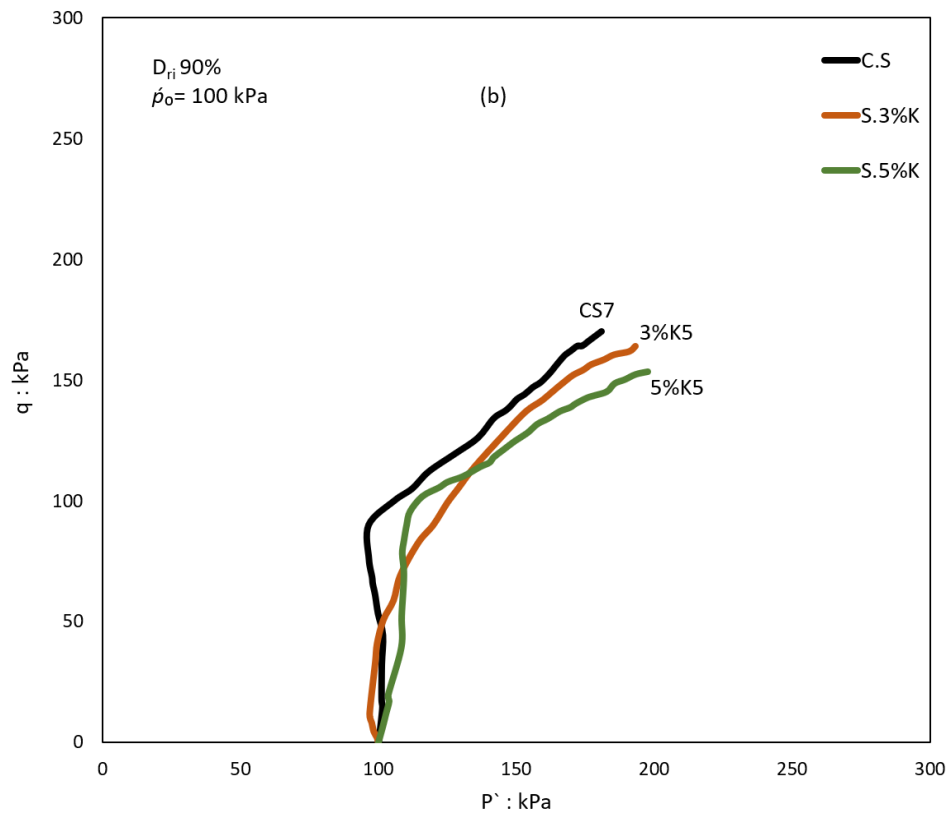
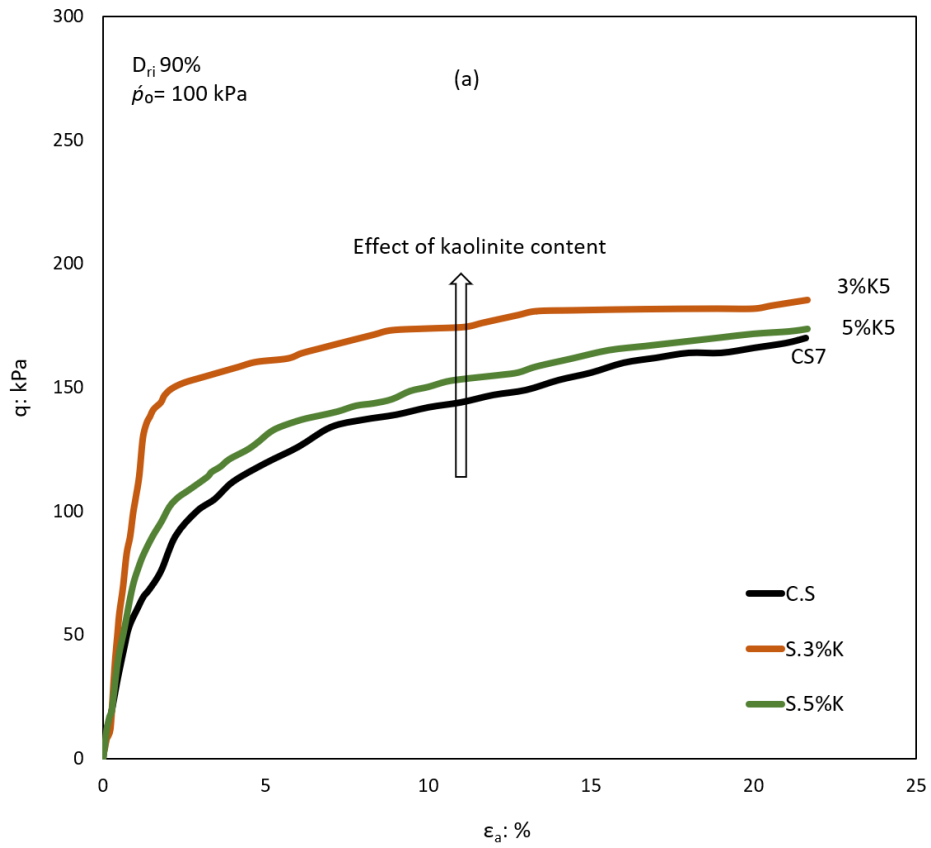


Figure 4.40 Undrained behaviour of sand–kaolinite samples prepared at the relative density of 50%: (a) stress–strain relationships, (b) effective stress paths, and (c) pore water pressure ratio–strain

The C.S sample showed limited liquefaction behaviour which was characterised by a reduction in the deviatoric stress after the initial peak deviatoric stress was attained; then, it increased slightly upwards toward a higher mean stress. However, the sand–kaolinite mixtures prepared at the same relative density ( $D_{ri} 50\%$ ) and tested under the same testing conditions showed a different behaviour trend. The sand–kaolinite mixtures showed a gradual increase in the deviatoric stress without any reduction until the end of the tests, which indicated non-flow behaviour. At the start of the test, the sample of 3%K showed abrupt increases in the deviatoric stress and the increment rate of the deviatoric stress was higher than 5%K. In contrast, both the 3%K and the 5%K samples showed a slight difference in the deviatoric stress at the end of the test.  $q_{peak}$  increased from 40.65 kPa in C.S to 56 kPa and 53 kPa when the sand was mixed with 3% kaolinite and 5% kaolinite, respectively. Figure 4.40(b) shows the effective stress paths of the three samples (C.S, 3%K, and 5%K) prepared at  $D_{ri} 50\%$ . It is apparent from this figure that effective stress paths moved to the left but did not reach zero. However, the samples of the sand–kaolinite mixtures moved to the left and then to the right with increases in the mean effective stress until the end of the test. Furthermore,

the slope of the effective stress path increased with increasing kaolinite content, and the sample of 3%K showed the highest value. The effect of increasing the relative density to 50% is shown in Figure 4.40(c) when the C.S sample showed a positive pore water pressure ratio  $R_u$  with a gradual increment until the maximum value was reached; it then decreased slightly until the end of the test. However, both the 3%K and the 5%K samples showed a significant reduction in  $R_u$  after attaining the initial peak value; the reduction in  $R_u$  was continuous until negative values were obtained at the end of the test. The negative pore water pressure ratio indicated non-flow behaviour.  $R_u$  decreased from 0.62 to 0.23 and 0.34 when the kaolinite content increased from 3% to 5%, respectively. Figures 4.41(a)–(c) show the results of tests conducted using C.S and the sand–slag mixtures prepared at  $D_{ri}$  90% and sheared at the initial confining pressure of 100 kPa. Figure 4.41(a) presents the stress–strain relationships of the dense ( $D_{ri}$  90%) sand–kaolinite mixtures. It is apparent from this figure that the three samples (C.S, 3%K, and 5%K) showed a non-flow behaviour which was characterised by a gradual increment in the deviatoric stresses until the maximum value was reached at the end of the test. Furthermore, the deviatoric stresses increased with increasing kaolinite content, and the sample of 3%K showed the highest value. Next,  $q_{peak}$  increased from 170 kPa in C.S to 185.43 kPa and 175 kPa when the kaolinite content increased to 3% and 5%, respectively. The effective stress paths of the dense samples are illustrated in Figure 4.41(b). It appears from this figure that the slope of the effective stress paths increased with increasing kaolinite content and that the sample of 3%K showed the highest value. The effective stress of 3%K directly moved to the right. However, the effective stress paths of the C.S and 5%K samples moved to the left and then to the right with an increase in the values of the mean effective confining pressure. The effect of the relative density on the liquefaction behaviour of the sand–kaolinite mixtures is pronounced in Figure 4.41(c). This figure presents the pore water pressure ratio  $R_u$ –strain relationships. It appears from Figure 4.41(c) that the three samples (C.S, 3%K, and 5%K) showed the initial peak values; then, it significantly decreased to the lowest value at the end of the test. The reduction rate of the pore water pressure ratio in the C.S sample was lower than in the other samples.  $R_u$  decreased from 0.336 in C.S to 0.15 and 0.204 when the kaolinite content increased to 3% and 5%, respectively. As mentioned in the previous sections, the negative values of  $R_u$  represent non-flow behaviour.



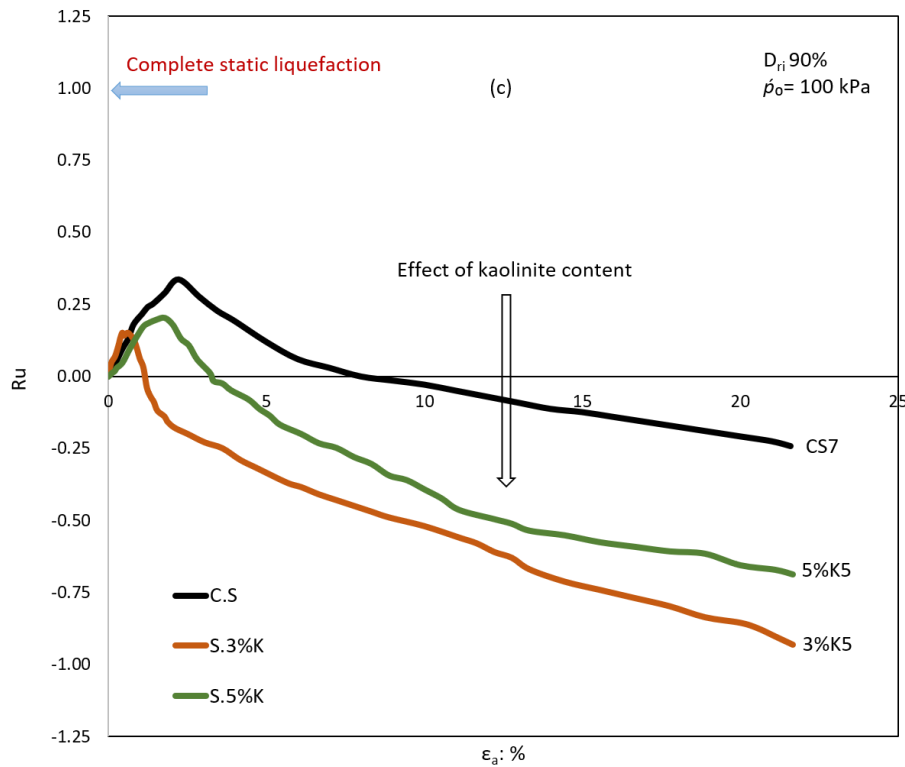


Figure 4.41 Undrained behaviour of sand–kaolinite samples prepared at the relative density of 90%: (a) stress–strain relationships, (b) effective stress paths, and (c) pore water pressure ratio–strain

Figure 4.42(a) shows the effect of the kaolinite content on the stress ratio ( $q_{min}/q_{peak}$ ) of the C.S and the sand–kaolinite samples prepared at three relative densities and sheared at the initial confining pressure 100 kPa. From this figure, we can see that the stress ratio ( $q_{min}/q_{peak}$ ) of all the samples substantially increased when the relative density increased from 10% to 50% and 90%. Furthermore, the effect of the kaolinite content was more pronounced at the loose state than at the medium and the dense states. This behaviour was apparently observed when the stress ratio ( $q_{min}/q_{peak}$ ) increased from zero in the C.S sample, which indicated the complete static liquefaction to 0.703 when the sand was mixed with 3% kaolinite. Then, it reduced to 0.474 when the kaolinite content increased to 5%. Nevertheless, there was little change in the stress ratio ( $q_{min}/q_{peak}$ ) when the relative density increased to 50%. The stress ratio ( $q_{min}/q_{peak}$ ) at the relative density of 50% increased from 0.88 in the C.S sample to 0.982 and 0.962 when the kaolinite content increased to 3% and 5%, respectively. In the dense state ( $D_{ri}$  90%), the change in the stress ratio ( $q_{min}/q_{peak}$ ) of all the samples was minimal and they exhibited almost the same values. The stress ratio ( $q_{min}/q_{peak}$ ) at the relative

density of 90% increased from 0.994 in the C.S sample to 0.998 and 0.996 when the kaolinite content increased to 3% and 5%, respectively.

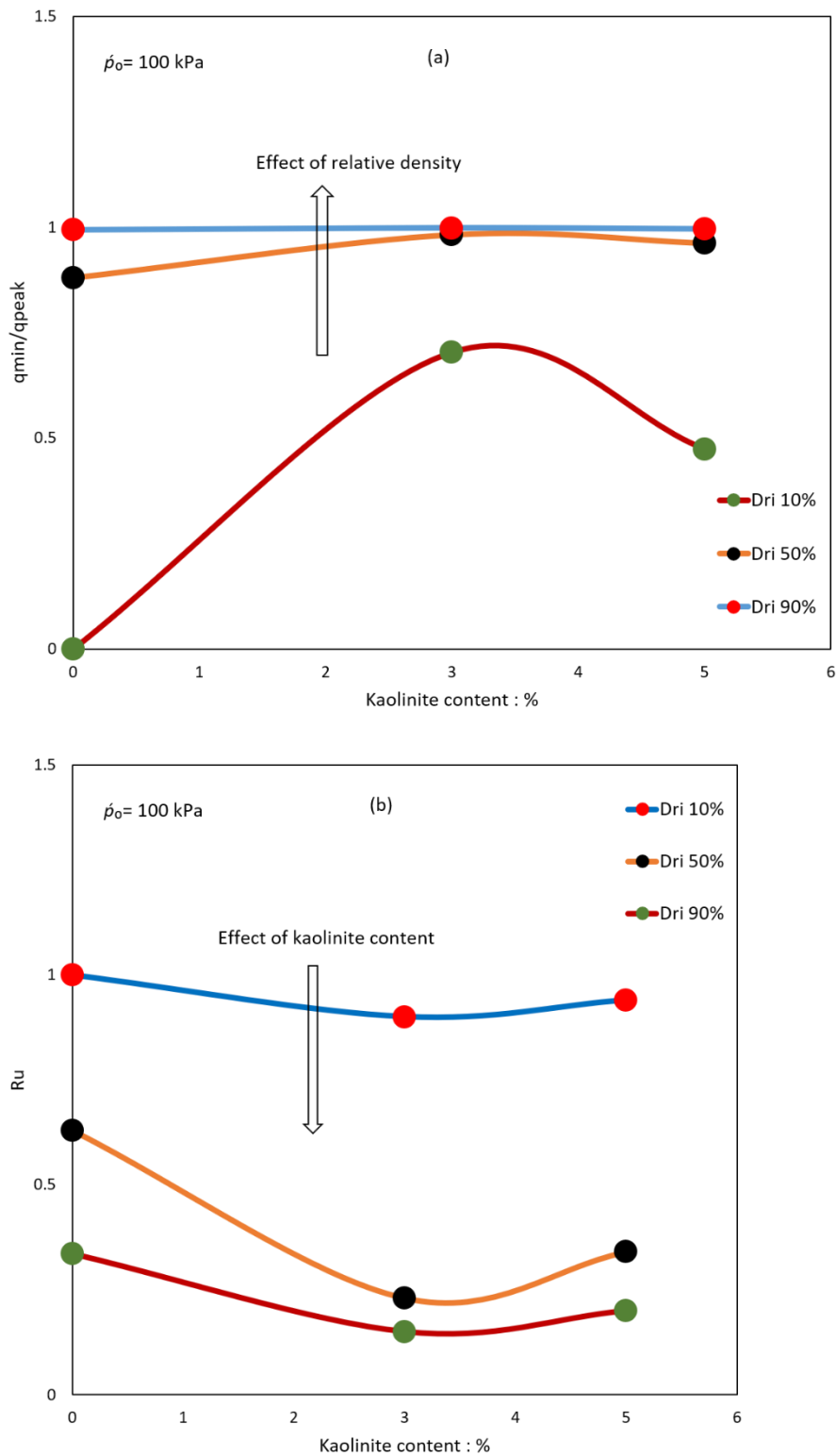


Figure 4.42 Effect of kaolinite content on undrained behaviour of sand–kaolinite mixtures: (a) stress ratio vs. kaolinite content and (b) pore water pressure ratios vs. kaolinite content

The above behaviour proved that the increasing relative density hindered the effect of kaolinite on the liquefaction behaviour of sandy soil. This is illustrated in Figure 4.42(b) when the pore water pressure ratios  $R_u$  of all the mixtures significantly reduced with increasing relative density and the pore water pressure ratios  $R_u$  in the dense state changed only slightly with the increasing kaolinite content. Furthermore, the pore water pressure ratios  $R_u$  at the three relative densities decreased when the sand was mixed with 3% kaolinite and then increased when the kaolinite content increased to 5%. Figure 4.42(b) illustrates that the amount of reduction in  $R_u$  decreased with increasing kaolinite content and that the samples of sand–3% kaolinite exhibited the lowest  $R_u$  values at the three relative densities. The pore water pressure ratios  $R_u$  reduced from 0.9 for the loose 3%K ( $D_{ri}$  10%) to 0.23 and 0.15 when  $D_{ri}$  increased to 50% and 90%, respectively. However,  $R_u$  decreased from 0.94 for loose 5%K ( $D_{ri}$  10%) to 0.34 and 0.204 when  $D_{ri}$  increased to 50% and 90%, respectively.

The liquefaction susceptibility represented by the brittleness index  $I_B$  of the sand–kaolinite mixtures prepared at  $D_{ri}$  10% and sheared at the three confining pressures of 100, 150, and 200 kPa is shown in Figure 4.43(a). It is apparent from this figure that the liquefaction susceptibility of all of the mixtures decreased with an increase in the initial confining pressure and that the reduction rate of the brittleness index  $I_B$  in the C.S samples was higher than that in the sand–bentonite mixtures. Furthermore, the liquefaction susceptibility of sandy soil decreased when the sand was mixed with 3% kaolinite and then increased when the kaolinite content increased to 5% but was still lower than  $I_B$  in the clean sand samples. The results of samples sheared at the initial confining pressure  $p'_o$  showed that the  $I_B$  value of the C.S sample decreased from 1 to 0.297 and 0.526 when the kaolinite content increased to 3% and 5%, respectively. However, at  $p'_o = 200$  kPa, the values of  $I_B$  of C.S decreased from 0.358 to 0.164 when the sand was mixed with 3% kaolinite and then increased to 0.375 when the kaolinite content increased to 5%. This behaviour was in line with the so-called ‘reverse behaviour’, as represented by a reduction in the liquefaction susceptibility with an increase in the initial confining pressure  $p'_o$ . Further, we found that the presence of kaolinite in sandy soil reduced the ability of the sandy soil to generate the ‘reverse behaviour’.

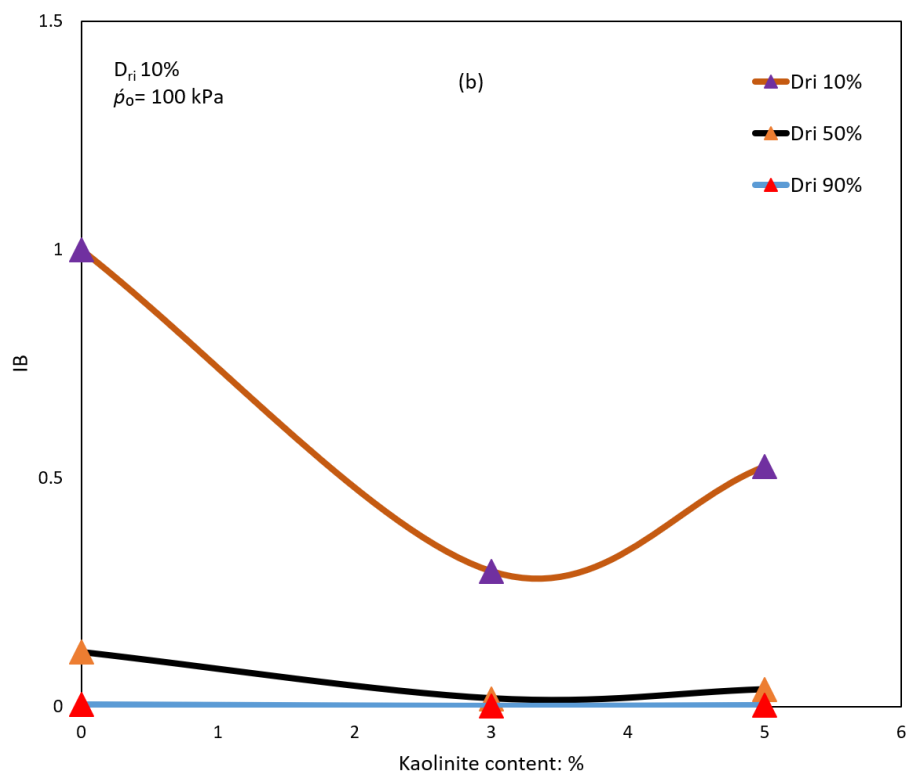
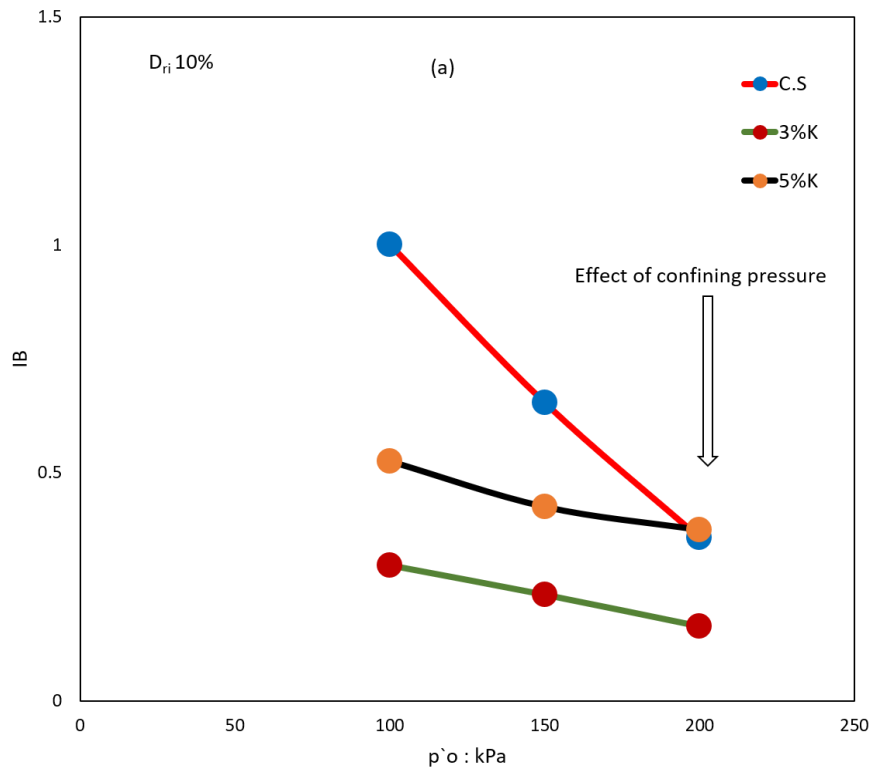


Figure 4.43 Effect of kaolinite content on brittleness index of sand–kaolinite mixtures: (a) brittleness index vs. initial confining pressure and (b) brittleness index vs. kaolinite content

Figure 4.43(b) shows the relationship between the brittleness index  $I_B$  and the relative density of the sand–kaolinite mixtures prepared at the three considered relative densities and tested at the initial confining pressure  $p'_o$  of 100 kPa. From this figure, we can see that the liquefaction susceptibility of all the mixtures decreased considerably with an increase in the relative density and the effect of the kaolinite content on the liquefaction susceptibility was more pronounced in the very loose state ( $D_{ri}$  10%) than in the medium and dense states ( $D_{ri}$  50% and 90%). The  $I_B$  values of the medium-state samples ( $D_{ri}$  50%) decreased from 0.12 in the C.S sample to 0.018 and 0.038 when the kaolinite content increased to 3% and 5%, respectively. However, the dense samples ( $D_{ri}$  90%) showed almost the same values of  $I_B$ ; the  $I_B$  value of the dense sand decreased from 0.006 to 0.002 and 0.004 when the sand was mixed with 3% and 5% kaolinite, respectively. The effect of the relative density on the liquefaction susceptibility may prove that the relative density hindered the effect of the kaolinite percentages on the liquefaction susceptibility of sandy soil.

The liquefaction susceptibility of the sand–kaolinite mixtures was also investigated by examining the relationships between the state parameter at the start of the tests ( $\Psi_o$ ) of very loose samples ( $D_{ri}$  10%) and the initial confining pressure and brittleness index  $I_B$ , as shown in Figures 4.44(a) and (b). Figure 4.44(a) shows that all of the loose mixtures exhibited positive values of  $\Psi_o$  and that these values increased with increasing initial confining pressures  $p'_o$ , which implied that the compressibility of the mixtures increased with increasing  $p'_o$ . The positive values of  $\Psi_o$  indicated the flow behaviour; however, negative values indicated non-flow behaviour. Furthermore,  $\Psi_o$  decreased when the sand was mixed with 3% kaolinite and then increased but was still lower than that of clean sand when the kaolinite content increased to 5%. The  $\Psi_o$  value of C.S decreased from 0.0035 to 0.0021 and 0.0028 when the sand was mixed with 3% and 5% kaolinite, respectively. Figure 4.44(b) shows that the relationships between  $I_B$  and  $\Psi_o$  of the three loose mixtures tested at  $p'_o = 100$  kPa weakened with a decrease in  $\Psi_o$ ; these relationships shifted downward with increasing kaolinite content, and the samples of 3%K showed the lowest liquefaction susceptibility. This behaviour indicated that  $\Psi_o$  decreased with an increase in the kaolinite content. Consequently, the liquefaction susceptibility decreased with an increase in the kaolinite content. Moreover, the C.S samples showed a higher reduction rate of the liquefaction susceptibility than the sand–kaolinite mixtures which may support the findings



reported in the previous sections and prove that the presence of kaolinite reduced the ability of sandy soil to induce flow behaviour.

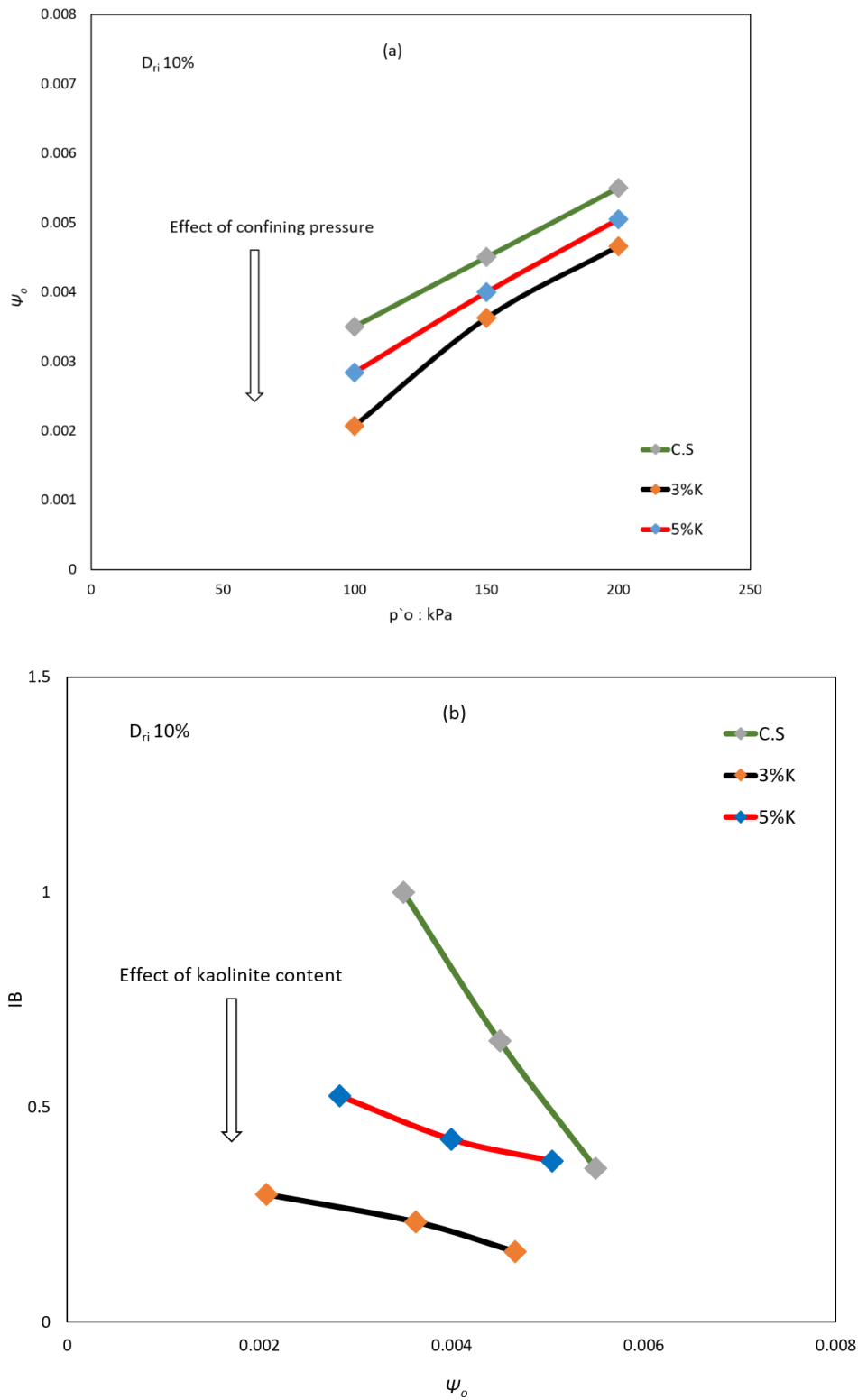


Figure 4.44 Effect of kaolinite content on state parameter at start of the test of sand–kaolinite mixtures: (a) state parameter at start of the test vs. confining pressure and (b) brittleness index vs. state parameter at start of the test

Figures 4.45(a) and (b) show the effect of the kaolinite content on the stress ratio at the instability line  $\eta$  of the very loose ( $D_{ri}$  10%) samples tested under the three initial confining pressures  $p'_o$  (100, 150, and 200 kPa). The data presented in Figure 4.45(a) revealed a slight increase in  $\eta$  with an increase in the kaolinite content. Furthermore,  $\eta$  increased with increasing  $p'_o$ , and the samples of 3%K showed the highest value. The values of  $\eta$  at  $p'_o = 100$  kPa increased from 0.129 in C.S to 0.133 when the kaolinite content was 3%; then, it decreased to 0.126 when the kaolinite content increased to 5%. However, the values of  $\eta$  of the loose 3%K samples increased from 0.133 at  $p'_o = 100$  kPa to 0.142 and 0.177 when  $p'_o$  increased to 150 kPa and 200 kPa, respectively. Table 4.7 shows that the  $\eta$  values of both the mixtures of 3%K and 5%K significantly increased with an increase in the relative density and that the samples of 3%K exhibited the highest values. Furthermore, increasing the relative density reduced the effect of the kaolinite content on  $\eta$ . Figure 4.45(b) shows the relationships between  $\eta$  of the very loose mixtures and the state parameter at the start of the test  $\Psi_o$ . It is apparent from this figure that the curves of the mixtures shifted to the left and that sand–3% kaolinite showed the most significant movement. Although the curve of 5%K moved to the right, it was still higher than that of the C.S samples. This behaviour proved that the presence of kaolinite enhanced the stability of the sand fabric by increasing the contact between the sand particles. Furthermore, the platen shape of the kaolinite particles played an important role in this development of the sand fabric. The results of sand–5% kaolinite also support the findings of Bayat et al. (2014) who concluded that the presence of up to 20% of kaolinite reduced the shear strength of mixtures and increased the pore water pressure generation. Furthermore, Koester (1994) found that the cyclic liquefaction resistance of soil reduced when the kaolinite content increased up to 20%.

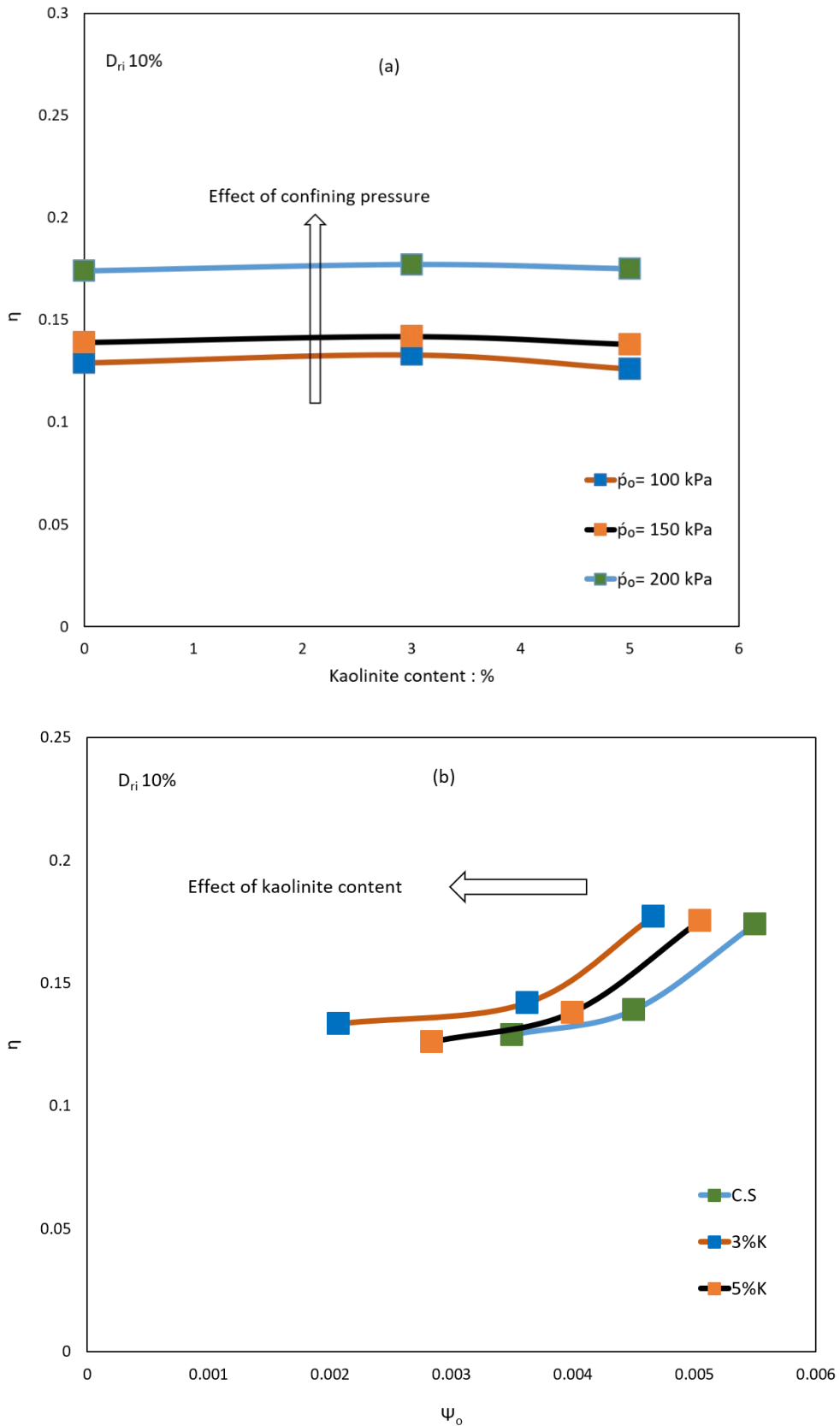


Figure 4.45 Effect of kaolinite content on stress ratio at instability line of sand–kaolinite mixtures: (a) stress ratio at instability line vs. kaolinite content and (b) stress ratio at instability line vs. state parameter at start of the test

## 4.6. Influence of clay mineralogy on liquefaction susceptibility of sandy soils

To examine whether the liquefaction behaviour of sand–clay mixtures is affected by clay mineralogy, the results of monotonic undrained compression triaxial tests conducted on the sand–bentonite and sand–kaolinite mixtures with the same clay percentages of 3% and 5% are replotted in Figures 4.46 and 4.47. Figure 4.46(a) presents the clay content against the brittleness index  $I_B$  of the sand–clay mixtures prepared at three different relative densities and sheared at the initial confining pressure  $p'_o$  of 100 kPa. This figure shows that the liquefaction susceptibility represented by the brittleness index  $I_B$  of the sand–kaolinite mixtures was less than that of the sand–bentonite mixtures at all of the considered relative densities. The samples of the sand–kaolinite mixtures tended to reduce the liquefaction susceptibility more than the sand–bentonite mixtures. However,  $I_B$  of all the mixtures significantly reduced with increasing relative density. The liquefaction susceptibility of both bentonite– and kaolinite–sand mixtures reduced when the clay content was 3% and then increased when it was increased to 5%. The  $I_B$  values of loose sand–kaolinite mixtures reduced from 1 at 0% clay content to 0.297 and 0.526 when the kaolinite content increased to 3% and 5%, respectively. At the same bentonite content,  $I_B$  reduced from 1 to 0.665 and 0.868. Note from Figure 4.46(a) that the increasing relative density hindered the effect of the kaolinite content on the liquefaction susceptibility of sandy soil as inferred from the slight change in  $I_B$  when the relative density increased to 50% and 90%. However, the sand–bentonite mixtures showed a continuous increase in  $I_B$  with increasing bentonite content when the relative density increased to 50% and 90%. The effect of the clay type on the liquefaction susceptibility of sandy soil is shown in Figure 4.46(b). This figure shows a clear trend of the decreasing pore water pressure ratio  $R_u$  of the sand–kaolinite mixtures with increasing relative density. Moreover, at three relative densities, the  $R_u$  values of the sand–kaolinite mixtures decreased when the sand was mixed with 3% kaolinite and then increased when the kaolinite content was increased to 5%. Nonetheless, samples of sand–bentonite mixtures at three relative densities showed continuous increases in  $R_u$  when the bentonite content increased to 3% and 5%.

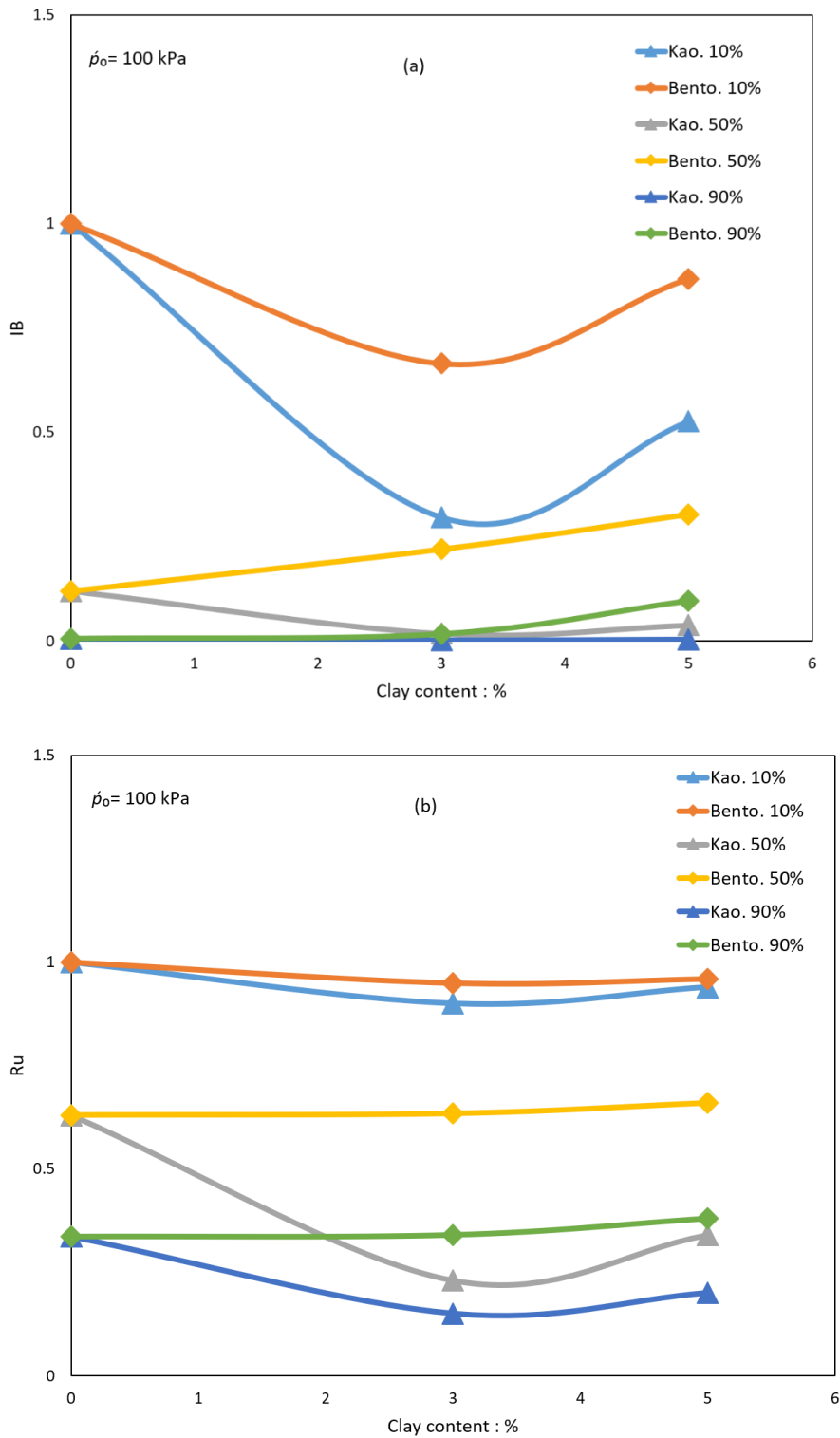
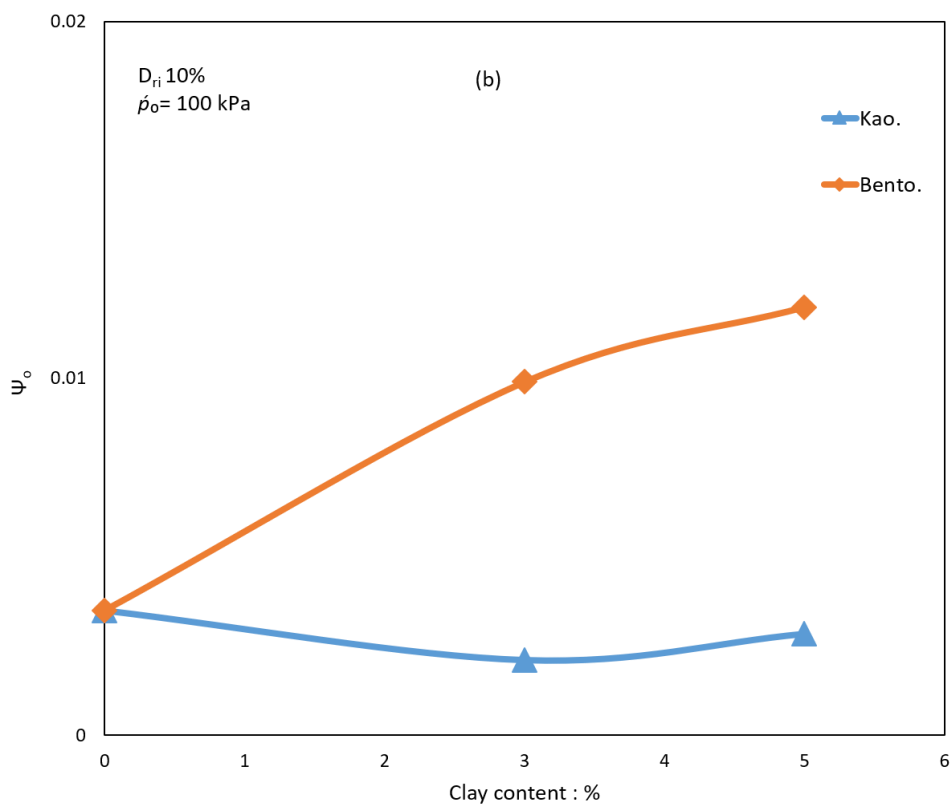
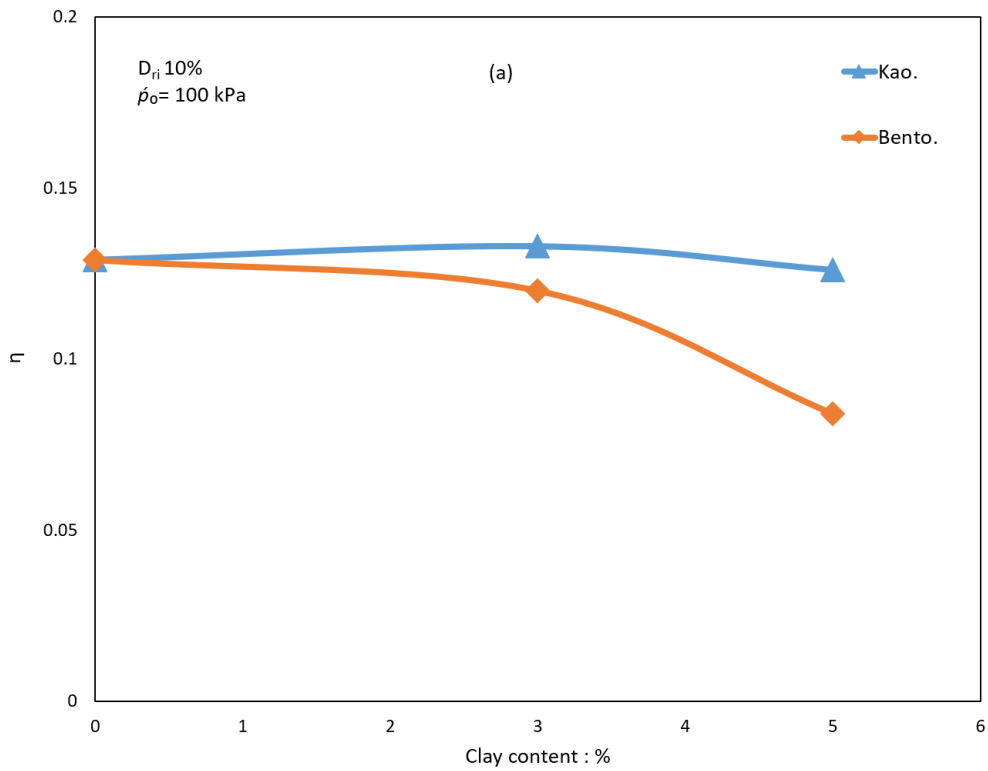


Figure 4.46 Effect of clay type on liquefaction behaviour of sandy soil: (a) brittleness index vs. clay content and (b) pore water pressure ratio vs. clay content

Figure 4.47(a) compares the effects of kaolinite and bentonite on the stress ratio at the instability line  $\eta$  of very loose sand–clay mixtures tested at an initial confining pressure  $p_o$  of 100 kPa. Here, the sand–kaolinite mixtures showed higher  $\eta$  values than the

sand–bentonite mixtures, while both the sand–clay mixtures showed increases in  $\eta$  when the clay content was 3%; then,  $\eta$  reduced when the clay content increased to 5%. The reduction rate of  $\eta$  of the sand–bentonite mixtures was higher than that of the sand–kaolinite mixtures. The effect of the clay type on the state parameter at the start of the test ( $\Psi_0$ ) is presented in Figure 4.47(b). As shown in Figure 4.47(b),  $\Psi_0$  reduced at the kaolinite content of 3% and then slightly increased when the kaolinite content increased to 5%. In contrast, the sand–bentonite mixtures showed a clear trend of increasing  $\Psi_0$  with increasing bentonite content. The findings proved that the liquefaction susceptibility of sandy soils was considerably dependent on the clay mineralogy. The presence of bentonite enhanced the liquefaction susceptibility of sandy soil by increasing the values of the brittleness index and the pore water pressure ratio, and reducing the stress ratio at the instability line. The negative effect of the bentonite content on the liquefaction susceptibility of sandy soils might be attributed to the fact that the presence of bentonite produces unstable fabric. The bentonite particles occupied the voids between the sand grains and reduced the contact between the sand particles which increased the compressibility of sandy soil and increased the pore water pressure. In addition, the characteristic of bentonite to swell when in contact with water may also play a significant role in generating unstable fabric. Gratchev et al. (2007) argued that the presence of bentonite may generate an open micro fabric structure in the sand–clay mixtures with low-strength ‘Clay Bridge’. They also added that the clayey soils have a complex mechanism of liquefaction and the clay content and distribution in the soil are the primary factors controlling the tendency of soils to liquefy. In contrast, the presence of kaolinite may produce a stable fabric and enhance the contact between the sand grains which reduce the ability of sand to liquefy.



**Figure 4.47** Effect of clay content on liquefaction behaviour of sandy soil: (a) stress ratio at instability line vs. clay content and (b) state parameter at start of the test vs. clay content

## 4.7 Summary

A series of undrained static triaxial compression tests were conducted to investigate the effect of the fines content and type on the liquefaction behaviour of sandy soils. The experiments were implemented on four types of materials, namely clean sand specimens, sand–(2%, 4%, and 6%) slag mixtures, sand–(3% and 5%) bentonite mixtures, and sand–(3% and 5%) kaolinite mixtures at three relative densities (10%, 50%, and 90%) and three initial confining pressures (100, 150, and 200 kPa). The experimental program also included two tests of partially saturated very loose clean sand specimens to examine the effect of the degree of saturation on the liquefaction behaviour of sandy soils. The results of the clean sand specimens showed that the samples prepared at the lowest relative density (10%) and sheared under the lowest initial confining pressure (100 kPa) exhibited complete static liquefaction characterised by zero deviatoric stress and the unity value of the pore water pressure ratio. However, the liquefaction susceptibility of sand samples reduced with increasing initial confining pressure and relative density. The results of the clean sand specimens also demonstrated that the liquefaction susceptibility of sandy soil reduced with a decrease in the degree of saturation. This was observed when the deviatoric stresses increased and the pore water pressure decreased with a decrease in the degree of saturation. The test results of the sand–fines mixtures showed that the liquefaction susceptibility of sandy soil was considerably dependent on the type of fines and the fines content. The liquefaction susceptibility of the sand–slag mixtures reduced when the slag content increased up to 4% and then increased when the slag content increased to 6%. However, the clay mineralogy played a significant role in the liquefaction susceptibility of sand–clay mixtures. This was observed when the liquefaction susceptibility reduced for sand mixed with 3% and 5% of bentonite. Moreover, the presence of 3% of kaolinite reduced the liquefaction susceptibility of clean sandy soil. Furthermore, at the same bentonite and kaolinite contents, the sand–kaolinite mixtures showed lower liquefaction susceptibility than the sand–bentonite mixtures. Based on the experimental results of present work the mixture of sand and 4% slag could be considered the best mixture for improving liquefaction resistance of sandy soil. The results of the sand–fines mixtures showed that the increasing relative density hindered the effect of the fines on the liquefaction behaviour of clean sandy soils.



# Chapter 5: Static Liquefaction Behaviour of Sand–Slag–Clay Mixtures

## 5.1 Introduction

As mentioned in Chapter 2, several experimental investigations have reported that the effect of fines on the static liquefaction behaviour of sandy soils has attracted considerable controversy and uncertainty. The complexity of this matter could be related to the nature of sand and fines. Some studies have found that the presence of fines reduced the liquefaction susceptibility of sandy soils (Pitman et al., 1994; Seed et al., 1983). In contrast, Rahman and Lo (2014); Thevanayagam and Martin (2002); Yang, Lacasse, and Sandven (2006) stated that the presence of fines increased the compressibility of sand–fines mixtures by reducing the contact between the sand particles. Consequently, the liquefaction susceptibility was increased. Other studies proposed a threshold around which the percentage of the fines content has positive or negative effects (Belhouari et al., 2015; Yamamuro & Covert, 2001; Yang & Wei, 2012). However, few studies have examined the effects of mixing two types of fines on the liquefaction behaviour of sandy soils under undrained conditions. Therefore, the primary objective of this chapter is to explore the effect of a combination of two different fines on the behaviour of sandy soil under undrained static loading. Therefore, we conducted strain-controlled, undrained, static, triaxial compression tests on isotropically consolidated samples of Perth sand mixed with different slag and clay contents. The tests were performed in a very loose state and sheared under a single confining pressure (100 kPa) because the results reported in Chapter 4 showed that complete static liquefaction only occurred in samples prepared in the loose state and sheared under a confining pressure of 100 kPa. The investigation emphasised the effect of slag on the liquefaction behaviour of sand that had a low clay content. Firstly, the undrained behaviour of the loose sand–slag–bentonite mixtures was investigated. The following tests were performed to examine the liquefaction behaviour of the sand–slag mixtures mixed with kaolinite clay and tested under the same testing conditions in the first stage.

## 5.2 Liquefaction behaviour of sand–slag–bentonite mixtures

A series of undrained isotropically consolidated monotonic triaxial tests were conducted to characterise the liquefaction behaviour of sand–slag–bentonite mixtures. Tests were performed on soil specimens prepared by mixing Perth sand with 2%, 4%, and 6% slag and two different bentonite contents (3% and 5%) by the dry weight of sand, giving six triple mixtures. The physical properties of mixtures used in the present work are shown in Table 5.1.

Table 5.1 Physical properties of sand–slag–bentonite mixtures

Materials	Symbol	$E_{max}$	$e_{min}$	$C_u$	$G_s$
Sand + 2% slag + 3% bentonite	3BS2	0.574	0.514	2.263	2.650
Sand + 4% slag + 3% bentonite	3BS4	0.565	0.497	2.333	2.680
Sand + 6% slag + 3% bentonite	3BS6	0.562	0.478	2.562	2.695
Sand + 2% slag + 5% bentonite	5BS2	0.665	0.458	2.444	2.673
Sand + 4% slag + 5% bentonite	5BS4	0.663	0.455	2.470	2.688
Sand + 6% slag + 5% bentonite	5BS6	0.667	0.444	2.560	2.710

Table 5.1 shows that the maximum void ratio ( $e_{max}$ ) and the minimum void ratio ( $e_{min}$ ) of clayey sand decreased with increasing slag content. However, the specific gravity ( $G_s$ ) and the coefficient of uniformity ( $C_u$ ) of clayey sand increased with increasing slag content. Table 5.1 also shows that the physical properties such as  $e_{max}$ ,  $C_u$ , and  $G_s$  of the mixtures increased with an increase in the bentonite content from 3% to 5%. The undrained monotonic triaxial tests were run on fully saturated ( $B \geq 0.95$ ) samples, at the same relative density ( $D_{ri} = 10\%$ ) with shearing commencing from the initial confining pressure of 100 kPa. Samples prepared by mixing sand with 2%, 4%, and 6% of slag and 3% bentonite were labelled 3BS2, 3BS4, and 3BS6, respectively. However, samples prepared by mixing sand with 2%, 4%, and 6% of slag and 5% bentonite were labelled 5BS2, 5BS4, and 5BS6, respectively. The results of these tests are presented in Table 5.2.

Table 5.2 List of undrained tests conducted on sand–slag–bentonite mixtures

Test name	$p'_o$	$e_o$	$e_{cs}$	$q_{peak}$	$R_u$	$q_{min}/q_{peak}$	$I_B$
<b>3BS2</b>	100	0.5680	0.5660	20.430	0.570	0.979	0.021
<b>3BS4</b>	100	0.5582	0.5540	39.720	0.320	0.989	0.011
<b>3BS6</b>	100	0.5536	0.5520	32.150	0.330	0.958	0.042
<b>5BS2</b>	100	0.6442	0.6417	15.200	0.880	0.551	0.449
<b>5BS4</b>	100	0.6420	0.6388	24.820	0.620	0.693	0.307
<b>5BS6</b>	100	0.6445	0.6415	19.160	0.720	0.570	0.430

The results of three isotropically consolidated undrained triaxial tests (3BS2, 3BS4, and 3BS6) prepared at a very loose state ( $D_{ri}$  10%) are presented in Figures 5.1 and 5.2. Figure 5.1(a) shows the stress–strain relationships of the sand–slag–bentonite mixtures tested under  $p'_o = 100$  kPa. From the data presented in Figure 5.1(a), it is apparent that the three blends (i.e. 3BS2, 3BS4, and 3BS6) exhibited non-flow behaviour characterised by a gradual increase in the deviatoric stress until the maximum value was reached at the end of the test. However, under the same test conditions, the clean sand sample exhibited a complete static liquefaction response characterised by a sudden reduction in the deviatoric stress after attaining the initial peak value  $q_{peak}$ ; the reduction continued until the deviatoric stress was zero at the end of the tests. Figure 5.1(a) also shows that the deviatoric stress of the mixtures increased with an increase in the slag content to 4%; then, it reduced when the slag content increased to 6%. Further,  $q_{peak}$  increased from 7 kPa in the clean sand sample to 20.43 kPa, 39.72 kPa, and 32.15 kPa when the slag content increased to 2%, 4%, and 6%, respectively. Figure 5.1(b) shows the effective stress paths of clean sand and the sand–3% bentonite–slag mixtures. In this figure, there is a clear trend of an increasing slope of the effective stress paths of the mixtures as compared to the clean sand sample. The stress path of the C.S sample showed flow behaviour when it plummeted toward the origin of the stress path after reaching its characteristic peak deviatoric stress. In contrast, the effective stress paths of the three mixtures moved to the left and then slightly upwards toward a higher mean stress. The slope of the effective stress paths increased with an increase in the slag content to 4% and then reduced when the slag content increased to 6%, but the mixture of 3BS6 exhibited a higher slope of the effective stress path than 3BS2 did.

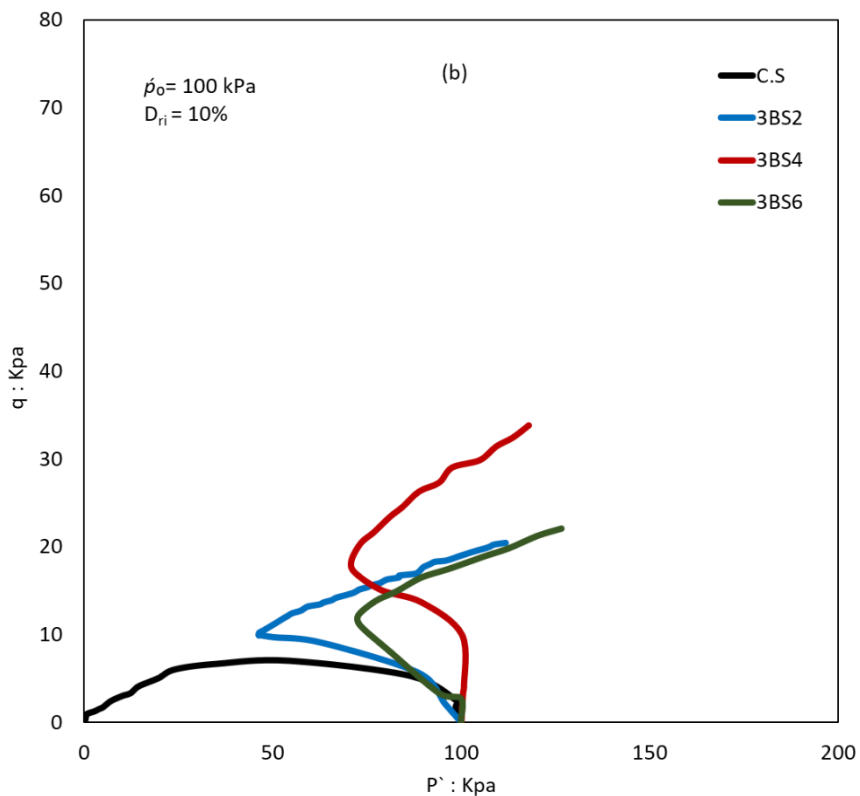
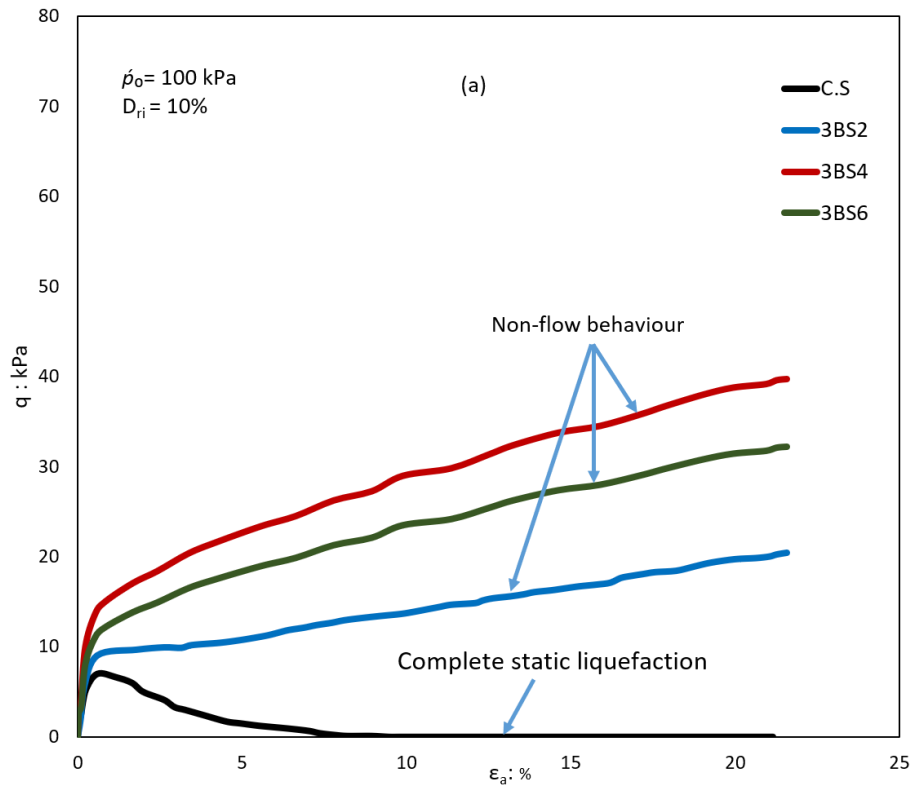
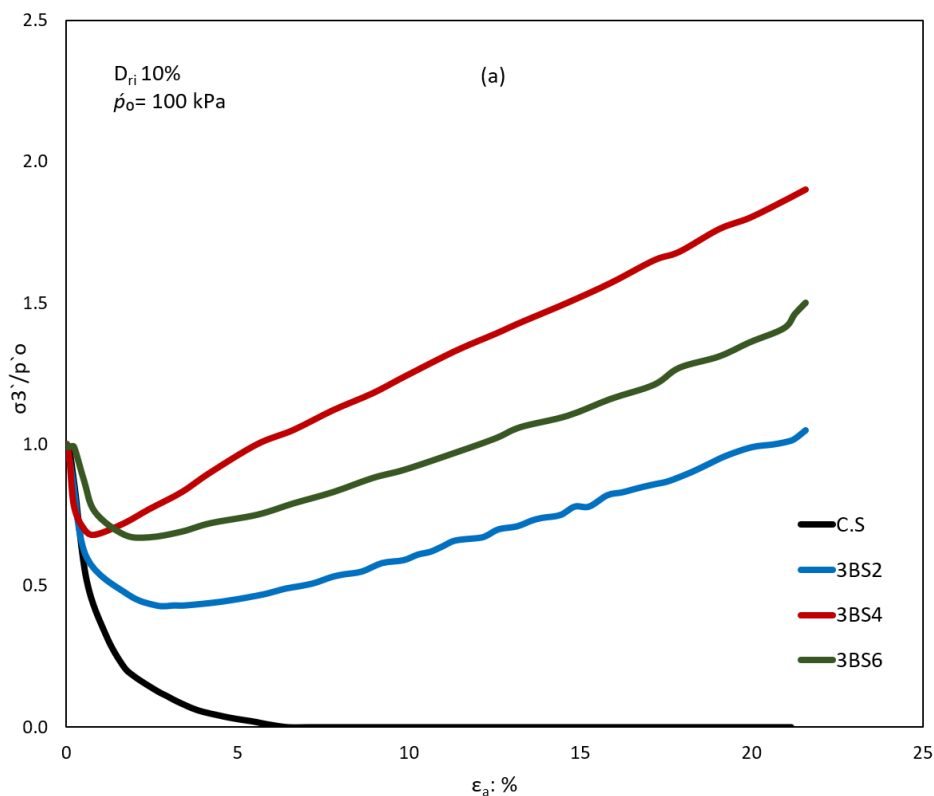


Figure 5.1 Undrained behaviour of very loose sand–3% bentonite–slag samples: (a) stress vs. strain curves with  $p'_o = 100$  kPa, and (b) effective stress path with  $p'_o = 100$  kPa

The non-flow behaviour of the three samples (3BS2, 3BS4, and 3BS6) can be observed by examining the effective stress and the excess pore water pressure ratios curves. Figure 5.2(a) shows the relationships between the effective stress ratios against the axial strain. Here, the effective stress ratio is the ratio of the effective stress to the initial confining pressure ( $\sigma'_3/p_o$ ). From Figure 5.2(a), we can see that the effective stress in C.S dramatically decreased from 1 at the start of the test to zero at a slight axial strain; however, 3BS2, 3BS4, and 3BS6 showed gradual reductions followed by increases in the effective stress ratio until the end of the tests. The effective stress ratios of 3BS2, 3BS4, and 3BS6 decreased from 1 to 0.43, 0.68, and 0.67, respectively. 3BS4 showed the highest effective stress ratio value at the end of the test. Figure 5.2(b) illustrates that the C.S sample showed abrupt increases in the pore water pressure ratio ( $R_u$ ) until it reached unity values, which indicated complete static liquefaction behaviour. However, mixing sand with 3% bentonite and the three different slag contents significantly reduced the pore water pressure ratios. Furthermore, for the three blends, the change in the pore water pressure ratios was considerably negative toward the end of the tests. The negative pore water pressure ratio indicated the non-flow behaviour. The pore water pressure  $R_u$  decreased from 1 in the C.S sample to 0.57, 0.32, and 0.33 in 3BS2, 3BS4, and 3BS6, respectively.



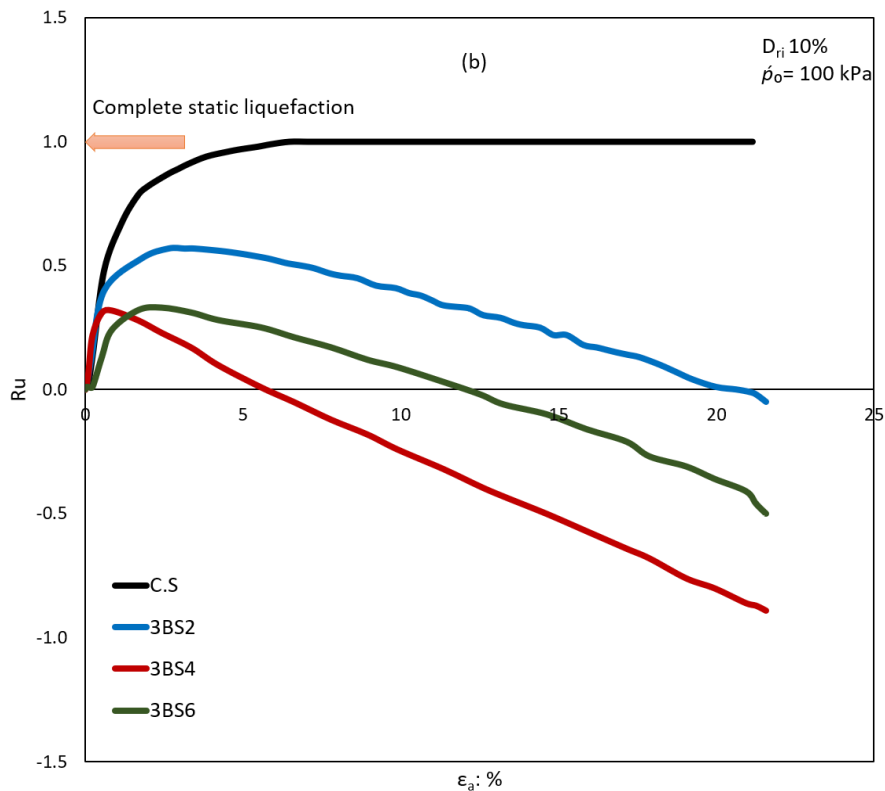
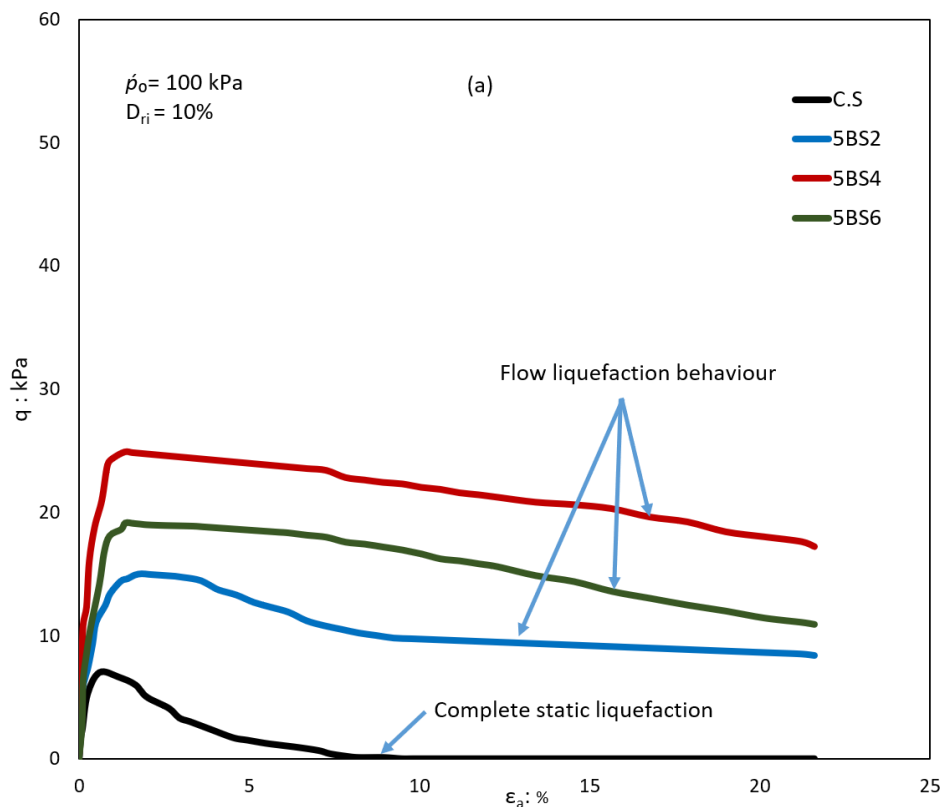


Figure 5.2 Undrained behaviour of very loose sand–slag–3% bentonite mixtures: (a) effective stress ratios vs. strain with  $p_0 = 100 \text{ kPa}$  and (b) pore water pressure ratio vs. strain with  $p_0 = 100 \text{ kPa}$

The reduction rate of the pore water pressure ratio increased with an increase in the slag content to 4% and then reduced with an increase in the slag content to 6%. The rate of excess pore pressure generation in the mixtures was lower than that for C.S, because of the potential improvement of the sand fabric when mixed with two different fines. The results of the three isotropically consolidated undrained tests for 5BS2, 5BS4, and 5BS6 with shearing commencing from  $p_0 = 100 \text{ kPa}$  are presented in Figures 5.3 and 5.4. Figure 5.3(a) showed that all the samples exhibited a reduction in the deviatoric stresses after reaching the initial peak deviatoric stress  $q_{peak}$  indicating the flow behaviour. The C.S sample showed abrupt decreases in the deviatoric stress until it reached zero at the end of the test, while mixtures of sand–slag–5% bentonite showed a gradual reduction in the deviatoric stress and the rate of reduction in the deviatoric stress decreased with an increase in the fines content. The initial peak deviatoric stress of sand–slag–5% bentonite increased when the slag content increased to 4% and then reduced when the slag content increased to 6%. Further,  $q_{peak}$  increased from 7 kPa in C.S to 15.2 kPa, 24.82 kPa, and 19.16 kPa in 5BS2, 5BS4, and 5BS6,

respectively. The minimum deviatoric stress  $q_{min}$  of the mixtures of sand–slag–5% bentonite also increased with an increase in the slag content to 4% and then reduced when the slag content increased to 6%. Moreover,  $q_{min}$  increased from 0 kPa in the CS1 test to 8.38 kPa, 17 kPa, and 10.92 kPa in the 5BS2, 5BS4, and 5BS6 tests, respectively. The resultant effective stress paths of CS1, 5BS2, 5BS4, and 5BS6 are shown in Figure 5.3(b). The effective stress path of the clean sand sample plummeted to the origin of the  $p'$ – $q$  plane after reaching the representative peak deviatoric stress; this indicated complete static liquefaction behaviour. However, the resultant effective stress paths of the sand–fines mixtures also plummeted, but they did not reach zero, indicating the flow liquefaction behaviour. Furthermore, the slope of the effective stress paths increased with increasing fines content, and 5BS4 showed the highest value.



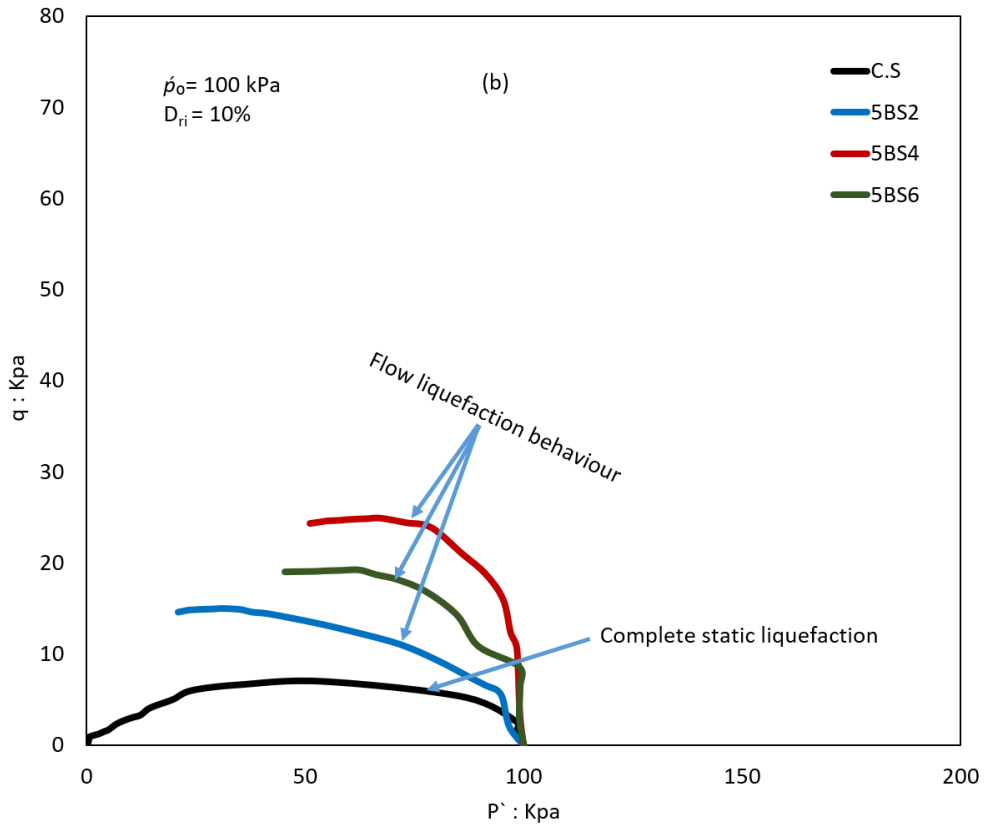
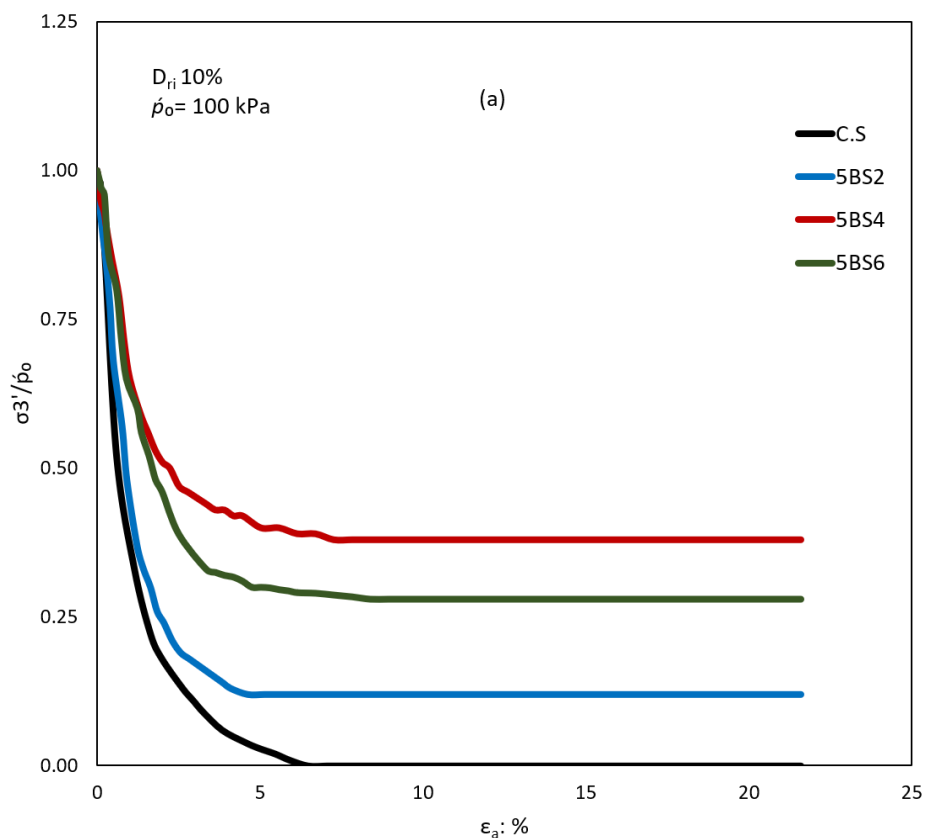


Figure 5.3 Undrained behaviour of very loose sand–5% bentonite–slag samples: (a) stress vs. strain curves with  $p_0 = 100$  kPa and (b) effective stress path with  $p_0 = 100$  kPa

The effect of the presence of 5% bentonite on the liquefaction behaviour of the sand–slag mixtures is shown in Figures 5.4(a) and (b). It is apparent from these figures that all of the loose samples (i.e. C.S, 5BS2, 5BS4, and 5BS6) that were sheared under the initial confining pressure  $p_0$  of 100 kPa showed flow behaviour characterised by a rapid reduction in the effective stress ratio and the positive pore water pressure ratio  $R_u$ . The C.S sample exhibited a rapid reduction in the effective stress ratio until the effective stress was zero, indicating complete static liquefaction behaviour. However, none of the other mixtures (5BS2, 5BS4, and 5BS6) showed zero effective stress ratios and the effective stress ratios increased with increasing fines content. A mixture of 5BS4 showed the highest effective stress ratio as shown in Figure 5.4(a). Figure 5.4(b) shows that the clean sand sample and the sand–fines samples exhibited a positive pore water pressure ratio, which indicated flow liquefaction behaviour. The pore water pressure ratio  $R_u$  of the clean sand sample abruptly increased, until it reached a unity value which implied that the excess pore water pressure was equal to the initial confining pressure, and herein, the effective stress was equal to zero (indicating



complete static liquefaction). In contrast, the samples of the sand–fines mixtures showed a slight increase in the pore water pressure ratios, but none of them reached the unity value of the pore water pressure ratios. Furthermore, the pore water pressure ratio reduced when the slag content increased to 4% and then increased when the slag content increased to 6%. The pore water pressure ratio  $R_u$  was reduced from 1 in the clean sand sample to 0.88, 0.62, and 0.72 in the mixtures of 5BS2, 5BS4, and 5BS6, respectively. The abovementioned behaviour of the sand–slag– bentonite mixtures indicated that increasing the bentonite content from 3% to 5% enhanced the flow liquefaction behaviour of the sand–slag mixtures. This was manifested when the behaviour of sand–slag–3% bentonite completely changed from the non-flow behaviour to the flow liquefaction behaviour. The deviatoric stresses and the effective stress ratios of the sand–slag–bentonite mixtures reduced when the bentonite content increased from 3% to 5%. Note from Figures 5.1 to 5.4 that the mixtures 3BS4 and 5BS4 exhibited the highest deviatoric stresses and effective stress ratios. The undrained behaviour of loose ( $D_{ri}$  10%) sand–fines mixtures containing 3% bentonite was compared with that of 5% bentonite in Figures 5.5 to 5.7.



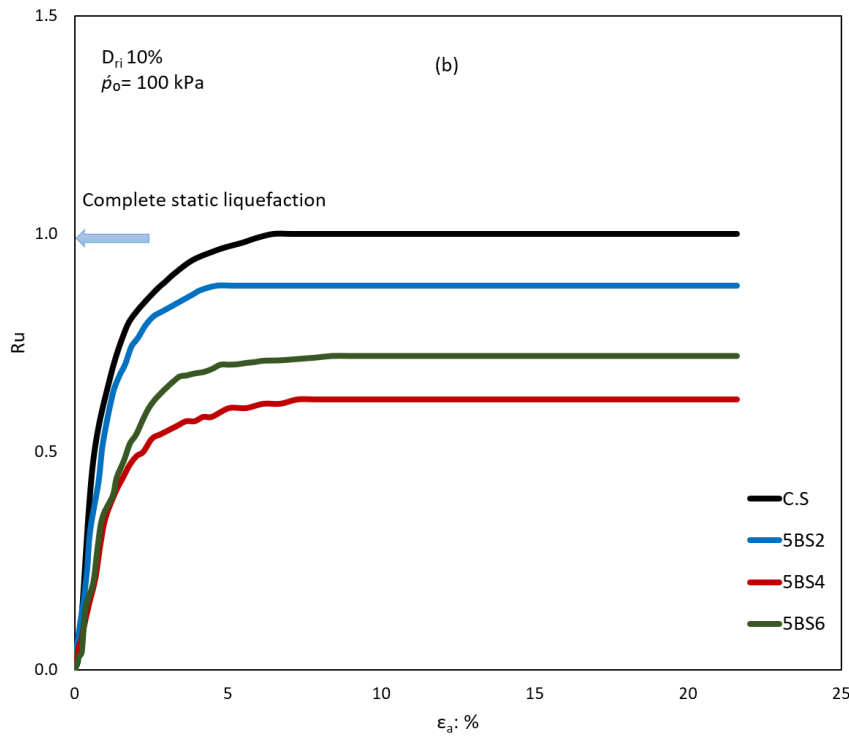


Figure 5.4 Undrained behaviour of very loose sand–slag–5% bentonite mixtures: (a) effective stress ratios vs. strain with  $p_o = 100$  kPa and (b) pore water pressure ratio vs. strain with  $p_o = 100$  kPa

The undrained shear of all the tests commenced from the same effective stress defined by  $p_o = 100$  kPa. Figure 5.5 shows a clear trend of increasing stress ratios ( $q_{min}/q_{peak}$ ) of the sand–slag–bentonite mixtures when sand and slag were mixed with 3% bentonite. Moreover, the mixtures of 3BS2, 3BS4, and 3BS6 showed almost the same values of the stress ratios. The values of the stress ratios of 3BS2, 3BS4, and 3BS6 were 0.979, 0.989, and 0.958, respectively. However, the stress ratio decreased when the bentonite content increased to 5% bentonite. The values of the stress ratios of 5BS2, 5BS4, and 5BS6 were 0.551, 0.693, and 0.570, respectively. The stress ratio ( $q_{min}/q_{peak}$ ) increased from 0 in the C.S sample, which indicated complete static liquefaction, to 0.989 in 3BS4. In contrast, the stress ratio for the same mixture reduced to 0.693 when the bentonite content increased to 5%. Figure 5.6 presents the liquefaction susceptibility of the sand–slag–bentonite mixtures. It is apparent from this figure that undrained brittleness index  $I_B$  significantly reduced when the sand was mixed with different percentages of fines. The clean sand sample showed complete liquefaction behaviour with  $I_B = 1$ . The  $I_B$  values of the mixtures decreased when the sand–slag mixtures were mixed with 3% bentonite and increased with when the

bentonite content increased to 5%. The  $I_B$  values of 3BS2, 3BS4, and 3BS6 were 0.021, 0.011, and 0.042, respectively. However, these values increased to 0.449, 0.307, and 0.430, respectively, when the bentonite content increased to 5%. A marked feature of Figure 5.6 is that the mixtures of sand + slag + 3% bentonite showed low liquefaction susceptibility with  $I_B \leq 0.05$ , while the liquefaction susceptibility of the same sand–slag mixtures increased to  $I_B \geq 0.3$  when bentonite increased to 5%. Furthermore, the mixture of sand + 4% slag + 3% bentonite (3BS4) exhibited a liquefaction susceptibility lower than that of the other mixtures. The effect of the combination of the two fines contents on the liquefaction behaviour of sandy soils can be observed by examining Figure 5.7, which shows the pore water pressure ratios  $R_u$  of very loose sand–slag–bentonite mixtures sheared at a single initial confining pressure  $p'_o$  of 100 kPa. From the data presented in Figure 5.7, we can see that the pore water pressure ratio considerably decreased when the sand was mixed with various slag contents and 3% bentonite. However, the pore water pressure ratios reduced slightly when the same sand–slag mixtures were mixed with 5% bentonite. The  $R_u$  values of 3BS2, 3BS4, and 3BS6 were 0.57, 0.32, and 0.33, respectively. However, these values increased to 0.88, 0.62, and 0.72 when the bentonite content increased to 5%. The effect of bentonite on the behaviour of the sand–slag mixtures was related to its role in affecting the soil fabric. At 3% bentonite, the behaviour of the sand–fines mixtures was dominated by the slag content. Therefore, the soil fabric might be improved by the presence of both slag and bentonite. However, at 5% bentonite content, the behaviour of the sand–fines mixtures was dominated by the bentonite content which made the sand grains slippery and increased compressibility. Furthermore, the negative effect of 5% bentonite on the liquefaction susceptibility of the sand–slag mixtures could be related to the ability of bentonite to swell when brought in contact with water. Consequently, the contact between sand grains reduced, which led to an increase in the compressibility of the samples. This finding was consistent with the findings reported by Tang, Ma, and Shao (2013); Tang, Ma, and Dieudonné (2013), and (El Mohtar et al., 2013); they reported that the liquefaction potential increased at bentonite contents of  $<5\%$ . However, (Gratchev et al., 2006) noted that artificial clay–sand mixtures exhibited rapid liquefaction when the bentonite content was  $\leq 7\%$ , while the liquefaction susceptibility was reduced when the bentonite content was  $\geq 11\%$ .

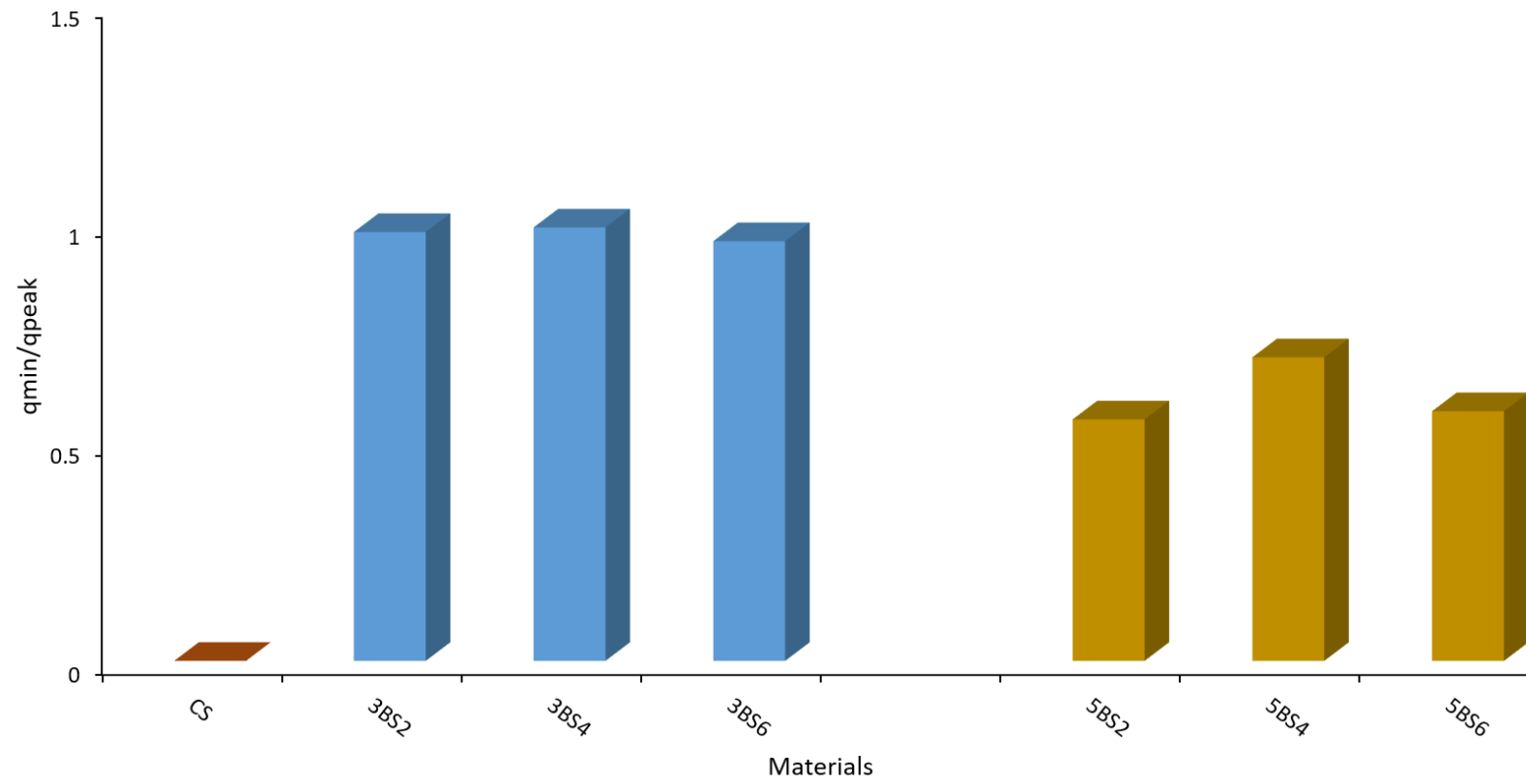


Figure 5.5 Stress ratios of sand-slag-bentonite mixtures

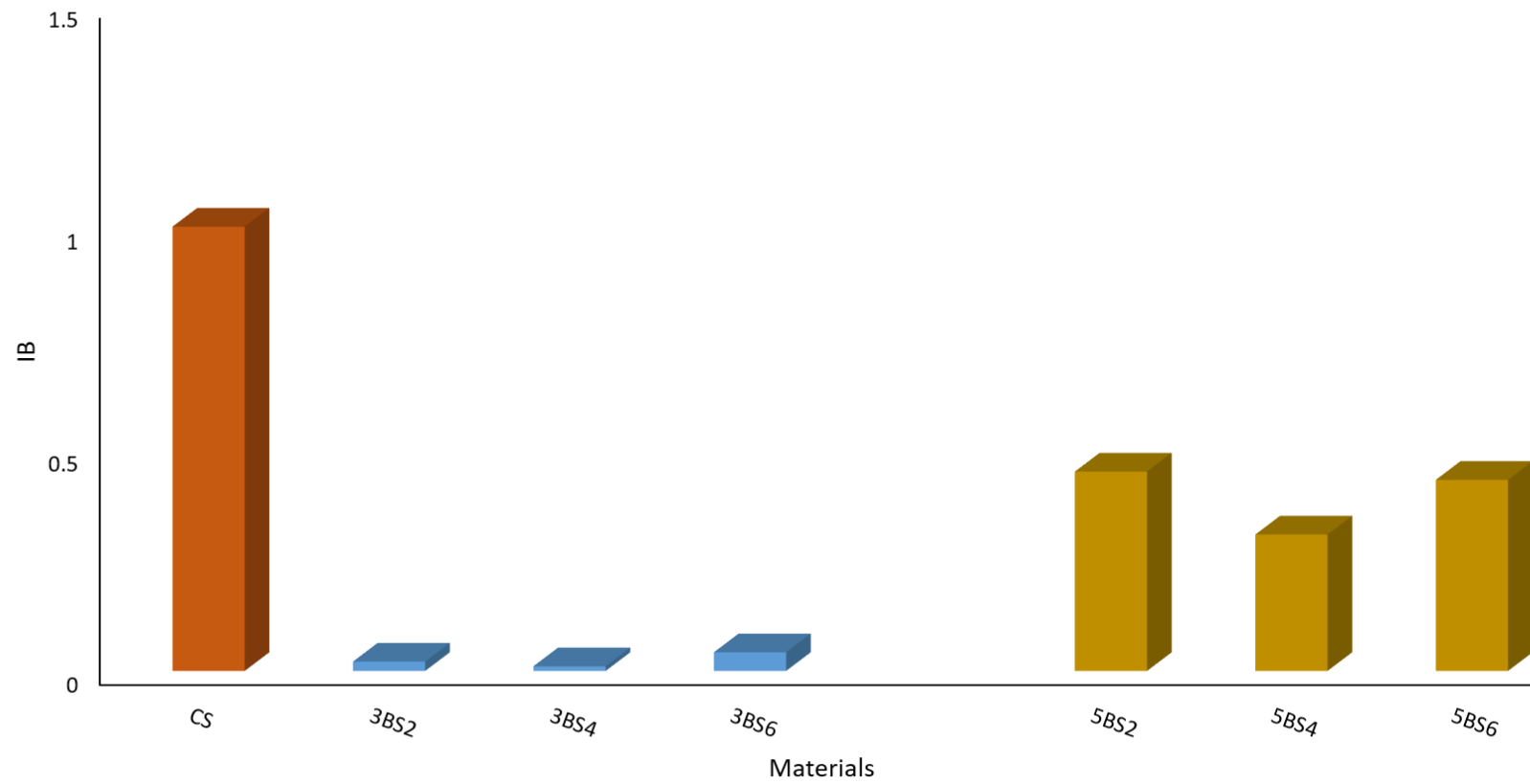


Figure 5.6 Undrained brittleness index of sand-slag-bentonite mixtures

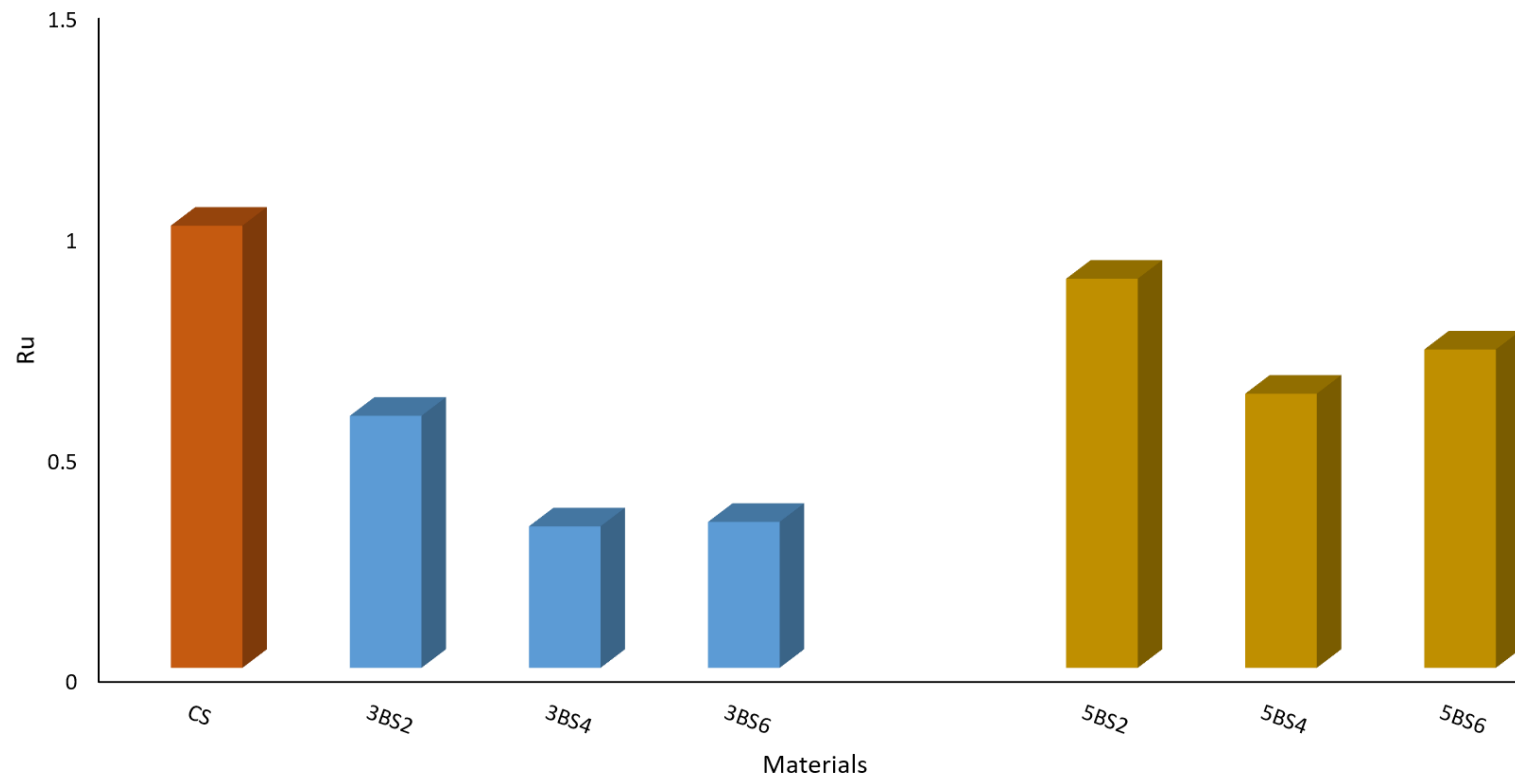


Figure 5.7 Pore water pressure ratios of sand-slag-bentonite mixtures

### 5.3 Liquefaction behaviour of sand–slag–kaolinite mixtures

In the present study, six series of undrained triaxial compression tests were performed on fully saturated sand–slag–kaolinite clay mixtures to investigate the effect of the combination of slag and kaolinite clay on the liquefaction behaviour of sandy soil. All the samples were formed by mixing sandy soil with three proportions of slag (2%, 4%, and 6%) and two proportions (3% and 5%) of kaolinite clay by the dry weight of sand, giving six triple mixtures as shown in Table 5.3.

Table 5.3 Physical properties of sand–slag–kaolinite mixtures

Materials	Symbol	$e_{max}$	$e_{min}$	$C_u$	$G_s$
Sand + 2% slag + 3% kaolinite	3KS2	0.708	0.486	1.92	2.671
Sand + 4% slag + 3% kaolinite	3KS4	0.706	0.468	2.04	2.688
Sand + 6% slag + 3% kaolinite	3KS6	0.702	0.450	2.25	2.692
Sand + 2% slag + 5% kaolinite	5KS2	0.736	0.472	1.62	2.68
Sand + 4% slag + 5% kaolinite	5KS4	0.728	0.433	1.92	2.686
Sand + 6% slag + 5% kaolinite	5KS6	0.722	0.394	2	2.69

Table 5.3 shows that the maximum void ratio ( $e_{max}$ ), specific gravity ( $G_s$ ), and coefficient of uniformity ( $C_u$ ) of the mixtures increased with increasing kaolinite content. However, the minimum void ratio ( $e_{min}$ ) of the mixtures decreased with increasing kaolinite content. Table 5.3 also shows that the  $e_{max}$ ,  $C_u$  and  $G_s$  values of the mixtures increased with increasing slag content in each mixture.

Each sample was monotonically sheared in compression under undrained conditions. Samples were prepared in the loose state ( $D_{ri}$  10%) with shearing starting from single initial confining pressures  $p'_o$  of 100 kPa. Tests conducted on samples prepared by mixing sand with 2%, 4%, and 6% slag and 3% kaolinite were labelled 3KS2, 3KS4, 3KS6, respectively. However, tests conducted on samples prepared by mixing sand with 2%, 4%, and 6% slag and 5% kaolinite were labelled 5KS2, 5KS4, and 5KS6 respectively. The results of these tests are listed in Table 5.4.

Table 5.4. Results of undrained tests conducted on sand–slag–kaolinite mixtures

Test name	$\rho_o$	$e_o$	$e_{cs}$	$q_{peak}$	$R_u$	$q_{min}/q_{peak}$	$I_B$
3KS2	100	0.686	0.684	68.69	0.44	0.997	0.003
3KS4	100	0.682	0.679	74.85	0.31	0.999	0.001
3KS6	100	0.677	0.674	93.6	0.23	0.999	0.001
5KS2	100	0.710	0.708	26.86	0.78	0.789	0.211
5KS4	100	0.698	0.696	31.59	0.57	0.802	0.198
5KS6	100	0.689	0.687	39.75	0.53	0.942	0.058

Figure 5.8(a) shows the stress–strain relationships of CS1, 3KS2, 3KS4, and 3KS5 sheared under initial confining pressures  $\rho_o$  of 100 kPa. It is apparent that mixing sandy soil with different slag contents and 3% kaolinite clay enhanced the undrained behaviour of the mixtures as compared to the clean sand. Three tests (3KS2, 3KS4, and 3KS5) exhibited gradual increases in the deviatoric stress until the maximum deviatoric stress was reached at the end of the test, which indicated non-flow behaviour. However, the clean sand sample showed a sudden reduction in the deviatoric stress after attaining the initial peak deviatoric stress  $q_{peak}$ , which indicated complete static liquefaction. As shown in Figure 5.8(a), there is a significant difference between the deviatoric stress of clean sand and that of the sample sand–fines mixtures. Furthermore, the deviatoric stresses of the sand–slag–3% kaolinite clay mixtures increased with increasing slag content, and the 3KS6 mixture exhibited the highest value. The deviatoric stress of the clean sand sample increased from 7 kPa to 68.5 kPa, 74.85 kPa, and 93.6 kPa in the mixtures of 3KS2, 3KS4, and 3KS6, respectively. The following effective stress paths of CS1, 3KS2, 3KS4, and 3KS6 are shown in Figure 5.8(b). The effective stress paths of the tests show a significant difference between the effective stress paths of the clean sand and those of the sand–fines mixtures. The resultant effective stress path of CS1 plummeted toward the origin of the  $q$ – $p'$  plane after reaching the characteristic peak deviatoric stress, which indicated complete static liquefaction behaviour. However, 3KS2, 3KS4, and 3KS6 showed different behaviour trends when the effective stress paths of these tests moved to the left and then moved upwards toward the higher mean stresses. The slope of the effective stress paths increased with increasing slag content, and the 3KS6 test showed the highest value. Figure 5.8(b) also shows the difference between the effective stresses paths that reduced with increasing slag content.



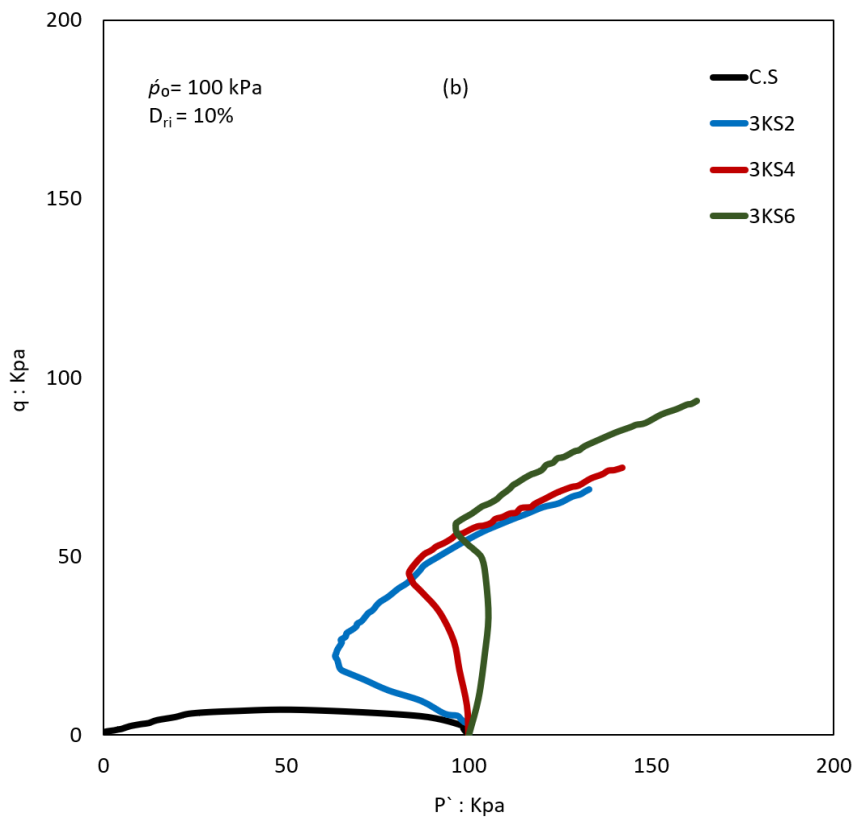
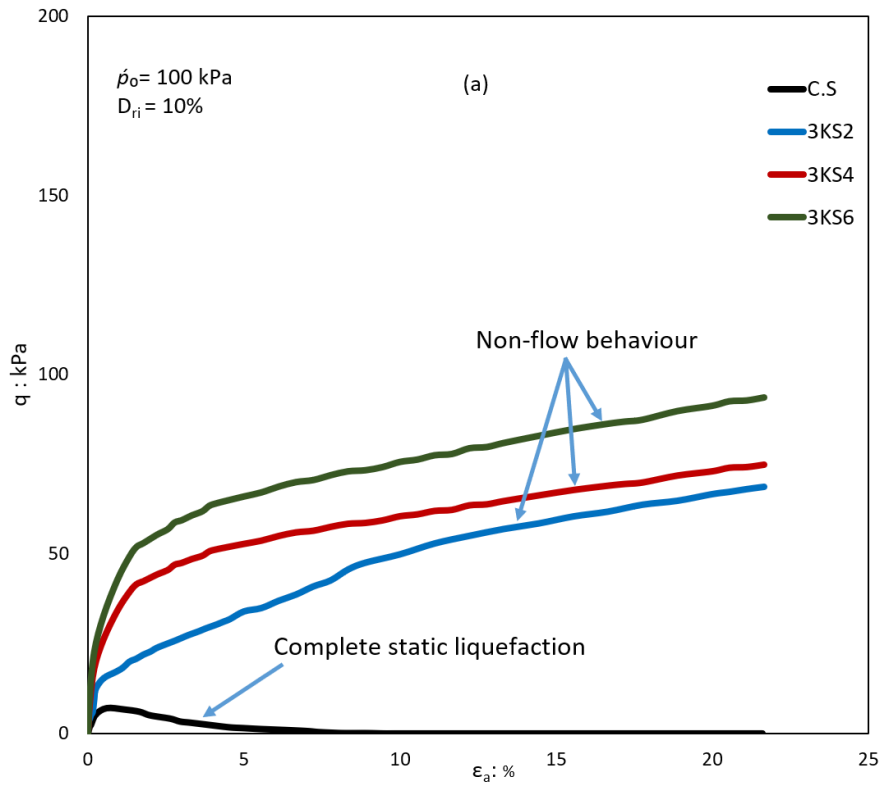
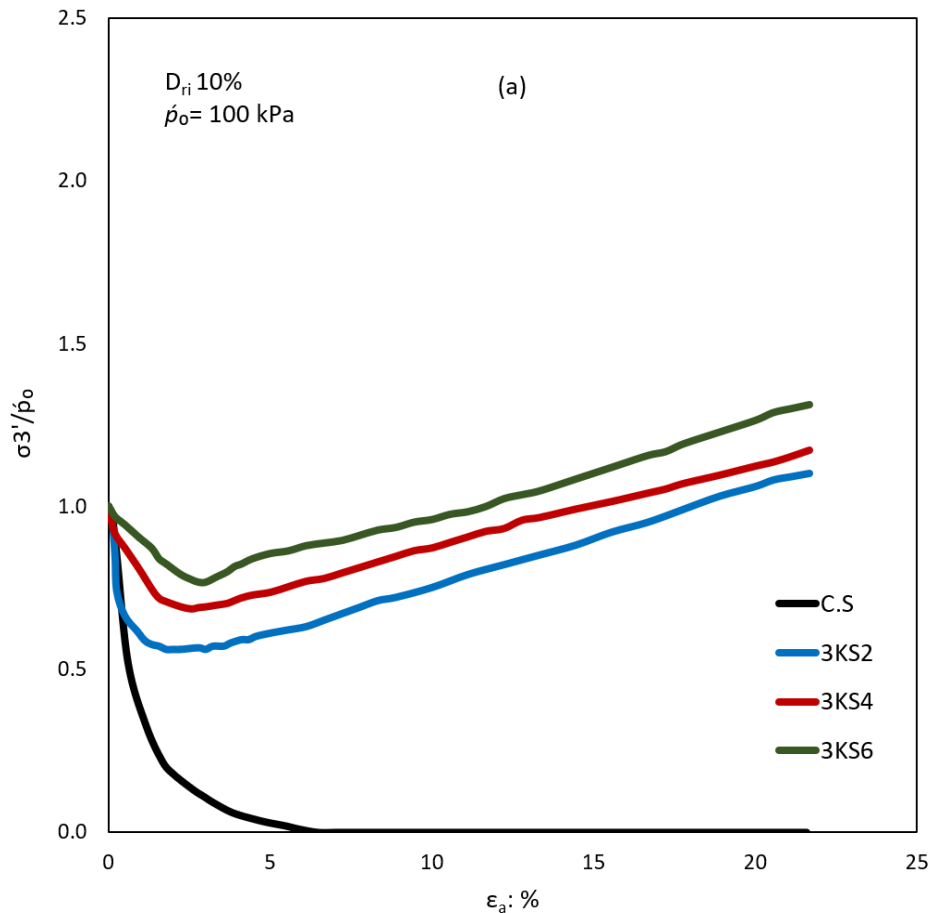


Figure 5.8 Undrained behaviour of very loose sand–slag–kaolinite samples: (a) stress vs. strain with  $p_0 = 100$  kPa and (b) effective stress path with  $p_0 = 100$  kPa

The effect of the combination of two types of fines on the liquefaction behaviour of sandy soils can be observed by examining Figures 5.9(a) and (b), which present the effective stress ratio versus axial strain and the pore water pressure ratios  $R_u$  versus the axial strain of CS1, 3KS2, 3KS4, and 3KS6. From the data shown in Figure 5.9(a), we can infer that the clean sand sample showed an abrupt reduction in the effective stress ratio until zero effective stress ratio was reached at a small strain (indicating complete static liquefaction). However, when the clean sand was mixed with different slag contents and 3% kaolinite, the behaviour of the effective stress ratios changed completely. Further, 3KS2, 3KS4, and 3KS6 exhibited a slight reduction in the effective stress ratio followed by a gradual increase toward a higher effective stress ratio at the end of the tests. The reduction in the effective stress ratio of the mixtures slowed down with increasing slag content. The effective stress ratio increased from zero in the CS1 test to 1.1, 1.17, and 1.312 in the 3KS2, 3KS4, and 3KS6 tests, respectively.



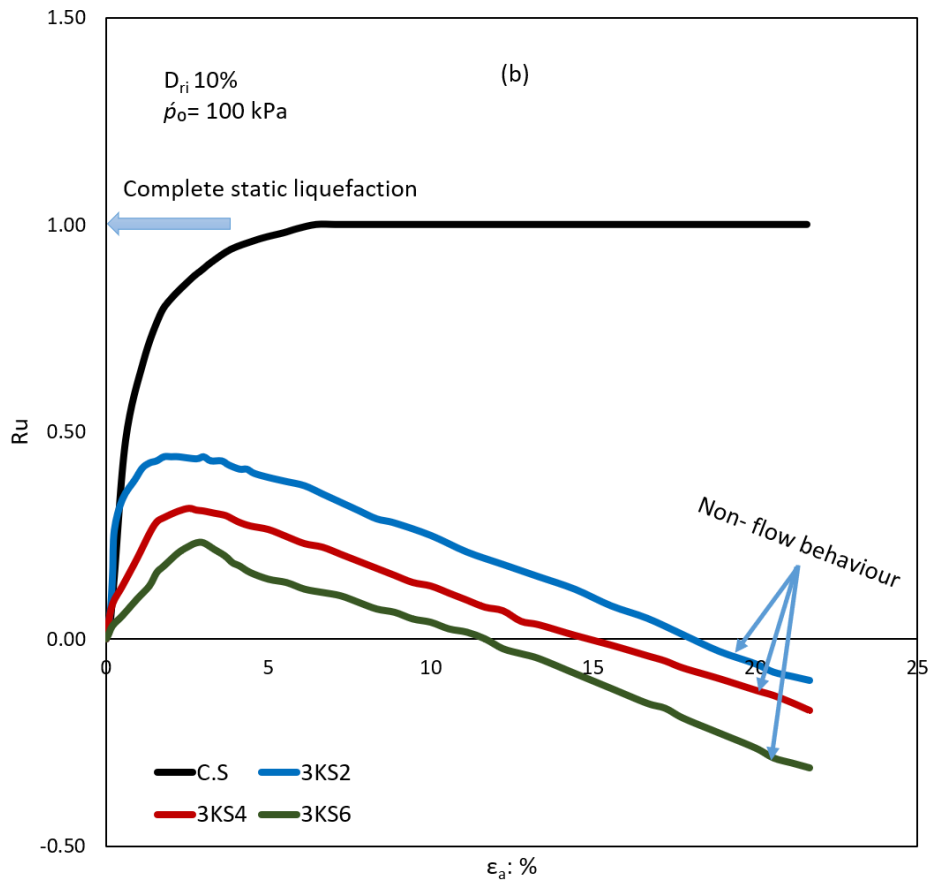


Figure 5.9 Undrained behaviour of very loose sand–slag–3% kaolinite mixtures: (a) effective stress ratios vs. strain with  $\dot{p}_o = 100$  kPa and (b) pore water pressure ratio vs. strain with  $\dot{p}_o = 100$  kPa

From the data shown in Figure 5.9(b), it is apparent that the pore water pressure ratio  $R_u$  significantly reduced when the sand was mixed with the fines. The clean sand sample exhibited an abrupt increase in the pore water pressure ratio until the unity value was reached, which indicated complete static liquefaction. However, when sand was mixed with slag and 3% kaolinite, the pore water pressure ratio significantly reduced after attaining the initial peak value. In the 3KS2, 3KS4, and 3KS6 tests, the change in the pore water pressure ratio was significantly negative toward the end of the test. The pore water pressure ratio reduced when the slag content in the mixtures increased up to 6%. The pore water pressure ratio  $R_u$  reduced from 1 in the CS1 test to 0.44, 0.31, and 0.23 in the 3KS2, 3KS4, and 3KS6 tests, respectively. The above behaviour trend (Figures 5.8 and 5.9) indicated that mixing the sand with different slag contents and 3% kaolinite clay enhanced the soil fabric, which improved the shear strength of the soil. Consequently, all the mixtures showed non-flow behaviour with low pore water pressure ratios.

The other three tests, namely 5KS2, 5KS4, and 5KS6, were conducted in the present study to examine the effect of increasing the kaolinite content to 5% on the liquefaction behaviour of the sand–slag–kaolinite mixtures. The results of three isotropically consolidated undrained tests 5KS2, 5KS4, and 5KS6 with shearing commencing from  $p'_o$  of 100 kPa are presented in Figures 5.10 and 5.11. Figure 5.10(a) presents the stress–strain relationships of the CS1, 5KS2, 5KS4, and 5KS6 tests; from this figure, we can infer that mixing the sand with fines enhanced the undrained behaviour of sandy soil by changing the behaviour trend from complete static liquefaction in the clean sand sample to flow and limited flow behaviour when the sand was mixed with both slag and 5% kaolinite. The CS1, 5KS2, and 5KS4 tests revealed a reduction in the deviatoric stresses after reaching the initial peak deviatoric stress  $q_{peak}$ , indicating flow behaviour. The CS1 test showed abrupt decreases in the deviatoric stress until the stress became zero at the end of the test, while the 5KS2 and 5KS4 tests showed a gradual reduction in the deviatoric stress, but in both of them, the stress did not reduce to zero at the end of the test. Furthermore, the rate of reduction of the deviatoric stress decreased with increasing slag content. The 5KS6 test showed a reduction in the deviatoric stress after attaining the initial peak deviatoric stress; then, it slightly increased toward a higher deviatoric stress. The initial peak deviatoric stress of the mixtures increased when the slag content increased up to 6%. Moreover,  $q_{peak}$  increased from 7 kPa in C.S to 26.86 kPa, 31.59 kPa, and 39.75 kPa in 5KS2, 5KS4, and 5KS6, respectively. The resultant effective stress paths of CS1, 5KS2, 5KS4, and 5KS6 are shown in Figure 5.10(b). The effective stress path of the clean sand sample plummeted to the origin of the  $p'$ – $q$  plane after reaching their representative peak deviatoric stress; this indicated complete static liquefaction behaviour. The resultant effective stress paths of 5KS2 and 5KS4 also plummeted, but they did not reach the zero values, indicating flow liquefaction behaviour. The effective stress path of 5KS6 consisted of three sections initially tracing toward a peak deviatoric stress, then plummeting after attaining the peak deviatoric stress, and finally bending slightly upwards toward the higher mean stresses. Furthermore, the slope of the effective stress paths increased with increasing fines content, and 5KS6 showed the highest value.

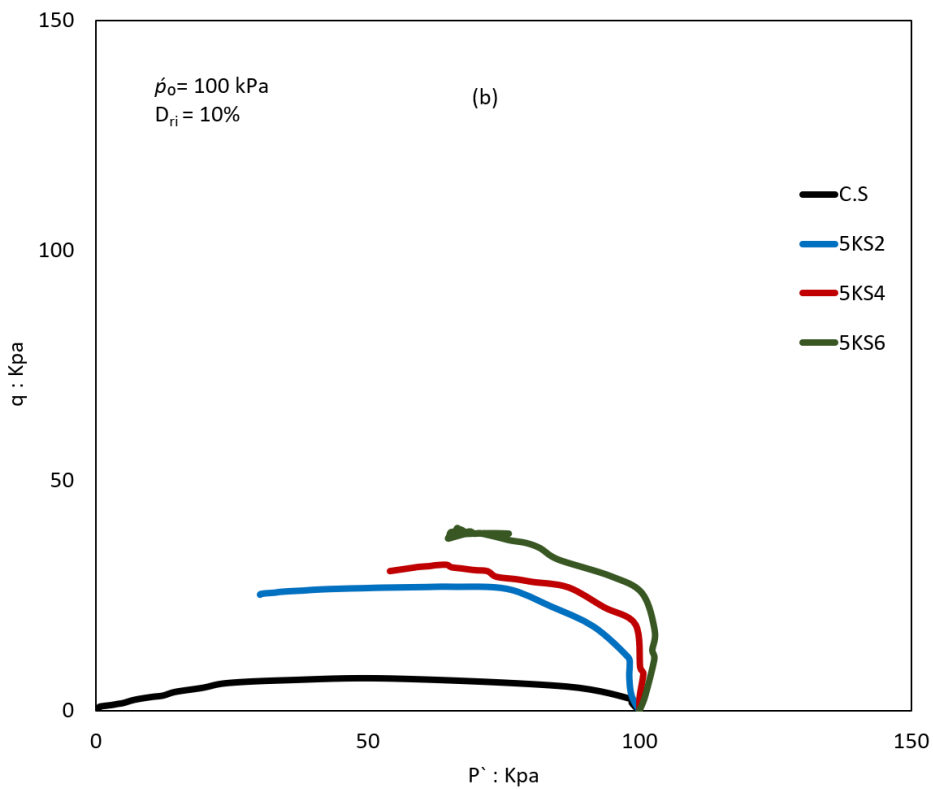
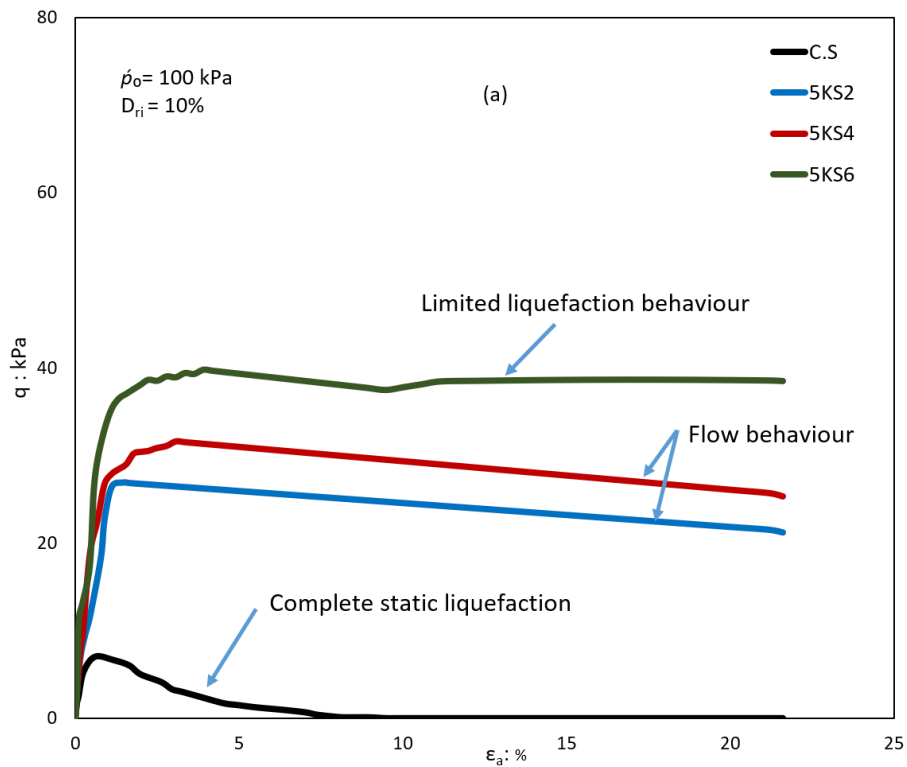


Figure 5.10 Undrained behaviour of very loose sand–5% kaolinite–slag samples: (a) stress vs. strain curves with  $p_o = 100$  kPa and (b) effective stress path with  $p_o = 100$  kPa

The effect of the combination of slag and 5% kaolinite on the liquefaction behaviour of the sand–slag mixtures is also shown in Figures 5.11(a) and (b). It is apparent from these figures that all the loose samples (i.e. C.S1, 5KS2, 5KS4, and 5KS6) sheared under initial confining pressure  $p'_o$  of 100 kPa showed flow behaviour characterised by a reduction in the effective stress ratio and a positive pore water pressure ratio  $R_u$ . The C.S sample exhibited a rapid reduction in the effective stress ratio until the effective stress was zero, indicating complete static liquefaction behaviour. However, 5KS2 and 5BS4 also exhibited a reduction in the effective stress ratio, but the reduction did not continue until the stress became zero. The 5KS6 test showed different behaviour characterised by a reduction in the effective stress ratio and then a slight increase with further strain. The reduction in the effective stress ratio reduced with increasing fines content, and the mixture of 5KS6 showed the highest value of the effective stress ratio, as shown in Figure 5.11(a). Figure 5.11(b) shows that the clean sand sample and the sand–fines samples exhibited a positive pore water pressure ratio, indicating flow liquefaction behaviour. The pore water pressure ratio  $R_u$  of the clean sand sample abruptly increased until it reached unity, which implied that the excess pore water pressure was equal to the initial confining pressure and the effective stress was equal to zero (indicating complete static liquefaction). In contrast, the sand–slag–5% kaolinite mixtures showed a different behaviour trend. The pore water pressure ratio  $R_u$  of 5KS2 and 5KS4 increased with increasing axial strain but none of them reached unity. 5KS4 exhibited a slight reduction in the pore water pressure ratio after reaching a peak value. Furthermore, the pore water pressure ratio reduced when the slag content increased up to 6%.  $R_u$  was reduced from 1 in the clean sand sample to 0.78, 0.57, and 0.53 in the mixtures of 5KS2, 5KS4, and 5KS6, respectively. The above behaviour of the sand–slag–bentonite mixtures indicated that increasing the kaolinite content from 3% to 5% enhanced the flow liquefaction behaviour of the sand–slag mixtures. This was manifested when the behaviour of sand–slag–3% kaolinite completely changed from non-flow behaviour to flow liquefaction behaviour. The deviatoric stresses and the effective stress ratios of the sand–slag–kaolinite mixtures reduced when the kaolinite content increased from 3% to 5%. Note from Figures 5.8–5.11 that the mixtures 3KS6 and 5KS6 exhibited the highest deviatoric stresses and effective stress ratios.

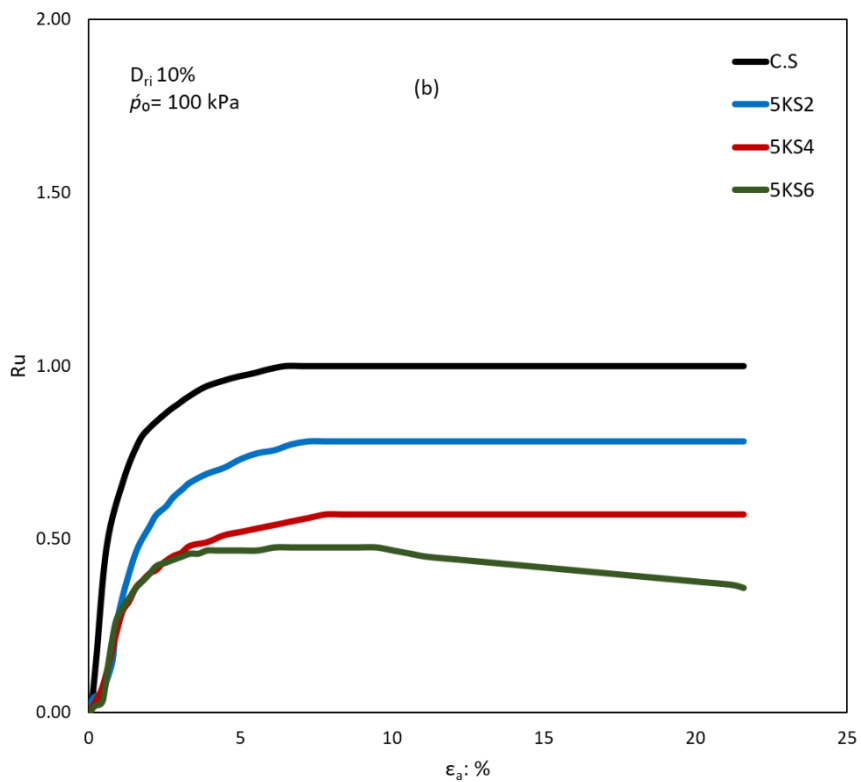
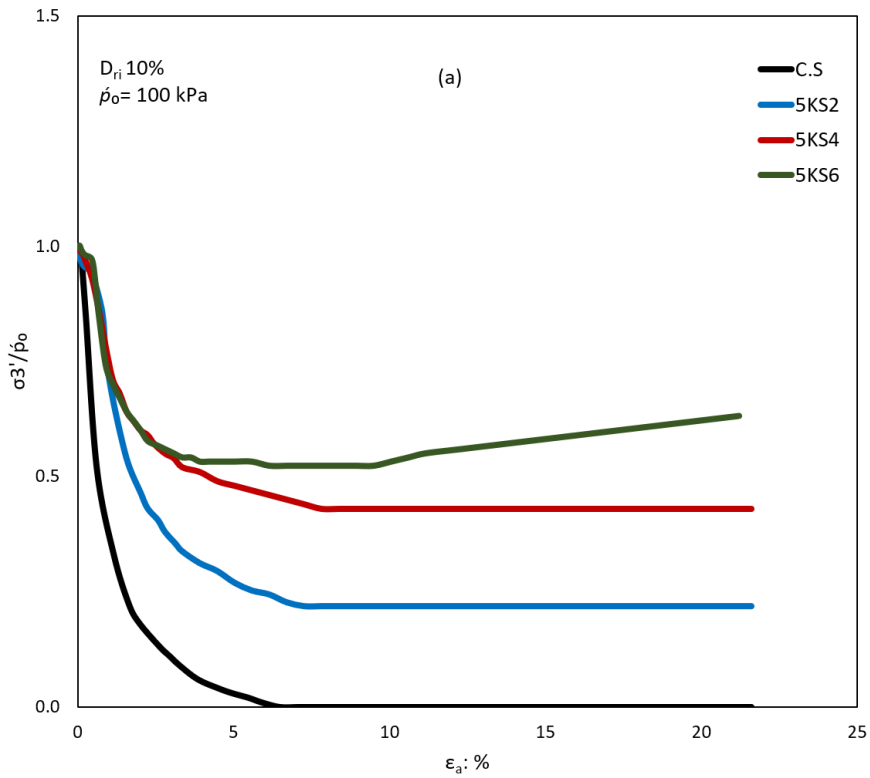


Figure 5.11 Undrained behaviour of very loose sand–slag–5% kaolinite mixtures: (a) effective stress ratios vs. strain with  $\dot{p}_0 = 100$  kPa and (b) pore water pressure ratio vs. strain with  $\dot{p}_0 = 100$  kPa

The undrained behaviour of the loose sand–slag–kaolinite clay mixtures containing 3% bentonite is compared with that of 5% bentonite in Figures 5.12–5.14. The undrained shear of all of the tests commenced from the same effective stress defined by  $p'_o = 100$  kPa. Figure 5.12 shows a clear trend of increasing stress ratios ( $q_{min}/q_{peak}$ ) of the sand–slag–kaolinite mixtures when the sand and the slag were mixed with 3% kaolinite. Moreover, the mixtures of 3KS2, 3KS4, and 3KS6 showed a slight difference in the stress ratios. The stress ratios of 3KS2, 3KS4, and 3KS6 were 0.997, 0.998, and 0.999, respectively. However, when the kaolinite content increased to 5%, the sand–fines mixtures exhibited a reduction in the stress ratio. The stress ratios of 5KS2, 5KS4, and 5KS6 were 0.788, 0.801, and 0.941, respectively. The stress ratio ( $q_{min}/q_{peak}$ ) of all the mixtures that contained 3% and 5% kaolinite increased with increasing slag content up to 6%, and 3KS6 showed the highest values. The stress ratio increased from 0 in the C.S sample, which indicated complete static liquefaction, to 0.999 in 3KS6. In contrast, the stress ratio for the same mixture reduced to 0.941 when the kaolinite content increased to 5%. Figure 5.13 presents the liquefaction susceptibility of the sand–slag–kaolinite mixtures. It is apparent from this figure that the undrained brittleness index  $I_B$  significantly reduced when the sand was mixed with different percentages of fines. The clean sand sample showed complete liquefaction behaviour with  $I_B = 1$ . The  $I_B$  values of the mixtures decreased when the sand–slag mixtures were mixed with 3% kaolinite and increased with an increase in the kaolinite content to 5%. The  $I_B$  values of 3KS2, 3KS4, and 3KS6 were 0.0277, 0.001, and 0.000534, respectively. However, these values increased to 0.24, 0.198, and 0.058 when the kaolinite content increased to 5%. A marked feature of Figure 5.6 is that the mixtures of sand + slag + 3% kaolinite showed low liquefaction susceptibility with  $I_B \leq 0.000534$ , while the liquefaction susceptibility of the same sand–slag mixtures increased to  $I_B \geq 0.058$  when the kaolinite content increased to 5%. Furthermore, the mixture of sand + 6% slag + 3% kaolinite (3KS6) exhibited lower liquefaction susceptibility than the other mixtures. The effect of the combination of two fines contents on the liquefaction behaviour of sandy soils can be observed from Figure 5.14, which presents the pore water pressure ratios  $R_u$  of very loose sand–slag–kaolinite mixtures sheared under single initial confining pressures of  $p'_o = 100$  kPa. From the data presented in Figure 5.14, we can see that the pore water pressure ratio considerably decreased when the sand was mixed with various slag contents and 3% kaolinite. However, the pore water pressure ratios increased when the same sand–slag



mixtures were mixed with 5% kaolinite. The  $R_u$  values of 3KS2, 3KS4, and 3KS6 were 0.44, 0.31, and 0.23, respectively. However, these values increased to 0.78, 0.57, and 0.53, respectively, when the kaolinite content increased to 5%. The improvement in the behaviour of the sand–slag–kaolinite mixtures was related to the role of the fines in enhancing the soil fabric. At 3% kaolinite, the behaviour of the sand–fines mixtures was dominated by the slag content. Therefore, the soil fabric was improved by the presence of both slag and kaolinite. However, at 5% kaolinite, the behaviour of the sand–fines mixtures was dominated by the kaolinite content. Furthermore, the fines particles occupied the voids between the sand grains which reduced the contact between the soil particles. Consequently, the compressibility of the sand–fines mixtures was increased. This finding is consistent with the findings of Bayat et al. (2014), who concluded that the presence of up to 20% kaolinite reduced the shear strength of mixtures and increased the pore water pressure generation. Furthermore, Koester (1994) found that the cyclic liquefaction resistance of soil reduced with increasing kaolinite content of up to 20%.

To examine whether the liquefaction behaviour of the sand–slag–clay mixtures was affected by clay mineralogy, the results of monotonic undrained compression triaxial tests conducted on the sand–slag–bentonite and sand–slag–kaolinite mixtures with the same clay percentages of 3% and 5% were replotted in Figures 5.15 and 5.16. Figure 5.15 presents the brittleness index  $I_B$  of all the mixtures prepared at the relative density of 10% and sheared under initial confining pressure  $p_o$  of 100 kPa. It is apparent from this figure that the liquefaction susceptibility represented by the brittleness index  $I_B$  of the sand–slag–kaolinite mixtures was less than that of the sand–slag–bentonite mixtures at both clay contents. The samples of the sand–slag–kaolinite mixtures showed a higher tendency to reduce the liquefaction susceptibility than the sand–slag–bentonite mixtures. However, the  $I_B$  of all the mixtures significantly reduced with increasing fines content. The liquefaction susceptibility of mixtures reduced when the clay content was 3% and then increased when the clay content increased to 5%. Note from Figure 5.15 that the mixtures of sand–slag–kaolinite showed consistent behaviour characterised by the reducing  $I_B$  values with increasing slag content. However, the mixtures of sand–slag–bentonite showed a reduction in the liquefaction susceptibility when the slag content increased up to 4% and then increased when the slag content increased to 6%. The effect of the clay type on the liquefaction susceptibility of the

sand–slag–clay mixtures is clearly seen in Figure 5.16. In this figure, there is a clear trend of the decreasing pore water pressure ratio  $R_u$  of the sand–slag–clay mixtures when the clay content was 3% and then an increasing trend when the clay content increased to 5%. At both kaolinite contents, namely 3% and 5%, the pore water pressure ratio reduced with increasing slag content and the mixtures of 6% slag showed the lowest values. However, at both bentonite contents, namely 3% and 5%, the pore water pressure ratio decreased with increasing slag content of up to 4% and then increased with increasing slag content of up to 6%. This discrepancy in the results of the liquefaction susceptibility of the sand–slag–clay mixtures proved the substantial effect of clay mineralogy on the liquefaction behaviour of the sand–slag–clay mixtures which could be related to the role played by the kaolinite clay in producing a more stable soil fabric than sand–slag–bentonite. The findings reported here are consistent with those reported in Chapter 4, which showed that the sand–kaolinite mixtures were less susceptible to liquefy than the sand–bentonite mixtures.

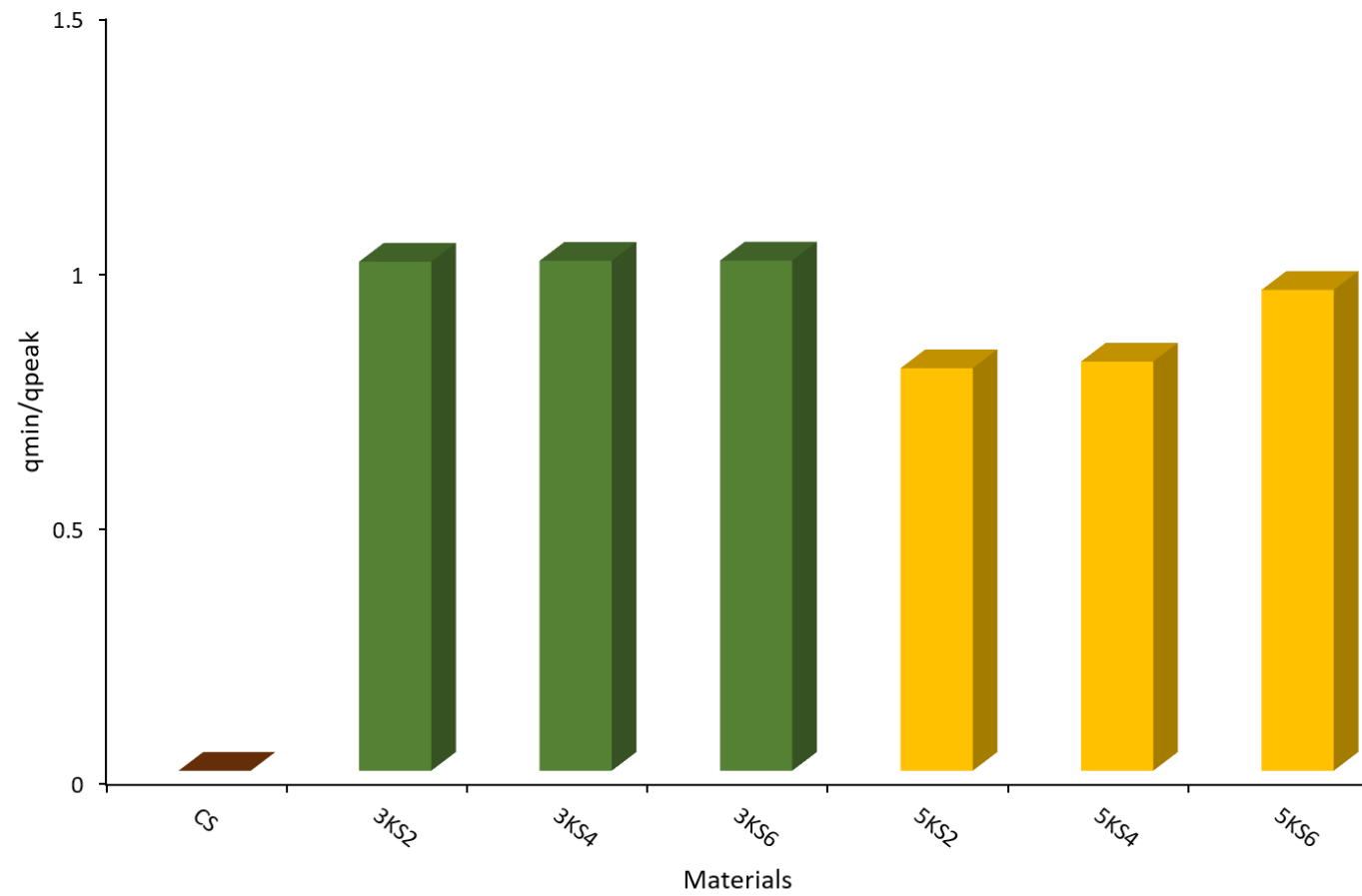


Figure 5.12 Stress ratios of sand-slag-kaolinite mixtures

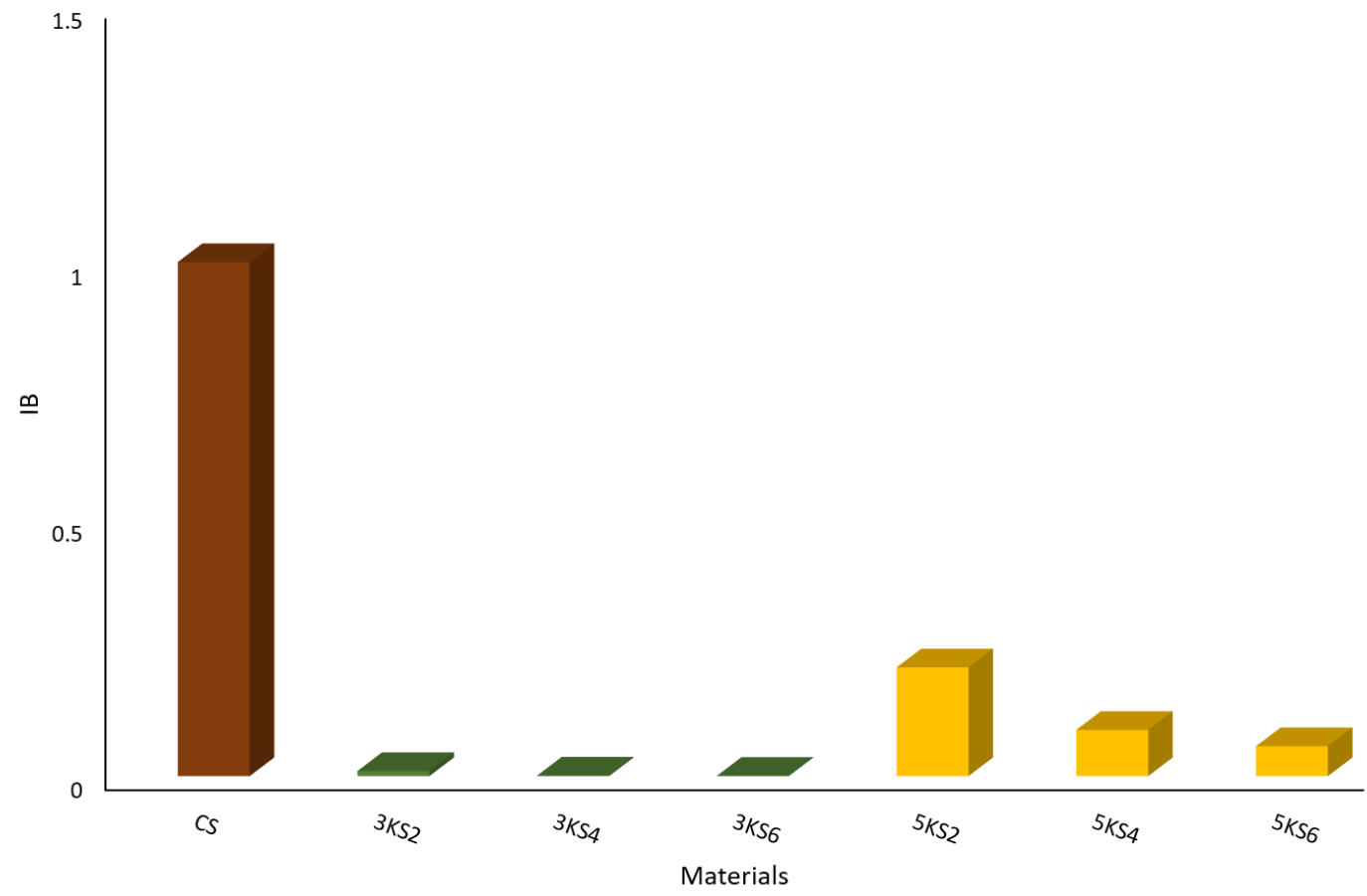


Figure 5.13 Undrained brittleness index of sand-slag-kaolinite mixtures

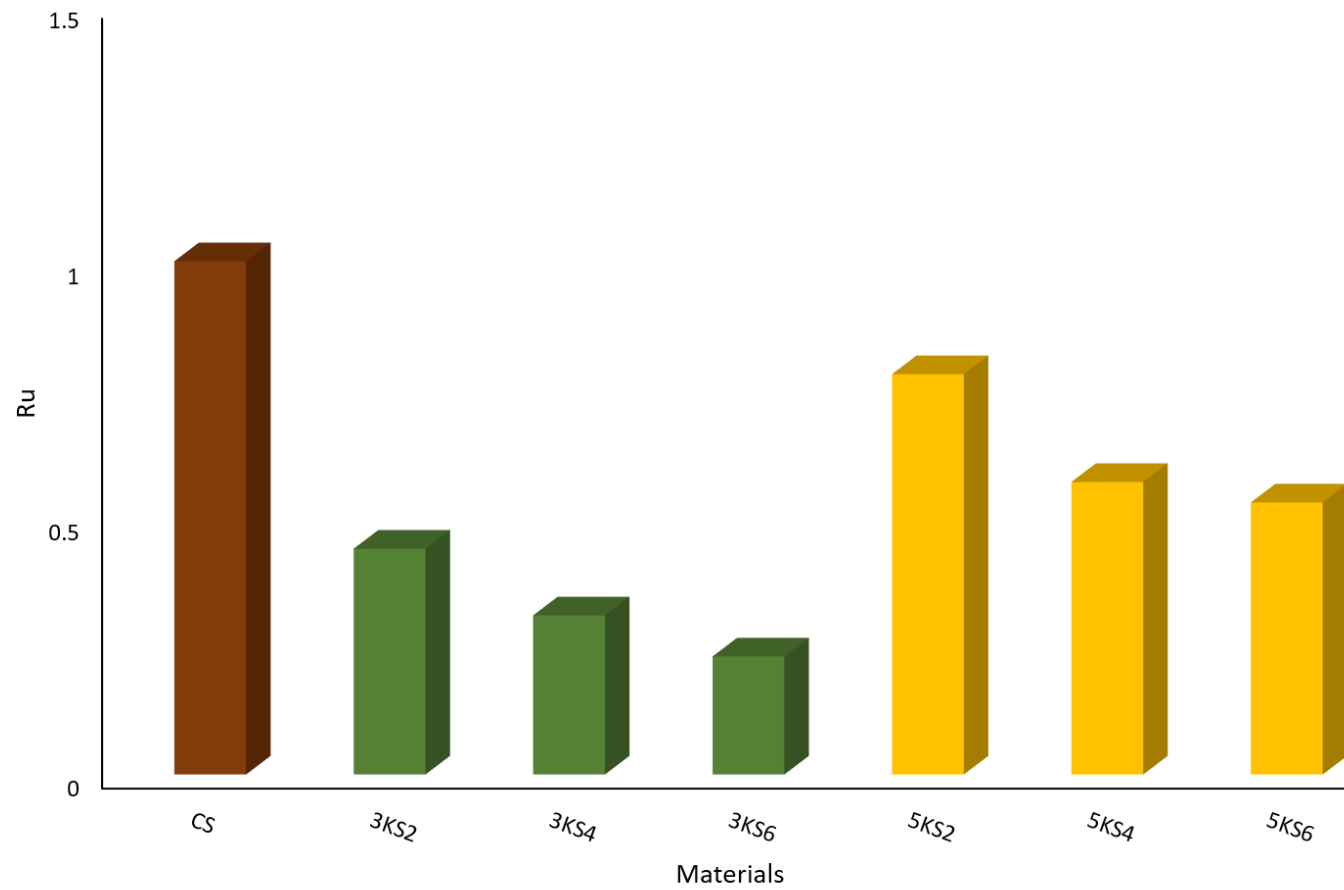
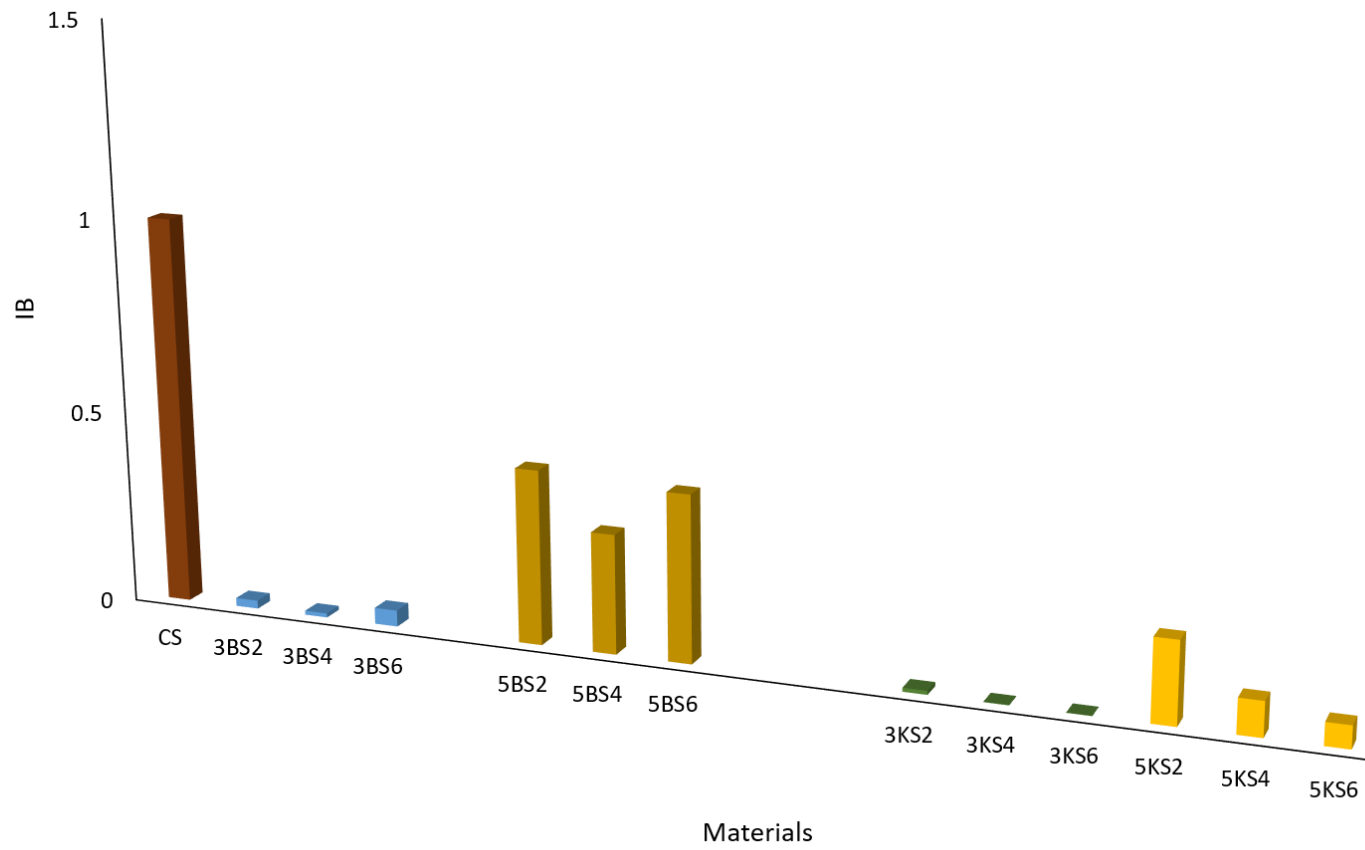
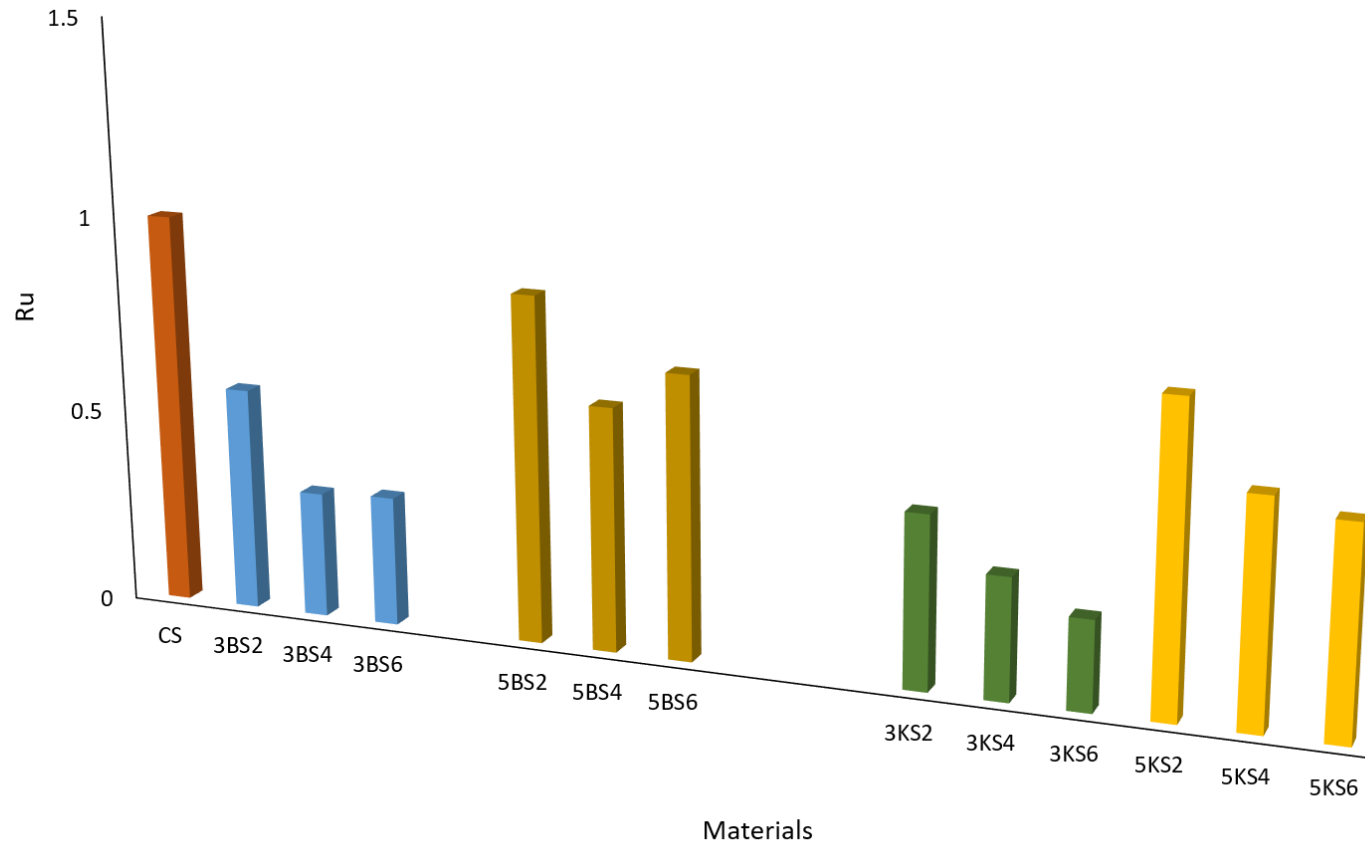


Figure 5.14 Pore water pressure ratio of sand-slag-bentonite mixtures



0 Figure 5.15 Undrained brittleness index of all the mixtures



1 Figure 5.16 Pore water pressure ratio of all the mixtures





## 5.4 Summary

Undrained triaxial compressions tests were conducted to investigate the effect of the combination of two types of fines on the liquefaction behaviour of sandy soils. Tests were carried out on loose samples prepared by mixing sand with various slag contents (2%, 4%, and 6%) and various clay contents (3% and 5% of bentonite and kaolinite). The test results of the sand–slag–bentonite mixtures showed that the liquefaction susceptibility of sandy soil significantly decreased when the sand–slag mixtures were mixed with 3% bentonite. However, the liquefaction susceptibility increased when the sand–slag mixtures were mixed with 5% bentonite. The undrained brittleness index and the pore water pressure ratio of sand–slag–bentonite reduced when the bentonite content was 3% and then increased when the bentonite content increased to 5%. The results of the sand–slag–bentonite mixtures also showed that the behaviour of these mixtures was inconsistent with increasing slag content. The brittleness index and the pore water pressure reduced with an increase in the slag content up to 4% and then increased with an increase in the slag content to 6%. The results of the sand–slag–kaolinite mixtures showed that the liquefaction susceptibility of sandy soil considerably reduced when the kaolinite content was 3% and then increased when the same sand–slag mixtures were mixed with 5% kaolinite. The undrained brittleness index and the pore water pressure ratio of sand–slag–kaolinite reduced when the bentonite content was 3% and then increased when the kaolinite content increased to 6%. The response of the sand–slag–kaolinite mixtures at the two kaolinite contents was consistent with the increasing slag content characterised by reducing the liquefaction susceptibility with an increase in the slag content to 6%. The mixtures of sand–6% slag–3% kaolinite and sand–6% slag–5% kaolinite exhibited the lowest undrained brittleness index and pore water pressure ratio. Furthermore, the results of the sand–slag–clay mixtures showed that the clay mineralogy might play a significant role in the behaviour of the sand–fines mixtures when the sand–slag–kaolinite mixtures at the two kaolinite contents (3% and 5%) exhibited less susceptibility to liquefy than the sand–slag–bentonite mixtures. This could be related to the effect of the clay type on the stability of the sand–fines mixtures. The mixture of sand–6% slag–3% kaolinite was the could be the best mixture for improving liquefaction resistance.

# Chapter 6: Modelling of Liquefaction Susceptibility Using Artificial Intelligence Approaches

## 6.1 Introduction

In the recent years, there has been an increasing amount of literature on the use of AI approaches such as ANN and GP for solving many of the geotechnical engineering problems. Most of the previous studies on AI approaches focused on developing models for the prediction of the seismic liquefaction potential relied on *in situ* tests and seismic records (Banimahd, Yasrobi, & Woodward, 2005; Das & Muduli, 2011; Goh, 1994; Muduli & Das, 2014a; Muduli & Das, 2014b; Young-Su & Byung-Tak, 2006). However, studies on the prediction of the static liquefaction susceptibility of clean sandy soil and sand–fines mixtures are rare. Moreover, the use of datasets including experimental parameters may provide another precise way to understand the static loading response of soils in an essential manner. Therefore, in this chapter, two different AI models are developed for predicting the static liquefaction susceptibility of clean sand and sand–fines mixtures on the basis of the experimental results. The first approach is ANN, which is used to predicate the stress ratio ( $q_{min}/q_{peak}$ ) (stress ratio is defined as the ratio of the minimum deviatoric stress to the peak deviatoric stress) on the basis of various combinations of input data. Complete static liquefaction (zero effective stress) is associated with a  $q_{min}/q_{peak}$  ratio of zero, and the non-flow behaviour with complete dilation is associated with a  $q_{min}/q_{peak}$  ratio of 1 (Yamamuro & Lade, 1997b). The  $q_{min}/q_{peak}$  ratio can be used to compute the liquefaction potential defined as  $(q_{peak} - q_{min})/q_{peak} = 1 - q_{min}/q_{peak}$ . The second method is symbolic regression via GP using the HeuristicLab software to correlate the stress ratio ( $q_{min}/q_{peak}$ ) to the initial soil parameters on the basis of one of the ANN models that led to the best estimation. For the clean sand models, the results of various undrained monotonic triaxial tests on the clean sand were collected carefully from the previously published work with different initial characteristics. However, the modelling of the sand–fines mixtures was based on the results of the undrained static triaxial tests discussed in

Chapters 4 and 5. Parametric methods used to evaluate the accuracy of the models are also included in this chapter. The results will also be used in the initial assessments of the liquefaction susceptibility of clean sandy soils and sand–fines mixtures under static loading before the final liquefaction evaluation.

## **6.2 Modelling of liquefaction susceptibility of clean sand soils**

### **6.2.1 Artificial neural network (ANN) models**

The input data of ANN models were collocated by investigating the published research that includes the results of both anisotropically and isotropically consolidated monotonic triaxial tests on clean sand soils. The results of the experimental studies conducted by Belhouari et al. (2015); Della et al. (2011); Della, Arab, Belkhatir, and Missoum (2009); Jafarian, Ghorbani, et al. (2013); Murthy et al. (2007); Rahman and Lo (2014); Verdugo and Ishihara (1996); Yamamuro and Lade (1997b); Yang and Wei (2012) have been used to create the database. Table 6.1 lists the key characteristics of these laboratory tests. According to Table 6.1, most of the samples were prepared using the moist tamping method, while the other samples were prepared using some other sample preparation method. Although the abovementioned tests were performed under different test conditions, two significant parameters, namely relative density and initial confining pressure, were broadly varied in these tests. The static liquefaction database included the results of 135 undrained static triaxial tests correlating the ratio of  $q_{min}/q_{peak}$  with different initial characteristics of clean sandy soils. The coefficient of uniformity ( $C_u$ ), mean diameter ( $D_{50}$ ), maximum void ratio ( $e_{max}$ ), minimum void ratio ( $e_{min}$ ), void ratio ( $e$ ), relative density ( $D_r$ ), initial confining pressure ( $p'_o$ ), ratio of the initial shear stress to the initial effective confining pressure ( $\alpha$ ), and Skempton's coefficient B were selected in this study as they have been considered to be the primary factors affecting the static behaviour of sandy soil in previous research. The criterion for complete static liquefaction in this database, and accordingly in this study, is the  $q_{min}/q_{peak}$  ratio of zero. Notwithstanding, the unity and the range of 0 to 1 of the ratio of  $q_{min}/q_{peak}$  are associated with the non-flow behaviour and limited liquefaction, respectively. Table 6.2 presents the statistical distribution of the input parameters. In the present work, nine parameters were used as the input data of the ANN models,

while one variable was used as the output data, as shown in Figure 6.1. The ANN models were generated using MATLAB's Neural Network Toolbox. The ANN models were based on the Levenberg–Marquardt back-propagation algorithm and had two layers of feed-forward back-propagation, and seven hidden neurons. The number of hidden neurons was set after many trials until the minimum root mean square error (RMSE) was reached. All of the datasets were normalised by using MATLAB's normalisation function, which is a requirement of ANN modelling. The dataset in this study was split into three groups, namely training, testing, and validation, and their data contents were 70%, 15%, and 15%, respectively. The best performance of the ANN models was obtained through trial and error until a coefficient of determination  $R^2$  value of around 90% was obtained. After completing the training and testing the model, a sample dataset was used to test the accuracy of the model. Nine parameters were used as the input dataset to run the ANN models. These included  $C_u$ ,  $D_{50}$ ,  $e_{max}$ ,  $e_{min}$ ,  $e$ ,  $D_{ri}$ ,  $\dot{p}_o$ ,  $\alpha$ , and  $B$ .

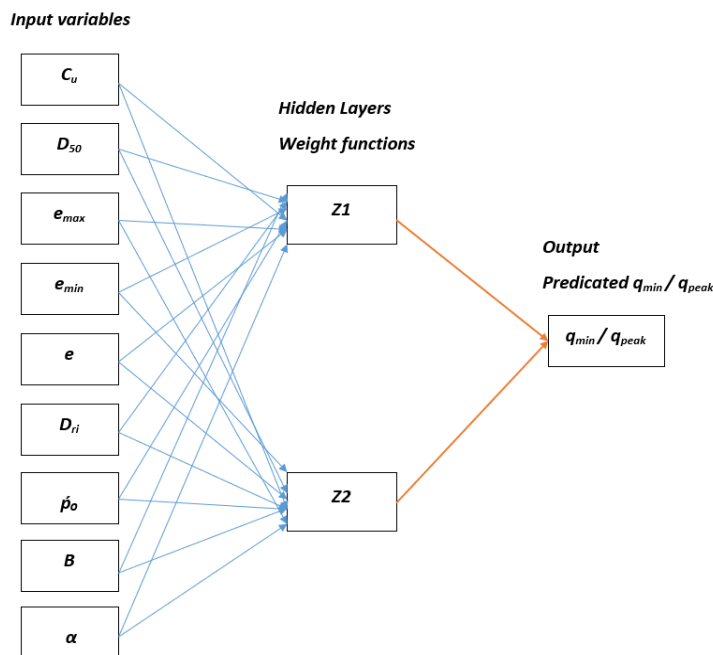


Figure 6.1 Schematic representation of an artificial neural network

Table 6.1 Properties of the sands used

<i>Sand type</i>	<i>Sample preparation method</i>	$C_u$	$D_{50}$	$Dr\%$	$p'_o$ (MPa)	<i>Reference</i>
Ottawa	Slurry deposition, moist tamping, and water pluviation	1.43	0.39	18–65	0.148–0.653	(Murthy et al., 2007)
Nevada and Ottawa	Funnel deposition and moist tamping	1.83 2.317	0.18 0.205	0–20	0.025–0.5	(Yamamuro & Lade, 1997b)
Babolsar	Moist tamping	1.8	0.24	8.5–68	0.04–0.41	(Jafarian, Ghorbani, et al., 2013)
Chlef	Wet deposition and funnel deposition	3.2	0.45	50	0.05–0.2	(Della et al., 2011)
Chlef	Wet deposition and funnel deposition	3.2	0.45	29, 80	0.05–0.2	(Della et al., 2009)
Sydney	Modified moist tamping	1.2	0.3	0–41	0.1–0.85	(Rahman & Lo, 2014)
Toyoura	Wet tamping	1.7	0.17	18.5, 37	0.1–3	(Verdugo & Ishihara, 1996)
Mostaganem	Dry funnel	1.704	0.32	15, 45	0.1–0.3	(Belhouari et al., 2015)
Toyoura and Fujian	Moist tamping	1.392 1.532	0.216 0.397	0–34	0.1–0.5	(Yang & Wei, 2012)

Table 6.2 Statistical distribution of each parameter in the database

<b>Parameters</b>	$C_u$	$D_{50}$	$e_{max}$	$e_{min}$	$e$	$Dr\%$	$p'_o$ (MPa)	$B$	$\alpha$
Mean	1.85	0.31	0.88	0.55	0.78	30.72	0.34	0.94	0.03
Standard error	0.05	0.01	0.01	0.00	0.01	1.75	0.03	0.01	0.01
Median	1.70	0.30	0.86	0.55	0.78	29.00	0.21	0.95	0.00
Mode	1.80	0.24	0.81	0.56	0.77	50.00	0.10	0.95	0.00
Standard deviation	0.63	0.10	0.09	0.05	0.10	20.32	0.38	0.07	0.09
Sample variance	0.40	0.01	0.01	0.00	0.01	412.91	0.15	0.00	0.01
Range	2.00	0.28	0.24	0.21	0.39	80.00	2.98	0.68	0.40
Minimum	1.20	0.17	0.78	0.48	0.58	0.00	0.03	0.32	0.00
Maximum	3.20	0.45	1.02	0.69	0.97	80.00	3.00	1.00	0.40

Input variables have been chosen according to the previous experimental studies that pointed out that the static behaviour of sandy soil depends considerably on many factors such as physical properties, relative density, initial effective confining pressure, degree of saturation, and consolidation type. Note that the effect of the sample preparation method was not considered in the input dataset because a majority of the samples used in the present work were deposited by using the moist tamping technique, as listed in Table 6.1. The stress ratio  $q_{min}/q_{peak}$  was used to identify which of the input data were superior in estimating the liquefaction susceptibility of sandy soil. The number of input variables was varied, and five ANN models were investigated. Figures 6.2–6.7 compare the measured stress ratio  $q_{min}/q_{peak}$  and the ANN predictions for the overall dataset, whereas Table 6.3 presents the  $R^2$  and RMSE values for the overall data, training, testing, and validation of each model. Further, it shows the identity in the statistical significance values for testing and validation in all the models. Figures 6.2–6.7 and Table 6.3 show that model 1 when all the input variables were used showed a good prediction with the highest  $R^2$  values of 0.865, 0.846, and 0.864 for the overall data, testing, and training, respectively. The lowest  $R^2$  values for the overall data (0.733) and the training set (0.722) were obtained in model 4 when the variables  $\alpha$  and  $B$  were eliminated, while the lowest  $R^2$  value for the testing set was obtained in model 5. In the present study, the efficiency of five models was evaluated with respect to the testing dataset as reported by (Das & Basudhar, 2008; Muduli & Das, 2014a). These researchers stated that the performance of the testing dataset should be used in the evaluation of the efficiency of the different developed ANN models. Thus, we found that the performance of model 1 with an  $R^2$  value of 0.864 for the testing set was the highest among the considered models, which indicated a good agreement between the measured and the predicted values of  $q_{min}/q_{peak}$ . However, model 5 showed the lowest  $R^2$  value of 0.707 for the testing set with some difficulty in predicting the ratio of  $q_{min}/q_{peak}$ . The results presented in Figure 6.7 and Table 6.3 also showed a slight reduction in the  $R^2$  values of the testing and the overall datasets for model 3 when Skempton's coefficient  $B$  was eliminated, as compared to model 1. This behaviour could be related to the fact that almost all of the test samples were thoroughly saturated and the  $B$  values were more than 0.95. The significant reduction in the  $R^2$  (0.707) value of the testing dataset for model 5 indicated the high influence of  $e_{max}$ ,  $e_{min}$ , and  $\alpha$  on the liquefaction susceptibility of sandy soils. The results of models 1–4 indicated that the significant effect of  $C_u$ ,  $D_{50}$ ,  $e_{max}$ ,  $e_{min}$ ,  $D_r$ , and  $\sigma'_{3c}$  on the

undrained static behaviour of sandy soils. A similar conclusion was observed and reported by Young-Su and Byung-Tak (2006); they reported that the use of data including  $C_u$ ,  $D_{50}$ ,  $e_{max}$ ,  $e_{min}$ ,  $D_r$ , and  $\sigma_{3c}$  increased the ability of an ANN model to capture the liquefaction resistance ratio of sandy soils. Banimahd et al. (2005) also reported that the relative density, effective confining pressure, fines content, and fines shape had a considerable effect on the ability of the ANN models to predict the undrained static stress–strain behaviour and the excess pore water pressure of sandy soils. Figure 6.7 shows a comparison of the five ANN models implemented in the present work; as can be seen, the results of the five models are quite close, which exhibited a relatively high prediction performance of the ANN models.

Table 6.3 Performance and details of the ANN models

Model no.	Input parameters	No. of hidden layers	Datasets	Performance	
				R <sup>2</sup>	RMSE
1	$(C_u), (D_{50}), (e_{max}), (e_{min}), (e), (D_r), (\sigma_{3c}), (\alpha), B$	2	Overall data	0.865	0.0993
			Training	0.846	0.1000
			Testing	0.864	0.0905
			Validation	0.883	0.0993
			Overall data	0.791	0.1247
2	$(C_u), (D_{50}), (e_{max}), (e_{min}), (e), (D_r), (\sigma_{3c}), B$	2	Training	0.789	0.1539
			Testing	0.828	0.1000
			Validation	0.828	0.1225
			Overall data	0.830	0.1062
3	$(C_u), (D_{50}), (e_{max}), (e_{min}), (e), (D_r), (\sigma_{3c}), (\alpha)$	2	Training	0.809	0.1283
			Testing	0.860	0.1534
			Validation	0.931	0.1062
			Overall data	0.733	0.1430
4	$(C_u), (D_{50}), (e_{max}), (e_{min}), (e), (D_r), (\sigma_{3c})$	2	Training	0.722	0.1524
			Testing	0.748	0.2097
			Validation	0.783	0.1414
			Overall data	0.762	0.1612
5	$(C_u), (D_{50}), (e), (D_r), (\sigma_{3c})$	2	Training	0.779	0.1414
			Testing	0.707	0.2302
			Validation	0.756	0.1612
			Overall data	0.762	0.1612

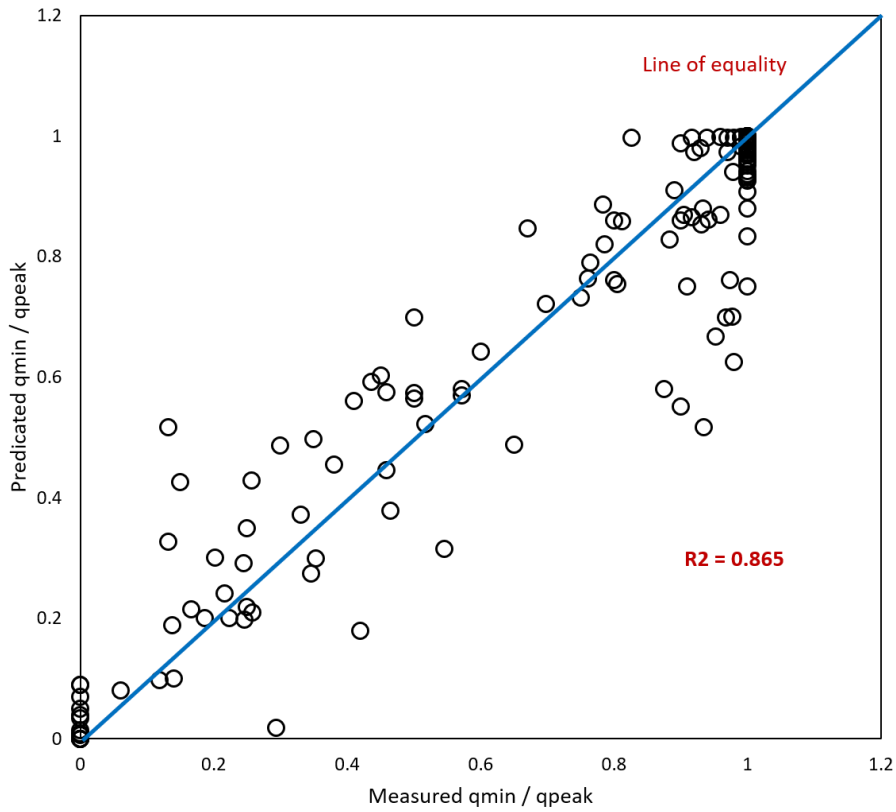


Figure 6.2 Measured vs. predicted stress ratio for ANN model 1

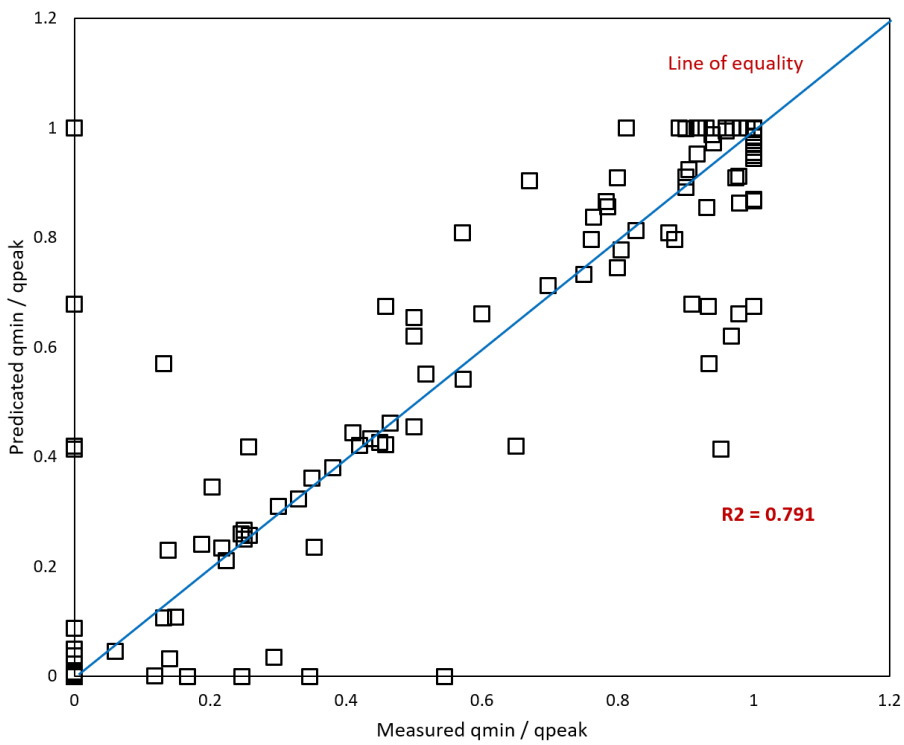


Figure 6.3 Measured vs. predicted stress ratio for ANN model 2



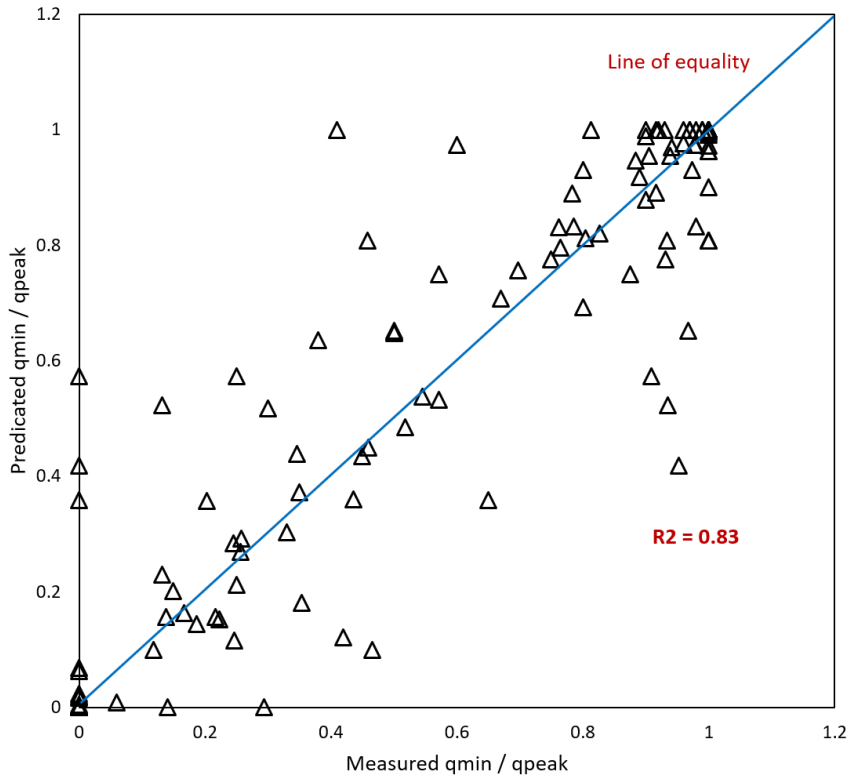


Figure 6.4 Measured vs. predicted stress ratio for ANN model 3

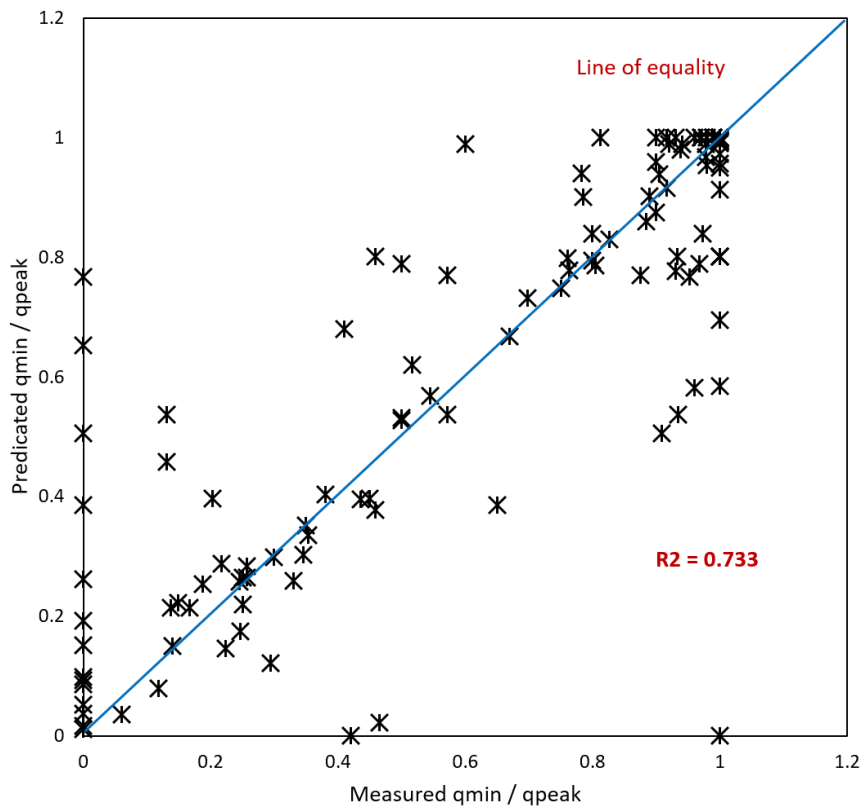


Figure 6.5 Measured vs. predicted stress ratio for ANN model 4

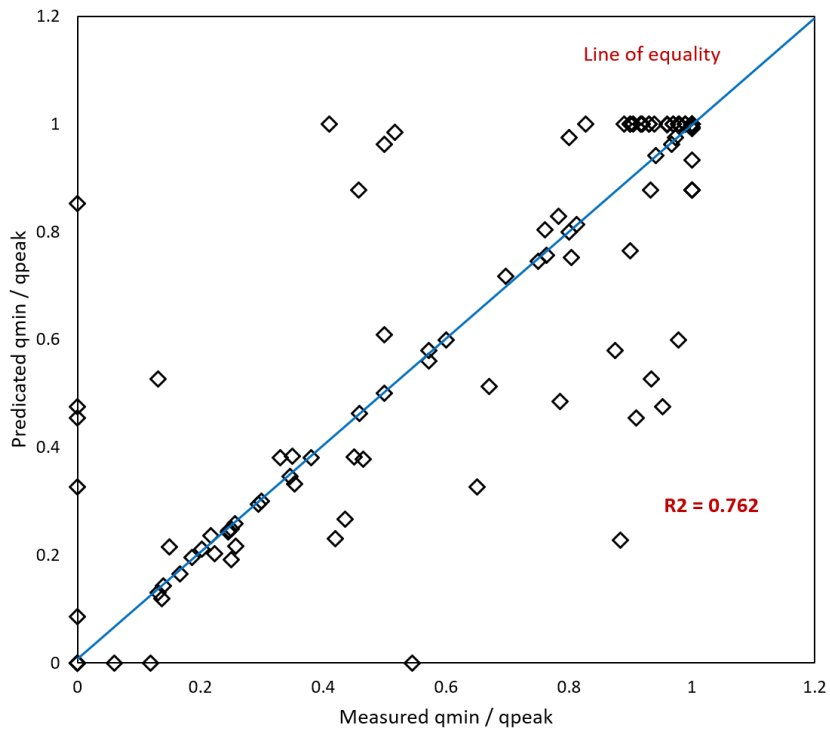


Figure 6.6 Measured vs. predicted stress ratio for ANN model 5

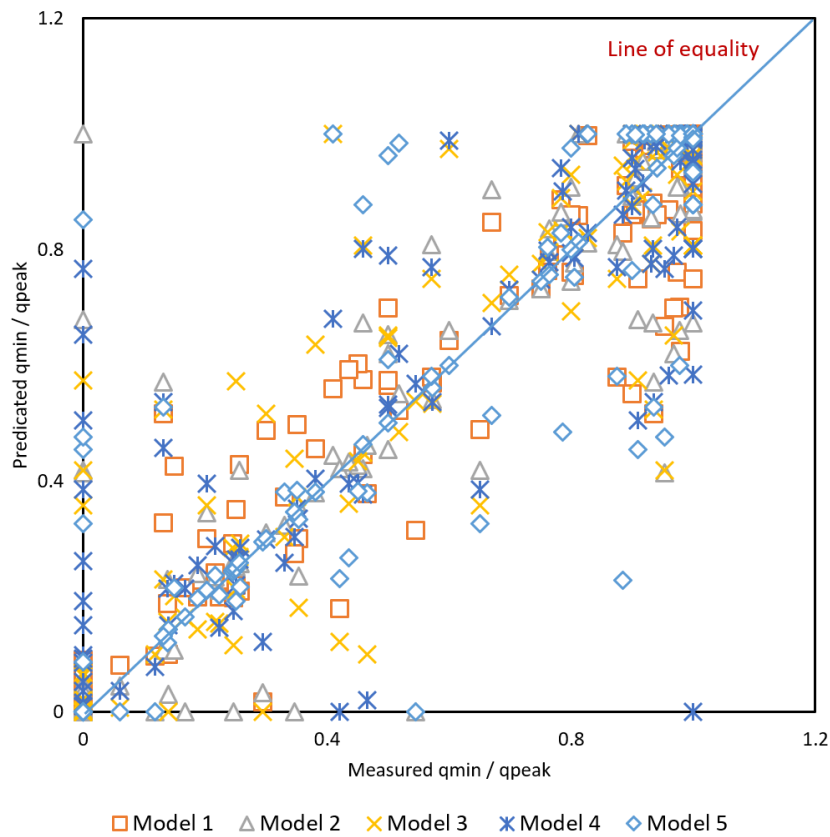


Figure 6.7 Measured vs. predicted stress ratio for all the ANN models

## 6.2.2 Genetic programming model

In the present work, the HeuristicLab software was used to develop a functional relationship for the stress ratio  $q_{min}/q_{peak}$  of clean sandy soils on the basis of symbolic regression via genetic programming (GP). The input data were chosen on the basis of the best results in ANN modelling as described in Part 3, which showed that model 1 with nine input variables exhibited the best prediction with the highest value of  $R^2$ . Nine parameters were used as the inputs to the GP model. These included  $C_u$ ,  $D_{50}$ ,  $e_{max}$ ,  $e_{min}$ ,  $e$ ,  $D_r$ ,  $\sigma'_{3c}$ ,  $\alpha$ , and B, while one parameter, the stress ratio  $q_{min}/q_{peak}$ , is used as the output. The input data were loaded into the software; thereafter, a symbolic regression by GP was performed with the variable set listed in Table 6.4.

Table 6.4 Symbolic regression parameters

Parameters	Value
Population size	1000
Maximum number of generations	75
Parent selection	Tournament (group size 7)
Replacement	1-Elitism
Crossover	Sub-tree-swapping
Mutation rate	15%
Fitness function	$R^2$ and RMSE
Function set	+, -, *, /, exp, ln
Terminal set	Constant, variable

The input data were divided as 67% for training and 33% for testing. The software approached the better model of the stress ratio  $q_{min}/q_{peak}$  with the highest values of  $R^2$  for training and testing, after a cycle of 75 generations. Therefore, the following equation was formulated to connect the stress ratio  $q_{min}/q_{peak}$  of clean sandy soils to nine input parameters:

$$q_{min}/q_{peak} = (7.314 * \text{EXP}(19.980 / ((0.027 * -13.896 - (c_1 * e_{min} + c_2 * D_{50}))) / ((6.146 * -0.83 / (1.100) - c_3 * C_u / (1.670)))) / ((6.146 * (13.875 * -13.283 / (c_4 * e) + (\text{EXP}(((c_5 * D_r + c_6 * e_{max}) + 5.780)) - (c_5 * D_r + c_6 * e_{max}))) - \text{LN}(\text{LN}(\text{EXP}((c_5 * D_r + c_6 * e_{max}))) * (c_7 * D_r + c_8 * \sigma'_{3c}) / ((c_9 * D_{50} - 6.544)) * 18.994 * (c_{10} * D_r + -0.187)))))) * -1.864 + 14.832$$

(6-1)

The values of coefficients  $c_1$  to  $c_{10}$  are listed in Table 6.5.

Table 6.5 Coefficients of Equation (6-1).

$c_1$	$c_2$	$c_3$	$c_4$	$c_5$	$c_6$	$c_7$	$c_8$	$c_9$	$c_{10}$
1.9215	0.7856	2.4800	1.0416	1.5366	0.2935	3.0886	1.7902	1.1763	0.2620

The developed model (Equation (6-1)) was more sensitive to changes in the physical properties and the initial state than the other parameters. The same results were reported in ANN modelling where the performance of the ANN model was affected by the change in  $C_u$ ,  $D_{50}$ ,  $e_{max}$ ,  $e_{min}$ ,  $D_r$ , and  $\sigma_{3c}$ . This finding was consistent with the findings of (Banimahd et al., 2005; Young-Su & Byung-Tak, 2006). Note that the effect of  $C_u$ ,  $D_{50}$ ,  $e_{max}$ ,  $e_{min}$ ,  $D_r$ , and  $\dot{p}_o$  on the liquefaction susceptibility of sandy soil has been reported in many previous experimental studies (Jafarian, Ghorbani, et al., 2013; Salamatpoor & Salamatpoor, 2014; Yamamuro & Lade, 1997b). The developed  $q_{min}/q_{peak}$  equation ignored certain parameters such as the ratio of the initial shear stress to the initial effective confining pressure ( $\alpha$ ), and Skempton's coefficient B. This was attributed to the fact that these values are considered barely useful because the experimental tests were almost fully saturated and isotropically consolidated with values of around 1 and 0 for B and  $\alpha$ , respectively. Moreover, Equation (4) does not take into account the effect of certain field factors such as ageing, strain history, cementation, and stratification due to the difficulties in mimicking these conditions in the experimental work. Figure 6.7 shows the measured values of the stress ratio  $q_{min}/q_{peak}$  versus the equivalent values as predicted by Equation (6.1). This figure shows that the data of the training and the testing sets were closely distributed around the bisector line, which indicated the good prediction ability of the developed model. The performance of the HeuristicLab model was examined using statistical precision parameters such as RMSE and  $R^2$ . Table 6.6 presents the  $R^2$  and RMSE values of the proposed model for the training and testing sets. Figure 6.8 illustrates the plot of the normalised  $q_{min}/q_{peak}$  (i.e. the ratio of the measured to the estimated  $q_{min}/q_{peak}$  values) versus the estimated  $q_{min}/q_{peak}$  values for all the datasets. The figure shows that the almost normalised  $q_{min}/q_{peak}$  values were distributed around 1, which indicated a good agreement between the measured and the predicted values. Figure 6.9 shows the tree of the developed model. In comparison, the classification accuracy of the ANN model

1 was 0.846 and 0.864 for the training and the testing sets, respectively. Similarly, the classification accuracy for the GP model was 0.868 and 0.842 for the training and the testing sets, respectively. Thus, we found a good agreement between the two models in predicting the  $q_{min}/q_{peak}$  ratio.

Table 6.6 Performance of the  $q_{min}/q_{peak}$  model for the training and testing datasets.

Dataset	Performance	
	R <sup>2</sup>	RMSE
Training	0.868	0.12
Testing	0.842	0.17

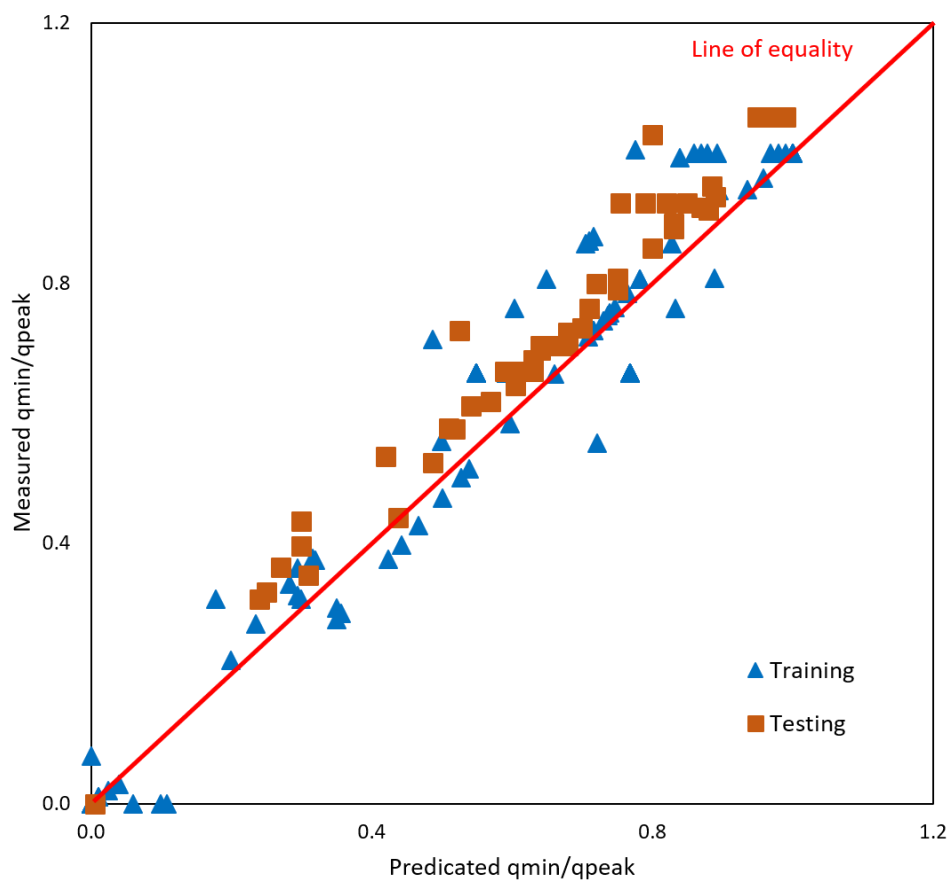


Figure 6.8 Measured values of the stress ratio vs. those predicted by the developed GP model

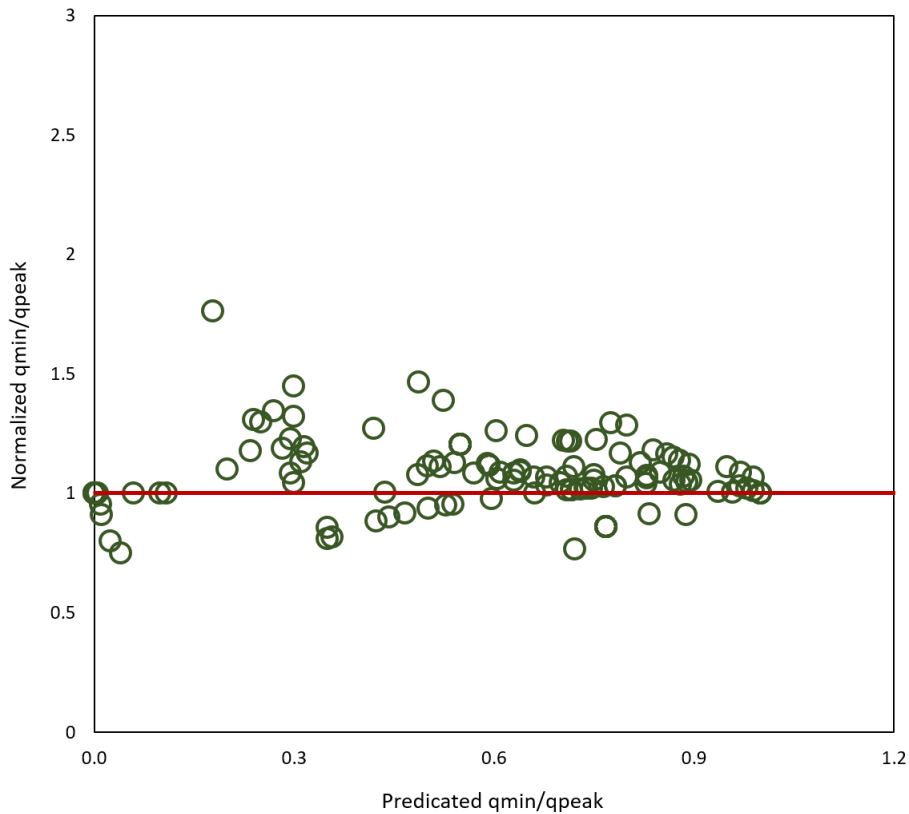


Figure 6.9 Normalised stress ratio vs. that predicted by the developed GP model for all the datasets

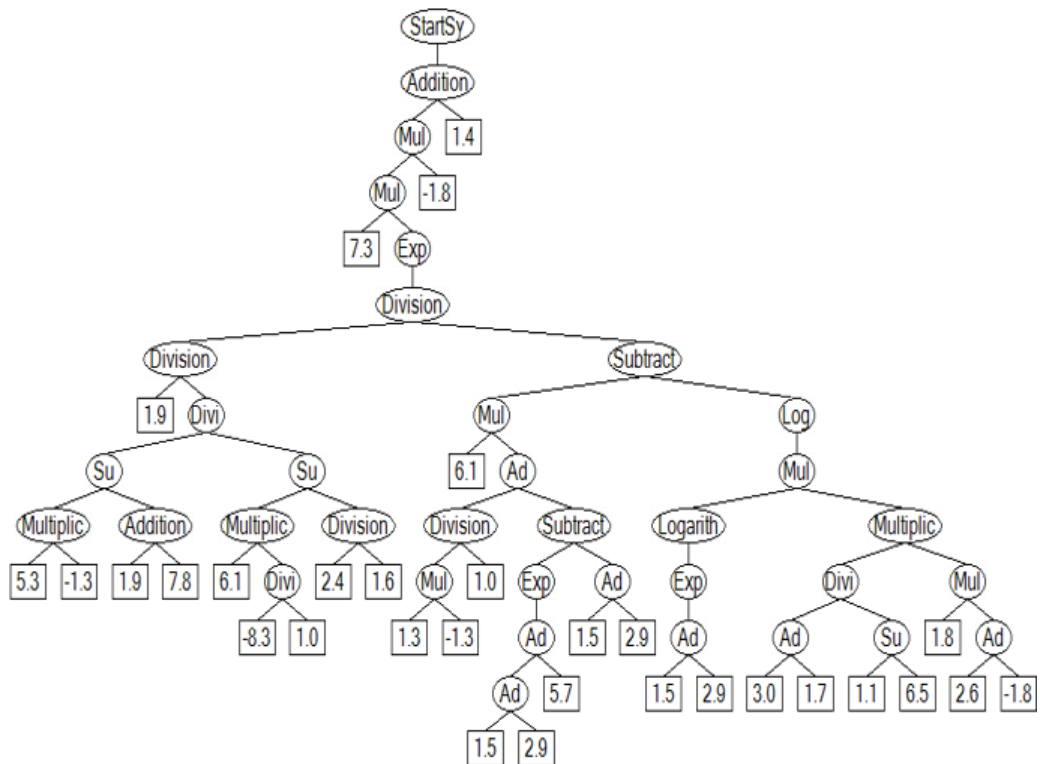


Figure 6.10 Tree of the developed GP model

### 6.2.3 Parametric study

The efficiency of the newly proposed models with respect to the prediction of the static liquefaction susceptibility of sandy soils requires one to compare it with that of other modelling methods or experimental results. Thus, in the present work, a systematic parametric study was implemented for the verification of the success rate for Equation (6.1) in the estimation of the stress ratio  $q_{min}/q_{peak}$ , taking into consideration its physical meaning. In this parametric study, the findings of three undrained static triaxial tests were compared with the results of Equation (6.1). Static undrained compression triaxial tests were performed on the soil samples deposited by the moist tamping technique and isotropically consolidated under three different confining pressures, namely 100, 150, and 200 kPa. The sand used for the experiments was clean sand, and  $C_u$ ,  $D_{50}$ ,  $e_{max}$ ,  $e_{min}$ ,  $e$ ,  $D_r$ ,  $B$ , and  $\alpha$  were equal to 2.235, 0.35, 0.675, 0.544, 0.6615, 10%, 0.95, and zero, respectively. The stress ratio of  $q_{min}/q_{peak}$  was calculated by the GP model using Equation (6.1) and experimental tests. According to the comparison presented in Figure 6.11, a good agreement between the experimental results and the modelling results at a confining pressure of 100 and 150 kPa. However, a slight difference was observed at a confining pressure of 200 kPa. This was related to the developed equation which was more suitable for low confining pressures than high confining pressures. Moreover, the applicability and validity of the developed equation were dependent on the range of variables in the input data, which were collected from previous studies. Furthermore, the parametric study demonstrated that the stress ratio  $q_{min}/q_{peak}$  increased with increasing confining pressure. This has been reported in many experimental studies which showed that the liquefaction susceptibility of very loose samples decreased with increasing relative density and confining pressure. Thus, the current GP model was observed to be equally efficient in predicting the stress ratio  $q_{min}/q_{peak}$  when compared to the experimental methods.

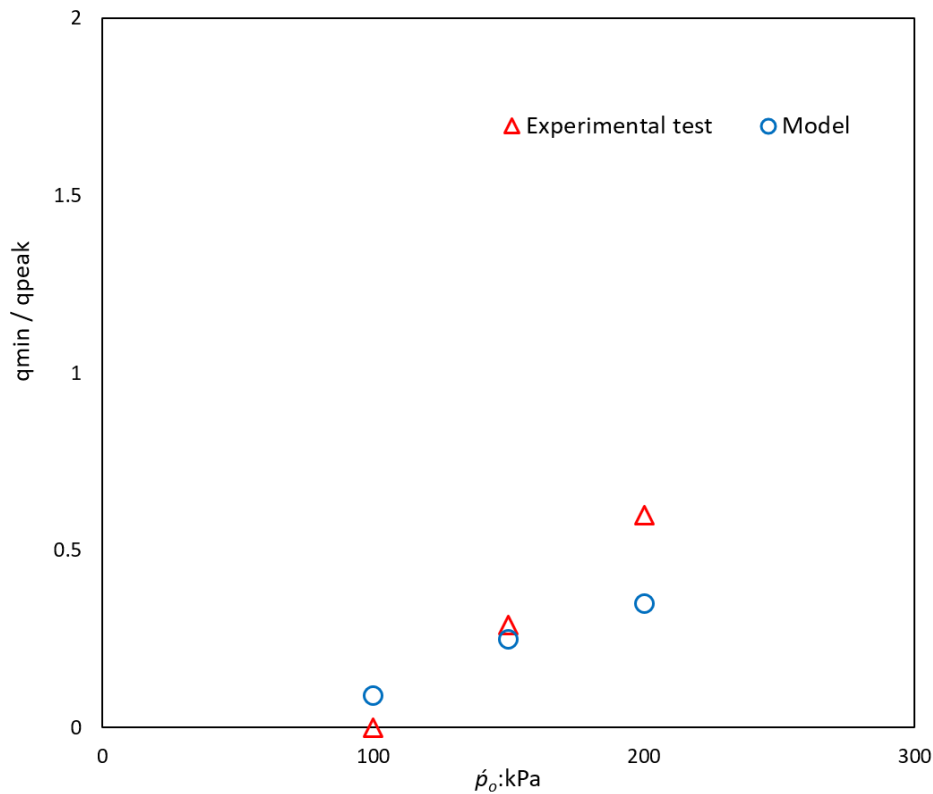


Figure 6.11 Stress ratio measured by experimental tests vs. that predicted by the developed GP model

## 6.3 Modelling of liquefaction susceptibility of sand–fines mixtures

### 6.3.1 Artificial neural network (ANN) models

The input data of the ANN models were collocated from the experimental tests conducted in the present work that included the results of isotropically consolidated monotonic triaxial tests on the clean sand and sand–fines mixtures. Table 6.7 lists the key characteristics of these laboratory tests. All the samples were prepared by using the moist tamping method performed under different test conditions; almost all the parameters were broadly varied in these tests. The static liquefaction of the sand–fines database involved the results of 67 undrained static triaxial tests correlating the stress ratio ( $q_{min}/q_{peak}$ ) with the different initial characteristics of the sand–fines soils. Table 6.8 presents the statistical distribution of the input parameters.



Table 6.7 Details of tests included in the database for modelling the liquefaction susceptibility of sand–fines mixtures

<i>No.</i>	<i>Test name</i>	$P_o'$	$B$	$C_u$	$D_{50}$	$G_s$	$e_{max}/e_{min}$	$e_o$	$q_{peak}$	$S_c$	$B_c$	$K_c$	$q_{min}/q_{peak}$
1	CS1	100	0.9500	2.2350	0.3500	2.5800	1.2408	0.6615	6.9900	0.0000	0.0000	0.0000	0.0000
2	CS2	150	0.9500	2.2350	0.3500	2.5800	1.2408	0.6615	9.0900	0.0000	0.0000	0.0000	0.3460
3	CS3	200	0.9500	2.2350	0.3500	2.5800	1.2408	0.6615	19.0000	0.0000	0.0000	0.0000	0.6421
4	CS4	100	0.9500	2.2350	0.3500	2.5800	1.2408	0.6095	40.6500	0.0000	0.0000	0.0000	0.8800
5	CS5	150	0.9500	2.2350	0.3500	2.5800	1.2408	0.6095	63.9400	0.0000	0.0000	0.0000	0.8524
6	CS6	200	0.9500	2.2350	0.3500	2.5800	1.2408	0.6095	84.5900	0.0000	0.0000	0.0000	0.8275
7	CS7	100	0.9500	2.2350	0.3500	2.5800	1.2408	0.5572	170.0000	0.0000	0.0000	0.0000	0.9941
8	CS8	150	0.9500	2.2350	0.3500	2.5800	1.2408	0.5572	266.0000	0.0000	0.0000	0.0000	0.9925
9	CS9	200	0.9500	2.2350	0.3500	2.5800	1.2408	0.5572	358.0000	0.0000	0.0000	0.0000	0.9888
10	CS10	100	0.5000	2.2350	0.3500	2.5800	1.2408	0.6615	21.2000	0.0000	0.0000	0.0000	0.5646
11	CS11	100	0.2500	2.2350	0.3500	2.5800	1.2408	0.6615	30.0000	0.0000	0.0000	0.0000	0.7967
12	CS12	100	0.9500	2.2350	0.3500	2.5800	1.2408	0.6487	15.6000	0.0000	0.0000	0.0000	0.8200
13	2%S1	100	0.9500	2.2090	0.3900	2.6130	1.1843	0.6389	12.5900	2.0000	0.0000	0.0000	0.8697
14	2%S2	150	0.9500	2.2090	0.3900	2.6130	1.1843	0.6389	13.3200	2.0000	0.0000	0.0000	0.9535
15	2%S3	200	0.9500	2.2090	0.3900	2.6130	1.1843	0.6389	21.9600	2.0000	0.0000	0.0000	0.9517
16	2%S4	100	0.9500	2.2090	0.3900	2.6130	1.1843	0.5988	58.1500	2.0000	0.0000	0.0000	0.9871
17	2%S5	100	0.9500	2.2090	0.3900	2.6130	1.1843	0.5581	177.6200	2.0000	0.0000	0.0000	0.9988
18	4%S1	100	0.9500	1.9020	0.4220	2.6300	1.1832	0.6360	16.5900	4.0000	0.0000	0.0000	0.9343
19	4%S2	150	0.9500	1.9020	0.4220	2.6300	1.1832	0.6360	16.6500	4.0000	0.0000	0.0000	0.9970
20	4%S3	200	0.9500	1.9020	0.4220	2.6300	1.1832	0.6360	26.9100	4.0000	0.0000	0.0000	0.9922
21	4%S4	100	0.9500	1.9020	0.4220	2.6300	1.1832	0.5959	99.5000	4.0000	0.0000	0.0000	0.9990
22	4%S5	100	0.9500	1.9020	0.4220	2.6300	1.1832	0.5560	204.0000	4.0000	0.0000	0.0000	0.9985
23	6%S1	100	0.9500	1.9300	0.4220	2.6400	1.1838	0.6340	11.3200	6.0000	0.0000	0.0000	0.8004

<b>No.</b>	<b>Test name</b>	<b><math>p_o'</math></b>	<b><math>B</math></b>	<b><math>C_u</math></b>	<b><math>D_{50}</math></b>	<b><math>G_s</math></b>	<b><math>e_{max}/e_{min}</math></b>	<b><math>e_o</math></b>	<b><math>q_{peak}</math></b>	<b><math>S_c</math></b>	<b><math>B_c</math></b>	<b><math>K_c</math></b>	<b><math>q_{min}/q_{peak}</math></b>
24	6%S2	150	0.9500	1.9300	0.4220	2.6400	1.1838	0.6340	14.7000	6.0000	0.0000	0.0000	0.9796
25	6%S3	200	0.9500	1.9300	0.4220	2.6400	1.1838	0.6340	17.5600	6.0000	0.0000	0.0000	0.9681
26	6%S4	100	0.9500	1.9300	0.4220	2.6400	1.1838	0.5940	88.0000	6.0000	0.0000	0.0000	0.9886
27	6%S5	100	0.9500	1.9300	0.4220	2.6400	1.1838	0.5540	189.0000	6.0000	0.0000	0.0000	0.9947
28	3%B1	100	0.9500	2.2500	0.4000	2.6140	1.3354	0.6404	5.6100	0.0000	3.0000	0.0000	0.3351
29	3%B2	150	0.9500	2.2500	0.4000	2.6140	1.3354	0.6404	7.1200	0.0000	3.0000	0.0000	0.4635
30	3%B3	200	0.9500	2.2500	0.4000	2.6140	1.3354	0.6404	9.7700	0.0000	3.0000	0.0000	0.6039
31	3%B4	100	0.9500	2.2500	0.4000	2.6140	1.3354	0.5738	35.9100	0.0000	3.0000	0.0000	0.7797
32	3%B5	100	0.9500	2.2500	0.4000	2.6140	1.3354	0.5085	70.0000	0.0000	3.0000	0.0000	0.9829
33	5%B1	100	0.9500	2.3000	0.4100	2.6700	1.3446	0.6574	3.7800	0.0000	5.0000	0.0000	0.1323
34	5%B2	150	0.9500	2.3000	0.4100	2.6700	1.3446	0.6574	5.4000	0.0000	5.0000	0.0000	0.3500
35	5%B3	200	0.9500	2.3000	0.4100	2.6700	1.3446	0.6574	6.4000	0.0000	5.0000	0.0000	0.5938
36	5%B4	100	0.9500	2.3000	0.4100	2.6700	1.3446	0.5883	27.6000	0.0000	5.0000	0.0000	0.6971
37	5%B5	100	0.9500	2.3000	0.4100	2.6700	1.3446	0.5196	73.0000	0.0000	5.0000	0.0000	0.9041
38	3%K1	100	0.9500	1.8820	0.4400	2.6440	1.4899	0.7147	6.8400	0.0000	0.0000	3.0000	0.7032
39	3%K2	150	0.9500	1.8820	0.4400	2.6440	1.4899	0.7147	11.7800	0.0000	0.0000	3.0000	0.7674
40	3%K3	200	0.9500	1.8820	0.4400	2.6440	1.4899	0.7147	20.9000	0.0000	0.0000	3.0000	0.8364
41	3%K4	100	0.9500	1.8820	0.4400	2.6440	1.4899	0.6181	56.0000	0.0000	0.0000	3.0000	0.9821
42	3%K5	100	0.9500	1.8820	0.4400	2.6440	1.4899	0.5204	185.4300	0.0000	0.0000	3.0000	0.9977
43	5%K1	100	0.9500	1.6330	0.4600	2.6770	1.5279	0.7406	5.8000	0.0000	0.0000	5.0000	0.4741
44	5%K2	150	0.9500	1.6330	0.4600	2.6770	1.5279	0.7406	8.7000	0.0000	0.0000	5.0000	0.5747
45	5%K3	200	0.9500	1.6330	0.4600	2.6770	1.5279	0.7406	17.9000	0.0000	0.0000	5.0000	0.6257
46	5%K4	100	0.9500	1.6330	0.4600	2.6770	1.5279	0.6343	53.0000	0.0000	0.0000	5.0000	0.9623
47	5%K5	100	0.9500	1.6330	0.4600	2.6770	1.5279	0.5297	174.9000	0.0000	0.0000	5.0000	0.9960
48	3BS2	100	0.9500	2.5630	0.3900	2.6500	1.1167	0.5680	20.4300	2.0000	3.0000	0.0000	0.9790

<i>No.</i>	<i>Test name</i>	$p_o'$	<i>B</i>	$C_u$	$D_{50}$	$G_s$	$e_{max}/e_{min}$	$e_o$	$q_{peak}$	$S_c$	$B_c$	$K_c$	$q_{min}/q_{peak}$
49	3BS2	150	0.9500	2.5630	0.3900	2.6500	1.1167	0.5680	22.9900	2.0000	3.0000	0.0000	0.9810
50	3BS2	200	0.9500	2.5630	0.3900	2.6500	1.1167	0.5680	25.5400	2.0000	3.0000	0.0000	0.9870
51	3BS2	100	0.9500	2.5630	0.3900	2.6500	1.1167	0.5680	45.0000	2.0000	3.0000	0.0000	0.9990
52	3BS4	100	0.9500	2.3330	0.3800	2.6800	1.1368	0.5582	39.7200	4.0000	3.0000	0.0000	0.9894
53	3BS4	150	0.9500	2.3330	0.3800	2.6800	1.1368	0.5582	31.0000	4.0000	3.0000	0.0000	0.9910
54	3BS4	200	0.9500	2.3330	0.3800	2.6800	1.1368	0.5582	38.0000	4.0000	3.0000	0.0000	0.9930
55	3BS4	100	0.9500	2.3330	0.3800	2.6800	1.1368	0.5582	58.0000	4.0000	3.0000	0.0000	0.9990
56	3BS6	100	0.9500	2.5620	0.3900	2.6950	1.1757	0.5536	32.1500	6.0000	3.0000	0.0000	0.9580
57	3BS6	150	0.9500	2.5620	0.3900	2.6950	1.1757	0.5536	24.0000	6.0000	3.0000	0.0000	0.9600
58	3BS6	200	0.9500	2.5620	0.3900	2.6950	1.1757	0.5536	13.1800	6.0000	3.0000	0.0000	0.9700
59	5BS2	100	0.9500	2.4440	0.3900	2.6730	1.4520	0.6442	15.2000	2.0000	5.0000	0.0000	0.5513
60	5BS4	100	0.9500	2.4700	0.3700	2.6880	1.4571	0.6420	24.8200	4.0000	5.0000	0.0000	0.6930
61	5BS6	100	0.9500	2.5600	0.3600	2.7100	1.5023	0.6445	19.1600	6.0000	5.0000	0.0000	0.5699
62	3KS2	100	0.9500	1.9200	0.4300	2.6710	1.4568	0.6857	68.6900	2.0000	0.0000	3.0000	0.9972
63	3KS4	100	0.9500	2.0400	0.4200	2.6880	1.5085	0.6821	74.8500	4.0000	0.0000	3.0000	0.9989
64	3KS6	100	0.9500	2.2500	0.4100	2.6920	1.5600	0.6767	93.6000	6.0000	0.0000	3.0000	0.9995
65	5KS2	100	0.9500	1.6200	0.4300	2.6800	1.5593	0.7096	26.8600	2.0000	0.0000	5.0000	0.7885
66	5KS4	100	0.9500	1.9200	0.4100	2.6860	1.6813	0.6984	31.5900	4.0000	0.0000	5.0000	0.8015
67	5KS6	100	0.9500	2.0000	0.4050	2.6900	1.8325	0.6890	39.7500	6.0000	0.0000	5.0000	0.9419

Table 6.8 Statistical analysis of input dataset

<i>Parameters</i>	<i>P<sub>o</sub>'</i> (MPa)	<i>B</i>	<i>C<sub>u</sub></i>	<i>D<sub>50</sub></i> (mm)	<i>G<sub>s</sub></i>	<i>e<sub>max</sub>/e<sub>min</sub></i>	<i>e<sub>o</sub></i>	<i>q<sub>peak</sub></i> (MPa)	<i>Slag content</i> (%)	<i>Bentonite content</i> (%)	<i>Kaolinite content</i> (%)
<i>Mean</i>	0.129	0.933	2.147	0.400	2.642	1.309	0.621	0.053	2.060	1.313	0.955
<i>Standard error</i>	0.005	0.012	0.032	0.004	0.005	0.020	0.007	0.008	0.282	0.227	0.218
<i>Median</i>	0.100	0.950	2.235	0.400	2.644	1.241	0.634	0.026	2.000	0.000	0.000
<i>Mode</i>	0.100	0.950	2.235	0.390	2.580	1.241	0.662	0.007	0.000	0.000	0.000
<i>Standard deviation</i>	0.040	0.101	0.265	0.032	0.039	0.161	0.059	0.068	2.309	1.860	1.787
<i>Sample variance</i>	0.002	0.010	0.070	0.001	0.001	0.026	0.003	0.005	5.330	3.461	3.195
<i>Range</i>	0.100	0.700	0.943	0.110	0.130	0.716	0.232	0.354	6.000	5.000	5.000
<i>Minimum</i>	0.100	0.250	1.620	0.350	2.580	1.117	0.509	0.004	0.000	0.000	0.000
<i>Maximum</i>	0.200	0.950	2.563	0.460	2.710	1.832	0.741	0.358	6.000	5.000	5.000
<i>Sum</i>	8.650	62.500	143.844	26.795	176.983	87.686	41.629	3.590	138.000	88.000	64.000
<i>Count</i>	67.000	67.000	67.000	67.000	67.000	67.000	67.000	67.000	67.000	67.000	67.000

The initial confining pressure ( $p_o'$ ), Skempton's coefficient ( $B$ ), coefficient of uniformity ( $C_u$ ), mean diameter ( $D_{50}$ ), ratio of the maximum void ratio to the minimum void ratio ( $e_{max}/e_{min}$ ), initial void ratio ( $e_o$ ), peak deviatoric stress ( $q_{peak}$ ), slag content ( $S_c$ ), bentonite content ( $B_c$ ), and kaolinite content ( $K_c$ ) were selected in this section as they were considered to be the primary factors affecting the static behaviour of sand–fines mixtures in the previous studies. Table 6.8 presents the statistical distribution of the input parameters. In the present work, 11 parameters were used as the input data of the ANN models, while 1 variable was used as the output data, as shown in Figure 6.12.

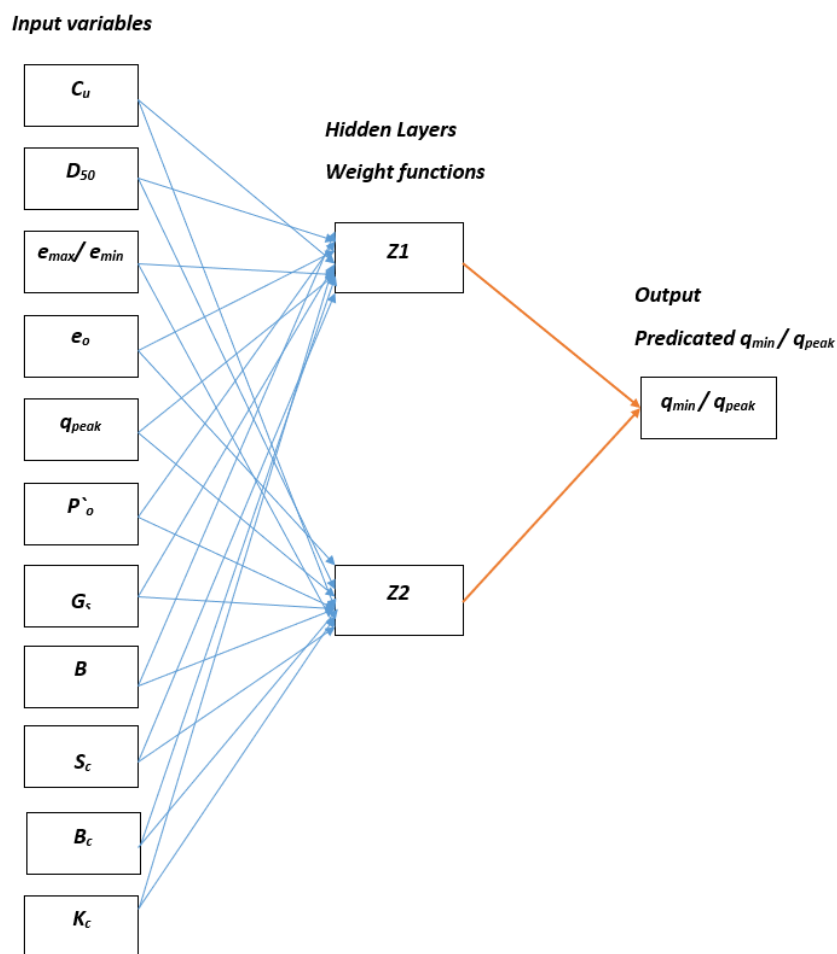


Figure 6.12 Schematic representation of the structure of ANN

The ANN models were generated using MATLAB's Neural Network Toolbox. The models were based on the Levenberg–Marquardt back-propagation algorithm and had two layers of feed-forward back-propagation and seven hidden neurons. The number

of hidden neurons was set after many trials conducted until the minimum RMSE was obtained. All the datasets were normalised by using MATLAB's normalisation function, which is a requirement of ANN modelling. The dataset in this study was split into three groups, namely training, testing, and validation, and their data percentage was 70%, 15%, and 15%, respectively. The best performance of the ANN models was obtained through trial and error until an  $R^2$  value of around 90% was obtained. After completing the training and testing of the models, a sample dataset was used to test the accuracy of the models. Eleven parameters were used as the input dataset to the ANN models. These included  $p_o'$ ,  $B$ ,  $C_u$ ,  $D_{50}$ ,  $e_{max}/e_{min}$ ,  $e_o$ ,  $q_{peak}$ ,  $S_c$ ,  $B_c$ , and  $K_c$ . Five ANN models were investigated in this section to identify which of the variables were superior in predicting the liquefaction susceptibility of sand–fines mixtures on the basis of the stress ratio  $q_{min}/q_{peak}$ . The number of input variables in each model was varied. Figures 6.13–6.18 show a comparison of the measured stress ratio  $q_{min}/q_{peak}$  and the predicated stress ratio for the overall datasets, whereas Table 6.9 presents the  $R^2$  and RMSE values for the overall, training, testing, and validation data of each model. Figures 6.13–6.18 and Table 6.8 show that model 1 when all the input variables were used showed a good prediction with the highest  $R^2$  value of 0.98 for the overall, testing, and training data. The lowest  $R^2$  value for the overall data (0.876) was obtained in model 2 when the variable  $e_o$  was eliminated. However, the lowest  $R^2$  value for the training set (0.880) was obtained in model 5 when the variable  $q_{peak}$  was eliminated. The lowest  $R^2$  value for the testing set was obtained in model 3 when the variable  $C_u$  was eliminated. The efficiency of the five models was examined using the testing datasets. Therefore, the performance of model 1 with the  $R^2$  value for the testing set of 0.98 was found to be the highest among the considered models, which indicated a good agreement between the measured and predicted stress ratio  $q_{min}/q_{peak}$ . However, model 2 showed the lowest  $R^2$  value of 0.865 for the testing set with some difficulty in predicting the liquefaction susceptibility of the sand–fines mixtures. Table 6.9 also shows a significant reduction in the  $R^2$  values of the testing and the overall datasets for model 2 when the initial void ratio was eliminated as compared to model 1. The significant reduction in the  $R^2$  value (0.865) of the testing dataset for model 2 indicated the considerable effect of the initial void ratio  $e_o$  on the liquefaction susceptibility of the sand–fines mixtures. The results of models 1–5 indicated the significant effect of the initial state and the physical properties of the mixtures on the liquefaction susceptibility of the sand–fines mixtures. Furthermore, Banimahd et al. (2005);

Young-Su and Byung-Tak (2006) concluded that the initial state (i.e. initial void ratio) and the physical properties (mean diameter and coefficient of uniformity) of the soil increased the ability of the ANN model to capture the liquefaction resistance ratio of sandy soils. From the data shown in Figure 6.18, it was apparent that the results of the five models were quite close, which indicated a higher prediction performance of the ANN models.

Table 6.9 Performance of ANN models of sand–fines mixtures

Model no.	Input parameters	No. of hidden layers	Datasets	Performance	
				R <sup>2</sup>	RMSE
1	$(p_o'), (B), (C_u), (D_{50}), (e_{max}/e_{min}), (G_s), (e_o), (q_{peak}), (S_c), (B_c), (K_c)$	2	Overall data	0.980	0.0137
			Training	0.980	0.0186
			Testing	0.980	0.0280
			Validation	0.980	0.0186
2	$(p_o'), (B), (C_u), (D_{50}), (e_{max}/e_{min}), (G_s), (q_{peak}), (S_c), (B_c), (K_c)$	2	Overall data	0.876	0.091
			Training	0.921	1.64*10 <sup>-8</sup>
			Testing	0.865	0.208
3	$(p_o'), (B), (D_{50}), (e_{max}/e_{min}), (G_s), (e_o), (q_{peak}), (S_c), (B_c), (K_c)$	2	Validation	0.846	0.145
			Overall data	0.910	0.014
			Training	0.914	2.36*10 <sup>-8</sup>
			Testing	0.884	0.327
4	$(p_o'), (B), (C_u), (e_{max}/e_{min}), (G_s), (e_o), (q_{peak}), (S_c), (B_c), (K_c)$	2	Validation	0.992	0.321
			Overall data	0.956	0.017
			Training	0.935	0.017
5	$(p_o'), (B), (C_u), (D_{50}), (e_{max}/e_{min}), (G_s), (e_o), (S_c), (B_c), (K_c)$	2	Testing	0.966	0.244
			Validation	0.976	0.0753
			Overall data	0.893	0.029
			Training	0.880	1.32*10 <sup>-6</sup>
			Testing	0.908	0.326
			Validation	0.978	0.353

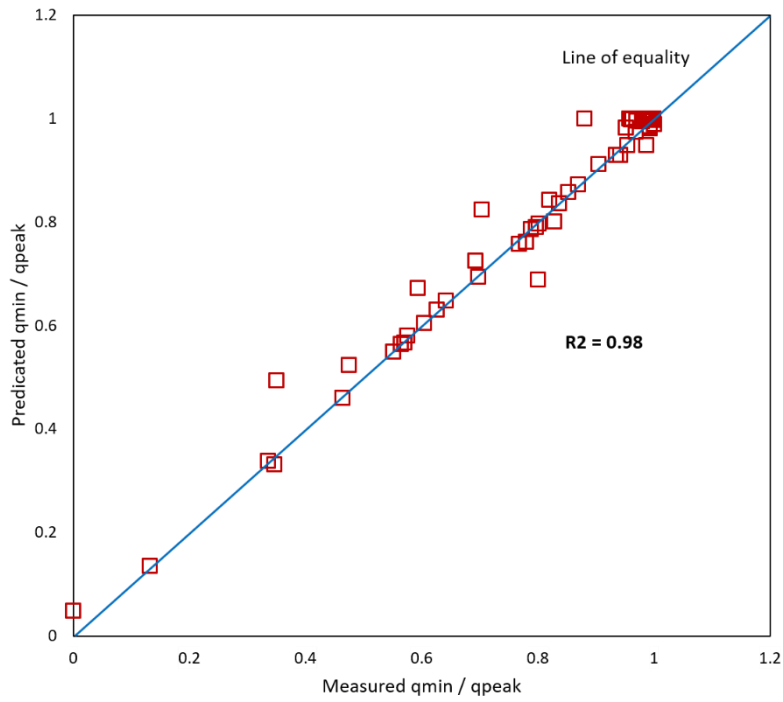


Figure 6.13 Measured vs. predicted stress ratio for ANN model 1 of sand–fines mixtures

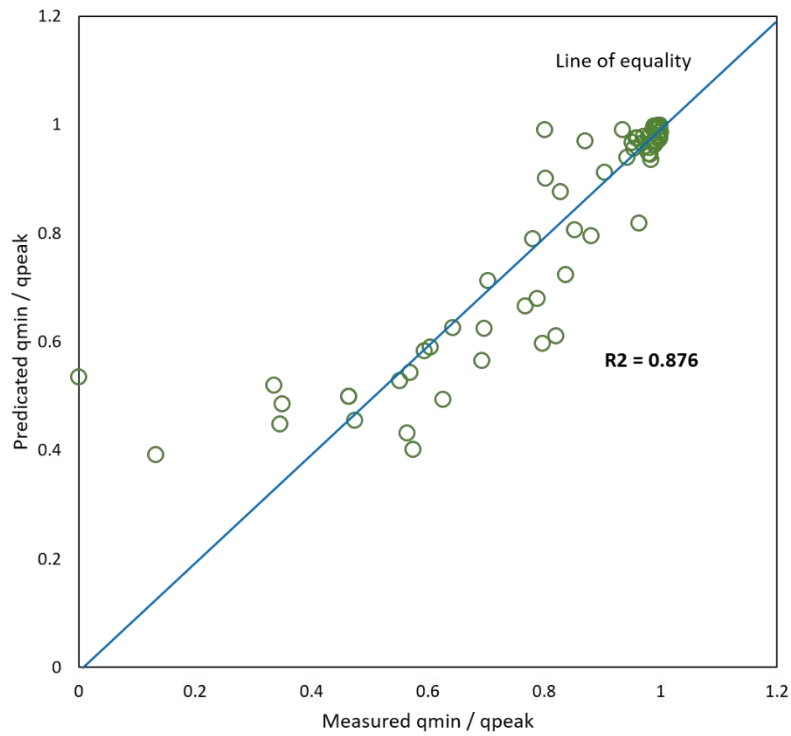


Figure 6.14 Measured vs. predicted stress ratio for ANN model 2 of sand–fines mixtures



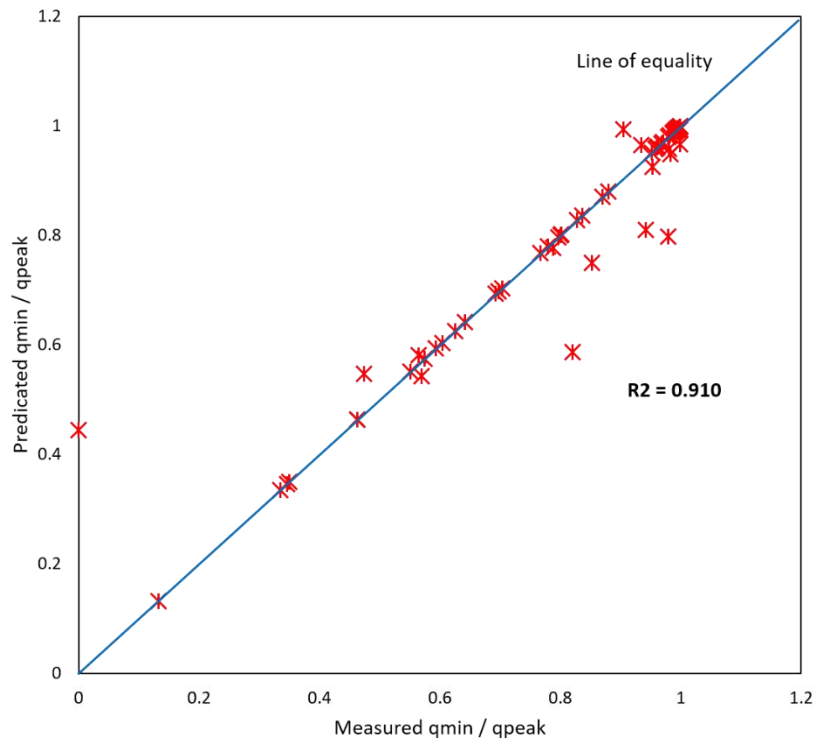


Figure 6.15 Measured vs. predicted stress ratio for ANN model 3 of sand–fines mixtures

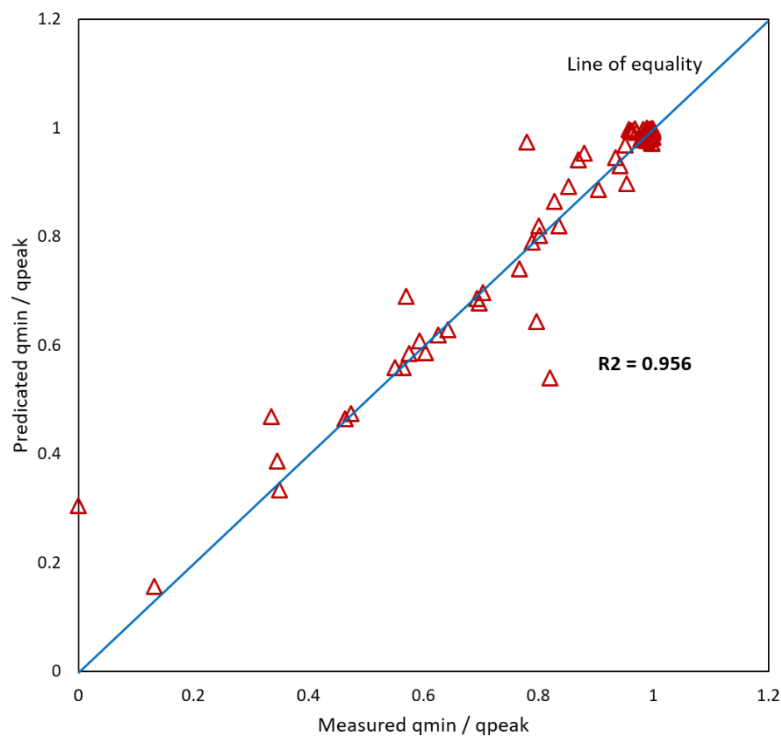


Figure 6.16 Measured vs. predicted stress ratio for ANN model 4 of sand–fines mixtures

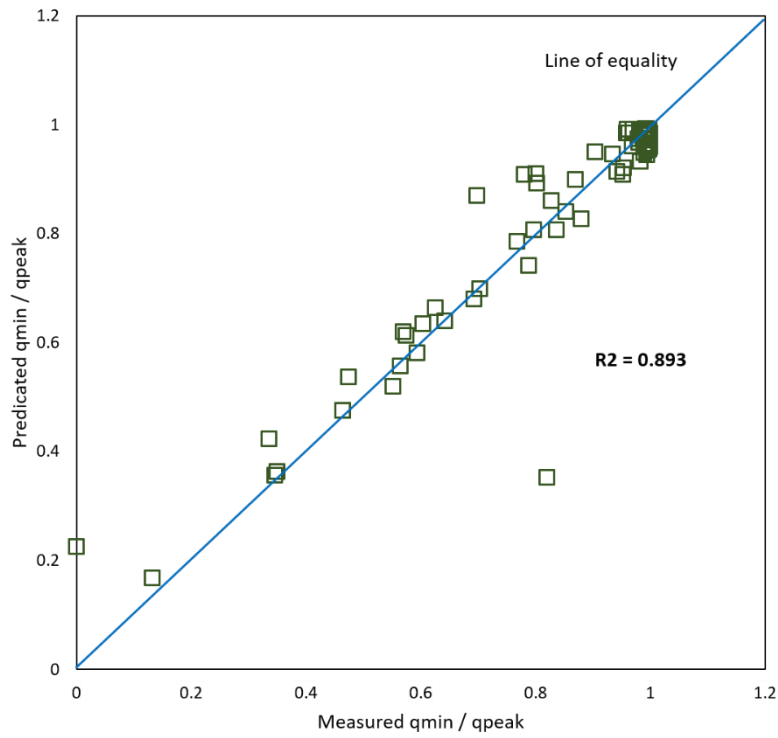


Figure 6.17 Measured vs. predicted stress ratio for ANN model 5 of sand–fines mixtures

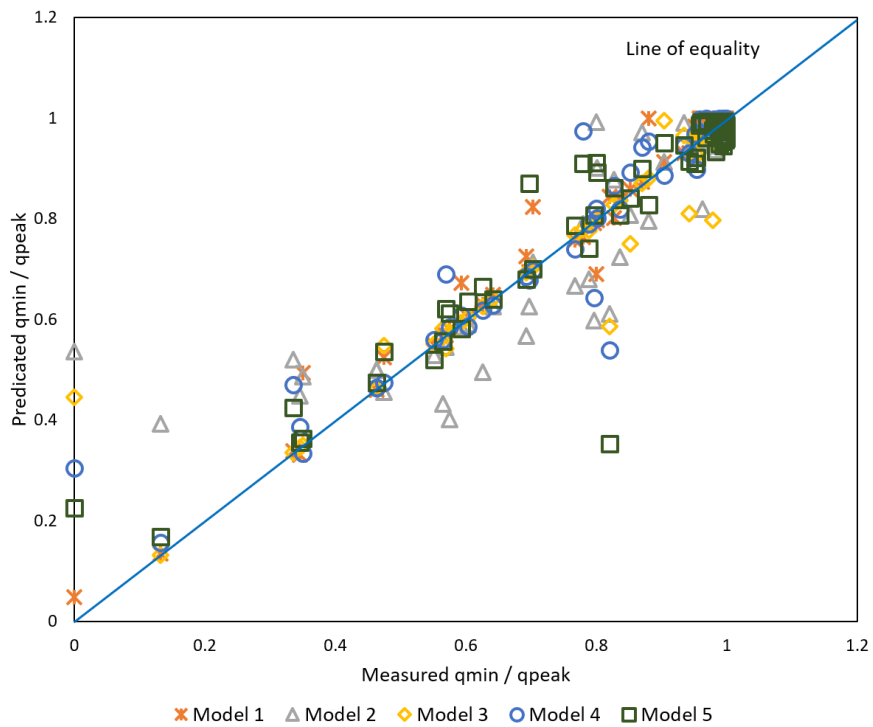


Figure 6.18 Measured vs. predicted stress ratio for all the ANN models of sand–fines mixtures

### 6.3.2 Genetic programming model of sand–fine mixtures

The HeuristicLab software was used to develop a functional relationship for the stress ratio  $q_{min}/q_{peak}$  of the sand–fines mixtures on the basis of symbolic regression via GP. The input data were chosen on the basis of the best results of the ANN modelling as described in Section 6.3.1, which showed that model 1 with 11 input parameters showed the best prediction with the highest value of  $R^2$ . The input dataset included  $p_o'$ ,  $B$ ,  $C_u$ ,  $D_{50}$ ,  $e_{max}/e_{min}$ ,  $e_o$ ,  $q_{peak}$ ,  $S_c$ ,  $B_c$ , and  $K_c$ , while one variable, the stress ratio  $q_{min}/q_{peak}$ , was used as output dataset. Symbolic regression by GP was performed with the variable set listed in Table 6.10. The input data were divided into 67% for training and 33% for testing. The software approached the better model of the stress ratio  $q_{min}/q_{peak}$  with the highest values of  $R^2$  for training and testing, after a cycle of 75 generations.

Table 6.10 Symbolic regression parameters

Parameters	Value
Population size	1000
Maximum number of generations	75
Parent selection	Tournament (group size 7)
Replacement	1-Elitism
Crossover	Sub-tree-swapping
Mutation rate	15%
Fitness function	$R^2$ and RMSE
Function set	+, -, *, /, exp, ln
Terminal set	Constant, variable

Therefore, the following equation was formulated to connect the stress ratio  $q_{min}/q_{peak}$  of the sand–fines mixtures to the input parameters:

$$\begin{aligned}
 q_{min}/q_{peak} = & (((EXP(c_1 * e_{max}/e_{min}) + 18.26) * LN(c_2 * D_{50}) + 1/(c_3 * C_u)) * LN(c_2 * D_{50})^{-11.24} / ((c_4 * S_c + \\
 & 1 * e_{max}/e_{min} * 1 * q_{peak} * 2.084 / (LN(c_2 * D_{50})) + 2.22267) * \\
 & (EXP(c_1 * e_{max}/e_{min}) * c_5 + 5.124)) + EXP((c_6 * e_{max}/e_{min} + 1/(c_7 * q_{peak}) + 11.02) * LN(c_2 * D_{50})) * (c_8 * p'_o \pm \\
 & c_9 * G_s) * 15.259 / (1 * D_{50} * (-17.3011 * D_{50} \pm 3.08744 * q_{peak} \pm 94.81933)) * (-3.6617703 * D_{50} \pm \\
 & 0.653456 * q_{peak} + 1 / (EXP(c_1 * e_{max}/e_{min}) * -0.00102)) * 1.793162)) * -1.19203 + 2.20934
 \end{aligned}$$

(6-2)

The values of coefficients  $c_1$  to  $c_9$  are listed in Table 6.11.

Table 6.11 Coefficients of Equation (6-2)

$c_1$	$c_2$	$c_3$	$c_4$	$c_5$	$c_6$	$c_7$	$c_8$	$c_9$
2.345	1.218	0.005	839.344	2.019	0.973	0.214	1.225	1.856

From the developed model (Equation 6-2), we can see that the initial state, physical properties, and fines content played a significant role in determining the liquefaction susceptibility of the sand–fines mixtures. The ANN models also demonstrated the substantial effect of the initial state and the physical properties of the sand–fines mixtures on the liquefaction susceptibility of these mixtures. Note that the effects of the initial state, physical properties, and fines content on the liquefaction susceptibility of sandy soil have been reported in many previous experimental studies (Jafarian, Ghorbani, et al., 2013; Salamatpoor & Salamatpoor, 2014; Yamamuro & Lade, 1997b). Figure 6.19 shows the measured values of the stress ratio  $q_{min}/q_{peak}$  versus the equivalent values as predicted by the GP model. It is apparent from this figure that the data of the training and the testing sets were closely distributed around the bisector line, which indicated the good prediction ability for the developed model. The performance of the HeuristicLab model was examined by using RMSE and  $R^2$ . Table 6.12 presents the  $R^2$  and RMSE values of the proposed model for the training and testing sets. Figure 6.20 shows the plot of the normalised stress  $q_{min}/q_{peak}$  versus the estimated  $q_{min}/q_{peak}$  values for all the datasets. The figure shows that the almost normalised  $q_{min}/q_{peak}$  values are distributed around 1, which indicated a good agreement between the measured and the predicted values. Figure 6.21 shows the tree of the developed model. The results of the ANN models and the GP models demonstrated that a good agreement might exist between the two AI approaches with respect to the prediction of the stress ratio  $q_{min}/q_{peak}$ .

Table 6.12 Performance of the  $q_{min}/q_{peak}$  model for the training and testing datasets

Dataset	Performance	
	$R^2$	RMSE
Training	0.953	0.000156
Testing	0.923	0.000197

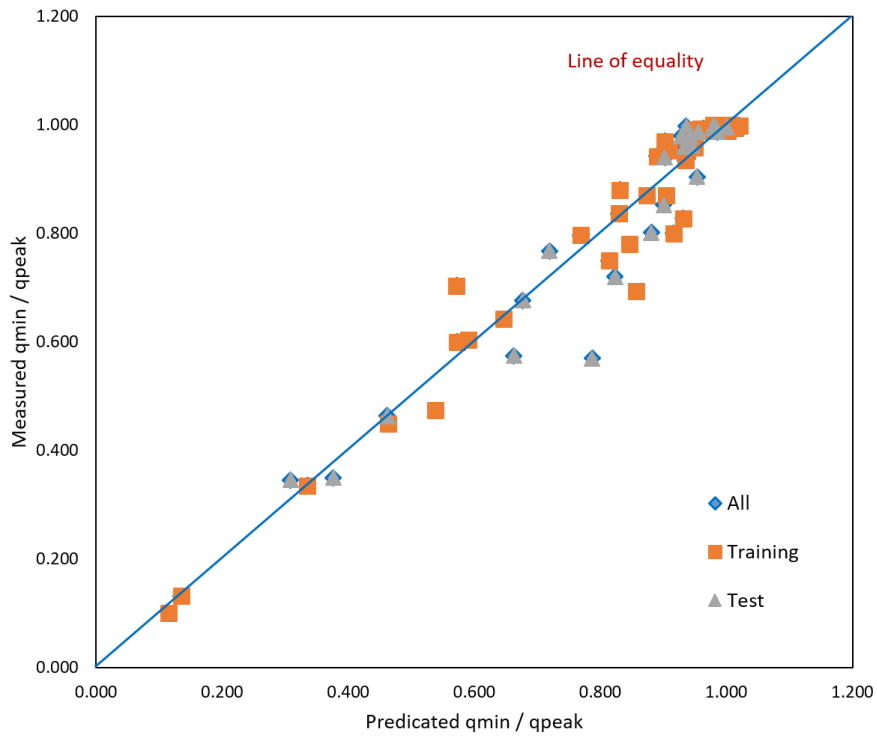


Figure 6.19 Measured values of the stress ratio vs. those predicted by the developed GP model of sand–fines mixtures

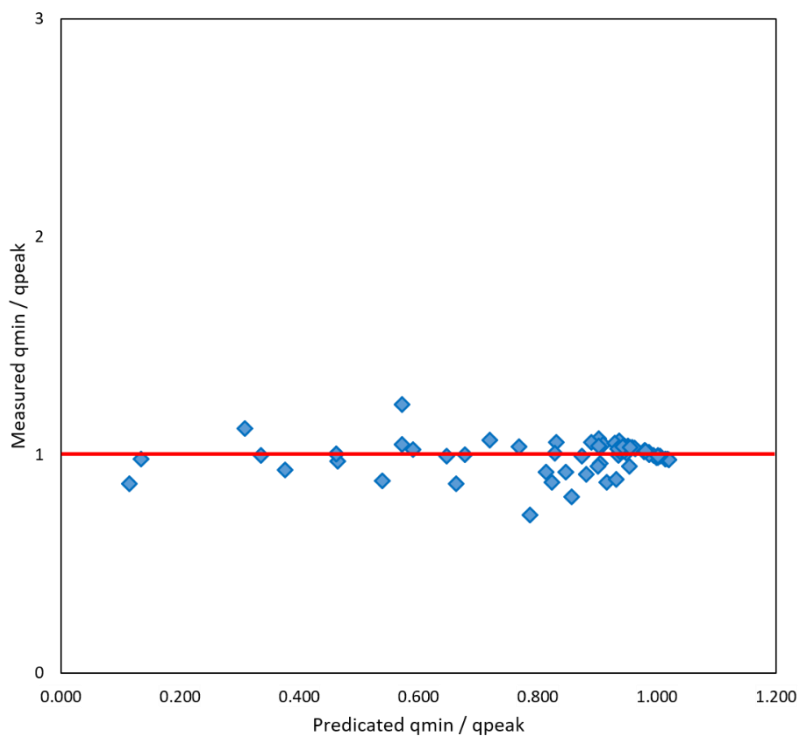


Figure 6.20 Normalised stress ratio vs. that predicted by the developed GP model for all the datasets of sand–fines mixtures

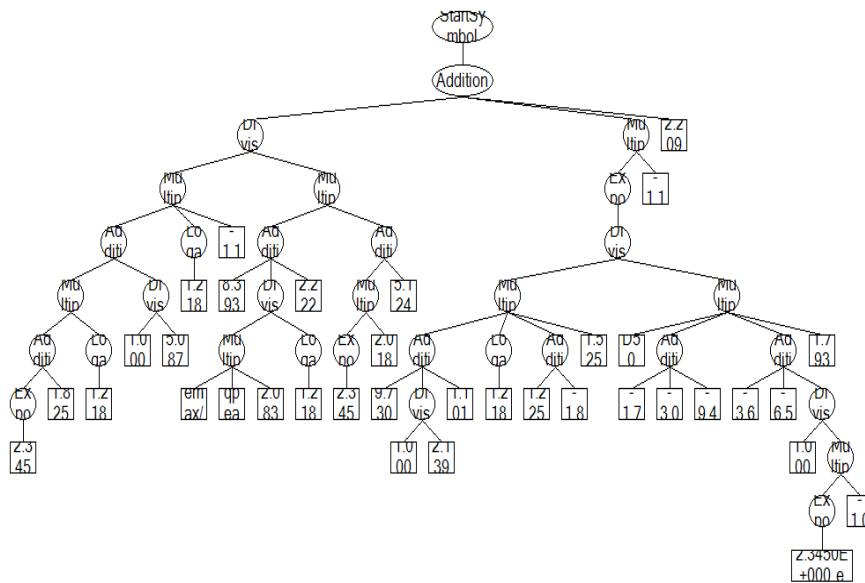


Figure 6.21 Tree of the developed GP model of sand–fines mixtures

## 6.4 Summary

Two AI approaches were used in this chapter to predict the liquefaction susceptibility of clean sand and sand–fines mixtures. For this purpose, ANN and GP were used for the prediction of the stress ratio  $q_{min}/q_{peak}$  of both the clean sand and the sand–fines mixtures. For modelling the liquefaction susceptibility of the clean sand, the dataset was obtained from previously published work. In contrast, the results of experimental tests conducted in the present study were used for modelling the liquefaction susceptibility of the sand–fines mixtures. The dataset of the clean sand models included nine input parameters, namely  $C_u$ ,  $D_{50}$ ,  $e_{max}$ ,  $e_{min}$ ,  $e$ ,  $D_r$ ,  $p_o'$ ,  $\alpha$ , and  $B$ , and one target parameter called the ratio of  $q_{min}/q_{peak}$ . The dataset of the sand–fines mixtures included 11 input parameters, namely  $p_o'$ ,  $C_u$ ,  $D_{50}$ ,  $G_s$ ,  $e_o$ ,  $e_{max}/e_{min}$ ,  $q_{peak}$ ,  $B$ ,  $S_c$ ,  $B_c$ , and  $K_c$  and one target parameter called the ratio of  $q_{min}/q_{peak}$ . The results demonstrated that the use of all the input parameters increased the ability of the ANN to predict the liquefaction susceptibility of both the clean sand and the sand–fines mixtures with a high coefficient of determination ( $R^2$ ) for the testing set. However, the accuracy of the ANN models decreased when the parameters of the initial state and the physical properties were eliminated. Symbolic regression via GP was used to develop a new equation for the determination of the liquefaction susceptibility of the clean sand and

the sand–fines mixtures with respect to the ratio of  $q_{min}/q_{peak}$ . The results presented in this chapter showed that the liquefaction susceptibility of the clean sand and the sand–fines mixtures depended considerably on the initial state (i.e. initial relative density (void ratio)), physical properties (i.e. mean diameter and coefficient of uniformity), and fines content. Furthermore, the results indicated a good agreement between the ANN and the GP approaches with respect to the prediction of the stress ratio of  $q_{min}/q_{peak}$ . Although the ANN models and the GP model were successful in predicting the ratio of  $q_{min}/q_{peak}$ , the proposed models still had certain limitations.

# Chapter 7: Conclusions and Recommendations

## 7.1 General

The effect of fines on the liquefaction behaviour of sandy soils has been investigated widely in the previous studies. However, research on the effect of waste materials on the liquefaction susceptibility of sandy soils is very limited. Furthermore, studies on the effect of a combination of two different types of fines on the liquefaction behaviour of sandy soils are very limited. Therefore, this study set out to determine how the presence of different slag contents affected the liquefaction behaviour of clean sandy soils. To accomplish this goal, a series of experimental and analytical tests were conducted on the sand–slag mixtures in a certain range of the slag content, initial confining pressure, and initial relative densities. Moreover, the relationship between sand purity and the effect of the slag content on the behaviour of sandy soils was investigated by conducting undrained tests on the sand–clay–slag mixtures. This allowed us to develop the current state of knowledge by giving more details about the effect of the fines on the liquefaction behaviour of sandy soils and to develop models for predicting the liquefaction susceptibility of sandy soils that can be used in the initial assessment of the liquefaction susceptibility.

## 7.2 Conclusions

- 1- In the undrained triaxial tests under static shearing, very loose saturated samples exhibited complete static liquefaction behaviour ( $q = 0$ ) at the lowest level of the initial confining pressure (100 kPa). However, the behaviour of the specimens prepared at the same relative density changed to flow behaviour when the initial confining pressure increased. This behaviour was called ‘*anomalous behaviour*’ and was in contrast to the normal behaviour of soils, where their resistance decreases with increasing confining pressure. These responses were attributed to the densification of the samples, as the compressibility of very loose samples increased with increasing confining



pressure and led to stable soil fabrics. Moreover, the pore pressure ratio decreased as the confining pressure increased.

- 2- The ability of specimens to generate '*anomalous behaviour*' decreased with increasing relative density of the sample. The flow behaviour was associated with very low-to-medium states. However, the non-flow behaviour was associated with the dense state. The behaviour of the sample significantly changed from complete static liquefaction at a very low relative density to limited liquefaction and non-flow behaviour when the initial relative density changed to the medium state and the dense state, respectively. An increase in the relative density shifted the behaviour of the sandy soil to the normal behaviour. The effect of increasing the relative density could be attributed to the stability of the sand fabric, which increased with increasing relative density. Furthermore, an increase in the initial relative density of the samples hindered the effect of the initial confining pressure on the undrained behaviour of clean sandy soils.
- 3- The degree of saturation had a significant effect on the undrained behaviour of clean sandy soils. The fully saturated very loose sample tested at the initial confining pressure of 100 kPa showed complete static liquefaction. However, a decrease in the degree of saturation of the sample significantly shifted the behaviour from complete static liquefaction to flow behaviour. Both the peak deviatoric stress and the minimum deviatoric stress increased with a decrease in the degree of saturation. Furthermore, the pore water pressure in the partially saturated samples was lower than that in the fully saturated samples because the presence of a compressible gas reduced the ability of the sample to generate pore water pressure. Consequently, the stability of the sand samples improved.
- 4- The experimental results showed that the undrained brittleness index  $I_B$ , stress ratio at the instability line  $\eta$ , and the state parameter at the start of the test  $\Psi_o$  could efficiently be used to evaluate the liquefaction susceptibility of clean sandy soils. The results also demonstrated that there was a good correlation among these parameters.
- 5- The undrained brittleness index  $I_B$  was used to determine the amount of reduction in the deviatoric stress during liquefaction. The undrained brittleness index  $I_B$  of the samples tested at the lowest initial confining

pressure (100 kPa) significantly reduced when the initial relative density increased from 10% to 90%. However, in the dense ( $D_{ri}$  90%) state, the tests showed a slight increase in the undrained brittleness index  $I_B$  with the increasing initial confining pressure indicating that the behaviour of the clean sandy soil shifted to normal behaviour in the dense state.

- 6- The stress ratio at the instability line  $\eta$  was used to identify the relationship between the instability and the liquefaction behaviour of sandy soils. The correlation between the undrained brittleness index  $I_B$  and the stress ratio at the instability line  $\eta$  showed that the instability of the clean sandy soil was dominated more by the relative density than by the initial confining pressure. This was observed when the loose sample exhibited significant increases in the stress ratio at the instability line with an increase in the initial confining pressure. However, the  $\eta$  value of the dense samples slightly decreased with an increase in the initial confining pressure. The positive effect of the relative density on the instability of sandy soils was attributed to the soil fabric; it improved with an increase in the relative density.
- 7- The results of this study showed that the state parameter at the start of the tests  $\Psi_o$  significantly reduced when the relative density increased from 10% to 90%. Very loose sand samples exhibited positive  $\Psi_o$ . However, dense samples showed negative values. The relationships between  $\Psi_o$  and the pore water pressure ratio  $R_u$  demonstrated that the  $\Psi_o - R_u$  space could be divided into three sections on the basis of the values of both  $\Psi_o$  and  $R_u$ . The first section was the complete static liquefaction section which was associated with positive  $\Psi_o$  and the unity value of  $R_u$ . The second section was the limited liquefaction section (lower right quarter) which was associated with positive  $\Psi_o$  and  $1 \leq R_u \leq 0.6$ . The negative values of  $\Psi_o$  and  $R_u \leq 0.3$  were associated with the third section called the non-flow section (lower left quarter). Furthermore, the results of the very loose clean sand samples exhibited a scattering trend across the correlation line.
- 8- The liquefaction behaviour of clean sandy soil significantly improved when sand was mixed with three different slag contents (2%, 4%, and 6%). The deviatoric stresses increased and the pore water pressure ratio decreased when the slag content increased up to 4%. However, the deviatoric stress reduced and the pore water pressure increased when the slag content

increased to 6%. Samples prepared by mixing sand with 4% slag exhibited the highest deviatoric stress and the lowest pore water pressure ratio. The very loose sand–slag mixtures showed different behaviours when the relative density increased to 50% and 90%.

- 9- Increasing the relative density reduced the effect of the slag content on the liquefaction behaviour of the sand–slag mixtures. The results showed that the presence of the slag content enhanced the ability of the samples to generate ‘anomalous behaviour’. The undrained brittleness index  $I_B$  and the state parameter at the start of the test  $\Psi_o$  significantly reduced when the slag content increased up to 4%. In contrast, the stress ratio at the instability line  $\eta$  of the very loose samples significantly increased when the slag content increased up to 4% and then reduced when the slag content increased to 6%.
- 10- The effect of the slag content on the liquefaction susceptibility of sandy soil could be related to the role of the slag particles in occupying the voids between the sand grains, which increased the contact between the sand grains and consequently, improved the soil fabric. However, the stability of the soil fabric reduced when the slag content increased to 6% because the slag particles reduced the contact between the sand grains. Furthermore, the angular shape of the slag particles positively influenced the sand fabric, which reduced the liquefaction susceptibility.
- 11- The presence of both 3% and 5% bentonite increased the liquefaction susceptibility of sandy soils. The mixtures of sand–3% bentonite showed lower liquefaction susceptibility than the mixtures of sand–5% bentonite. Furthermore, the presence of bentonite improved the ability of the soil to generate reverse behaviour. However, the mixtures of sand–5% bentonite exhibited slight increases in the deviatoric stress with increasing initial confining pressures.
- 12- At a very low relative density, the undrained brittleness index  $I_B$  decreased when the bentonite content increased up to 3% and then increased when the bentonite content increased to 5%. However, at the medium and dense states, the undrained brittleness index  $I_B$  increased with an increase in the bentonite content and the increase rate decreased with an increase in the relative density. The sand–bentonite mixtures showed a positive state parameter at the start of the tests  $\Psi_o$ , and its value increased with an increase in the

bentonite content, which indicated that the liquefaction susceptibility of sandy soils increased when sand was mixed with bentonite. Furthermore, the stress ratio at the instability line  $\eta$  reduced with increasing bentonite content. The negative effect of bentonite on the liquefaction susceptibility of sandy soils could be attributed to the role of bentonite in creating an unstable sand fabric.

- 13- The undrained results for the sand–kaolinite mixtures showed that the presence of 3% kaolinite improved the liquefaction behaviour of sandy soil by increasing the deviatoric stresses and reducing the pore water pressures. However, the deviatoric stresses reduced and the pore water pressure ratio increased when the kaolinite content increased to 5%. The results also demonstrated that the presence of kaolinite enhanced the ability of the sandy soil to generate reverse behaviour as represented by an increase in the deviatoric stresses with an increase in the initial confining pressures.
- 14- The undrained brittleness index  $I_B$  of then very loose sand–kaolinite mixtures significantly reduced with an increase in the initial confining pressures, and sand–3% kaolinite exhibited the lowest values. At a very low relative density, the liquefaction susceptibility reduced when the kaolinite content increased to 3% and then significantly increased when the kaolinite content increased to 5%. However, the effect of the kaolinite content on the undrained brittleness index reduced with an increase in the relative density. The sand–kaolinite mixtures showed a positive state parameter at the start of the tests  $\Psi_o$ , and its value decreased with an increase in the kaolinite content, which indicated that the liquefaction susceptibility of the sandy soils decreased when sand was mixed with kaolinite. Furthermore, the stress ratio at the instability line  $\eta$  decreased with an increase in the kaolinite content. The positive effect of kaolinite on the liquefaction susceptibility of sandy soils could be attributed to the role of kaolinite in creating a stable sand fabric.
- 15- The results of the undrained tests conducted on the sand–clay mixtures showed that the liquefaction behaviour of the sand–clay mixtures depended considerably on the clay mineralogy. This was observed when the presence of the bentonite content enhanced the liquefaction susceptibility by reducing the deviatoric stresses and increasing the pore water pressure ratios.

However, the liquefaction susceptibility for the sample prepared by mixing sandy soil with different clay types (kaolinite) and tested under the same test conditions as those of the sand–bentonite mixtures reduced when the kaolinite content increased up to 3%. In both the sand–bentonite and the sand–kaolinite mixtures, the presence of 5% clay increased the undrained brittleness index and the pore water pressure ratios, but the mixtures of sand–5% kaolinite exhibited the lowest values.

- 16- One of the more significant findings of this study was that mixing clean sandy soil with various slag and clay contents positively affected the liquefaction behaviour of sandy soil. All the mixtures of sand–slag–clay prepared at a very low relative density and tested at the lowest initial confining pressure (100 kPa) exhibited lower liquefaction susceptibility than the clean sandy soils tested under the same conditions. The undrained brittleness index  $I_B$  of the sand–slag–bentonite mixtures significantly reduced when the bentonite content was 3% and then increased when the bentonite content increased to 5%, and at both the bentonite contents, the mixtures of sand–4% slag–3% bentonite showed the lowest values. The mixtures of sand–slag–kaolinite showed more stable behaviour than the sand–slag–bentonite mixtures. This was observed when the undrained brittleness index significantly reduced with an increase in the kaolinite content of up to 3% and then slightly increased when the kaolinite content increased to 5%. At both kaolinite contents, the mixture of sand–6% slag–3% kaolinite showed the lowest value. Furthermore, the mixtures of sand–slag–kaolinite showed a consistent behaviour characterised by the increase in  $I_B$  upon an increase in the slag content. However, the sand–slag–bentonite mixtures showed inconsistent behaviour with increasing slag content. The undrained brittleness index  $I_B$  reduced when the slag content increased up to 4% and then increased when the slag content increased to 6%.
- 17- The second significant finding of this study was that the effect of the fines on the liquefaction susceptibility of clean sandy soils was considerably dependent on the type and content of the fines. The presence of non-plastic fines decreased the liquefaction susceptibility of sandy soils. However, the effect of plastic fines on the liquefaction susceptibility was considerably dependent on the clay mineralogy. This was observed when the sand–

bentonite mixtures showed higher liquefaction susceptibility than the sand–kaolinite mixtures. Furthermore, the presence of non-plastic fines improved the liquefaction resistance of sandy soils more than that of plastic fines. The results also showed that mixing sandy soils with non-plastic and plastic fines considerably reduced the liquefaction susceptibility of the soils.

18- The results of the AI approaches revealed that ANN and GP could efficiently capture the liquefaction susceptibility of the clean sand and the sand–fines mixtures with a high  $R^2$  value and the lowest RMSE. The results also indicated a good agreement between the ANN and the GP approaches in predicting the liquefaction susceptibility of the clean sand and the sand–fines mixtures. Although the ANN models and the GP model were successful in predicting the ratio of  $q_{min}/q_{peak}$  of the clean sand and the sand–fines mixtures, the proposed models still have certain limitations. The limitations in the present work might be related to some sources such as the properties of the database, amount of data, method of sample deposition, type of software, and type of regression analysis. Therefore, the findings of this work should be used carefully to account for the limitations presented above.

### 7.3 Recommendations

The experimental and empirical work performed in this thesis was limited to the study of the behaviour of sand mixed with specific fines contents. Therefore, the following areas need to be investigated further:

- 1- Further experimental study on the effect of extra slag, bentonite, and kaolinite content on the liquefaction behaviour of sandy soils is required. Moreover, the effect of the curing time of sand mixed with slag, bentonite, or kaolinite also required.
- 2- Further interpretations of the results of the undrained static triaxial tests of the sand–fines mixtures within the critical state framework and the steady-state frameworks are highly recommended.
- 3- The liquefaction behaviour of the sand–fines mixtures in anisotropic consolidations and under triaxial extension (static and cyclic) loading has

not been investigated in this thesis. Therefore, additional investigations considering these conditions are required.

- 4- Further experimental investigations on the effect of additional factors such as soil structure and liquefaction history on static liquefaction resistance of clean sandy soils and sand-fine mixtures.
- 5- With the view that the sample preparation method may affect the liquefaction behaviour of sandy samples, an additional study can be conducted by using different sample preparation methods.
- 6- Further ANN and GP modelling by using other software programs and a wide range of input datasets is required.

# References

- Abedi, M., & Yasrobi, S. S. (2010). Effects of plastic fines on the instability of sand. *Soil Dynamics and Earthquake Engineering*, 30(3), 61-67.
- Alarcon-Guzman, A., Leonards, G., & Chameau, J. (1988). Undrained monotonic and cyclic strength of sands. *Journal of Geotechnical engineering*, 114(10), 1089-1109.
- Andrade, J. (2009). A predictive framework for liquefaction instability. *Geotechnique*, 59(8), 673.
- Arthur, J., & Menzies, B. (1972). Inherent anisotropy in a sand. *Geotechnique*, 22(1), 115-128.
- Australian Slag Association. (2011). Blast Furnace Slag Aggregate and Cementitious products. *Reference data sheet 1*.
- Banimahd, M., Yasrobi, S., & Woodward, P. (2005). Artificial neural network for stress-strain behavior of sandy soils: Knowledge based verification. *Computers and Geotechnics*, 32(5), 377-386.
- Bayat, E., & Bayat, M. (2013). Effect of grading characteristics on the undrained shear strength of sand: review with new evidences. *Arabian journal of geosciences*, 6(11), 4409-4418.
- Bayat, M., Bayat, E., Aminpour, H., & Salarpour, A. (2014). Shear strength and pore-water pressure characteristics of sandy soil mixed with plastic fine. *Arabian journal of geosciences*, 7(3), 1049-1057.
- Baziar, M., & Nilipour, N. (2003). Evaluation of liquefaction potential using neural-networks and CPT results. *Soil Dynamics and Earthquake Engineering*, 23(7), 631-636.
- Beaty, M. H., & Byrne, P. M. (2008). Liquefaction and Deformation Analyses Using a Total Stress Approach. *Journal of Geotechnical and Geoenvironmental Engineering*, 134(8), 1059-1072.
- Been, K., & Jefferies, M. (2004). Stress dilatancy in very loose sand. *Canadian Geotechnical Journal*, 41(5), 972-989.
- Been, K., Jefferies, M., & Hachey, J. (1991). Critical state of sands. *Geotechnique*, 41(3), 365-381.
- Been, K., & Jefferies, M. G. (1985). *State parameter for sands*. Paper presented at the International Journal of Rock Mechanics and Mining Sciences and Geomechanics Abstracts.
- Belhouari, F., Bendani, K., Missoum, H., & Derkaoui, M. (2015). Undrained Static Response of Loose and Medium Dense Silty Sand of Mostaganem (Northern Algeria). *Arabian Journal for Science and Engineering*, 40(5), 1327-1342.
- Benahmed, N., Canou, J., & Dupla, J. (2004). Initial structure and static liquefaction properties of sand. *Comptes Rendus Mécanique*, 332(11), 887-894.
- Bishop, A. W. (1966). The strength of soils as engineering materials. *Geotechnique*.
- Bishop, A. W. (1971). *Shear strength parameters for undisturbed and remoulded soil specimens*. Paper presented at the Proceedings of the Roscoe Memorial Symposium, Cambridge University, Cambridge, Mass.
- Bjerrum, L. (1971). Subaqueous slope failures in Norwegian fjords. *Norwegian Geotechnical Institute Publ*(88).
- Bjerrum, L., Kringstad, S., & Kummeneje, O. (1961). *The shear strength of a fine sand*: Norges Geotekniske Institutt.
- Bobei, D. (2004). *Static liquefaction of sand with a small amount of fines*: University of new South Wales, Australian Defence Force Academy, School of Aerospace, Civil and Mechanical Engineering.



- Bobei, D., Lo, S., Wanatowski, D., Gnanendran, C., & Rahman, M. M. (2009). Modified state parameter for characterizing static liquefaction of sand with fines. *Canadian Geotechnical Journal*, 46(3), 281-295.
- Boulanger, R. W., Meyers, M. W., Mejia, L. H., & Idriss, I. M. (1998). Behavior of a fine-grained soil during the Loma Prieta earthquake. *Canadian Geotechnical Journal*, 35(1), 146-158.
- Bray, J. D., Sancio, R. B., Durgunoglu, T., Onalp, A., Youd, T. L., Stewart, J. P., . . . Karadayilar, T. (2004). Subsurface Characterization at Ground Failure Sites in Adapazari, Turkey. In: ASCE.
- Budihardjo, M. A., Chegenizadeh, A., & Nikraz, H. (2015). Application of Wood to Sand-slag and its Effect on Soil Strength. *Procedia Engineering*, 102, 640-646.
- Byrne, P. M. (1991). *A model for predicting liquefaction induced displacement*. Paper presented at the Second International Conference on Recent Advances in Geotechnical Earthquake Engineering and Soil Dynamics, St. Louis.
- Byrne, P. M., Jitno, H., & Salgado, F. (2004). *Earthquake induced displacements of soil-structures systems*. Paper presented at the Proceedings of the Tenth World Conference on Earthquake Engineering: 19-24 July 1992, Madrid, Spain.
- Casagrande, A. (1940). Characteristics of Cohesionless Soils Affecting the Stability of Slopes and Earth Fills, *Contrib. SM, Boston Soc. CE*, 72-126.
- Casagrande, A. (1975). *Liquefaction and cyclic deformation of sand*. Paper presented at the A Critical Review. V<sup>o</sup> Panamerican Conference on Soil Mechanics and Foundation Engineering, Buenos Aires, Argentina.
- Casagrande, A. (1976). *Liquefaction and Cyclic Deformation of Sands: A Critical Review; Presented at Fifth Panamerican Conference on Soil Mechanics and Foundation Engineering, Buenos Aires, Argentina, November 1975*: Pierce Hall.
- Castro, G. (1969). *Liquefaction of sands*: Harvard Univ., Division of Engineering and Applied Mechanics.
- Castro, G. (1975). Liquefaction and cyclic mobility of saturated sands. *Journal of the Geotechnical Engineering Division*, 101(6), 551-569.
- Castro, G., & Poulos, S. (1980). FACTORS AFFECTING LIQUEFACTION AND CYCLIC MOBILITY-CLOSURE. *Journal of Geotechnical and Geoenvironmental Engineering*, 106(ASCE 112994).
- Castro, G., & Poulos, S. J. (1977). Factors affecting liquefaction and cyclic mobility. *Journal of Geotechnical and Geoenvironmental Engineering*, 103(6).
- Chang, K. (1978). An analysis of damage of slope sliding by earthquake on the Paiho Main Dam and its earthquake strengthening. *Tseng-hua Design Section, Department of Earthquake-Resistant Design and Flood Control Command of Miyna Reservoir, Peoples Republic of China*.
- Chang, N. (1990). Influence of fines content and plasticity on earthquake-induced soil liquefaction. *Contract Report to US Army Engineer Waterways Experiment Station, Vicksburg, MS, Contract No. DACW3988-C-0078*.
- Chern, J.-C. (1985). *Undrained response of saturated sands with emphasis on liquefaction and cyclic mobility*. University of British Columbia,
- Chheda, T., Quigley, M., Duffy, B., Borella, J., HAMPTON, S., BORELLA, M., & GRAVLEY, D. M. (2014). *The Physics and Mechanics of Liquefaction*. Paper presented at the 2014 GSA Annual Meeting in Vancouver, British Columbia.
- Choobasti, A., Farrokhzad, F., & Barari, A. (2009). Prediction of slope stability using artificial neural network (case study: Noabad, Mazandaran, Iran). *Arabian journal of geosciences*, 2(4), 311-319.
- Chu, J. (1995). An experimental examination of the critical state and other similar concepts for granular soils. *Canadian Geotechnical Journal*, 32(6), 1065-1075.
- Chu, J., & Leong, W. (2002). Effect of fines on instability behaviour of loose sand. *Geotechnique*, 52(10), 751-755.
- Chu, J., Lo, S.-C., & Lee, I. K. (1993). Instability of granular soils under strain path testing. *Journal of Geotechnical engineering*, 119(5), 874-892.

- Cokca, E., Yazici, V., & Ozaydin, V. (2009). Stabilization of expansive clays using granulated blast furnace slag (GBFS) and GBFS-cement. *Geotechnical and Geological Engineering*, 27(4), 489.
- Cornforth, D., Worth, E., & Wright, W. (1974). *Observations and analysis of a flow slide in sand fill*. Paper presented at the Proceedings of the Symposium on Field Instrumentation in Geotechnical Engineering.
- Cramer, N. L. (1985). *A representation for the adaptive generation of simple sequential programs*. Paper presented at the Proceedings of the first international conference on genetic algorithms.
- Dafalias, Y. F., & Manzari, M. T. (2004). Simple plasticity sand model accounting for fabric change effects. *Journal of Engineering mechanics*, 130(6), 622-634.
- Das, B. M., & Sobhan, K. (2014). *Principles of geotechnical engineering* (Eight ed.). Stamford, USA: Cengage Learning.
- Das, S. K. (2013). 10 Artificial Neural Networks in Geotechnical Engineering: Modeling and Application Issues. *Metaheuristics in Water, Geotechnical and Transport Engineering*, 231.
- Das, S. K., & Basudhar, P. K. (2008). Prediction of residual friction angle of clays using artificial neural network. *Engineering geology*, 100(3), 142-145.
- Das, S. K., & Muduli, P. K. (2011). *Evaluation of liquefaction potential of soil using genetic programming*. Paper presented at the Proc. Golden Jubilee Indian Geotechnical Conference, 15-17 December 2011, Kochi, India.
- Dawson, R., Morgenstern, N., & Stokes, A. (1998). Liquefaction flowslides in Rocky Mountain coal mine waste dumps. *Canadian Geotechnical Journal*, 35(2), 328-343.
- Delia, N. (2010). Laboratory testing of the Monotonic behavior of partially saturated sandy soil. *Earth Sciences Research Journal*, 14(2), 181-186.
- Della, N., Arab, A., & Belkhatir, M. (2011). Influence of specimen-reconstituting method on the undrained response of loose granular soil under static loading. *Acta Mechanica Sinica*, 27(5), 796-802.
- Della, N., Arab, A., Belkhatir, M., & Missoum, H. (2009). Identification of the behavior of the Chlef sand to static liquefaction. *Comptes Rendus Mécanique*, 337(5), 282-290.
- Demuth, H., Beale, M., & Hagan, M. (2008). *Neural network toolbox™ 6. User's guide*, 37-55.
- Eckersley, J. (1985). Flowslides in stockpiled coal. *Engineering geology*, 22(1), 13-22.
- El Mohtar, C., Bobet, A., Drnevich, V., Johnston, C., & Santagata, M. (2013). Pore pressure generation in sand with bentonite: from small strains to liquefaction. *Geotechnique*, 64(2), 108-117.
- ELE. (2004). *Operating Instructing Triaxial cells*. In. England: ELE International
- Elhag, T. M., & Wang, Y.-M. (2007). Risk assessment for bridge maintenance projects: Neural networks versus regression techniques. *Journal of computing in civil engineering*, 21(6), 402-409.
- Erzin, Y., & Cetin, T. (2012). The use of neural networks for the prediction of the critical factor of safety of an artificial slope subjected to earthquake forces. *Scientia Iranica*, 19(2), 188-194.
- Eseller-Bayat, E., Yegian, M. K., Alshawabkeh, A., & Gokyer, S. (2013). Liquefaction Response of Partially Saturated Sands. I: Experimental Results. *Journal of Geotechnical and Geoenvironmental Engineering*, 863, 871.
- Evans, M. D., & Seed, H. B. (1987). *Undrained cyclic triaxial testing of gravels: the effect of membrane compliance*: College of Engineering, University of California.
- Farrokhzad, F., Choobbasti, A., & Barari, A. (2010). Artificial neural network model for prediction of liquefaction potential in soil deposits.
- Farrokhzad, F., JanAliZadeh, A., & Barari, A. (2008). Prediction of Slope Stability Using Artificial Neural Network (Case Study: Noabad, Mazandaran, Iran).
- Ferreira, C. (2006). *Gene expression programming: mathematical modeling by an artificial intelligence* (Vol. 21): Springer.

- Fourie, A., Blight, G., & Papageorgiou, G. (2001). Static liquefaction as a possible explanation for the Merriespruit tailings dam failure. *Canadian Geotechnical Journal*, 38(4), 707-719.
- Frydman, S., Zeitlen, J., & Alpan, I. (1973). The membrane effect in triaxial testing of granular soils. *Journal of Testing and Evaluation*, 1(1), 37-41.
- Gandomi, A. H., & Alavi, A. H. (2011). Multi-stage genetic programming: a new strategy to nonlinear system modeling. *Information Sciences*, 181(23), 5227-5239.
- Gandomi, A. H., & Alavi, A. H. (2012). A new multi-gene genetic programming approach to non-linear system modeling. Part II: geotechnical and earthquake engineering problems. *Neural Computing and Applications*, 21(1), 189-201.
- Garga, V. K., & Zhang, H. (1997). Volume changes in undrained triaxial tests on sands. *Canadian Geotechnical Journal*, 34(5), 762-772.
- Georgiannou, V. (2006). The undrained response of sands with additions of particles of various shapes and sizes. *Geotechnique*, 56(9), 639-649.
- Georgiannou, V., Burland, J., & Hight, D. (1990). The undrained behaviour of clayey sands in triaxial compression and extension. *Geotechnique*, 40(3), 431-449.
- Goh, A. T. (1994). Seismic liquefaction potential assessed by neural networks. *Journal of Geotechnical engineering*, 120(9), 1467-1480.
- Goh, A. T. (1996). Neural-network modeling of CPT seismic liquefaction data. *Journal of Geotechnical engineering*, 122(1), 70-73.
- Goh, A. T., Kulhawy, F. H., & Chua, C. (2005). Bayesian neural network analysis of undrained side resistance of drilled shafts. *Journal of Geotechnical and Geoenvironmental Engineering*, 131(1), 84-93.
- Goto, S., & Tatsuoka, F. (1988). Influence of several testing conditions in triaxial compression tests on sands and gravels. *Soil Mechanics and Foundation Engineering*, 36(9), 13-18.
- Gratchev, I. B., Sassa, K., Osipov, V. I., Fukuoka, H., & Wang, G. (2007). Undrained cyclic behavior of bentonite-sand mixtures and factors affecting it. *Geotechnical and Geological Engineering*, 25(3), 349.
- Gratchev, I. B., Sassa, K., Osipov, V. I., & Sokolov, V. N. (2006). The liquefaction of clayey soils under cyclic loading. *Engineering geology*, 86(1), 70-84.
- Hagan, M. T., Demuth, H. B., & Beale, M. H. (2002). *Neural network design*. Singapore: Thomson Learning.
- Han, C., & Vardoulakis, I. (1991). Plane-strain compression experiments on water-saturated fine-grained sand. *Geotechnique*, 41(1), 49-78.
- Hanna, A. M., Ural, D., & Saygili, G. (2007). Neural network model for liquefaction potential in soil deposits using Turkey and Taiwan earthquake data. *Soil Dynamics and Earthquake Engineering*, 27(6), 521-540.
- Hazen, A. (1918). A study of the slip in the Calaveras Dam. *Engineering News Record*, 81(26), 1158-1164.
- Hazen, A. (1920). Hydraulic-fill dams. *Transactions of the American Society of Civil Engineers*, 83(1), 1713-1745.
- Head, K. (2014). *Manual of soil laboratory testing: volume 3: Effective Stress Tests* (Third ed.). Scotland, UK: Whittles Publishing.
- Head, K., & Epps, R. (2011). *Manual of Soil Laboratory Testing, Volume 2: Permeability, Shear Strength, and Compressibility Tests* (Vol. 2). Scotland, UK: Whittles Publishing.
- Hird, C., & Hassona, F. (1990). Some factors affecting the liquefaction and flow of saturated sands in laboratory tests. *Engineering geology*, 28(1), 149-170.
- Hossein Alavi, A., & Hossein Gandomi, A. (2011). A robust data mining approach for formulation of geotechnical engineering systems. *Engineering Computations*, 28(3), 242-274.
- Hsiao, D.-H., & Phan, V. T.-A. (2016). Evaluation of static and dynamic properties of sand-fines mixtures through the state and equivalent state parameters. *Soil Dynamics and Earthquake Engineering*, 84, 134-144.

- Hutchinson, J. (1986). A sliding–consolidation model for flow slides. *Canadian Geotechnical Journal*, 23(2), 115-126.
- Hyodo, M., Tanimizu, H., Yasufuku, N., & Murata, H. (1994). Undrained cyclic and monotonic triaxial behaviour of saturated loose sand. *Soils and foundations*, 34(1), 19-32.
- Ibsen, L. B. (1998). *The mechanism controlling static liquefaction and cyclic strength of sand*. Retrieved from
- Igwe, O., Sassa, K., & Fukuoka, H. (2004). Liquefaction potential of granular materials using differently graded sandy soils.
- Ika Putra, A. (2014). *Stabilisation of expansive subgrade soils with slag and cement for road construction*. (Master's thesis),
- Ishihara, K. (1985). *Stability of natural deposits during earthquakes*. Paper presented at the Proc., 11th Int. Conf. on Soil Mechanics and Foundation Engineering.
- Ishihara, K. (1993). Liquefaction and flow failure during earthquakes. *Geotechnique*, 43(3), 351-451.
- Ishihara, K., & Koseki, J. (1989). *Discussion on the cyclic shear strength of fines-containing sands*. Paper presented at the Earthquake Geotechnical Engineering, Proc., XII Int. Conf. on Soil Mechanics.
- Ishihara, K., Troncoso, J., Kawase, Y., & Takahashi, Y. (1980). Cyclic strength characteristics of tailings materials. *Soils and foundations*, 20(4), 127-142.
- Ishihara, K., Tsuchiya, H., Huang, Y., & Kamada, K. (2001). *Recent studies on liquefaction resistance of sand effect of saturation*. Paper presented at the Proc. 4th Conf. Recent Advances in Geotech. Earth. Engg., Keynote Lecture.
- Ishihara, K., Tsukamoto, Y., & Kamada, K. (2004). *Undrained behavior of near-saturated sand in cyclic and monotonic loading*. Paper presented at the Proc. Conf., Cyclic Behavior of Soils and Liquefaction Phenomena.
- Ishihara, K., Verdugo, R., & Acacio, A. A. (1991). *Characterisation of cyclic behaviour of sand and post-seismic stability analysis*. Paper presented at the 9th Asian Regional Conference on Soil Mechanics and Foundation Engineering, Bangkok, Thailand.
- Jafarian, Y., Ghorbani, A., Salamatpoor, S., & Salamatpoor, S. (2013). Monotonic triaxial experiments to evaluate steady-state and liquefaction susceptibility of Babolsar sand. *Journal of Zhejiang University SCIENCE A*, 14(10), 739-750.
- Jafarian, Y., Vakili, R., & Abdollahi, A. S. (2013). Prediction of cyclic resistance ratio for silty sands and its applications in the simplified liquefaction analysis. *Computers and Geotechnics*, 52, 54-62.
- Javadi, A. A., Rezaia, M., & Nezhad, M. M. (2006). Evaluation of liquefaction induced lateral displacements using genetic programming. *Computers and Geotechnics*, 33(4), 222-233.
- Jefferies, M., & Been, K. (2015). *Soil liquefaction: a critical state approach*: Crc Press.
- Jeyapalan, J. K., Duncan, J. M., & Seed, H. B. (1983). Analyses of flow failures of mine tailings dams. *Journal of Geotechnical engineering*, 109(2), 150-171.
- Johari, A., Habibagahi, G., & Ghahramani, A. (2006). Prediction of soil–water characteristic curve using genetic programming. *Journal of Geotechnical and Geoenvironmental Engineering*, 132(5), 661-665.
- Kaya, A. (2010). Artificial neural network study of observed pattern of scour depth around bridge piers. *Computers and Geotechnics*, 37(3), 413-418.
- Kenney, T. (1977). *Residual strengths of mineral mixtures*. Paper presented at the 9th International Conference on Soil Mechanics and Foundation Engineering, Tokyo.
- Kim, Y.-S., & Kim, B.-T. (2008). Prediction of relative crest settlement of concrete-faced rockfill dams analyzed using an artificial neural network model. *Computers and Geotechnics*, 35(3), 313-322.
- Koester, J. P. (1994). *The influence of fines type and content on cyclic strength*. Paper presented at the Ground failures under seismic conditions.

- Kokusho, T., Hara, T., & Hiraoka, R. (2004). Undrained shear strength of granular soils with different particle gradations. *Journal of Geotechnical and Geoenvironmental Engineering*, 130(6), 621-629.
- Konrad, J.-M. (1988). Interpretation of flat plate dilatometer tests in sands in terms of the state parameter. *Geotechnique*, 38(2), 263-277.
- Konrad, J.-M. (1990). Minimum undrained strength of two sands. *Journal of Geotechnical engineering*, 116(6), 932-947.
- Konrad, J. (1993). Undrained response of loosely compacted sands during monotonic and cyclic compression tests. *Geotechnique*, 43(1), 69-89.
- Koza, J. R. (1990). *Genetic programming: A paradigm for genetically breeding populations of computer programs to solve problems*: Stanford University, Department of Computer Science.
- Koza, J. R. (1992). *Genetic programming: on the programming of computers by means of natural selection* (Vol. 1): MIT press.
- Kramer, S. L. (1996). *Geotechnical earthquake engineering*: Prentice Hall, Upper Saddle River (NJ).
- Kramer, S. L., & Seed, H. B. (1988). Initiation of soil liquefaction under static loading conditions. *Journal of Geotechnical engineering*, 114(4), 412-430.
- Krim, A., el Abidine Zitouni, Z., Arab, A., & Mostéfa, B. (2013). Identification of the behavior of sandy soil to static liquefaction and microtomography. *Arabian journal of geosciences*, 6(7), 2211-2224.
- Kuerbis, R., Negussey, D., & Vaid, Y. (1988). *Effect of gradation and fines content on the undrained response of sand*. Paper presented at the Hydraulic fill structures.
- Lade, P. V. (1992). Static instability and liquefaction of loose fine sandy slopes. *Journal of Geotechnical engineering*, 118(1), 51-71.
- Lade, P. V. (1993). Initiation of static instability in the submarine Nerlerk berm. *Canadian Geotechnical Journal*, 30(6), 895-904.
- Lade, P. V., & Hernandez, S. B. (1977). Membrane penetration effects in undrained tests. *Journal of the Geotechnical Engineering Division*, 103(2), 109-125.
- Lade, P. V., Nelson, R. B., & Ito, Y. M. (1988). Instability of granular materials with nonassociated flow. *Journal of Engineering mechanics*, 114(12), 2173-2191.
- Lade, P. V., & Pradel, D. (1990). Instability and plastic flow of soils. I: Experimental observations. *Journal of Engineering mechanics*, 116(11), 2532-2550.
- Lade, P. V., & Yamamuro, J. A. (2011). Evaluation of static liquefaction potential of silty sand slopes. *Canadian Geotechnical Journal*, 48(2), 247-264.
- Lee, S., Lee, S., & Kim, Y. (2003). An approach to estimate unsaturated shear strength using artificial neural network and hyperbolic formulation. *Computers and Geotechnics*, 30(6), 489-503.
- Leong, W., Chu, J., & Teh, C. (2000). Liquefaction and instability of a granular fill material. *Geotechnical Testing Journal*, 23(2).
- Li, X.-S., & Wang, Y. (1998). Linear representation of steady-state line for sand. *Journal of Geotechnical and Geoenvironmental Engineering*, 124(12), 1215-1217.
- Liu, J., Wang, G., Kamai, T., Zhang, F., Yang, J., & Shi, B. (2011). Static liquefaction behavior of saturated fiber-reinforced sand in undrained ring-shear tests. *Geotextiles and Geomembranes*, 29(5), 462-471.
- Lu, J., Modmoltin, C., & Onitsuka, K. (2004). Stabilization effects of surplus soft clay with cement and GBF slag. *Journal of Environmental Sciences*, 16(3), 397-403.
- Luong, M. (1980). *Stress-strain aspects of cohesionless soils under cyclic and transient loading*. Paper presented at the Proc., Int. Symp. on Soils under Cyclic and Transient Loading.
- Maier, H. R., & Dandy, G. C. (2000). Application of Artificial Neural Networks to Forecasting of Surface Water Quality Variables: Issues, Applications and Challenges. In R. S. Govindaraju & A. R. Rao (Eds.), *Artificial Neural Networks in Hydrology* (pp. 287-309). Dordrecht: Springer Netherlands.

- Matsuda, H., Shinozaki, H., Ishikura, R., & Kitayama, N. (2008). *Application of granulated blast furnace slag to the earthquake resistant earth structure as a geo-material*. Paper presented at the Proceedings of the 14th World Conference on Earthquake Engineering Beijing, China.
- Mitchell, J. K. (1976). *Fundamentals of soil behavior*. New York: New York : Wiley.
- Miura, S., & Toki, S. (1982). A sample preparation method and its effect on static and cyclic deformation-strength properties of sand. *Soils and foundations*, 22(1), 61-77.
- Miura, S., Yagi, K., & Kawamura, S. (1995). Liquefaction damage of sandy and volcanic grounds in the 1993 Hokkaido Nansei-Oki earthquake.
- Mogami, T., & Kubu, K. (1953). *The behavior of soil during vibration*. Paper presented at the 3rd international conference on Soil Mechanics and Foundation Engineering Zurich.
- Mohamad, R., & Dobry, R. (1986). Undrained Monotonic and Cyclic Triaxial Strength of Sand. *Journal of Geotechnical engineering*, 112(10), 941-958. doi:10.1061/(ASCE)0733-9410(1986)112:10(941)
- Monkul, M. M., Etmnan, E., & Şenol, A. (2016). Influence of coefficient of uniformity and base sand gradation on static liquefaction of loose sands with silt. *Soil Dynamics and Earthquake Engineering*, 89, 185-197.
- Muduli, P., & Das, S. (2014a). Evaluation of liquefaction potential of soil based on standard penetration test using multi-gene genetic programming model. *Acta Geophysica*, 62(3), 529-543.
- Muduli, P. K., & Das, S. K. (2014b). CPT-based seismic liquefaction potential evaluation using multi-gene genetic programming approach. *Indian Geotechnical Journal*, 44(1), 86-93.
- Muhammad, K. (2012). Case history - based analysis of liquefaction in sloping ground. In S. M. Olson, J. Long, G. Mesri, & E. Tutumluer (Eds.): ProQuest Dissertations Publishing.
- Mulilis, J., Townsend, F., & Horz, R. (1978). Triaxial testing techniques and sand liquefaction. *ASTM STP*, 654, 265-279.
- Mulilis, J. P., Arulanandan, K., Mitchell, J. K., Chan, C. K., & Seed, H. B. (1977). Effects of sample preparation on sand liquefaction. *Journal of the Geotechnical Engineering Division*, 103(2), 91-108.
- Murthy, T., Loukidis, D., Carraro, J., Prezzi, M., & Salgado, R. (2007). Undrained monotonic response of clean and silty sands. *Geotechnique*, 57(3), 273-288.
- Newland, P., & Allely, B. (1959). Volume changes during undrained triaxial tests on saturated dilatant granular materials. *Geotechnique*, 9(4), 174-182.
- Ni, Q., Tan, T., Dasari, G., & Hight, D. (2004). Contribution of fines to the compressive strength of mixed soils. *Geotechnique*, 54(9), 561-569.
- NRC, N. R. C. (1985). *Liquefaction of soils during earthquakes* (Vol. 1): National Academies.
- Odom, I. (1984). Smectite clay minerals: properties and uses. *Philosophical Transactions of the Royal Society of London. Series A, Mathematical and Physical Sciences*, 391-409.
- Olson, S. M. (2001). Liquefaction analysis of level and sloping ground using field case histories and penetration resistance. In T. D. Stark (Ed.): ProQuest Dissertations Publishing.
- Olson, S. M., & Stark, T. D. (2002). Liquefied strength ratio from liquefaction flow failure case histories. *Canadian Geotechnical Journal*, 39(3), 629-647.
- Olson, S. M., & Stark, T. D. (2003). Yield strength ratio and liquefaction analysis of slopes and embankments. *Journal of Geotechnical and Geoenvironmental Engineering*, 129(8), 727-737.
- Olson, S. M., Stark, T. D., Walton, W. H., & Castro, G. (2000). 1907 static liquefaction flow failure of the north dike of Wachusett dam. *Journal of Geotechnical and Geoenvironmental Engineering*, 126(12), 1184-1193.
- Omar, T. (2013). *Specimen size effect on shear behavior of loose sand in triaxial testing*. (Master thesis), Western University, London, Canada.
- Ouf, M. E.-S. A. R. (2001). *Stabilisation of clay subgrade soils using ground granulated blastfurnace slag*. University of Leeds,

- Park, S.-S., Choi, S.-G., & Nam, I.-H. (2014). A Study on Cementation of Sand Using Blast Furnace Slag and Extreme Microorganism. *Journal of the Korean Geotechnical Society*, 30(1), 93-101.
- Park, S.-S., & Jeong, S. W. (2015). Effect of Specimen Size on Undrained and Drained Shear Strength of Sand. *Marine Georesources & Geotechnology*, 33(4), 361-366.
- Perlea, V., Koester, J., & Prakash, S. (1999). *How liquefiable are cohesive soils*. Paper presented at the Proceedings of the 2nd International Conference on Earthquake Geotechnical Engineering.
- Perlea, V. G. (2000). Liquefaction of cohesive soils. In *Soil Dynamics and Liquefaction 2000* (pp. 58-76).
- Pitman, T., Robertson, P., & Segoo, D. (1994). Influence of fines on the collapse of loose sands. *Canadian Geotechnical Journal*, 31(5), 728-739.
- Polito, C. P., & Martin, J. R. (2003). A reconciliation of the effects of non-plastic fines on the liquefaction resistance of sands reported in the literature. *Earthquake Spectra*, 19(3), 635-651.
- Poorooshasb, H. B. (1989). Description of flow of sand using state parameters. *Computers and Geotechnics*, 8(3), 195-218.
- Poulos, S., Castro, G., & France, J. (1988). Closure to discussion: Liquefaction evaluation procedure. *Journal of Geotechnical Engineering, ASCE*, 114(2), 251-259.
- Poulos, S. J. (1981). The steady state of deformation. *Journal of Geotechnical and Geoenvironmental Engineering*, 107(ASCE 16241 Proceeding).
- Poulos, S. J., Castro, G., & France, J. W. (1985). Liquefaction evaluation procedure. *Journal of Geotechnical engineering*, 111(6), 772-792.
- Pradel, D., & Lade, P. V. (1990). Instability and plastic flow of soils. II: Analytical investigation. *Journal of Engineering mechanics*, 116(11), 2551-2566.
- Rabbani, P., Daghigh, Y., Atrechian, M. R., Karimi, M., & Tolooyan, A. (2012). The potential of lime and grand granulated blast furnace slag (GGBFS) mixture for stabilisation of desert silty sands. *Journal of Civil Engineering Research*, 2(6), 108-119.
- Rahman, M. M., Lo, S.-C., & Dafalias, Y. (2014). Modelling the static liquefaction of sand with low-plasticity fines. *Geotechnique*, 64(11), 881-894.
- Rahman, M. M., & Lo, S. (2014). Undrained behavior of sand-fines mixtures and their state parameter. *Journal of Geotechnical and Geoenvironmental Engineering*, 140(7), 04014036.
- Rahman, M. M., Lo, S., & Gnanendran, C. (2008). On equivalent granular void ratio and steady state behaviour of loose sand with fines. *Canadian Geotechnical Journal*, 45(10), 1439-1456.
- Rapti, I. (2016). *Numerical modeling of liquefaction-induced failure of geostuctures subjected to earthquakes*. Université Paris-Saclay-CentraleSupélec,
- Rezania, M., & Javadi, A. A. (2007). A new genetic programming model for predicting settlement of shallow foundations. *Canadian Geotechnical Journal*, 44(12), 1462-1473.
- Riemer, M. F., & Seed, R. B. (1997). Factors affecting apparent position of steady-state line. *Journal of Geotechnical and Geoenvironmental Engineering*, 123(3), 281-288.
- Riemer, M. F., Seed, R. B., Nicholson, P. G., & Jong, H.-L. (1990). Steady state testing of loose sands: limiting minimum density. *Journal of Geotechnical engineering*, 116(2), 332-337.
- Robertson, P. (2004). *Evaluating soil liquefaction and post-earthquake deformations using the CPT*. Paper presented at the Proc. 2nd Int. Conf. on Site Characterization ISC.
- Robertson, P. (2009). Evaluation of flow liquefaction and liquefied strength using the cone penetration test. *Journal of Geotechnical and Geoenvironmental Engineering*, 136(6), 842-853.
- Robertson, P., & Fear, C. (1995). *Liquefaction of sands and its evaluation*. Paper presented at the Proceedings of the 1st International Conference on Earthquake Geotechnical Engineering, Tokyo.

- Roscoe, K., Schofield, A., & Thurairajah, A. (1963). An evaluation of test data for selecting a yield criterion for soils with discussion. *ASTM Special Technical Publications*(361).
- Roscoe, K. H., Schofield, A., & Wroth, C. (1958). On the yielding of soils. *Geotechnique*, 8(1), 22-53.
- Sadrekarimi, A. (2014a). Effect of soil contraction tendency on static liquefaction triggering analysis. *Geotechnique*, 64(4), 325.
- Sadrekarimi, A. (2014b). Effect of the mode of shear on static liquefaction analysis. *Journal of Geotechnical and Geoenvironmental Engineering*, 140(12), 04014069.
- Sadrekarimi, A. (2014c). Static liquefaction-triggering analysis considering soil dilatancy. *Soils and foundations*, 54(5), 955-966.
- Saikia, R., & Chetia, M. (2014). Critical Review on the Parameters Influencing Liquefaction of Soils. *International Journal of Innovative Research in Science, Engineering and Technology*, 3(Special Issue 4), 110-116.
- Salamatpoor, S., & Salamatpoor, S. (2014). Evaluation of Babolsar Sand Behaviour by Using Static Triaxial Tests and Comparison with Case History. *Open Journal of Civil Engineering*, 2014.
- Salem, M., Elmamlouk, H., & Agaiby, S. (2013). Static and cyclic behavior of North Coast calcareous sand in Egypt. *Soil Dynamics and Earthquake Engineering*, 55, 83-91.
- Sasitharan, S., Robertson, P., Sego, D., & Morgenstern, N. (1994). State-boundary surface for very loose sand and its practical implications. *Canadian Geotechnical Journal*, 31(3), 321-334.
- Schofield, A., & Wroth, P. (1968). *Critical state soil mechanics*. London: McGraw-Hill.
- Seed, H. B. (1968). Landslides during earthquakes due to liquefaction. *Journal of Soil Mechanics & Foundations Div.*
- Seed, H. B. (1987). Design problems in soil liquefaction. *Journal of Geotechnical engineering*, 113(8), 827-845.
- Seed, H. B., Idriss, I., & Arango, I. (1983). Evaluation of liquefaction potential using field performance data. *Journal of Geotechnical engineering*, 109(3), 458-482.
- Seed, H. B., & Lee, K. L. (1966). Liquefaction of saturated sands during cyclic loading. *Journal of Soil Mechanics & Foundations Div*, 92(ASCE# 4972 Proceeding).
- Seed, H. B., & Lee, K. L. (1967). Undrained strength characteristics of cohesionless soils. *Journal of Soil Mechanics & Foundations Div.*
- Seed, H. B., Lee, K. L., Idriss, I. M., & Makdisi, F. I. (1975). The slides in the San Fernando dams during the earthquake of February 9, 1971. *Journal of Geotechnical and Geoenvironmental Engineering*, 101(ASCE# 11449 Proceeding).
- Sinha, S. K., & Wang, M. C. (2008). Artificial neural network prediction models for soil compaction and permeability. *Geotechnical and Geological Engineering*, 26(1), 47-64.
- Sivathayalan, S., & Vaid, Y. (2002). Influence of generalized initial state and principal stress rotation on the undrained response of sands. *Canadian Geotechnical Journal*, 39(1), 63-76.
- Sivathayalan, S., & Vaid, Y. (2004). EVALUATION OF STATIC LIQUEFACTION POTENTIAL USING UNDISTURBED SAND SPECIMENS.
- Sladen, J., D'hollander, R., & Krahn, J. (1985). The liquefaction of sands, a collapse surface approach. *Canadian Geotechnical Journal*, 22(4), 564-578.
- Sladen, J., D'Hollander, R., Krahn, J., & Mitchell, D. (1985). Back analysis of the Nerlerk berm liquefaction slides. *Canadian Geotechnical Journal*, 22(4), 579-588.
- Srbulov, M. (2008). *Geotechnical earthquake engineering: simplified analyses with case studies and examples* (Vol. 9): Springer Science & Business Media.
- Stark, T. D., & Mesri, G. (1992). Undrained shear strength of liquefied sands for stability analysis. *Journal of Geotechnical engineering*, 118(11), 1727-1747.
- Stark, T. D., & Olson, S. M. (1995). Liquefaction resistance using CPT and field case histories. *Journal of Geotechnical engineering*, 121(12), 856-869.



- Tang, X., Ma, L., & Shao, Q. (2013). Experimental Investigation on Effect of Bentonite Content to the Liquefaction Potential in Saturated Sand. *Electronic Journal of Geotechnical Engineering*, 18, 1409-1417.
- Tang, X. W., Ma, L., & Dieudonné, S. (2013). *Influence of Bentonite Content on the Static Liquefaction Behavior of Sand*. Paper presented at the Advanced Materials Research.
- Terzaghi, K., & Peck, R. B. (1948). *Soil mechanics in engineering practice*. New York: John Wiley and Sons.
- Thevanayagam, S. (1998). Effect of fines and confining stress on undrained shear strength of silty sands. *Journal of Geotechnical and Geoenvironmental Engineering*, 124(6), 479-491.
- Thevanayagam, S., & Martin, G. R. (2002). Liquefaction in silty soils—screening and remediation issues. *Soil Dynamics and Earthquake Engineering*, 22(9), 1035-1042. doi:[http://dx.doi.org/10.1016/S0267-7261\(02\)00128-8](http://dx.doi.org/10.1016/S0267-7261(02)00128-8)
- Thevanayagam, S., & Mohan, S. (2000). Intergranular state variables and stress-strain behaviour of silty sands. *Geotechnique*, 50(1), 1-23.
- Thevanayagam, S., Ravishankar, K., & Mohan, S. (1996). Steady-state strength, relative density, and fines content relationship for sands. *Transportation Research Record: Journal of the Transportation Research Board*(1547), 61-67.
- Thevanayagam, S., Shenthana, T., Mohan, S., & Liang, J. (2002). Undrained fragility of clean sands, silty sands, and sandy silts. *Journal of Geotechnical and Geoenvironmental Engineering*, 128(10), 849-859.
- Tsuchida, H. (1970). *Prediction and countermeasure against the liquefaction in sand deposits*. Paper presented at the Abstract of the seminar in the Port and Harbor Research Institute.
- Tung, A. T., Wang, Y. Y., & Wong, F. S. (1993). Assessment of liquefaction potential using neural networks. *Soil Dynamics and Earthquake Engineering*, 12(6), 325-335.
- Ural, D. N., & Saka, H. (1998). Liquefaction assessment by neural networks. *Electronic Journal of Geotechnical Engineering*, 3.
- Uthayakumar, M., & Vaid, Y. (1998). Static liquefaction of sands under multiaxial loading. *Canadian Geotechnical Journal*, 35(2), 273-283.
- Vaid, Y., & Chern, J. (1983a). Mechanism of deformation during cyclic undrained loading of saturated sands. *International Journal of Soil Dynamics and Earthquake Engineering*, 2(3), 171-177.
- Vaid, Y., & Chern, J. (1985). *Cyclic and monotonic undrained response of saturated sands*. Paper presented at the Advances in the Art of Testing Soils Under Cyclic Conditions:.
- Vaid, Y., Chung, E., & Kuerbis, R. (1990). Stress path and steady state. *Canadian Geotechnical Journal*, 27(1), 1-7.
- Vaid, Y., & Sivathayalan, S. (2000). Fundamental factors affecting liquefaction susceptibility of sands. *Canadian Geotechnical Journal*, 37(3), 592-606.
- Vaid, Y., & Thomas, J. (1995). Liquefaction and postliquefaction behavior of sand. *Journal of Geotechnical engineering*, 121(2), 163-173.
- Vaid, Y. P., & Chern, J.-C. (1983b). Effect of static shear on resistance to liquefaction. *Soils and foundations*, 23(1), 47-60.
- Vaid, Y. P., Sivathayalan, S., & Stedman, D. (1999). Influence of specimen-reconstituting method on the undrained response of sand.
- Veith, G. (2000). Essay competition: Green, ground and great: soil stabilization with slag. *Building Research & Information*, 28(1), 70-72.
- Verdugo, R., & Ishihara, K. (1996). The steady state of sandy soils. *Soils and foundations*, 36(2), 81-91.
- Wagner, S., Kronberger, G., Beham, A., Kommenda, M., Scheibenpflug, A., Pitzer, E., . . . Dorfer, V. (2014). Architecture and design of the heuristiclab optimization environment. In *Advanced Methods and Applications in Computational Intelligence* (pp. 197-261): Springer.
- Wanatowski, D., & Chu, J. (2007). Static liquefaction of sand in plane strain. *Canadian Geotechnical Journal*, 44(3), 299-313.

- Wang, J., & Rahman, M. S. (1999). A neural network model for liquefaction-induced horizontal ground displacement. *Soil Dynamics and Earthquake Engineering*, 18(8), 555-568.
- Wang, W. (1979). *Some findings in soil liquefaction*: Earthquake Engineering Department, Water Conservancy and Hydroelectric Power Scientific Research Institute.
- Wang, Z.-L., Dafalias, Y. F., Li, X.-S., & Makdisi, F. I. (2002). State pressure index for modeling sand behavior. *Journal of Geotechnical and Geoenvironmental Engineering*, 128(6), 511-519.
- Wei, L., & Yang, J. (2014). On the role of grain shape in static liquefaction of sand–fines mixtures. *Geotechnique*, 64(9), 740-745.
- Wood, F. M., Yamamuro, J. A., & Lade, P. V. (2008). Effect of depositional method on the undrained response of silty sand. *Canadian Geotechnical Journal*, 45(11), 1525-1537.
- Xenaki, V., & Athanasopoulos, G. (2003). Liquefaction resistance of sand–silt mixtures: an experimental investigation of the effect of fines. *Soil Dynamics and Earthquake Engineering*, 23(3), 1-12.
- Xia, H., & Hu, T. (1991). Effects of saturation and back pressure on sand liquefaction. *Journal of Geotechnical engineering*, 117(9), 1347-1362.
- Yadu, L., & Tripathi, R. (2013). Effects of granulated blast furnace slag in the engineering behaviour of stabilized soft soil. *Procedia Engineering*, 51, 125-131.
- Yamamuro, J. A., Abrantes, A. E., & Lade, P. V. (2011). Effect of strain rate on the stress-strain behavior of sand. *Journal of Geotechnical and Geoenvironmental Engineering*, 137(12), 1169-1178.
- Yamamuro, J. A., & Covert, K. M. (2001). Monotonic and cyclic liquefaction of very loose sands with high silt content. *Journal of Geotechnical and Geoenvironmental Engineering*, 127(4), 314-324.
- Yamamuro, J. A., & Lade, P. V. (1997a). Instability of granular materials at high pressures. *Soils and foundations*, 37(1), 41-52.
- Yamamuro, J. A., & Lade, P. V. (1997b). Static liquefaction of very loose sands. *Canadian Geotechnical Journal*, 34(6), 905-917.
- Yamamuro, J. A., & Lade, P. V. (1998). Steady-state concepts and static liquefaction of silty sands. *Journal of Geotechnical and Geoenvironmental Engineering*, 124(9), 868-877.
- Yamamuro, J. A., & Wood, F. M. (2004). Effect of depositional method on the undrained behavior and microstructure of sand with silt. *Soil Dynamics and Earthquake Engineering*, 24(9), 751-760.
- Yamamuro, J. A., Wood, F. M., & Lade, P. V. (2008). Effect of depositional method on the microstructure of silty sand. *Canadian Geotechnical Journal*, 45(11), 1538-1555.
- Yang, J. (2002). Non-uniqueness of flow liquefaction line for loose sand. *GEOTECHNIQUE-LONDON-*, 52(10), 757-760.
- Yang, J., Savidis, S., & Roemer, M. (2004). Evaluating liquefaction strength of partially saturated sand. *Journal of Geotechnical and Geoenvironmental Engineering*, 130(9), 975-979.
- Yang, J., Sze, H., & Heung, M. (2009). *Effect of initial static shear on cyclic behavior of sand*. Paper presented at the Proceedings of the 17th International Conference on Soil Mechanics and Geotechnical Engineering.
- Yang, J., & Wei, L. (2012). Collapse of loose sand with the addition of fines: the role of particle shape. *Geotechnique*, 62(12), 1111-1125.
- Yang, J., & Wei, L. (2015). Static Liquefaction of Granular Soils: The Role of Grain Shape and Size. In *Bifurcation and Degradation of Geomaterials in the New Millennium* (pp. 199-205): Springer.
- Yang, S., Lacasse, S., & Sandven, R. (2006). Determination of the transitional fines content of mixtures of sand and non-plastic fines. *Geotechnical Testing Journal*, 29(2), 102.
- Yang, S., Sandven, R., & Grande, L. (2006). Instability of sand–silt mixtures. *Soil Dynamics and Earthquake Engineering*, 26(2), 183-190.
- Yasuda, S., Wakamatsu, K., & Nagase, H. (1994). *Liquefaction of artificially filled silty sands*. Paper presented at the Ground Failures under Seismic Conditions.

- Yi, Y., Liska, M., & Al-Tabbaa, A. (2014). Properties of two model soils stabilized with different blends and contents of GGBS, MgO, lime, and PC. *Journal of Materials in Civil Engineering*, 26(2), 267-274.
- Yoshimine, M., & Ishihara, K. (1998). Flow potential of sand during liquefaction. *Soils and foundations*, 38(3), 189-198.
- Yoshimine, M., Robertson, P., & Wride, C. (1999). Undrained shear strength of clean sands to trigger flow liquefaction. *Canadian Geotechnical Journal*, 36(5), 891-906.
- Youd, T., Harp, E., Keefer, D., & Wilson, R. (1985). The Borah Peak, Idaho earthquake of October 28, 1983—liquefaction. *Earthquake Spectra*, 2(1), 71-89.
- Young-Su, K., & Byung-Tak, K. (2006). Use of artificial neural networks in the prediction of liquefaction resistance of sands. *Journal of Geotechnical and Geoenvironmental Engineering*, 132(11), 1502-1504.
- Zlatovic, S., & Ishihara, K. (1997). Normalized behavior of very loose non-plastic soils: Effects of fabric. *Soils and foundations*, 37(4), 47-56.
- Zlatović, S., & Ishihara, K. (1995). *On the influence of nonplastic fines on residual strength*. Paper presented at the First International Conference on Earthquake Geotechnical Engineering.

Every reasonable effort has been made to acknowledge the owner of the copyright material. I would be pleased to hear from any copyright owner who has been omitted or incorrectly acknowledged.

# Appendix



Available online at [www.sciencedirect.com](http://www.sciencedirect.com)

ScienceDirect

Soils and Foundations 57 (2017) 341–356



[www.elsevier.com/locate/sandf](http://www.elsevier.com/locate/sandf)

## Static liquefaction of very loose sand–slag–bentonite mixtures

Ayad Salih Sabbar, Amin Chegenizadeh\*, Hamid Nikraz

*Department of Civil Engineering, Curtin University, Perth, Australia*

Received 18 April 2016; received in revised form 22 December 2016; accepted 25 January 2017  
Available online 17 May 2017

### Abstract

Static liquefaction is a highly destructive mechanism in the failure of soil deposits caused by a sudden loss of effective stress accompanied by vast deformations and a rapid build-up of pore water pressure that can cause soils to behave like liquids. This study examined liquefaction phenomena in saturated clean Perth sand, sand containing 3% bentonite, sand containing slag (2%, 4%, and 6%), and sand containing both 3% bentonite and slag (2%, 4%, and 6%). Undrained static triaxial compression tests were implemented on very loose mixtures at three initial confining pressures (100, 150, and 200 kPa). Static liquefaction (zero deviatoric stress and zero effective confining pressure) was observed at the lowest relative density and the lowest confining pressure. The liquefaction potential of the clean sand and the sand mixtures decreased with increases in confining pressure and relative density. The slag reduced the liquefaction susceptibility by reducing the inter-particle voids and producing a stable fabric. The optimum slag content was found to be 4%. Mixing clean sand with 3% bentonite produced a vulnerable fabric which exhibited high compressibility and a high level of excess pore water pressure. All sand–slag–bentonite mixtures showed non-flow behaviour and low excess pore water pressure. The mixture of sand with 4% slag and 3% bentonite exhibited the highest effective stress and the lowest excess pore pressure. It was revealed that the normalisation between the maximum and the minimum deviatoric stresses, namely, the brittleness index, can be used to quantify the liquefaction potential of clean sand and sand–slag–bentonite mixtures.

© 2017 Production and hosting by Elsevier B.V. on behalf of The Japanese Geotechnical Society. This is an open access article under the CC BY-NC-ND license (<http://creativecommons.org/licenses/by-nc-nd/4.0/>).

**Keywords:** Clean sand; Slag; Bentonite; Static liquefaction; Limited liquefaction; Non-flow behaviour; Brittleness index

### 1. Introduction

Liquefaction is one of the most complicated and debated topics in geotechnical engineering because it is used to define various contrasting, but related, phenomena (Kramer, 1996). Liquefaction has been widely studied, and researchers have devised a common definition for it. Liquefaction is a phenomenon involving a significant reduction in effective stress; it is accompanied by excessive strain and a build-up of pore water pressure when saturated soils are subjected to undrained static or cyclic loading (Castro, 1969; El Mohtar et al., 2013; Hird and Hassona, 1990;

Jafarian et al., 2013; Kramer, 1996; NRC, 1985; Vaid and Sivathayalan, 2000; Verdugo and Ishihara, 1996; Yamamuro and Lade, 1997). The criteria for liquefaction failure can be divided into two main groups depending on the type of loading: flow liquefaction and cyclic mobility (Kramer, 1996; NRC, 1985). Flow liquefaction may occur when the static shear stresses applied to a soil are greater than the shear strength of the soil in its liquefied state (Kramer, 1996; NRC, 1985). Cyclic mobility may occur during cyclic loading; however, it is not considered here. Flow liquefaction produces the most devastating effects of all liquefaction types, and massive instabilities are termed ‘flow failures’ (Kramer, 1996; NRC, 1985). The flow failure mechanism requires a triggering method to initiate the liquefaction and undrained strain-softening (Sadrekarimi, 2014). Liquefaction flow failures have been

Peer review under responsibility of The Japanese Geotechnical Society.

\* Corresponding author.

*E-mail address:* [amin.chezenizadeh@curtin.edu.au](mailto:amin.chezenizadeh@curtin.edu.au) (A. Chegenizadeh).

<http://dx.doi.org/10.1016/j.sandf.2017.05.003>

0038-0806/© 2017 Production and hosting by Elsevier B.V. on behalf of The Japanese Geotechnical Society.

This is an open access article under the CC BY-NC-ND license (<http://creativecommons.org/licenses/by-nc-nd/4.0/>).

## Prediction of Liquefaction Susceptibility of Clean Sandy Soils Using Artificial Intelligence Techniques

Ayad Salih Sabbar<sup>1</sup> · Amin Chegenizadeh<sup>1</sup> · Hamid Nikraz<sup>1</sup>

Received: 14 March 2017 / Accepted: 2 November 2017  
© Indian Geotechnical Society 2017

**Abstract** The liquefaction susceptibility of sandy soil is generally characterised by some parameters in the static liquefaction potential evaluation. These parameters are usually measured by static laboratory tests on distributed and undistributed samples under different test conditions. This study performs the ANN and genetic programming to estimate the static liquefaction susceptibility of clean sand soils based on experimental results to predict and develop an equation for the ratio of  $q_{min}/q_{peak}$  which is considered as the static liquefaction criterion. The  $q_{min}/q_{peak}$  model is a function of the minimum and maximum void ratios, relative density, initial effective confining pressure, and some other parameters. The findings of this study demonstrated that a good agreement between ANN and symbolic regression in predicting the ratio of  $q_{min}/q_{peak}$  based on laboratory tests. The possible application of the proposed  $q_{min}/q_{peak}$  equation is restricted by some limitations. The outcomes of the present work can be used in the preliminary liquefaction assessment of clean sandy soils prior to the complementary experimental studies.

**Keywords** Static liquefaction · ANN · Symbolic regression · Genetic programming ·  $q_{min}/q_{peak}$

### Abbreviations

AI	Artificial intelligent
ANN	Artificial neural network
B	Skempton's coefficient
$C_u$	Uniformity coefficient

✉ Amin Chegenizadeh  
amin.chegenizadeh@curtin.edu.au

<sup>1</sup> Department of Civil Engineering, Curtin University, Perth, Australia

CPT	Cone Penetration Test
$D_r$	Relative density
$D_{50}$	Mean grains size
$e_{max}$	Maximum void ratio
$e_{min}$	Minimum void ratio
$e$	Void ratio
GP	Genetic programming
MGGP	Multi-Gene Genetic Programming
$I$	Number of input variables
$q_{min}$	Minimum deviatoric stress
$q_{peak}$	Initial peak deviatoric stress
RMSE	Root mean square error
$R^2$	Coefficient of determination
SPT	Standard Penetration Test
$\alpha$	The ratio of initial shear stresses to the initial effective confining pressure
$\sigma'_{3c}$	Initial effective confining pressure
$\sigma_1$	Axial stress
$\sigma_{3c}$	Confining pressure

### Introduction

When saturated cohesionless soils were subjected to the undrained static or cyclic loading, the pore water pressure developed abruptly, and the effective stress reduced dramatically leading to a loss in shear strength or liquefaction [1–5]. The static liquefaction has been considered one of the biggest disastrous failure mechanisms in saturated sandy soils because when it occurs, the resistance of the soil reduces, and the ability of a soil layer to sustain many of geotechnical applications such as foundations of buildings and bridges, earth dams, slopes, and embankments is

# A REVIEW OF THE EXPERIMENTAL STUDIES OF THE CYCLIC BEHAVIOUR OF GRANULAR MATERIALS: GEOTECHNICAL AND PAVEMENT ENGINEERING

Ayad Salih Sabbar<sup>1</sup>, Amin Chegenizadeh<sup>2</sup> and Hamid Nikraz<sup>3</sup>

<sup>1</sup>PhD candidate of the Department of Civil Engineering, Curtin University, Perth, Australia

<sup>2</sup>Researcher at the Department of Civil Engineering, Curtin University, Perth, Australia,

Corresponding author: [amin.chegenizadeh@curtin.edu.au](mailto:amin.chegenizadeh@curtin.edu.au)

<sup>3</sup>Professor at the Department of Civil Engineering, Curtin University, Perth, Australia

## ABSTRACT

The cyclic behaviour of granular materials has become a critical issue in many civil engineering applications, especially in seismic hazard areas, offshore projects and pavements. Cyclic loading has a detrimental effect on the soil layers under foundations of buildings because it can generate unacceptable deformations and excess pore water pressure in these soil layers. This paper presents the results of research on the behaviour of granular materials under cyclic loading in geotechnical engineering. The cyclic behaviour of granular materials is investigated by using different testing devices as well as various testing conditions. Also, this paper provides a comparison between the response of granular materials in geotechnical aspect under cyclic and monotonic loadings. Moreover, the influence of factors such as drainage conditions, sample preparation method, confining pressure, relative density, frequency, loading type, and stress level on the cyclic behaviour of granular materials was reviewed.

**Keywords:** Sand, cyclic loading, liquefaction, cyclic strength, cyclic resistance, cyclic behaviour.

## 1 INTRODUCTION

Cyclic loading has become crucial for the design of building foundations due to many structures being located in offshore or seismic activity zones (Andersen, 2009). The term cyclic loading is defined as a system of repeated loads that shows a constancy rate in amplitude and frequency (Andersen & Lawitzsen, 1988; Das & Ramana, 2010; O'Reilly & Brown 1991; Presti *et al.* 1997). Cyclic loading can be generated from environmental or anthropogenic origins. There are many types of environmental cyclic loadings such as seasons, waves, tide, currents, the wind, earthquakes and ice sheets. Anthropogenic cyclic loading can occur from traffic, blasting operations and plant operations or rotating machinery (Shajarati *et al.*, 2012). Peralta (2010) classified soil cyclic loadings according to the frequency; the frequency of cyclic loading is 0-1 Hz, whereas the frequency of dynamic loading is more than 10 Hz. There are three types of cyclic loading that can affect soil elements: symmetrical (two-ways), non-symmetrical with reversal loading (two-ways), and non-symmetrical without reversal loading (one-way). Initial static shear stress plays a considerable role in the classification of the above three types of cyclic loading. Symmetrical loading is presented as a case where no initial static shear takes action on level planes of elements of soil, in other words, in level ground conditions. However, in many cases soil elements are subjected to initial static shear on the horizontal level before cyclic loading is applied, such as in embankments, slopes, or earth dams (Yang & Sze, 2011). Two parameters could be used to evaluate cyclic stresses in soil elements. The first is cyclic stress ratio (CSR), which is defined as the ratio of the applied cyclic stresses to the initial confining pressure. The second parameter is the cyclic resistance ratio (CRR), which is defined as the ability of soil to resist the cyclic loading. Different methods were used to define the failure caused by cyclic loading. Salem, Elmamlouk and Agaiby (2013) defined the failure as the number of loading cycles required to reach liquefaction or an axial strain of 5% in double amplitude. Andersen (2009) argued that the failure caused by cyclic loading is at 15% of permanent shear strain, or 15% cyclic shear strain. A considerable amount of literature has been published on the cyclic behaviour of sand soil and the factors affecting it. These studies have examined the strength of sandy soil under cyclic loading by using different materials and techniques, and it was found that cyclic loading had a detrimental effect on sand soil, and the strength of sand under cyclic loading was less than under monotonic loading with the same stress amplitude. Cyclic loading generates excessive deformations in soil elements, and these strains accumulate with increasing number of cycles, causing damage to building foundations due to differential settlement of the ground underneath (Erken & Ulker, 2007; Lombardi *et al.*, 2014; Nguyen, Francois & Degrande, 2014; Shajarati *et al.*, 2012; Wichtmann, Niemann & Triantafyllidis, 2005). Recent evidence shows that the type of soil plays a significant role in soil response under cyclic loading and that deformation of sandy soil under cyclic loading was much more rapid than for clay soil. In addition, a number of studies have found that the cyclic behaviour of sand soils is influenced by factors such as drainage conditions, confining pressure, frequency, stress level, load types and relative density (Cabalar, Dulundu & Tuncay, 2013; Flora, Lirer & Silvestri, 2012; Katzenbach & Festag, 2004; Sitharam, Raju & Murthy, 2004; Sze & Yang, 2014).

# Effect of Slag and Bentonite on Shear Strength Parameters of Sandy Soil

Ayad Salih Sabbar <sup>a</sup>, Amin Chegenizadeh <sup>\*</sup>, Hamid Nikraz <sup>b</sup>

*Department of Civil Engineering, Faculty of Science and Engineering, Curtin University, Australia*

(Received , Revised , Accepted )

**Abstract.** A series of direct shear tests were implemented on three different types of specimens (i.e. clean Perth sand, sand containing 10, 20 and 30% bentonite, sand containing 1, 3 and 5% slag, and sand containing 10, 20 and 30% bentonite with increasing percentages of added slag (1%, 3% and 5%). This paper focuses on the shear stress characteristics of clean sand and sand mixtures. The samples were tested under different three normal stresses (100, 150 and 200 kPa) and three curing periods of no curing time, 7 and 14 days. It was observed that the shear stresses of clean sand and mixtures were increased with increasing normal stresses. In addition, the use of slag has improved the shear strength of the sand-slag mixtures; the shear stresses rose from 128.642 kPa in the clean sand at normal stress of 200 kPa to 146.89 kPa, 154 kPa and 161.14 kPa when sand was mixed with 1%, 3% and 5% slag respectively and tested at the same normal stress. Internal friction angle increased from 32.74° in the clean sand to 34.87°, 37.12° and 39.4° when sand was mixed with 1%, 3% and 5% slag respectively and tested at 100, 150, and 200 kPa normal stresses. The cohesion of sand-bentonite mixtures increased from 3.34 kPa in 10% bentonite to 22.9 kPa, 70.6 kPa when sand was mixed with 20% and 30% bentonite respectively. All the mixtures of clean sand, different bentonite and slag contents showed different behaviour; some mixtures exhibited shear stress more than clean sand whereas others showed less than clean sand. The internal friction angle increased, and cohesion decreased with increasing curing time.]

**Keywords:** sand; bentonite; slag; shear strength; shear strength parameters; direct shear test

## 1. Introduction:

Shear strength of soil is one of the essential factors to be considered in analysing and designing many of geotechnical applications such as shallow foundations, roads, embankments, earth dams and slopes (Das and Sobhan 2014). Cohesion and internal friction angle are the major parameters used to assess the shear strength of soil (Budhu 2010). There are various apparatuses which can be used to determine the shear strength parameters such as the direct shear box, ring shear, laboratory vane, cone penetrometer, triaxial apparatus and plain strain device. Sandy soil covers broad areas around the globe, and it has many properties which may create problems during construction such as variation in density and strength in various positions, high permeability that increase the possibility of failure, low bearing capacity, and high ground water level (Shooshpasha and Shirvani 2015). Numerous studies have investigated the effects of mixing sandy soil with additives such as cement, lime, fly ash, bitumen, and clay or mixtures of these additives on shear strength parameters.

\* Corresponding author, Research Fellow, E-mail: [Amin.Chegenizadeh@curtin.edu.au](mailto:Amin.Chegenizadeh@curtin.edu.au)

a Ph.D. Candidate, E-mail: [ayadsaleh2000@yahoo.com](mailto:ayadsaleh2000@yahoo.com)

b Professor, E-mail: [H.Nikraz@curtin.edu.au](mailto:H.Nikraz@curtin.edu.au)

# Effect of Fines on Liquefaction Susceptibility of Sandy Soil

Ayad Salih Sabbar, Amin Chegenizadeh, Hamid Nikraz

**Abstract**—Investigation of liquefaction susceptibility of materials that have been used in embankments, slopes, dams, and foundations is very essential. Many catastrophic geo-hazards such as flow slides, declination of foundations, and damage to earth structure are associated with static liquefaction that may occur during abrupt shearing of these materials. Many artificial backfill materials are mixtures of sand with fines and other composition. In order to provide some clarifications and evaluations on the role of fines in static liquefaction behaviour of sand sandy soils, the effect of fines on the liquefaction susceptibility of sand was experimentally examined in the present work over a range of fines content, relative density, and initial confining pressure. The results of an experimental study on various sand-fines mixtures are presented. Undrained static triaxial compression tests were conducted on saturated Perth sand containing 5% bentonite at three different relative densities (10, 50, and 90%), and saturated Perth sand containing both 5% bentonite and slag (2%, 4%, and 6%) at single relative density 10%. Undrained static triaxial tests were performed at three different initial confining pressures (100, 150, and 200 kPa). The brittleness index was used to quantify the liquefaction potential of sand-bentonite-slag mixtures. The results demonstrated that the liquefaction susceptibility of sand-5% bentonite mixture was more than liquefaction susceptibility of clean sandy soil. However, liquefaction potential decreased when both of two fines (bentonite and slag) were used. Liquefaction susceptibility of all mixtures decreased with increasing relative density and initial confining pressure.

**Keywords**—Bentonite, brittleness index, liquefaction, slag.

## I. INTRODUCTION

TERM liquefaction includes all situations involving sudden losses in soil strength; it is accompanied by rapid development in pore water pressure and large deformation when saturated soil are subjected to undrained monotonic or cyclic loadings [1]-[7]. The sudden increment of pore water pressure is related to loss the contact between soil particles during shearing. The sand-water mixture behaves as a viscous liquid under loading, which able to rise through soil mass [1]. Depending on loading type the failure criteria for liquefaction can be divided into two types: flow failure and cyclic mobility [5], [6]. Under static loading, the failure criterion is known as flow liquefaction. However, it is recognised as cyclic mobility under cyclic loading. Cyclic mobility is out of the scope of the present study. There are many catastrophic geo-hazards associated with static liquefaction such as flow slides,

declination of foundations, damage to earth structure, and disruption of services [8]. These hazards make the investigation of liquefaction susceptibility of embankments, slopes, dams, and foundations materials very essential. There are many examples of flow slides triggered by static liquefaction such as failures of slopes at Sau Mau Ping in Hong Kong on August 25, 1976, and Shenzhen in China on September 18, 2002. A significant amount of literature has been published on liquefaction behaviour of sandy soils. These studies reported that flow liquefaction of clean sandy soils is profoundly affected by many factors such as initial state (i.e., relative density and initial confining pressure), stress mode, sample preparation method, the degree of saturation, compositional characteristics, and fines content [4], [7], [9]-[15]. However, several experimental investigations have reported that the impact of fines on static liquefaction behaviour of sandy soils is located in the area of considerable controversy and uncertainty. The complexity of this matter is related to the nature of sand and fines, both of them are granular materials, and they individually interact with each other during loading. Some studies have found that the presences of fines reduced the liquefaction susceptibility of sandy soils [16], [17]. In contrast, [18]-[20] stated that the presence of fines increased the compressibility of sand-fine mixtures by reducing the contact between sand particles. Consequently, the liquefaction susceptibility was increased. Other studies proposed a threshold around which is the percentage of fines content has positive or negative impacts [21]-[23]. Liquefaction susceptibility of granular materials has been extensively investigated by experimental, theoretical, and empirical methods, few geological studies and field observations have been reported in the literature [4], [7], [11], [14]. Many parameters have been proposed in previous studies to evaluate the liquefaction susceptibility of soil such as state parameter, relative contractiveness and stress ratio (minimum deviator stress to initial peak deviator stress). Sadrekarimi [14] used the brittleness index,  $I_B$  which proposed by Bishop [24] to characterize the amount of reduction in undrained shear strength during liquefaction. The undrained brittleness index,  $I_B$ , can be expressed by:

$$I_B = \frac{q_{peak} - q_{min}}{q_{peak}} \quad (1)$$

where  $q_{peak}$  = peak deviator stress and  $q_{min}$  = minimum deviator stress.

The values of  $I_B$  are in the range 0-1, and non-flow or non-brittle behaviour (where a non-strength decline occurs during undrained static shear) is observed when  $I_B = 0$ . However,

Ayad Salih Sabbar is Ph.D. candidate of the Department of Civil Engineering, Curtin University, Perth, Australia (phone: +61424673252; e-mail: Ayad.sabbar2000@yahoo.com).

Amin Chegenizadeh is Lecturer and Hamid Nikraz is Professor at the Department of Civil Engineering, Curtin University, Perth, Australia (e-mail: Amin.Chegenizadeh@curtin.edu.au, H.Nikraz@curtin.edu.au).



## Experimental Investigation on the Shear Strength Parameters of Sand-Slag Mixtures

Ayad Salih Sabbar, Amin Chegenizadeh, Hamid Nikraz

**Abstract**—Utilizing waste materials in civil engineering applications has a positive influence on the environment by reducing carbon dioxide emissions and issues associated with waste disposal. Granulated blast furnace slag (GBFS) is a by-product of the iron and steel industry, with millions of tons of slag being annually produced worldwide. Slag has been widely used in structural engineering and for stabilizing clay soils; however, studies on the effect of slag on sandy soils are scarce. This article investigates the effect of slag content on shear strength parameters through direct shear tests and unconsolidated undrained triaxial tests on mixtures of Perth sand and slag. For this purpose, sand-slag mixtures, with slag contents of 2%, 4%, and 6% by weight of samples, were tested with direct shear tests under three normal stress values, namely 100 kPa, 150 kPa, and 200 kPa. Unconsolidated undrained triaxial tests were performed under a single confining pressure of 100 kPa and relative density of 80%. The internal friction angles and shear stresses of the mixtures were determined via the direct shear tests, demonstrating that shear stresses increased with increasing normal stress and the internal friction angles and cohesion increased with increasing slag. There were no significant differences in shear stresses parameters when slag content rose from 4% to 6%. The unconsolidated undrained triaxial tests demonstrated that shear strength increased with increasing slag content.

**Keywords**—Direct shear, shear strength, slag, UU test.

### I. INTRODUCTION

SHEAR strength is one of the most important soil characteristics required for analysing and designing geotechnical applications, such as foundations, slopes, embankments and retaining walls [1]. Shear strength refers to the maximum stress that a soil can withstand before reaching failure conditions [2]. In granular soils, shear strength is a combined effect of friction and interlocking forces between soil grains. Conversely, in fine soils, the shear strength is produced from soil particles cementing together, or in other words, their cohesion. Shear strength characteristics, for instance the internal friction angle and cohesion, have been extensively investigated by the implementation of both in situ and laboratory tests, such as the direct shear box, ring shear, cone penetrometer and triaxial apparatus. Variations in strength and density, low bearing capacity and high permeability are negative properties of sandy soils which can cause problems for construction [3]. Numerous studies have researched methods to reduce the negative properties of sandy

soil by mixing it with additives such as cement, lime, clay, and fly ash. There has been recent interest globally in the use of slag in different civil engineering applications, due to the environmental and economic advantages. Using Slag has a positive influence on the environment, as it reduces carbon dioxide emissions and other issues associated with waste disposal; most countries in the world, including Australia, are manufacturing millions of tons of slag annually [4], [5]. The production of one ton of Portland cement generates 0.95 tons of CO<sub>2</sub>; however, production of the same amount of slag produces 0.07 tons of CO<sub>2</sub> [6]. Additionally, using slag in construction engineering may reduce the cost of building and conserve resources. Slag is a by-product of the iron and steel industries which can be classified into different types based on the production method used. Blast furnace slag is a by-product of iron made in a blast furnace, which can be divided into three categories (those being air-cooled, granulated, and expanded slag). Slag has been widely utilized in structural engineering, but has more recent application in geotechnical engineering [6], [7]. According to the Australian Slag Association [8], 80% of the 3.4 million tons of slag which was produced in Australia in 2009 was used in the construction of buildings and roads. In geotechnical engineering, slag has been utilized widely for improving the properties of clay soils, but published research on the use of slag (without other additives) for improving sandy soils is limited. Slag reacts to water contact in the same way as Portland cement; however, it takes a long time to complete its chemical reaction, which is why it is sometimes blended with a chemical activator [9]. According to [10], the geotechnical characteristics of GBFS, such as a high internal friction angle, light weight, and high permeability, make it useful for the backfilling of quay-wells, sand mats, and lightweight embankments. Many researchers have found that the shear strength of slag-stabilized sand was increased by using a chemical activator with the slag [6], [11], [12]. The present study was recently started by the authors in collaboration with an investigation into the effects of slag content on the shear strength characteristics of sandy soils. The aim was to examine the possibility of improving the shear strength of sandy soils by using waste materials, such as slag. It is apparent from the literature review that numerous investigations have been conducted on the effects of slag contents on clay soils, while research into the effect of slag on the shear strength of sandy soils is limited. Therefore, this study aimed to explore the properties of clean sand compared to sand mixed with various slag contents (2%, 4%, and 6%, by weight), using direct shear tests and unconsolidated undrained triaxial tests. Additionally, this work is a part of ongoing

Ayad Salih Sabbar is Ph.D. candidate at the Department of Civil Engineering, Curtin University, Perth, Australia (phone: +61424673252; e-mail: Ayadsalih.sabbar@postgrad.curtin.edu.au).

Amin Chegenizadeh, Researcher, and Hamid Nikraz, Professor, are with the Department of Civil Engineering, Curtin University, Perth, Australia (e-mail: Amin.Chegenizadeh@curtin.edu.au, H.Nikraz@curtin.edu.au).

# Experimental Investigation on the Shear Strength Parameters of Sand-Slag Mixtures

Ayad Salih Sabbar, Amin Chegenizadeh, Hamid Nikraz

**Abstract**—Utilizing waste materials in civil engineering applications has a positive influence on the environment by reducing carbon dioxide emissions and issues associated with waste disposal. Granulated blast furnace slag (GBFS) is a by-product of the iron and steel industry, with millions of tons of slag being annually produced worldwide. Slag has been widely used in structural engineering and for stabilizing clay soils; however, studies on the effect of slag on sandy soils are scarce. This article investigates the effect of slag content on shear strength parameters through direct shear tests and unconsolidated undrained triaxial tests on mixtures of Perth sand and slag. For this purpose, sand-slag mixtures, with slag contents of 2%, 4%, and 6% by weight of samples, were tested with direct shear tests under three normal stress values, namely 100 kPa, 150 kPa, and 200 kPa. Unconsolidated undrained triaxial tests were performed under a single confining pressure of 100 kPa and relative density of 80%. The internal friction angles and shear stresses of the mixtures were determined via the direct shear tests, demonstrating that shear stresses increased with increasing normal stress and the internal friction angles and cohesion increased with increasing slag. There were no significant differences in shear stresses parameters when slag content rose from 4% to 6%. The unconsolidated undrained triaxial tests demonstrated that shear strength increased with increasing slag content.

**Keywords**—Direct shear, shear strength, slag, UU test.

## I. INTRODUCTION

**S**HEAR strength is one of the most important soil characteristics required for analysing and designing geotechnical applications, such as foundations, slopes, embankments and retaining walls [1]. Shear strength refers to the maximum stress that a soil can withstand before reaching failure conditions [2]. In granular soils, shear strength is a combined effect of friction and interlocking forces between soil grains. Conversely, in fine soils, the shear strength is produced from soil particles cementing together, or in other words, their cohesion. Shear strength characteristics, for instance the internal friction angle and cohesion, have been extensively investigated by the implementation of both in situ and laboratory tests, such as the direct shear box, ring shear, cone penetrometer and triaxial apparatus. Variations in strength and density, low bearing capacity and high permeability are negative properties of sandy soils which can cause problems for construction [3]. Numerous studies have researched methods to reduce the negative properties of sandy

soil by mixing it with additives such as cement, lime, clay, and fly ash. There has been recent interest globally in the use of slag in different civil engineering applications, due to the environmental and economic advantages. Using Slag has a positive influence on the environment, as it reduces carbon dioxide emissions and other issues associated with waste disposal; most countries in the world, including Australia, are manufacturing millions of tons of slag annually [4], [5]. The production of one ton of Portland cement generates 0.95 tons of CO<sub>2</sub>; however, production of the same amount of slag produces 0.07 tons of CO<sub>2</sub> [6]. Additionally, using slag in construction engineering may reduce the cost of building and conserve resources. Slag is a by-product of the iron and steel industries which can be classified into different types based on the production method used. Blast furnace slag is a by-product of iron made in a blast furnace, which can be divided into three categories (those being air-cooled, granulated, and expanded slag). Slag has been widely utilized in structural engineering, but has more recent application in geotechnical engineering [6], [7]. According to the Australian Slag Association [8], 80% of the 3.4 million tons of slag which was produced in Australia in 2009 was used in the construction of buildings and roads. In geotechnical engineering, slag has been utilized widely for improving the properties of clay soils, but published research on the use of slag (without other additives) for improving sandy soils is limited. Slag reacts to water contact in the same way as Portland cement however, it takes a long time to complete its chemical reaction, which is why it is sometimes blended with a chemical activator [9]. According to [10], the geotechnical characteristics of GBFS, such as a high internal friction angle, light weight, and high permeability, make it useful for the backfilling of quay-wells, sand mats, and lightweight embankments. Many researchers have found that the shear strength of slag-stabilized sand was increased by using a chemical activator with the slag [6], [11], [12]. The present study was recently started by the authors in collaboration with an investigation into the effects of slag content on the shear strength characteristics of sandy soils. The aim was to examine the possibility of improving the shear strength of sandy soils by using waste materials, such as slag. It is apparent from the literature review that numerous investigations have been conducted on the effects of slag contents on clay soils, while research into the effect of slag on the shear strength of sandy soils is limited. Therefore, this study aimed to explore the properties of clean sand compared to sand mixed with various slag contents (2%, 4%, and 6%, by weight), using direct shear tests and unconsolidated undrained triaxial tests. Additionally, this work is a part of ongoing

Ayad Salih Sabbar is Ph.D. candidate at the Department of Civil Engineering, Curtin University, Perth, Australia (phone: +61424673252; e-mail: Ayadsalih.sabbar@postgrad.curtin.edu.au).

Amin Chegenizadeh, Researcher, and Hamid Nikraz, Professor, are with the Department of Civil Engineering, Curtin University, Perth, Australia (e-mail: Amin.Chegenizadeh@curtin.edu.au, H.Nikraz@curtin.edu.au).

# Effect of Fines on Liquefaction Susceptibility of Sandy Soil

Ayad Salih Sabbar, Amin Chegenizadeh, Hamid Nikraz

**Abstract**—Investigation of liquefaction susceptibility of materials that have been used in embankments, slopes, dams, and foundations is very essential. Many catastrophic geo-hazards such as flow slides, declination of foundations, and damage to earth structure are associated with static liquefaction that may occur during abrupt shearing of these materials. Many artificial backfill materials are mixtures of sand with fines and other composition. In order to provide some clarifications and evaluations on the role of fines in static liquefaction behaviour of sand sandy soils, the effect of fines on the liquefaction susceptibility of sand was experimentally examined in the present work over a range of fines content, relative density, and initial confining pressure. The results of an experimental study on various sand-fines mixtures are presented. Undrained static triaxial compression tests were conducted on saturated Perth sand containing 5% bentonite at three different relative densities (10, 50, and 90%), and saturated Perth sand containing both 5% bentonite and slag (2%, 4%, and 6%) at single relative density 10%. Undrained static triaxial tests were performed at three different initial confining pressures (100, 150, and 200 kPa). The brittleness index was used to quantify the liquefaction potential of sand-bentonite-slag mixtures. The results demonstrated that the liquefaction susceptibility of sand-5% bentonite mixture was more than liquefaction susceptibility of clean sandy soil. However, liquefaction potential decreased when both of two fines (bentonite and slag) were used. Liquefaction susceptibility of all mixtures decreased with increasing relative density and initial confining pressure.

**Keywords**—Bentonite, brittleness index, liquefaction, slag.

## I. INTRODUCTION

TERM liquefaction includes all situations involving sudden losses in soil strength; it is accompanied by rapid development in pore water pressure and large deformation when saturated soil are subjected to undrained monotonic or cyclic loadings [1-7]. The sudden increment of pore water pressure is related to loss the contact between soil particles during shearing. The sand-water mixture behaves as a viscous liquid under loading, which able to rise through soil mass [1]. Depending on loading type the failure criteria for liquefaction can be divided into two types: flow failure and cyclic mobility [5, 6]. Under static loading, the failure criterion is known as flow liquefaction. However, it is recognized as cyclic mobility under cyclic loading. Cyclic mobility is out of the scope of the present study. There are many catastrophic geo-hazards associated with static liquefaction such as flow slides, declination of foundations, damage to earth structure, and disruption of services [8]. These hazards make the investigation of liquefaction

susceptibility of embankments, slopes, dams, and foundations materials very essential. There are many examples of flow slides triggered by static liquefaction such as failures of slopes at Sau Mau Ping in Hong Kong on August 25, 1976, and Shenzhen in China on September 18, 2002. A significant amount of literature has been published on liquefaction behaviour of sandy soils. These studies reported that flow liquefaction of clean sandy soils is profoundly affected by many factors such as initial state (i.e., relative density and initial confining pressure), stress mode, sample preparation method, the degree of saturation, compositional characteristics, and fines content [4, 7, 9-15]. However, several experimental investigations have reported that the impact of fines on static liquefaction behaviour of sandy soils is located in the area of considerable controversy and uncertainty. The complexity of this matter is related to the nature of sand and fines, both of them are granular materials, and they individually interact with each other during loading. Some studies have found that the presences of fines reduced the liquefaction susceptibility of sandy soils [16, 17]. In contrast, Rahman and Lo [18], Thevanayagam and Martin [19], Yang et al. [20] stated that the presence of fines increased the compressibility of sand-fine mixtures by reducing the contact between sand particles. Consequently, the liquefaction susceptibility was increased. Other studies proposed a threshold around which is the percentage of fines content has positive or negative impacts [21-23]. Liquefaction susceptibility of granular materials has been extensively investigated by experimental, theoretical, and empirical methods, few geological studies and field observations have been reported in the literature [24-26]. Many parameters have proposed in previous studies to evaluate the liquefaction susceptibility of soil such as state parameter, relative contractiveness and stress ratio (minimum deviator stress to initial peak deviator stress). Some studies Sadrekarimi [27] used the brittleness index,  $I_B$  which proposed by Bishop [28] to characterize the amount of reduction in undrained shear strength during liquefaction. The undrained brittleness index,  $I_B$ , can be expressed by:

$$I_B = \frac{q_{peak} - q_{min}}{q_{min}} \quad (1)$$

Where  $q_{peak}$  = peak deviator stress and  $q_{min}$  = minimum deviator stress.

The values of  $I_B$  are in the range 0-1, and non-flow or non-brittle behaviour (where a non-strength decline occurs during undrained static shear) is observed when  $I_B = 0$ . However, brittle soil behaviour or complete static liquefaction is associated with  $I_B = 1$ . Using waste materials in various engineering applications may positively impact on the environment by decreasing greenhouse gas emissions and problems related to disposal. Rising amount of waste

Ayad Salih Sabbar is Ph.D. candidate of the Department of Civil Engineering, Curtin University, Perth, Australia (phone: +61424673252; e-mail: Ayadsaleh2000@yahoo.com).

Amin Chegenizadeh is Lecturer and Hamid Nikraz is Professor at the Department of Civil Engineering, Curtin University, Perth, Australia (e-mail: Amin.Chegenizadeh@curtin.edu.au, HNikraz@curtin.edu.au).

## Influence of slag content on liquefaction susceptibility of sandy soils

Ayad Salih Sabbar<sup>1,\*</sup>, Amin Chegenizadeh<sup>2</sup>, Hamid Nikraz<sup>3</sup>

<sup>1,2,3</sup>Curtin University, Kent St, Bentley WA 6102, Australia

\*Corresponding author: [ayadsalih.sabbar@postgrad.curtin.edu.au](mailto:ayadsalih.sabbar@postgrad.curtin.edu.au)

**Abstract:** This study experimentally investigated the liquefaction susceptibility of clean Perth sand and sand containing three different slag contents (2%, 4% and 6%). Undrained static triaxial compression tests were performed on saturated samples at three initial confining pressure (100, 150, and 200 kPa) and three relative densities (10%, 50%, and 90%). Samples were prepared by using moist tamping method. The brittleness index and excess pore water pressure ratio were used to quantify the liquefaction susceptibility of mixtures. The results showed that the complete static liquefaction (zero effective stress) was observed at the lowest confining pressure and lowest relative density. In addition, the liquefaction susceptibility of mixtures reduced with increasing initial confining pressure and relative density. Slag reduced the liquefaction susceptibility of sand by filling the voids between sand grains which reduces the rate of pore water pressure generation. Samples of sand with 4% slag exhibited the lowest brittleness index and lowest excess pore water pressure ratio. Sample with 90% relative density exhibited negative excess pore water pressure ratio that indicates the strain hardening behaviour.

**Keywords:** clean sand, slag, brittleness index, liquefaction

### 1. INTRODUCTION

Liquefaction is a phenomenon of a sudden reduction in shear strength due to an abrupt increase in pore water pressure in saturated cohesionless soils when subjected to undrained monotonic or cyclic loading so that it moves as a viscous liquid (Castro, 1969, Kramer, 1996, NRC, 1985, Yamamuro and Lade, 1997). The criterion for liquefaction failure under cyclic loading is called cyclic mobility and known as flow liquefaction under static loading (Kramer, 1996, NRC, 1985). In the field, the cyclic liquefaction occurs more than static liquefaction but the consequences of static liquefaction usually far more severe (Kramer, 1996). Flow liquefaction can exist when the static shear stresses subjected to the soil mass exceed the shear strength of the soil in its liquefied condition (NRC, 1985). Cyclic mobility is not examined here. The induced pore water pressure may reduce the bearing capacity of the sandy soil, accordingly jeopardise the stability of geotechnical applications. Based on the initial state of saturated sandy soils the liquefaction behaviour can be classified into four categories: complete static liquefaction, flow failure, limited liquefaction and non-flow behaviour as demonstrated in (Fig. 1). Previous studies on static liquefaction of sandy soils reported that the liquefaction behaviour of clean sandy soils is profoundly affected by many factors such as initial state (i.e., relative density and initial confining pressure), stress mode, sample preparation method, the degree of saturation, compositional characteristics, and fines content (Georgiannou et al., 1990, Igwe et al., 2004, Ishihara, 1993, Ishihara et al., 2004, Konrad, 1993, Sadrekarimi, 2014, Thevanayagam, 1998, Vaid and Sivathayalan, 2000, Yamamuro and Lade, 1997). The determination of liquefaction susceptibility is one of the soil stability analysis techniques. However, different methods were used in the literature. Liquefaction susceptibility

of sandy soils is generally examined in two ways: (1) utilizing experimental tests on undisturbed and remoulded specimens and adapting the collected results to equivalent parameters such as state parameter, undrained brittleness index, liquefaction potential, pore pressure ratio, and the ratio of minimum of deviatoric stress to the initial peak deviatoric stress and (2) using the empirical relations based on the correlation between the field tests and laboratory tests. The liquefaction susceptibility of soils can be evaluated by using brittleness index,  $I_b$  which proposed by Bishop (1971) to characterise the amount of reduction in undrained shear strength during liquefaction. The undrained brittleness index,  $I_b$ , can be expressed by using the equation shown below:

$$I_b = \frac{q_{peak} - q_{min}}{q_{peak}} \quad (1)$$

Where  $q_{peak}$  is initial peak deviator stress, and  $q_{min}$  is the minimum deviatoric stress as shown in Fig. 1. The values of  $I_b$  are in the range of 0 to 1, non-flow or non-brittle behaviour (where a non-strength decline occurs during undrained static shear) is observed when  $I_b = 0$ . However, brittle soil behaviour or complete static liquefaction is associated with  $I_b = 1$ . The influence of fines content on the response of sandy soil under monotonic and cyclic loading is an area of uncertainty due to differing results being obtained by previous studies. Some studies reported that the presence of fines content reduced the liquefaction susceptibility of sandy soils. In contrast, other studies concluded that the strength of sandy soil reduces with increasing fines content, as its presence elevates soil compressibility by reducing contact between coarse particles. Today, there is a global interest in utilising waste materials for different engineering applications due to the huge amount of these materials that are produced and their